Phononics 2023

6th International Conference on Phononic Crystals/Metamaterials/ Metasurfaces, Phonon Transport, and Topological Phononics

June 12 - 16, 2023 – Manchester, England

Book of Abstracts

6th International Conference on Phononic Crystals/Metamaterials/ Metasurfaces, Phonon Transport, and Topological Phononics

June 12 - 16, 2023 – Manchester, England

Welcome to Phononics 2023!

Prof. William J. Parnell
University of Manchester
Chair

Dr. Olga Umnova
University of Salford
Co-chair

Prof. Richard Craster
Imperial College London
Co-chair

Contents

Welcome from the Chair

I am absolutely delighted to bring the Phononics community back together again in Manchester following a pause in the conference since 2019 given the COVID-19 pandemic. It was a great shame that we did not get to experience the delights that Marrakech has to offer in 2021. It is a real honour to host this international conference in the UK and to showcase the latest research in the broad field of Phononics. Manchester has a rich history in Science, Engineering and Mathematics (see page 12 for a brief history of this). I hope that delegates get to learn more about this whilst here in the UK. The city of Manchester has changed enormously over the last 20 years, becoming a modern, diverse European city with a strong local economy and vibrant cultural scene. Everyone will no doubt be aware of its rich musical and sporting heritage but it's also worth noting the many areas of outstanding natural beauty that are close by. I hope that delegates get to experience some of the many exciting local attractions within the city but also some of the areas of further afield, outside the city.

I would like to thank all delegates for their support of the Phononics 20XX series and for making the effort to travel to Manchester. I am aware that the last few years has been a struggle for many and getting back into the swing of international travel is not necessarily easy, or inexpensive. However I hope that all delegates will benefit from being together in one venue again, which brings forth so many more benefits over and above the virtual meetings and conferences, as we know well.

I have many people to thank for their help in the organisation of the conference. Mahmoud Hussein (International Phononics Society - IPS) has been a constant source of support, energy and encouragement and without him I am not sure we would have got here! I am amazed by his ability to work around the clock to make things happen and to motivate others. I am also sincerely grateful to Mehmet Su, who cannot be here in Manchester unfortunately but has worked tirelessly behind the scenes for the IPS and for the conference on the website and technical matters. I also thank Ihab El-Kady for general matters relating to the IPS.

Locally I would like to thank our students Eleanor, Elena, Tom, and Valentin for various administrative matters, Lisa Jepson for help with hotels, and Anna Healy, who was incredibly responsive on all matters relating to the e-store. For all things of a printed and merchandise nature I thank Sam Pearson from Chapel Press, whose enthusiasm and helpfulness knows no bounds! Brookdale Bees, a local company in Manchester, supplied the honey. I'm grateful to them for stepping in at the last minute to help with

this. The fantastically creative John Cooper created our video. We have worked with John now for some years and I am always impressed by his imaginative approach, as well as his genuine interest in the science. Thanks to Eleanor Russell for her creative contributions to the programme covers and to my close colleague Raphael Assier, who listens very well and always offers thoughtful suggestions. Thanks in advance to our local helpers, who will be wearing yellow T-shirts all week. Do feel free to ask them for help if you need it. They will try to assist!

Thanks to Jane and Julie from the Manchester Conference Team for putting up with my persistent questions about every aspect of conference organisation. I am also grateful to the conference sponsors, listed on page 15, for their financial support.

Finally, thanks to my family for their understanding. As we all know it's not a 9 to 5 profession and certainly not when organising a large international conference!

Have a fabulous week in Manchester.

William J. Parnell
Professor of Applied Mathematics
Department of Mathematics
University of Manchester

Who's who at Phononics 2023

Conference Chair

William J. Parnell
University of Manchester, UK

Conference Co-chairs

Olga Umnova
University of Salford, UK

Richard Craster
Imperial College London, UK

IPS International Organising Committee

Bernard Bonello
Sorbonne Université (France)

Pierre Deymier
University of Arizona

Bahram Djafari-Rouhani
Université Lille 1 (France)

Ihab El-Kady
Sandia National Laboratories/University of New Mexico (USA)

Mahmoud I. Hussein
University of Colorado Boulder (USA)

Abdelkrim Khelif
Université de Franche-Comté-Besançon (France)

Baowen Li
University of Colorado Boulder (USA) and Southern UST, Shenzen (China)

Charles M. Reinke
Sandia National Laboratories (USA)

José Sánchez-Dehesa
Universidad Politecnica de Valencia (Spain)

Clivia M.S. Torres
Catalan Institute of Nanoscience & Nanotech. (Spain)

Ying Wu
King Abdullah University of Science and Technology (Saudi Arabia)

University of Manchester Student and Postdoc Helpers

Fatmeh Alsalami
Georgia Bradshaw
Charlotte Charlton
Sean Donner
Erik Garcia-Neefjes
Valentina Kunz
Hollie Lloyd
Daniel McKinnell
Elena Medvedeva
Frank Millward
Matt Nethercote
Ekaterina Nguyen
Aidan Retallick
James Shemilt
Tom White

A very brief history of Science, Engineering and Mathematics at the University of Manchester

The city of Manchester has made significant contributions to the fields of science, engineering and mathematics, dating back to the industrial revolution in England in the 18th and 19th centuries. During this time it became a modern hub for textile manufacturing and engineering. Engineers and inventors in Manchester pioneered the development of machinery and infrastructure that powered the industrialisation process. The city's canals, railways and mills became symbols of progress and innovation. One of Manchester's most notable scientists was John Dalton, an English chemist who formulated the atomic theory. His work revolutionised our understanding of matter and laid the foundations of modern chemistry.

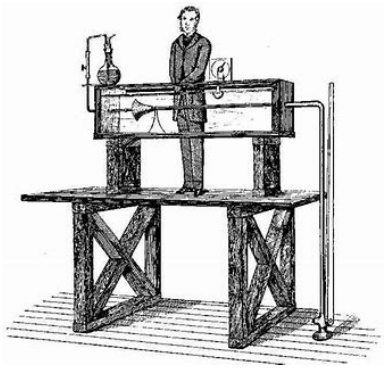

Reynolds and his famous transition-to-turbulence experimental apparatus.

In the 19th century Osborne Reynolds, a prominent engineer and applied mathematician, conducted groundbreaking experiments on fluid dynamics in Manchester. His research on fluid flow along channels established the concept of the *Reynolds number*, fundamental to the transition between turbulent and laminar flow. Reynolds' experimental apparatus is still kept in the basement of the old engineering buildings in Manchester.

Of great relevance to wave mechanics is the work of Horace Lamb, who held the Beyer Chair in Applied Mathematics in Manchester from 1888 until 1920. Lamb was a renowned mathematician, with notable contributions to hydrodynamics, elasticity theory, and acoustics, among others. He is of course very well known for the waves in plates that bear his name. His famous furniture is still located in the Horace Lamb room in the Alan Turing building, home to the Department of Mathematics.

Sir Horace Lamb, who held the Beyer Chair at Manchester from 1888-1920.

During the late 19th and early 20th centuries the University of Manchester's Physics department was home to some of the giants of Physics including Rutherford, Bohr (briefly), WL Bragg and JJ Thomson, amongst others. Rutherford conducted his famous experiments that led to the discovery of the atomic nucleus whilst in Manchester.

He conducted these experiments between 1907 and 1919, bombarding thin metal foils, including gold, with positively charged alpha particles. Rutherford's observations led to the conclusions that most of the mass of an atom is concentrated in a small dense region (which he called the nucleus.....). This discovery revolutionised our understanding of the atom and laid the foundation for the development of nuclear physics.

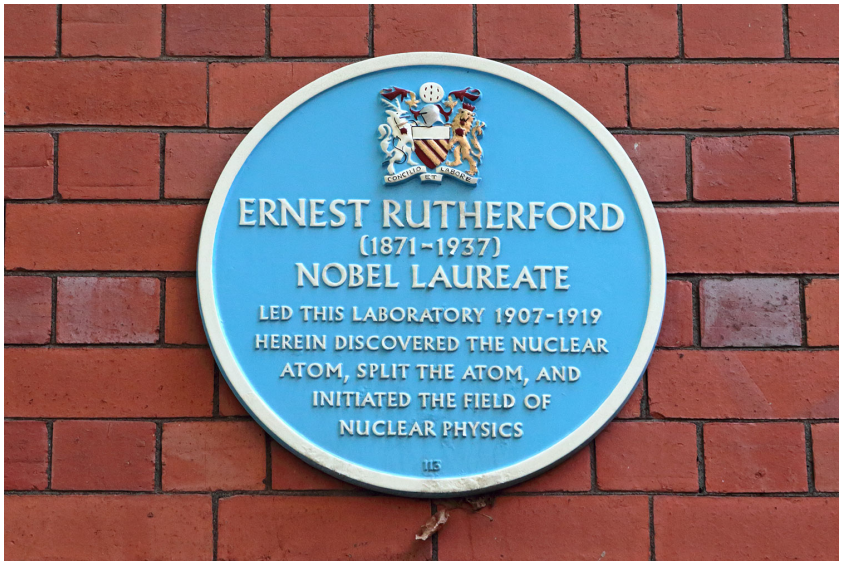

When Rutherford returned to Cambridge in 1919, Manchester appointed William Lawrence Bragg, who had shared a Nobel Prize with his father for inventing x-ray crystallography and the famous Bragg scattering effect. He was succeeded by Patrick Blackett, who won a Nobel Prize for his work on cosmic rays. Interestingly, it was work on cosmic rays that led to radio astronomy and the University's world famous 'big dish', a radio telescope created by Bernard Lovell at Jodrell Bank in the 1950s (the venue of our social excursion on Wednesday morning).

Moving back to the area of fluid dynamics, James Lighthill spent much of his career at Manchester. Lighthill made significant contributions to aerodynamics, acoustics and general mathematical aspects of wave motion. He also served as the Director of the Royal Aircraft Establishment.

In the 1960s the physics department moved to a new building, named after Schuster, on Brunswick Street. The old physics building was given over to psychology and now houses part of the University administration. Electrical engineering was initially linked with physics but became a separate department, from which developed Britain's first department of computer science, based on a series of pioneering computers, beginning with the *Manchester Baby*. This machine, built in 1948 by Freddie Williams and Tom Kilburn, is widely considered to be the world's first stored-program computer.

Working with Williams and Kilburn was, of course the Mathematician Alan Turing. His life and legacy is critically important to city and the University.

Turing is widely known for his concept of the Turing machine, a theoretical device that laid the groundwork for the study of computability and algorithms. Turing's work on code-breaking during World War II at Bletchley Park, and particularly his efforts in cracking the Enigma code, played a crucial role in the second world war. His contributions to the field of artificial intelligence were also groundbreaking. He proposed the idea of a *universal machine* capable of mimicking any other machine, which later became known as the Universal Turing Machine. This concept provided the theoretical underpinnings for the development of AI and computability.

In modern times Manchester has become well known for its research in graphene. Geim and Novoselov discovered a simple and effective method to isolate and study graphene, for which they were awarded the Nobel prize in Physics in 2010.

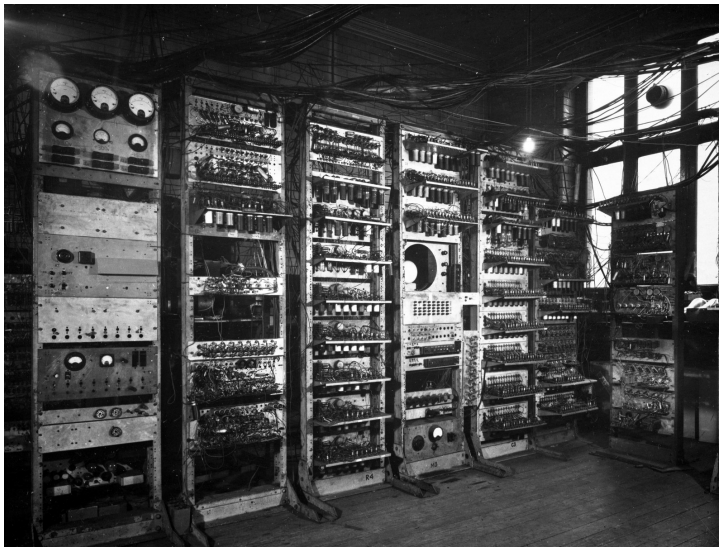

The Manchester baby, widely acknowledged to be the world's first stored program computer.

The Alan Turing memorial, located in Sackville Gardens, in central Manchester.

Sponsors

Manchester Mathematical Sciences

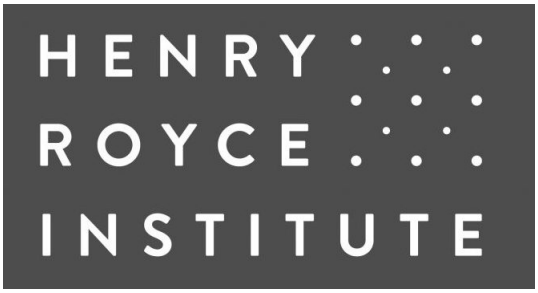

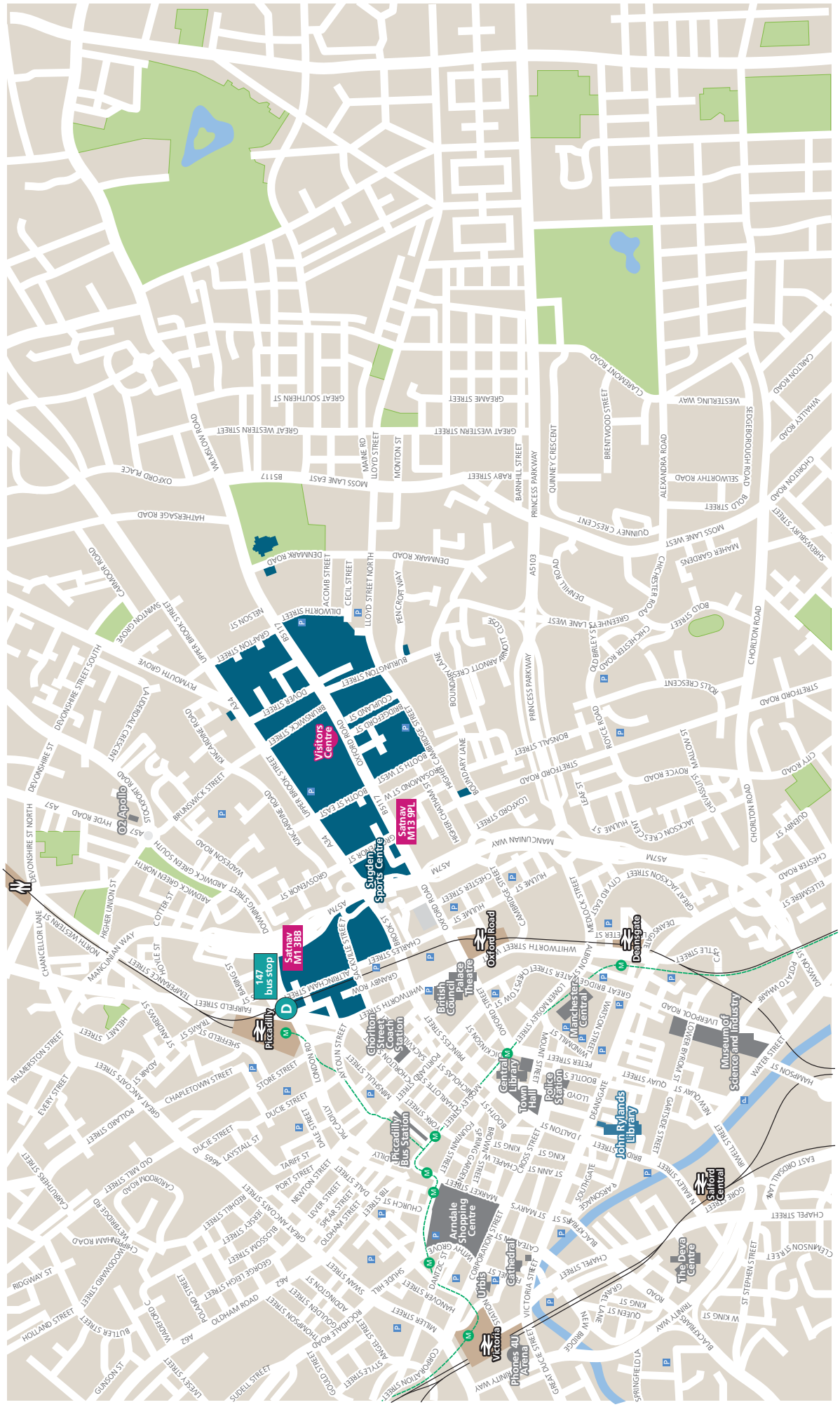 Visitors Centre
Satnav M13 9PL
Satnav M1 3BB
Sugden Sports Centre
147 bus stop
D
Piccadilly
O2 Apollo
Oxford Road
Deansgate
British Council
Palace Theatre
Manchester Central
Chorlton Street Coach Station
Central Library
Town Hall
Police Station
John Rylands Library
Museum of Science and Industry
Piccadilly Bus Station
Arndale Shopping Centre
Cathedral
Urbis
Victoria
Phones 4U Arena
Salford Central
The Deva Centre
GREAT WESTERN STREET
MOSS LANE EAST
OXFORD PLACE
HATHERSAGE ROAD
DENMARK ROAD
UPPER BROOK STREET
GRAFTON STREET
DILWORTH STREET
BURLINGTON STREET
DOVER STREET
BRUNSWICK STREET
OXFORD ROAD
BOOTH ST EAST
BOOTH ST WEST
CAMBRIDGE STREET
BOUNDARY LANE
PRINCESS PARKWAY
MANCUNIAN WAY
A57M
HULME ST
CHESTER STREET
WHITWORTH STREET
PRINCESS STREET
PORTLAND STREET
LONDON RD
PICCADILLY
DEANSGATE
LIVERPOOL ROAD
QUAY STREET
CORPORATION STREET
WITHY GROVE
ROCHDALE ROAD
OLDHAM ROAD
GREAT ANCOATS STREET
CHAPEL STREET
BLACKFRIARS ROAD
STRETFORD ROAD
CHORLTON ROAD
CITY ROAD
MOSS LANE WEST
ALEXANDRA ROAD
QUINNEY CRESCENT
WESTERLING WAY
CLAREMONT ROAD
A34
A57
A6
A665
A62
A5103
B5117

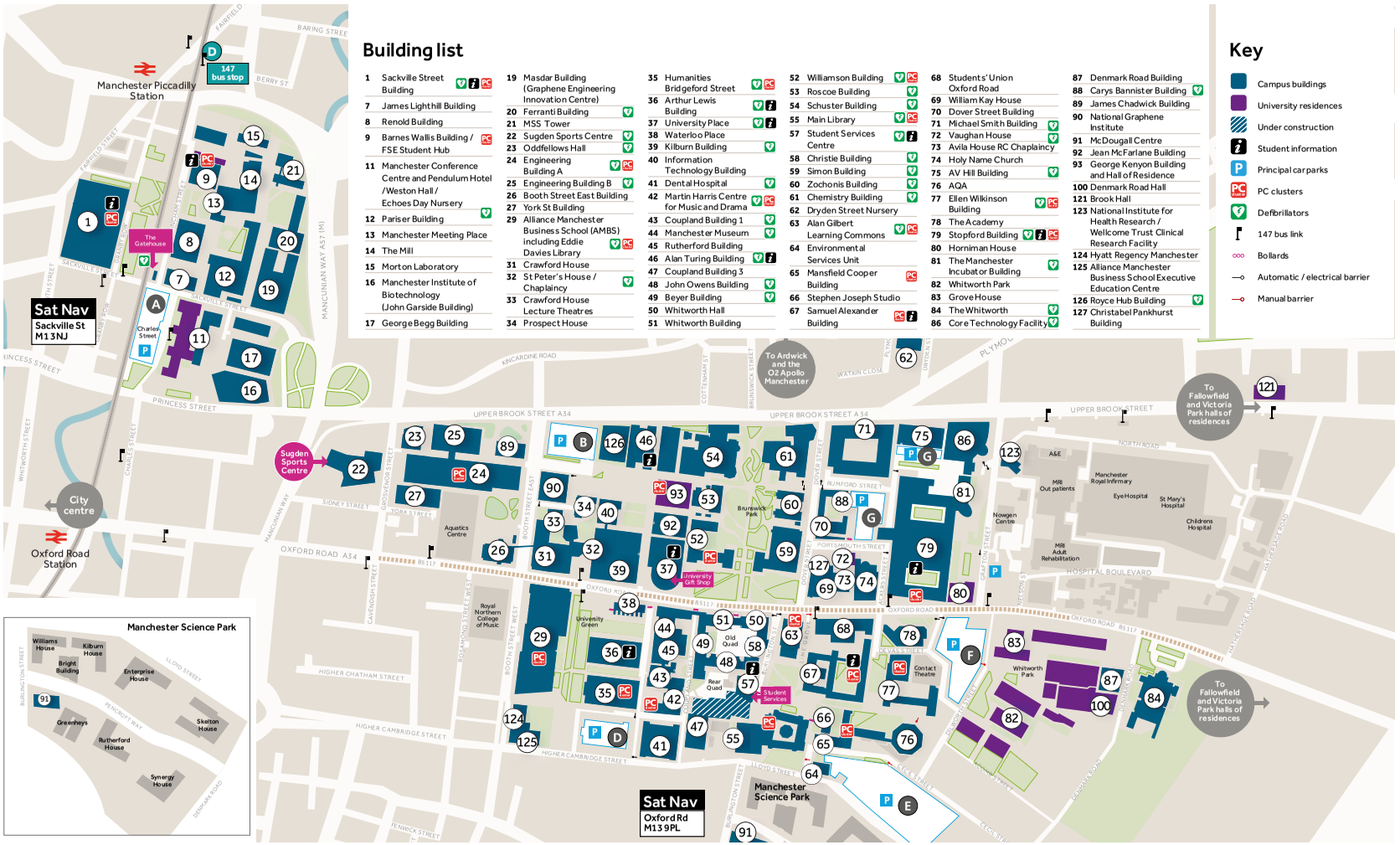

Building list

1 Sackville Street Building
7 James Lighthill Building
8 Renold Building
9 Barnes Wallis Building / FSE Student Hub
11 Manchester Conference Centre and Pendulum Hotel /Weston Hall / Echoes Day Nursery
12 Pariser Building
13 Manchester Meeting Place
14 The Mill
15 Morton Laboratory
16 Manchester Institute of Biotechnology (John Garside Building)
17 George Begg Building
19 Masdar Building (Graphene Engineering Innovation Centre)
20 Ferranti Building
21 MSS Tower
22 Sugden Sports Centre
23 Oddfellows Hall
24 Engineering Building A
25 Engineering Building B
26 Booth Street East Building
27 York St Building
29 Alliance Manchester Business School (AMBS) including Eddie Davies Library
31 Crawford House
32 St Peter's House / Chaplaincy
33 Crawford House Lecture Theatres
34 Prospect House
35 Humanities Bridgeford Street
36 Arthur Lewis Building
37 University Place
38 Waterloo Place
39 Kilburn Building
40 Information Technology Building
41 Dental Hospital
42 Martin Harris Centre for Music and Drama
43 Coupland Building 1
44 Manchester Museum
45 Rutherford Building
46 Alan Turing Building
47 Coupland Building 3
48 John Owens Building
49 Beyer Building
50 Whitworth Hall
51 Whitworth Building
52 Williamson Building
53 Roscoe Building
54 Schuster Building
55 Main Library
56 Student Services Centre
58 Christie Building
59 Simon Building
60 Zochonis Building
61 Chemistry Building
62 Dryden Street Nursery
63 Alan Gilbert Learning Commons
64 Environmental Services Unit
65 Mansfield Cooper Building
66 Stephen Joseph Studio
67 Samuel Alexander Building
68 Students' Union Oxford Road
69 William Kay House
70 Dover Street Building
71 Michael Smith Building
72 Vaughan House
73 Avila House RC Chaplaincy
74 Holy Name Church
75 AV Hill Building
76 AQA
77 Ellen Wilkinson Building
78 The Academy
79 Stopford Building
80 Horniman House
81 The Manchester Incubator Building
82 Whitworth Park
83 Grove House
84 The Whitworth
86 Core Technology Facility
87 Denmark Road Building
88 Carys Bannister Building
89 James Chadwick Building
90 National Graphene Institute
91 McDougall Centre
92 Jean McFarlane Building
93 Christabel Pankhurst Building
100 Denmark Road Hall
121 Brook Hall
123 National Institute for Health Research / Wellcome Trust Clinical Research Facility
124 Hyatt Regency Manchester
125 Alliance Manchester Business School Executive Education Centre
126 Royce Hub Building
127 Christabel Pankhurst Building

Key

Campus buildings
University residences
Under construction
Student information
Principal car parks
PC clusters
Defibrillators
147 bus link
Bollards
Automatic / electrical barrier
Manual barrier

A

78 Academy
37 Access Summit Assessment Centre at The University of Manchester
83 Accommodation Office
7 Aerospace Research Centre (UMARI)
63 Alan Gilbert Learning Commons
46 Alan Turing Building
29 Alliance Manchester Business School (AMBS) including Eddie Davies Library
125 AMBS Executive Education Centre
65 Art and Archaeology Library
29 AMBS People Management Organisations
29 AMBS Innovation, Management & Policy
36 Applied Social Sciences
76 AQA
65 Archaeology
35 Architecture and Planning
65 Art History and Visual Studies
36 Arthur Lewis Building
1 Association of University Administrators (AUA)
46 Astrophysics
69 Athletic Union
75 AV Hill Building
73 Avila House (RC Chaplaincy)

B

9 Barnes Wallis Building
49 Beyer Building
79 Biology, Medicine and Health (see also 43, 47,52, 59, 60, 71, 72, 75, 77, 81, 86, 88 & 92)
59 Biology, Medicine and Health Faculty Admin Offices (see also 60,71, 75, 79, 86, 88 & 92)
54 Blackett Lecture Theatre
26 Booth Street East Building
54 Braddick Library
54 Bragg Lecture Theatre
121 Brook Hall
36 Brookes World Poverty Institute

C

86 Cardiovascular Sciences (see also 71, 75 & 79)
49 Car Park Permit Office (Beyer Building)
31 Careers and Employability Division Administration (via Booth St East)
37 Careers Service
88 Carys Bannister Building
35 Cathie Marsh Centre for Census and Survey Research (CCSR)
71 Cell Matrix Biology and Regenerative Medicine (see also 75 & 79)
49 Central Services Unit
77 Centre for English Language Studies in Education (CELSE)
59 Centre for the History of Science, Technology and Medicine (CHSTM)
65 Centre for New Writing
1 Centre for Process and Integration
14 Chemical Engineering and Analytical Sciences (see also 89)
61 Christabel Pankhurst Institute
61 Chemistry Building
67 Chinese Studies
58 Christie Building/Bistro
12 Civil and Construction Engineering
67 Classics and Ancient History
48 Communications, Marketing and Student Recruitment
39 Computer Science
13 Conference Office (see also 49)
38 Confucius Institute
35 Cordingley Lecture Theatre
86 Core Technology Facility
42 Cosmo Rodewald Concert Hall
1 Council Chamber (Sackville Street)
51 Council Chamber (Whitworth Building)
68 Council Chamber (Students' Union)
31 Counselling Service
43 Coupland Building 1
47 Coupland Building 3
31 Crawford House
33 Crawford House Lecture Theatres
48 Curriculum Innovation

D

12 Dalton Nuclear Institute
87 Denmark Road Building
41 Dental Hospital
47 Dentistry (see also 41)
48 Development and Alumni Relations
71 Developmental Biology and Medicine (see also 79)
75 Diabetes, Endocrinology and Gastroenterology (see also 71 & 86)
37 Disability Advisory Support Services
37 Disability Support Office
70 Dover Street Building
42 Drama

E

52 Earth Sciences
67 East Asian Studies
11 Echoes Day Nursery
1 Electrical and Electronic Engineering
27 E&EE High Voltage (see also 20)
36 Economics
77 Ellen Wilkinson Building
24 Engineering Building A
25 Engineering Building B
1 Engineering Doctorate Centre
67 English and American Studies
36 Environment, Education and Development
64 Environmental Services Unit
48 Equality and Diversity Office
49 Estates and Facilities Directorate
88 Eurolens Research
71 Evolution and Genomic Sciences (see also 79)

F

20 Ferranti Building
48 Finance Office
67 French Studies
9 FSE Student Hub (Barnes Wallis)

G

36 Geography
52 Geology
17 George Begg Building
93 George Kenyon Building and Hall of Residence
67 German Studies
67 Goethe Institute
36 Government
36 Granada Centre for Visual Anthropology
19 Graphene Engineering Innovation Centre (Masdar Building)
35 Graphics Support Workshop
52 GM Geological Unit
83 Grove House

H

59 Health and Safety Services
34 Higher Education Careers Service Unit
67 History
74 Holy Name RC Church
80 Horniman House
59 HR Services
77 Human Communication, Development and Hearing (see also 43 & 60)
35 Humanities Bridgeford Street
38 Humanities Faculty Office
124 Hyatt Regency Manchester

I

48 Income Office
86 Infection, Immunity and Respiratory Medicine (see also 71, 75 & 79)
72 Informatics, Imaging and Data Sciences (see also 71, 79 & 92)
40 Information Technology Building
36 Institute for Development Policy and Management (IDPM)
12 International Centre for Advanced Materials (ICAM)
29 International Centre for Labour Studies
45 International Development
68 International Society
67 Italian Studies

J

89 James Chadwick Building
7 James Lighthill Building
67 Japanese Studies
92 Jean McFarlane Building
16 John Garside Building
48 John Owens Building
42 John Thaw Studio

K

44 Kanaris Lecture Theatre
51 Keepers Room
48 Ken Kitchen Committee Room
39 Kilburn Building
50 Knowles Committee Room

L

67 Language Centre
52 Law
63 Learning Commons
38 Legal Advice Centre
42 Lenagan Library
67 Linguistics

M

55 Main Library
29 Management and Leisure
86 Manchester Collaborative Centre for Inflammation Research
11 Manchester Conference Centre
41 Manchester Dental Education Centre (MANDEC)
36 Manchester eResearch Centre (MeRC)
81 Manchester Incubator Building
31 Manchester Institute for the Deaf
35 Manchester Institute for Collaborative Research on Ageing (MICRA)
16 Manchester Institute of Biotechnology (John Garside Building)
77 Manchester Institute of Education
29 Manchester Institute of Innovation Research
13 Manchester Meeting Place
44 Manchester Museum
79 Manchester Surgical Skills and Simulation Centre
8 Manchester University Press
39 Manchester Visualisation Centre
65 Mansfield Cooper Building
42 Martin Harris Centre for Music and Drama, and Electro Acoustic Studio
29 Masood Entrepreneurship Centre
46 Mathematics
91 McDougall Centre
17 Mechanical, Aerospace and Civil Engineering (MACE)
35 Media Centre
79 Medical Education
71 Michael Smith Building
67 Middle Eastern Studies
67 Modern Languages
71 Molecular and Cellular Function (see also 79)
71 Molecular and Clinical Cancer Sciences
15 Morton Laboratory
54 Moseley Lecture Theatre
21 MSS Tower
79 Musculoskeletal and Dermatological Sciences (see also 75)
42 Music
1 Muslim Prayer Hall North
91 Muslim Prayer Hall South

N

90 National Graphene Institute
60 Neuroscience and Experimental Psychology (see also 71, 75, 79, 88 & 92)
92 Nursing, Midwifery and Social Work
42 Novars Research Centre

O

31 Occupational Health
23 Oddfellows Hall
38 Office for Social Responsibility
88 Optometry Clinics
48 Owens' Committee Room

P

12 Pariser Building
43 Pear Lecture Theatre
79 Pharmacy
36 Philosophy
46 Photon Science Research Institute
54 Physics and Astronomy
35 Planning and Environmental Management
36 Politics
79 Population Health, Health Services Research and Primary Care (see also 52, 77 & 92)
29 Precinct Library
48 President and Vice Chancellor's Offices
40 Prospect House
43 Psychology and Mental Health (see also 60, 79 & 92)

R

48 Regional and Economic Affairs
48 Registrar and Secretary
67 Religions and Theology
8 Renold Building
58 Research and Business Engagement Support Services
53 Roscoe Building
126 Royce Hub Building
67 Russian Studies
45 Rutherford Building
54 Rutherford Lecture Theatre

S

32 St Peter's Chaplaincy
1 Sackville Street Building
67 Samuel Alexander Building
71 School of Biological Sciences (see also 60, 75, 79, 86, 88 & 92
79 School of Health Sciences (see also 43, 52, 60, 71, 72, 75, 77, 88 & 92)
79 School of Medical Sciences (see also 41, 47, 59, 71, 75 & 86)
1 Science and Engineering Faculty Office
1 Science and Engineering Foundation Studies
54 Schuster Building
59 Simon Building
36 Social Anthropology
92 Social Work
36 Sociology
67 Spanish and Portuguese Studies
60 Speech and Language Therapy
77 Speech Pathology
69 Sports Directorate
53 Staff Learning and Development
66 Stephen Joseph Studio
79 Stopford Building
79 Stopford Library
37 Student Communications and Marketing
45 Student Experience Directorat
31 Student Health Centre
24 Student Hub
57 Student Services Centre
37 Student Support, Advice and Guidance
48 Student System Office
68 Students' Union Oxford Rd
9 Students' Union Sackville St
37 Studying and Working Abroad
22 Sugden Sports Centre
38 Sustainable Consumption Institute

T

48 Teaching, Learning and Support Office
1 Textiles
37 The Atrium
14 The Mill

U

7 UMARI
86 UMIP
67 University Centre for Academic English
1 University College Union
37 University Place

V

72 Vaughan House
88 Vision Science

W

38 Waterloo Place
59 Wellbeing Room
11 Weston Hall
84 The Whitworth
51 Whitworth Building
50 Whitworth Corridor Committee Rooms
50 Whitworth Hall
82 Whitworth Park
69 William Kay House
52 Williamson Building

Y

27 York St Building

Z

60 Zochonis Building

The Conference Space and Events Details

We are using essentially *three* spaces for the conference inside the MECD building at Manchester. These are all accessible on the 2nd floor of the MECD building (see floor maps on pages to follow) and they are:

- Eventspace 3: Rooms 2A.011, 2A.012, 2A.013, 2A.014 and foyer space.
- Main Lecture Theatre A: 2A.040.
- Blended Lecture Theatre: 2B.020

Eventspace 3 is where the registration desk is located, and is where all refreshment and lunch breaks will take place. The cloakroom is also located here.

The majority of the talks will be held in the Main Lecture Theatre A: 2A.040. The *back* of this lecture theatre is accessible from the 2nd floor. The front of the theatre can be accessed from the 1st floor.

When we switch to two parallel sessions on Monday, Tuesday and Friday, in addition to 2A.040 we will also use our third space, the Blended Lecture Theatre, 2B.020. This is located in Building B, which is accessible across the Link Bridge on the second floor, midway between Eventspace 3 and the Main Lecture Theatre along the main walkway. **All three spaces are highlighted in red on the 2nd floor map.**

We advise you to enter the MECD building via either the north or south entrances. Our helpers will also be located at these entrances to guide you to the right place.

Welcome Drinks Reception - Monday 12th June - 18:45-20:30

This will be held in the Manchester museum on Oxford Road. Building number 44 on the Campus Map (page 18).

The Conference Dinner - Tuesday 13th June - 19:30-end

Tickets to this should have been purchased in advance. You will have been issued with your ticket(s) at registration. A pre-dinner drinks reception will be held from 19:30-20:00 in Christie's Bistro, building number 58 on the Campus Map (page 18), before we move into the historic Whitworth Hall (building number 50 on the Campus Map) for the dinner at 20:00.

Social Excursion - Wednesday 14th June

Tickets to this should have been purchased in advance. You will have been issued with your ticket(s) at registration. Buses will depart from in front of the Hyatt Regency Manchester Hotel (Building number 124 on the Campus Map) at 9am on Wednesday morning. **Please do not be late!**

General Interest Lecture - Wednesday 14th June - 18:00-19:00

Prof. Trevor Cox will be giving the general interest lecture in the Main Lecture Theatre A (2A.040), with a drinks reception held in advance 17:15-18:00.

A Celebration of Architectural Acoustic Aberrations

Professor Trevor Cox, Acoustic Research Centre, University of Salford

Acoustic consultants try to make sure rooms do not have problems such as focussed echoes from domes, excessive reverberation and flutter echoes from parallel walls. But in this paper, I will celebrate these acoustic 'defects' and other extraordinary architectural sounds.

The science behind some historical examples, such as the whispering gallery in St Paul's in London, was solved around a century ago, but others, like the underneath of Echo Bridge in Massachusetts, which was debated in the scientific literature in the 1940s, have never had the physics

fully resolved until recently. Some have suggested that Stonehenge should have extraordinary sounds due to the concave arrangement of the stones, but measurements on a 1:12 acoustic scale model of the site show this is unlikely. Mathematicians use billiards to explore dynamical systems, but real-life audio examples are rare. One of those is the abandoned Thurgoland railway tunnel near Penistone, UK that has an extraordinary metallic flutter arising from closed orbits. The acoustic phenomena play with our perception of sound: in the spherical radome on top of the disused Cold War spy station at Teufelsberg near Berlin, you can whisper into your own ears. Included in the sites to be present will be the disused World War II oil tank which Guinness awarded with the record for the 'longest echo'. Details of acoustic measurements in the space will be presented, where the reverberation time is 112 seconds at 125 Hz, along with discussions of why it is so reverberant. Remarkable architectural sound effects usually arise by chance, being an accidental by-product of geometry. Using prediction models, the paper will also explore what sound effects could be created if designers deliberately set out to maximise acoustic aberrations.

Biography

Trevor Cox is Professor of Acoustic Engineering at the University of Salford where he directs the Acoustic Research Centre. He is a past president of the UK's Institute of Acoustics and was awarded the IoA Tyndall Medal. His research covers architectural acoustics, psychoacoustics and audio. He has been PI/CI on 10 EPSRC projects on built environment acoustics. Current EPSRC projects include two on machine learning challenges to improve hearing aids. Trevor co-wrote the definitive text on room Acoustic Absorbers and Diffusers (CRC Press). He was an EPSRC Senior Media Fellow. He has presented 26 documentaries for BBC radio including: The Physicist's Guide to the Orchestra. He won an ASA Science Writing Award for his popular science book Sonic Wonderland. The book describes the oil tank where he broke the Guinness World record for the longest echo. His latest popular science book is Now You're Talking.

Early career Workshop - Thursday 15th June - 17:00-18:30

This event, focussed on Early Career Researchers, will be held in the Blended Lecture Theatre (2B.020). It will be led by the Engineering and Physical Sciences Research Council (EPSRC) UK Metamaterials Network. The session will consist of talks from members from the Network about its mission and objectives, and the EPSRC about general funding scheme and approaches to obtaining funding, from a general perspective. The session will close with a session on storytelling in science, led by Anna Ploszajski (www.annaploszajski.com).

If you are a PhD student, postdoctoral research, research fellow or in any way deem yourself to be at an early career stage, we would highly encourage you to attend this event, which forms an important part of the conference!

2 SECOND FLOOR

2B.020

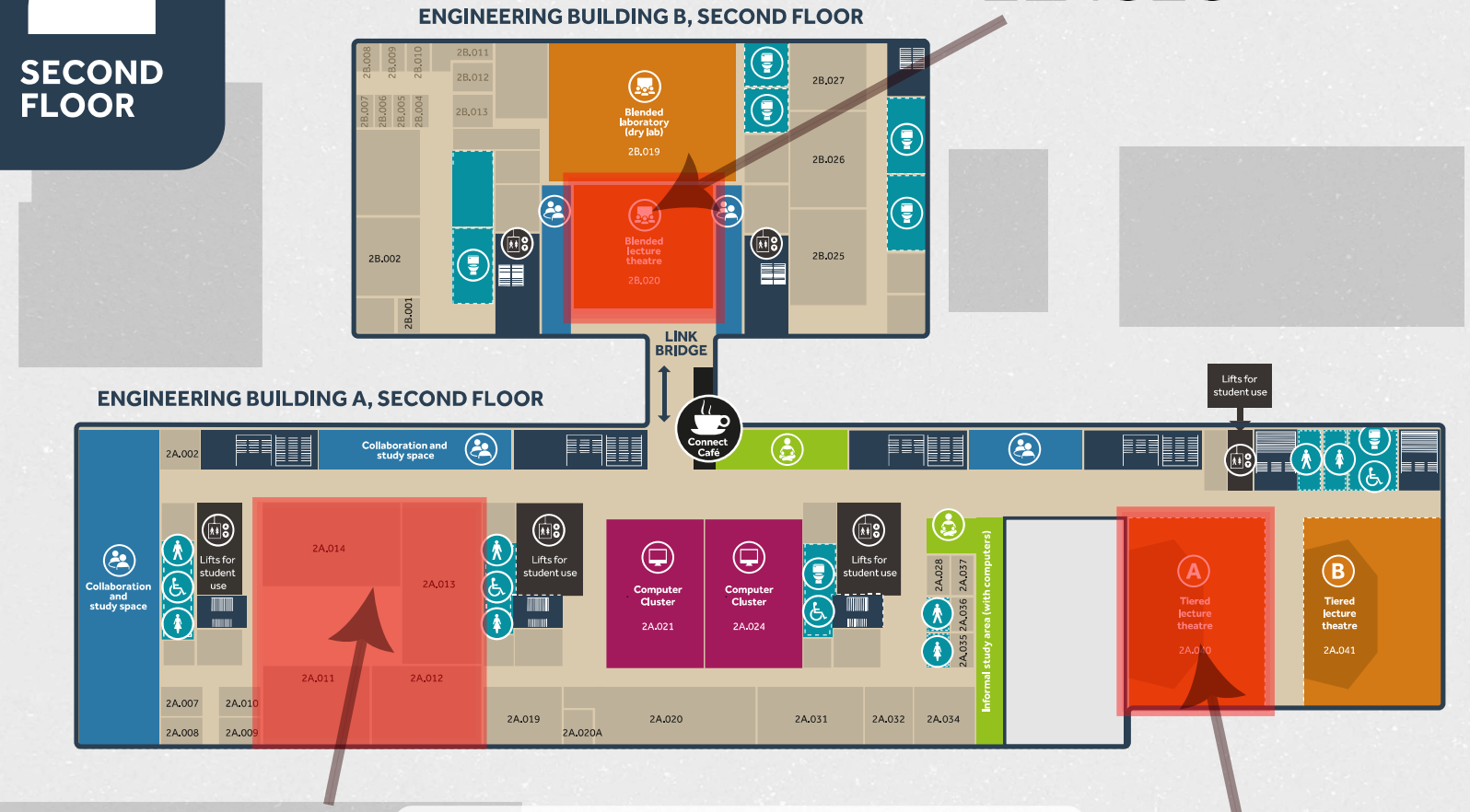

EVENTSPACE 3

2A.040

- Female Toilet
- Male Toilet
- Accessible Toilet
- All Gender Toilet
- Lift
- Café
- Student Support Hub
- Makerspace
- Computer Cluster
- Blended Lecture Theatre
- Tiered Lecture Theatre A
- Tiered Lecture Theatre B
- Workspace
- Collaboration and Study Space
- Informal Study Space
- Swipe card access

1 FIRST FLOOR

ENGINEERING BUILDING B, FIRST FLOOR

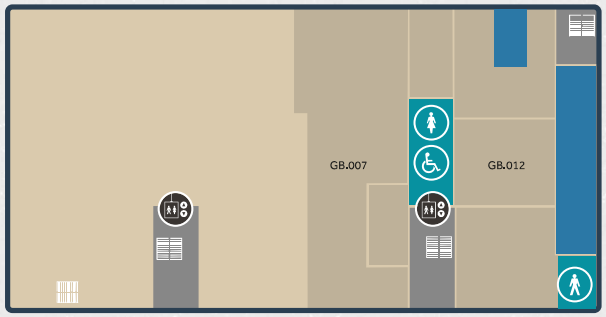

GOOGLE MAP

Access the Google Map for our building by scanning the QR code

ENGINEERING BUILDING A, FIRST FLOOR

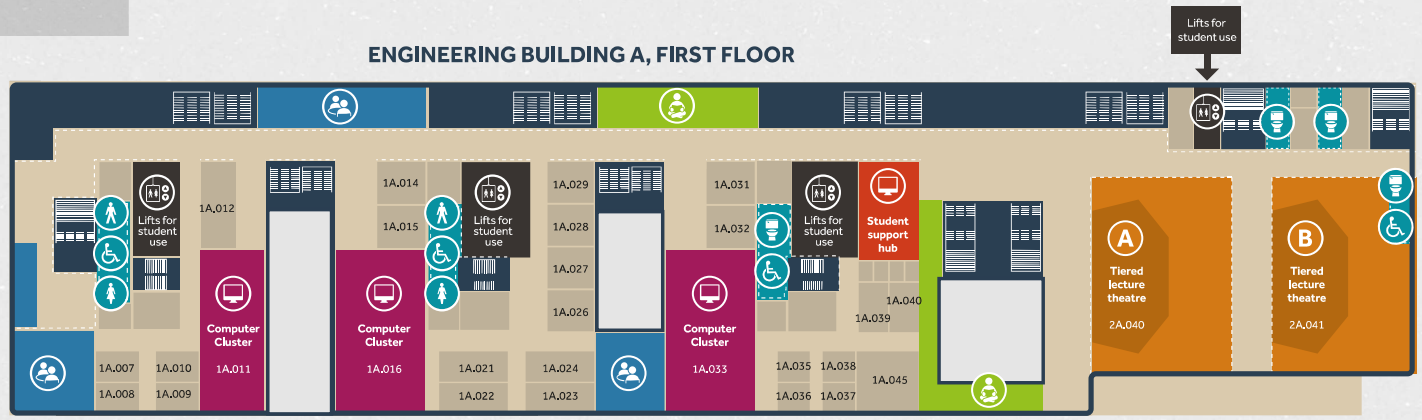

- Female Toilet
- Male Toilet
- Accessible Toilet
- All Gender Toilet
- Lift
- Café
- Student Support Hub
- Makerspace
- Computer Cluster
- Blended Lecture Theatre
- Tiered Lecture Theatre A
- Tiered Lecture Theatre B
- Workspace
- Collaboration and Study Space
- Informal Study Space
- Swipe card access

OPENING HOURS

For building opening hours, visit our Instagram page @uom_mecd

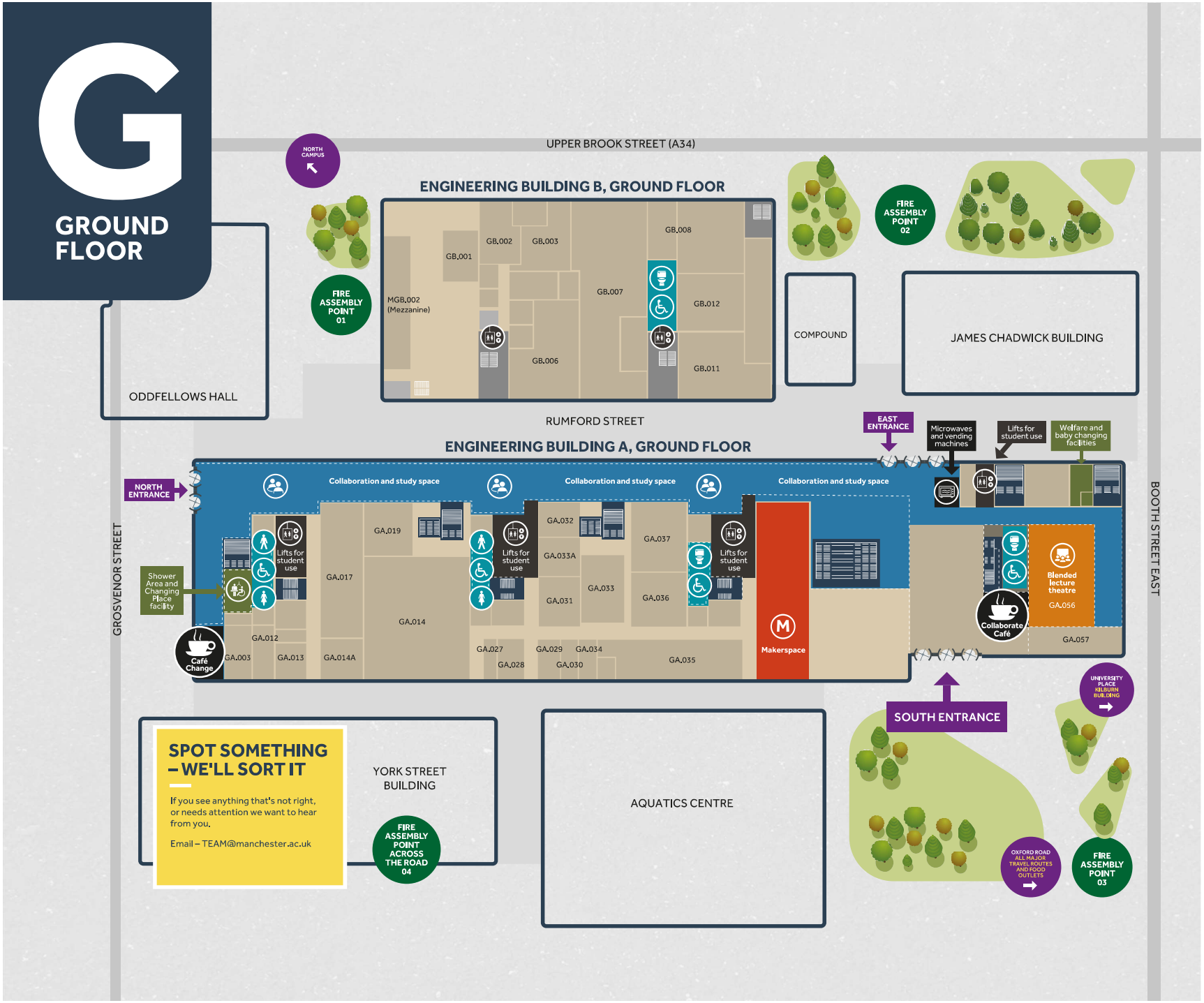
G
GROUND FLOOR
NORTH CAMPUS
UPPER BROOK STREET (A34)
ENGINEERING BUILDING B, GROUND FLOOR
GB.001
GB.002
GB.003
GB.008
MGB.002 (Mezzanine)
GB.007
GB.012
GB.006
GB.011
FIRE ASSEMBLY POINT 01
FIRE ASSEMBLY POINT 02
COMPOUND
JAMES CHADWICK BUILDING
ODDFELLOWS HALL
RUMFORD STREET
EAST ENTRANCE
Microwaves and vending machines
Lifts for student use
Welfare and baby changing facilities
ENGINEERING BUILDING A, GROUND FLOOR
NORTH ENTRANCE
Collaboration and study space
Collaboration and study space
Collaboration and study space
GROSVENOR STREET
BOOTH STREET EAST
Lifts for student use
Lifts for student use
Lifts for student use
Shower Area and Changing Place facility
GA.019
GA.017
GA.014
GA.012
GA.003
GA.013
GA.014A
GA.032
GA.033A
GA.031
GA.033
GA.037
GA.036
GA.027
GA.028
GA.029
GA.030
GA.034
GA.035
Makerspace
Blended lecture theatre
GA.056
GA.057
Collaborate Café
Café Change
SOUTH ENTRANCE
UNIVERSITY PLACE KILBURN BUILDING
OXFORD ROAD ALL MAJOR TRAVEL ROUTES AND FOOD OUTLETS
FIRE ASSEMBLY POINT 03
SPOT SOMETHING – WE'LL SORT IT
If you see anything that's not right, or needs attention we want to hear from you.
Email – TEAM@manchester.ac.uk
YORK STREET BUILDING
FIRE ASSEMBLY POINT ACROSS THE ROAD 04
AQUATICS CENTRE

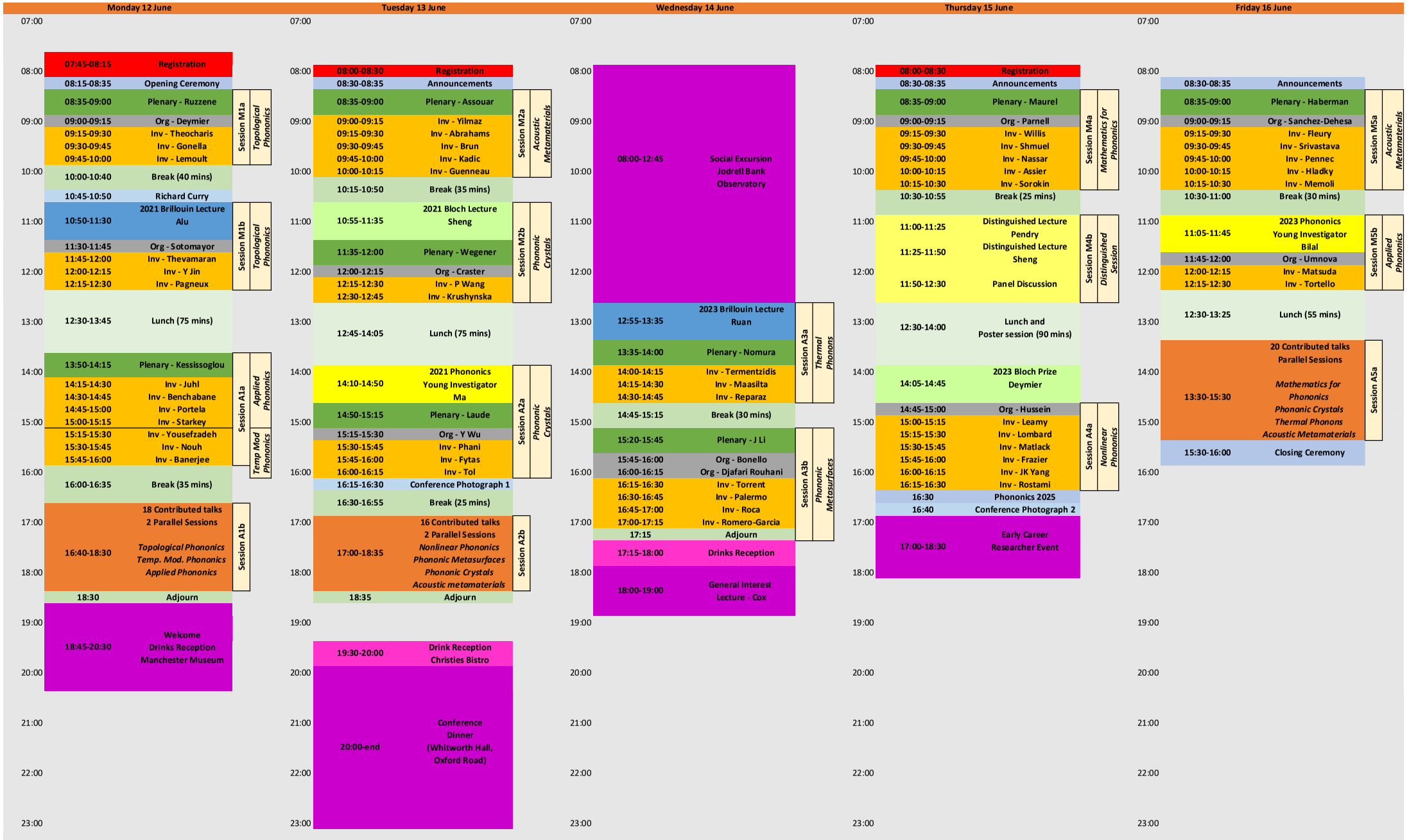
Monday 12 June
07:45-08:15 Registration
08:15-08:35 Opening Ceremony
08:35-09:00 Plenary - Ruzzene
09:00-09:15 Org - Deymier
09:15-09:30 Inv - Theocharis
09:30-09:45 Inv - Gonella
09:45-10:00 Inv - Lemoult
Session M1a Topological Phononics
10:00-10:40 Break (40 mins)
10:45-10:50 Richard Curry
10:50-11:30 2021 Brillouin Lecture Alu
11:30-11:45 Org - Sotomayor
11:45-12:00 Inv - Thevamaran
12:00-12:15 Inv - Y Jin
12:15-12:30 Inv - Pagneux
Session M1b Topological Phononics
12:30-13:45 Lunch (75 mins)
13:50-14:15 Plenary - Kessissoglou
14:15-14:30 Inv - Juhl
14:30-14:45 Inv - Benchabane
14:45-15:00 Inv - Portela
15:00-15:15 Inv - Starkey
Session A1a Applied Phononics
15:15-15:30 Inv - Yousefzadeh
15:30-15:45 Inv - Nouh
15:45-16:00 Inv - Banerjee
Temp Mod Phononics
16:00-16:35 Break (35 mins)
16:40-18:30 18 Contributed talks 2 Parallel Sessions Topological Phononics Temp. Mod. Phononics Applied Phononics
Session A1b
18:30 Adjourn
18:45-20:30 Welcome Drinks Reception Manchester Museum
Tuesday 13 June
08:00-08:30 Registration
08:30-08:35 Announcements
08:35-09:00 Plenary - Assouar
09:00-09:15 Inv - Yilmaz
09:15-09:30 Inv - Abrahams
09:30-09:45 Inv - Brun
09:45-10:00 Inv - Kadic
10:00-10:15 Inv - Guenneau
Session M2a Acoustic Metamaterials
10:15-10:50 Break (35 mins)
10:55-11:35 2021 Bloch Lecture Sheng
11:35-12:00 Plenary - Wegener
12:00-12:15 Org - Craster
12:15-12:30 Inv - P Wang
12:30-12:45 Inv - Krushynska
Session M2b Phononic Crystals
12:45-14:05 Lunch (75 mins)
14:10-14:50 2021 Phononics Young Investigator Ma
14:50-15:15 Plenary - Laude
15:15-15:30 Org - Y Wu
15:30-15:45 Inv - Phani
15:45-16:00 Inv - Fytas
16:00-16:15 Inv - Tol
Session A2a Phononic Crystals
16:15-16:30 Conference Photograph 1
16:30-16:55 Break (25 mins)
17:00-18:35 16 Contributed talks 2 Parallel Sessions Nonlinear Phononics Phononic Metasurfaces Phononic Crystals Acoustic metamaterials
Session A2b
18:35 Adjourn
19:30-20:00 Drink Reception Christies Bistro
20:00-end Conference Dinner (Whitworth Hall, Oxford Road)
Wednesday 14 June
08:00-12:45 Social Excursion Jodrell Bank Observatory
12:55-13:35 2023 Brillouin Lecture Ruan
13:35-14:00 Plenary - Nomura
14:00-14:15 Inv - Termentzidis
14:15-14:30 Inv - Maasilta
14:30-14:45 Inv - Reparaz
Session A3a Thermal Phonons
14:45-15:15 Break (30 mins)
15:20-15:45 Plenary - J Li
15:45-16:00 Org - Bonello
16:00-16:15 Org - Djafari Rouhani
16:15-16:30 Inv - Torrent
16:30-16:45 Inv - Palermo
16:45-17:00 Inv - Roca
17:00-17:15 Inv - Romero-Garcia
Session A3b Phononic Metasurfaces
17:15 Adjourn
17:15-18:00 Drinks Reception
18:00-19:00 General Interest Lecture - Cox
Thursday 15 June
08:00-08:30 Registration
08:30-08:35 Announcements
08:35-09:00 Plenary - Maurel
09:00-09:15 Org - Parnell
09:15-09:30 Inv - Willis
09:30-09:45 Inv - Shmuel
09:45-10:00 Inv - Nassar
10:00-10:15 Inv - Assier
10:15-10:30 Inv - Sorokin
Session M4a Mathematics for Phononics
10:30-10:55 Break (25 mins)
11:00-11:25 Distinguished Lecture Pendry
11:25-11:50 Distinguished Lecture Sheng
11:50-12:30 Panel Discussion
Session M4b Distinguished Session
12:30-14:00 Lunch and Poster session (90 mins)
14:05-14:45 2023 Bloch Prize Deymier
14:45-15:00 Org - Hussein
15:00-15:15 Inv - Leamy
15:15-15:30 Inv - Lombard
15:30-15:45 Inv - Matlack
15:45-16:00 Inv - Frazier
16:00-16:15 Inv - JK Yang
16:15-16:30 Inv - Rostami
Session A4a Nonlinear Phononics
16:30 Phononics 2025
16:40 Conference Photograph 2
17:00-18:30 Early Career Researcher Event
Friday 16 June
08:30-08:35 Announcements
08:35-09:00 Plenary - Haberman
09:00-09:15 Org - Sanchez-Dehesa
09:15-09:30 Inv - Fleury
09:30-09:45 Inv - Srivastava
09:45-10:00 Inv - Pennec
10:00-10:15 Inv - Hladky
10:15-10:30 Inv - Memoli
Session M5a Acoustic Metamaterials
10:30-11:00 Break (30 mins)
11:05-11:45 2023 Phononics Young Investigator Bilal
11:45-12:00 Org - Umnova
12:00-12:15 Inv - Matsuda
12:15-12:30 Inv - Tortello
Session M5b Applied Phononics
12:30-13:25 Lunch (55 mins)
13:30-15:30 20 Contributed talks Parallel Sessions Mathematics for Phononics Phononic Crystals Thermal Phonons Acoustic Metamaterials
Session A5a
15:30-16:00 Closing Ceremony

CONTRIBUTED TALKS

	MONDAY A1b	Room 2A.040		MONDAY A1b	Room 2B.020	
16:40-16:52	De Ponti	Jacopo	TOPOLOGICAL PHONONICS	Tessier Brothelande	Sarah	TEMPORALLY MODULATED PHONONICS
16:52-17:04	Ma	Jihong Aafia		Gliozzi	Antonio	
17:04-17:16	Rosa	Matheus		Riva	Emanuele	
17:16-17:28	Wiltshaw	Richard		Dhiman	Anuj Kumar	
17:28-17:40	Florez	Omar		Hall	Andrew	APPLIED PHONONICS
17:40-17:52	Hatanka	Daiki		Cutanda Henriquez	Vicente	
17:52-18:04	Achilleos	Vassos		Kianfar	Armin	
18:04-18:16	Otsuka	Paul		Feng	Gao	
18:16-18:28	Iglesias Martínez	Julio Andrés		Alcorta Galvan	Ricardo	
	TUESDAY A2b	**Room 2A.040**		**TUESDAY A2b**	**Room 2B.020**	
17:00-17:12	Smith	Elizabeth	NONLINEAR PHONONICS	Dass	Chandriker	PHONONIC CRYSTALS
17:12-17:24	Bae	Myung Hwan		Graczykowski	Bartlomiej	
17:24-17:36	Ioannou Sougleridis	Ioannis		Marburg	Steffen	
17:36-17:48	Alu	Andrea	PHONONIC METASURFACES	Calius	Emilio	ACOUSTIC METAMATERIALS
17:48-18:00	Bosia	Federico		Clarke	Claudia	
18:00-18:12	Lee	Sung-Won		Rosafalco	Luca	
18:12-18:24	Dorn	Charles		Skvortsov	Alex	
18:24-18:36	Muhammad	Muhammad		Zhang	Quan	
	FRIDAY A5a	**Room 2A.040**		**FRIDAY A5a**	**Room 2B.020**	
13:30-13:42	Kisil	Anastasia	MATHEMATICS FOR PHONONICS	Geng	Zhuoran	THERMAL PHONONS
13:42-13:54	Bhatt	Abhigna		Beardo	Albert	
13:54-14:06	Touboul	Marie		Ordonez-Miranda	Jose	
14:06-14:18	Vial	Benjamin		Roshdy	Mohamed Eid	ACOUSTIC METAMATERIALS
14:18-14:30	Davies	Bryn		Röntgen	Malte	
14:30-14:42	Lazaro	Mario		Keogh	Melanie	
14:42-14:54	Morini	Lorenzo	PHONONIC CRYSTALS	Meng	Yang	
14:54-15:06	Liang	Yu-Jui		Giannini	Daniele	
15:06-15:18	Hales Swift	Stephen		Fossat	Pascal	
15:18-15:30	Xu	Changqing		Reda	Jana	

CONTRIBUTED POSTER SESSION THURSDAY 12.30-14.00 EVENT SPACE 3		POSTER NUMBER	
Kogani	Ali	1	*Nonlinear Phononics*
Kamruzzaman	Md	17	
Paliovaios	Apostolos	23	
Jang	Sang Vin	3	*Phononic Metasurfaces*
Shin	YeJeong	32	
Korkiamaki	Tatu Antti Santeri	4	*Phononic Crystals*
Gattin	Max	8	
Beoletto	Paolo Han	14	
Nistri	Fabio	20	
Patino	Nicholas	24	
Diaz	Jon Canosa	33	
Belahurau	Yauheni	43	
Das	Rishab	5	*Acoustic Metamaterials*
Adham	Ali Ishan	6	
Cominelli	Sebastiano	7	
Kim	Gihyun	10	
Vasconcelos	Ana	12	
Saatchi	Daniel	13	
Panda	Susmita	28	
Patro	Somya Ranjan	29	
Sethi	Muskaan	31	
Piva	Paulo Sergio	37	
Rodriguez Gomez	Sara Elena	41	
Poulous	Markos	15	*Thermal Phonons*
Ma	Jihong Aafia	16	
Rawte	Prajit	38	
Kim	Namjeong	18	*Applied Phononics*
Clark	Monty Edward	22	
Harris	Adam	39	
Hales Swift	Stephen	40	
Krasikova	Mariia	42	
Djafari Rouhani	Bahram	21	*Topological Phononics*
Lee	Myung-Joon	27	

Scientific Programme

Monday 12th June

M1a [MECD, Main Lecture Theatre A (2A.040)]

08:15-08:35		Opening Ceremony

Topological Phononics

08:35-09:00	Plenary	**Dynamics of Modulated Media and Acoustic Temporal Metagratings** M. Ruzzene
09:00-09:15	Organisers' Colloquium	**Topological Acoustics Sensing** P.A. Deymier, Trevor D. Lata, M. Arif Hasan, Keith Runge
09:15-09:30	Invited	**Topological Mechanical Metamaterials Revealed By Higher-order Coordinate Transformations** F. Allein, A. Anastasiadis, R. Chaunsali, I. Frank, N. Boechler, F. Diakonos, G. Theocharis
09:30-09:45	Invited	**Topologically Polarized Maxwell Lattices: beyond the Kagome Paradigm** M. Charara, S. Gonella
09:45-10:00	Invited	**Guided Waves in Soft Elastomers: Non-Linear Control and Topological Properties** A. Delory, F. Lemoult, M. Lanoy, A. Eddi, C. Prada

[MECD, Event Space 3]

10:00-10:40		Break

M1b [MECD, Main Lecture Theatre A (2A.040)]

10:45-10:50		Prof. Richard Curry, Dean of Research, Faculty of Science and Engineering, University of Manchester

Topological Phononics

10:50-11:30	2021 Brillouin	**Non-Reciprocal and Topological Phononics** A. Alu, R. Fleury, Sounas, D.
11:30-11:45	Organisers' Colloquium	**Towards Phononic Circuits: Components and Signal Protection** C.M. Sotomayor Torres, G. Madiot, R.C. Ng, D. Navarro-Urrios, G. Arregui, M. Albrechtsen, O. Florez, A. Martinez, S. Stobbe, P.D. Garcia, J. Ahopelto
11:45-12:00	Invited	**Non-Hermitian Elastodynamic Metamaterials** A. Gupta, A. Kurnosov, T. Kottos, R. Thevamaran
12:00-12:15	Invited	**Topological states in Hermitian and non-Hermitian beams** Y. Jin, L. He, W. Wang, R. Cai, W. Zhong, X. Zhuang, T. Rabczuk, Y. Pennec, B. Djafari-Rouhani
12:15-12:30	Invited	**Invisibility of Defects in Chiral and Mirror Symmetric Networks** A. Coutant, L.Y Zheng, V. Achilleos, O. Richoux, G. Theocharis, V. Pagneux

[MECD, Event Space 3]

12:30-13:45		Lunch

A1a [MECD, Main Lecture Theatre A (2A.040)]

Applied Phononics

13:50-14:15	Plenary	**Acoustic Coatings for Maritime Applications** C. Lin, G.S. Sharma, A. Skvortsov, I. MacGillivray, N. Kessissoglou
14:15-14:30	Invited	**Flow Transition Delay by Multi-Input Multi-Output Phononic Subsurface** C.L. Willey, C.J. Barnes, V.W. Chen, K. Rosenberg, A. Medina, A.T. Juhl,
14:30-14:45	Invited	**Hybridizing Surface Acoustic Waves and Mechanical Resonators for Phononic Information Processing** S. Benchabane, M. Baranski, R. Chacon, J. Chatellier, J.-M. Friedt, A. Khelif
14:45-15:00	Invited	**Leveraging and Tuning Acoustic-Wave Propagation in Micro-Architected Materials** R. Sun, Y. Kai, T. Pezeril, W. DeLima, C.M. Portela
15:00-15:15	Invited	**Realizing Beyond-Nearest-Neighbour Coupling in Acoustic and Elastic Metamaterials on a Benchtop Scale** T.A. Starkey, D.B. Moore, I.R. Hooper, J.R. Sambles, A.P. Hibbins, G.J. Chaplain

Temporally Modulated Phononics

15:15-15:30	Invited	**Dynamics of Spatiotemporally Modulated Materials** B. Yousefzadeh
15:30-15:45	Invited	**Temporally Modulated Phase Gradient Systems: Towards Frequency-selective Acoustic Wave Beaming** M. Moghaddaszadeh, R. Adlakha, M.A. Attarzadeh, A. Aref, M. Nouh
16:00-16:00	Invited	**Nonreciprocal Metamaterial from Piezo-electric Sensing and Actuation** A. Banerjee, K.K. Bera

[MECD, Event Space 3]

16:00-16:35		Break

A1a [MECD, Main Lecture Theatre A (2A.040)]

Topological Phononics

16:40-16:52	Contributed	**Tailored Protected Edge Waves via Chiral Hierarchical Metamaterials** J.M. De Ponti, L. Iorio, G.J. Chaplain, A. Corigliano, R.V. Craster, R. Ardito
16:52-17:04	Contributed	**Topological Edge States in Su-Schrieffer-Heeger Phononic Crystals: An Experimental Study** A.R. Alisepahi, K. Sun, J. Ma
17:04-17:16	Contributed	**Interface States in Dimerized Quasicrystal Lattices with Broken Inversion Symmetry** M.I.N. Rosa, D. Beli, L. Lomazzi, C.M. Junior, M. Ruzzene
17:16-17:28	Contributed	**Analytical Solutions for Bloch Waves and Topological Mode Steering in a Meta-Plate** R. Wiltshaw , J.M. De Ponti, R.V. Craster
17:28-17:40	Contributed	**A Topological Phononic Waveguide Above 10 GHz** O. Florez, M. Poblet, S. Pourjamal, J. Ahopelto, C.M. Sotomayor-Torres
17:40-17:52	Contributed	**Control of Ultrahigh Frequency Phonon Transport in Valley Topological Ring Resonator-Waveguide Systems** D. Hatanaka, H. Takeshita, M. Kataoka, M. Misaawa, H. Okamoto, H. Yamaguchi, and K. Tsuruta
17:52-18:04	Contributed	**Experiments in an exact acoustic analogue of the Hatano-Nelson model** A. Maddi , V. Achilleos, G. Penelet, V. Pagneux, Y. Aurégan
18:04-18:16	Contributed	**Imaging a Topological Phononic Crystal in Real and k-Space** P.H. Otsuka, K. Nishimata1, M. Tomoda1, D. Hatanaka, H. Yamaguchi, K. Tsuruta, O. Matsuda
18:16-18:28	Contributed	**Non-Hermitian topological disclination defect in a valley-Hall sonic lattice** J.A. Iglesias Martínez, R. Pernas, M. Kadic, J. Christensen

A1a [MECD, Blended Lecture Theatre (2B.020)]

Temporally Modulated Phononics

16:40-16:52	Contributed	**Experimental study of piezoelectric phononic crystals with space-time modulation in the sub-sonic and sonic regimes** S. Tessier Brothelande, C. Croënne, F. Allein, J.O. Vasseur, B. Dubus
16:52-17:04	Contributed	**Tunable topological edge-modes in photo-responsive periodic structures** G.J. Chaplain, A.S. Gliozzi, B. Davies, D. Urban, F. Bosia, R.V. Craster
17:04-17:16	Contributed	**Surface to Bulk Conversion of Elastic Waves by Temporal Modulation** J. Santini, X. Pu, A. Palermo, F. Braghin, E. Riva
17:16-17:28	Contributed	**Frequency- and Momentum-Resolved Detection of Laser-Excited Acoustic Phonons in Nanomembranes** T. Vasileiadis, A. Kumar Dhiman, K. Sympoura, M. Pochylski, B. Graczykowski

Applied Phononics

17:28-17:40	Contributed	**Multiple layers, phononic arrays and surface variations to suppress the bending wave coincidence effect in panels** A. Hall, G. Schmid, V. Sorokin, G. Dodd
17:40-17:52	Contributed	**Phononic Crystal and Resonator-Based Metasurface Combination for Wide-Angle Sound Absorption** D.M. Garza-Agudelo, V. Cutanda Henríquez, C.-H. Jeong, P.R. Andersen, M. Ibarias, J. Sánchez-Dehesa, F. Lucklum
17:52-18:04	Contributed	**Local flow stabilization/destabilization by phononic subsurfaces over an extended spatial domain** A. Kianfar, M.I. Hussein
18:04-18:16	Contributed	**Locally Resonant Phononic biosensors** A. Khelif, F. Gao, S. Benchabane, A. Bermak
18:16-18:28	Contributed	**Application of Periodic Electrical Boundary Conditions as a Means of Achieving Tunable RF SAW Devices** R. Alcorta Galván, C. Croënne, B. Dubus, B. Loiseaux, E. Eustache, M. Bertrand, A.-C. Hladky

Scientific Programme

Tuesday 13th June

M2a [MECD, Main Lecture Theatre A (2A.040)]

08:30-08:35		Announcements

Acoustic Metamaterials

08:35-09:00	Plenary	**Phononic Skyrmions: a new horizon to structure acoustic and elastic waves?** B. Assouar, L. Cao, S. Wan, Y. Zeng, Y. Zhu
09:00-09:15	Invited	**Ultrawide Phononic Band Gaps** C. Yilmaz
09:15-09:30	Invited	**Acoustic Wave Propagation through Resonant Meta-Materials; an Asymptotic Analysis** I.D. Abrahams, M.J.A. Smith
09:30-09:45	Invited	**Lamb waves in discrete waveguides: unidirectional waves and mechanical switching networks** G. Carta, M.J. Nieves, M. Brun
09:45-10:00	Invited	**Shape Morphing and Elastic waves in Metamaterials** L. Wang, K. Dudek, J. Iglesias, G. Ulliac, V. Laude, M. Kadic,
10:00-10:15	Invited	**Active Thermal Cloaking** M. Cassier, T. DeGiovanni, S. Guenneau, F. Guevara Vasquez

[MECD, Event Space 3]

10:15-10:50		Break

M2b [MECD, Main Lecture Theatre A (2A.040)]

Phononic Crystals

10:55-11:35	2021 Bloch	**Causality and the Development of Tunable Acoustic Metamaterial Absorbers** P. Sheng
11:35-12:00	Plenary	**Roton-like Dispersion Relations in Designed Elastic Crystals** M. Wegener
12:00-12:15	Organisers' Colloquium	**Phononic crystals for elastic wave control** R.V. Craster
12:15-12:30	Invited	**Drawing Dispersion Curves: Band Customization by Non-local Phononic Crystals** A. Kazemi, K.J. Deshmukh, F. Chen, S. Paul, B. Deng, H.C. Fu, P. Wang
12:30-12:45	Invited	**Acoustic Wave Steering in Disordered Networks by Rational Pruning** A.O. Krushynska, M. van Hecke

[MECD, Event Space 3]

12:45-14:05		Lunch

A2a [MECD, Main Lecture Theatre A (2A.040)]

Phononic Crystals

14:05-14:50	2021 Phononics YIA	**Non-Hermitian Extended Topological Modes** G. Ma
14:50-15:15	Plenary	**Guided Waves in Glide-Reflection Symmetric Phononic Crystal Interfaces** J.A Iglesias, N. Laforge, M. Kadic1, E. Prodan, V. Laude
15:15-15:30	Organisers' Colloquium	**From Effective Medium Theory to Acoustic Double-Zero-Index Materials** K. Lyu, C. Xu, M. Farhat, G. Ma, Y. Lai, Y. Wu
15:30-15:45	Invited	**Dissipation Driven Bloch Wave Degeneracies** A.S. Phani
15:45-16:00	Invited	**Hypersonic Metamaterials Based on Architected Hybrid Colloids** Y. Cang, R. Sainidou, P. Rembert, K. Matyjaszewski, M.R. Bockstaller, B. Graczykowski, G. Fytas
16:00-16:15	Invited	**Subwavelength Imaging of Flexural Waves Beyond the Diffraction Limit** H. Danawe, S. Tol

[MECD, Staircase, Outside 1st Floor entrance to Main Lecture Theatre A (2A.040)]

16:15-16:30	Conference Photograph 1

[MECD, Event Space 3]

16:30-16:55	Break

A2b [MECD, Main Lecture Theatre A (2A.040)]

Nonlinear Phononics

17:00-17:12	Contributed	**Wave Propagation in a Phononic Material with Asymmetric Bilinear Stiffness** E.J. Smith, K.H. Matlack
17:12-17:24	Contributed	**Tunable Mid Gap in Monoatomic-diatomic Convertible Phononic Crystal with Odd-even Alternating Nonlinearity** M.H. Bae, S.H. Kim, H.M. Seung, J.H. Oh
17:24-17:36	Contributed	**Nonlinear Propagation in 1D and 2D Acoustic Networks** I. Ioannou Sougleridis, O. Richoux, V. Achilleos, G. Theocharis, C. Desjouy, D.J. Frantzeskakis

Phononic Metasurfaces

17:36-17:48	Contributed	**Hyperbolic Shear Elastodynamic Waves** S. Yves, E. Galiffi, E.M. Renzi, X. Ni, A. Alu
17:48-18:00	Contributed	**Auxeticity enables tuning of topological waveguiding in metamaterial plates** F. Bosia, G. Carta, M. Morvaridi, V.F. Dal Poggetto, A.S. Gliozzi, M. Miniaci, N. Pugno
18:00-18:12	Contributed	**Elastic Metasurface for Multi-Modes** S.-W. Lee, S.-I. Kim, H.-M. Seung, J.-H. Oh
18:12-18:24	Contributed	**Conformally Graded Metamaterials for Wave Attenuation** C. Dorn, D.M. Kochmann
18:24-18:36	Contributed	**Design and Manufacturing of Monolithic Mechanical Metastructure with Ultrawide Bandgap for Low Frequency Vibration and Noise Control** Muhammad, J. Kennedy, C.W. Lim

A2b [MECD, Blended Lecture Theatre (2B.020)]

Phononic Crystals

17:00-17:12	Contributed	**Tapered Resonator-Based Phononic Crystal: Avoided Level Crossings, Robust Self-Collimation, and Bi-Refringence** D. Das, C.K. Dass, P.J. Shah, R. Bedford, L.R. Ram-Mohan
17:12-17:24	Contributed	**Breaking the symmetry: Do imperfect Phononic Crystals work?** V. Babacic, M. Sledzinska, T. Vasileiadis, C.M. Sotomayor Torres, B. Graczykowski
17:24-17:36	Contributed	**Engineering phononic crystals – always finite and never perfectly periodic** S. Marburg, F. Kronowetter

Acoustic Metamaterials

17:36-17:48	Contributed	**Vibroacoustic Metamaterial Systems as Transformation Mechanisms: Towards Multi-Scale and Non-Periodicity** S.E. Rodriguez, E.P. Calius, A. Hall, R. Das
17:48-18:00	Contributed	**Dispersion Behaviour of a Non-Resonant Elastic Metamaterial** J.D. Smith, C.L. Clarke
18:00-18:12	Contributed	**Reinforcement Learning Guiding the Design Optimization of Graded Metamaterials for Energy Harvesting** L. Rosafalco, J.M. De Ponti, L. Iorio, R.V. Craster, R. Ardito, A. Corigliano
18:12-18:24	Contributed	**Acoustic Wave Scattering by a Lattice of Scatterers in a Soft Medium: Homogenisation Approach** A. Skvortsov, G.S. Sharma, I. MacGillivray, N. Kessissoglou
18:24-18:36	Contributed	**Hard-Magnetic Soft Elastic Metamaterials for Tunable Wave Manipulation** Q. Zhang, S. Rudykh

Scientific Programme

Wednesday 14th June

A3a [MECD, Main Lecture Theatre A (2A.040)]

Thermal Phonons

12:55-13:35	2023 Brillouin	**General Formulation, Computational Method, and Significance of Four-Phonon Scattering** X. Ruan, T. Feng
13:35-14:00	Plenary	**Behavior of Thermal Phonons in Contrast to Photons** M. Nomura,
14:00-14:15	Invited	**Phonons and Nanomaterials, New Era** K. Termentzidis
14:15-14:30	Invited	**Acoustic Phonon Tunneling Across a Vacuum Gap between Piezoelectric Crystals** Z. Geng, I.J. Maasilta
14:30-14:45	Invited	**Determination of the In-plane Thermal Diffusivity Using Beam-Offset Frequency-Domain Thermoreflectance with a One-Dimensional Optical Heat Source** K. Xu, J.S. Reparaz

[MECD, Event Space 3]

14:45-15:15		Break

A3b [MECD, Main Lecture Theatre A (2A.040)]

Phononic Metasurfaces

15:20-15:45	Plenary	**Non-reciprocal amplification using Willis coupling** J. Li,
15:45-16:00	Organisers' Colloquium	**Localization of Elastic Energy on Metasurfaces with Resonators** T. Deletang, A. Noual, R. Buisine, B. Djafari-Rouhani, Y. Pennec, L. Carpentier, B. Bonello
16:00-16:15	Organisers' Colloquium	**Focusing and Imaging of Flexural Lamb Waves by Pillared Metasurfaces** L. Carpentier, Y. Jin, W. Wang, J. Iglesias, A. Khelif, Y. Pennec, B. Bonello, B. Djafari-Rouhani
16:15-16:30	Invited	**Tailoring Bound States in the Continuum by Circular Clusters of Scatterers** M. Martí-Sabaté, J. Li, S. Cummer, B. Djafari-Rouhani, D. Torrent
16:30-16:45	Invited	**A Multiple Scattering Approach for Elastic Metasurfaces: from Quasi-Periodicity to Space-Time Modulation** X. Pu , A. Palermo, A. Marzani
16:45-17:00	Invited	**Coupled Resonances Mechanisms to Broaden Low-Frequency Bandgaps in Acoustic Metamaterials** D. Roca, G. Sal, D. Yago, J. Cante, J. Oliver, M.I. Hussein
17:00-17:15	Invited	**Target scattering properties with correlated disorder** S. Kuznetsova, L.M. Garcia-Raffi, J.-P. Groby, V. Romero-García

Scientific Programme

Thursday 15th June

M4a [MECD, Main Lecture Theatre A (2A.040)]

08:30-08:35		Announcements

Mathematics Underpinning Phononics

08:35-09:00	Plenary	**Acoustic diffraction grating with space-time modulation** A. Maurel, K. Pham
09:00-09:15	Organisers' Colloquium	**Emergence of Willis constitutive coupling in elastodynamic heterogeneous media** W.J. Parnell, P.A. Cotterill, D. Nigro
09:15-09:30	Invited	**Energy Transmission and Reflection at the Boundary of a Composite with Random Microgeometry** J.R. Willis
09:30-09:45	Invited	**Discrete One-dimensional Models for the Electromomentum Coupling** K. Muhafra, M.R. Haberman, G. Shmuel
09:45-10:00	Invited	**Strong Passive Willis Coupling** P. Brucks, H. Nassar
10:00-10:15	Invited	**Wave asymptotics in two-dimensional periodic media** R.C. Assier, A. Shanin, A. Korolkov, O. Makarov
10:15-10:30	Invited	**Bi-orthogonality Relations in the Waveguide Theory** S.V. Sorokin, L.S. Ledet

[MECD, Event Space 3]

10:30-10:55		Break

M4a [MECD, Main Lecture Theatre A (2A.040)]

Distinguished Speaker Session

11:00-11:25	Distinguished	**Waves in Time-Dependent Systems** J. Pendry
11:25-11:50	Distinguished	**Underwater Acoustic Absorption by Using Impedance Matched Composites** P. Sheng
11:50-12:30		**Panel Discussion**

[MECD, Event Space 3]

12:30-14:00		Lunch and Poster Session

[MECD, Event Space 3]

Nonlinear Phononics

12:30-14:00	Poster 1	**Phase Nonreciprocity in a Periodic Material with a Nonlinear Asymmetric Unit Cell** A. Kogani, B. Yousefzadeh
12:30-14:00	Poster 17	**Contact Stiffness Evaluation and Wave Response Study of Engineered Contact-Based Nonlinear Phononic Material** M. Kamruzzaman, G.U. Patil, K.H. Matlack
12:30-14:00	Poster 23	**Non-Linear Waves in Bistable Mechanical Metamaterials and Transition Waves** A. Paliovaios, V. Achilleos, G. Theocharis, V. Tournat, N. Stefanou

Phononic Metasurfaces

12:30-14:00	Poster 3	**Asymmetric Elastic Metasurface between Different Media** S.V. Jang, S.W. Lee, J.-H. Oh
12:30-14:00	Poster 32	**Fluid-like Elastic Metasurface** Y.-J. Shin, H.-M. Seung, J.-H. Oh

Phononic Crystals

12:30-14:00	Poster 4	**Controlling Thermal Transport with Pillar-Based Phononic Crystals** T.A.S. Korkiamäki, T.A. Puurtinen, T. Loippo, I.J. Maasilta
12:30-14:00	Poster 8	**Characterization of biphasic architectured media towards ultrasound monitoring applications** M. Gattin, N. Bochud, G. Rosi, Q. Grossman, D. Ruffoni, S. Naili
12:30-14:00	Poster 14	**Design and characterization of Snell Lenses with Gradient Index Phononic Crystals** P.H. Beoletto , Fabio Nistri, Antonio S. Gliozzi, Federico Bosia,
12:30-14:00	Poster 20	**Metamaterial-based barriers for railway-generated ground borne vibration** F. Nistri, R.M. Cosentini, V.F. Dal Poggetto, P. Charkaluk, N. Pugno, M. Miniaci, A. Gliozzi, F. Bosia
12:30-14:00	Poster 24	**Elastic Hyperbolic Strips** N.H. Patino, L. Lomazzi, L. De Beni, M. Ruzzene
12:30-14:00	Poster 33	**Silicon Based Suspended Thermometry Device Fabrication for Phonon Ballistic and Coherent Regimes Study** J. Canosa Diaz, H. Ikzibane, B. Brisuda, C. Polanco Garcia, L. Saminadayar, N. Mingo, O. Bourgeois, E. Dubois, J.-F. Robillard

Acoustic Metamaterials

12:30-14:00	Poster 5	**Metapile: Resonator Impregnated Pile Towards Enhanced Passive Vibration Control** R. Das, A. Banerjee, B. Manna
12:30-14:00	Poster 6	**Acoustic attenuation bands using graded metamaterials** A.I. Adham, V. Sorokin, B. Mace, A. Hall
12:30-14:00	Poster 7	**Weight Reduction Strategies for Underwater Acoustic Cloaking** S. Cominelli, D.E. Quadrelli, G. Cazzulani, F. Braghin
12:30-14:00	Poster 10	**Full Ultrasound Transmission in the Metal-Water-Metal System using Elastic Metamaterials** G. Kim, J. Lee, J.H. Cho, M. Kweun, Y.Y. Kim
12:30-14:00	Poster 12	**Multi-Objective Design Optimization of a Metamaterial-Based Interface** A.C.A. Vasconcelos, A.M. Aragon, D.L. Schott, J. Jovanova
12:30-14:00	Poster 13	**Data Driven Geometric Design of Biomimetic Minimal Surface Metamaterial for Elastic to Acoustic Band Gaps** D. Saatchi , I.-K. Oh
12:30-14:00	Poster 28	**Vibration Control of Beams under the Action of Moving Loads using Inertial Amplifier** S. Panda , A. Banerjee, B. Manna
12:30-14:00	Poster 29	**Flexural wave propagation of Metamaterial inspired Rigid Elastic metastructures** S.R. Patro, A. Banerjee, G.V. Ramana
12:30-14:00	Poster 31	**Vibration attenuation in a mass in mass frictional metamaterial: An analytical investigation** M. Sethi, A. Banerjee, B. Manna
12:30-14:00	Poster 37	**Mathematical Model for Layered Acoustic Materials with Random Particulate Microstructure** P.S. Piva, K.K. Napal, A.L. Gower
12:30-14:00	Poster 41	**Automated design of multiscale mechanical metamaterials** S.E. Rodriguez, R. Das, E.P. Calius

Thermal Phonons

12:30-14:00	Poster 15	**Thermal Rectification using Asymmetrically Perforated Graphene** M. Poulos, K. Termentzidis
12:30-14:00	Poster 16	**Phonon Transport in Defected Bi-Layer Graphene Nanoribbons** T. Boriwaye, J. Ma
12:30-14:00	Poster 38	**Propagation Characteristics of Narrowband Thermal Phonons under Atomic-scale Local Resonance Conditions** A. Beardo, P. Desmarchelier, C.-N. Tsai, P. Rawte, K. Termentzidis, M.I. Hussein

Applied Phononics

12:30-14:00	Poster 18	**Sensing 6G Communication Ultra-high Frequency Radio Waves via Phononic Crystal** N.J. Kim, Y.J. Shin, S.W. Lee, H.W. Park, M.H. Bae, J.H. Oh
12:30-14:00	Poster 22	**Apertures for Generating Spatial Superoscillations of Coherent Acoustic Phonons** M.E. Clark, K.A. Benedict, K. Sellami, A.V. Akimov, J. Bailey, R.P. Campion, A.J. Kent
12:30-14:00	Poster 39	**Design of 3D Printable Phononic Subsurfaces based on Locally Resonant Elastic Metamaterials** A.R. Harris, T. Calascione, J.A.N. Farnsworth, M.I. Hussein
12:30-14:00	Poster 40	**Phononic Dispersion Coupling as Flowmeter** S. Hales Swift, I.F. El-Kady

Topological Phononics

12:30-14:00	Poster 21	**Flat Band Induced Topological Tamm States in One-Dimensional Comb-like Structures** S. Khattou, Y. Rezzouk, M. Amrani, M. El Ghafiani, E.H. El Boudouti, A. Talbi, Y. Jin, B. Djafari-Rouhani
12:30-14:00	Poster 27	**Tailoring Valley Displacement in Valley Topological Mechanical Honeycomb Lattice** M.-J. Lee, I.-K. Oh

A4a [MECD, Main Lecture Theatre A (2A.040)]

Nonlinear Phononics

14:05-14:45	2023 Bloch	**Quantum-inspired Acoustic Computing** P. Deymier
14:45-15:00	Organisers' Colloquium	**Harmonics dispersion relation: Inner makings of a time evolving strongly nonlinear wave** M.I. Hussein, R. Khajehtourian
15:00-15:15	Invited	**A Perturbation Approach for Interfaced Transmission Between Linear and Nonlinear Monatomic Lattices** L. Fang, M.J. Leamy
15:15-15:30	Invited	**Effective Dynamics for Low-Amplitude Transient Elastic Waves in a 1D Periodic Array of Non-Linear Interfaces** C. Bellis, B. Lombard, M. Touboul, R. Assier
15:30-15:45	Invited	**Nonlinear wave propagation through phononic materials with rough contact interfaces** G.U. Patil, K.H. Matlack
15:45-16:00	Invited	**Mechanical Multi-level Memory** J.E. Pechac, M.J. Frazier
16:00-16:15	Invited	**Origami-based Metamaterial: A New Type of Versatile Mechanical Waveguide** H. Yasuda, Y. Miyazawa, P. Kevrekidis, J. Yang
16:15-16:30	Invited	**Acoustogalvanic Effect in Dirac Materials** H. Rostami
16:30-16:40		**Phononics 2025 Host Announcement**

[MECD, Staircase, Outside 1st Floor entrance to Main Lecture Theatre A (2A.040)]

16:40-16:50	Conference Photograph 2

Scientific Programme

Friday 16th June

M5a [MECD, Main Lecture Theatre A (2A.040)]

08:30-08:35		Announcements

Acoustic Metamaterials

08:35-09:00	Plenary	**Non-reciprocal Sound Scattering with Spatiotemporally Modulated Acoustic Metasurfaces** M.R. Haberman
09:00-09:15	Organisers' Colloquium	**Shannon Entropy as a Characterization Tool in Acoustics** J. Sánchez-Dehesa
09:15-09:30	Invited	**Nonlocally-Resonant Elastic Metamaterials** A. Bossart, R. Fleury
09:30-09:45	Invited	**On the Nature of Boundaries and Interfaces in Metamaterials and Phononic Crystals** A. Srivastava
09:45-10:00	Invited	**Propagation of Elastic Waves in Randomly Distributed Pillars on Metamaterial Phononic Plate** Y. Pennec, L. Carpentier, R. Cai, Y. Jin, A. Noual, B. Djafari-Rouhani, T. Deletang, B. Bonello
10:00-10:15	Invited	**Design of Metamaterials for Acoustic Stealth Using Optimization Tools** L. Roux, C. Croënne, M. Pouille, C. Audoly, A.-C. Hladky
10:15-10:30	Invited	**Spherical aberration in a 2D sound delivery system** C. Rajguru, G. Memoli

[MECD, Event Space 3]

10:30-11:00		Break

M5a [MECD, Main Lecture Theatre A (2A.040)]

Applied Phononics

11:05-11:45	2023 Phononics YIA	**Tunable Nonlinear Magnetic Lattices as a Platform for Controlling Waves** O. Bilal
11:45-12:00	Organisers' Colloquium	**Sound Attenuation by Pancake structures and Acoustic Black Holes in Linear and Nonlinear regimes** O. Umnova , D. Brooke, P. Leclaire, T. Dupont
11:45-12:00	Invited	**Optical generation and detection of GHz compression/ dilatation and shear acoustic waves in transparent medium with two-dimensional metallic grating structure** O. Matsuda, K. Momiyama, M. Tomoda, G. Vaudel, V. Gusev
12:00-12:15	Invited	**Multiscale Mechanical Study of Marine Seashells and Implications in the Design of Bioinspired Structures for Advanced Vibration Control** Y. Liu, M. Lott, S.F. Seyyedizadeh, I. Corvaglia, G. Greco, V.F. Dal Poggetto, A.S. Gliozzi, R. Mussat Sartor, N. Nurra, C. Vitale-Brovarone, N.M. Pugno, F. Bosia, M. Tortello

[MECD, Event Space 3]

12:30-13:25		Lunch

A5a [MECD, Main Lecture Theatre A (2A.040)]

Mathematics Underpinning Phononics

13:30-13:42	Contributed	**Discrete Helmholtz equation on a square lattice with corners** A. Kisil
13:42-13:54	Contributed	**Wave Dispersion in Monocoupled System with Inertial Amplifier and Embedded Resonator** A.S. Bhatt, A. Banerjee
13:54-14:06	Contributed	**High-frequency Homogenization of Dispersive Media** M. Touboul, B. Vial, R. Assier, S. Guenneau, R.V. Craster
14:06-14:18	Contributed	**Modeling and optimization of discrete phononic lattices** B. Vial, R.V. Craster
14:18-14:30	Contributed	**Joining the Dots to Understand the Spectral Convergence of Finite-Sized Acoustic Metamaterials** H. Ammari, B. Davies, E.O. Hiltunen
14:30-14:42	Contributed	**Frequency Spectrum of Sturmian Quasiperiodic Tilings** M. Lázaro , A. Niemczynowicz, P. Siemaszko, L.M. García-Raffi

Phononic Crystals

14:42-14:54	Contributed	**Negative refraction in canonical quasicrystalline-generated phononic metamaterials** Z. Chen, L. Morini, M. Gei
14:54-15:06	Contributed	**The Topological Valley Edge State of the Archimedean Tilings Phononic Crystal** Y.-J. Liang, P.-J. Guo, D.-H. Jhu, L.-W. Chen
15:06-15:18	Contributed	**Principles Underlying 2-D Phononic Pseudocrystal Isolators** S. Hales Swift, I.F. El-Kady, R.A. Kellogg
15:18-15:30	Contributed	**Broad-angle Coherent Perfect Absorption-Lasing in twodimensional non-Hermitian Phononic Crystals** C. Xu, Y. Wu

A5a [MECD, Blended Lecture Theatre (2B.020)]

Thermal Phonons

13:30-13:42	Contributed	**Piezoelectrically Mediated Acoustic Phonon Heat Transfer Across a Vacuum Gap** Z. Geng, I.J. Maasilta
13:42-13:54	Contributed	**Universal Behavior of Highly-Confined Heat Flow in Semiconductor Nanosystems: from nanomeshes to metalattices** B. McBennett, A. Beardo, E. Nelson, B. Abad, T. Frazer, A. Adak, Y. Esashi, B. Li, H. Kapteyn, M. Murnane, J. Knobloch
13:54-14:06	Contributed	**Net heat current at zero mean temperature gradient** J. Ordonez-Miranda, R. Anufriev, M. Nomura, S. Volz

Acoustic Metamaterials

14:06-14:18	Contributed	**Three-dimensions auxetic metamaterials with tunable ferroelectric properties for guiding elastic waves** M. Roshdy, T. Chen, S. Nakhmanson, O.R. Bilal
14:18-14:30	Contributed	**Latent Symmetries in Acoustic Systems** M. Röntgen , C.V. Morfonios, P. Schmelcher, V. Pagneux
14:30-14:42	Contributed	**Dynamically Tunable Metamaterial for Controlling Airborne Sound in Real-time** M. Keogh, M. Kheybari, O.R. Bilal
14:42-14:54	Contributed	**Subwavelength Broadband Perfect Absorption for Unidimensional Open-Duct Problems** Y. Meng, V. Romero-García, G. Gabard, J.-P. Groby, C. Bricault, S. Goudé
14:54-15:06	Contributed	**Efficient analysis of sound insulation in locally resonant metamaterial panels using an effective medium model** D. Giannini , E.P.B. Reynders
15:06-15:18	Contributed	**Wave propagation characterization of 2D structures through an algebraic identification technique** X. Li, M. Ichchou, A. Zine, N. Bouhaddi, P. Fossat
15:18-15:30	Contributed	**A Non-Linear Delayed Acoustic Resonator for Mimicking the Hearing Haircells** J. Reda, M. Fink, F. Lemoult

[MECD, Event Space 3]

15:30-16:00		Closing Ceremony

Delegate list

Abrahams, David	University of Cambridge	UK
Achilleos, Vassos	Laboratoire d'Acoustique de l'Université du Mans	France
Adham, Ali Ishan	The University of Auckland	New Zealand
Ahopelto, Jouni	VTT	Finland
Alcorta Galvan, Ricardo	CNRS, IEMN	France
Alsalami, Fatmeh	University of Manchester	UK
Alu, Andrea	City University of New York	USA
Assier, Raphael	University of Manchester	UK
Assouar, Badreddine	University of Lorraine	France
Bae, Myung Hwan	Ulsan National Institute of Science and Technology	Korea
Banerjee, Arnab	Indian Institute of Technology Delhi	India
Beardo, Albert	University of Colorado Boulder	USA
Belahurau, Yauheni	Technical University of Denmark	Denmark
Benchabane, Sarah	Université de Franche-Comté	France
Beoletto, Paolo Han	Politecnico di Torino	Italy
Bhatt, Abhigna	Indian Institute of Technology Delhi	India
Bilal, Osama	University of Connecticut	USA
Bonello, Bernard	CNRS Institut des Nanosciences de Paris	France
Bosia, Federico	Politecnico di Torino	Italy
Bradshaw, Georgia	University of Manchester	UK
Brun, Michele	University of Cagliari	Italy
Calius, Emilio	Computed Materiality, Auckland	New Zealand
Cazzaluni, Gabriele	Politecnico di Milano	Italy
Chaplain, Greg	University of Exeter	UK
Charlton, Charlotte	University of Manchester	UK
Chisari, Letizia	University of Sussex	UK
Clark, Monty Edward	University of Nottingham	UK
Clarke, Claudia Louise	DSTL	UK
Cominelli, Sebastiano	Politecnico di Milano	Italy
Cotterill, Philip	University of Manchester	UK
Cox, Trevor	University of Salford	UK
Craster, Richard	Imperial College London	UK
Croenne, Charles	CNRS, IEMN	France
Cutanda Henriquez, Vicente	Technical University of Denmark	Denmark
Das, Rishab	Indian Institute of Technology Delhi	India
Dass, Chandriker	Air Force Research Lab	USA
Davey, Robert	Thales UK	UK
Davies, Bryn	Imperial College London	UK
De Ponti, Jacopo	Politecnico di Milano	Italy
De Santis, Lorenzo	Politecnico di Milano	Italy
Deymier, Pierre	University of Arizona	USA
Diaz, Jon Canosa	JUNIA/IEMN	France
Djafari Rouhani, Bahram	CNRS, IEMN	France
Donner, Sean	University of Manchester	UK
Dorlot, Florent	Institute Langevin	France
Dorn, Charles	ETH Zurich	Switzerland
El-Kady, Ihab	Sandia National Labs	USA
Feng, Gao	Université de Bourgogne-Franche-Comté	France
Fleury, Romain	École Polytechnique Fédérale de Lausanne	Switzerland
Florez, Omar	ICN2	Spain
Fossat, Pascal	FEMTO-ST	France
Foxell, Emma	EPSRC	UK

Frazier, Michael	University of California	USA
Fytas, George	Max Planck Institute for Polymer Research	Germany
Gattin, Max	Univ Paris Est Creteil, Univ Gustave Eiffel	France
Geng, Zhuoran	University of Jyvaskyla	Finland
Giannini, Daniele	KU Leuven	Belgium
Gliozzi, Antonio	Politecnico di Torino	Italy
Gonella, Stefano	University of Minnesota	USA
Gower, Artur	University of Sheffield	UK
Graczykowski, Bartlomiej	Adam Mickiewicz University	Poland
Guenneau, Sebastien	Imperial College London	UK
Gupta, Ankush	ASML	USA
Haberman, Michael	University of Texas at Austin	USA
Hales Swift, Stephen	Sandia National Laboratories	USA
Hall, Andrew James	University of Auckland	New Zealand
Harris, Adam	University of Colorado Boulder	USA
Hatanaka, Daiki	NTT Basic Research Laboratories	Japan
Hladky, Anne-Christine	CNRS, IEMN	France
Hussein, Mahmoud	University of Colorado Boulder	USA
Iglesias Martinez Julio Andres	FEMTO-ST	France
Jang, Sang Vin	Ulsan National Institute of Science and Technology	Korea
Jin, Yabin	Tongji University	China
Juhl, Abby	Air Force Research Lab	USA
Kadic, Muamer	Université de Franche-Comté	France
Kamruzzaman, Md	University of Illinois at Urbana-Champaign	USA
Kasprzak, Scott	NSWCCD	USA
Keogh, Melanie	University of Connecticut	USA
Kessissoglou, Nicole	UNSW Sydney	Australia
Kheybari, Majid	University of Connecticut	USA
Kianfar, Armin	University of Colorado Boulder	USA
Kim, Dohyeong	Ulsan National Institute of Science and Technology	Korea
Kim, Gihyun	Seoul National University	Korea
Kim, Namjeong	Ulsan National Institute of Science and Technology	Korea
Kim, Seung Han	Ulsan National Institute of Science and Technology	Korea
Kisil, Anastasia	University of Manchester	UK
Kogani, Ali	Concordia University, Montreal	Canada
Korkiamaki, Tatu Antti Santeri	University of Jyväskylä	Finland
Krasikova, Mariia	Technical University of Munich	Germany
Krushynska, Anastasiia	University of Groningen	The Netherlands
Kumar, Amit	EPSRC	UK
Kumar Dhiman, Anuj	Adam Mickiewicz University	Poland
Kunz, Valentin	University of Manchester	UK
Lam, Wei Kit	University of Sheffield	UK
Laude, Vincent	Université de Franche-Comté	France
Lazaro, Mario	Universitat Politècnica de València	Spain
Leamy, Michael	Georgia Institute of Technology	USA
Lee, Myung-Joon	Korea Advanced Institute of Science and Technology	Korea
Lee, Sung-Won	Ulsan National Institute of Science and Technology	Korea
Lemoult, Fabrice	Institut Langevin, ESPCI Paris, Université PSL	France
Li, Jensen	Hong Kong University of Science and Technology	Hong Kong
Li, Qingming	University of Manchester	UK
Liang, Yu-Jui	National Cheng Kung University	Taiwan
Lloyd, Hollie	University of Manchester	UK
Lombard, Bruno	CNRS, Laboratoire de Mécanique et d'Acoustique	France
Ma, Guancong	Hong Kong Baptist University	Hong Kong
Ma, Jihong Aafia	University of Vermont	USA
Ma, Pyung Sik	Korea Institute of Machinery and Materials	Korea

Maasilta, Ilari	University of Jyväskylä	Finland
Marburg, Steffen	Technical University of Munich	Germany
Matlack, Kathryn	University of Illinois Urbana-Champaign	USA
Matsuda, Osama	Hokkaido University	Japan
Maurel, Agnes	Institut Langevin, ESPCI Paris, Université PSL	France
McKinnel, Danel	University of Manchester	UK
Medvedeva, Elena	University of Manchester	UK
Meier, Johanna	FEMTO-ST	France
Memoli, Gianluca	University of Sussex	UK
Meng, Yang	Laboratoire d'Acoustique de l'Université du Mans	France
Millward, Frank	University of Manchester	UK
Morini, Lorenzo	Cardiff University	UK
Muhammad Muhammad	Trinity College Dublin; City University, Hong Kong	Ireland; Hong Kong
Nasser, Hussein	University of Missouri, Columbia	USA
Nethercote, Matthew	University of Manchester	UK
Nguyen, Ekaterina	University of Manchester	UK
Nigro, David	Thales UK	UK
Nistri, Fabio	Politecnico di Torino	Italy
Nomura, Masahiro	University of Tokyo	Japan
Nouh, Mostafa	University at Buffalo (SUNY)	USA
Oh, Joo Hwan	Ulsan National Institute of Science and Technology	Korea
Ordonez-Miranda, Jose	University of Tokyo	Japan
Otsuka, Paul	Hokkaido University	Japan
Pagneux, Vincent	Laboratoire d'Acoustique de l'Université du Mans	France
Palermo, Antonio	University of Bologna	Italy
Panda, Susmita	Indian Institute of Technology Delhi	India
Parnell, William J.	University of Manchester	UK
Patino, Nicholas	University of Colorado Boulder	USA
Patro, Somya Ranjan	Indian Institute of Technology Delhi	India
Pavliovaios, Apostolos	Laboratoire d'Acoustique de l'Université du Mans	France
Pendry, John	Imperial College London	UK
Pennec, Yan	Université de Lille	France
Pham, Kim	ENSTA Paris	France
Phani, Srikantha	University of British Columbia	Canada
Piva, Paulo Sergio	University of Sheffield	UK
Portela, Carlos	Massachusetts Institute of Technology	USA
Poulos, Markos	INSA-Lyon	France
Rawte, Prajit	University of Colorado Boulder	USA
Reda, Jana	Institut Langevin, ESPCI Paris, Université PSL	France
Reparaz, Sebastian	Materials Science Institute of Barcelona	Spain
Riva, Emanuele	Politecnico di Milano	Italy
Roca, David	Universitat Politècnica de Catalunya	Spain
Romero-Garcia, Vicente	Universitat Politècnica de València	Spain
Röntgen, Malte	Laboratoire d'Acoustique de l'Université du Mans	France
Rosa, Matheus	University of Colorado Boulder	USA
Rosafalco, Luca	Politecnico di Milano	Italy
Roshdy, Mohamed	University of Connecticut	USA
Rostami, Habib	University of Bath	UK
Ruan, Xiulin	Purdue University	USA
Russell, Eleanor	Thales UK	UK
Ruzzene, Massimo	University of Colorado Boulder	USA
Saatchi, Daniel	Korea Advanced Institute of Science and Technology	Korea
Sanchez-Dehesa, Jose	Universitat Politècnica de Valencia	Spain
Sethi, Muskaan	Indian Institute of Technology Delhi	India
Shemilt, James	University of Manchester	UK
Sheng, Ping	Hong Kong University of Science and Technology	Hong Kong

Shin, Ye Jeong	Ulsan National Institute of Science and Technology	Korea
Shmuel, Gal	Technion–Israel Institute of Technology	Israel
Skvortsov, Alex	Defence Science & Technology Group	Australia
Smith, Elizabeth	University of Illinois at Urbana Champaign	USA
Smith, John	DSTL	UK
Sorokin, Sergei	Aalborg University	Denmark
Sotomayor, Clivia	Catalan Institute of Nanoscience and Nanotechnology	Spain
Sougleridis, I. Ioannou	Laboratoire d'Acoustique de l'Université du Mans	France
Srivastava, Ankit	Illinois Institute of Technology	USA
Starkey, Tim	University of Exeter	UK
Tessier Brothelande, Sarah	CNRS, IEMN	France
Theocharis, Georgios	Laboratoire d'Acoustique de l'Université du Mans	France
Thevamaran, Ramathasan	University of Wisconsin, Madison	USA
Termentzidis, Konstantinos	CNRS, INSA-Lyon	France
Titovich, Aleksey	NSWCCD	USA
Tol, Serife	University of Michigan	USA
Torrent, Daniel	Universitat Jaume I	Spain
Tortello, Mauro	Politecnico di Torino	Italy
Touboul, Marie	Imperial College London	UK
Umnova, Olga	University of Salford	UK
Vasconcelos, Ana	Delft University of Technology	The Netherlands
Vial, Benjamin	Imperial College London	UK
Wang, Pai	University of Utah	USA
Wang, Wan	FEMTO-ST	France
Wegener, Martin	Karlsruhe Institute of Technology	Germany
White, Tom	University of Manchester	UK
Willey, Carson	UES Inc	USA
Willis, John	University of Cambridge	UK
Wiltshaw, Richard	Imperial College London	UK
Wu, Ying	King Abdullah University of Science and Technology	Saudi Arabia
Xu, Changqing	Nanjing Normal University	China
Yamaguchi, Hiroshi	NTT Basic Research Labs	Japan
Yang, Jinkyu	Seoul National University	Korea
Yilmaz, Cetin	Bogazici University	Turkey
Yousefzadeh, Behrooz	Concordia University, Montreal	Canada
Zhang, Quan	University of Galway	Ireland
Zhao, Zile	University of Manchester	UK

Monday 12th June

PHONONICS 2023: 6th International Conference on Phononic Crystals/Metamaterials/Metasurfaces, Phonon Transport, and Topological Phononics
Manchester, England, June 12-16, 2023
PHONONICS-2023-0197

Dynamics of Modulated Media and Acoustic Temporal Metagratings

Massimo Ruzzene[1]

[1] *Department of Mechanical Engineering, University of Colorado Boulder, 1111 Engineering Dr., USA, Massimo.ruzzene@colorado.edu*

Abstract: This talk will describe numerical and experimental studies on the dynamics of acoustic temporal metagratings. The proposed implementation leverages an acoustic waveguide with Helmholtz resonators whose frequencies are smoothly varied in time. In analogy with space metagratings, we illustrate functionalities such as frequency conversion, temporal compression, and the temporal rainbow effect.

The concept of a space metagrating – a metamaterial whose resonating units are smoothly varied in space - has been long studied and its features are now well-established. A spatial variation of resonances leads to effects such as rainbow trapping[1] and spatial signal compression[2,3], which are related to a gradual spatial wavenumber variation occurring at fixed temporal frequencies. We introduce the temporal analogue of such gratings and explore the resulting wave phenomena emerging by virtue of time modulation. In contrast to space metagratings, which feature time invariant and spatially varying resonances, time metagratings employ spatially invariant and smoothly time-varying resonances, as conceptually illustrated in Fig. 1.

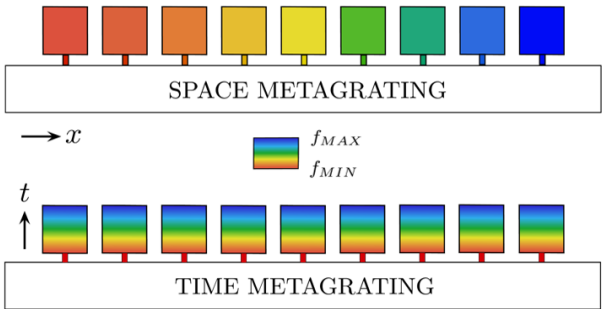

Figure 1 Conceptual illustration of space and time metagratings.

While the concept can be generally applied within multiple physical domains, in our implementation we consider an acoustic waveguide endowed with tuneable Helmholtz resonators. A schematic of the unit cell is depicted in Fig. 2a, illustrating a Helmholtz resonator of volume V_r connected to a pipe of cross-sectional area A. A temporal variation of the resonator's frequency is achieved through a temporal modulation of the connecting area, e.g., $A_r = A_r(t)$. The practical implementation of the concept is illustrated in Fig. 2b, which leverages a tube with open pockets that can be rotated with respect to a fixed base containing the resonating chambers. The rotation angle α therefore controls the resonances of all chambers in the pipe simultaneously, allowing for its smooth variation in time.

The talk will describe the results of numerical simulations and experimental studies, unveiling key functionalities inherently present in such a system when the properties of the resonators are gradually varied over time. In analogy with space metagratings, we demonstrate frequency conversion, and the temporal rainbow effect, which are suitable to produce fast-and-compressed or slow-and-dilated versions of impinging temporal signals. Figure 2c shows one key numerical result demonstrating a simultaneous frequency conversion and temporal compression of an input wave packet. Such behavior is the result of a smooth evolution of the wave-packet spectral content following a slow evolution of the dispersion properties of the system, as illustrated in the frequency-wavenumber plots of Fig. 2d. The input wave-packet targets a nearly flat region of the dispersion band right before the gap for an angle near the closed configuration ($\alpha = 1°$). As the pipe slowly rotates, the resonance frequency of the chambers slowly increases until the final configuration near the totally open state ($\alpha = 10°$). In the same way a space metagrading induces a spatial wavenumber transformation at constant frequency, here the smooth temporal variation leads to a smooth temporal frequency conversion that preserves the fixed wavenumber content of the wave-packet[4]. Therefore, when the rotation finishes, the wave-packet exhibits a broader frequency content that lies on the almost linear dispersion band, with an increase in central frequency, and corresponding to a narrower (compressed) temporal signal. Similarly, a variation in the opposite direction (e.g. open to closed) leads to a conversion from higher to lower frequency accompanied by a temporal signal decompression.

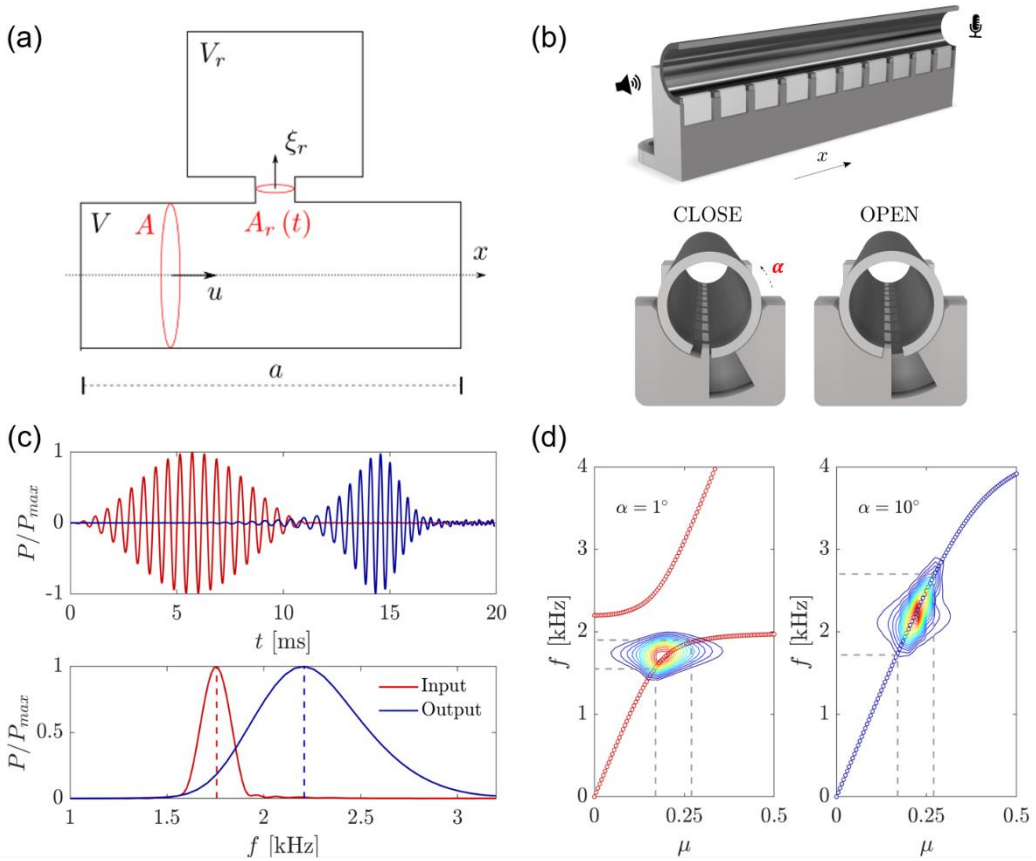

Figure 2 Temporal compression in acoustic time metagrating. **(a)** Unit cell of acoustic waveguide featuring a time modulated Helmholtz resonator with varying connecting area $\boldsymbol{A_r(t)}$. **(b)** Implementation of time-varying resonators through rotation of the acoustic pipe with respect to the fixed base containing the acoustic chambers. **(c)** Input and output wave-packets illustrating a frequency shift and temporal signal compression due to time varying resonances. **(d)** Frequency-wavenumber content of input and output wavepackets (colormaps), superimposed to the dispersion bands of the initial ($\boldsymbol{\alpha = 1}$°) and final ($\boldsymbol{\alpha = 10}$°) configurations.

The results in the talk outline the key features of temporal metagratings that leverage the synergistic interplay between local resonance and time modulation, offering exquisite control of the underlying dispersion properties. The presented frameworks may open new avenues in the context of time-varying phononics, with applications to communication, sound isolation, and energy conversion.

References

[1] K. L. Tsakmakidis, A. D. Boardman, and O. Hess. *Nature*, ***450***, 397-401, (2007).
[2] Y. Chen, H. Liu, M. Reilly, H. Bae, and M. Yu. *Nature communications*, ***5***, 5247, (2014).
[3] X. Wang, J. Li, J. Yang, B. Chen, S. Liu, and Y. Chen. *Applied Acoustics*, ***204***, 109246, (2023).
[4] V. Pacheco-Peña and N. Engheta. *Optica*, **7**, 323-331, (2020).

PHONONICS 2023: 6th International Conference on Phononic Crystals/Metamaterials/Metasurfaces, Phonon Transport, and Topological Phononics
Manchester, England, June 12-16, 2023
PHONONICS-2023-0128

Topological Acoustics Sensing

Pierre A. Deymier[1], Trevor D. Lata[1], M. Arif Hasan[2], Keith Runge[1]

[1] *Department of Materials Science and Engineering, University of Arizona, Tucson AZ 85721, USA*
deymier@arizona.edu, tlata157@arizona.edu, krunge@bellsouth.net
[2] *Department of Mechanical Engineering, Wayne State University, Detroit, MI 4820, USA*
hasan.arif@wayne.edu

Abstract: Topological acoustic sensing exploits the sharp topological features (e.g., twists, singularities, etc.) in the manifold spanned by the geometric phase of an acoustic wave upon parametric exploration of its Hilbert space, to achieve high sensitivity to defects or perturbations in the supporting medium. The geometric phase is a sensitive global metric for the wave-scattering environment that can be used to develop practical, low-cost acoustic sensing modalities.

The conventional approach to acoustic sensing has relied on the spectral or intensity response of a system or environment's sound field to some perturbation. The geometric phase of acoustic waves (η) has hitherto been excluded from sensing approaches. Therefore, incorporating η in sensing modalities may reinvigorate the field of acoustic sensing and consequently create the new field of topological acoustic (TA) sensing.

There is an intimate connection between an acoustic wave's η and its Green's function[1]. The acoustic Green's function is the point displacement response of a system given an impulse at another point in

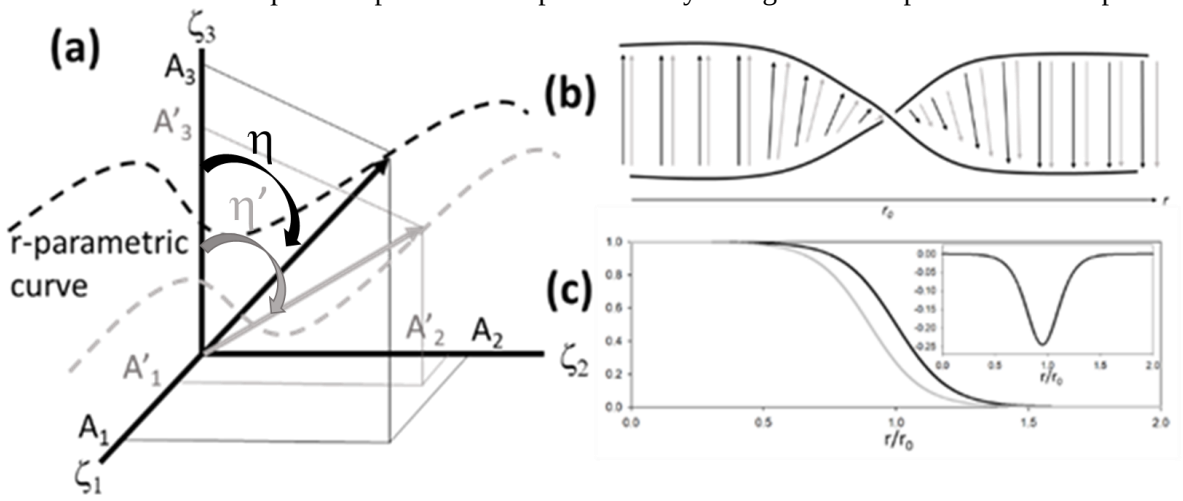

Figure 1 Navigating the Green's function Hilbert space by varying the driving parameter r. (a) The state vectors in the absence and presence of a perturbation (black and grey arrows, respectively) are expressed in a basis ζ_1, ζ_2, and ζ_3, and span the paths shown as dashed lines. (b) Schematic of the corresponding topological manifold as a twisted-ribbon supporting the state vector of the unperturbed (black arrows) and perturbed (grey arrows) systems as r is varied. The additional rotation in Hilbert space for a given r due to the effect of the perturbation, leading to an effective translation to the right on the manifold (grey arrows) along the r axis. (c) Schematic of the rotation angle of the state vectors (η) (in units of π) for the unperturbed (black line) and perturbed (grey line) systems. Inset shows large sensitivity to the perturbation near the twist.

the system, which depends on the response and stimulus positions. An external driver produces a stimulus that is controllable through parameters such as the magnitude and distribution of applied forces, frequency, and/or time. On an orthonormal basis, the Green's function is a vector in a multi-dimensional complex Hilbert space and η depends on the state vector direction (Fig. 1(a)). By varying a driver controllable parameter, *r*, the state vector parametrically spans a path in the Hilbert space. η accumulating along a parametric path is the change in direction (or "angle") of the vector state in the Hilbert space. The variation of the state vector can be depicted as a geometric manifold whose topology may not be conventional (e.g., near resonance). Due to scattering, perturbations such as imperfections, structural defects, or local or global changes in properties of the system/environment lead to an additional rotation of the state vector, which will follow another parametric path and span a different

part of the topological manifold (Fig. 1(b)). Manifold regions with sharp non-conventional topological features, such as twists, offer high sensitivity to the presence of perturbations (Fig. 1(c)). The power of TA sensing lies in η being a sensitive global metric for the wave-scattering environment. There is no theoretical limit to the magnitude of detectable perturbations. From an experimental viewpoint, the sensitivity will depend on the accuracy of the phase measurement. The choice of basis (i.e., the mathematical representation of the Green's function determines the sharpness of topological features in its Hilbert space) can also help maximize the TA sensing modality's sensitivity. Dissipation may affect sensitivity through smearing of the sharpness of topological features, e.g., for resonant scattering.

We will describe three examples of applicability of TA sensing.

In the first example, by exploiting η, TA can serve as a sensing modality for the remote, direct, and continuous monitoring of arctic forested areas using long-wavelength seismic waves[2,3]. Here, the parameter, *r*, is the frequency of seismic waves. Few-tens of Hz seismic waves interact strongly with trees by resonant scattering that changes η. The ground stiffness influences this phase change, which relates to subsurface temperatures changes for permafrost and/or forest-floor moisture levels. Preliminary studies predict large detectable changes in geometric phase due to changes in ground stiffness/temperature (up to $3\pi/1^{o}$C) for frequencies near tree resonances, versus current seismic sensing approach based on wave velocity change of only 2–3%/1–3^{o}C.

The second example deals with the experimental demonstration of TA sensing using the geometric phase of non-separable superpositions of acoustic waves, i.e., "classically entangled" elastic waves in externally driven parallel arrays of coupled one-dimensional metallic acoustic waveguides[4]. These superpositions of states lie in the tensor product Hilbert space of the two-dimensional subspaces associated with the degrees of freedom along and across the waveguide array. We report the effect of mass defects (i.e., mass scatterers attached locally to the waveguides) on the non-separable superpositions of product states. Here, the parameter *r* enables us to tune the probing superposition of states. We show experimentally that mass scatterers effectively rotate the state vector of the non-separable wave in its Hilbert space. The geometrical phase associated with this rotation is demonstrated experimentally to be a very sensitive metric for detecting the presence of the scatterers. A 1% mass perturbation results in a geometric phase change of $\eta \sim 44^{o}$ while the change in magnitude of the amplitude is only ~ 13%.

The third example addresses parametric exploration of a system's Hilbert space in time. Dynamical simulations of an externally harmonically driven model granular metamaterial composed of four linearly and nonlinearly coupled granules show that the nonlinear normal mode can be expressed in a linear normal mode orthonormal basis with time dependent complex coefficients. These coefficients form the components of a state vector that spans a 2^2 dimensional Hilbert space parametrically with time. Local π jumps in the phase of these components occurring periodically are indicative of twist-like topological features in the manifold spanned by the geometric phase of the vibrational state of the granular metamaterial. These topological features can be exploited to realize mass sensors with sensitivity of approximately 10^{-5} times the mass of one granule.

These examples, show that TA sensing could forge practical, predictive, high-sensitivity, multi-scale low-cost sensing modalities for continuous monitoring of built and/or natural environments.

Acknowledgements: PAD, TDL, and KR are grateful for financial support from General Dynamics Mission Systems. M.A.H. received support from Wayne State University Startup funds.

References

[1] P.A. Deymier & K. Runge, *Phase properties of elastic waves in systems constituted of adsorbed diatomic molecules on the (001) surface of a simple cubic crystal*, J. of Appl. Phys. 123, 125106 (2018).
[2] T. D. Lata, P. A. Deymier, K. Runge, F.-M. Le Tourneau, R. Ferrière, F. Huettmann, *Topological Acoustic Sensing of Tree Spatial Patterns in a Model Forest*, Ecological Modelling 419, 108964 (2020).
[3] T.D. Lata, P.A. Deymier, K. Runge, F.-M. Le Tourneau, R. Ferrière, F. Huettmann, *Resonant topological acoustic sensing of permafrost thawing*, Cold Region Science & Tech. 199,103569 (2022).
[4] T. D. Lata, P A. Deymier, K. Runge, and W. Clark, *Topological acoustic sensing using nonseparable superpositions of acoustic waves*, Vibration 5, 513 (2022).
[5] M. A. Hasan and P. A. Deymier, *Modelling and Simulations of a Nonlinear Granular Metamaterial: Application to Geometric Phase-based Mass Sensing*, Modelling Simul. Mater. Sci. Eng. 30, 074002 (2022).

Topological Mechanical Metamaterials Revealed By Higher-order Coordinate Transformations

F. Allein[1], A. Anastasiadis[2], R. Chaunsali[3], I. Frank[4], N. Boechler[4], F. Diakonos[5], G. Theocharis[2]

[1] *Univ. Lille, CNRS, Centrale Lille, Univ. Polytechnique Hauts-de-France, Junia, UMR 8520-IEMN, F-59000 Lille, France*

[2] *Laboratoire d'Acoustique de l'Université du Mans (LAUM), UMR 6613, Institut d'Acoustique - Graduate School (IA-GS), CNRS, Le Mans Université, France*

[3] *Department of Aerospace Engineering, Indian Institute of Science, Bangalore 560012, India*

[4] *Department of Mechanical and Aerospace Engineering, University of California, San Diego, La Jolla, CA 92093, USA*

[5] *Department of Physics, University of Athens, 15784 Athens, Greece*

georgios.theocharis@univ-lemans.fr

Abstract: We introduce a new family of systems whose topological properties are revealed only under higher-order coordinate transformations (deformation). We present two examples in detail: (i) the canonical mass dimer and (ii) a new mechanical analogue of the Kitaev chain. Both systems have hidden chiral and particle-hole symmetries and support topological edge modes at free boundaries.

The field of condensed matter physics has advanced considerably with the recent discovery of topological quantum matter, including topological insulating and superconducting materials. Many topological phenomena have also moved from the quantum to the classical domain[1,2] despite the fundamental differences between electrons (fermions) and photons or phonons (bosons). Either in quantum or classical topological matter, the bulk-boundary correspondence is a central concept which associates a non-trivial bulk topology of the material with the existence of localized topological states at its boundaries.

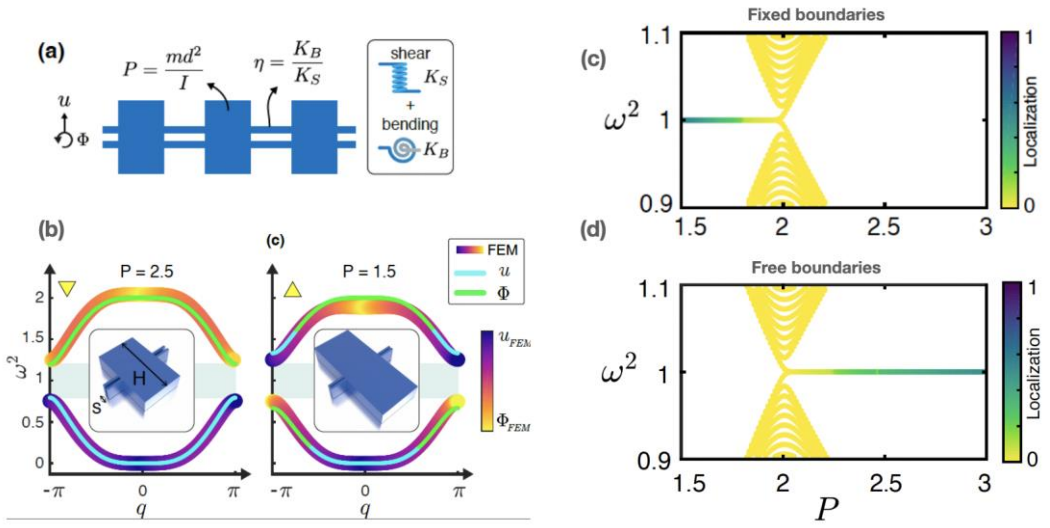

Figure 1 (a) A mechanical chain with transverse and rotational degrees of freedom maps to the Kitaev chain (particle mass *m*, lattice constant *d*, and particle mass moment of inertia *I*. **(b)** Dispersion diagrams for P= 1.5 and P = 2.5 are obtained in two ways: Analytically, via the lumped-mass model, and numerically, using the finite element method. **(c)** Evolution of the spectrum of finite chain with an even number of particles (200) and fixed boundaries as we change P. Edge states emerge for $P < 2$. **(d)** Same as in (c) but with both boundaries free. Localized edge states emerge in the band gap for $P > 2$.

In particular for finite-frequency mechanical metamaterials[3], the bulk-boundary correspondence has so far been described in terms of displacements, which requires fixed boundaries to support topologically protected edge modes. Here[4], we present a new family of finite-frequency mechanical metamaterials

whose topological properties emerge in deformation coordinates and for free boundaries. We present two examples, the first being the canonical mass-dimer, for which the bulk-boundary correspondence in deformation coordinates reveals the previously unknown topological origin of its edge modes. Second, we present a new mechanical analog of the Kitaev chain, see Figure 1. We show theoretically and experimentally that this mechanical chain supports edge states for both free and fixed boundaries, where the bulk-boundary correspondence is established in deformations and displacements, respectively. Our results suggest the existence of a class of topological edge modes not previously discovered, including in other contexts such as electrical circuits and optics, and for more complex and tailored boundaries.

References

[1] T. Ozawa, H. M. Price, A. Amo, N. Goldman, M. Hafezi, L. Lu, M. C. Rechtsman, D. Schuster, J. Simon, O. Zilberberg, and I. Carusotto, Topological photonics, Rev. Mod. Phys. **91**, 015006 (2019).
[2] R. Susstrunk and S. D. Huber, Classification of topological phonons in linear mechanical metamaterials, Proc. Natl. Acad. Sci. USA 113, EA767 (2016).
[3] S. D. Huber, Topological mechanics, Nat. Phys. 12, 621 (2016); Y. Barlas and E. Prodan, Topological classification table implemented with classical passive metamaterials, Phys.Rev. B 98 , 094310 (2018).
[4] F. Allein, A. Anastasiadis, R. Chaunsali, I. Frank, N. Boechler, F. Diakonos, G. Theocharis, Strain Topological Metamaterials, arxiv: 2212.10942

PHONONICS 2023: 6th International Conference on Phononic Crystals/Metamaterials/Metasurfaces, Phonon Transport, and Topological Phononics
Manchester, England, June 12-16, 2023
PHONONICS-2023-0064

Topologically Polarized Maxwell Lattices: beyond the Kagome Paradigm

Mohammad Charara, Stefano Gonella

Department of Civil, Environmental, and Geo- Engineering, University of Minnesota, 500 Pillsbury Dr. SE, Minneapolis, MN, 55455 USA
chara043@umn.edu, sgonella@umn.edu

Abstract: Topological Maxwell lattices display a polarized response that results in the ability to localize stress and deformation on opposing edges. In two dimensions, such polarization has been mostly studied within the realm of the kagome and square lattices. Here, we introduce a generalized family of topological lattices, obtained via mirror augmentations of the primitive kagome cell, which display full in-plane polarization. We corroborate our results via full-scale simulations and experiments on a lattice prototype assembled from 3D-printed links.

Maxwell lattices are characterized by an equal number of degrees of freedom and constraints in the bulk. They display the ability to host zero-energy (floppy) modes that involve site displacements without straining of the bonds, thus not costing energy. Finite Maxwell lattices with open boundary conditions localize zero modes at the edges due to a local imbalance between degrees of freedom and constraints. Specifically, certain Maxwell lattices have been shown to localize deformation and stress on opposite edges, a feature referred to as *topological polarization*, which is protected against defects by the momentum space topology of their bulk[1-3]. This polarization manifests as an excess of zero modes (and softness) at the so-called floppy edge, while the opposite edge remains rigid. In two dimensions (2D), studies have largely been restricted to deformed variations of the canonical square and kagome configurations. A gap exists in the study of topological lattices with increased cell geometry complexity and kinematics. While complex Maxwell configurations encompassing non-conventional assemblies of triangular and quadrilateral elements, e.g., the hexagonal cupola[4], have been investigated, to the authors' best knowledge no explicit effort has been devoted to investigate the potential of these structures to be polarized.

In this work, we address this shortcoming by considering Maxwell lattices characterized by higher geometric complexity, with the objective of stretching the design parameter available while designing polarized configurations. In general, the task of generating augmented unit cells adhering to Maxwell conditions is non-trivial, as configurations resulting from the process may be over- or under-coordinated. A promising path consists of leveraging known unit cells amenable to topological polarization as elementary building blocks. One option consists of adopting a kagome cell as a *primitive* geometry and *augmenting* it through a series of *mirror-folding* operations. We can document analytically an emergent topological polarization associated with this augmentation process, and explore parametrically its robustness upon changes in geometry. We validate our results via experiments on a prototype assembled from 3D-printed mechanical links.

Starting from a primitive topologically polarized single kagome (SK) lattice, we obtain an augmented bi-kagome (BK) cell by mirroring the SK cell about an axis passing through two of its sites, as shown in Fig. 1(a). We investigate the polarization of the augmented cell by exploring the null space of the compatibility matrix $\mathbf{C}$ of a unit cell in momentum space. The analysis reveals the existence of four zero modes, all featuring decay rates with the same sign and therefore localized on the same edge. This picture is corroborated by Bloch analysis of a supercell, which displays four zero-frequency branches associated with mode shapes characterized by an excess of floppiness at the same edge. Winding number calculations confirm that such polarization is topologically protected. To study the dependence of the polarization upon the geometric parameters of the cell, we sweep the tilt angle γ of a bond, as shown in Fig. 1(a), which effectively results in a deformation of the top triangle. We observe an interesting phase transition, whereby small values of γ yield polarized cells, whereas larger γ produce trivial non-polarized configurations.

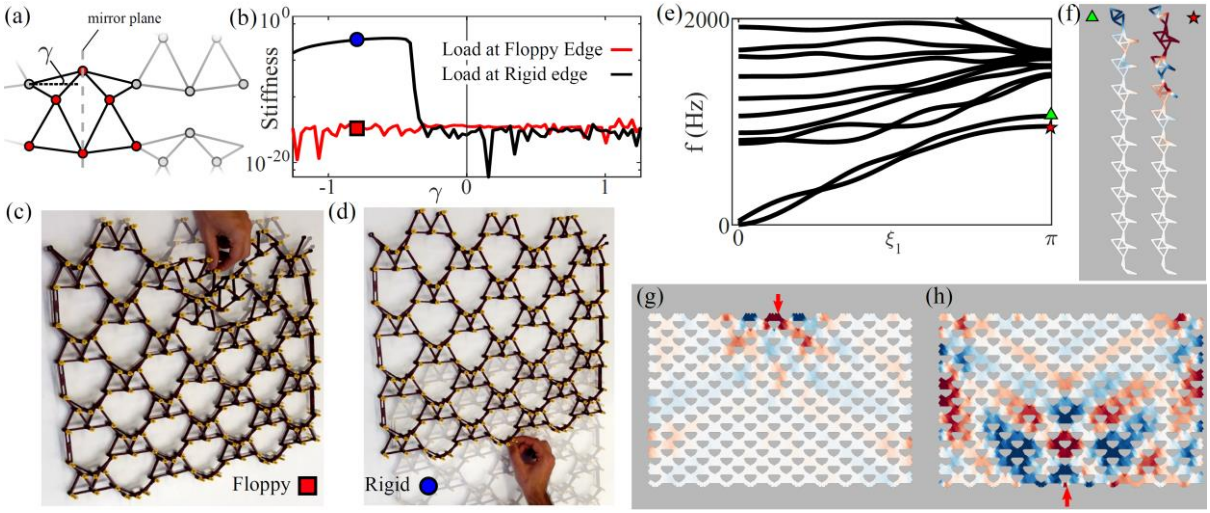

Figure 1 (a) Unit cell of bikagome (BK) lattice; **(b)** Comparison of stiffness on opposite edges for different BK configurations; **(c-d)** Static testing of BK lattice prototype loaded from the floppy and rigid edge, respectively; **(e)** Supercell band diagram for BK made of beams, revealing two edge modes; **(f)** Mode shapes of lowest two modes at wavenumber $\xi_1=\pi$, confirming localization on same edge (polarization); **(g-h)** Simulation of finite-frequency edge excitation of beam BK lattice, revealing edge-bound propagation at the floppy edge and propagation into the bulk form the rigid edge.

We quantify the asymmetry of the response by performing full-scale static simulations of a finite domain, loaded by a concentrated load applied at the top (bottom) edge. We infer edge stiffness by dividing the force by the resulting point displacement. We repeat this exercise for a spectrum of γ values, with the stiffness of the rigid (floppy) edge shown in black (red) in Fig. 1(b). For low γ values, the gap between the two curves denotes asymmetric edge stiffness. For γ above a certain threshold, the stiffness curves coalesce, marking the transition to a non-polarized regime. We construct a mechanical prototype with slender 3D-printed links connected with nearly frictionless rod-like hinges of Lego® axles and bushings. Loading from the floppy edge, as shown in Fig. 1(c), yields strong localization of deformation. In contrast, loading from the rigid edge, as illustrated in Fig. 1(d), results in rigid body motion of the entire lattice.

While the theory underpinning topological polarization is applicable to *ideal lattices* (i.e., spring-mass systems or trusses of rods connected by perfect hinges that allow free relative rotation of the bonds), it inspires a question of practical relevance: are the polarization predictions robust against transition to *structural lattices* (as practically achievable via manufacturing)?. This exercise has been performed for 2D kagome lattices deforming in-plane[5] and for topological lattice bilayers undergoing in-plane and out-of-plane deformation[6], revealing that polarization is in general preserved, albeit diluted (in strength and "multi-modality"), by the loss of ideality. Fig. 1(e), depicting the supercell band diagram of a BK lattice of beams, shows two low-frequency modes that represent the dynamical counterparts of the four zero modes of the ideal BK lattice. Their mode shapes in Fig. 1(f), evaluated at the edge of the Brillouin zone, display localization on the same edge, a signature of full polarization. Full-scale simulations of a finite domain excited at the edges with tone bursts with carrier frequency falling in the range of the edge modes, produce the dichotomy of scenarios depicted in Fig. 1(g-h): an excitation prescribed at the floppy edge results in a wave localized at the excitation edge, while exciting the rigid edge produces a bulk mode. This behavior endows the lattice with an ability to switch between isolating and conducting mode that is controlled solely by the edge selection.

References

[1] C. Kane and T.C. Lubensky, *Nat. Phys.* **10**, 39-45 (2014).
[2] X. Mao and T. Lubensky, *Ann. Rev. Cond. Matt. Phys.* **9**, 413 (2018).
[3] D. Rocklin, S. Zhou, K. Sun and X. Mao, *Nat. Comm.* **8**, 14201 (2017).
[4] T.N. Pronk, C. Ayas, and C. Tekoglu, *J. Mech. Phys. Sol.* **105**, 199-216 (2017).
[5] J. Ma, D. Zhou, K. Sun, X. Mao and S. Gonella, *Phys Rev. Lett.* **121**, 094301 (2018).
[6] M. Charara, J. McInerney, K. Sun, X. Mao and S. Gonella, *Proc. Natl. Acad. Sci.* U.S.A. **119**, e2208051119 (2022).

PHONONICS 2023: 6th International Conference on Phononic Crystals/Metamaterials/Metasurfaces, Phonon Transport, and Topological Phononics
Manchester, England, June 12-16, 2023
PHONONICS-2023-0017

Guided Waves in Soft Elastomers: Non-Linear Control and Topological Properties

Alexandre Delory[1], Fabrice Lemoult[1], Maxime Lanoy[2], Antonin Eddi[3], Claire Prada[1]

[1] Institut Langevin, ESPCI Paris, Université PSL, CNRS, 75005 Paris, France,
Alexander.delory@espci.psl.eu, fabrice.lemoult@espci.psl.eu, claire Prada@espci.psl.eu
[2] LAUM, CNRS, Le Mans Université, 72085 Le Mans, France
maxime.lanoy@univ-lemans.fr
[3] PMMH, CNRS, ESPCI Paris, Université PSL, Sorbonne Université, Université de Paris, 75005, Paris, France
Antonin.eddi@espci.psl.eu

Abstract: Mechanical waves propagating in soft materials play an important role in physiology. They can be natural, as in the cochlear wave in the mammalian inner ear, or controlled, as in elastography in the context of medical imaging. We will present a detailed description of the experimental set-up we developed to investigate the propagation of guided waves in such media. The versatility of the experimental platform is exploited to experimentally illustrate original features of modern wave physics such as the appearance of a Dirac cone, chiral waves and the possibility to modify the propagation with an external control.

The propagation of elastic waves in nearly incompressible material is characterized by a velocity V_L of longitudinal waves which is much higher than the velocity V_T of transverse waves. Guiding waves in a thin plate leads to the so-called Lamb modes. In the low frequency domain, only three independent modes coexist. For nearly incompressible media, among them, SH_0 and S_0 are non dispersive and have mostly an in-plane displacement. While SH_0 propagates at V_T, S_0 propagates at the plate velocity $V_P = 2V_T$, which is independent from the longitudinal velocity V_L despite its apparent longitudinal polarization.

We propose an experimental setup to measure those velocities in a soft plate made of a commercial silicone elastomer Ecoflex©, with a contrast in velocities $V_L/V_T \approx 200$ [1] (Figure 1). A monochromatic (1-300 Hz) source generates waves in a 60 cm x 60 cm plate and a camera mounted with a narrow angle lens records a movie. Making use of common image post-processing techniques, the full in-plane displacement field is extracted. The two guided modes with their respective phase velocities V_T and V_P

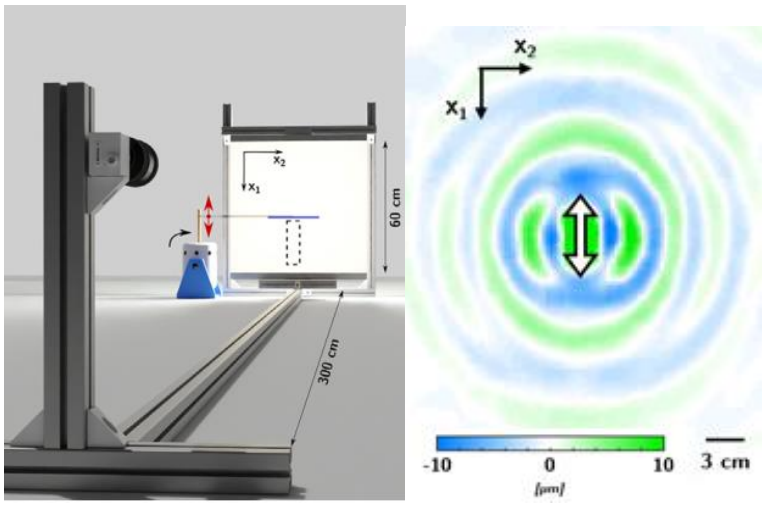

Figure 1 - Experimental setup and a typical 2D displacement maps. (left) A camera is used to stroboscopically monitor the local displacement on a soft nearly incompressible elastic plate. (right) Typical snapshot of the local displacement for a vertically polarized point source at 200 Hz. Two wavelengths are evidenced in the two main direction of the plate.

are nicely observed. Then, starting from this very simple experimental setup two different experiments are realized to tackle modern wave physics phenomena: (i) a static stress can be applied in order to modify the wave propagation, (ii) new boundaries can be added in order to generate new guided modes that present some topological features.

For the first experiment, the soft plate is subjected to a uniaxial tension with a stretch ratio reaching $\lambda = 2.5$. An induced anisotropy is observed and the new phase velocities at play present relatively complex dependence on the stretch ratio. To explain those changes, one needs to take into account the acoustoelastic effect [2]. It is derived from a hyperelastic constitutive law, which is based on a strain energy density function. For low stretch ratios ($\lambda \lesssim 1.1$), the experimental observations can be explained by the simplest model, *ie.* the NeoHookean model. However, for larger deformations, a more sophisticated hyperelastic model, involving the second principal invariant is needed. Such non-linearly induced anisotropy can be exploited in more complex scenario to transform an isotropic medium onto more specific devices such as lenses.

The second experiment relies on adding new boundaries to the elastic waveguide [3]. The plate is cut onto a soft strip with fixed or free edges. An elegant analogy with the Lamb wave in a plate with an equivalent longitudinal velocity of $V_L' = V_P$ permits to easily find the in-plane guided waves in such a geometry. Experimentally, more modes are involved at each frequency in the studied spectral range, but the full dispersion diagram of in-plane guided modes in a soft strip can also be measured. Due to the factor 2 between the plate velocity and the transverse one, the existence of a Dirac cone at $k = 0$ in the dispersion diagram is evidenced. Exploiting this degeneracy, it can be demonstrated that one can generate unidirectional propagation by exploiting the chirality of a source (Figure 2).

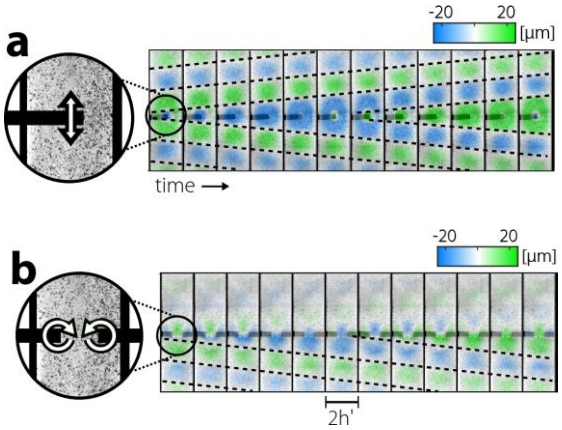

Figure 2 - Selective excitation at 136 Hz – The strip is excited in a symmetrical manner (a) Linear excitation. The source is placed in the centre of the strip and shaken vertically: waves travel to the the bottom and the top of the strip. (b) With a chiral excitation the energy is directed toward the bottom only.

The work is not over and many more complex guiding geometries can be envisioned. The nearly incompressible nature of the medium being a property shared with most of the biological tissues, analogies with elastic waves existing in the living world can be made. At least 3 different waveguides in the human body are already identified. The cochlear wave inside the inner ear of mammalians is supported by the basilar membrane which strongly resembles the clamped strip studied here. The vocal cords, whose vibrations are responsible of sound control, could be the support of complex stationary fields. And, arteries or neuronal axons are fluid filled circular soft waveguides which could also be the support of interesting wave phenomena.

References

[1] A. Delory, F. Lemoult, M. Lanoy, A. Eddi & C. Prada, "Soft elastomers: A playground for guided waves," *The Journal of the Acoustical Society of America*, vol. 151, n°5, pp. 3343-3358. (2022).
[2] A. Delory, F. Lemoult, A. Eddi & C. Prada, "Guided elastic waves in a highly-stretched plate," *arXiv:2209.00926* (2022).
[3] M. Lanoy, F. Lemoult, A. Eddi & C. Prada, "Dirac cones and chiral selection of elastic waves in a soft strip," *Proceedings of the National Academy of Sciences*, vol. 117, n°48, pp. 30186-30190 (2020).

PHONONICS 2023: 6th International Conference on Phononic Crystals/Metamaterials/Metasurfaces, Phonon Transport, and Topological Phononics
Manchester, England, June 12-16, 2023
PHONONICS-2023-0217

Towards Phononic Circuits: Components and Signal Protection

Clivia M. Sotomayor Torres[1,2], Guilhem Madiot[1], Ryan C. Ng[1], Daniel Navarro-Urrios[3], Guillermo Arregui[4], Marcus Albrechtsen[4], Omar Florez[1], Alejandro Martinez[5], Soren Stobbe[4], P. David Garcia[1] and Jouni Ahopelto[6]

[1] *Catalan Institute of Nanoscience and Nanotechnology (ICN2), CSIC and BIST, Campus UAB, Bellaterra, 08193, Barcelona, Spain*
clivia.sotomayor@icn2.cat, guilhem.madiot@icn2.cat, ryan.ng@icn2.cat, omar.florez@icn2.cat, pd.garcia@csic.es
[2] *ICREA, Pg. Lluís Companys 23, 08010 Barcelona, Spain*
[3] *MIND-IN2UB, Departament d'Electrònica, Facultat de Física, Universitat de Barcelona, Martí i Franquès 1, 08028 Barcelona, Spain*
dnavarro@ub.eu
[4] *Dept. Electrical and Photonics Engineering, Technical University of Denmark, 2800 Kgs. Lyngby, Denmark.*
guibra@dtu.dk, marcus.albrechtsen@gmail.com, ssto@dtu.dk
[5] *Nanophotonics Technology Center, Universitat Politècnica de Valencia, Spain*
amartinez@ntc.upv.es
[6] *VTT Technical Research Centre of Finland Ltd., P.O. Box 1000, Espoo, VTT FI-02044, Finland*
jouni.ahopelto@vtt.fi

Abstract: The search for lower energy tokens of information has turned towards phononics. Here we summarise the state of the art of three approaches involving phonons towards this goal. The first is room temperature optomechanics in NOEMS structures, the second is photonic crystal waveguides and sources and the third, topological protection, all in silicon platforms for GHz phonons.

The majority of information transmission, conversion and processing takes place using charge and photons and in some cases, as in storage, spins. We investigate the possibility to use phonons for these functions along three pathways.

Our initial Ansatz was the design, realization and test of a nano-opto-electromechanical system (NOEMS) structure operating at room temperature based on silicon, where the optomechanical interaction transduces THz photons to GHz phonons or mechanical modes. These endeavours led to the realisation of a laboratory-scale phononic circuit operating at 2GHz[1], which incorporated a phonon source, a photonic-phononic waveguide to co-localise photons and phonons and both, an optical driver in the form of an adjacent photonic crystal waveguide and another using surface acoustic waves. The simulations yielded the band structure conditions for the optomechanical interaction[2] and these were validated experimentally[3].

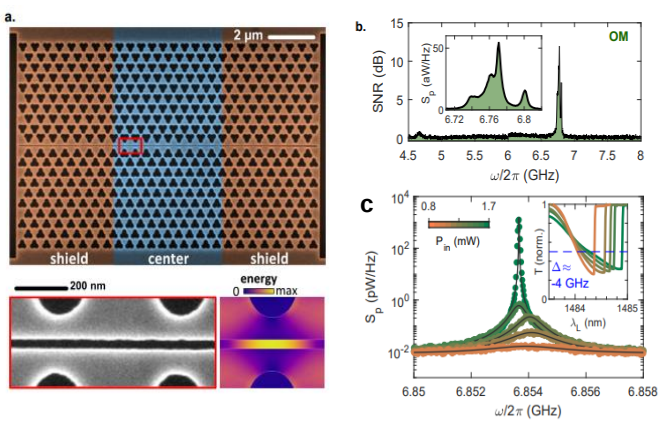

Figure 1. A phonon source. (a-top) SEM image of the optomechanical cavity waveguide and (a-bottom left) the central air-slot region. Magnified SEM image of the center slot highlighted above in red (a-bottom right). The electromagnetic energy density. (b) Mechanical mode probed with a tapered fiber loop. Inset: magnified spectrum of the same mode. (c) Radio-frequency spectrum of transmitted light showing the mechanical mode. Dynamical back-action is observed leading to mechanical lasing. Colour scale indicates laser power in mW. Inset: driven optical mode exhibits a thermo-optic shift with increasing power.

The experimental platform exhibited phonon generation in the form of a frequency comb[4] based on self-pulsing and a myriad of non-linear physical phenomena such as reversible chaotic behaviour[5], synchronization of two optomechanical resonators[6], modulation of coherent phonons[7] and injection locking into coherent phonon modes[8].

The role of Anderson localization was explored, primarily considering the deviations from the critical dimensions in the nanofabricated structures, first focusing on the opto-mechanical coupling[9] and subsequently on its modulation[10]. The random deviations from the designed structures size and shapes inevitable present sites for phonon localization since these are in the few nm length scale.

Extending the studies from silicon-on-insulators (SOI) to nanocrystalline silicon (nc-Si) yielded the surprise of higher mechanical cavity Q factors in nc-Si[11] and another angle of thermal parameters[12], this time related to the size of nanocrystallite and grain boundary, which are commensurate with the acoustic phonon wavelength of a few nanometres[13].

An alternative to the optomechanical nanobeam was explored, namely, phononic crystal waveguides formed at the interface of two phononic crystals with mirror symmetry at an interface (see figure 1), which also performed as a coherent phonon source[14] giving rise to frequency combs[15]. However, despite performance above 10 GHz, the integration of such waveguides in a circuit poses serious challenges.

Phonon signals departing slightly form the coherent regime need protection of intensity and phase, if they are to be used in in-chip interconnects. To this end the last approach is the exploration of topological protection[16,17] We have already obtained a mechanical gap at around 8 GHz with two guided mechanical modes[18]. However, topological protection is predicted for non-trivial topological waveguides and this is work in progress[19] aiming at both 2 and 10 GHz. Latest results will be discussed.

Thus, we demonstrated a classical Si-compatible phononic circuit. The next step is the topological version for lower energy use.

References

[1] D. Navarro-Urrios et al., *ACS Photonics* **9**, 413 (2022).
[2] M. Oudich et al., *Phys. Rev. B* **89**, 245122 (2014).
[3] J. Gomis-Bresco et al., *Nature Comms.* **5**, 4452 (2014).
[4] D. Navarro-Urrios et al., *Scientific Reports* **5**, 15733 (2015).
[5] D. Navarro-Urrios et al., *Nature Comms*. **8**, 14965 (2017).
[6] M.F. Colombano et al., *Phys. Rev. Lett.* **123**, 017402 (2019).
[7] J. Maire et al., *APL Photonics*, **3**, 126102 (2018).
[8] G. Arregui et al., *Nanophotonics*, **10** (4) 1319 (2021).
[9] P D Garcia et al., *Phys. Rev B*, **95** (11) 115129 (2017).
[10] G. Arregui et al., *Phys. Rev. B*, **98**, 180202(R) (2018).
[11] D. Navarro-Urrios et al., *Optics Express*, **26** (8) 9829 (2018).
[12] J. Maire et al., *Adv. Funct. Mater.*, **32**, 2105767 (2022).
[13] D. Navarro Urrios et al., *Nanophotonics*, **9** (16) 4819 (2020).
[14] G. Madiot et al., *Phys. Rev. Lett.*, **130**, 106903 (2023).
[15] R.C. Ng et al., arXiv:2210.16370.
[16] G. Arregui et al., *Phys. Rev. Lett.*, **122** (4) 043903) 2019.
[17] G. Arregui et al., *Appl. Phys. Photonics*, **4**, 030805 (2019).
[18] O. Florez et al., *Nature Nanotech*., **17**, 947 (2022)
[19] O. Florez et al., this conference.

Non-Hermitian Elastodynamic Metamaterials

Abhishek Gupta[1], Arkady Kurnosov[2], Tsampikos Kottos[2], Ramathasan Thevamaran[1,*]

[1]Department of Mechanical Engineering, University of Wisconsin-Madison, Madison, WI, 53706, USA
[2]Wave Transport in Complex Systems Lab, Physics Department, Wesleyan University, Middletown, CT 06459, USA
**thevamaran@wisc.edu*

Abstract: We study the requisites on frequency-dependent viscoelastic properties of dissipative materials to support the formation of exceptional points in passive non-Hermitian elastodynamic metamaterials and demonstrate their ramification in achieving an unusual enhancement of actuation force (emissivity). We further extend this work to magnetically damped systems that also offer the potential to achieve balanced gain and loss to create Parity-Time symmetry.

Potential of non-Hermitian physics and the notion of exceptional points has recently been exploited to generate exotic wave phenomenon such as unidirectional invisibility [1], dynamical mode-switching [2], asymmetric transport [3], hypersensitivity [4], and most recently enhanced emissivity [5-6] in optics, acoustics, and elastodynamics. Until now, wave transport properties of elastodynamic metamaterials such as locally resonant structures mostly rely on geometric symmetries of periodically arranged meta-atoms, and impedance mismatch achieved by combining materials with dissimilar densities and modulus [7-8]. In contrast, non-Hermitian metamaterials utilize hidden (dynamical) symmetries such as parity-time (PT) symmetry encoded in the governing dynamical equations of motion achieved by spatially distributed complex impedances with amplification (gain) and attenuation (loss) mechanisms (imaginary part). Non-Hermitian metamaterials can lead to exceptional points (EPs)—branch point singularities where distinct eigenvalues and the corresponding eigenvectors of the system coalesce and become degenerate. Small perturbations to a system's parameter such as gain and loss intensity in the vicinity of an EP results in spontaneous sublinear bifurcation of eigenvalues, a characteristic exploited in developing hypersensitive sensors [4].

While loss or damping occurs naturally in various material systems, gain is achieved by creating active positive feedback control drives that can make systems bulkier. Non-Hermitian systems with passive differential losses (no gain) have also been shown to exhibit EPs. Here, we present the design of a passive non-Hermitian metamaterial that supports the formation of an EP in elastodynamic framework and exploit it to achieving an unusual enhancement of actuation force (emissivity) [5]. We attain a six times enhancement of applied input actuation force when the system is operating at the EP as compared to only a three times enhancement when it is operating away from the EP. Thus, by bringing our system close to the EP, we boost the enhancement factor beyond its standard Purcell effect expectation by two-fold while maintaining a constant quality factor of the signal [5]. Purcell effect was first described in quantum electrodynamics and is governed by the Fermi's Golden Rule which links emission rate of a source to the local density of states of its surroundings.

To achieve differential loss (non-Hermiticity), we coupled an undamped mechanical oscillator with a damped oscillator via a coupling spring of stiffness κ (Figure 1(a)). We designed and fabricated a compliant aluminum spring (k) that follows Hooke's law for the undamped oscillator, and we used a viscoelastic material with complex dynamic modulus for the damped oscillator. By investigating different viscoelastic material models, we found that the EP emerges only when the frequency-dependent loss tangent of a viscoelastic material remains almost constant in the frequency range of operation [9]. Such type of loss-tangent occurs in materials that follow Kelvin-Voigt fractional derivative (KVFD) model (Figure 1(b)). Whereas, materials that follow Kelvin-Voigt model or Standard Linear Solid (SLS) model exhibit strong dependence of loss-tangent on frequency and thus cannot be used to achieve EP (Figure 1(b)). By conducting broadband dynamic mechanical analysis (DMA) on various viscoelastic materials, we found that materials like polydimethylsiloxane (PDMS) and polyurethane follows KVFD model (Figure 1(c)). In contrast, natural rubber has an almost linear dependence of loss-tangent on frequency,

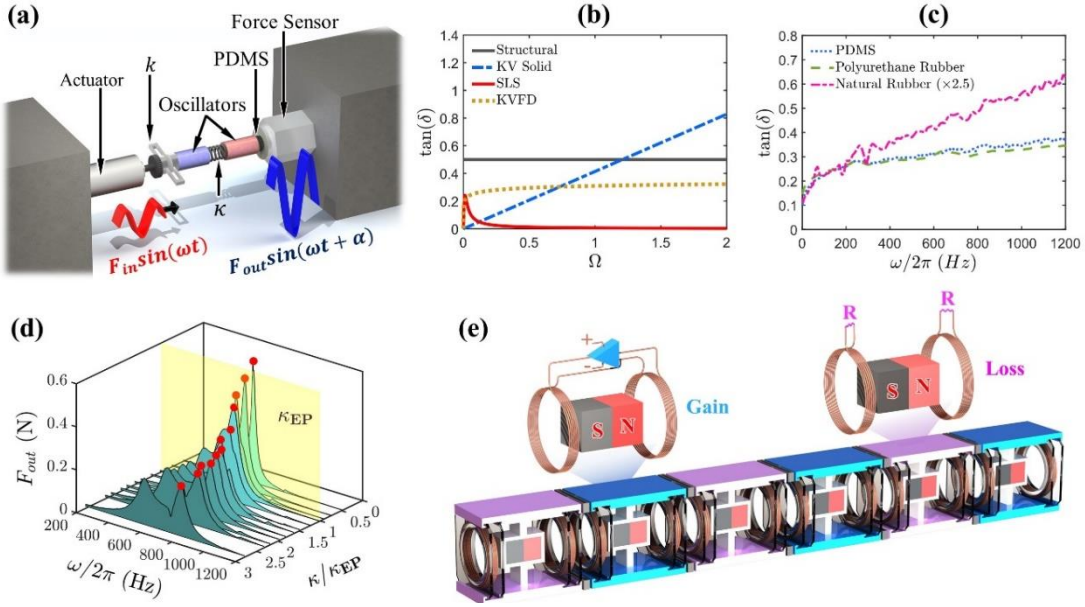

Figure 1 (a) A schematic of experimental setup showing coupled oscillator non-Hermitian metamaterial mounted between the piezoelectric actuator and the dynamic force sensor. (b) Frequency dependent loss-tangent of various viscoelastic material models. (c) Experimentally measured loss-tangent of three different viscoelastic materials. (d) Experimentally measured reaction force output at the fixed end [5]. (e) Schematic of a periodic non-Hermitian metamaterial with magnetic loss and gain).

so it does not follow the KVFD model and cannot support the formation of EP. We chose the dimensions of the PDMS sample such that the real part of stiffness is equivalent to that of the Hookean aluminum spring (k). Figure 1(a) shows an illustration of the experimental setup with our non-Hermitian metamaterial mounted on a custom built dynamic mechanical analyzer. The setup consists of a piezoelectric actuator (PI-841.10) which imparts a prescribed displacement actuation of a fixed amplitude on the undamped oscillator side and a dynamic force sensor (PCB208C01) which measures the dynamic force output (F_{out}) at the fixed end on the damped oscillator side. Figure 1(d) shows experimentally measured frequency response of the force output (F_{out}) as a function of the coupling spring's stiffness κ. As the coupling spring's stiffness decreases, two broad resonant peaks—corresponding to two modes of the system—coalesce to form a single narrow peak at the EP $(\kappa = \kappa_{EP})$. Clearly, the amplification factor is boosted by two-fold near the EP $(\kappa/\kappa_{EP} = 1)$ compared to when the system was operating away from the EP $(\kappa/\kappa_{EP} \approx 3)$. In contrast to conventional Purcell enhancement where amplification results in decay of signal quality, EP-based enhancement maintains a constant Q-Factor (linewidth) of the signal. This enhancement factor can be further increased in active non-Hermitian metamaterials with balanced gain and loss. Figure 1(e) shows an illustration of a periodic non-Hermitian metamaterial with alternate loss achieved by eddy-current damping and gain achieved by creating a feedback loop that amplifies and reverse the induced current by the oscillating magnet to create gain. Our work expands the applications of EP-degeneracies in achieving actuation enhancement at constant Q-Factor which has applications in developing novel robotic actuators, biomedical devices, and a new class of indenters for materials hardness measurements.

References

[1] Z. Lin, H. Ramezani, T. Eichelkraut, T. Kottos, H. Cao, and D. N. Christodoulides, Phys Rev Lett 106, (2011)
[2] J. Doppler, A. A. Mailybaev, J. Böhm, U. Kuhl, A. Girschik, F. Libisch, T. J. Milburn, P. Rabl, N. Moiseyev, and S. Rotter, Nature 537, 76 (2016)
[3] Thevamaran R., Branscomb R.M., Makri E., Anzel P., Christodoulides D., Kottos T., Thomas E.L. J Acoust Soc Am, 146, 863 (2019)
[4] R. Kononchuk, J. Cai, F. Ellis, R. Thevamaran, and T. Kottos, Nature 607, (2022)
[5] A. Gupta, A. Kurnosov, T. Kottos, and R. Thevamaran, Extreme Mech Lett 59, 101979 (2023)
[6] V. Dominguez-Rocha, R. Thevamaran, F. M. Ellis, and T. Kottos, Phys Rev Appl **13**, 14060 (2020)
[7] Z. Liu, X. Zhang, Y. Mao, Y. Y. Zhu, Z. Yang, C. T. Chan, and P. Sheng, Science (1979) **289**, 1734 (2000)
[8] M. I. Hussein, M. J. Leamy, and M. Ruzzene, Appl Mech Rev **66**, (2014)
[9] A. Gupta and R. Thevamaran, *arXiv:2209.04960* (2022)

PHONONICS 2023: 6th International Conference on Phononic Crystals/Metamaterials/Metasurfaces, Phonon Transport, and Topological Phononics
Manchester, England, June 12-16, 2023
PHONONICS-2023-0091

Topological states in Hermitian and non-Hermitian beams

Yabin Jin[1], Liangshu He[1], Wan Wang[1], Runcheng Cai[2], Wenxin Zhong[1], Xiaoying Zhuang[2,3], Timon Rabczuk[4], Yan Pennec[5], Bahram Djafari-Rouhani[5]

[1] *School of Aerospace Engineering and Applied Mechanics, Tongji University, Shanghai, P.R.China,*
[2] *School of Civil Engineering and Applied Mechanics, Tongji University, Shanghai, P.R.China,*
[3]*IOP, Department of Mathematics and Physics, Leibniz University Hannover, Hannover, Germany*
[4]*Institute of Structural Mechanics, Bauhaus-Universität Weimar, Weimar, Germany*
[5] *IEMN-UMR CNRS 8520 Department of Physics, University of Lille, Lille, France*
Corresponding author: 083623jinyabin@tongji.edu.cn

Abstract: Recently, the studies of topological insulators with topological protection edge states have been extended to elastic wave systems. We take the elastic phononic beam as the basic model to study a series of topological phenomena in Hermitian and non-Hermitian systems, including asymmetric transmission, robust Fano resonance, skin effect and Weyl physics.

Topological insulators are an emerging topic in condensed matter physics that can provide anomalous properties like direction selective propagation, back scattering free and high robustness. As the most basic one-dimensional structure, phononic beams provide an important platform for the study of elastic wave phenomena.

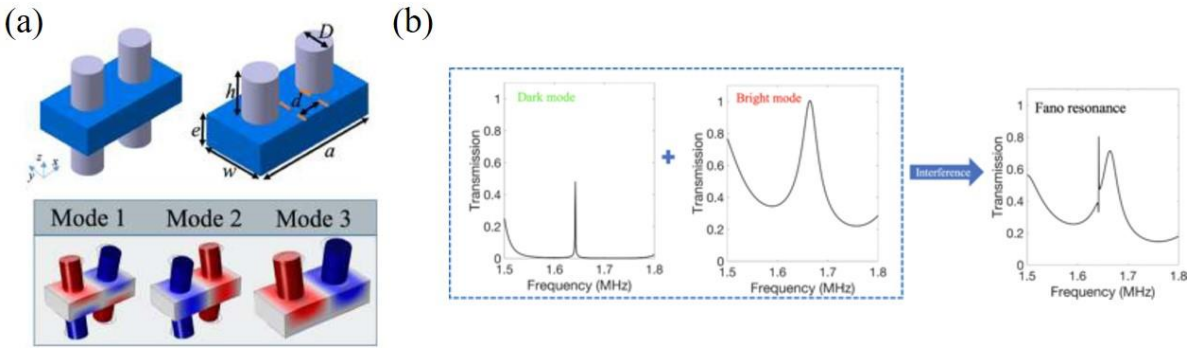

Fig.1 (a) Double- and single-sided pillared unit cells. The decoupling (Mode1 and Mode2) and coupling (Mode3) of torsional and shear waves. (b) The formation of topological Fano resonance.

The phononic beam structure has four wave modes: longitudinal, flexural, shear and torsional, which are coupled with each other. We proposed the fully described of the coupling or decoupling effects with the four wave modes by means of the analysis of the structural symmetry relation of the beam vibration. For a pillared single-side beam, the torsional and shear modes, or the longitudinal and flexural modes are coupled to each other; For a two-sided pillared beam, the four modes can be decoupled from each other, as shown in Fig. 1(a). By combining a single side pillared beam with a double side pillared beam, we can realize one-way transmission of torsional wave incidence[1]. Further, by enlarging or narrowing the distance between the pillars in a two-sided pillared beam, the shear wave signal passing through can be highly robust. The asymmetric topological state opens opportunities for designing topological solid devices with high performance, such as robust filter.

Fano resonance refers to the asymmetric spectral peaks in wave scattering. We achieve a robust Fano mechanical resonance with topological protection by engineering band inversion of two different vibrating symmetries of a pillared beam. The Fano resonance results from the constructive and destructive interferences between topological dark and bright modes[2], as shown in Fig. 1(b). It is further demonstrated that the Fano asymmetric shape of the transmission peak and its frequency are robust against random perturbations in the pillars' position as long as the symmetry is conserved. The robustness of Fano resonance can support the design of topological high-Q resonance in sensing applications.

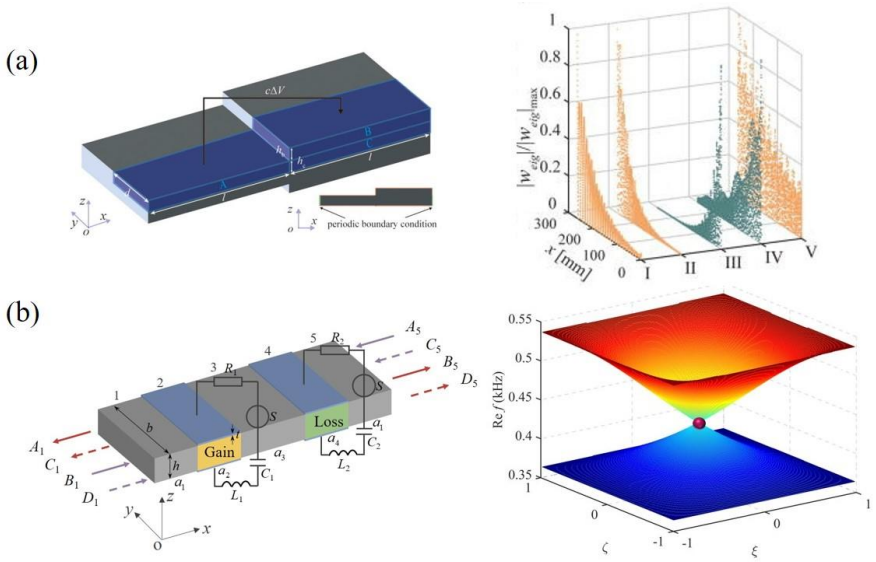

Fig.2 Realization of (a) skin effect and (b) Weyl physics using piezoelectric phononic beam.

Skin effect is shown as the localization of all bulk modes in a specific frequency range at a given boundary, with an unconventional bulk-boundary correspondence. We propose to realize the skin effect for flexural waves in a non-Hermitian piezoelectric phononic beam with feedback control between a sensor and an actuator in each unit cell, as shown in Fig. 2(a). By implementing a non-Hermitian parameter, effective gain and loss can be achieved in the phononic beam characterized by complex eigen frequencies, and non-reciprocal pass bands are obtained. The localization degree of the skin mode manifested by the enhanced beam's vibration energy at one boundary is related to the strength of the non-reciprocity, and the skin mode can be always excited regardless of the source position[3,4]. Our results provide a potential platform to introduce non-Hermiticity into phononic or metamaterial systems with novel functions for elastic waves such as topological insulators, vibration attenuation or amplification, and energy harvesting.

The evolution of Weyl point caused by the introduction of non-Hermiticity into Weyl semimetals has aroused great research interest. We consider elastic flexural wave propagation in a phononic beam containing piezoelectric materials and introduce the non-Hermiticity through active regulation of external circuits, as shown in Fig. 2(b). Considering a synthetic parameter space constituted by the 1D Bloch wavevector and two geometrical parameters, we demonstrate that a double Weyl point arises at the band crossing. Then, we study its evolution from the Hermitic to non-Hermitic situation under the effect of the active piezoelectric materials. We find that the double Weyl point in the Hermitic case evolve into a Weyl degenerate line and a Weyl hollow ring as concerns the real and imaginary parts of the Weyl frequencies respectively. The formation mechanisms of the double Weyl points, lines and rings are explained through the Hamiltonian of the system. Further, we observe the changes of double Weyl point and degenerate line in the transmission spectra of finite structures. Finally, we discuss the synthetic Fermi arc interface states through the analysis of the reflected phase vortices[5]. Our work provides insights for the high-dimensional Hermitian and non-Hermitian physics in elastic wave systems using synthetic dimensions.

References

[1] Y. Jin, W. Wang, B. Djafari-Rouhani, Int. J. Mech. Sci. 186, 105897,2020

[2] W. Wang, Y. Jin, W. Wang, B. Bonello, B. Djafari-Rouhani, R. Fleury, Phys. Rev. B 101 (2), 024101,2020

[3] R. Cai, Y. Jin, T. Rabczuk, Y. Pennec, B. Djafari-Rouhani, X. Zhuang, Physical Review Applied 18 (1), 014067,2022

[4] Y. Jin, W. Zhong, R. Cai, X. Zhuang, Y. Pennec, B. Djafari-Rouhani, Applied Physics Letters 121 (2), 022202,2022

[5] L. He, Y. Li, B. Djafari-Rouhani, Y. Jin, under review.

PHONONICS 2023: 6th International Conference on Phononic Crystals/Metamaterials/Metasurfaces, Phonon Transport, and Topological Phononics
Manchester, England, June 12-16, 2023
PHONONICS-2023-0191

Invisibility of Defects in Chiral and Mirror Symmetric Networks

A. Coutant[1], L.Y Zheng[2], V. Achilleos[3], O. Richoux[3], G. Theocharis[3], V. Pagneux[3]

[1]Aix Marseille Univ., CNRS, Centrale Marseille, LMA UMR 7031, Marseille, France, coutant@lma.cnrs-mrs.fr
[2] School of Science, Shenzhen Campus of Sun Yat-sen University, Shenzhen, China zhengly27@mail.sysu.edu.cn
[3]Laboratoire d'Acoustique de l'Université du Mans (LAUM), UMR 6613, Institut d'Acoustique - Graduate School (IA-GS), CNRS, Avenue O. Messiaen, F-72085 Le Mans Cedex 9, France, Achilleos.Vassos@univ-lemans.fr,olivier.richoux@univ-lemans.fr,Georgios.Theocharis@univ-lemans.fr, vincent.pagneux@univ-lemans.fr

Abstract: Network waveguides with mirror and chiral symmetry are considered: it is shown that, in these systems, scattering is very particular in the sense that defects respecting the symmetries are invisible (perfect transmission with no phase delay) at zero pseudo-energy. Application to acoustic waveguides is presented.

One signature of topological phases in periodic materials is the existence of propagating modes that benefit from topological protection which renders them immune to backscattering over defects or disorder. This has attracted a lot of works in the classical wave context[1-3] such as in photonics or acoustics, however total immunity to backscattering has not been achieved so far. In this work, we show how to obtain perfect transmission of topological edge waves by exploiting the combination of chiral and mirror symmetry. This guarantees a unit transmission coefficient of edge waves across symmetry preserving defects or disorder. We illustrate this result in the context of the Kekule model. It consist in a graphene lattice with a modulation of the intersite coupling that preserves the hexagonal symmetry of the system. This model possesses topological edge waves protected by chiral and mirror symmetries. We show that these waves propagate without reflection on defects or disorder. We also show how to realize Kekule structures in acoustic networks of waveguides. One numerical result is displayed in figure 1, where a typical symmetric defect is invisible (T=1), other defects of any shape or disorder with the same symmetry would as well be invisible.

Figure 1 Numerical computation of the scattering in an acoustic waveguide network (absolute value of the pressure). Perfect transmission and invisibility of a defect with mirror and chiral symmetry.

References

[1] T. Ozawa, H. M. Price, A. Amo, N. Goldman, M. Hafezi, L. Lu, M. C. Rechtsman, D. Schuster, J. Simon, O. Zilberberg, et al., "Topological photonics," Reviews of Modern Physics 91 no. 1, 015006 (2019)
[2] G. Ma, M. Xiao, and C. T. Chan, "Topological phases in acoustic and mechanical systems," Nature Reviews Physics 1 no. 4, 281–294 (2019)
[3] S. Yves, X. Ni, and A. Alu, "Topological sound in two dimensions," Annals of the New York Academy of Sciences, 1517(1), 63-77 (2022)

PHONONICS 2023: 6th International Conference on Phononic Crystals/Metamaterials/Metasurfaces, Phonon Transport, and Topological Phononics
Manchester, England, June 12-16, 2023
PHONONICS-2023-0195

Acoustic Coatings for Maritime Applications

C. Lin[1], G.S. Sharma[2], A. Skvortsov[2], I. MacGillivray[2], N. Kessissoglou[1]

[1] School of Mechanical and Manufacturing Engineering, UNSW Sydney, Sydney, NSW, Australia, cikai.lin@unsw.edu.au, n.kessissoglou@unsw.edu.au
[2] Maritime Division, Defence Science and Technology Group, Melbourne, VIC, Australia gyani.sharma@defence.gov.au, alex.skvortsov@defence.gov.au, ian.macgillivray@defence.gov.au

Abstract: We investigate sound scattering by an array of resonant scatterers in a soft material, utilized as an acoustic coating on a submerged cylindrical shell for mitigation of underwater noise. We model the coating as an equivalent fluid and employ a homogenization approach to represent the layer of inclusions with effective material and geometric properties.

Acoustic coatings for underwater noise control applications are generally manufactured using a soft viscoelastic material with an impedance that closely matches that of the surrounding water. Resonant inclusions embedded in the soft material facilitate conversion of subwavelength sound to shear waves, resulting in strong sound attenuation. Multiple wave scattering between inclusions in proximity further enhances sound dissipation within the coating. A plethora of studies on the acoustic performance of planar coatings have been reported, for example, see Refs. 1-6 and references therein. These studies have provided notable insight into the influence of the shape of inclusions (cylinders, spheres, disks, superellipsoids), their material (cavities, hard scatterers), filling fraction of the inclusions and their lattice arrangement.

We study a regular distribution of resonant scatterers embedded in a soft elastic medium as an external coating on a marine vessel which is modelled as a structurally excited, submerged elastic shell. We consider inclusions that are vacuous cavities or hard steel scatterers that respectively yield monopole and dipole scattering responses. The problem has been treated using an effective medium theory, viz., the layer of inclusions at a circumferential location of half the coating thickness is modelled as a homogenized layer with some effective properties, as shown in Figure 1.

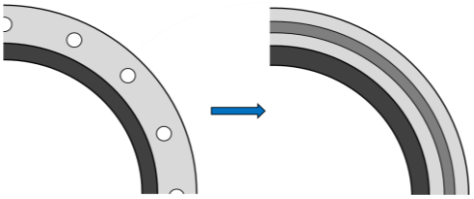

Figure 1 Homogenization scheme applied to the coated cylindrical shell embedded with equispaced resonant inclusions.

Figure 2 compares the radiated sound power from an elastic shell with a soft rubber coating embedded with a single layer of inclusions composed of cavities or hard scatterers, with the sound power from an uncoated shell and with a homogeneous rubber coating (in the absence of resonant inclusions). We consider a steel shell of radius 1 m and thickness 0.01 m. The coating has thickness 0.1 m and the inclusion diameter is 0.05 m. For a coating with cavities, we used the coating material properties from Ref. 7 and similarly, for a coating with hard scatterers we used the material properties from Ref. 8. The monopole and dipole resonances were tuned by varying the number of equispaced inclusions.

The radiated sound power for an uncoated shell or with a homogeneous coating both follow a similar trend to the sound power due to a dipole. A homogeneous coating increases the sound power with increasing frequency compared to the uncoated shell, attributed to an increase in coupling between the shell and water[9]. Figure 2(a) shows a strong reduction in sound power around monopole resonance of the voids corresponding to 486 Hz for 50 cavities and 706 Hz for 67 cavities. The low frequency peak around 70 Hz is attributed to a spring-mass resonance associated with elasticity contributed by the layer of cavities and mass provided by the shell[7]. Subsequent peaks in sound power correspond to the shell circumferential resonances, analogous to those of a shell in air as the layer of cavities effectively decouples the shell from the surrounding water[10]. Increasing the monopole resonance frequency by increasing the number of cavities leads to further global reduction in radiated sound power. In Figure 2(b), the influence of the ring frequency of the shell at 865 Hz and its harmonic are clearly observed, showing a slight reduction in the sound power due to trapping of acoustic energy along the shell circumference. The ring frequency has a significant impact on the performance of a coating with hard

scatterers, as evidenced when the dipole resonance frequency is tuned to a frequency below or above the ring frequency. For a dipole resonance frequency below the ring frequency at 494 Hz, the reduction in sound power occurs in a narrow frequency range and the sound power for the locally resonant coated shell converges to that for a homogeneous coating above the ring frequency. Tuning the dipole resonance frequency to 1425 Hz yields a plateau in sound power for a broad frequency range between the ring frequency and its harmonic.

Figure 3 presents the acoustic pressure for a coating with cavities or hard scatterers as a function of frequency and distance from the shell surface. For a coating with cavities (Figure 3(a)), high sound pressure at low frequencies around the spring-mass resonance and around the shell circumferential resonances occurs. The layer of voids results in strong blocking of sound transmission. For a coating with hard scatterers (Figure 3(b)), the lowest radiated sound occurs around the dipole resonance frequency.

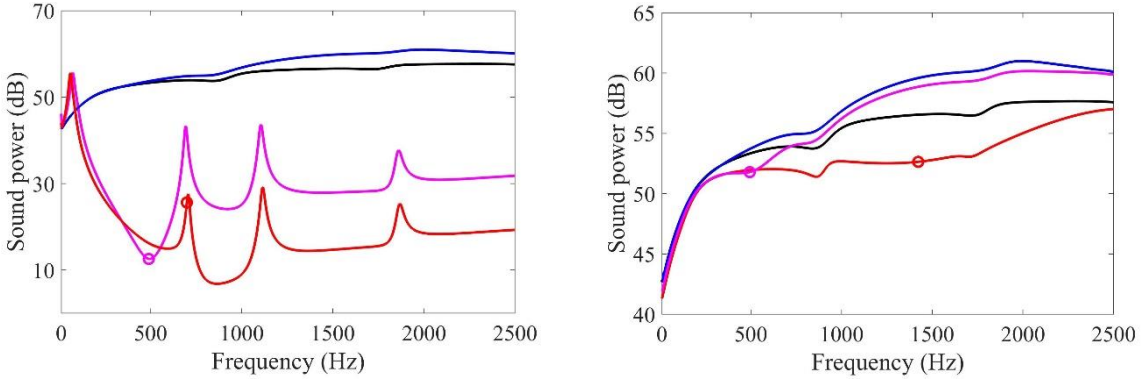

Figure 2 Radiated sound power (dB ref 1 pW) from an uncoated shell (black line), a shell with a homogeneous coating (blue lines), a locally resonant coated shell with **(a)** 50 cavities (pink line) or 67 cavities (red line), **(b)** 60 hard scatterers (pink line) or 110 hard scatterers (red line). The corresponding monopole and dipole resonances are indicated by pink and red circles.

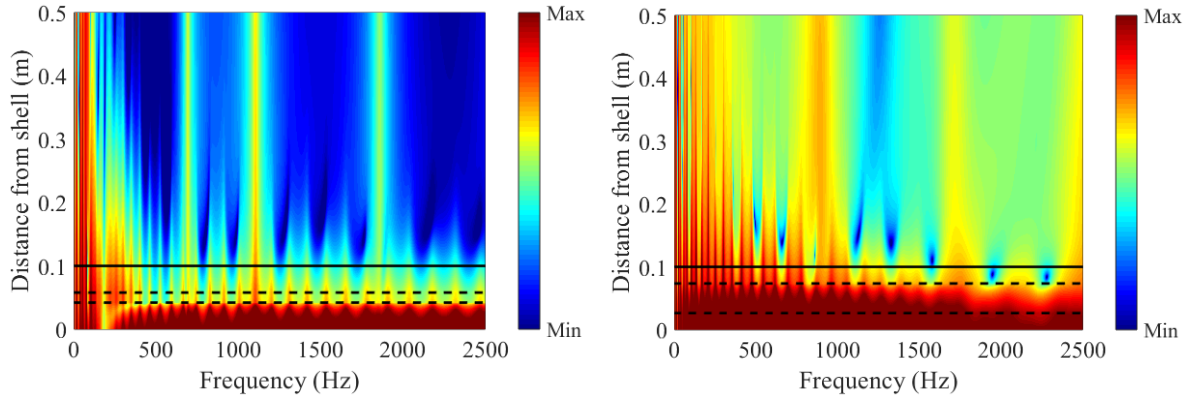

Figure 3 Acoustic pressure (dB ref 1 μPa) as a function of distance from the shell surface for a locally resonant coated shell with **(a)** 50 cavities and **(b)** 110 hard scatterers. The exterior surface of the coating is indicated by a black solid line. The homogenized layer of inclusions is indicated by black dashed lines.

References

[1] J. Wen, H. Zhao, L. Lv, B. Yuan, G. Wang, and X. Wen, *J. Acoust. Soc. Am.*, **130**, 1201–1208 (2011).
[2] S.M. Ivansson, *J. Acoust. Soc. Am.* **131**, 2622-2637 (2012).
[3] P. Méresse, C. Audoly, C. Croënne, and A.-C. Hladky-Hennion, *Comptes Rendus Mécanique*, **343**, 645–655 (2015).
[4] C. Ye, X. Liu, F. Xin, and T.J. Lu, *J. Sound Vib.*, **426**, 54–74 (2018).
[5] G.S. Sharma, A. Skvortsov, I. MacGillivray, and N. Kessissoglou, *Appl. Acoust.*, **143**, 200–210 (2019).
[6] Z. Zhang, Y. Zhao, and N. Gao, *Eng. Rep.*, e12627 (2023).
[7] G.S. Sharma, A. Marsick, L. Maxit, A. Skvortsov, I. MacGillivray, and N. Kessissoglou, *J. Acoust. Soc. Am.*, **150**, 4308–4314 (2021).
[8] G.S. Sharma, A. Skvortsov, I. MacGillivray, and N. Kessissoglou, *J. Sound Vib.*, **443**, 652–665 (2019).
[9] E.A. Skelton and J.H. James, *Theoretical Acoustics of Underwater Structures*, World Scientific, London, UK (1997).
[10] C. Lin, G.S. Sharma, D. Eggler, L. Maxit, A. Skvortsov, I. MacGillivray, and N. Kessissoglou, *Int. J. Mech. Sci.*, **232**, 107479 (2022).

PHONONICS 2023: 6th International Conference on Phononic Crystals/Metamaterials/Metasurfaces, Phonon Transport, and Topological Phononics
Manchester, England, June 12-16, 2023
PHONONICS-2023-0061

Flow Transition Delay by Multi-Input Multi-Output Phononic Subsurface

Carson L. Willey[1,2], Caleb J. Barnes[3], Vincent W. Chen[1,2], Kevin Rosenberg[2,3], Albert Medina[2], Abigail T. Juhl[2]

[1] UES, Inc., Dayton, OH 45432, USA
carson.willey.ctr@us.af.mil, vincent.chen.2.ctr@us.af.mil
[2] Air Force Research Laboratory, Wright-Patterson AFB, OH, 45433, USA
caleb.barnes.1@us.af.mil, alberto.medina.3@us.af.mil, abigail.juhl.1@us.af.mil
[3]Spectral Energies, LLC., Dayton, OH 45432, USA
kevin.rosenberg.2.ctr@us.af.mil

Abstract: This work addresses delaying the onset of turbulence by allowing a portion of a flow bounded surface to displace according to a receptance. A forced motion study determined conditions of the phase and magnitude of the receptance to cause transition delay. A multi-input multi-output phononic subsurface was designed to exhibit the proper response at each fluid-structure interaction surface.

Passive flow control by compliant surfaces has been studied since the early 1950's, but has been difficult to realize by conventional materials/structures[1]. Recently, M. I. Hussein put forward the concept of a phononic subsurface (PSub) that acts as a passive actuator for flow control[2]. That work was followed up by the development of a miniaturized PSub that worked on the same principle as the original[3]. In both cases, the PSubs operate by exchanging energy with the flow through a single interaction surface, whose responses are governed by the interaction surface receptance and may be classified as single-input single-output (SISO) PSubs. In an undamped PSub, the phase of the response will shift between 0° and 180° at the anti/resonances. A strong, out-of-phase response can be engineered by situating a truncation resonance just before the desired frequency of operation, and since this resonance is within a bandgap, the phase is assured to be relatively stable across the bandgap range. The result of this design strategy is that the kinetic energy of the flow nearby the flow-PSub interaction surface drops below the case without a PSub (i.e. rigid case), but this effect is highly localized.

The first part of this work was a detailed forced motion study using computational fluid dynamics (CFD) simulations and linear stability analysis to study Tollmien–Schlichting (T-S) wave flow instabilities. T-S waves are a type of well-ordered flow structure that arise during the transition between laminar and turbulent flow. Analysis determined that there is a range of receptance phases of a flow bounded surface that cause downstream (DS) reductions in flow kinetic energy, as opposed to a reduction in flow kinetic energy local to the PSub. Table 1 contains the receptance phase limits given by each analysis type. These results show that there is a need for a response whose displacement will lead the forcing imposed on each interaction surface by the T-S wave pressure. The phase of undamped SISO PSubs is limited to 0° and 180°, such that they are ill-suited to the task of reducing the total flow kinetic energy DS which is necessary to delay the onset of turbulence over an airfoil.

Analysis	ϕ_{min}	$\phi_{optimal}$	ϕ_{max}
Lin. Stability	-10°	90°	170°
CFD	-20°	57°	161°

Table 1 Single point receptance phase bounds for T-S wave

A primary objective of this work is to passively reduce the flow kinetic energy DS from the flow interaction surface attached to the passive actuator, as in the case of the SISO PSub[2,3]. This was achieved by allowing the flow to interact with the PSub at multiple points, making it a multi-input/multi-output (MIMO) system. In this context, inputs are the forces exerted on the PSub by the original T-S wave associated with flow transition, and outputs are the displacements of the PSub degrees of freedom associated with the upstream (US) and DS flow-PSub interaction locations, as shown in Figure 1 a. Here the PSub is a three unit cell structure with two types of rigid masses situated along a beam that is clamped at either end. The dispersion curves and component receptances of the diatomic beam-based

PSub are shown in Figure 1 b and c respectively. Note, the component receptances are collocated and cross receptances when the MIMO PSub is excited by a single force at either the US or DS locations. In the forced motion CFD analysis, and the linear stability analysis, it was determined that a positive receptance phase is required to delay transition, but the phase response (Figure 1 c) shows that only 0° or -180° can be achieved by the component receptances. Considering the receptance matrix of the MIMO PSub, and that the T-S wave has a known phase shift between the US and DS locations, apparent collocated receptances (ACR) are calculated for multiple values of the US/DS forcing phase shift and plotted in Figure 1 d and e, along with the CFD phase value requirements given in Table 1. The ACR are shown to have a broad region of stabile phase inside the band gap that fall within the region for T-S wave attenuation.

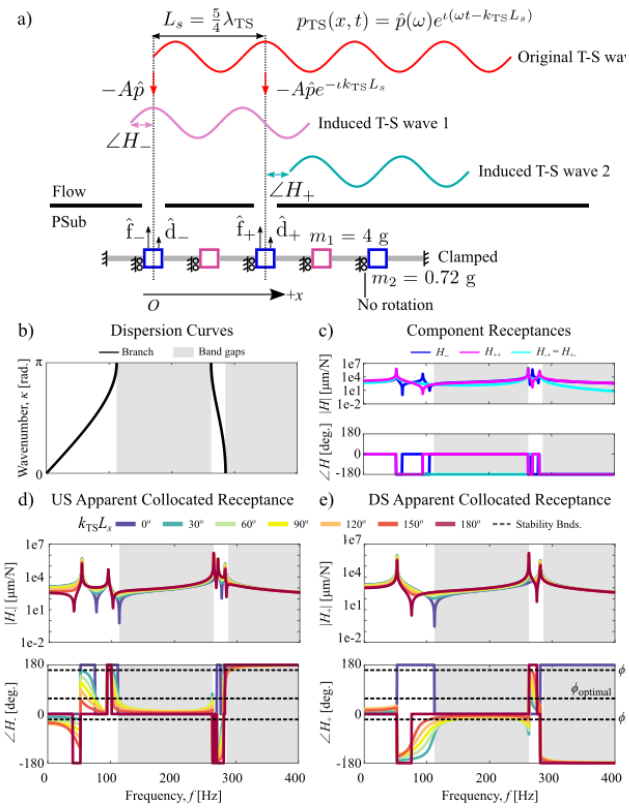

Figure 1 T-S wave interaction with MIMO PSub. Original (red), induces two T-S waves (magenta and cyan) a) according to the dispersion characteristics b), and component reacceptances c) of the PSub. Apparent collocated receptances at the US d) and DS e) positions, are determined by combining collocated reacceptances, taking into account the phase shift between T-S wave forcing at US/DS.

The result of this is demonstrated in Figure 2, which shows the flow vortex formation for a spanwise periodic three-dimensional CFD simulation, without (top panel) and with (bottom panel) MIMO PSub passive control. A clear delay in the DS onset of turbulence. This result indicates that a MIMO PSub passive controller has the ability to reduce the skin friction drag and therefore extend flight times due to lower fuel consumption. Note, current results assume the interaction surface is broad in the spanwise direction in order to provide a sufficiently strong forcing on the PSub. Work remains to boost the displacement amplitude so that the interaction surface size can be reduced.

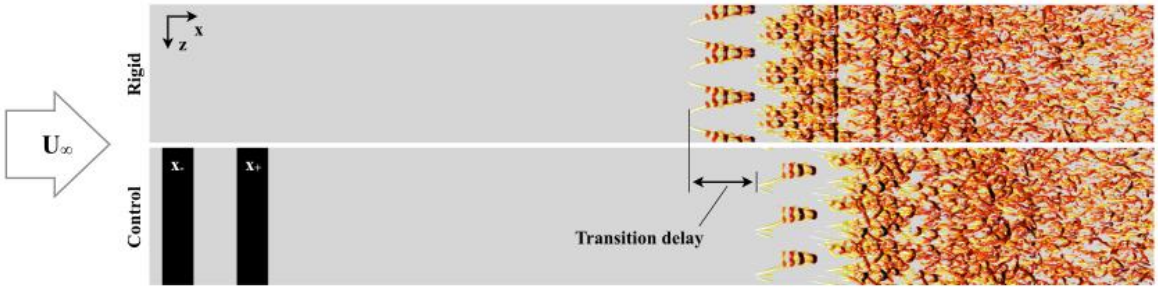

Figure 2 Flow vortex formation. Boundary layer transition occurs earlier in the rigid case (top panel) than in the case with passive MIMO PSub control (bottom panel).

References

[1] M. O. Kramer, *J. Aerosp. Sci.* **27**(1), 69 (1959).
[2] M. I. Hussein, S. Biringen, O. R. Bilal, and A. Kucala, *Proc. R. Soc. A* **471**, 20140928 (2015).
[3] C. J. Barnes, C. L. Willey, K. Rosenberg, A. Medina and A. T. Juhl, AIAA Scitech 2021, 1–23 (2021).

PHONONICS 2023: 6th International Conference on Phononic Crystals/Metamaterials/Metasurfaces, Phonon Transport, and Topological Phononics
Manchester, England, June 12-16, 2023
PHONONICS-2023-0178

Hybridizing Surface Acoustic Waves and Mechanical Resonators for Phononic Information Processing

Sarah Benchabane, Maciej Baranski, Reinaldo Chacon, Jules Chatellier, Jean-Michel Friedt and Abdelkrim Khelif

[1] *FEMTO-ST, Université de Franche-Comté, CNRS, 15b avenue des Montboucons, F-25000 Besançon, France. sarah.benchabane@femto-st.fr*

Abstract: The implementation of scalable phononic circuits has become an appealing prospect in view of increasing the versatility of radio-frequency signal processing devices, both in the classical and quantum regime. Here, we propose to exploit hybridisation between surface acoustic waves and micropillars in view of implementing various phononic circuit elements in the linear or non-linear regime.

Guided elastic waves are powerful information carriers standing at the core of modern telecommunication devices. Surface acoustic waves (SAW), in particular, have been industrially used as radio-frequency filters or delay lines since the 1970s[1] and remain relevant in current wireless standard technologies. More recently, the scope of their potential application fields has expanded covering fields as diverse as life science and quantum information technology[2]: SAWs are mechanical vibrations, and as such, can coherently couple to a number of physical systems. This intrinsic property has recently pushed towards the development of hybrid electromechanical or phonon-based devices. In this context, the implementation of scalable phononic circuits has become an appealing prospect in view of increasing the versatility of electro-acoustic devices. Recent demonstrations have made convincing steps towards this objective by proposing phononic architectures inspired by photonic integrated circuits[3] or combining the rich dynamics of micro- and nano-electromechanical (MEMS/NEMS) resonators with propagating elastic waves[4].

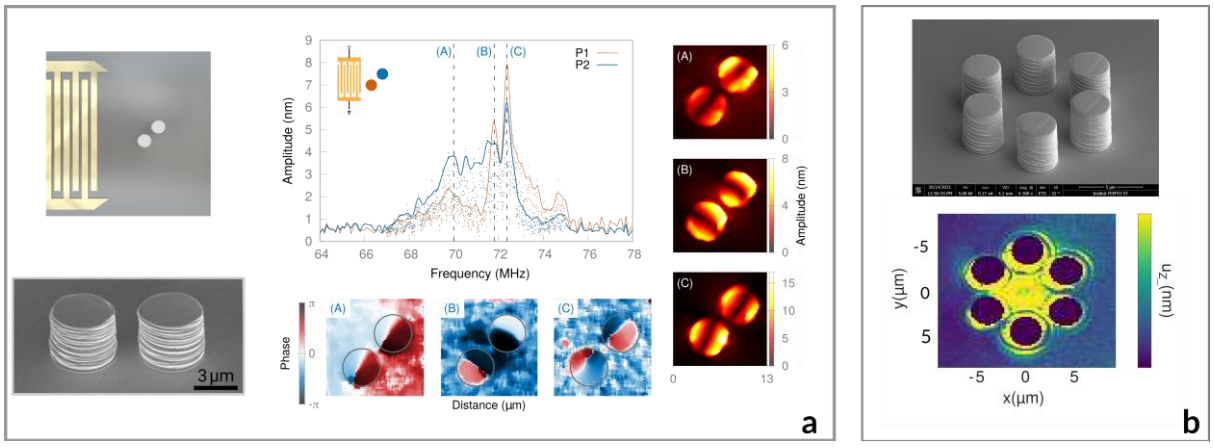

Figure 1 Examples of coupled SAW-mechanical resonator structures. **(a)** Pair of micropillars interrogated by a propagating SAW. The interaction results in the occurrence of a dipole-dipole-like coupled state[5]. **(b)** Phononic confinement resulting from the coupling of six resonators arranged hexagonally. The mode area is if the order of λ/10. In both cases, the resonators are made of ion-beam-deposited platinum and have a diameter between 3 and 4 µm and a height of 4 µm.

In this work, we propose to show how the interaction between surface guided waves and locally-resonant, micro- or nano-mechanical resonators can be exploited not only to control elastic wave propagation at the sub-wavelength scale but also to govern mechanical states of motion in various resonator arrangements. We implement these experimental demonstrations in an integrated platform combining interdigital transducers (IDTs) and sub-wavelength micropillars deposited on a piezoelectric substrate. We investigate different resonator arrangements — single, isolated micropillars; periodical arrays of resonators and different coupled resonator schemes — to illustrate the capabilities of-

fered by such hybrid systems. In all cases, the elastic field distribution is directly imaged by laser scanning heterodyne interferometry, hence granting access to a rich set of features characterising the interactions. Our experiments further reveal that such SAW-coupled micromechanical resonators are prone to exhibit rich non-linear dynamics, even at low drive powers and for low resonator quality factors. This potentially allows for an increasing number of signal processing functionalities, including e.g. parametric amplification or mechanical logic.
The fabricated devices operate at 70 MHz to ease the characterisation process but are readily scalable to higher frequencies, which opens up possibilities to reach sub-micrometer scale confinement and field enhancement in gigahertz locally-resonant cavities. They illustrate the potential of SAW-based architectures for the implementation of densely-integrated phononic-NEMS circuits and are particularly relevant in view of implementing efficient and low-footprint opto-electro-mechanical transduction devices integrated on-chip.

References

[1] D. Morgan and E. G. S. Paige, in *Surface Acoustic Wave Filters* (Second Ed.) Academic Press, UK, (2007).
[2] P. Delsing *et al.*, J. Phys. D: Appl. Phys. **52**, 353001, (2019).
[3] Fu et al., Nature Commun. 10, 2743 (2019).
[4] Kurosu et al., Nature Commun. 9, 1331 (2018).
[5] L. Raguin *et al.*, Nat. Commun. **10**, 4583, (2019).

PHONONICS 2023: 6th International Conference on Phononic Crystals/Metamaterials/Metasurfaces, Phonon Transport, and Topological Phononics
Manchester, England, June 12-16, 2023
PHONONICS-2023-0214

Leveraging and Tuning Acoustic-Wave Propagation in Micro-Architected Materials

Rachel Sun[1], Yun Kai[1], Thomas Pezeril[2], Washington DeLima[3], Carlos M. Portela[1]

[1] Department of Mechanical Engineering, Massachusetts Institute of Technology, 77 Massachusetts Ave., Cambridge, MA 02139, USA,
rmsun@mit.edu, ykai@mit.edu, cportela@mit.edu
[2] Institut de Physique de Rennes, UMR CNRS 6251, Université Rennes, Rennes, France,
thomas.pezeril@univ-rennes1.fr
[3] Kansas City National Security Campus, Department of Energy, Kansas City, MO 64147, USA,
wdelima@kcnsc.doe.gov

Abstract: Three-dimensional (3D) architected materials have enabled unique combinations of mechanical properties in the static regime, such as their extreme stiffness-to-density ratios or auxetic responses. However, their dynamic response—particularly at the microscale—has remained largely unexplored. Here, we present our progress towards (i) leveraging acoustic waves in the MHz regime to mechanically characterize micro-architected materials, and (ii) understanding the role of 3D architecture in controlling wave propagation characteristics.

Architected materials with user-defined 3D morphologies at the nano- to microscale have demonstrated properties unachievable by their underlying constituent materials—unveiling a rich mechanical property space with exotic responses such as extreme stiffness-to-weight ratios[1]. Most of these explorations have focused on static properties such as stiffness and strength, while their 3D nano- and microstructures are hypothesized to exhibit exotic properties in dynamic realms ranging from elastic wave propagation[2] to extreme conditions such as impact[3,4]. However, challenges associated with scalable fabrication of architected materials and characterization of their response in dynamic regimes have precluded progress in these topics. Namely, characterization of architected materials has relied on nanomechanical tools such as nanoindenters to provide force-displacement measurement with sufficient spatial resolution, while advances in improving their temporal resolution and thus capturing responses with nanometer and nanosecond resolution are still in their infancy. To expand our knowledge of the potential of architected materials in dynamic regimes such as acoustic wave propagation—towards the design of novel acoustic metamaterials—new versatile characterization techniques are required.

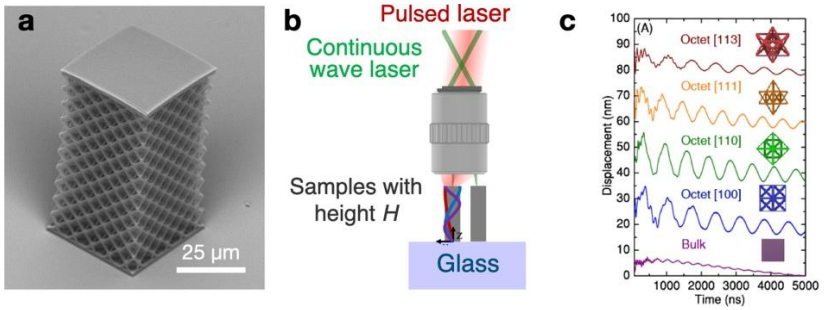

Figure 1 Laser-induced acoustic wave propagation method in architected materials. **(a)** Architected material sample fabricated via two-photon lithography, with features down to ~1 μm. **(b)** Schematic of characterization technique, consisting of a pump (pulsed) laser and probe (continuous wave) laser. **(c)** Sample displacement responses for bulk polymer samples and architected materials at different orientations.

As an alternative to classical contact-based characterization, we present a framework for excitation and measurement of small-amplitude mechanical waves in architected materials via laser pump-probe schemes. This technique thus enables measurement of acoustic waves propagating in microscopic architected material samples, enabling systematic explorations of the role of 3D geometry on wave propagation characteristics in acoustic metamaterials. We employ our proposed characterization method to (i) leverage propagation of acoustic waves in the MHz regime to infer dynamic mechanical properties of architected materials, and (ii) to uncover the influences of microinertia on the wave propagation response of architected materials.

First, we leverage our characterization method to access dynamic properties of periodic architected materials, enabling high-throughput, non-contact measurement of their dynamic elastic properties. We

fabricate architected materials using two-photon lithography with feature sizes on the order of ~1 µm and unit cells of ~10 µm, out of an acrylate-based photoresist (Figure 1a). Specifically, we select the octet and tetrakaidecahedron morphologies as representative stretching- and bending-dominated geometries. To characterize their effective elastic constants, we induce photoacoustic stimuli in a pump-probe scheme at the top of the sample to dynamically excite elastic waves in the architected materials and thereby determine the dominant modal response using a common-path interferometric setup (Figure 1b). Using the time-dependent oscillations on the samples (Figure 1c), we extract the frequency content of the resonant modes to construct an experimental partial dispersion relation (by varying the wavenumber of the induced excitations) and thus calculate an effective wave velocity in the architected materials. Using various crystallographic orientations of the architected materials, we then extract their full dynamic elastic tensor and compute their direction-dependent stiffness. Given the viscoelastic nature of the constituent acrylate-based polymer, we demonstrate viscoelastic effects such as dynamic stiffening and damping in the architected materials. Lastly, we demonstrate quantification of invisible defects in microscopic samples by measuring shifts in resonant frequencies as a function of defect densities. These efforts open the door to acoustic-wave propagation as a characterization technique for linear dynamic properties in microscopic architected materials, enabling rapid non-destructive characterization.

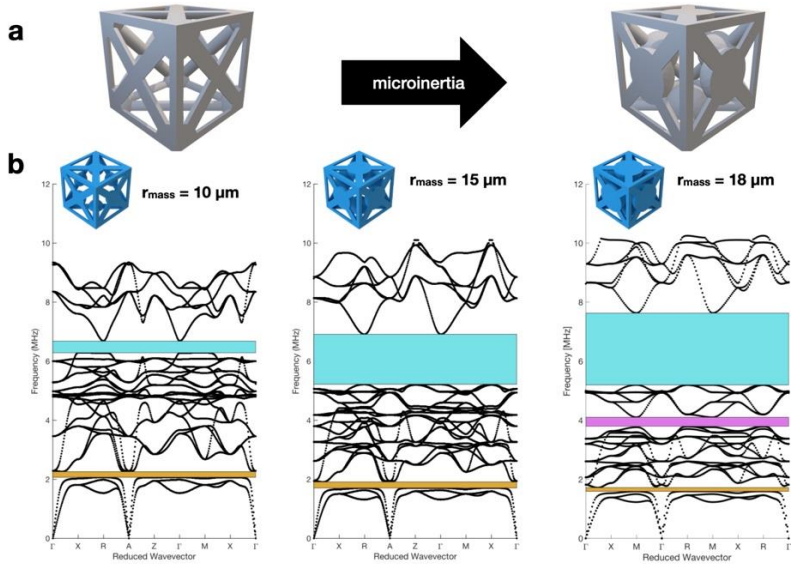

Figure 2 Acoustic metamaterials with engineered microinertia. **(a)** Schematic of braced cubic geometry with and without microinertia, selected to be a sphere at the center of edge braces. **(b)** Representative dispersion relations for the architected material as a function of microinertia size. Full band gaps are depicted as teal, yellow, and magenta regions.

Second, we design, fabricate, and characterize micro-architected materials with tunable acoustic properties through engineered placement of microinertia in 3D morphologies. Using our laser-based characterization technique, we perform a systematic exploration of a braced cubic morphology with varying sizes of lumped masses, placed at different locations of the unit cell (Figure 2a). Using our measurements, supported by Bloch wave analysis on the unit cells, we construct their partial dispersion relation and discuss the effect of microinertia and local resonance on long-wavelength-limit group velocity and band gap formation (Figure 2b). Using static computational homogenization, we also connect the observed dynamic response of the architected materials to the competing stretching and bending deformation within a unit cell. Our results provide a baseline to attain tunable acoustic metamaterials through use of inertia at the microscale and in the MHz regime. We envision these materials to have important implications in acoustic devices in microelectromechanical systems, medical ultrasound imaging, and microscale waveguides.

References

[1]Meza, L. R. *et al. Acta Mater.* **140**, 424–432 (2017).
[2]Patil, G. U. & Matlack, K. H. *J. Acoust. Soc. Am.* **145**, 1259–1269 (2019).
[3]Mueller, J., Matlack, K. H., Shea, K. & Daraio, C. *Adv. Theory Simulations* **2**, 1900081 (2019).
[4]Portela, C. M. *et al.* Supersonic impact resilience of nanoarchitected carbon. *Nat. Mater.* **20**, 1491–1497 (2021).

Realizing Beyond-Nearest-Neighbour Coupling in Acoustic and Elastic Metamaterials on a Benchtop Scale

Timothy A. Starkey[1*], Daniel B. Moore[1], Ian R. Hooper[1], J. Roy Sambles[1], Alastair P. Hibbins[1], Gregory J. Chaplain[1]

[1] *Centre for Metamaterial Research and Innovation, University of Exeter, Exeter, United Kingdom*
[*] *t.a.starkey@exeter.ac.uk*

Abstract: Engineering the dispersion of acoustic or elastic waves using coupling terms that spatially reach beyond the immediate local environment, or unit cell, is an 'emerging topic' in metamaterial design. In this talk, we present experimental studies in acoustic and elastic systems that realize beyond-nearest-neighbour coupling to introduce dispersion relations with extrema within the first Brillouin zone. In acoustics, we use mixed waveguide-surface wave coupling, whilst in elastics we develop an elastic scaffold with reconfigurable coupling elements and demonstrate the effects of structural symmetries on these exotic dispersion relations.

A chain of masses connected by springs is a staple for elementary courses on wave propagation because it demonstrates fundamental aspects of wave dispersion for electrons, phonons, and photons moving in periodic potentials. Usually, the springs connect masses directly to their neighbours, providing a 'local' interaction, and textbook physics ensues. By connecting masses with springs that reach-around their neighbouring masses, a beyond-nearest-neighbour (BNN) interaction introduces interesting wave effects such as backward energy propagation. Here, tailored wave dispersions resulting from nearest and BNN coupling are realized in an elastic metamaterial assembled in Meccano™ and in a 3D-printed acoustic metasurface with embedded waveguide channels. These designs enable the control of waves of long wavelength with compact unit cells.

The concept of BNN coupling is not unique to metamaterials or other periodic analogs. Indeed, it is commonplace to account for additional (sometimes "non-local") interactions when considering substantially more complex electronic band structures, for instance in tight-binding models, **k·p** perturbation theory, and density-functional theory. A coalescence of the ideas surrounding BNN interactions has recently been realized in the acoustic and elastic metamaterial communities. Specifically, next-next-nearest neighbours [1,2], have also been described as non-local metamaterials [3]. The intricately designed structures of Ref. [1] interconnect one unit cell with a physical join that extends to three unit-cells away, providing an additional degree of interaction and an alternative channel for power flow. The maxima and minima of the modal dispersion within the first Brillouin zone are associated with these competing channels, resulting in a characteristic dispersion relation that shows some analogies to that of a Roton.

The dispersion relation can be altered by including BNN coupling; as discussed by Brillouin [4]. For interactions extending to the L^{th} nearest neighbour, the form of the dispersion relation

"[· · ·] will be expressed as a polynomial of degree L."

And so, for interactions with the L^{th} nearest neighbor, there will be $L - 1$ extrema within the first Brillouin

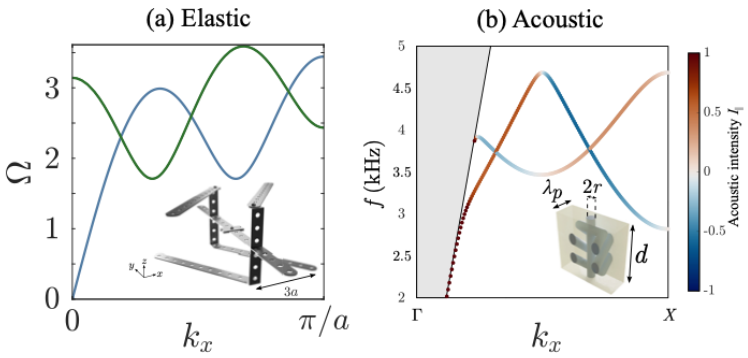

Figure 1 – Dispersion relations and corresponding unit cell schematics for benchtop (a) elastic and (b) acoustic BNN coupling demonstrations. (a) Toy-model results for a mass-spring system that approximates the elastic modes for the inset unit cell. (b) FEM model dispersion for the inset acoustic metasurface unit cell. Colour scale shows calculated acoustic intensity demonstrating regions of forward and backward group velocity for positive phase velocity.

zone, resulting in regions with altering signs of the group velocity, $v_g \equiv \partial\omega/\partial k$. For the case of NN-only interactions, the singular extrema occurs at the band edge owing to the formation of standing waves via the Bragg condition.

Elastic realization

We design, simulate, and experimentally characterize a reconfigurable elastic metamaterial with beyond-nearest-neighbor (BNN) coupling [5]. The structure is composed from the popular British model-construction system Meccano™ and supports backward waves with opposite directions of phase and group velocities. Figure 1(a) displays an extended unit-cell schematic and dispersion relations with symmetric and antisymmetric eigenmodes. In the talk we present the experimental results and verify three distinct configurations of the Meccano sample by acoustically inferring their spatial vibration spectra. Figure 2(a) shows the render schematic of one sample.

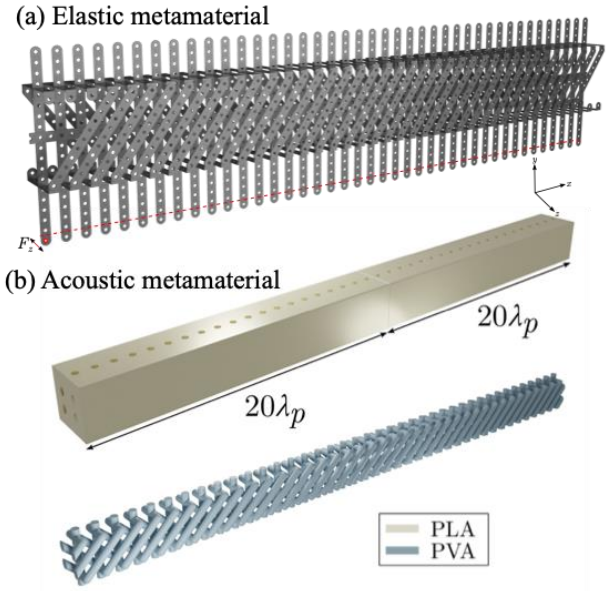

Figure 2 - Rendered schematic diagrams of (a) Elastic metamaterial design comprised of Meccano-like steel parts. (b) Acoustic metamaterial showing (top) the solid substrate, and (bottom) the embedded waveguide paths which enable the BNN acoustic coupling.

Acoustics realization

We design, simulate, and experimentally characterize an acoustic metasurface comprised of a 1D array of open, sound-hard, cavities, modulated with beyond-nearest-neighbor (BNN) couplings in the form of additional connecting cavities embedded beneath the surface [6]. The hidden complex structure is realized readily with additive manufacturing techniques (3D printing). Figure 1(a) shows the unit-cell schematic and computed bandstructure; nearest-neighbour coupling is achieved via diffraction from vertical pipes, and BNN coupling occurs via-waveguided fields between the pipes within the structure. The dispersive properties of the supported localized acoustic surface waves are influenced by competing power-flow channels provided by the BNN couplings that generate extrema in the dispersion spectra within the first Brillouin zone. The structure supports negatively dispersing 'backwards' waves that we experimentally verify. Figure 2(b) top shows the acoustically rigid material that comprises the metasurface; Figure 2(b) bottom shows the air channels within the metasurface, that mediate the BNN couplings.

References

[1] Y. Chen, M. Kadic, and M. Wegener, *Nat. Comms.* **12**, 1 (2021).
[2] J.A.I. Martínez, M. F. Groß, Y. Chen, T. Frenzel, V. Laude, M. Kadic, and M. Wegener, *Sci. Adv.* **7** (2021).
[3] K. Wang, Y. Chen, M. Kadic, C. Wang, and M. Wegener, *Comm. Mat.* **3**, 1 (2022).
[4] L. Brillouin, Wave propagation in periodic structures: electric filters and crystal lattices, 2nd ed. (Dover, New York, 1953).
[5] G.J. Chaplain, I.R. Hooper, A.P. Hibbins, and T.A. Starkey, *Phys. Rev. Appl.*, (accepted 2023).
[6] D.B. Moore, J.R. Sambles, A.P. Hibbins, T.A. Starkey, and G.J. Chaplain, *Phys. Rev. B,* (accepted 2023).

PHONONICS 2023: 6th International Conference on Phononic Crystals/Metamaterials/Metasurfaces, Phonon Transport, and Topological Phononics
Manchester, England, June 12-16, 2023
PHONONICS-2023-0061

Dynamics of Spatiotemporally Modulated Materials

Behrooz Yousefzadeh[1]

[1] *Department of Mechanical, Industrial and Aerospace Engineering, Concordia University, Montreal, QC, Canada*
behrooz.yousefzadeh@concordia.ca

Abstract: Spatiotemporally modulated materials possess effective properties that change periodically in space and time. These materials exhibit nonreciprocal wave propagation characteristics. We explore and review these properties, with a focus on nonreciprocal phase shifts and vibration transmission in short mechanical systems.

Materials with spatiotemporally modulated properties exhibit wave propagation characteristics that are not typical of regular materials. In particular, they have a demonstrated ability to restrict the propagation of waves to only one direction[1]. Such nonreciprocal transmission properties have the potential to lead to new vibration mitigation devices and energy harvesting techniques. Understanding the nonreciprocal dynamics of these materials has therefore attracted the attention of many researchers[2].

Nonreciprocity is predominantly identified by a left-to-right transmission amplitude that is different from the right-to-left transmission amplitude; a significant difference in the transmitted amplitudes is often desirable in this context. In this work, we review the nonreciprocal vibration transmission characteristics of discrete mechanical systems with spatiotemporally modulated elasticity. We focus exclusively on short systems, starting with the extreme case of two degrees of freedom (Figure 1).

Purely temporal modulation of the stiffness parameters ($\phi = 0$) results in the appearance of sideband resonances in the steady-state response of the system. For weak modulation amplitudes, and light damping, these extra resonances occur at $\omega_n \pm p\omega_m$, where ω_n is the *n*-th natural frequency of the unmodulated system, ω_m is the modulation frequency and $p = 0,1,2,$ .... The presence of spatiotemporal modulation ($\phi \neq 0$) does not alter the location of the sideband resonance, but the transmission characteristics are no longer reciprocal in this case. Remarkably, the main contributor to nonreciprocity is not that the transmitted vibrations have different amplitudes (or energy) in the left-to-right (L-R) configuration compared to the right-to-left (R-L) configuration. It is instead the difference between the transmitted phases that contributes to breaking of reciprocity in very short systems[3].

For passive (not modulated) nonlinear system, efficient numerical techniques exist for computing the nonreciprocal dynamics of the system and for identifying response regimes that are characterized by a nonreciprocal phase shift while maintaining equal transmitted amplitudes[4]. In contrast, the linear response of a temporally modulated material to external harmonic drive is quasiperiodic; i.e. characterized by two or more incommensurate frequencies. This makes the numerical analysis of the problem very costly compared to materials without temporal modulation. To bridge this gap, we utilize the envelope of the response: while the response of temporally modulated systems is quasiperiodic, its envelope is periodic in time. We can therefore use the response envelopes to identify nonreciprocal dynamics and response regimes that are identified by nonreciprocal phase shifts.

Figure 2 (a) shows an example of phase nonreciprocity in a weakly modulated system ($k_m = 0.1k_g$): the transmitted amplitudes of the L-R and R-L configurations are equal, but the response is nonreciprocal because of the relative phase shift between the two displacement outputs (solid curves). The corresponding response envelopes (dashed curves) are identical except for a phase shift. This nonreciprocal phase shift is illustrated in Figure (b) by shifting the R-L output such that there is no phase shift between the two response envelopes.

The response envelopes in Figure 2 are typically obtained using the rotating wave approximation[5], which result in harmonic envelope equations. The limitation of this classical approach is that the predicted envelopes are harmonic. We have observed in our simulations of spatiotemporally modulated materials that the response envelopes are harmonic in a very limited range of parameters, in particular for very weak modulations. To overcome this shortcoming, we obtain the response envelopes using the averaging method. Figure 3 shows the response of a moderately modulated system ($k_m = 0.7k_g$). Note in panel (a) that the response envelope is no longer harmonic – the envelope remains periodic. The

transmitted amplitudes of the L-R and R-L configurations are equal, even though the response is clearly nonreciprocal. Panel (b) indicates that indeed the difference between the anharmonic response envelopes is caused merely by a phase shift.

In summary, we present the application of response envelopes in analysing the steady-state quasiperiodic response of spatiotemporally modulated materials. We will discuss the influence of the size of the system (number of degrees of freedom) on the transmission characteristics in terms of both amplitude and phase. Furthermore, we will discuss parametric instabilities caused by the temporal modulation. Finally, we show that the formulation of the problem in terms of response envelopes presents a computationally viable path for exploring the role of nonlinearity on nonreciprocal transmission characteristics in spatiotemporally modulated materials.

References

[1] K. A. Lurie, *An Introduction to the Mathematical Theory of Dynamic Materials*, Springer, (2017).
[2] H. Nassar, B. Yousefzadeh, R. Fleury, M. Ruzzene, A. Alù, C. Daraio, A. N. Norris, G. Huang and M. R. Haberman, *Nature Reviews Materials*, **5**, 667-685 (2020).
[3] J. Wu and B. Yousefzadeh, Proceedings of the Canadian Society of Mechanical Engineers International Congress, 1-6 (2022).
[4] B. Yousefzadeh, *Journal of Computational Dynamics*, **9 (3)**, 451-464 (2022).
[5] A.H. Nayfeh and D.T. Mook, *Nonlinear Oscillations*, Wiley (1995).

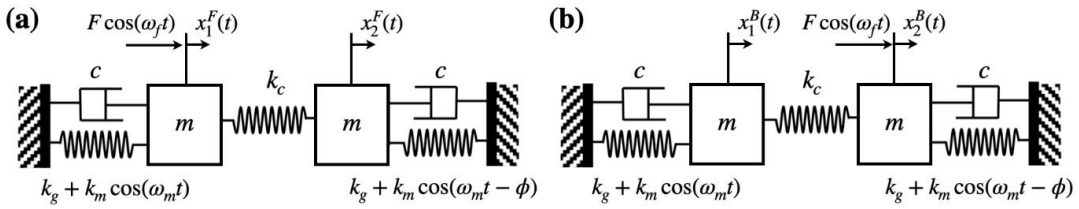

Figure 1 Schematic of the system with two degrees of freedom: (a) left-to-right configuration, (b) right-to-left configuration.

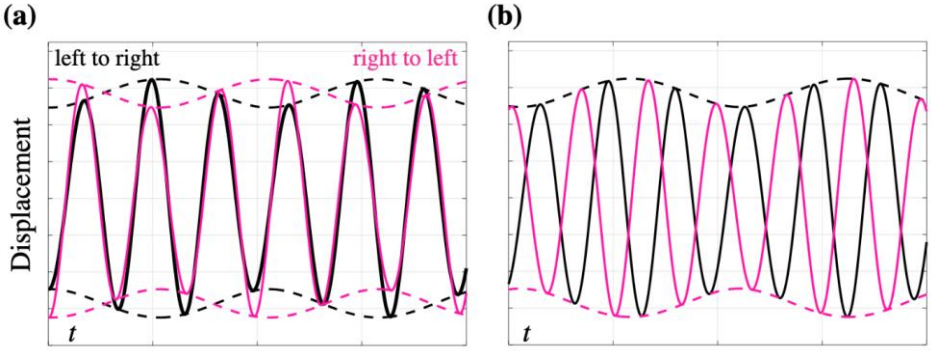

Figure 2 Phase nonreciprocity in a weak modulated system **($k_m = 0.1k_g$)**: (a) original response, (b) phase-shifted response to highlight phase nonreciprocity.

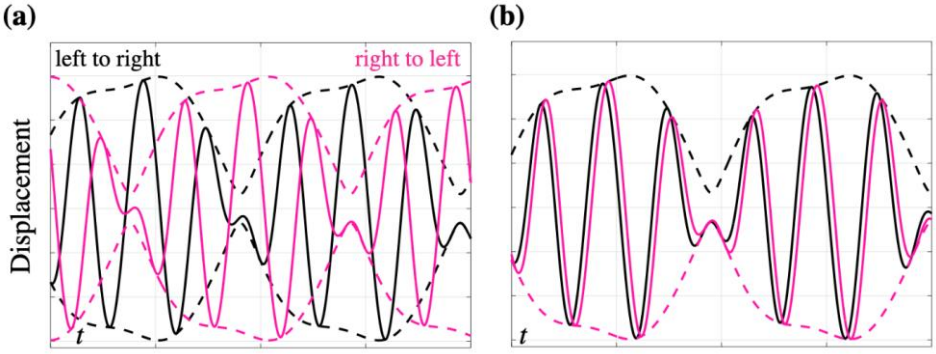

Figure 3 Phase nonreciprocity in a moderately modulated system **($k_m = 0.7k_g$)**: (a) original response, (b) phase-shifted response to highlight phase nonreciprocity.

PHONONICS 2023: 6th International Conference on Phononic Crystals/Metamaterials/Metasurfaces, Phonon Transport, and Topological Phononics
Manchester, England, June 12-16, 2023
PHONONICS-2023-0113

Temporally Modulated Phase Gradient Systems: Towards Frequency-selective Acoustic Wave Beaming

M. Moghaddaszadeh[1,2] ,R. Adlakha[1], M. A. Attarzadeh[1], A. Aref[2], M. Nouh[1]

[1] Dept. of Mechanical and Aerospace Engineering, Univ at Buffalo (SUNY), Buffalo, NY 14260, USA, mmoghadd@buffalo.edu, revantad@buffalo.edu, mattarza@buffalo.edu, mnouh@buffalo.edu

[2] Dept. of Civil, Structural and Environmental Engineering, Univ at Buffalo (SUNY), Buffalo, NY 14260, USA, aaref@buffalo.edu

Abstract: Beam forming using phase gradient structures forms the basis of several sonar and biomedical imaging applications. We report on a class of temporally-modulated elastoacoustic phased arrays which operate independently within different directions and frequency channels, and exercise a degree of unprecedented control over its beamed waves ranging from tunable directivity, nonreciprocal transmission, and selective suppression of up or down harmonics.

Acoustic phased arrays (APAs) have been a cornerstone of non-destructive evaluation, wave beaming, and medical imaging for decades. In their most general form, phased arrays can be thought of as a coalescence of multiple wave transmitting/receiving components, also known as transceivers, which share a common excitation/collection port. The hallmark feature of phased arrays, which sets them apart from antennas, is an additionally imparted phase angle on each of its individual transceivers. As such, during transmission (TX), conventional arrays work by utilizing a static phase gradient across a set of acoustic transducers to steer a self-created wavefront in a desired direction. In reception (RX) mode, they abide by basic reciprocity principles and exhibit the strongest gain for waves incident from the same direction to which they transmit. The first part of this talk introduces the notion of dynamic phase gradients, i.e., a phase shift between neighbouring transceivers which also varies in time. We will show that these temporally-modulated APAs are capable of (a) generating multiple scattered harmonics of a single-frequency voltage input which simultaneously propagate in different directional lanes, and (b) exhibiting non-identical TX/RX patterns. We will show that such lanes emerge in the form of artificially-synthesized directional channels each with a distinct frequency signature that can be predicted a priori. To achieve this, we devise a class of phase shifters which augment the array elements with a dynamic phase modulation using an array of piezo-wafer discs bonded to an elastic medium. The scattered beams propagate simultaneously in the transmitted wave field but can be visualized using an FFT of the time-transient measurements via laser Doppler vibrometry. The experimental realization illustrates the array's ability to guide incident waves within tunable frequency channels that are commensurate with the modulation rate and along the intended directions.

The relationship between the spectral content of the transmitted waves and their corresponding principal directions can be elegantly predicted from the array's time-variant dynamics. However, owing to the Hermitian (real) nature of the spatiotemporal phase gradient, the emergent waves are still bound to symmetrically send energy into up- and down-converted frequency channels, thus impeding our ability to selectively mitigate or even entirely suppress either up- or down-converted harmonics. Seeking to push this boundary, the second part of the talk will present a class of non-Hermitian acoustic phased arrays which exercise a degree of unprecedented control over the multi-directional transmitted waves through an interplay between gain, loss, and coupling between individual components. The non-Hermitian APA structure provides a unique platform for unconventional scattering features, loss compensation, and wave amplification with minimal power consumption. Here, a complex phase profile under two special symmetries, PT and anti-PT, is introduced that enables the modulation of the amplitude of various harmonics and decouples up- and down-converted harmonics of the same order. We show that both PT- and anti-PT-symmetric phase profiles along the array exhibit a transition from "exact" to "broken phase" at the exceptional point -- a degeneracy in the parameter space where the system's eigenvalues and eigenvectors coalesce. The exceptional point is shown to support selective, on-demand suppression of up or down-converted harmonics. This theoretical prediction is validated

using several finite element simulations and is further verified experimentally. Scattered beams propagating simultaneously in the transmitted wave field of the non-Hermitian array are visualized using scanning laser Doppler vibrometry and are inspected in tandem via FFTs of the measured time-transient displacements. The theory of non-Hermitian APAs and their experimental realization unlocks rich opportunities in precise elastic/acoustic wave manipulation and opens up the possibility of simultaneous control over frequency and directional channels that can be tailored for a diverse range of engineering applications.

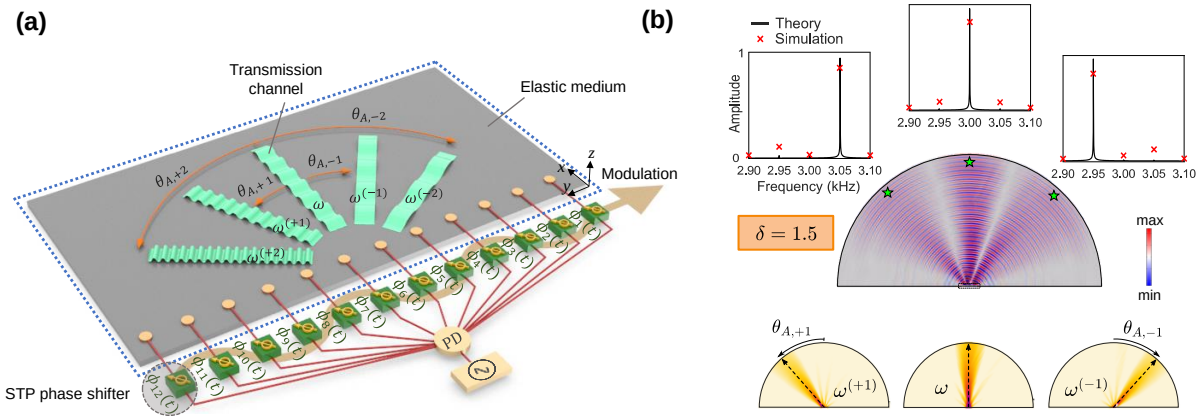

Figure 1 (a) Conceptual schematic and (b) Frequency-selective beaming in temporally-modulated acoustic phased arrays.

PHONONICS 2023: 6th International Conference on Phononic Crystals/Metamaterials/Metasurfaces, Phonon Transport, and Topological Phononics
Manchester, England, June 12-16, 2023
PHONONICS-2023-0150

Nonreciprocal Metamaterial from Piezo-electric Sensing and Actuation

A. Banerjee[1], K.K. Bera[2]

[1] *Department of Civil Engineering, Indian Institute of Technology Delhi, Hauz Khas, India, abanerjee@iitd.ac.in,*
[2] *Department of Civil Engineering, National Institute of Technology Tiruchirappalli, India kamal@nitt.edu*

Abstract: A unique strategy by harnessing the concept of feedback control between the piezo-electric bimorph sub-cells which are acting as sensor and actuator is conceptualized in this paper. In the unit cell, voltages from the sensing bimorph are fed back to actuate another bimorph. The analytical formulation employing transfer matrix method is adopted to obtain the dispersion diagram. Behavior of bandgap is studied for different gain. Non-reciprocal behavior of the lattice is observed due to the directionality induced via electrical coupling arising from the dependence of the actuating bimorph on the sensing bimorph. The decaying waves in either direction give rise to an almost uninterrupted attenuation bandgap starting at very low free wave frequency.

Non-reciprocity in a lattice provides another means of obtaining the wider attenuation band. Two types of definitions of non-reciprocal unit is available. Non-reciprocal transmission is reported in linear graded metamaterial in which the dispersion diagram remains symmetric only the frequency response functions alter. However, non-reciprocity in dispersion diagram can be acquired either by temporal and/or spatial modulation, or by introducing flow into the medium [1, 2]. Wave propagation through the beam with periodically bonded piezoelectric actuator-sensor pair is considered [3], in which the sensing voltage form the bottom piezoelectric patch is fed back to the top piezoelectric patch for actuation. This provides additional active stiffness to the system and thereby improves the stability and bandgaps behaviour. The bandwidth increment is marginal in this top-bottom pairing configuration of sensor/actuator bimorph as it primarily depends on the Bragg phenomenon. The properties of a shunted circuit piezoelectric bimorph beam are modulated by an inductive circuit to realize non-reciprocity [4]. However, feedback of voltages from a sensing bimorph to actuate another bimorph within a single unit cell is not persuaded so far. In this study, a unique strategy involving periodically placed piezoelectric sensing and actuation is developed. The novelty of the paper lies in realizing the non-reciprocal system and developing the solution procedure to obtain the dispersion relationship using transfer matrix method for a bimorph actuated by the feedback-controlled voltage received from the sensing bimorph located in the same unit cell.

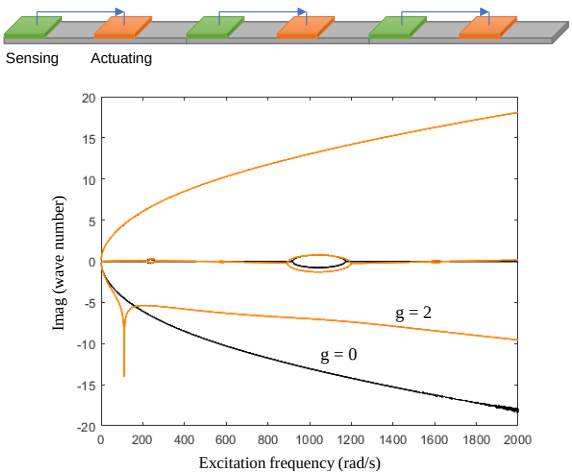

Figure 1: Realization of nonreciprocal piezo-electric bimorph. Dispersion diagram showing influence of gain.

Equation of motion of the piezo-electric coupled bimorph for the sensing and actuated conditions are derived. For example, the governing equation of the actuating sub-cell is written as [5]

$$m_e \frac{\partial^2 w_a}{\partial t^2} + (k_e + 2k_s)\frac{\partial^4 w_a}{\partial x^4} + g k_s \frac{\partial^4 w_s}{\partial x^4} = 0 \quad (1)$$

Here, m_e is the mass per unit length of the bimorph, w_s and w_a are the transverse flexural displacements of the sensing and actuation sub-cells, $(k_e + 2k_s)$ is the total stiffness contribution of the main beam and piezo patches, and g is the feedback control gain. Transfer matrix has been formulated after solving the coupled partial differential equation. Finally, Bloch theorem is applied for obtaining the dispersion

relationship. The detail derivation is omitted here for brevity. For a non-reciprocal lattice, an important characteristic of the transfer matrix is that it is being complex. Additionally, the dispersion relationship is non-palindromic. With the application of gain, transfer matrix becomes complex, and it made the system non-reciprocal. It can be noticed in the dispersion plot given in Figure 1 that imaginary part of the wave numbers is non-symmetric. The non-reciprocity is dependent on the gain as well as the free wave frequency. Attenuation of low frequency wave can be achieved with the application of small gain.

Uncommon wave phenomena, such as completely unsymmetrical dispersion diagram and an ultra-wide attenuation band covering entire frequency domain even for very low value of the feedback gain, are obtained due to the non-reciprocity. The non-reciprocity introduces attenuation band for a free wave frequency near to zero. This shows the promise of the system to be capable for used in several application associated with low frequency excitation.

References

[1] Z. Lu, A. N. Norris, Unilateral and nonreciprocal transmission through bilinear spring systems, 394 Extreme Mech. Lett. 42 (2021) 101087. 395

[2] J. Achenbach, J. Achenbach, Reciprocity in elastodynamics, Cambridge University Press, 2003.

[3] F. Li, C. Zhang, C. Liu, Active tuning of vibration and wave propagation in elastic beams with 463 periodically placed piezoelectric actuator/sensor pairs, J. Sound Vib. 393 (2017) 14–29

[4] C. Sugino, M. Ruzzene, A. Erturk, Nonreciprocal piezoelectric metamaterial framework and circuit 473 strategies, Phys. Rev. B 102 (1) (2020) 014304.

[5] A. Banerjee, K. K. Bera, Emergence of non-reciprocity in metabeam exploiting piezoelectric sensing and actuation, International Journal of Mechanical Sciences 236 (2022) 107765.

PHONONICS 2023: 6th International Conference on Phononic Crystals/Metamaterials/Metasurfaces, Phonon Transport, and Topological Phononics
Manchester, England, June 12-16, 2023
PHONONICS-2023-0003

Tailored Protected Edge Waves via Chiral Hierarchical Metamaterials

J. M. De Ponti[1], L. Iorio[1], G. J. Chaplain[2], A. Corigliano[1], R. V. Craster[3], R. Ardito[1],

[1] *Department of Civil and Environmental Engineering, Politecnico di Milano, Piazza Leonardo da Vinci, 32, 20133 Milano, Italy,*

[2] *Centre for Metamaterial Research and Innovation, Department of Physics and Astronomy, University of Exeter, Exeter EX4 4QL, United Kingdon*

[3] *Department of Mathematics, Imperial College London, 180 Queen's Gate, South Kensington, London SW7 2AZ*

E-mail: jacopomaria.deponti@polimi.it

Abstract: Precise manipulation of vibrational wave energy is a key demand in wave physics and engineering. We tailor protected edge states using a tetrachiral lattice with the addition of micro-resonators that impose tuneable symmetry breaking and reconfigurable mass. This allows us to achieve precise positional control, opening opportunities for robust signal transport and vibration control.

The investigation of topological states of matter has attracted growing interest with multiple realizations in photonics[1] and phononics[2]. Initiated from the field of topological insulators in quantum-mechanical systems, protected edge (or interfacial) surface states have now percolated into the physical platforms of classical wave propagation.

Within the passive topological materials framework, we tailor protected edge states in the elastic frame shown in Figure 1. Given the necessity of developing edge modes that propagate in the frequency region defined by the band gaps of the bulk modes, we opt for a tetrachiral structure, that allows for large band gaps in the low frequency spectrum[3].

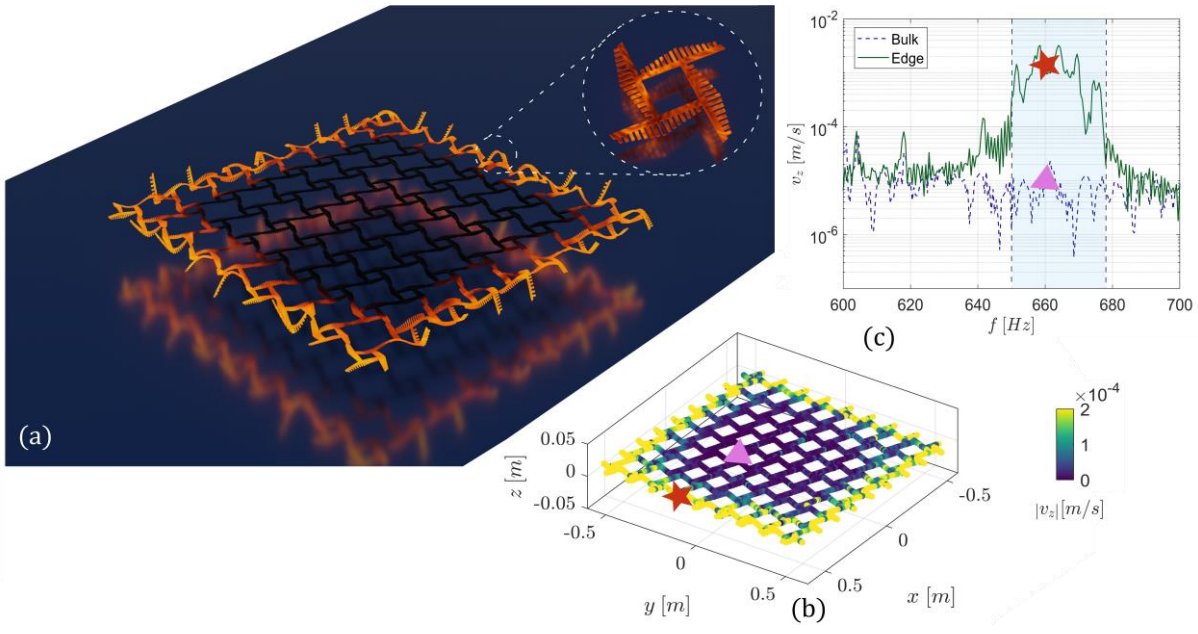

Figure 1 (a) Rendering from the numerical solution of the displacement field of the edge mode at the boundary of the lattice, together with an enlargement on the unit cell. The lattice is excited using an out-of-plane force on the edge, able to activate flexural wave propagation. (b) Experimental results obtained with a Scanning Laser Doppler Vibrometer (SLDV) on the real specimen, confirming strong agreement with numerical simulations. Experimental tests are performed by suspending the structure on a frame and providing the input using an electrodynamic shaker. (c) Logarithmic amplitude of the experimental displacement field depending on frequency. The two curves report the bulk (blue) and the edge (green) solutions. Dashed vertical lines denotes the central part of the bulk band gap.

We demonstrate that tetrachiral lattices do not only possess peculiar static features, but also non-trivial topological states motivated by the extension of well-known topological properties of hexagonal lattices to square lattices[4,5]. In addition, the obtained edge states can be precisely tuned leveraging graded arrays of masses within each unit cell. By doing so, we introduce a hierarchy of levels allowing us to design the internal microstructure of the unit cell to obtain highly controllable edge bands.

Separate from topological wave physics, another recent advance has been to take photonic or phononic crystals and then grade them spatially to create rainbow trapping or reflection devices[6]. Once robust edge states are established, the combination of these with such graded structures fulfils a requirement of vibrational devices, that is to deliver maximum energy to pre-allocated positions within the lattice. We take these concepts to exemplify the advantages of the proposed design in tailoring edge waves.

References

[1] A. B. Khanikaev, S. H. Mousavi, W.-K. Tse, M. Kargarian, A. H. MacDonald, and G. Shvets, Photonic topological insulators, *Nat. Mater.* **12**, 233–239 (2013).
[2] S. D. Huber, Topological mechanics, *Nat. Phys.* **12**, 621–623 (2016).
[3] A. Bacigalupo and L. Gambarotta, Simplified modelling of chiral lattice materials with local resonators, *Int. J. Solids Struct.* **83**, 126 (2016).
[4] M. P. Makwana, R. V. Craster, and S. Guenneau, Topological beam-splitting in photonic crystals, *Opt. Express* **27**, 1 (2019).
[5] W. Jiang, M. Kang, H. Huang, H. Xu, T. Low and F. Liu, Topological band evolution between Lieb and Kagome lattices, *Phys. Rev. B* **99**, 125131 (2019).
[6] J. M. De Ponti, L. Iorio, E. Riva, R. Ardito, F. Braghin and A. Corigliano, Selective mode conversion and rainbow trapping via graded elastic waveguides, *Phys. Rev. Appl.* **16**, 034028 (2021).

PHONONICS 2023: 6th International Conference on Phononic Crystals/Metamaterials/Metasurfaces, Phonon Transport, and Topological Phononics
Manchester, England, June 12-16, 2023
PHONONICS-2023-0052

Topological Edge States in Su-Schrieffer-Heeger Phononic Crystals: An Experimental Study

Amir Rajabpoor Alisepahi[1], Kai Sun[2], Jihong Ma[1,3,4,*]

[1] *Department of Mechanical Engineering, University of Vermont, Burlington, Vermont 05405, USA*
[2] *Department of Physics, University of Michigan, Ann Arbor, Michigan 48109, USA*
[3] *Department of Physics, University of Vermont, Burlington, Vermont 05405, USA*
[4] *Materials Science Program, University of Vermont, Burlington, Vermont 05405, USA*
[*] *Corresponding Author: Jihong.Ma@uvm.edu*

Abstract: Topological edge states in phononic crystals have been widely studied. Using laser-assisted experimental characterization, we explore the topological features of one-dimensional phononic crystals with beyond-nearest-neighbor interactions and make correct predictions on the number of topologically protected edge states with our newly proposed methodology.

Phononic crystals (PnCs) and acoustic metamaterials (AMMs) are artificially architected materials endowed with the capabilities of wave manipulation, which have attracted attention for emerging technological applications. Recently, the concept of topological insulators (TIs) originates from quantum physics, in which a topological invariant is often used to describe a category of materials or structures that present the same types of confined conductive states.

One simple example of using topological invariant to determine the nontrivial topologically protected edge states (TPES) would be the one-dimensional (1D) Su-Schrieffer-Heeger (SSH) model [1,2], as shown in **Fig. 1**. Initially introduced to understand solitons in polyacetylene, the SSH model was later adapted in mechanical systems to identify TPES via the winding number, *n*.

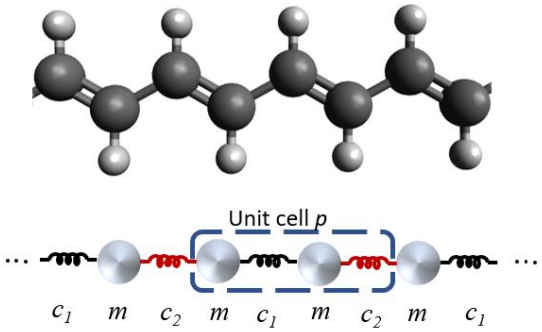

Figure 1 Top: Energetically relaxed polyacetylene using the universal force field. The alternating double-single covalent bonds can be simplified using the schematic spring-mass system shown at the bottom with alternating spring constants, c_1 and c_2.

The two arrangements of isomers with nonidentical spring stiffness c_1 and c_2 in **Fig. 1** represent two topologically different phases. When $c_1 > c_2$, n=0, signifying a trivial intra-cell hopping phase. In contrast, when $c_1 < c_2$, n=1, indicating a topologically nontrivial inter-cell hopping phase. These gauge-dependent winding numbers can also be evaluated via the Zak phase [3], which measures the rotation of eigenvectors in the unit cell.

All the studies thus far can be simplified using mass-spring systems considering only the nearest neighbor interactions. Recently, arising attention has been devoted to mechanical metamaterials with lattice interactions beyond nearest-neighbors (BNN), allowing the achievement of roton-like acoustical dispersion relations under ambient conditions similar to those observed in correlated quantum systems at low temperatures [4,5]. In addition to the unusual dispersion relation providing broadband acoustical backward waves and the multiple coexisting acoustical modes with the same polarization at one frequency due to the BNN interactions, interesting topological states also arise due to such BNN coupling.

In this work, we investigate the TPES in1D SSH structures with the third nearest neighbor interactions and have discovered the breakdown of the Chern number TPES prediction. In Ref [6], we prove theoretically and experimentally that, under certain circumstances, the number of TPES can be greater than *n*. We then further verify our theories using 3D-printed specimens and characterize the velocity field with a Polytec PSV-500 scanning Laser Doppler Vibrometer. More details on theories, simulations, and experiments can be found in Ref [6].

We then perform a discrete Fourier transform to the experimentally measured velocity field of our 3D-printed specimens with the third nearest neighbours. As can be seen from **Fig. 2 (a)**, the experimental measurement fits very well with the unit cell analysis from the 3D simulation. We then sampled

the locations near the interface (zero, one, and two cells away from the interface) about which the arrangement of the nearest-neighbour spring constants is symmetric. Our experimental measurement reveals three distinct interface modes appearing within the bandgap frequency range, as shown in **Fig. 2 (c)**. As a comparison, we also measure the velocity fields at the same locations for the 3D-printed structure without the interface.

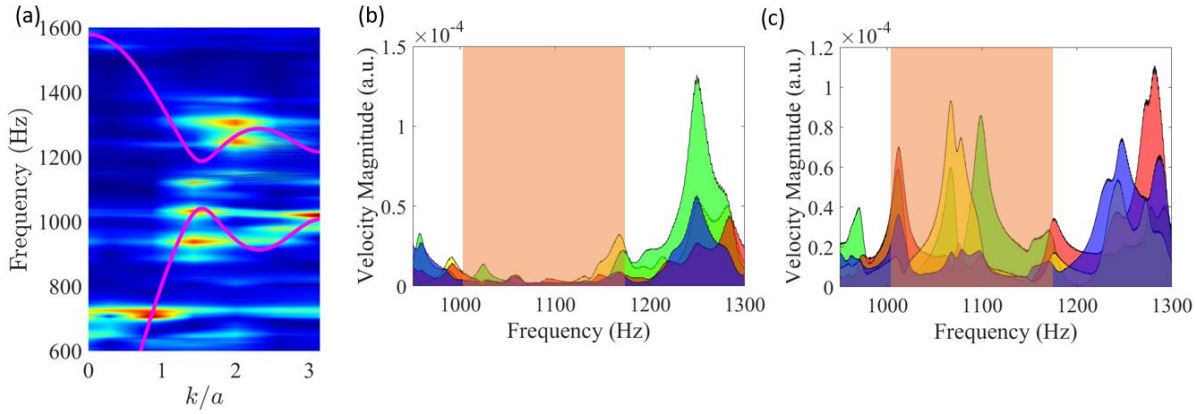

Figure 2 (a) Discrete Fourier transform of the experimentally measured velocity fields in a 3D-printed SSH structure. The magenta curves are the acoustic and optical phonon bands obtained from a unit cell analysis from a 3D simulation. (b) and (c): Experimentally measured frequency responses of the velocity fields in a 3-D printed SSH structure (b) without and (c) with an interface, about which the arrangement of the nearest-neighbour spring constants is symmetric. The orange-shaded region is the bulk bandgap between acoustic and optical phonon bands. The red, yellow, and green frequency response curves denote the velocity magnitudes at the zeroth, first, and second unit cells away from the interface. For the structure without the interface, the velocity fields are measured at the same locations as the one with the interface. The purple curves represent the velocity magnitude in the bulk. All figures are taken from Ref [6].

In conclusion, our experimental characterization presents unequivocal evidence to prove the breakdown of the Chern number prediction. Our newly proposed method to predict the number of TPES is detailed in Ref [6].

References

[1] Su, W., Schrieffer, J. R., & Heeger, A. J. (1979). Solitons in polyacetylene. *Physical Review Letters*, *42*(25), 1698.
[2] Su, W. P., Schrieffer, J. R., & Heeger, A. J. (1980). Soliton excitations in polyacetylene. *Physical Review B*, *22*(4), 2099.
[3] Zak, J. (1989). Berry's phase for energy bands in solids. *Physical Review Letters*, *62*(23), 2747.
[4] Chen, Y., Kadic, M., & Wegener, M. (2021). Roton-like acoustical dispersion relations in 3D metamaterials. *Nature Communications*, *12*(1), 3278.
[5] Iglesias Martínez, J. A., Groß, M. F., Chen, Y., Frenzel, T., Laude, V., Kadic, M., & Wegener, M. (2021). Experimental observation of roton-like dispersion relations in metamaterials. *Science Advances*, *7*(49), eabm2189.
[6] Rajabpoor Alisepahi, A., Sun, K., & Ma, J. (2021). Breakdown of Conventional Winding Number Calculation in Lattices with Interactions Beyond Nearest Neighbors. *In Submission.*

PHONONICS 2023: 6th International Conference on Phononic Crystals/Metamaterials/Metasurfaces, Phonon Transport, and Topological Phononics
Manchester, England, June 12-16, 2023
PHONONICS-2023-0019

Interface States in Dimerized Quasicrystal Lattices with Broken Inversion Symmetry

Matheus I. N. Rosa[1] , Danilo Beli[2], Luca Lomazzi[3], Carlos M. Junior[2], Massimo Ruzzene[1]

[1] Department of Mechanical Engineering, University of Colorado Boulder, 1111 Engineering Dr., USA, Matheus.rosa@colorado.edu, Massimo.ruzzene@colorado.edu
[2] Department of Aeronautical Engineering, University of Sao Paulo, Avenida Joao Danone 1100, Brazil beli.danilo@gmail.com, demarqui@sc.usp.br
[3] Department of Mechanical Engineering, Politecnico di Milano, Via La Masa 1, Italy Luca.lomazzi@polimi.it

Abstract: In this talk we investigate the existence of interface states induced by broken inversion symmetries in quasicrystal lattices. We consider a lattice of resonators attached to an elastic plate and introduce a mass dimerization to form domain-wall interfaces separating regions of opposite inversion symmetry. The features of the interface states are demonstrated both numerically and experimentally.

The discovery of topological insulators has inspired the development of topological states in classical wave platforms such as in photonic[1] and acoustic/elastic[2] metamaterials. The examples realized so far illustrate a wealth of strategies for the design of backscattering-free waveguides with a high degree of immunity to defects, a feature deemed promising for technological applications and devices. Typically, these phenomena are unlocked by engineering the band structure of periodic lattices, for example by nucleating degeneracies and opening band gaps through the careful manipulation and selective breaking of their symmetries. A well-known example is the group of analogues to the Valley-Hall effect (VHE)[3], which allows for topological states to be exploited in passive systems by simple procedures cantered at breaking real-space inversion symmetries.

We here investigate the existence of valley-like interface states in quasicrystal (QC) lattices. While they lack translational periodicity, QCs have long-range order and form a particularly interesting class of aperiodic lattices since they may exhibit symmetries which are forbidden in periodic crystals, such as 5, 7, 8 and 10-fold rotational symmetries. The interplay between their unique symmetries and the concepts of topological physics is a subject of ongoing investigations[4], with limited progress achieved in the context of passive systems that preserve time reversal symmetry. Inspired by the VHE, which has so far been limited to periodic lattices, we here propose a framework to achieve interface states by breaking the inversion symmetry of QC lattices.

We introduce a QC lattice with 10-fold rotational symmetry (C_{10}) whose broken inversion symmetry is achieved through a dimerization that produces two 5-fold symmetric (C_5) sub-lattices, depicted as blue and red points in Fig. 1a. The color of the points may represent a property such as mass, leading to a convenient dimerization where red and blue masses are respectively parametrized as $m_0(1+\beta)$ and $m_0(1-\beta)$, with m_0 being the baseline mass, and β the dimerization parameter. Notice that the positions of the masses alone define a C_{10} QC lattice, whose symmetry is maintained when $\beta = 0$ and the masses are equal to m_0. However, when $\beta > 0$, a QC with broken inversion symmetry is formed due to the contrast between blue and red masses. The dimerization conveniently allows the creation of domain-wall interfaces by connecting two regions with β values of opposite signs, as illustrated in Fig.1b for the case of a straight interface parallel to the y axis. This parametrization is inspired by similar procedures applied to hexagonal lattices in the context of the VHE, where β is used to break the inversion symmetry of C_6 lattices into C_3, and forms the basis for the creation of symmetry-breaking interfaces.[3]

The talk will describe the key features of interface states in the QC lattices uncovered by our numerical simulations and experimental studies. In particular, we consider a lattice of resonators attached to an

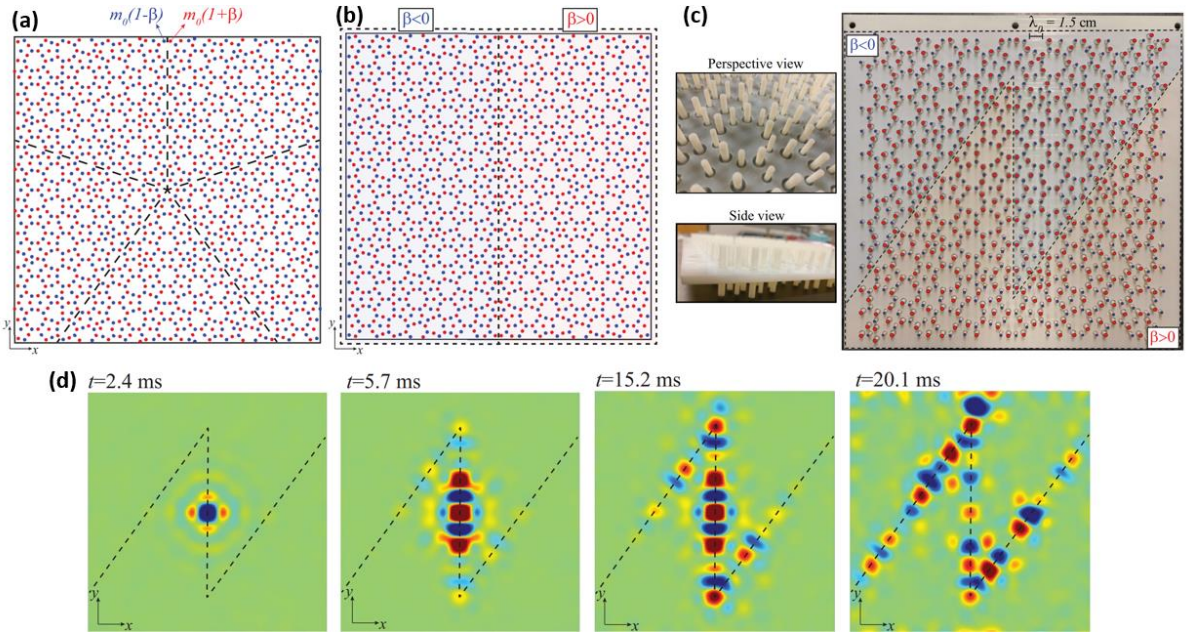

Figure 1 Observation of interface states in dimerized quasicrystal lattices. **(a)** The QC lattice with broken inversion symmetry through a mass dimerization, and **(b)** the creation of a straight interface by contrasting domains with opposite dimerization parameters $\boldsymbol{\beta}$. **(c)** Photographs of plate prototype featuring a QC lattice of membrane-pillar resonators and a zig-zag interface. **(d)** Snapshots of experimentally measured recorded wave-field illustrating the propagation of interface states along the interface.

elastic plate, but our results may be extended to other platforms such as quantum, photonic and acoustic lattices. Our numerical simulations show the emergence of bands of interface states that accompany a band inversion of the quasicrystal spectrum as a function of the dimerization parameter. These bands are filled by modes which are localized along symmetry-breaking interfaces separating domains with opposite dimerization parameters. We exploit these states to numerically and experimentally demonstrate wave-guiding along a zig-zag interface with sharp turns of 36 degrees, which goes beyond the limitation of 60 degrees associated with 6-fold symmetric lattices. Figure 1c shows photographs of our experimental prototype, fabricated through additive manufacturing, which features a QC lattice of membrane-pillar resonators forming a zig-zag interface. The motion of the plate is recorded by a Scanning Laser Doppler Vibrometer (SLDV) as it is excited by a piezoelectric patch attached to its centre. Figure 1d shows subsequent snapshots of the recorded plate motion following from a transient wave packet, illustrating wave propagation along the interface with no noticeable backscattering at the sharp turns.

Our results suggest that an analogue to the VHE may also exist in quasicrystals, providing new opportunities for symmetry-based quasicrystalline topological waveguides that don't require time-reversal symmetry breaking, and that allow for higher freedom in the design of their waveguiding path by leveraging higher-order rotational symmetries.

References

[1] L. Lu, J. D. Joannopoulos, and M. Soljacic, *Nature Photonics*. **8**, 821-829 (2014).
[2] G. Ma, M. Xiao, and C. T. Chan. *Nature Reviews Physics*. **1**, 281–294, (2019).
[3] R. K. Pal and M. Ruzzene, *New Journal of Physics*. **19**, 025001, (2017).
[4] J. Fan and H. Huang, *Frontiers of Physics*.**17**, 13203, (2022).

PHONONICS 2023: 6th International Conference on Phononic Crystals/Metamaterials/Metasurfaces, Phonon Transport, and Topological Phononics
Manchester, England, June 12-16, 2023
PHONONICS-2023-0114

Analytical Solutions for Bloch Waves and Topological Mode Steering in a Meta-Plate

R. Wiltshaw[1*], J. M. De Ponti[2], R. V. Craster[1]

[1] *Department of Mathematics, Imperial College London, London, SW7 2AZ, United Kingdom,*
[2] *Department of Civil and Environmental Engineering, Politecnico di Milanos Piazza Leonardo da Vinci, 32, 20133 Milano, Italy*
[*] *(r.wiltshaw17@imperial.ac.uk)*

Abstract: We discuss our recently[1] proposed analytical solutions for a thin elastic plate patterned with arrays of Euler-Bernoulli beams. The beams are approximated by monopole and dipole point source terms applied to the neutral plane of the plate. We consider eigensolutions for Floquet-Bloch wave propagation, and apply Foldy's method to consider scattering from finite arrays - both of which involve singular Green's functions. The methods will be demonstrated by designing deep-subwavelength topologically protected states arising from gapped symmetry induced degeneracies.

Metamaterial concepts provide an incredibly popular design paradigm for researchers in all fields of wave physics. These concepts, introduced in photonics, have proved very general and spawned mass interest within acoustics, seismology and elastic settings, to manipulate the propagation of waves over subwavelength scales. Within these fields, topological designs - originating from quantum mechanics - are widely used to create robust effects, e.g. achieving topological mode steering or energy splitting[2].

We consider doubly periodic arrays of elastic beams attached to the surface of an elastic plate, as shown in fig. 1. The arrays are defined by the lattice vectors $\boldsymbol{\alpha}_1$ and $\boldsymbol{\alpha}_2$ in physical space. We utilise: Floquet-Bloch theory to derive eigensolutions for arrays of infinite extent to determine dispersion or eigenmodes, and generalised Foldy's method[3] to consider scattering from finite arrays. The beams are approximated as regular and singular perturbations to the neutral plane of the elastic plate. We show how to exploit the flexural resonances of the beams to create deep-subwavelength Dirac cones.

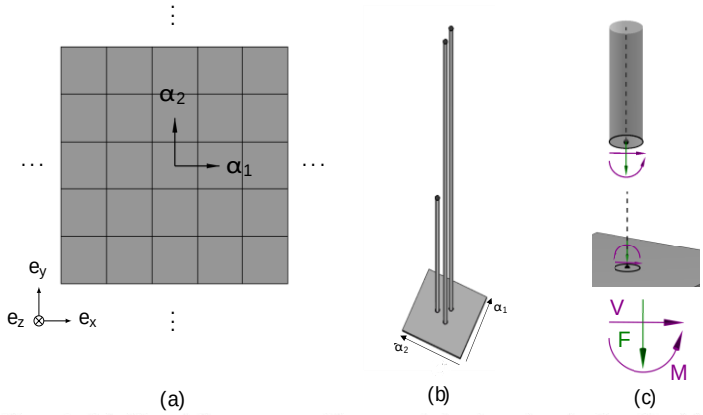

Figure 1: A doubly periodic arrangement of beams attached to the surface of a plate. Here (*a*) shows the plate in physical space, where the coordinate system is chosen such that the neutral plane of the plate is spanned by $\mathbf{e}_x$ and $\mathbf{e}_y$ Cartesian basis vectors with $\mathbf{e}_z$ out of the plane. The phononic crystal is formed by tessellating the fundamental cell by the primitive lattice vectors $\boldsymbol{\alpha}_1$ and $\boldsymbol{\alpha}_2$. In (*b*) we show an example arrangement of $P = 3$ beams per cell. Panel (*c*) shows the point forces and moments arising from the compressional ($\mathbf{F}$) and shear ($\mathbf{V}$) forces, and moments ($\mathbf{M}$) within a beam interacting with the plate.

The plate is modelled using Kirchhoff–Love thin plate theory, and the beams using Euler–Bernoulli beam theory. The beams can be replaced by point forces and moments, as such we consider the following expression governing the displacement field of the plate.

$$\left[\nabla^4 - \Omega^2\right]\mathbf{w} = \frac{1}{D}\sum_{I=1}^{N}\sum_{J=1}^{P} L\mathbf{F}_{IJ}\delta(\mathbf{x}-\mathbf{X}_{IJ}) - \mathbf{M}_{IJ}\times\nabla\delta(\mathbf{x}-\mathbf{X}_{IJ}), \tag{1}$$

We respectively denote I and J as the Ith cell and Jth beam within said cell, and denote quantities belonging to the IJth beam by subscripts. In equation (1), $\mathbf{w} = w\,\mathbf{e}_z$ describes the flexural displacement field of the plate, $\mathbf{x} = x\mathbf{e}_x + y\mathbf{e}_y$ denotes the in-plane position vector, Ω denotes the dimensionless frequency parameter, and δ denotes the Dirac delta function. $\mathbf{F}_{IJ}$ and $\mathbf{M}_{IJ}$ denote the compressional force and flexural moment arising from the IJth beam applied to the surface of the plate.

$$\mathbf{F}(\Omega) = -\hat{S}\hat{E}\frac{\partial\hat{\mathbf{w}}}{\partial z}\Big|_{z=\frac{\hbar}{2L}} = \hat{S}\hat{E}\hat{\alpha}\Omega\tan(\hat{\alpha}\Omega\hat{\ell})\mathbf{w}(\mathbf{X}), \tag{2}$$

$$\mathbf{M}(\Omega) = \frac{\hat{E}\hat{I}}{L}\frac{\partial}{\partial z}\left[\nabla\times\hat{\mathbf{u}}\right]\Big|_{z=\frac{\hbar}{2L}} = \\ = \frac{\hat{E}\hat{I}}{L}\frac{\hat{\beta}\sqrt{\Omega}\left[\nabla\times\mathbf{w}\right]\Big|_{\mathbf{x}=\mathbf{X}}\left\{\frac{\hbar}{2L}\hat{\beta}\sqrt{\Omega}\sin\hat{\beta}\sqrt{\Omega}\hat{\ell}\tanh\hat{\beta}\sqrt{\Omega}\hat{\ell} + 2\left(\sin\hat{\beta}\sqrt{\Omega}\hat{\ell} - \cos\hat{\beta}\sqrt{\Omega}\hat{\ell}\tanh\hat{\beta}\sqrt{\Omega}\hat{\ell}\right)\right\}}{\cos\hat{\beta}\sqrt{\Omega}\hat{\ell} + \operatorname{sech}\hat{\beta}\sqrt{\Omega}\hat{\ell}}. \tag{3}$$

Here $\mathbf{F}_{IJ}$ and $\mathbf{M}_{IJ}$ are deduced such that continuity of displacements, rotations, forces and moments occur where the beams meet the plate,

and we apply free end conditions at the free end of the beams. As such, one finds[1] equations (2) and (3), where $\hat{\mathbf{w}} = \hat{w}\,\mathbf{e}_z$ and $\hat{u} = \hat{u}_x\,\mathbf{e}_x + \hat{u}_y\,\mathbf{e}_y$ respectively describe the out-of-plane and in-plane displacement fields of the beams. Other parameters denote quantities belonging to the plate or the beams - see[1] for all details.

When seeking eigensolutions for doubly periodic infinite arrays, one can apply Floquet-Bloch theory and seek solutions in the form of a Fourier series expansion

$$w = W(\mathbf{x})\exp(i\boldsymbol{\kappa}\cdot\mathbf{x}), \quad \text{where} \quad W(\mathbf{x}) = W(\mathbf{x}+\boldsymbol{\alpha}_1+\boldsymbol{\alpha}_2) = \sum_{\mathbf{G}} W_{\mathbf{G}}\exp(i\mathbf{G}\cdot\mathbf{x}) \qquad (4)$$

Here W(**x**) denotes a periodic function, whose fundamental period coincides with that of the array, and **κ** denotes the Bloch wavevector. Also, $W_{\mathbf{G}}$ denotes the Fourier coefficients of the expanded variable, and the summation is over the reciprocal lattice vector **G**. For finite arrays, one can utilize the Fourier transform to deduce the following Green's function appropriate for the IJth beam (summed over to consider the array)

$$w = \frac{L}{D}\mathbf{F}_{IJ}(\Omega)\cdot\mathbf{e}_z\left[H_0(r_{IJ}\sqrt{\Omega}) - H_0(ir_{IJ}\sqrt{\Omega})\right]\frac{i}{8\Omega} - \frac{\mathbf{e}_{\theta\,IJ}\cdot\mathbf{M}_{IJ}(\Omega)}{8D\sqrt{\Omega}}\left[iH_1(r_{IJ}\sqrt{\Omega}) + H_1(ir_{IJ}\sqrt{\Omega})\right]. \qquad (5)$$

Here H_n denotes the Hankel function of the first kind and nth order and $r_{IJ}=|\mathbf{x}-\mathbf{X}_{IJ}|$. Both expressions (4) and (5) contain logarithmic singularities when considering the gradient of w in the limit as $r_{IJ} \to 0$. The analytical nuances required to deal with the singular Green's functions are given in[1].

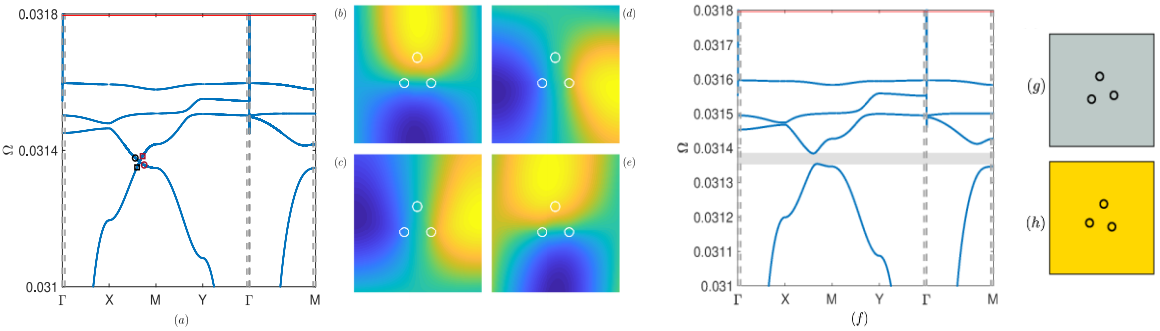

Figure 2: The Dirac point, in panel (a), observed by zooming in about the first flexural resonance found in the arrangement in fig. 1 (b), where the plate thickness is $h = 0.05$ m and the material parameters for aluminium were used. The dimensionless parameters (scaled with L) are $\boldsymbol{\alpha}_1 = \mathbf{e}_x$, $\boldsymbol{\alpha}_2 = \mathbf{e}_y$, $\mathbf{X}_{1J} = 0.125\left[\cos(\frac{2\pi(J-1)}{3}+\frac{\pi}{2})\mathbf{e}_x + \sin(\frac{2\pi(J-1)}{3}+\frac{\pi}{2})\mathbf{e}_y\right]$, $\epsilon_{1J} = 0.035$, for $J = 1,2,3$ and the beam heights were $\hat{\ell}_{11} = 4.50$, $\hat{\ell}_{12} = \hat{\ell}_{13} = 11.25$. Panels (b), (c), (d) and (e) show the eigenmodes at the respective points ○, □, □ and ○ from the bands in panel (a). Panel (f) shows the Floquet-Bloch dispersion branches of the primitive cell in (g). Cells (g) & (h) are obtained by perturbing the arrangement in fig.1(b) via rotations, setting $\mathbf{X}_{1J} = 0.125\left[\cos(\frac{2\pi(J-1)}{3}+\frac{\pi}{2}+\theta')\mathbf{e}_x + \sin(\frac{2\pi(J-1)}{3}+\frac{\pi}{2}+\theta')\mathbf{e}_y\right]$, the grey (g) and yellow (h) cells respectively correspond to positive and negative rotations in which $\theta' = \pm\frac{\pi}{20}$. The topological band gap is shaded in grey in (f).

Fig. 2 shows our eigensolutions from[1], they demonstrate how a symmetry protected accidental degeneracy is formed when considering a square cell with a sole vertical spatial symmetry. Breaking the vertical symmetry gaps the degeneracy and produces a topologically non-trival bandgap in which we expect topologically protected states to exist.

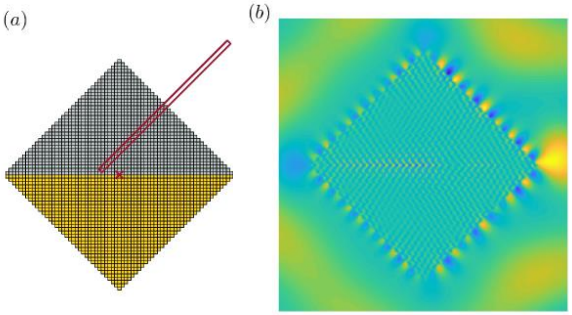

Figure 3: Generalised Foldy simulation (b) for the phononic crystal designs shown in the schematics of panel (a); here (a) is formed from 2450 cells, half grey and half yellow cells from fig. 2 (g) & (h), for a total of 7350 beams atop an elastic plate of infinite expanse. The incident sources, in (b), both consider monopoles placed at $\mathbf{x} = \mathbf{X}_{\text{inc}}$ marked by × in (a). The frequencies of the point-sources lie within the topological band gap of 2 (f), and consider $\Omega = 0.0313695$ for (b).

Fig 3. shows a scattering simulation from[1], in which we excite the quantum valley Hall modes known as zero line modes at the interface between the yellow and grey cells. The topological states between the phononic crystal and the free space are produced in accordance with the bulk-edge correspondence. These topologically protected modes are robust, and occur at the deep-subwavelength scattering regime. As such we demonstrate very low-frequency long-wave manipulation utilising our subwavelength structured designs; these concepts are very general, and show promise in aiding the design of robust devices to protect against or harvest energy from very long-wave disturbances.

References

[1] Wiltshaw R., De Ponti J. M., & Craster, R. V. *Analytical solutions for Bloch waves in resonant phononic crystals: Deep subwavelength energy splitting and mode steering between topologically protected interfacial and edge states*. arXiv **preprint arXiv:2207.13118**. (2022).
[2] Ozawa T., Price H. M., Amo A., Goldman N., Hafezi M., Lu L., Rechtsman M. C., Schuster D., Simon J., Zilberberg O., & Carusotto, l. *Topological photonics*. **Reviews of Modern Physics, 91(1), 015006**. (2019)
[3] Martin, P. A. *Multiple scattering: interaction of time-harmonic waves with N obstacles* **(No. 107). Cambridge University Press.** (2006)

PHONONICS 2023: 6th International Conference on Phononic Crystals/Metamaterials/Metasurfaces, Phonon Transport, and Topological Phononics
Manchester, England, June 12-16, 2023
PHONONICS-2023-0019

A Topological Phononic Waveguide Above 10 GHz

Omar Florez[1], Martin Poblet[1], Sara Pourjamal[2], Jouni Ahopelto[2] and Clivia M. Sotomayor-Torres[1,3]

[1]Catalan Institute of Nanoscience and Nanotechnology (ICN2), Campus UAB, 08193 Bellaterra, Spain,
[2] VTT Technical Research Centre of Finland Ltd., P.O. Box 1000, Espoo, VTT FI-02044, Finland
[3]Institució Catalana de Recerca i Estudis Avançats, 08010 Barcelona, Spain
omar.florez@icn2.cat

Abstract: We present the design of a topological phononic waveguide suitable for fabrication in silicon-on-insulator. The waveguide is simulated and found to exhibit an isolated topological mode at 13.5 GHz inside a gap of 1 GHz. The samples have been recently fabricated and their characterization by Brillouin light scattering (BLS) spectroscopy are in progress.

Hexagonal two-dimensional crystals, such as graphene, exhibit a pair of degenerate states at the *K* and *K*' valleys in reciprocal space [1]. In the solid state, the valley electrons have non-trivial Berry curvatures which results in anomalous quantum Hall states in graphene [2]. The same analogy can be applied to mechanical waves to obtain protected transport of phonons at kHz [3], MHz [4] and GHz [5] frequencies. Such two-dimensional chiral states are topologically protected as long as there is no inter-valley scattering generated by geometrical defects. In figure 1(a) top, the unit cell of the Valley-Hall phononic crystal with periodic distance *a* is shown. It is composed of two rounded and inverted triangles connected by three equally spaced bars. The crystal is designed for fabrication in silicon-on-insulator (SOI) wafers of 220 nm thickness and with a periodic distance *a* of the crystal of 381 nm. Figure 1(a) bottom shows the dispersion relation calculated along the entire first Brillouin zone for the two phononic bands that shows Dirac points in each vertex of the reciprocal space. The frequency of this Dirac point is approximately 13.5 GHz.

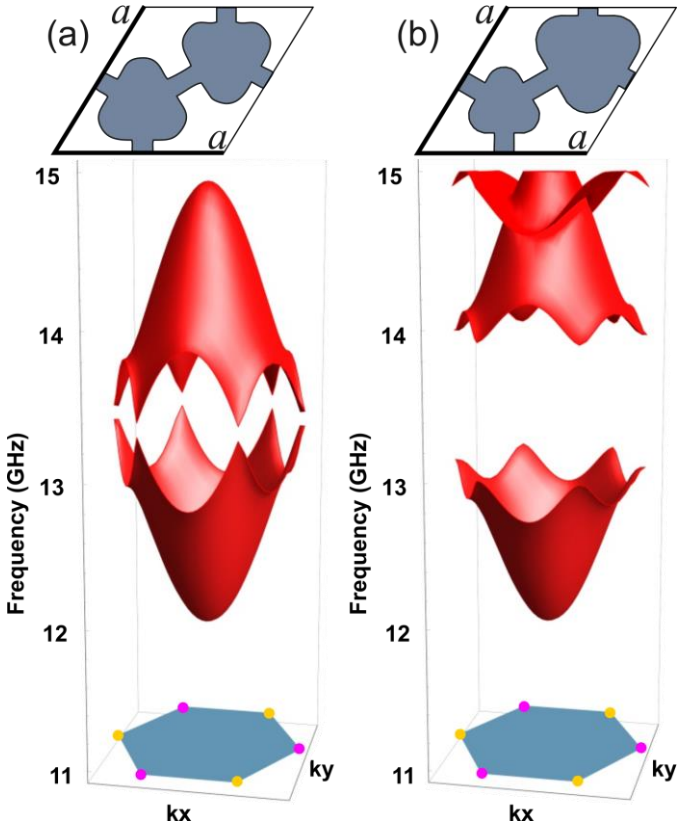

Figure 1. Topological phononic crystal. (a) Unit cell and phononic dispersion relation for the designed Valley-Hall Phononic crystal. The two phononic bands considered possess Dirac cones at the edges of the first Brillouin zone. By perturbing the unit cell design as shown in **(b)**, it is possible to create a 1 GHz gap centred at 13.5 GHz that allows the further design of topological waveguides.

A phononic gap at the Dirac point can be opened by perturbing the mass distribution of the original arrangement. In this case, modifying the size of the triangles composing the unit cell, so that one of them becomes larger and the other becomes smaller results in the opening of a gap spanning from 13 to 14 GHz as shown in Figure 1(b). Once the degeneracy in the Dirac points is lifted, it is possible to create topological waveguides by breaking the crystal symmetry, as shown in Figure 2(a). Flipping the unit cell to form two different crystals and joining them, a topological interface can be created as highlighted by the dashed line in Figure 2(a).

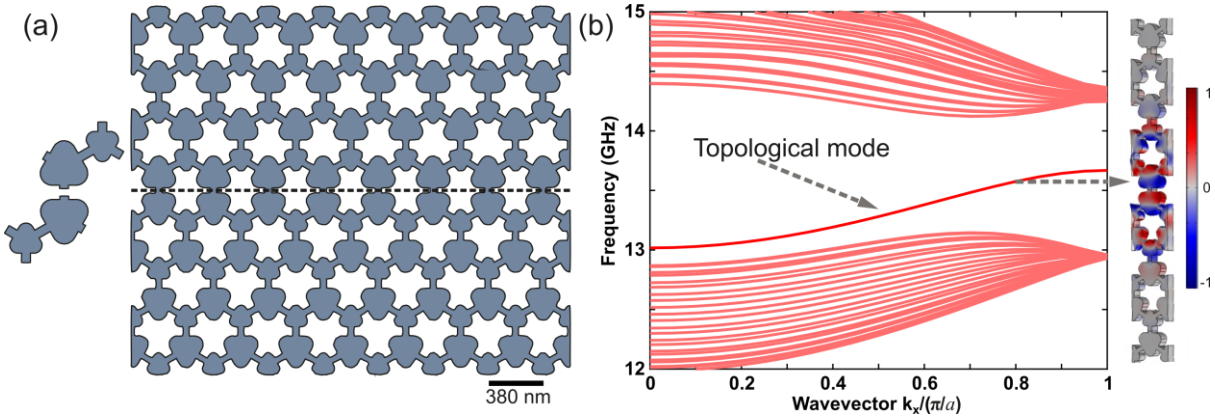

Figure 2. Topological waveguide. (a) Topological interface delimited by the union of the designed phonon crystal and its mirror image. **(b)** Phononic dispersion relation for the topological waveguide. An isolated mode inside the gap going from 13 GHz for $k_x=0$ to 13.7 GHz for $k_x=\pi/a$ is formed. The inset shows the mode profile of the topological mode, and the color bar indicates the out-of-plane displacement.

Figure 2(b) shows the simulated phononic dispersion relation for the geometry presented in figure 2(a). The considered material is the [110] crystalline silicon used in SOI wafers. There is an isolated mode inside the gap going from 13 GHz for $k_x = 0$, to 13.7 GHz for $k_x = \pi/a$. The inset on the right shows the mode profile of the topological guided mode for $k_x/(\pi/a) = 0.8$ and the color bar indicates the normalized out-of-plane displacement. This displacement is fully localized at the topological interface. Samples have been recently fabricated in SOI wafers and Brillouin light scattering experiments [6] are in progress.

References

[1] L. Ju et al, *Nature* **520**, 650-655 (2015).
[2] F. D. M. Haldane, and S. Raghu, *Phys. rev. Lett.* **100**, 013904 (2008).
[3] C. He et al, *Nat. Phys.* **12**, 1124-1129 (2016).
[4] J. Lu et al, *Nat. Phys.* **13**, 369-374 (2017).
[5] Q. Zhang et al, *Nat. Electron.* **5**, 157-163 (2022).
[6] O. Florez et al, *Nat. Nanotechnol.* **17**, 947-951 (2022).

PHONONICS 2023: 6th International Conference on Phononic Crystals/Metamaterials/Metasurfaces, Phonon Transport, and Topological Phononics
Manchester, England, June 12-16, 2023
PHONONICS-2023-0025

Control of Ultrahigh Frequency Phonon Transport in Valley Topological Ring Resonator-Waveguide Systems

D. Hatanaka[1], H. Takeshita[2], M. Kataoka[2], M. Misaawa[2], H. Okamoto[1], H. Yamaguchi[1], and K. Tsuruta[2]

[1] NTT Basic Research Laboratories, NTT Corporation, Atsugi-shi Kanagawa, Japan, daiki.hatanaka@ntt.com, hajime.okamoto.sd@hco.ntt.co.jp, hiroshi.yamaguchi.zc@hco.ntt.co.jp
[2] Department of Electrical and Electric Engineering, Okayama University, Okayama-shi Okayama, Japan pwto8ywj@s.okayama-u.ac.jp, pqf75c64@s.okayama-u.ac.jp, misawa@okayama-u.ac.jp, tsuruta@ec.okayama-u.ac.jp

Abstract: We develop ring resonator-waveguide coupled systems in a valley topological phononic crystal and demonstrate spatial control of ultrahigh frequency phonon transport. The valley pseudospin locked elastic waves are routed, filtered, and trapped in/through the ring resonator. The results reveal the capability of topological phononics technology in integrated phononic circuity for microwave signal processing application.

Acoustic phonons at microwave frequencies have attracted much attention as an alternative information carrier for signal processing in classical and even quantum regimes. This is because their fundamental properties such as short wavelength and low loss structure are appropriate for compact and energy efficient processing[1]. A key component to realize wave-based integrated circuits is a ring resonator-waveguide coupled system, which provides various functions such as filtering, trapping, and multiplexing of specific signals[2]. However, integration of the ring structure into such a tiny chip-scale system is difficult because circulating elastic waves in it easily lose the energy and are unintentionally localized due to significant back-scattering to surface imperfection and geometric variation. This has hindered flexible wave manipulation in the microwave phononic systems and circuits.

Topological phononics offers possible solution to this difficulty. Nontrivial bulk topology guarantees existence of a gapless edge state, where elastic waves are topologically protected and back-scattering immunity[3,4]. Despite the prospect, there have been a few reports on such ultrahigh frequency topological phononic systems[3,4]. Moreover, they focused on fundamental study of the topological phenomena on a simple phononic waveguide. Therefore, the capability of the topological technology in microwave phononics, where the coupling with the ring resonator plays the essential role, remains unexplored.

We fabricate a ring resonator-waveguide coupled system based on valley topological phononic crystals (PnCs) at microwave frequencies (Fig. a). The device is comprised from 1-μm GaAs free-standing membrane where a three-rotational symmetry hole cluster is arrayed with a periodic distance of $a =$ 3.65 μm to form triangular lattice. Its graphene-like phononic band dispersion has a Dirac degeneracy ($\theta = 0°$) at K/K' valleys and around 0.5 GHz. The Dirac point is degenerated by rotating each cluster by $\theta = 5°$ or $-5°$, giving rise to a bandgap due to breaking of inversion symmetry. The PnC hosts different valley Hall phase depending on the polarity of θ. Therefore, a gapless edge state can be formed in interface between the different valley PnCs (Fig. b), efficiently guiding elastic waves in the edge without significant reflection from arbitrary bends and structural disorders.

Figures c show real-space imaging of elastic wave propagations in ring resonator-waveguide systems with various separations ($d = c, 2c, 4c$ with $c = \sqrt{3}a/2$). The ring resonator is constructed by hexagonal edge channel loop and its radius is nearly $R = 2.5\lambda$ (SAW wavelength $\lambda = 5.7\sim5.9$ μm) which is much smaller than previous phononic ring resonators with a radius of a dozens of the wavelength[2]. When the separation is small ($d = c$), two structures are over-coupled where the energy transferring from the waveguide to the ring is dominant. The elastic waves at 0.504 GHz in the waveguide are routed to the ring, showing counterintuitive Ω-shaped profile. This clearly shows generation of valley pseudospin-locked transport (left panel). The phonon transport dynamics is largely changed when $d = 2c$. The decreased coupling strength is nearly satisfied with critical coupling condition, so elastic waves in and out of the ring are destructively interfered. Therefore, transferred elastic waves circulate in the ring but

the output of the waveguide disappears (middle panel), realizing a phonon wave filter. Further increasing separation makes these two structures weakly coupled ($d = 4c$). Partial vibrations are trapped and circulate in the ring resonator (right panel). Its quality factor is experimentally obtained as $Q = 1{,}700$ that is comparable with a line-defect PnC cavity whose Q-factor is limited by the intrinsic material loss[5]. This might indicate that back-scattering in the ring is relatively suppressed.

Our demonstrations firstly unveil the capability of the topological phononics technology for on-chip manipulations of ultrahigh frequency phonons. The robust transport property realizes efficient elastic wave circulation in the ring having a large curvature without significant back scattering. This topological ring resonator can be used as filtering and trapping of the elastic transmission. Thus, the topological PnC is a promising platform to design and construct integrated phononic circuits.

This work was supported by JSPS KAKENHI(S) Grant Number JP21H05020

References

[1] M .J. Schuetz, *et al.*, *Phys. Rev. X*, **5**, 031031 (2015).
[2] W. Fu *et al.*, *Nature Commun.* **10**, 2743 (2019).
[3] Q. Zhang *et al.*, *Nature Electron.* **5**, 157-163 (2022).
[4] Y. Nii and Y. Onose, *Phys. Rev. Appl.* **19**, 014001 (2022).
[5] D. Hatanaka and H. Yamaguchi, *Phys. Rev. Appl.* **13**, 024005 (2020).

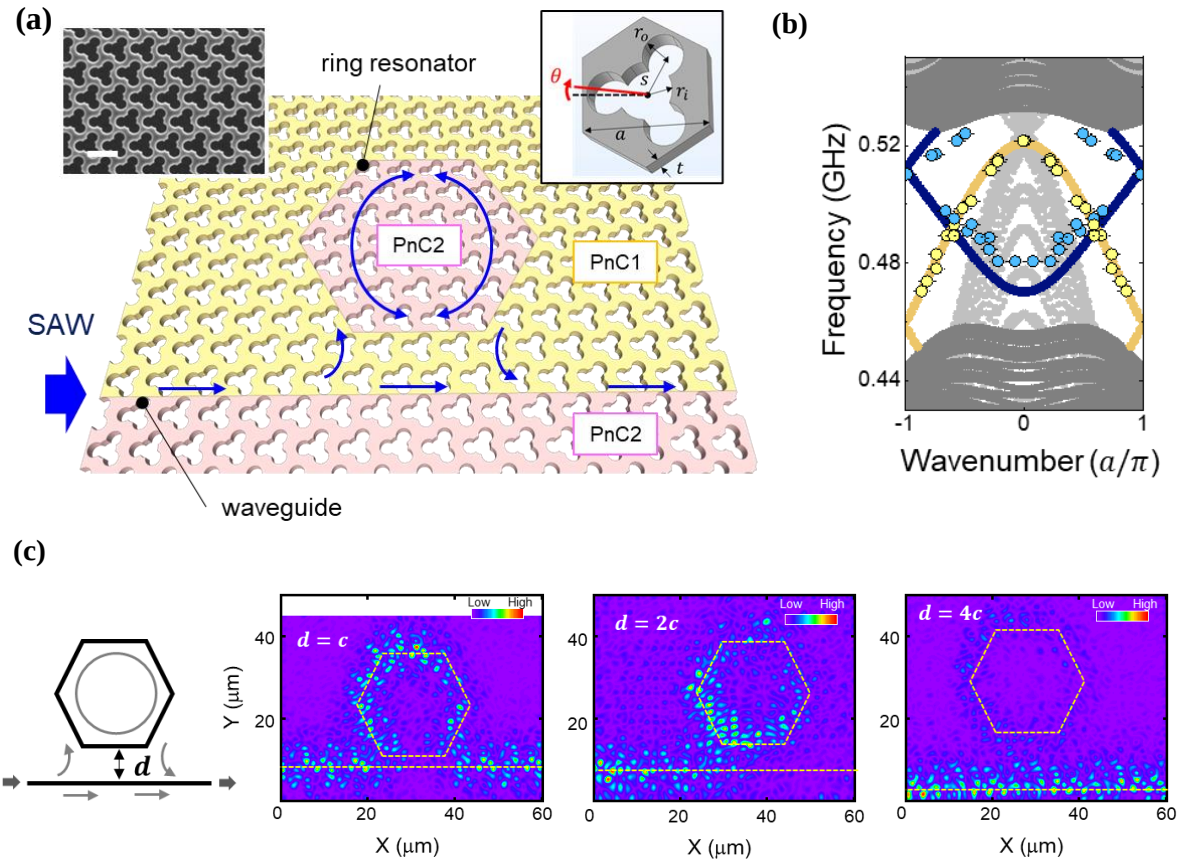

Figure (a) Schematic of a valley topological ring resonator-waveguide system. This is driven by injecting surface acoustic waves (SAWs) into the edge waveguide and the resultant vibrations are measured by an optical interferometer. The left unit shows an SEM image of the valley PnC. The white bar denotes 4 μm. The right inset shows the unit cell $a = 3.65\ \boldsymbol{\mu m}, r_i = 0.90\ \boldsymbol{\mu m}, r_o = 0.72$ μm, $s = 1.10$ μm, and $t = 1.00$ μm. PnC1 and PnC2 are realized by $\theta = 5°$ and $-5°$, respectively. **(b)** Dispersion relation of the interface of PnC1/PnC2 and PnC2/PnC1, where edge states are generated in the bandgap. The filled circles and solid lines are experimental and calculation results respectively. (c) Spatial profiles of elastic wave amplitude at 0.504, 0.495, and 0.518 GHz in the coupled systems with $d = c, 2c$, and $4c$, respectively. The left inset shows illustration of the ring resonator-waveguide system.

PHONONICS 2023: 6th International Conference on Phononic Crystals/Metamaterials/Metasurfaces, Phonon Transport, and Topological Phononics
Manchester, England, June 12-16, 2023
PHONONICS-2023-0123

Experiments in an exact acoustic analogue of the Hatano-Nelson model

A. Maddi[1] , V. Achilleos[1] , G. Penelet[1],V. Pagneux[1], Y. Aurégan [1]

[1] Laboratoire d'Acoustique de l'Université du Mans (LAUM), UMR 6613, Institut d'Acoustique - Graduate School (IA-GS), CNRS, Le Mans Université, France
Achilleos.Vassos@univ-lemans.fr

Abstract: In this work, using active acoustic elements we design an exact analogue of the nonreciprocal Hatano-Nelson, applying a simple transfer matrix formulation. Beyond the skin effect which we measure, due to the systems losses, we experimentally probe the transition from a line segment spectrum a loop shaped spectrum in the complex plane, avoiding instabilities. The sensitivity of the boundaries is also measured.

In recent years, the interest in the fascinating features of non-Hermitian models has increased extensively. Initially the interest was focused on the study of non-conservative systems, characterized by complex eigenenergies, that reflect the presence of gains/losses, and find applications in a plethora of fields. In the even more recent literature, there has been a surge of interest in the interplay of non-Hermiticity and topological phenomena given their promise for the unidirectional control of waves, and the development of enhanced sensors[1]. In this perspective, the topological phase of matter explores the relationship between the bulk properties of a lattice and its behavior at the boundary, using the so called topological invariants. This has led to the discovery of new non-Hermitian properties in nonreciprocal systems, such as the skin effect, occurring when transitioning from periodic boundary conditions (PBC) to open boundary conditions (OBC) localizing the systems modes at one boundary. This effect has been demonstrated both theoretically and experimentally in various physical systems, such as electronic, optic, acoustic[3,4,5,6,7].

The Hatano-Nelson (HN) model is one of the most prominent models in the field of non-Hermitian and nonreciprocal topology. This model describes a one-dimensional lattice where each site is coupled by a pair of asymmetric (nonreciprocal) hopping (see Fig. 1 (b)). It is the prototypical lattice to show the transition from a complex closed loop spectrum for PBC to a line segment spectrum for OBC. Since the breaking of reciprocity is a prerequisite in the HN, its experimental realization using waves and the ability to explore all its regimes is rather challenging, as it typically requires an external energy source that can lead to instabilities.

In this study, we propose an exact and broadband mapping of the HN model in a periodic acoustic waveguide which captures all of the associated phenomena. Our theoretical approach relies on a simple condition which is to achieve a unit cell with a transfer matrix M having a determinant $det(M) \neq 1$. In practice, we achieve that using a series of loudspeakers with a feedback loop[8]. By using only this assumption, the acoustic velocity at each unit-cell of the waveguide is described by the following equation

$$u_{n+1} + t\, u_{n-1} = E u_n \quad (1),$$

where $t = det(M)$ and $E = Tr(M)$ as schematically shown in see Fig. 1. In practice the eigenvalues $E = E(k)$, where $k = \omega/c_0$ with c_0 is the sound velocity and k the wavenumber, provide a mapping of the HN model eigenvalues to the acoustic eigenfrequencies. Owing to this mapping and the intrinsic losses of the acoustic system we are able to probe the complex closed loop spectrum of the HN model in a system with stable modes.

We perform experiments using a waveguide with closed walls which corresponds to the OBC, and observe the skin modes localized at one edge of the system [see Fig 2 (a)]. Furthermore, we build a ring waveguide and observe the closed curve complex spectrum corresponding to the PBC [see Fig 2 (b)].

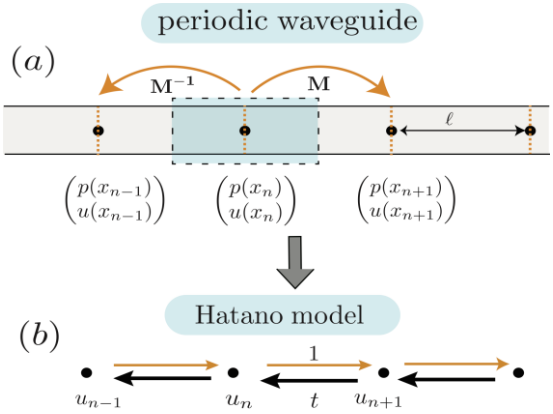

Figure 1 (a) Schematic of the acoustic waveguide and the transfer matrix action between consecutive cells. **(b)** The corresponding Hatano-Nelson model where the value of the acoustic velocity is retrieved at each unit cell and t=det(M).

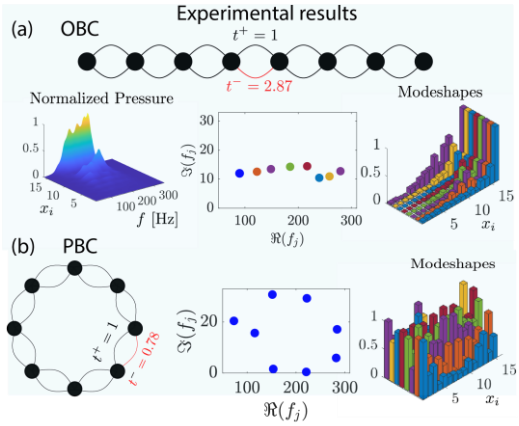

Figure 2: Experimental results for bot the OBC configuration and the PBC. **(a)** Left panel shows the measured acoustic pressure field with ht=2.87 as a function of frequency and space indicating the skin effect. Middle panel shows the obtained frequency of the N=8 modes and right panel shows the reconstruction of the modes. **(b)** Middle panel shows the measured spectrum for the PBC and with t=0.78 and the right panel illustrates the extended modes.

Going a step further, we experimentally probe the transition from PBC to OBC by adding a diaphragm in the looped waveguide and reducing the diaphragm's radius. Our result provides a direct observation of the associated sensitivity of the spectrum where the stable acoustic system corresponding to the OBC can become unstable (with real imaginary frequency) just by opening a tiny hole on the diaphragm inside the waveguide.

References

[1] O. Nobuyuki, and M. Sato, *Annual Review of Condensed Matter Physics* **14** (2022).
[2] A. Yuto, Z. Gong, and M. Ueda, *Advances in Physics* **69** (2020).
[3] L. Zang *et al*, Nat. Comm **12,** 6297 (2021)
[4] R. H Helbig, *et* al. Nat. *Phys.* **16,** 747 (2020).
[5] T. Hofmann, *et* al. PRResearch **2**, 023265 (2020) .
[6] A. Ghatak, *et* al. PNAS **117**, 29561 (2020).
[7] L. Xiao, *et* al. Nat. Phys. **16**, 761 (2020)61 (2020).
[8] G. Penelet, *et* al. Phys. Rev. Applied **16,** 064012 (2022).

PHONONICS 2023: 6th International Conference on Phononic Crystals/Metamaterials/Metasurfaces, Phonon Transport, and Topological Phononics
Manchester, England, June 12-16, 2023
PHONONICS-2023-0080

Imaging a Topological Phononic Crystal in Real and k-Space

Paul H. Otsuka[1], Katsuya Nishimata[1], Motonobu Tomoda[1], Daiki Hatanaka[2], Hiroshi Yamaguchi[2], Kenji Tsuruta[3], Osamu Matsuda[1]

[1] Faculty of Engineering, Hokkaido University, Sapporo 060-8628, Japan
paul@hokudai.eng.ac.jp, nishimata.katsuya.u3@elms.hokudai.ac.jp, omatsuda@eng.hokudai.ac.jp
[2] NTT Basic Research Laboratories, NTT Corporation, Atsugi-shi, Kanagawa 243-0198, Japan
daiki.hatanaka.hz@hco.ntt.co.jp, hiroshi.yamaguchi.zc@hco.ntt.co.jp
[3] Department of Electrical and Electronic Engineering, Okayama University, Okayama 700-8530, Japan
tsuruta@okayama-u.ac.jp

Abstract: We perform numerical simulations and optical measurements of phonon propagation in novel topological phononic crystal structures. We extract mode patterns and **k**-space images at different frequencies, and investigate the dispersion relations and conditions required for waveguiding.

Introduction

Topological insulators are materials that undergo a topological transition in their wavefunction upon some continuous change in their structure. Such materials are insulators in their bulk but can allow topologically protected edge states at interfaces between different topological phases, enabling efficient wave propagation that is highly resistant to imperfections and bending of the interface. Originally demonstrated in electronic materials, topological effects have recently been reproduced in acoustic materials[1].

A topological phase transition can be produced by the breaking of some symmetry in order to open a band gap at the Dirac points. In the acoustic case, producing topological effects is naturally done by adapting phononic crystal designs. Phononic crystals are periodic acoustic structures, which may include defects such as waveguides that can contain wave propagation. It should be relatively straightforward to extend the well-established methods of analysis to topological materials.

Previously we have performed experimental and numerical studies of waveguides formed by defects in phononic crystals based on optical pump-probe methods[2]. Here we perform numerical simulations and optical measurements of phonon propagation in a topological phononic crystal, particularly the guiding of bounded edge states. We analyse the mode patterns and investigate the **k**-space behaviour by Fourier analysis.

Experiment

The sample structure is based on a novel topological phononic crystal design provided by NTT Basic Laboratories. It consists of a hexagonal array of voids in a GaAs slab of 1μm thickness. Each void is composed of a central hole of radius 0.9 μm surrounded by three circular lobes, forming a unit cell with 3-fold symmetry. The unit cell spacing is 3.65 μm. Distinct regions are formed by rotating the individual unit cell orientations in the different regions by ±5° with respect to each other. Such rotation of the unit cell breaks the mirror symmetry of the cell, which has been shown to produce a topological phase transition[3]. We investigated various arrangements with different boundary geometries. Figure 1 (a) shows an example of a structure with three regions, with boundaries forming two linear interfaces that act as guiding paths. The inset shows the structure of the unit cell.

The samples provided for experiments are equipped with interdigital transducers (IDTs) with an accessible frequency range of 465 MHz to 495 MHz. Surface acoustic waves are excited at a single frequency by the IDTs. The resulting surface displacement is probed with periodic pulses from a mode-locked laser and detected by an interferometer. The probe position is scanned in order to produce a

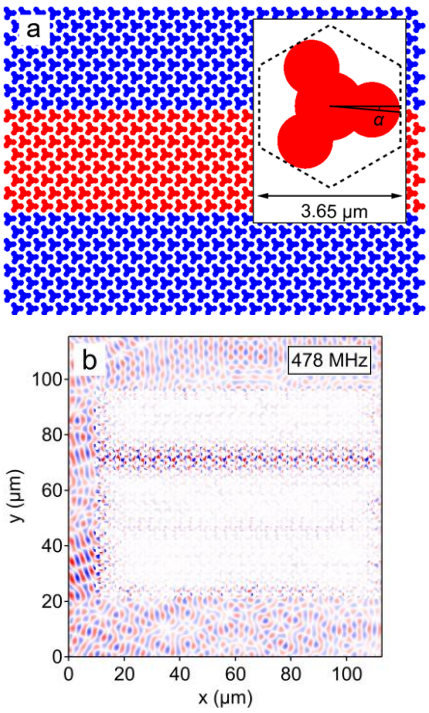

Figure 1 (a) Topological phononic crystal structure consisting of a hexagonal array of lobed holes with 3-fold symmetry. The blue top/bottom ($\alpha = +5°$) and red central ($\alpha = -5°$) regions differ by an in-plane rotation of the unit cell. Inset: geometry of the unit cell. **(b)** Snapshot of the time-domain simulation results at a constant frequency of 478 MHz.

two-dimensional image. Signal detection is assisted by a lock-in amplifier, synchronized with the laser by a heterodyne set-up so that we can extract the amplitude and phase of the surface motion[4].

Numerical model

Phonon propagation in the structures is investigated by numerical time-domain simulations. Surface phonons are excited by a line source placed 20 μm either to the right or to the left of the sample. An implosive force with a half-sine temporal function and a Gaussian spatial distribution produces an excitation with a broadband frequency distribution, simulating an optical laser pulse that would be produced in optical pump-probe experiments. Subsequent processing of the resulting time-domain signal by Fourier analysis provides a filtered representation of the propagation at fixed frequencies, corresponding to the signal that would be produced by the excitation of an IDT at a constant frequency.

Results

The imaging results allow us to follow the wave propagation along a waveguide and observe its ability to turn efficiently around bends. Figure 1 (b) shows an image of a simulation of phonons propagating in the above structure at 478 MHz, with excitation from the left. This frequency lies in the phononic crystal band gap. Phonons do not penetrate inside the material bulk, except for the localized guiding along the top interface. This demonstrates that this boundary is acting as a topological bound state.

Propagation along a particular interface depends not only on the structures of the two phases but also on the geometry of the insertion surface and the angle of the incident wave relative to the bulk. We discuss the conditions required for the excitation and propagation of a particular topological mode.

The frequency-resolved images can be animated by propagating the phase of the data, allowing us to observe the mode patterns. In addition, we take spatial Fourier transforms of the data to reveal the **k**-space behaviour and investigate the dispersion relations. Different regions of the samples are selectively analysed by spatially filtering the images. For example, **k**-space images of the horizontally-propagating sections of a waveguide are compared with angled sections.

Conclusion

By adapting established methods for imaging surface acoustic wave propagation, we performed numerical and experimental measurements of waveguiding in topological phononic crystals on the micrometer scale. The results demonstrated robust propagation in different waveguide configurations and should prove useful in the development of topological phononic crystals for practical devices.

References

[1] Y. Liu, X. Chen, and Y. Xu, *Adv. Funct. Mater*., **30**, 1904784 (2020).
[2] P. H. Otsuka, K. Nanri, O. Matsuda, M. Tomoda, D. M. Profunser, I. A. Veres, S. Danworaphong, A. Khelif, S. Benchabane, V. Laude, and O. B. Wright, *Sci. Rep*. **3**, 3351 (2013).
[3] J. Lu, C. Qiu, L. Ye, X. Fan, M. Ke, F. Zhang, and Z. Liu, *Nature Phys.* **13**, 369-374 (2017).
[4] O. Matsuda, H. Shono, S. Kato, S. Kaneko, S. Mezil, M. Tomoda, O. B. Wright, in Proceedings of the 22nd International Congress on Acoustics, Buenos Aires, Argentina, ICA2016-264 (2016).

PHONONICS 2023: 6th International Conference on Phononic Crystals/Metamaterials/Metasurfaces, Phonon Transport, and Topological Phononics
Manchester, England, June 12-16, 2023
PHONONICS-2023-0205

Non-Hermitian topological disclination defect in a valley-Hall sonic lattice

Julio Andrés Iglesias Martínez[1] , René Pernas[2], Muamer Kadic[1], Johan Christensen[3]

[1] Femto-st Institude, 15B avenue des Montboucons 25030 Besançon, France,
julio.iglesias@femto-st.fr, muamer.kadic@univ-fcomte.fr
[2] Universidad Carlos III de Madrid, Avenida de la Universidad 30 ,28911 Leganés, Madrid, Spain,
rpernas@fis.uc3m.es
[3] IMDEA Materials Institute, Calle Eric Kandel, 2, 28906, Getafe, Madrid, Spain
johan.christensen@imdea.org

In this contribution we focus on topological defects that are local kinks or obstructions in an order parameter field where domain walls, superconductor vortices or dislocations are few of many prominent examples. Topological bound states can form around these defects much in the same way edge and surface states bind to one- and two-dimensional interfaces, respectively. Here we discuss both numerical and experimental advanced in the context of topological acoustics, where a man-made lattice hosting a topological nontrivial phase is realized with added real-space lattice distortion and non-Hermiticity.

PHONONICS 2023: 6th International Conference on Phononic Crystals/Metamaterials/Metasurfaces, Phonon Transport, and Topological Phononics
Manchester, England, June 12-16, 2023
PHONONICS-2023-0085

Experimental study of piezoelectric phononic crystals with space-time modulation in the sub-sonic and sonic regimes

S. Tessier Brothelande[1] , C. Croënne[1], F. Allein[1], J. O. Vasseur[1], B. Dubus[1]

[1] *Univ. Lille, CNRS, Centrale Lille, Univ. Polytechnique Hauts-de-France, Junia, UMR 8520 – IEMN, F-59000 Lille, France, sarah.tessier@cnrs.fr, charles.croenne@isen.fr, florian.allein@junia.com, jerome.vasseur@univ-lille.fr, bertrand.dubus@junia.com*

Abstract: The study focuses on piezoelectric phononic crystals whose electrical boundary conditions are modulated in time through external circuits. We experimentally study wave propagation in a spatio-temporally modulated system for different modulation velocities, up to the sonic regime when modulation and wave velocities are similar.

Spatio-temporal modulation in phononic crystals is known to have some original wave propagation effects, such as non-reciprocity[1-3]. However, experimental implementation of such systems is rare since they require rapid temporal variation of material parameters. A good alternative is to use piezoelectric elements to introduce a spatio-temporal modulation through electrical conditions.

Our study is based on a piezoelectric phononic crystal whose electrical boundary conditions are periodically controlled by external circuits. This modulation can strongly modify phononic crystal dispersion properties. For instance, a periodic grounding of the electrodes reveals a Bragg band gap that does not exist when the electrodes have a floating potential condition[4]. When the electrical conditions of the electrodes are spatio-temporally modulated, nonreciprocal wave propagation may occur at some modulation velocities in specific frequency bands[1]. Since the control of the electrical conditions is made via a micro-processor, it is possible to apply high modulation velocity c_m compared to the velocity of the propagating waves in the crystal c_L, and thus to study the propagation of waves in the subsonic (when $c_m < c_L$) and sonic (when $c_m \approx c_L$) regimes. The sonic regime is of specific interest as the spectral degeneracy of the forward propagating modes is expected to lead to a broadband parametric amplification effect[5]. This regime has been rarely discussed in theoretical papers[6] and, to the best author's knowledge, never experimentally,

The experimental set-up is made up of a stack of piezoelectric rings separated by thin electrodes, as depicted in figure 1. The spatio-temporal modulation is achieved by shifting the position of the periodic grounded conditions of the electrodes versus time. The experimental dispersion curves are obtained using measurements of the normal displacement of the piezoelectric rings with a scanning laser vibrometer on the one hand, and of electrical potential of floating electrodes on the other hand. The change of dispersion curves as a function of modulation velocity, as depicted for example in figure 2, is analysed and compared to finite element simulation results.

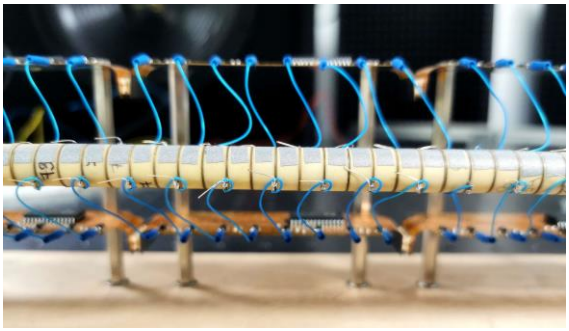

Figure 1 – Stack of piezoelectric rings separated by thin brass electrodes connected to printed circuit boards.

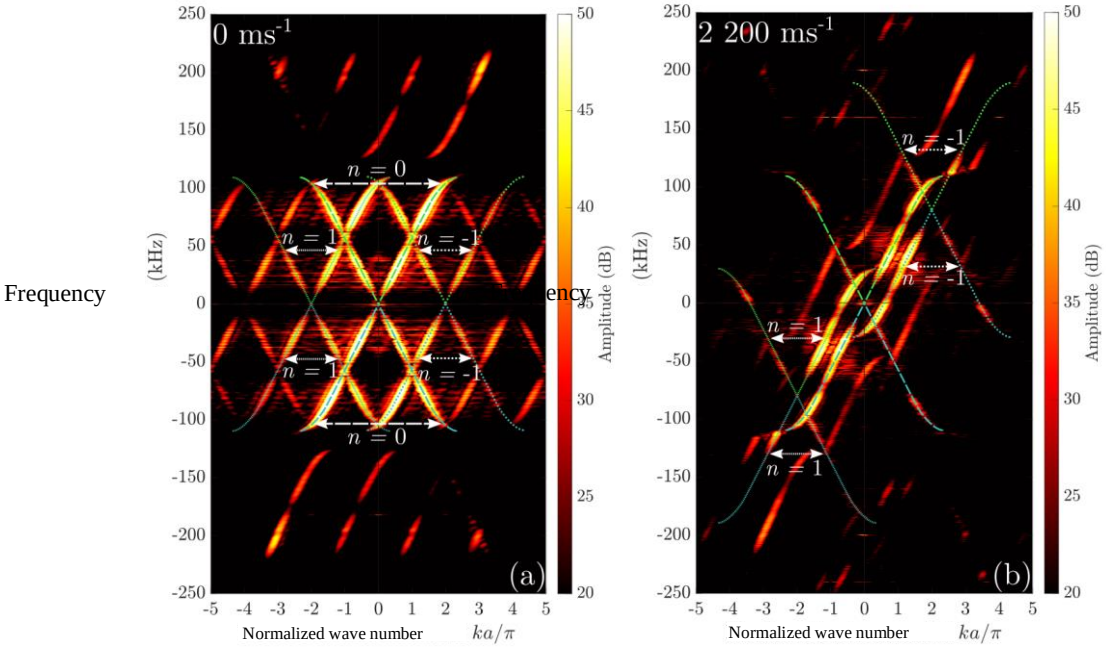

Figure 2 – Band diagrams obtained from experimental measurements for zero modulation velocity (a) and for a modulation velocity of $c_m=0.7c_L$ (b).

References

[1] Croënne et al., Jounal of Applied Physics, vol. 126 no. 14, 2019

[2] Nassar et al., Journal of the Mechanics and Physics of Solids, vol. 101, 2017

[3] Palacios et al., The Journal of the Acoustical Society of America 151, 2022

[4] Degraeve et al, Journal of Applied Physics, vol. 115, 2014

[5] Galiffi et al., Physical Review Letter, vol. 123 no. 20, 2019

[6] Cassedy et Olinar, Proceedings of IEEE, vol. 51 no. 10, 1963

PHONONICS 2023: 6th International Conference on Phononic Crystals/Metamaterials/Metasurfaces, Phonon Transport, and Topological Phononics
Manchester, England, June 12-16, 2023
PHONONICS-2023-0096

Tunable topological edge-modes in photo-responsive periodic structures

G. J. Chaplain[1], A.S. Gliozzi[2], B. Davies[3], D. Urban[4], F. Bosia[2], R.V. Craster[3]

[1]*Electromagnetic and Acoustic Materials Group, Department of Physics and Astronomy, University of Exeter, Exeter EX4 4QL, United Kingdom.*
G.J.Chaplain@exeter.ac.uk
[2] *Department of Applied Science and Technology, Politecnico di Torino, Corso Duca degli Abruzzi 24, Italy*
antonio.gliozzi@polito.it, federico.bosia@polito.it
[3]*Department of Mathematics, Imperial College London, South Kensington Campus, London SW7 2AZ, United Kingdom.*
bryn.davies@imperial.ac.uk , r.craster@imperial.ac.uk
[4]*Department of Electronic Systems, Norwegian University of Science and Technology, Trondheim, Norway.*
david.urban@ntnu.no

Abstract: Dynamic tunability of topological edge modes is achieved by using photo-responsive materials that experience a significant reduction in Young's modulus when illuminated by a laser. Topological edge modes are formed when symmetries are broken in a periodic system that has a topologically non-trivial band gap, creating an interface for waves of specific frequencies. We present a tunability strategy for the eigenfrequency of topological edge modes in a system based on the Su-Schrieffer-Heeger model.

Topological edge modes confine waves at specific frequencies, making them attractive for wave control devices. These modes occur when symmetries are broken in a periodic system, generating an interface for specific frequency waves, so that the waves are unable to propagate away from the interface, giving a strong waveguide. Topological waveguides are thus frequency-specific, so it is essential to design modes with specific eigenfrequencies for practical use, but once fabricated they cannot adapt to other specific frequencies. We propose here a tunability strategy for the eigenfrequency of a topological edge mode in a one-dimensional system using the Su-Schrieffer-Heeger (SSH) model [1]. The SSH model is realized by arranging paired elements with alternating coupling strengths (in our case realized by alternating "long" and "short" separation distances [2]). The unit cell comprises a horizontal elastic beam of thickness $t = 1.5$ *mm*, and width $a = 7$ *mm* and a set of elastic rods, each with a height of *20 mm* and a radius of *0.5 mm*, arranged periodically in a unit cell (see Fig. 1a). These rods are separated by a distance s_i from the center of the unit cell. We create two different kinds of cells depending on the separation distances s_1 and s_2 , respectively, which are related by $s_2 = a - s_1$. The total length of the beam is determined by the number of unit cells used in the arrangement. A periodic array with $s_1 = a/3.9$ is equivalent to one with s_2, due to the non-uniqueness of the unit cell. The unit cells have the same dispersion curves and share a common bandgap, and they are related to each other by a simple translation of s_2. The generation of edge modes is obtained by introducing a "defect" in the periodic structure, corresponding to an interface of Zak phases. This is realized by creating an interface between two distinct arrays, each containing 9 cells, with different central separations, s_1 and s_2 (see Fig. 1a). The interface supports a topologically protected mode due to the common bandgap and distinct Zak phase associated with the bands of each geometry.

We performed an experimental realization of this sample, using a 3D printing technique with the polymer Solflex SF650, W2P Engineering GmbH, which has, printed and polymerized with a UV process, with the following mechanical characteristics: Young's modulus E = 1.25 GPa, Poisson's ratio ν = 0.3, and mass density ρ = 1120 kg/m^3. In order to induce the possibility of tuning the mechanical properties of the sample [2], we add a photo-responsive azo-dye, the Disperse Red 1 methacrylate (DR1m), swelling the pre-cured structure, and thus permitting homogeneous dye dispersion. Finally, the swollen structure is dried for 1 hour until the pristine shape is recovered and the latter is UV-post-cured for 1 hour under all-around illumination in the wavelength range 320–450 nm. Our tunability strategy uses the photo-responsive material property described above to induce a reduction of the

Young's modulus when stimulated by a 405 nm-wavelength laser beam impinging laterally on the central region of the sample. The realized structure is then equipped with a piezo-transducer attached to the sample with super-glue and used to excite in the sample elastic waves, that propagate through the beam and can be detected by a laser Doppler vibrometer, that measures the out-of-plane particle velocity.
We then performed a set of experiments devoted to revealing the existence of the edge modes and the effects induced by tuning the elastic constants by illuminating with the laser beam.

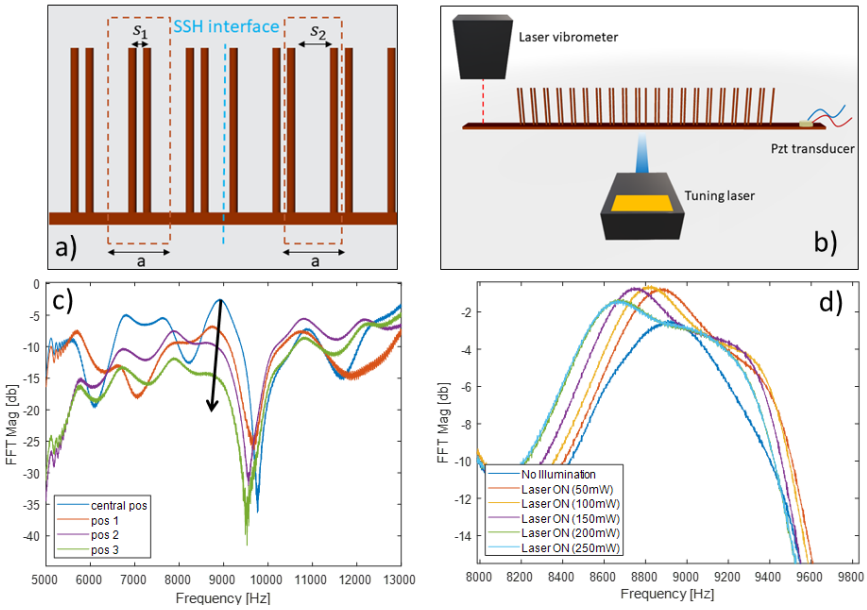

Figure 1: (a) Definition of the unit cell of dimension *a* in the two rod arrays, with separation distance s_1 and s_2 respectively**. (b)** Experimental set-up, with the polymeric sample excited by a piezoelectric transducer, the signal detected by a laser vibrometer and a second laser to induce the tuning of the elastic properties of the sample in the illuminated region. **(c)** The exponential decay of the edge-mode amplitude with the distance from the SSH interface. **(d)** The shift of the eigenfrequency of the edge mode at different levels of illumination of the tuning laser.

Figure 1(c) displays the Fast Fourier Transform (FFT) of the acquired signals, which clearly depicts the band gap region and an isolated peak that corresponds to the localized mode at approximately 9 kHz. When the signal detection point is moved from the central position to the lateral position 3 (as shown in Fig. 1(c)), the amplitude of the FFT peak exponentially decreases as predicted by theory. Additionally, by increasing the output power of the laser illumination in the central defect region, the peak relative to the localized mode shifts towards smaller frequency values (as shown in Fig. 1(d)), with a maximum variation of approximately 300 Hz observed at 250 mW compared to the original frequency. The frequency shift due to local illumination of the sample is linearly dependent on laser power and can reach the band gap edge, and is fully reversible when illumination is removed.
The present study demonstrates the potential of utilizing photo-responsive materials to generate topological edge modes that can be dynamically tuned. This approach complements existing techniques that rely on geometric manipulation to achieve tunability. Moreover, the principle underlying this work could be extended to multi-dimensional topological systems, enabling dynamic tuning of topological waveguides and energy splitters. The ability to dynamically modify the operating frequency of these devices would significantly enhance their versatility.

References

[1] W. P. Su, J. R. Schrieffer, and A. J. Heeger, "Solitons in polyacetylene,", Phys. Rev. Lett. 42, 1698–1701 (1979).
[2] G. J. Chaplain, J. M. De Ponti, G. Aguzzi, A. Colombi, and R. V. Craster, "Topological rainbow trapping for elastic energy harvesting in graded Su-Schrieffer-Heeger systems," Phys. Rev. Appl. 14, 054035 (2020).
[3] A. S. Gliozzi, M. Miniaci, A. Chiappone, A. Bergamini, B. Morin, and E. Descrovi, "Tunable photo-responsive elastic metamaterials," Nat. Commun. 11, 2576 (2020).

PHONONICS 2023: 6th International Conference on Phononic Crystals/Metamaterials/Metasurfaces, Phonon Transport, and Topological Phononics
Manchester, England, June 12-16, 2023
PHONONICS-2023-0045

Surface to Bulk Conversion of Elastic Waves by Temporal Modulation

Jonatha Santini[1], Xingbo Pu[2], Antonio Palermo[2], Francesco Braghin[1], Emanuele Riva[1]

[1] *Department of Mechanical Engineering, Politecnico di Milano, 20156, Italy, jonatha.santini@polimi.it, emanuele.riva@polimi.it, francesco.braghin@polimi.it*
[2] *Department of Civil, Chemical, Environmental and Materials Engineering, University of Bologna, 40033, Italy xingbo.pu2@unibo.it; antonio.palermo6@unibo.it*

Abstract: We investigate surface-to-bulk conversion in time-modulated metasurfaces. We observe that temporal gradings induce similar yet different phenomena as compared to the space counterpart. In particular, the wavenumber conversion, characteristic of space-graded metasurfaces, is replaced by frequency conversion, while a scattering process at constant wavenumber takes place in a way to convert Rayleigh waves into Bulk waves.

Introduction

Time modulated metasurfaces are of great interest in physics and engineering, due to a number of novel wave phenomena that can be triggered by the temporal degree of freedom. In this context, we explore the synergistic interplay between temporal modulations and surface acoustic waves, which can be functional to meet technological needs in SAW applications impossible to access via space-modulated materials.

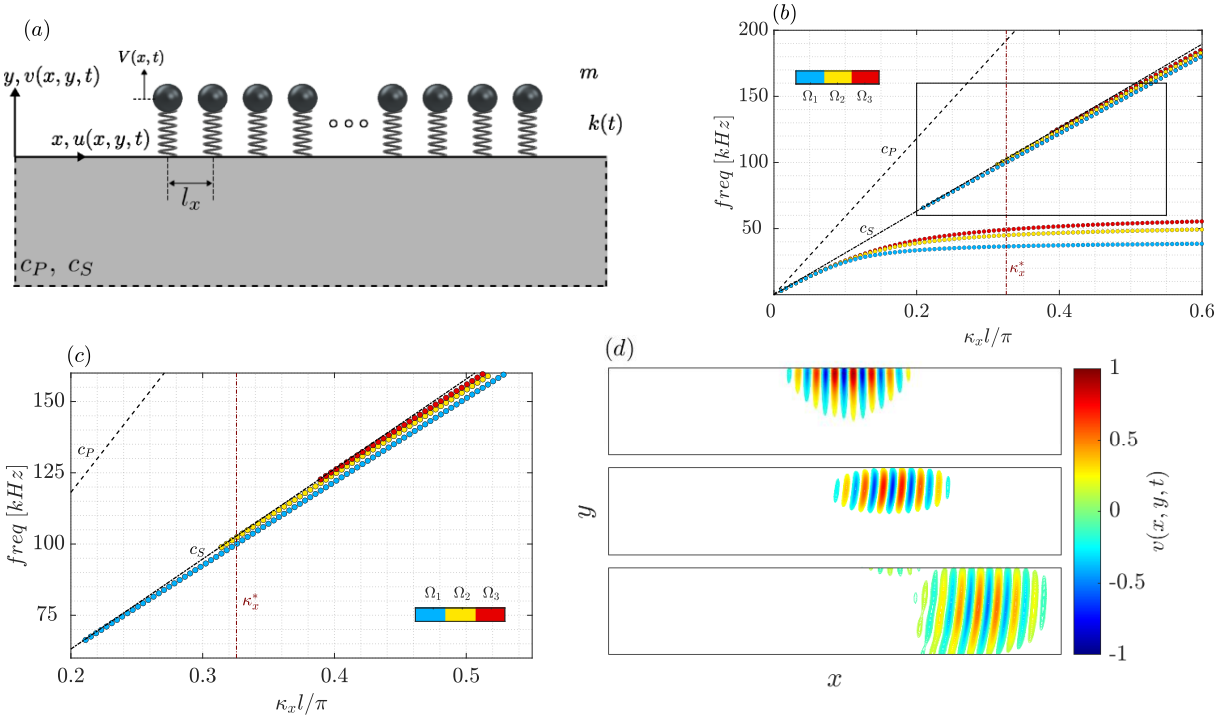

Figure 1: **(a):** Schematic representation of the elastic metasurface. The resonators with constant mass m and time-varying stiffness $k(t)$ are placed atop the surface spaced by a lattice constant l.The resonators move along the vertical direction. The elastic substrate supports pressure and shear waves with characteristic speed c_P and c_S, respectively. **(b)**: Metasurface dispersion relation[1] accounting for surface (coloured dots) and bulk (dashed and dash-dot lines) available modes for three different values of the resonators' natural frequency. **(c):** Zoomed view of Figure (b). **(d):** Normalized displacement field (only v is shown for convenience) evaluated for three different time instants.

Surface – to – bulk conversion

The underlying physics that takes place in such materials is briefly illustrated in what follows. Consider an elastic, isotropic, homogeneous half-space depicted in **Error! Reference source not found.**(a), where an array of time-varying spring-mass resonators is placed in correspondence with the top layer and constitutes the elastic metasurface. Each resonator is characterized by a tunable natural frequency $\Omega(t) = \sqrt{k(t)/m}$, which serves to induce time-dependent interactions. For such a system, the dispersion relation is illustrated in Figure 1(b) for three resonators' natural frequencies., where $\Omega_1 < \Omega_2 < \Omega_3$ are three relevant values for $\Omega(t)$. The coloured dots are relative to surface acoustic waves, while shear and pressure waves are represented with dashed lines. Time modulation is exploited to perform a frequency conversion of a surface waves. We show this through numerical simulations, where a Rayleigh wave is initially excited and characterized by an imaginary wavenumber along x, i.e. κ_x^*, and a real negative (evanescent) wavenumber along y, i.e. ${\kappa_y}^2$. This initial condition is represented in the upper panel of Figure 1(c), and in terms of energetic content, lies in the upper blue branch of Figure 1(b) for the impinging wavenumber κ_x^*. Depending on the modulation law, a number of behaviours can be achieved through transformations that preserve wavenumber ${\kappa_x}^3$:

1. *Frequency conversion*: when the modulation is sufficiently slow (adiabatic) and the final condition is represented by the yellow dots (Ω_2), the result is a propagating surface wave with greater frequency; The frequency conversion is accompanied by delocalization (greater penetration depth), but no mode conversion takes place.
2. *Frequency conversion with mode conversion*: if we target the red dispersion of Figure 1(b), the energy hits the bulk wave mode, and surface-to-shear wave mode conversion is achieved.
3. A combination of the two cases above depending on the spectral width of the wave packet and on the final condition for $\Omega(t)$.
4. Scattering between different modes: if the modulation is fast, a scattering process between the wave modes that populate the dispersion relation, including resonant modes (lower branch of the dispersion), counter propagating surface waves, and bulk modes.

Among all four cases listed above, we reported a simulation relative to case 4 (Figure 1(d)). The resonators are modulated with a step function, which drives the resonant frequency from Ω_1 to Ω_3, thereby inducing a scattering process. Indeed, in the second and third panels we can observe that part of the energy reaches the bulk of the material, while part remains localized on the surface, and consistently with transformations that preserve momentum $\kappa = \kappa_x^*$.

Conclusions

In this work, the role of time modulation techniques in elastic metagradings is discussed, with particular emphasis on wave mode and frequency conversion. We unfold a number of behaviours that are relatively unexplored in the context of surface acoustic wave devices and are analog yet different as compared to the space counterpart.

.

References

[1]A. Palermo, P. Celli, B. Yousefzadeh, C. Daraio, A. Marzani, *Journal of the Mechanics and Physics of Solids*, **145,** 104181 (2020).

[2] K. F. Graff, *Wave Motion in Elastic Solids*, *Oxford University Press* (1975).

[3] J. Santini and E. Riva, *New J. Phys.* **25** 013031 (2023).

PHONONICS 2023: 6th International Conference on Phononic Crystals/Metamaterials/Metasurfaces, Phonon Transport, and Topological Phononics
Manchester, England, June 12-16, 2023
PHONONICS-2023-0093

Frequency- and Momentum-Resolved Detection of Laser-Excited Acoustic Phonons in Nanomembranes

Thomas Vasileiadis[1], Anuj Kumar Dhiman[1], Kleoniki Sympoura[1], Mikołaj Pochylski[1], and Bartłomiej Graczykowski[1]

[1] *Faculty of Physics, Adam Mickiewicz University, Uniwersytetu Poznanskiego 2, 61-614 Poznan, Poland, thomas.vasileiadis@amu.edu.pl, anuj.dhiman@uwb.edu.pl, up1068656@upnet.gr, pochyl@amu.edu.pl, bartlomiej.graczykowski@amu.edu.pl.*

Abstract: Irradiation of opaque nanomembranes with optical pulses creates non-thermal Lamb waves that can be detected with frequency-domain Brillouin light scattering (BLS). These 'pumped' BLS spectra contain a continuum of background excitations, Fano resonances, Stoke/anti-Stokes asymmetries, and acoustic frequency combs, which can provide rich information on the physics of non-thermal Lamb waves.

The study of acoustic phonons under confinement and in non-equilibrium conditions is useful for developing future signal-processing applications and for efficient thermal management of nanodevices. However, the frequency-domain, laser-based detection of thermal, acoustic phonons in semiconducting nanostructures is limited to spontaneous inelastic light scattering by thermal phonons, while light absorption and the small mass of the investigated system lead to poor signal-to-noise ratio. Moreover, in non-equilibrium conditions, such as those established during a device's operation, acoustic phonons' properties can be modified due to interactions with other microscopic excitations, such as electron-hole pairs and plasmons. Thus, it is useful to develop methods for amplifying gigahertz signals and generating long-living, non-thermal, coherent states.

Recently, we have developed an all-optical method, termed pumped Brillouin Light Scattering (pumped-BLS), for excitation and frequency-, momentum-, and space-resolved detection of gigahertz acoustic waves in spatially confined semiconducting nanomembranes[1]. Using femtosecond laser pulses, we have excited GHz acoustic phonons, termed Lamb waves, in a bare silicon membrane and probed them with frequency-domain micro-Brillouin light spectroscopy [**Figure 1(a)**]. The population of photoexcited Lamb waves displays a hundredfold compared to thermal equilibrium, strongly asymmetric Fano resonances due to coupling between the electron-hole plasma and the phonons, and Stokes–anti-Stokes asymmetry due to directional phonon transport.

This contribution presents an ongoing investigation verifying these observations for various nanomaterials and bulk structures. For instance, we have demonstrated the connection between directional phonon transport and Stokes – anti-Stokes symmetry for metallic transducers on a silicon surface. Additionally, in a recent work, Białek *et al*. have shown that a gold-silicon nanomembrane exhibits a thousandfold enhancement of the BLS signal and the emergence of Fano resonances upon irradiation with femtosecond laser pulses[2]. Interestingly, the broken mid-plane symmetry of the membrane leads to the excitation of both symmetric and anti-symmetric Lamb modes with mode-dependent Fano-coupling parameters. This mode-dependence proves that the symmetry and generation mechanism of each phonon plays a key role in the observed Fano lineshape.

In addition to the above, we show how the BLS spectrum can be enhanced and controlled with two-pulse pumped-BLS experiments. The pump pulses – characterized by 780 nm wavelength, 150 fs duration, and 80 MHz repetition rate – are split into two branches, with the one passing from a delay stage. With this procedure, the broad background of the pumped-BLS spectra transforms into an acoustic frequency comb with the frequency spacing between peaks corresponding to the time delay between pump pulses. This observation can be used to interpret the inelastic background of pumped-BLS.

Based on our understanding, the femtosecond laser pulses primarily excite the electronic degrees of freedom and generate electron-hole (e-h) pairs. In our first work with pumped-BLS, we used time-

resolved THz spectroscopy to measure the dynamics and density of the e-h plasma[1]. For a pure silicon membrane, 260 nm-thick, the e-h pairs thermalize in the picosecond timescale and then slowly recombine with a time constant of about 5 ns. These e-h pairs enhance the BLS signal in two ways. First, the e-h pairs excite acoustic phonons via the thermoelastic effect (sudden expansion due to electron-phonon coupling) and the deformation potential mechanism (modified bonding in electronically excited solids)[3]. Second, e-h pairs modify the optical properties, modulate the reflectivity, and cause a broad incoherent background in the frequency domain. The coexistence of these two amplification mechanisms leads to a nonlinear fluence dependence[1] with an order slightly larger than 2.

With double pulse excitation, the broad incoherent BLS background transforms into an acoustic frequency comb [**Figure 1(b)**]. Noticeably, the appearance of the background alone cannot create Fano resonances. The emergence of asymmetric Fano shapes requires that the excited phonon phase is different from zero [**Figure 1(c)**]. This phase is determined by the interplay between impulsive and displacive phonon-excitation processes, *i.e.*, thermoelastic versus deformation potential mechanisms. For silicon, the phase can be negative – meaning that the photoexcited crystal is shrinking – and this leads to an asymmetric Fano shape where the dip is at higher frequencies than the peak maximum. In time-domain experiments, the arbitrary selection of a window for Fourier-transform removes the Fano lineshape, and instead, the phase information is retrieved from the direct observation of the first phonon period.

Understanding the physical mechanisms behind pumped-BLS can pave the way for its use in systems with acoustic Anderson localization, topological one-way transport, and acoustic diodes[4,5]. Moreover, the combination of pumped- and time-resolved BLS might be useful for studying the transient elastic properties of photoexcited materials.

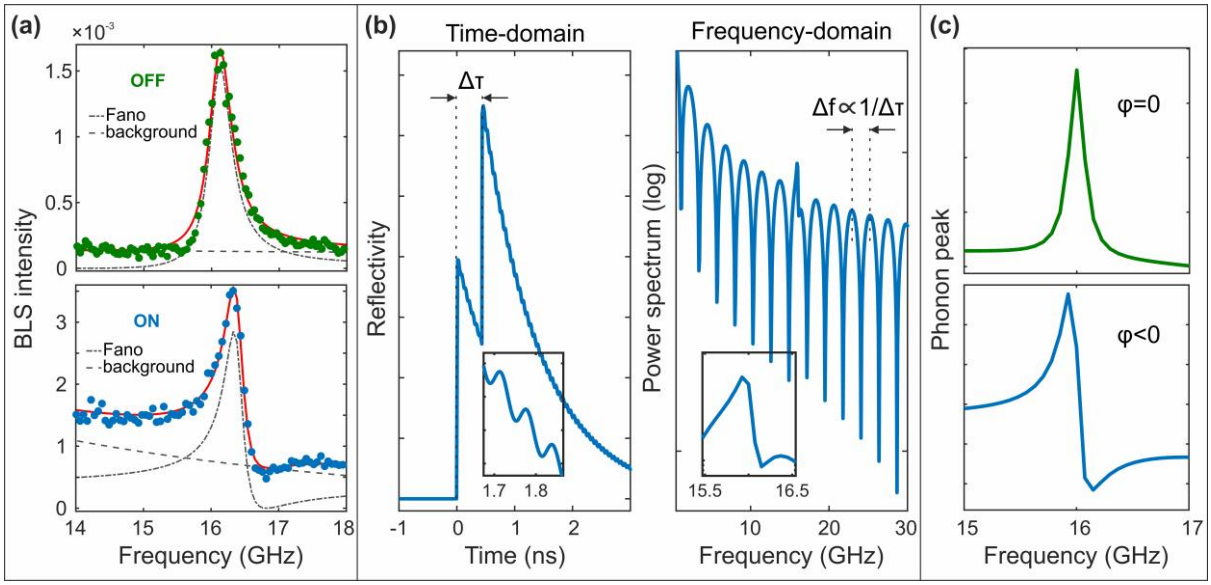

Figure 1 (a) BLS spectrum of dilatational Lamb standing waves in 260 nm-thick silicon with the femtosecond laser off (up) and on (down) adapted from Ref. 1. **(b)** A simple simulation in time- and frequency-domain of reflectivity modulation with exponential decay dynamics for a double pulse excitation. The insets show the oscillations and spectroscopic peak of a phonon with 16 GHz period. **(c)** The phonon lineshape for zero (up) and negative (down) phonon excitation phases.

References

[1] T. Vasileiadis, H. Zhang, H. Wang, B. Mischa, G. Fytas, and B. Graczykowski, *Science Advances* **6**(51), eabd4540 (2020).
[2] R. Białek, T. Vasileiadis, M. Pochylski, and B. Graczykowski, '*Fano meets Stokes: four-order-of-magnitude enhancement of asymmetric Brillouin light scattering spectra*', Photoacoustics 2023 (in review).
[3] P. Ruello, V. E. Gusev, *Ultrasonics* **56**, 21–35 (2015).
[4] T. Vasileiadis, J.S. Reparaz, and B. Graczykowski, *Journal of Applied Physics*, **131**(18), 180901 (2022).
[5] T. Vasileiadis, J. Varghese, V. Babacic, J. Gomis-Bresco, D. Navarro Urrios, and B. Graczykowski, *Journal of Applied Physics*, **131**(18), 180901 (2022).

PHONONICS 2023: 6th International Conference on Phononic Crystals/Metamaterials/Metasurfaces, Phonon Transport, and Topological Phononics
Manchester, England, June 12-16, 2023
PHONONICS-2023-0126

Multiple layers, phononic arrays and surface variations to suppress the bending wave coincidence effect in panels

A Hall; G Schmid; V Sorokin; G Dodd
Acoustics Research Centre, University of Auckland, Auckland 1142, New Zealand
Email: a.hall@auckland.ac.nz

Abstract: An investigation into three methods to improve the coincidence region including the addition of periodic/quasi-periodic inclusions, a multi-layer approach, and geometrical patterns on the surface of wall panels. Experimental and modeling results were in good qualitative agreement and see an improvement of attenuation within the targeted band.

The building acoustics industry has seen little development away from traditional homogeneous materials. With the inevitable densification of housing, the severity of noise pollution within residential living environments is escalating. While the transmission of high-frequency audible sound through walls is relatively manageable between 1 to 5kHz, the overall acoustic performance classification of a wall system suffers from a phenomenon known as the coincidence effect. This effect involves a more efficient coupling of the incident sound wave and the bending waves within the wall panel. This research [1,2] aims to find a cost-effective solution to improving the Sound reduction index (Rw) performance of wall systems, in this case constrained by the coincidence region between 2000-4000Hz.

The coincidence dip occurs where the wave speed of the dispersive bending waves in the material are equal to the projected wavelengths of the incident sound in the air as it is incident at particular angles [3]. The lowest frequency at which it happens is termed the critical frequency, fc, and is when the airborne sound is at grazing incidence. fc can be found from equation (1):

$$f_c = \frac{c_{plate}}{1.8h}\sqrt{\left(\frac{\rho(1-\nu^2}{E}\right)} \quad (1)$$

Three techniques were investigated. The first method shifts the coincidence region beyond 5kHz using multiple thinner layers, the second uses the creation of a band gap through impedance changes creating multiple scattering[4,5] and the third method combines shifting and supressing using panel surface variations. The first method utilized much thinner panels (e.g. 4.5mm MDF) which have a much higher coincidence frequency due to their lower stiffness. As shown in Figure 3, layers of 4.5mm MDF were glued together to ensure the panels felt rigid and could be handled easily as single panel for ease of construction. The combined panels were aimed at having a static stiffness of a normal panel but enabled shear action at higher frequencies where bending waves dominate the TL. The incident sound would encounter the layers as separate, independent layers.

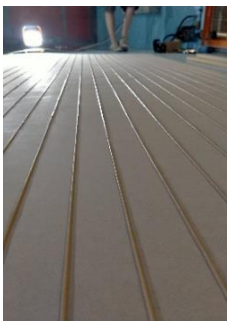

Figure 3 Glue lines between the layers of 4.5mm MDF

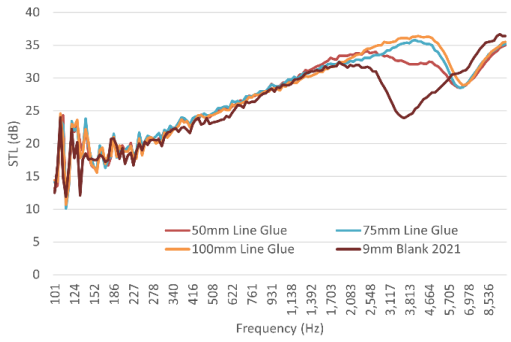

Figure 4 Sound transmission loss in 1/24th octs for panel unit with varying glue lines

Figure 4 shows testing results under diffuse field conditions for 3 different glue line spacings, 50, 75 and 100mm. This is compared to a control sample of a single 9mm layer. Results indicate that both 100 and 75mm samples act as a single unit following mass law at frequencies below f_c. At higher frequencies the panels act as individual panels allowing shear action.

The second method aims to use multiple scattering and interference of bending waves, causing attenuation bands (bandgaps). Impedance changes between two materials withing the material or structure causes reflections of the internal bending waves. These material changes can be more or less dense, such as a change from MDF to steel or alternatively MDF to an air cavity.

The spacing of the impedance periodic arrays of inclusions will determine the frequency position of the band gap. The band gaps were tuned to target the coincidence region based on the Mindlin plate theory.

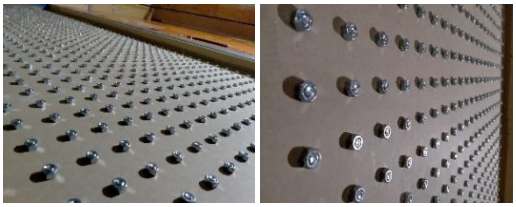

Figure 5 Periodic arrays of M8 nuts and bolts on a 9mm thick 2.4x1m MDF panel

The predicted frequency region of a complete bandgap for a 45mm square lattice was 3100 – 3900 Hz, and for the 50mm square lattice, 2800 – 3400 Hz.

Figure 5 shows a square lattice array of inclusions tested under diffuse field conditions. Figure 6 shows the results for three samples tested under diffuse field conditions with approximately the same mass. These are compared with a 9mm MDF panel and an 18mm MDF panels.

Results indicate a band gap is present at the predicted frequencies likely due to interference scattering of the bending waves in the panels from the inclusions. The 35mm spaced square lattice shows a remarkable improvement over that of the 9mm and 18mm sample up to 4664Hz with a removal of the coincidence region.

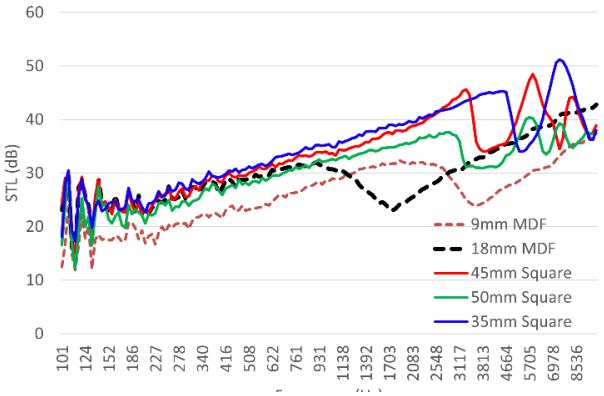

Figure 6 Diffuse field sound transmission loss measurements in 1/24th octaves for samples with periodic arrays inclusions

The final method combines both stiffness change and multiple scattering techniques to combat the coincidence region. Periodic surface variations were generated on a 9mm MDF panel by routing 4mm x 4.5mms (width x depth) channels panel in a number of individual patterns. The variations create a periodic impedance change in the panel due to the slots, whilst also lowering the dynamic stiffness of the panel at high frequencies in the coincidence region. Figure 7 shows a sample with slots cut in the panel at 4.5mm deep to create a square 50x50mm pattern. Wave finite element (WFE) modelling indicates a band gap around 3800Hz for this sample.

Figure 7 50x50mm routed slots in a panel mounted for diffuse field testing

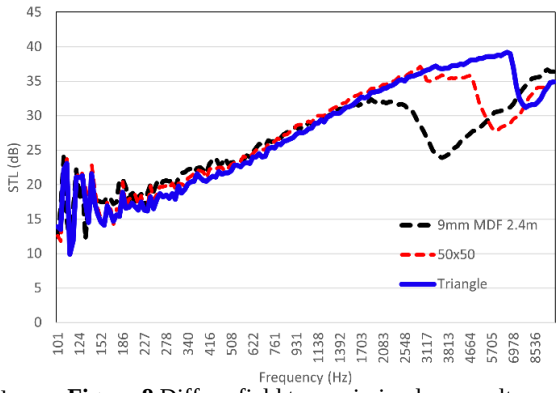

Figure 8 Diffuse field transmission loss results for individual panels routed in a square (red dashes) and triangular (blue) pattern.

Results shown in Figure 8 indicate that the coincidence region has been shifted higher in frequency from the hange in stiffness of the panel due to the routed patterns. Both the 50x50mm square design and the triangular pattern also indicate a band gap feature in this region.

Three practical methods for improving the coincidence region by either shifting or reducing the phenomenon. Multi-layer panels can significantly shift the coincidence region out of the STC and Rw range while impedance cahnges can scatter bending waves creating a band gap of attenuation. The panel surface variation method indicates a good system for both raising the frequency of f_c and narrowing the bandwidth of the coincidence region. Routing the panel reduces the amount of material in the panel whilst having little to no effect in the mass law region. We would like to acknowledge the MBIE Endeavour fund smart ideas grant for making this research possible.

[1] Hall A.J., Dodd G, Calius E.P., Multiplying resonances for attenuation in mechanical metamaterials: Part 2 Multilayer structures, Applied Acoustics, Volume 179, August 2021, 108041 DOI 10.1016/J.APACOUST.2021.108041
[2] Hall A.J., Dodd G, Calius E.P., Multiplying resonances for attenuation in mechanical metamaterials: Part 1 - Concepts, initial validation and single layer structures, Applied Acoustics, Volume 170, 15 December 2020, 107513, DOI 10.1016/J.APACOUST.2020.107513
[3] Frank Fahy. Sound and Structural Vibration: Radiation, Transmission and Response.Academic Press, Orlando, 1987.
[4] B.R. Mace. The vibration of plates on two-dimensionally periodic point supports. J. Sound Vib., 192(3), 629–643, 1996
[5] C.G. Poulton et al. Analytic theory of defects in periodically structured elastic plates.

Phononic Crystal and Resonator-Based Metasurface Combination for Wide-Angle Sound Absorption

Diana Maria Garza-Agudelo[1,2], Vicente Cutanda Henríquez[3], Cheol-Ho Jeong[2], Peter Risby Andersen[4], Martin Ibarias[5], José Sánchez-Dehesa[5], Frieder Lucklum[3]

[1] *Oticon A/S, Kongebakken 9, 2765 Smørum, Denmark*
dimg@demant.com
[2] *Acoustic Technology, Department of Electrical and Photonics Engineering, Technical University of Denmark, Ørsteds Plads, Building 352, Kongens Lyngby, 2800 Denmark*
chje@dtu.dk
[3] *Centre for Acoustic-Mechanical Microsystems, Department of Electrical and Photonics Engineering, Technical University of Denmark, Ørsteds Plads, Building 352, Kongens Lyngby, 2800 Denmark*
vcuhe@dtu.dk, fluc@dtu.dk
[4] *Audio Research, GN Audio A/S & Jabra, Lautrupbjerg 7, Ballerup, 2750, Denmark*
prandersen@jabra.com
[5] *Department of Electronic Engineering, Universitat Politècnica de València, Camino de Vera s.n., Building 7F, Valencia, ES-46022, Spain*
maibaal1@eln.upv.es, jsdehesa@upv.es

Abstract: A combination of a hexagonal lattice of close cylinders and a metasurface containing Helmholtz resonators (HRs) is presented in this contribution. The arrangement has been optimized to enhance sound absorption of plane waves arriving at a wide range of incidence angles. In room acoustics, this is useful for adapting the absorption performance to realistic sound field characteristics.

Room acoustic designs can benefit from materials that have high absorption over a wide range of sound wave incidence angles[1,2]. In the field of acoustic metamaterials, sound absorbers are often designed and optimized for normal incidence, with only a few examples where oblique incidence is examined in detail[3,4]. It has been shown in previous research that resonator-based sound absorbing metasurfaces that present a locally reacting impedance to the sound field cannot be tuned for high absorption at nearly-grazing incidence while maintaining a similarly high absorption at near-normal incidence angles[5].

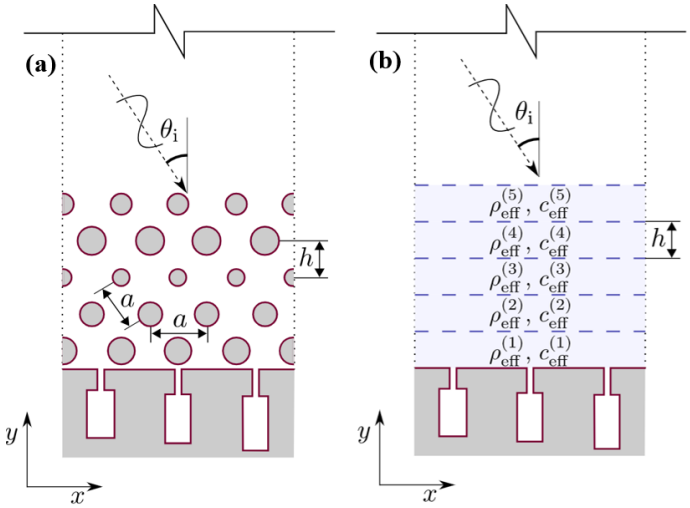

Figure 1 In **(a),** an arrangement of a metasurface with HRs and several layers of a hexagonal lattice of cylinders is shown. The version in **(b)** represents the equivalent homogenized medium used for optimization. A single periodic cell is shown.

The work presented here builds upon a two-dimensional metasurface formed by a periodic arrangement of Helmholtz slit resonators tuned to one or several frequencies. To overcome the aforementioned limitations on its angular absorption properties, a hexagonal lattice of cylinders is placed over the metasurface[6,7]. The lattice is then modeled as the superposition of several layers of homogenized medium that includes acoustic losses[8]. This allows the representation of the whole setup using the Transfer Matrix Method (TMM) as a one-dimensional physical system, as shown in Fig. 1[9,10]. The effective density and speed of sound in the homogenized layers and the dimensions of the resonators are then numerically optimized for a wide range of plane wave incidence angles[11]. The resulting design, shown in Fig. 2 for the

one-resonator case, is a single layer of homogenized cylinders, with an air layer separating it from the metasurface of HRs[12]. This optimized design outperforms an equivalent locally reacting material in terms of range of absorption at different angles (Fig. 2b) and frequency dependence (Fig. 2c). A similar design with multiple resonators has also been shown to perform well. In the present work, we introduce validation measurements made in an impedance tube as shown in Fig. 3. The samples have been produced with additive manufacturing in a modular assembly that snugly fits in the tube. The match with simulations at normal incidence (not shown here) is good. The possibility and difficulties of using porous materials will also be mentioned. Finally, extensions of this research will be examined, such as the measurement of finite samples at oblique incidence.

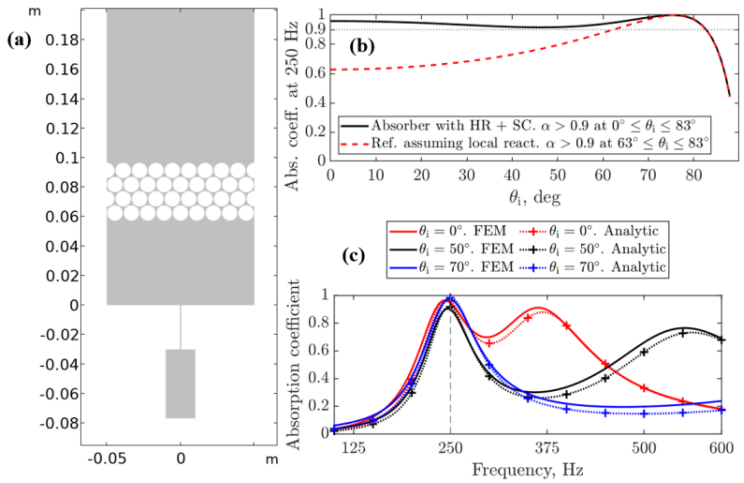

Figure 2 One-resonator arrangement, optimized for wide incidence angle. In **(a)**, geometrical representation; **(b)** is the absorption coefficient at the design frequency, 250 Hz, for all incidence angles; **(c)** is the dependence of frequency of the absorption coefficient for several incidence angles, validated with FEM.

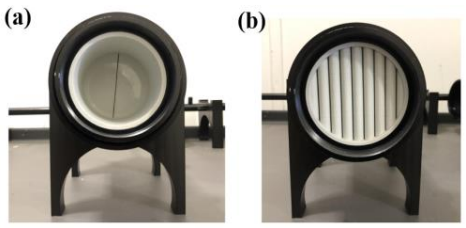

Figure 3 Pictures of the measurement setup in the impedance tube: **(a)** shows the slit resonator alone and in **(b)** the hexagonal cylinder lattice has been added.

References

[1] M. Hodgson, A. Wareing, *Comparisons of Predicted Steady-State Levels in Rooms with Extended- and Local-Reaction Bounding Surfaces*, Journal of Sound and Vibration 309 (2008) 167–177. https://doi.org/10.1016/j.jsv.2007.06.069.

[2] P. D'Antonio, T. J. Cox, *Acoustic Absorbers and Diffusers: Theory, Design and Application*, 3rd ed., CRC Press, London, 2017.

[3] T. Cavalieri, J. Boulvert, G. Gabard, V. Romero-García, M. Escouflaire, J. Regnard, J.-P. Groby, *Graded and Anisotropic Porous Materials for Broadband and Angular Maximal Acoustic Absorption*, Materials **13** (2020). https://doi.org/10.3390/ma13204605.

[4] N. Jiménez, V. Romero-García, V. Pagneux, J.-P. Groby, *Rainbow-Trapping Absorbers: Broadband, Perfect and Asymmetric Sound Absorption by Subwavelength Panels for Transmission Problems*, Scientific Reports **7** (2017) 13595, https://doi.org/10.1038/s41598-017-13706-4.

[5] D. M. Garza-Agudelo, V. Cutanda Henriquez, C. H. Jeong, P. R. Andersen, *Characterization and Optimization of the Angle Dependent Acoustic Absorption of 2D Infinite Periodic Surfaces of Helmholtz Resonators*, Journal of Theoretical and Computational Acoustics. https://doi.org/10.1142/S2591728522500104, accepted/In press.

[6] A. Climente, D. Torrent, J. Sánchez-Dehesa, *Sound Focusing by Gradient Index Sonic Lenses*, Applied Physics Letters **97** (2010) 104103. https://doi.org/10.1063/1.3488349.

[7] V. C. Henríquez, J. Sánchez-Dehesa,*Viscothermal Effects in a Two-Dimensional Acoustic Black Hole:a Boundary Element Approach*, Phys. Rev. Applied **15** (2021) 064057. URL: https://link.aps.org/doi/10.1103/PhysRevApplied.15.064057.

[8] M. Ibarias, Y. Zubov, J. Arriaga, A. A. Krokhin, *Phononic Crystal as a Homogeneous Viscous Metamaterial*, Physical Review Research **2** (2020) 022053. https://doi.org/10.1103/PhysRevResearch.2.022053.

[9] J. F. Allard, N. Atalla, *Propagation of Sound in Porous Media: Modelling Sound Absorbing Materials*, John Wiley and Sons, 2009. https://doi.org/10.1002/9780470747339.

[10] M. R. Stinson, *The Propagation of Plane Sound Waves in Narrow and Wide Circular Tubes, and Generalization to Uniform Tubes of Arbitrary Cross-Sectional Shape*, Journal of the Acoustical Society of America **89** (1991) 550–8. https://doi.org/10.1121/1.400379.

[11] P. R. Andersen, V. Cutanda Henríquez, N. Aage, *Shape Optimization of Micro-Acoustic Devices Including Viscous and Thermal Losses*, Journal of Sound and Vibration **447** (2019) 120–136. https://doi.org/10.1016/j.jsv.2019.01.047.

[12] D. M. Garza-Agudelo, V. Cutanda Henriquez, C. H. Jeong, P. R. Andersen, M. Ibarias, *Extending the Angle Range of High Absorption of Metasurfaces by Adding a Multilayered Medium*, Proceedings of the 24th International Congress of Acoustics, Gyeongju, Korea (2022).

PHONONICS 2023: 6th International Conference on Phononic Crystals/Metamaterials/Metasurfaces, Phonon Transport, and Topological Phononics
Manchester, England, June 12-16, 2023
PHONONICS-2023-0219

Local flow stabilization/destabilization by phononic subsurfaces over an extended spatial domain

Armin Kianfar[1], Mahmoud I. Hussein[1,2]

[1]Ann and H.J. Smead Department of Aerospace Engineering Sciences, University of Colorado Boulder, Boulder, Colorado 80303,
[2]Department of Physics, University of Colorado Boulder, Boulder, Colorado 80302,
armin.kianfar@colorado.edu, mih@colorado.edu

Abstract: Local phonon motion underneath a surface interacting with a flow may cause the flow to passively stabilize, or destabilize, as desired. This mechanism has been demonstrated for a spatial region on the order of the instability wavelength along the fluid-structure interface. Here we uncover fundamental relations between the behaviour of flow instabilities and the frequency response characteristics of the structure admitting the phonon motion, and use these relations to realize extensive spatial expansion of the control regime—possibly covering the entire surface exposed to the flow.

The interactions between a solid surface and a fluid flow underlie dynamical processes relevant to air, sea, and land vehicle performance and numerous other technologies. For example, skin-friction drag, flow transition, and flow separation may be engineered by control of these interactions. Key objects that influence these interactions are unstable flow disturbances, or perturbations, such as Tollmien–Schlichting (TS) waves. Active control of flow instabilities has been pursued by numerous techniques. However, these techniques require energy input as well as complex sensing and actuation devices[1]. To overcome these drawbacks, precise passive, and responsive, control of flow instabilities has been demonstrated using a phononic subsurface (PSub)[2-4].

A PSub comprises a finite phononic structure placed nominally perpendicular to the fluid-structure interface. An instability traveling within the flow excites this interface, triggering elastic waves in the PSub which reflect and return to the flow. The unit-cell and finite-structure characteristics of the PSub may be designed to passively enforce the returning waves to resonate and be out of phase when reentering the flow, causing significant destructive interference of the continuously incoming flow waves near the surface and subsequently their attenuation over the spatial region of the PSub-fluid interface. The outcome in this scenario is a local reduction in the skin-friction drag. Destabilization, which accelerates the transition to turbulence, is also possible, where, in contrast, the PSub is configured to induce constructive interference. Destabilization is beneficial for delaying flow separation or enhancing chemical mixing and combustion.

Phononic subsurfaces have been demonstrated over a characteristically narrow spatial domain, covering a streamwise distance on the order of the wavelength of the target flow instability wave[2,3]. In this work, we demonstrate the application of PSubs over extended special domains. We apply direct numerical simulation (DNS) to uncover a series of relationships between key features in the frequency response of a standalone PSub and key features in the responding spatially unstable flow disturbances for incompressible channel flows at Reynolds number 7,500 (based on the centerline velocity U_c). These relations reveal fundamental tradeoffs in the PSub performance, which must be understood to enable effective and sustained flow stabilization or destabilization over an extended spatial domain along the downstream direction when a series of contiguously arranged PSubs is applied.

For PSubs, the performance metric P is the primary quantity to measure the effectiveness of the passive control scheme. This quantity, introduced in Ref. (2), is obtained from the frequency response of the PSub structure under a harmonic force, uncoupled with the flow field. In Figure 1, the characterization and performance of different PSub designs are presented. We consider a PSub comprising a rod with a periodic array of spring-mass resonators. The resonator's mass m_{res} is perturbed by up to $\varepsilon = \pm 20\%$, causing shifts in the sub-hybridization resonance[4]. The value and sign of P, as well as the value of its derivative with respect to frequency $dP/d\Omega$, at the target frequency varies in response to perturbing the resonator mass. For example, as shown in Figure 1(a,b), a positive P corresponds to a local destabilization; in Fig. 1(B), K_p represents the wall-normal integral of the perturbation kinetic energy for the flow

field, x is the streamwise location, and δ is the half height of the channel. Note, the local stabilization (or destabilization) occurs exactly at the edges of the control region (dotted lines) where the PSub is installed at the bottom wall of the channel. Moreover, the reduction or enhancement strength depends on the value of $dP/d\Omega$; the higher the frequency derivatives, the stronger the control scheme.

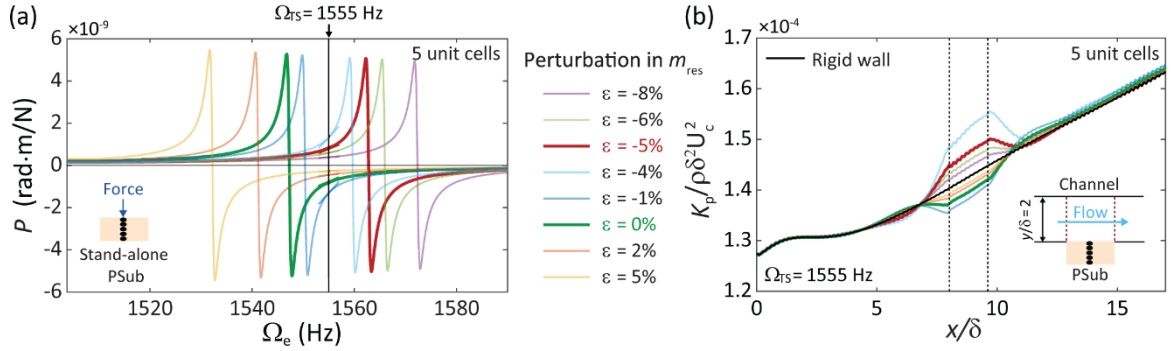

Figure 1 Characterization and performance of different PSub designs realized by varying the resonator mass: (a) Performance metric P with respect to the excitation frequency (standalone analysis done prior to the coupled fluid-structure simulations), and (b) kinetic energy of flow instability K_p as a function of the streamwise position when various PSub designs are employed (with all-rigid-wall case included for comparison), targeting TS wave frequency Ω_{TS} = 1555 Hz.

Figure 2(a,b) shows an extension of the control region by using five consecutive and independent PSubs. The basis of this extension is the local effect of this control mechanism on the flow disturbances. In Figure 1(a), K_p remains below the corresponding value for the all-rigid-wall case throughout the control region (region gray shading), whereas downstream of the control region (shaded gray) the disturbances recover from the PSub effect. Similarly, the friction drag D is plotted showing a sustained dip within the entire control region. Note, the drag reduction is small in this report because the contribution of disturbances to momentum flux is small compared with the mean (base) flow; however, it demonstrates a proof concept that in the future may be applied to multiple instability waves at once, in which case the accumulative effect would be more significant.

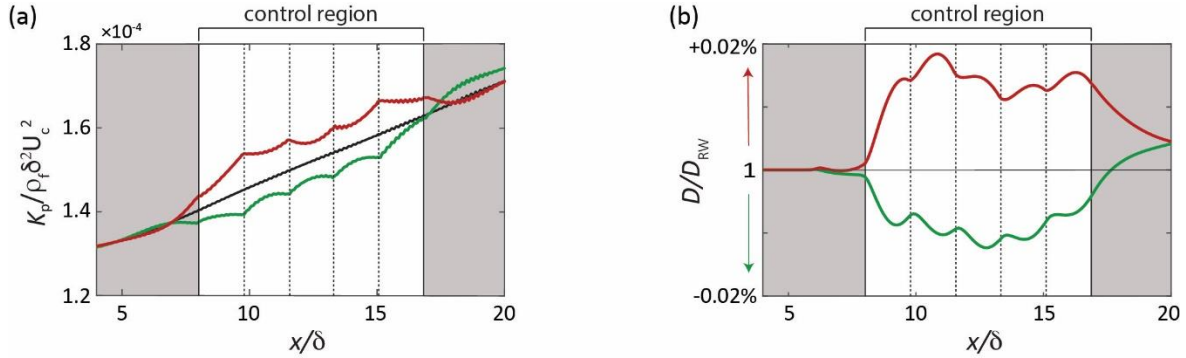

Figure 2 Extended control region with five consecutive PSubs installed: (a) Stabilization and destabilization as represented by (a) the kinetic energy of the flow instability K_p, and (b) friction drag D normalized by the that of the all-rigid-wall case D_{RW}.

References

[1] M. Gad-el-Hak, *Flow Control: Passive, Active, and Reactive Flow Management*, Cambridge University Press, UK (2000).
[2] M.I. Hussein, S. Biringen, O.R. Bilal, and A. Kucala, *Proc. R. Soc. A* **471**, 20140928, (2015).
[3] C.J. Barnes, C.L. Willey, K. Rosenberg, A. Medina, and A.T. Juhl, *AIAA Scitech 2021 Forum*, 2021–1454 (2021).
[4] A. Kianfar and M.I. Hussein, *New J. Phys.*, 10.1088/1367-2630/accbe5; *arXiv:2302.14330* (2023).

PHONONICS 2023: 6th International Conference on Phononic Crystals/Metamaterials/Metasurfaces, Phonon Transport, and Topological Phononics
Manchester, England, June 12-16, 2023
PHONONICS-2023-0166

Locally Resonant Phononic biosensors

Abdelkrim Khelif[1] , Feng Gao[1,2], Sarah Benchabane[1] and Amine Bermak[2]

[1] Institut FEMTO-ST, CNRS, Université de Bourgogne-Franche-Comté, Besançon, France
abdelkrim.khelif@femto-st.fr, feng.gao@femto-st.fr, sarah.benchabane@femto-st.fr
[2] College of Science and Engineering, Hamad Bin Khalifa University, Doha, Qatar
abermak@hbku.edu.qa

Abstract: This article presents a novel acoustic-radiation-free gravimetric biosensor based on the locally resonance of surface phononic crystal (SPC) constructed by periodic high aspect ratio electrodes on Lithium Niobate substrate. A mass sensitivity of 12.9 Hz/ng cm^2 was achieved with a SPC resonator operating around 110 MHz. It can boost the mass detection limit of many acoustic biosensors.

Mass-sensitive biosensors based on acoustic wave resonators are competitive alternatives to optical biosensors as they are low-cost, small-size and compatible for on-chip integration [1, 2]. However, acoustic wave resonators suffers from strong acoustic radiation in liquid, which reduces their quality factor and increases the signal noise. To maintain operation in liquid, acoustic wave resonators for biosensing are usually designed to work in shear horizontal mode. As the movement of the shear wave is in parallel with the liquid-solid interface, the mechanical motion transferred to water is reduced compared to the vertical polarized waves. Both bulk acoustic wave (BAW) and surface acoustic wave (SAW) can be polarized in shear mode. Quartz crystal microbalance (QCM) in thickness shear mode (TSM) is the simplest shear mode BAW resonator. It is usually made of an AT-cut quartz plate sandwiched by two metal electrodes. When alternating electric field is applied to the electrodes, TSM wave can be excited in the AT-cut quartz plate [3]. The mass sensitivity of TSM-QCM is relatively low due to their low operating frequency (a few megahertz). To achieve higher sensitivity, shear mode film bulk acoustic wave resonator (S-FBAR) was developed. S-FBAR is also a BAW device that exploits the same device structure and operation principle as TSM-QCM [4, 5]. The major limitation of S-FBAR is that it requires a relatively complex fabrication process involving the deposition of a tilted c-axis piezoelectric film. As achieving good homogeneity and crystallinity of the tilted c-axis piezoelectric film is difficult with existing technologies.

In this work, we exploit this idea for the realization of SAW resonators operating in liquid. By incorporating SPC with the IDTs, we find that the velocity of Rayleigh wave in water can be reduced to a value lower than the sound speed of water. This successfully stops the propagation of acoustic wave in water and thus eliminates acoustic radiation. Because of the complete suppression of radiation, the quality factor of the resonator is found to be improved by more than 15 times compared to a conventional Rayleigh wave resonator working at the same frequency range. In addition to this slowing down of the phase velocity, the SPC is shown to lead to almost zero-group velocity, hence suppressing energy propagation in the horizontal plane. This enables the use of zero or a small number of reflectors when constructing a resonator, therefore significantly reducing the sensor size and fabrication cost. Moreover, as the SPC made of high aspect ratio electrodes increases the surface to volume ratio of the device, the number of binding sites for target biomolecules in a unit area increases accordingly, which improves the mass sensitivity of the device. A mass sensitivity of 12.9 $Hz/(ng \cdot cm)$ in water was achieved with resonators operating around 110 MHz [6, 7]. The proposed SPC resonator was theoretically studied by finite element method (FEM) and experimentally implemented by the classical lithography, electroplating, and molding (LIGA) process. The experimental data agree well with the theoretical predictions. The proposed acoustic radiation suppression method can also be applied in other types of acoustic waves, which makes it a general technique that can significantly push forward the performance boundary of many acoustic biosensors.

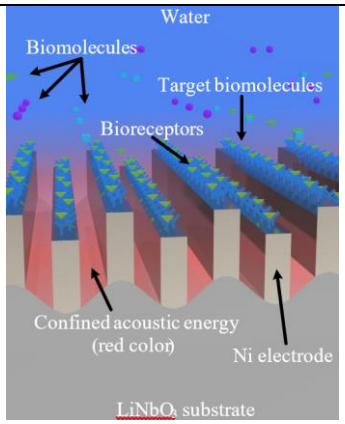

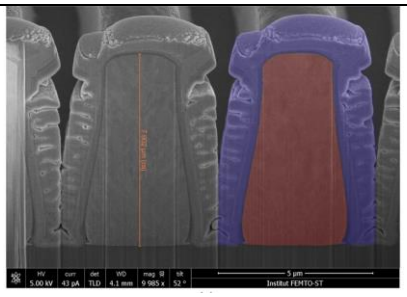

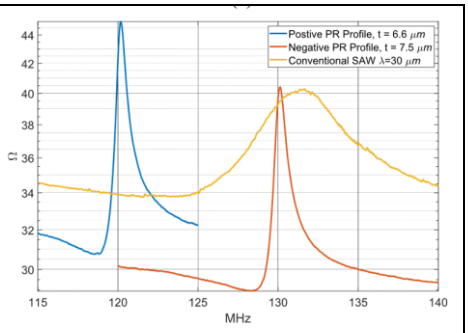

Figure 1: (left) Diagram of the SPC used for biomolecule detection. (Middle) SEM image of the Cross-section of SPC resonator with a high aspect ratio electrode fabricated with positive photoresist. (Right) Impedance magnitude curves of resonators and conventional Rayleigh SAW resonator in liquid

References

[1] I. Voiculescu, A. N. Nordin, Acoustic wave based mems devices for biosensing applications, Biosensors and Bioelectronics 33 (2012) 1–9.
[2] A. Mujahid, A. Afzal, F. L. Dickert, An overview of high frequency acoustic sensors—qcms, saws and fbars—chemical and biochemical applications, Sensors 19 (2019) 4395.
[3] G.N.Ferreira, A.-C.Da-Silva, B.Tomé, Acousticwavebiosensors: physicalmodelsandbiologicalapplicationsofquartzcrystalmicrobalance, Trends in biotechnology 27 (2009) 689–697.
[4] S. Song, D. Chen, H. Wang, C. Li, W. Wang, W. Yu, Y. Wang, Q. Guo, Shear mode bulk acoustic resonator based on inclined c-axis aln film for monitoring of human hemostatic parameters, Micromachines 9 (2018) 501.
[5] S. Song, D. Chen, H. Wang, Q. Guo, W. Yu, Shear mode bulk acoustic viscosity sensor for blood coagulation monitoring in oral anticoagulant therapy, Journal of nanoscience and nanotechnology 18 (2018) 8099–8104.
[6] Gao, F., Bermak, A., Benchabane, S. et al. Acoustic radiation-free surface phononic crystal resonator for in-liquid low-noise gravimetric detection. Microsyst Nanoeng 7, 8 (2021). https://doi.org/10.1038/s41378-020-00236-9
[7] F. Gao, A. Khelif, S. Benchabane and A. Bermak, "Shear Horizontal Phononic Metasurface for In-Liquid Gravimetric Biosensing," in *IEEE Electron Device Letters*, vol. 42, no. 6, pp. 915-918, June 2021, doi: 10.1109/LED.2021.3076046.

PHONONICS 2023: 6th International Conference on Phononic Crystals/Metamaterials/Metasurfaces, Phonon Transport, and Topological Phononics
Manchester, England, June 12-16, 2023
PHONONICS-2023-0073

Application of Periodic Electrical Boundary Conditions as a Means of Achieving Tunable RF SAW Devices

Ricardo Alcorta Galván[1], Charles Croënne[1], Bertrand Dubus[1], Brigitte Loiseaux[2], Etienne Eustache[2], Matthieu Bertrand[2], Anne-Christine Hladky-Hennion[1]

[1] Acoustics department, Univ. Lille, CNRS, Centrale Lille, Univ. Polytechnique Hauts-de-France, Junia, UMR 8520 - IEMN, 41 Bd Vauban, F-59000 Lille, France, ricardo.alcorta.g@gmail.com, charles.croenne@isen.fr, bertrand.dubus@isen.fr, anne-christine.hladky@isen.fr
[2] GRTM, Thales Research & Technology, 1 Av. Augustin Fresnel, 91120 Palaiseau, France, brigitte.loiseaux@thalesgroup.com, etienne.eustache@thalesgroup.com, matthieu-m.bertrand@thalesgroup.com

Abstract: Based on a single port SAW resonator, the reflection coefficient of its mirrors as a function of different periodic electrical boundary conditions is studied. Tunable Bragg band gaps as well as bands of high reflection coefficient due to electromechanical resonances of the mirror electrodes are shown. Finally, such tunable resonators are experimentally presented.

Switchable surface acoustic wave (SAW) devices are of major interest for telecommunication systems. Frequency bands for wireless communication are separated into frequency channels. Classically, a unique pass-band filter is needed for each channel that the receiver can address. The use of switchable pass-band filters which can address multiple frequency bands would allow for a significant reduction of the size of communication systems[1]. SAW filters, commonly used for these applications, are generally composed of inter-digital transducers inside of a cavity delimited by Bragg mirrors which allow the formation of resonant cavities in a given frequency band. These mirrors are formed by deposition of periodically spaced electrodes on the surface of a piezoelectric substrate.

The mirrors can thus be analysed as 1-D phononic crystals which present a Bragg band gap where propagation of elastic waves is prohibited. Previous research[2] have shown that for periodic structures composed of elastic/piezoelectric materials (piezoelectric phononic crystals), the band gap frequency is modified by the application of periodic electrical boundary conditions. In this presentation, the Electrical Bragg Band Gap concept is used to allow the commutability of SAW devices.

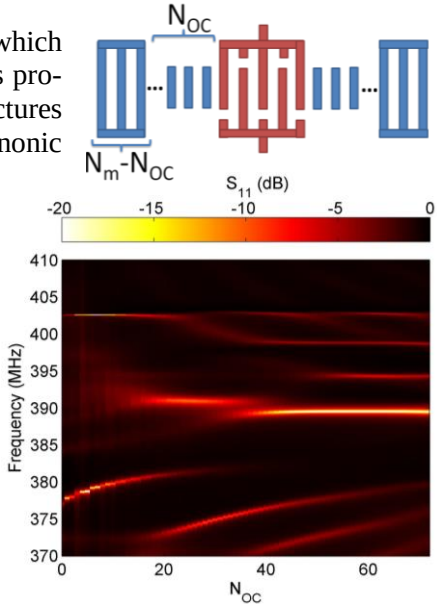

Figure 1 Proposed SAW resonator[3] (top) and S_{11} parameter of the device calculated by FEM simulations as a function of the number of floating potential electrodes N_{OC} (bottom).

A single port SAW resonator (Fig. 1-top) on $LiNbO_3$ substrate and working frequency of around 400 MHz was designed and finite element simulations are used to study the evolution of its resonance frequency as the mirror electrodes (72 in total) are switched from a grounded/short circuit (SC) to an floating potential/open circuit (OC) condition[3]. The resonator behaves like a classic Fabry-Perot cavity, resonance occurs when a phase condition between the transmission coefficient of the transducer at the center of the cavity and the reflection coefficient of the mirrors is met inside the bandgap for the mirrors (the bandgap frequencies for the SC and OC conditions are shown in Fig. 2, indicated by vertical dashed lines). At resonance, the electric S_{11} parameter (measured at the input of the transducer) presents a very low value since energy can be effectively injected into the cavity and converted into mechanical energy. Figure 1 presents the evolution of the S_{11} parameter as the 72 electrodes of both mirrors, on the right and on the left of the transducer, are switched one by one from a SC to an OC condition. Each vertical line of the figure shows the S_{11} parameter for a given number of OC electrodes from a fully grounded mirror (N_{OC} = 0) to a floating potential mirror (N_{OC} = 72). The resonance for the Rayleigh mode is present inside the SC bandgap when all the electrodes are grounded, at 377.4 MHz. As N_{OC} increases, the resonance shifts upwards

in frequency due to a modification of the phase of the mirror reflection coefficients. When N_{OC} = 40, the SC resonance is no longer present. Since a majority of the mirror presents the OC condition, the cavity resonance is near the upper edge of the OC bandgap, at around 389 MHz. It is thus possible to either perform a frequency shift or a frequency jump by changing the electrical condition of the mirror electrodes.

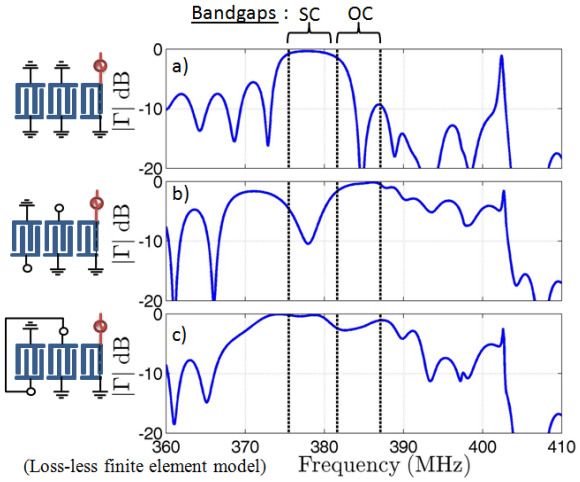

Figure 2 Schematic of the proposed interdigitated comb mirror SAW resonator for different electrical conditions (left) and mirror reflection coefficient for each electrical connection of the combs.

In order to reduce the number of switches required to perform a resonance frequency jump, resonators whose mirrors are made of interdigitated electrodes combs are now studied. The geometry of Figure 1 is conserved and the electrodes of the mirrors are grouped into a pair of 25 electrodes combs followed by a pair of 11 electrode combs (from the transducer outward). Figure 2 presents the reflection coefficient of such mirrors for 3 electrical conditions as well as a schematic of the resonator and the mirror connections. In figure 2a), the combs are connected to the ground. For figure 2b), one comb from each pair is left in floating potential. Finally in figure 2c), one of the 25 electrode combs and one of the 11 electrode combs are interconnected such that two contiguous electrodes in the mirror are interconnected and the resulting group is left in floating potential. As expected, in figure 2a), the mirror presents a high reflection coefficient inside the SC bandgap. By switching one comb from each pair to a floating potential, a sharp drop in the main lobe of the reflection coefficient occurs and, inside the OC bandgap, the reflection coefficient becomes higher. This should result in a jump of the resonance of the device, like in the case of figure 1. Interestingly in figure 2c) as expected, the reflection coefficient is high in a rather large band, larger than both the OC and GR bandgaps. This result is also in consistent with the electromechanical resonance of the floating potential comb which results in energy storage inside the cavity.

Figure 3 shows the measured S_{11} parameter of fabricated resonators presenting the electrical conditions of the mirrors of figure 2. The SC curve corresponds to the electrical condition of the mirror of figure 2a), S1 that of figure 2c) and OC that of figure 2b). Indeed a resonance frequency jump is clearly demonstrated by switching from between the SC and OC curves. For the S1 case, three resonances are present in the 376-390 MHz frequency range, which are indicative of a high reflection coefficient in this band, fully in agreement with the calculated mirror reflection coefficients presented in figure 2.

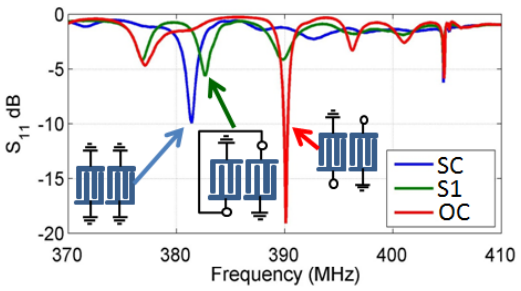

Figure 3 Measured S_{11} parameter of three fabricated resonators whose mirrors electrical conditions correspond to those shown in figures 2a-c).

References

[1] Hashimoto K., Tanaka S. and Esashi, "Tunable RF SAW/BAW filters: Dream or reality?," 2011 Joint Conference of the IEEE International Frequency Control and the European Frequency and Time Forum (FCS) Proceedings, pp. 1-8, 2011.
[2] Degraeve S., Granger C., Dubus B., Vasseur J., Pham Thi M., Hladky-Hennion A.-C., "Bragg band gaps tunability in an homogeneous piezoelectric rod with periodic electrical boundary conditions", J. Appl. Phys. 115, 194508 (2014).
[3] Alcorta Galván R., Croënne C., Dubus B., Loiseaux B., Eustache E., Bertrand M., and Hladky-Hennion A.-C., "Switchability of a single port SAW resonator using the electrical Bragg band gap," Applied Physics Letters 120, 203504 (2022).

Tuesday 13th June

PHONONICS 2023: 6th International Conference on Phononic Crystals/Metamaterials/Metasurfaces, Phonon Transport, and Topological Phononics
Manchester, England, June 12-16, 2023
PHONONICS-2023-0040

Phononic Skyrmions: a new horizon to structure acoustic and elastic waves ?

Badreddine Assouar, Liyun Cao, Sheng Wan, Yi Zeng & Yifan Zhu

Université de Lorraine, CNRS, Institut Jean Lamour, Nancy – France
badreddine.assouar@univ-lorraine.fr

Abstract: Skyrmion, a topologically stable three-component vector field, was initially developed in elementary particles and has since been demonstrated in condensed-matter systems. In this talk, I will report theoretically and experimentally on the existence of *phononic skyrmions* as new topological structures formed by the three-dimensional hybrid spin of elastic waves.

Elastic phonons form an excellent platform for carrying and processing information due to their unique advantages, including orders of magnitude lower phononic wavelength in comparison with photonic systems[1], scalability toward integrated devices[2], and extremely low losses[3]. The development of phonon physics has advanced the technology in high signal-to-noise information processing[3], high-sensitive remote sensing, and intense wave-matter interaction for future quantum networks[4]. Thus, in actual solid carriers with ubiquitous defects, realizing a new topological robust mode, i.e., phononic skyrmion, could lead to transformative phononic applications, especially in a generally concise configuration that can be scaled accordingly for future chip-scale technologies.

Recently, the hybrid spin induced by mixed transverse–longitudinal waves, which is responsible for abnormal phenomena beyond pure transverse waves and longitudinal waves (i.e., acoustic waves), has been uncovered in the elastic phononic system[5]. The hybrid spin can inspire strong spin-momentum locking of the elastic edge modes. However, the trivial topological invariant of the latter is not robust against defects[6]. In this talk, I will describe how to construct a new nontrivial topological structure of ultra-broadband phononic skyrmions based on the three-dimensional hybrid spin of elastic waves. It should, however, be pointed out that the formation of phononic and photonic skyrmions comes from different spin textures, with the latter being based on transverse wave spin.

In more details, I will talk about using spin angular momentum as a new degree of freedom to manipulate wave propagation. Some examples on photonic and acoustic systems generating skyrmions will be presented. I will then delineate the main part of this talk related to phononic/elastic skyrmions[7], and how we can use them as a powerful degree of freedom to generate more functionalities for engineering applications.

To illustrate the formation of phononic skyrmions by intrinsic hybrid spins, and to make the structure compact, we have built the skyrmion system in a thin plate model supporting the hybrid spin of the Lamb wave arising from the hybridization between the longitudinal wave and the transverse wave in the upper and lower plate interfaces. The three-dimensional hybrid spin field of plane Lamb waves can be expressed by the axial (out-of-plane) and transverse (in-plane) field components.

To produce the phononic skyrmions, we have designed a hexagonal meta-plate with pillared resonators (figure 1), and excited three pairs of counterpropagating plane Lamb waves with hybrid spins along with the directions of $\theta = 0°$, $60°$, and $-60°$, as shown in Fig. 1A. The corresponding wavenumber of these exciting plane waves can be presented by six points in the momentum space (the lower right corner of Fig. 1A). The interference of these wave fields constructs the three-dimensional skyrmion lattice configuration of the real wavefield.

The Ultra-broadband and tunable characteristic of phononic skyrmions have been also investigated. Actually, for classical waves, constructed photonic[8] or acoustic[9] Néel-type skyrmions, with the former based on transverse waves and the latter based on longitudinal waves, require an evanescent wave field to create the three-dimensional wave fields. Once their carrier structure is designed, these skyrmions have a limited bandwidth since the evanescent waves in the near field can be only visualized in

a narrow frequency band. In this talk, I will show that phononic skyrmions have an ultra-broadband topological robustness feature, due to the frequency-independent three-dimensional hybrid spin texture of the elastic wave (A0-mode wave).

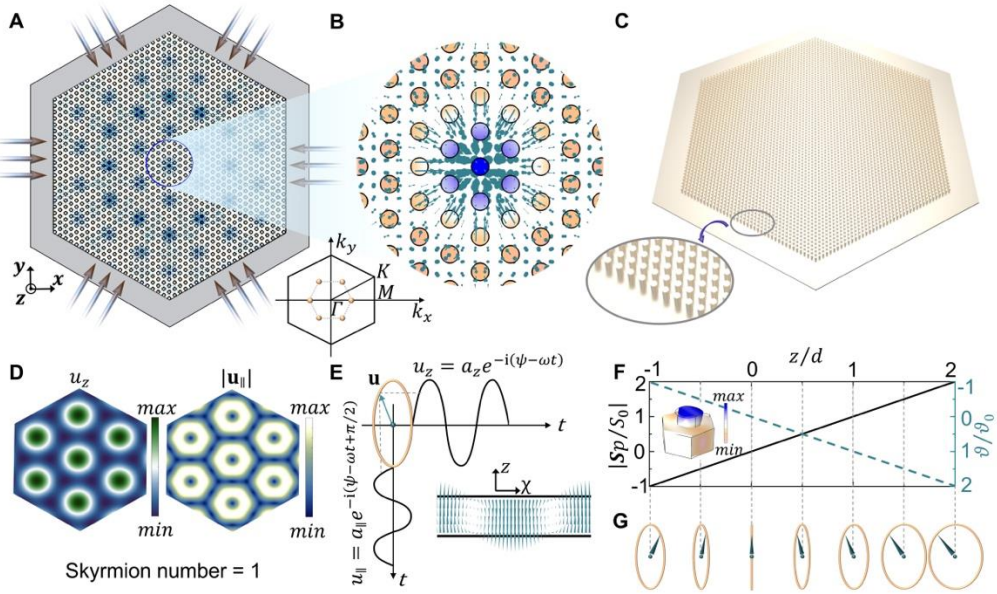

Figure 1: Formation of phononic skyrmions. (A) The interference of three pairs of counterpropagating plane Lamb waves with hybrid spins construct the phononic skyrmion lattice in a hexagonal elastic meta-plate. (B) Enlarged view of the local vector field. (C) The meta-plate with periodically pillared resonators. (D) The theoretical axial (out-of-plane) u_z and transverse $u_\parallel$ (in-plane) fields of the skyrmion lattices. (E) The axial and transverse fields have a phase difference of pi/2, creating a spiral spin geometry with an elliptical trajectory. The inset is a spin vector field at the plane formed by the z-axis and χ-axis (same as the direction vectors k). (F) The inset shows a unit structure with six-fold rotational symmetry, including an oscillating non-resonant pillared resonator on the hosting plate with a thickness of h. The resonator with the height of l (here $l = h/2 = d$ = 0.5 mm at the frequency of 8 kHz) can linearly amplify spin angular momentum and the polarization along the z-axis (-d<z<2d). The coordinate origin is on the neutral plane of the hosting plate. The S_0 and ϑ_0 are the spin angular momentum magnitude and the polarization on the plate surface (i.e., $z = d$). (G) The elliptical spin trajectories of different particles along the plate thickness.

References

[1] S. H. Mousavi, A. B. Khanikaev, Z. Wang, *Topologically protected elastic waves in phononic metamaterials. Nat. Commun.* **6**, 8682 (2015).
[2] R. H. Olsson Iii, I. El-Kady, *Microfabricated phononic crystal devices and applications. Measurement Science and Technology* **20**, 012002 (2008).
[3] S.-Y. Yu, C. He, Z. Wang, F.-K. Liu, X.-C. Sun, Z. Li, H.-Z. Lu, M.-H. Lu, X.-P. Liu, Y.-F. Chen, *Elastic pseudospin transport for integratable topological phononic circuits. Nat Commun.* **9**, 3072 (2018).
[4] B. Vermersch, P.-O. Guimond, H. Pichler, P. Zoller, *Quantum state transfer via noisy photonic and phononic waveguides*. *Phys Rev Lett* **118**, 133601 (2017).
[5] Y. Long, J. Ren, H. Chen, *Intrinsic spin of elastic waves*. *Proceedings of the National Academy of Sciences* **115**, 9951-9955 (2018).
[6] W. Yuan, C. Yang, D. Zhang, Y. Long, Y. Pan, Z. Zhong, H. Chen, J. Zhao, J. Ren, *Observation of elastic spin with chiral meta-sources. Nat Commun.* **12**, 6954 (2021).
[7] L. Cao, S. Wan, Y. Zeng, Y. Zhu & M. B. Assouar, *Observation of phononic skyrmions based on hybrid spin of elastic waves. Science Advances* **9**, eadf3652 (2023).
[8] S. Tsesses, E. Ostrovsky, K. Cohen, B. Gjonaj, N. H. Lindner, G. Bartal, *Optical skyrmion lattice in evanescent electromagnetic fields. Science* **361**, 993-996 (2018).
[9] H. Ge, X.-Y. Xu, L. Liu, R. Xu, Z.-K. Lin, S.-Y. Yu, M. Bao, J.-H. Jiang, M.-H. Lu, Y.-F. Chen, *Observation of Acoustic Skyrmions*. *Phys Rev Lett.* **127**, 144502 (2021).

PHONONICS 2023: 6th International Conference on Phononic Crystals/Metamaterials/Metasurfaces, Phonon Transport, and Topological Phononics
Manchester, England, June 12-16, 2023
PHONONICS-2023-0162

Ultrawide Phononic Band Gaps

Cetin Yilmaz[1]

[1] *Department of Mechanical Engineering, Bogazici University, 34342 Bebek, Istanbul, Turkey*
cetin.yilmaz@boun.edu.tr

Abstract: For phononic crystals and elastic metamaterials, a major and practical challenge is to obtain ultrawide phononic band gaps. Ultrawide phononic band gaps can be beneficial in vibration isolation, elastic wave shielding or seismic applications. This paper will comparatively investigate phononic crystals and elastic metamaterials that possess ultrawide phononic band gaps.

Periodic structures can be used to prevent the transmission of vibrations or elastic/acoustic waves in certain frequency ranges known as vibration stop bands or phononic band gaps. In the literature, Bragg scattering or local resonance methods are frequently used to obtain phononic band gaps[1]. In Bragg scattering[2,3], frequency of the lowest phononic band gap is determined by the ratio of the wave propagation speed to the size of the unit cell in a periodic structure. Hence, materials with low elastic modulus and high density or large size structures are necessitated to generate band gaps at low frequencies. Local resonators[4,5] can provide band gaps below the Bragg limit. However, heavy resonators are required to generate wide band gaps with this method[5,6]. Periodic structures that use Bragg scattering method are generally referred as phononic crystals, while the ones that utilize the local resonance method are generally referred as elastic metamaterials as band gaps can be obtained below the Bragg limit.

In 2007, an alternative band gap generation method based on inertial amplification was introduced[1]. In this method, the effective mass of a structure can be increased with embedded mechanisms. Essentially, when an inertially amplified structure is subject to vibrations, its effective mass can be orders of magnitude larger than its static mass. As heavy structures are hard to move, vibration or wave propagation can be very effectively hindered. Consequently, wide band gaps at low frequencies can be obtained[1,7]. Inertial amplification method allows to generate band gaps below the Bragg limit. Hence, periodic structures with embedded inertial amplification mechanisms are also considered as elastic metamaterials.

There are various studies with wide phononic band gaps in one-dimension[8-11], two-dimensions[12-16] and three-dimensions[17-21]. In order to compare the bandwidths in various studies, arithmetic mean normalized bandwidth (BW_a) or geometric mean normalized bandwidth (BW_g) can be used, i.e.,

$$BW_a = \frac{\omega_u - \omega_l}{(\omega_u + \omega_l)/2} \tag{1}$$

$$BW_g = \frac{\omega_u - \omega_l}{\sqrt{\omega_u \omega_l}} \tag{2}$$

where ω_u and ω_l are the upper and lower limits of the band gap. For narrow band gaps in which ω_u is at most 10% higher than ω_l, $BW_a \cong BW_g$. For wider band gaps, BW_a can be significantly different than BW_g. Note that as $\omega_u/\omega_l \to \infty$, $BW_a \to 200\%$. Although BW_a is commonly used in the literature, it is not very effective in differentiating very large bandwidths. On the other hand, as $\omega_u/\omega_l \to \infty$, $BW_g \to \infty$. Thus, BW_g can better characterize wide band gaps.

The lowest frequency phononic band gap in a structure can have a lower limit at zero frequency or at a higher frequency depending on the stiffness characteristics. In particular, when the unit cell of a periodic structure possesses zero stiffness along the excitation direction[22-23], then the first band gap can start at zero frequency ($\omega_l = 0$). As the upper limit of the band gap is finite, $\omega_u/\omega_l \to \infty$. Consequently, $BW_a \to 200\%$ and $BW_g \to \infty$. On the other hand, for some applications such as vibration or seismic isolation, zero stiffness may not be desirable as small static load changes may result in excessive deformations.

For a three-dimensional structure that possesses positive stiffness along all axes, there should be at least three branches (corresponding to one longitudinal mode and two transverse modes) below the first band gap. When the studies with very wide band gaps are considered[18-21], it can be seen that there are much more than three branches below their first band gaps. Hence, the unit cells in these studies experience several vibration modes until the first band gap appears. In essence, it is difficult to obtain an ultrawide phononic band gap at low frequencies. However, inertial amplification method can provide significant advantages when the aim is to obtain low-frequency ultrawide phononic band gaps.

In this invited talk, various structures with ultrawide phononic band gaps will be shown. Recent advances and challenges will be summarized and future outlook will be given.

Acknowledgement
Cetin Yilmaz acknowledges the support from the Turkish Academy of Sciences Distinguished Young Scientist Award (TUBA-GEBIP).

References

[1] C. Yilmaz, G.M. Hulbert, and N. Kikuchi, *Phys. Rev. B* **76** (5), 054309 (2007).
[2] M. M. Sigalas, *J. Sound Vib.* **158** (2) 377–382 (1992).
[3] M. Sigalas and E. N. Economou, *Solid State Commun.* **86** (3) 141–143 (1993).
[4] Z. Liu, X. Zhang, Y. Mao, Y. Y. Zhu, Z. Yang, C. T. Chan, and P. Sheng, *Science* **289** (5485) 1734–1736 (2000).
[5] C. Goffaux and J. Sanchez-Dehesa, *Phys. Rev. B* **67** (14) 144301 (2003).
[6] Z. Liu, C.T. Chan, and P. Sheng, *Phys. Rev. B* **65** (16), 165116 (2002).
[7] C. Yilmaz and G.M. Hulbert, *Phys. Lett. A* **374** (34), 3576–3584 (2010).
[8] J.H. Oh, S. Qi, Y.Y. Kim, and B. Assouar, *Phys. Rev. Appl.* **8** (5) 054034 (2017).
[9] S. Taniker and C. Yilmaz, *Int. J. Solids Struct.* **106** 129–138 (2017).
[10] H.W. Park, H.M. Seung, M. Kim, W. Choi, and J.H. Oh, *Phys. Rev. Appl.* **15** (2) 024008 (2021)
[11] S. Park and W. Jeon, *J. Sound Vib.* **499** 115977 (2021)
[12] O.R. Bilal and M.I. Hussein, *Phys. Rev. E* **84** (6) 065701 (2011).
[13] S. Jiang, H. Hu, and V. Laude, *Phys. Status Solidi (RRL)* **12** (2) 1700317 (2018).
[14] G. Wen, H. Ou, and J. Liu, *Mater. Today Commun.* **24**, 100977 (2020).
[15] O. Yuksel and C. Yilmaz, *Int. J. Solids Struct.* **203** 138-150 (2020).
[16] Y. Li, S. Yan, and Y. Peng, *Thin-Walled Struct.* **183** 110418 (2023).
[17] S. Taniker and C. Yilmaz, *Int. J. Solids Struct.* **72** 88–97 (2015).
[18] L. D'Alessandro, A. O. Krushynska, R. Ardito, N. M. Pugno, and A. Corigliano, *Sci. Rep.* **10** (1) 16403 (2020).
[19] Muhammad and C. W. Lim, *Arch. Civ. Mech. Eng.* **21** 1–11 (2021).
[20] Muhammad and C. W. Lim, *Sci. Rep.* **11** 1–11 (2021).
[21] J. Martinez, J. Moughames, G. Ulliac, M. Kadic, and V. Laude, *Appl. Phys. Lett.* **118** 063507 (2021).
[22] J.H. Oh and B. Assouar, *Sci. Rep.* **6** (1) 1-10 (2016).
[23] J.H. Oh, S.J. Choi, J.K. Lee, and Y.Y. Kim, *New J. Phys.* **20** (8) 083035 (2018).

PHONONICS 2023: 6th International Conference on Phononic Crystals/Metamaterials/Metasurfaces, Phonon Transport, and Topological Phononics
Manchester, England, June 12-16, 2023
PHONONICS-2023-0218

Acoustic Wave Propagation through Resonant Meta-Materials; an Asymptotic Analysis

I. David Abrahams[1] , Mike Smith[1]

[1] Department of Applied Mathematics and Theoretical Physics, University of Cambridge, Wilberforce Road, Cambridge CB3 0WA, United Kingdom
ida20@cam.ac.uk, smith.mike943@gmail.com

Abstract: This presentation will outline a model for two-dimensional resonant acoustic meta-materials. The simple geometry, and low frequency limit (scatterer size to acoustic wavelength), allows for asymptotic analysis to be employed to obtain explicit analytical expressions for both periodic and random materials. Results show the strong effects of resonance on wave propagation.

Introduction Reducing low-frequency noise is an ongoing challenge in all parts of industry, from wind turbines, fans and vacuum cleaners through to vehicle noise (engines, tyres, underwater and aero-acoustically generated sound). Although this subject has been a source of research going back to the time of Lord Rayleigh, there has been recent intense study on the shielding or isolation of noise via exotic composite structures, often referred to as meta-materials. Such materials, demonstrated in electromagnetic applications, can yield negative refractive index, band-gaps, strong anisotropy etc. The application of these ideas in acoustics or elasticity is less well developed due to some specific challenges related to the realization of mechanical metamaterials, and so such materials have not yet found wide application.

Recently the authors have developed an analytic approach for simple composites composed of resonant inclusions, that can exhibit strong behaviour even at very low frequencies. We broadly outline the solution procedure in our talk, for a periodic arrangement of cylindrical inclusions (Figure 1), and obtain an explicit form of the dispersion equation in the low frequency regime. Our methodology, which employs multipole expansions and matched asymptotic expansions, is easily generalizable to a wide choice of inclusions/host materials in many application areas, in both two and three dimensions. The explicit formulae that we derive allow rapid exploration of parameter space and hence help reduce prototyping overheads.

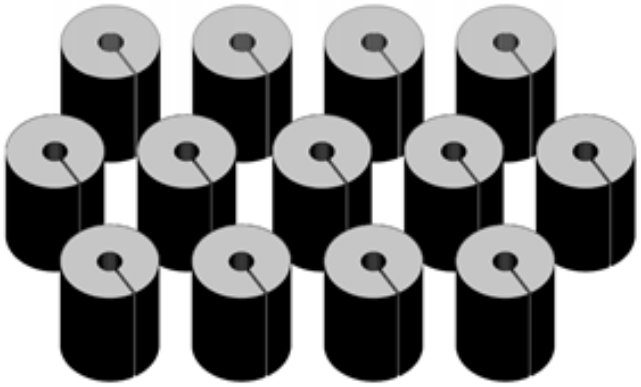

Figure 1 A periodic array of rigid walled cylinders containing a slit connecting the exterior to an interior cavity.

Single scatterer model We commence discussions with a single infinite cylinder[1], and examine its scattering of a monochromatic plane wave as we increase the incident wave frequency. The cylinder has a small slit, or aperture, which connects the exterior to an interior cavity, as shown in Figure 1. The exterior and interior fields are modelled using multipole methods and the two are related via asymptotic 'matching' to the field local to the aperture – this yields explicit expressions for the multipole coefficients. The cylinder is shown to act as a Helmholtz resonator (HHR), and so as the frequency is increased, the field passes through the HHR frequency as well as higher (interior) resonances. The scattering cross-section for this body, for particular values of the cylinder radius, slit width, and inner radius is plotted in Figure 2: one

can see the significant increase in scattering through the Helmholtz resonance compared with the scattering cross-section for a closed rigid cylinder (dashed line).

Multiple scattering model (periodic) The fundamental scatterer can be integrated into a periodic array using the same mathematical formulation[2,3]: multipole methods and matched asymptotic expansions, with the addition now of a lattice sum which accounts for the periodic arrangement of cylinders. The algebra is significantly more complicated, but at low frequency (i.e. cylinder radius and spacing small compared with the incident wavelength) explicit expressions can be deduced from which the band diagram can be plotted. The effect of the HHR is to create a gap (stop band) within the first band at very low frequencies as shown by the contrast between a closed cylinder (Figure 3) and open cylinder (Figure 4).

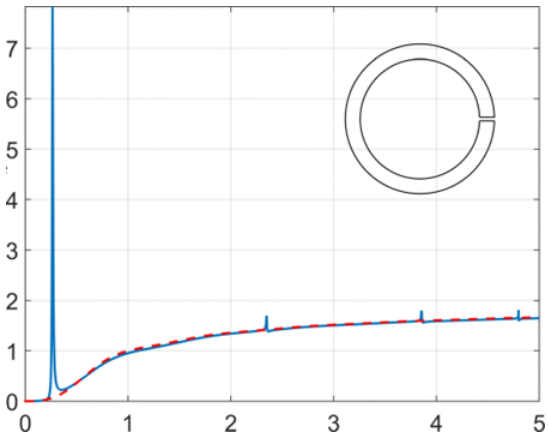

Figure 2 Scattering cross-section for single cylinder with small aperture (dashed line is that for a closed cylinder.)

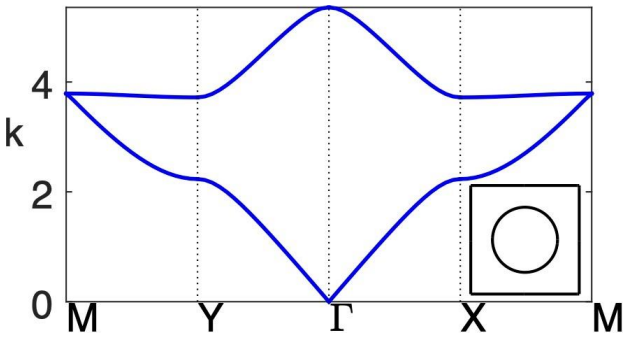

Figure 3 Band diagram for a square array of rigid closed (Neumann cylinders.)

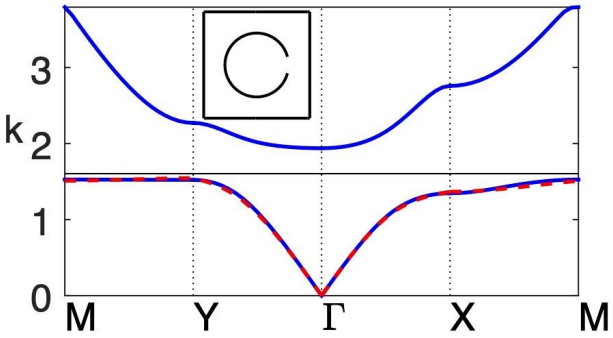

Figure 4 Band diagram for a square array of thin-walled resonant cylinders (dashed line is from a FE calculation.)

Multiple scattering model (random) Finally, we will present recent results for the propagation characteristics of infinite and semi-infinite acoustic meta-media composed of the aforementioned HHR cylinders, but now distributed randomly within the host. The approach for rigid closed (Neumann) cylinders[4,5] is generalised to the present HHR cylinder case; that is, the field is ensemble averaged over all inclusion locations, and then a quasi-crystalline approximation is made to close the system. The differences found between the media when composed of closed and open cylinders will be discussed, as will the variation between random and periodic distributions.

Future work The approach described above is generalizable to a wide range of geometries of both scatterer and distribution, in both two and three dimensions, and for elastic as well as acoustic models.

References

[1] M. J. A. Smith *et al.*, *Phil. Trans. R. Soc. A* **380**, 20210383 (2022). (http://doi.org/10.1098/rsta.2021.0383)
[2] M. J. A. Smith, and I. D. Abrahams, *Proc. R. Soc. A* **478**, 20220124 (2022). (http://doi.org/10.1098/rspa.2022.0124)
[3] M. J. A. Smith, and I. D. Abrahams, *Proc. R. Soc. A* **478**, 20220125 (2022). (http://doi.org/10.1098/rspa.2022.0125)
[4] A. L. Gower, W. J. Parnell, and I. D. Abrahams, *SIAM J. Appl. Math.* **79**(6), 2569-2592 (2019). (http://doi.org/10.1137/18M122306X)
[5] A. L. Gower, I. D. Abrahams, and W. J. Parnell, *Proc. R. Soc.* A **475**, 20190344 (2019). (http://doi.org/10.1098/rspa.2019.0344)

PHONONICS 2023: 6th International Conference on Phononic Crystals/Metamaterials/Metasurfaces, Phonon Transport, and Topological Phononics
Manchester, England, June 12-16, 2023
PHONONICS-2023-0177

Lamb waves in discrete waveguides: unidirectional waves and mechanical switching networks

Giorgio Carta[1], Michael J. Nieves[2], Michele Brun[1]

[1] *Department of Mechanical, Chemical and Materials Engineering, University of Cagliari, Italy*
giorgio_carta@unica.it, mbrun@unica.it
[2]*School of Computer Science and Mathematics Department, Institution, Address, Country*
m.nieves@keele.ac.uk

Abstract: Lamb wave propagation in either a monoatomic or a biatomic triangular lattice is considered. The vector problem of elasticity has been solved analytically for a generic number of rows within the waveguide thickness. The model is exploited to design a structured medium capable of manipulating wave modes, and, through conversion and selection, to generate unidirectional wave phenomena. Additionally, by introducing a gyroscopic effect due to the presence of attached spinners a *Mechanical Switching Network* (MSN) is obtained.

We consider a waveguide consisting of a triangular array of point masses connected by non-inertial elastic links. The masses can also be attached to gyroscopic spinners, which couple the in-plane displacement components of the masses. For small nutation angle the gyroscopic spinners are characterised mechanically by the constant "effective gyricity", denoted by Ω^*, sum of the initial precession and spin rates.

The in-plane vector problem of elasticity is solved analytically in the time-harmonic regime, the governing equations of the particles inside the bulk are accompanied by the free boundary conditions on the upper and lower boundaries for both the cases without[1] and with[2] gyroscopic spinners. The dispersion curves for the periodic strip exhibit a semi-infinite band-gap at higher frequencies and their number is finite and exactly equal to twice the number of the lattice rows. In the transient regime, the solution for a concentrated applied load is based on the use of Laplace and discrete Fourier transforms[2]. Homogenisation limits and the behavior for a large number of rows are analysed in detail.

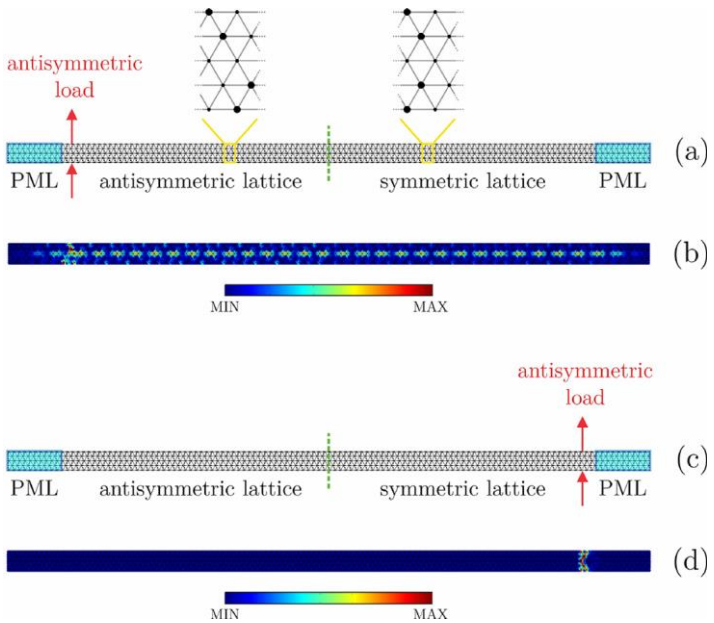

Figure 1 Antisymmetric lattice (left inset) and symmetric lattice (right inset). An antisymmetric time-harmonic load of frequency $\omega = 1.25$ is imposed at the (a) left and (c) right of the strip, as indicated by the arrows.

In Figure 1 it is shown how the structured medium, through conversion and selection, generates unidirectional wave phenomena. Two diatomic lattices are considered, joined at the center of the waveguide. In the insets of part (a) the antisymmetric and symmetric lattices are reported. In part (a), an antisymmetric time-harmonic load is applied at the left of the structure at the frequency $\omega = 1.25$ rad/s, that corresponds to a propagating hybrid mode in the antisymmetric lattice and a symmetric mode in the symmetric lattice. The wave generated by the antisymmetric load becomes hybrid when travels through the antisymmetric lattice and its symmetric component can propagate to the right. In part (c) the same load is applied near the right end of the strip. Being antisymmetric, it cannot propagate through the symmetric lattice since that frequency corresponds to a symmetric mode.

Alternatively, attaching a spinner to each mass it is possible to exploit non-reciprocity induced by gyroscopic effect[3,4] to design a network with an internal lattice structure, where the destination of Lamb waves generated by an external excitation can be chosen in order to create a *Mechanical Switching Network* (MSN)[2].

G.C. and M.B.'s work has been performed under the auspices of GNFM-INDAM. M.J.N. gratefully acknowledges the support of the EU H2020 grant MSCA-RISE-2020-101008140-EffectFact.

References

[1] G. Carta, M. J. Nieves and M. Brun, *Eur. J. Mech. A Solids*, 104695 (2022).
[2] G. Carta, M. J. Nieves and M. Brun submitted to *Eur. J. Mech. A Solids.*
[3] M. J. Nieves, G. Carta, V. Pagneux and M. Brun, *Int. J. Eng. Sci.*, **156**, 103365 (2020).
[4] M. J. Nieves, G. Carta, V. Pagneux and M. Brun, *Front. Mater.*, **7**, 602960 (2021).

PHONONICS 2023: 6th International Conference on Phononic Crystals/Metamaterials/Metasurfaces, Phonon Transport, and Topological Phononics
Manchester, England, June 12-16, 2023
PHONONICS-2023-0216

Shape Morphing and Elastic waves in Metamaterials

Lianchao Wang, Krzysztof Dudek, Julio Iglesias, Gwenn Ulliac, Vincent Laude, Muamer Kadic

Université de Franche-Comté, Institut FEMTO-ST, CNRS, 25000 Besançon, France

Abstract: In this talk, we will review auxetic metamaterials for shape morphing and for elastic waves. We will remind the reader of the general concept of auxeticity, the implication on waves, and how we can tune wave properties via shape morphing or external stimulus.

In continuum mechanics, one of the oldest meta properties is probably the auxeticity. It was first shown by Lakes in foams. Auxetics have a negative Poisson's ratio along one or more directions. From the general metamaterial aspect, they contract in the orthogonal one when compressed in a given direction (S). This static aspect is not directly translated to any wave property.

In this presentation, we will first show a few examples of auxetic metamaterials [1] which are good candidates for large strain deformations (see Figure 1). Then we will look at some auxetics which can be programmed in the spirit of shape morphing [2] and we will analyze their properties either when simply compressing them or by applying an external field such as the magnetic field [3].

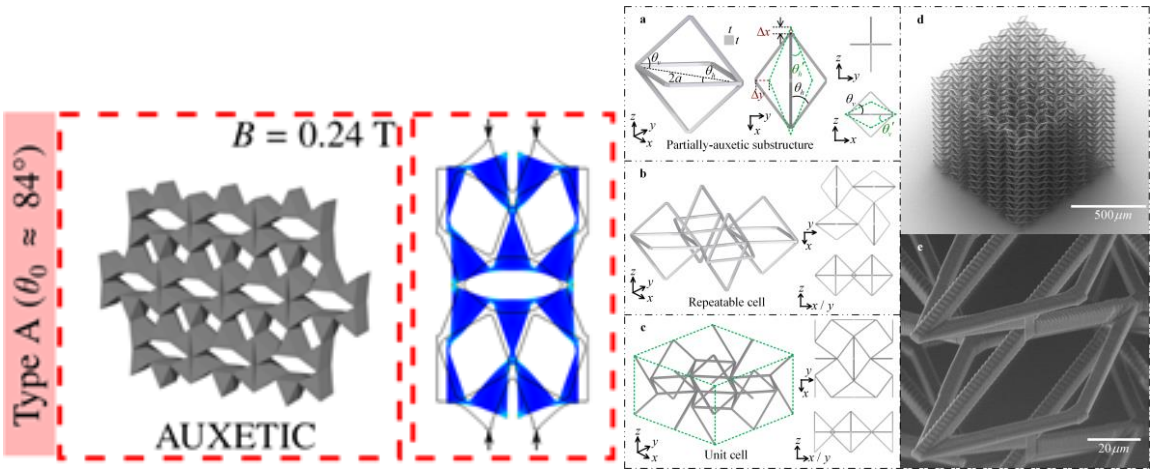

Figure 1: (left) auxetic structure deforming under an external magnetic field. (right) example of an auxetic structure with a continuous phase transition in elastic properties. Taken from [3] and [2].

References

[1] Dudek, Krzysztof K., et al. "Micro-scale auxetic hierarchical mechanical metamaterials for shape morphing." Advanced Materials 34.14, 2110115 (2022).
[2] Wang, Lianchao, et al. "3D Auxetic Metamaterials with Elastically-Stable Continuous Phase Transition." Advanced Science, 2204721 (2022).
[3] Dudek, Krzysztof K., et al., Advanced Materials, 2210993 (2023).

Active Thermal Cloaking

Maxence Cassier[1], Trent DeGiovanni[2], Sébastien Guenneau[3], Fernando Guevara Vasquez[2]

[1] *Aix-Marseille Univ, CNRS, Centrale Marseille, Institut Fresnel, 13397, Marseille, France*
maxence.cassier@fresnel.fr
[2] *University of Utah, Mathematics Department, Salt Lake City UT 84112, USA*
degiovan@math.utah.edu , fguevara@math.utah.edu
[3] *The Blackett Laboratory, Department of Physics, Imperial College London, London, SW7 2AZ, UK*
s.guenneau@imperial.ac.uk

Abstract: We propose two methods for cloaking objects from thermal measurements that rely on active sources instead of bulky metamaterials. One method deals with the parabolic heat equation, in which case active sources should completely surround the object to cloak. Another method, for which the sources need not completely surround the object to cloak, relies on a Helmholtz equation with complex wave numbers, counterpart of the heat equation in the frequency domain. This second method extends the active exterior cloaking for waves modelled with the Helmholtz equation from positive wavenumbers to complex ones, allowing for active cloaking in various physical contexts, including wave in dissipative and dispersive media.

Introduction

Control of heat diffusion at a macroscopic scale in so-called thermal metamaterials[1] can be modelled with the Fourier equation, wherein one assumes that the temperature field $u(x,t)$ of a homogeneous isotropic body satisfies the parabolic heat equation

$$\frac{\partial u}{\partial t} = \sigma \Delta u + h, \text{ for } t > 0, \tag{1}$$

with σ the thermal diffusivity (a scalar constant), h a source term and Δ the Laplacian in 2D. However, a deeper understanding of the physics at work in heat diffusion requires studying phonon propagation at an atomistic scale[2] and so there is a clear connection between thermal cloaking challenges and physical problems addressed by the research community of the Phononics conference series.

Cloaking of heat in the transient regime was first proposed via a coordinate change in (1) and this led to an anisotropic heterogeneous diffusivity[3]. Such transient thermal cloaking was experimentally confirmed with a metamaterial cloak[4]. Many research groups have contributed to the design of thermal metamaterials, including making use of deep learning algorithms[5] and this field of transformation thermodynamics is now quite mature[1]. However, managing thermal fields does not necessarily require the use of bulky metamaterials. Let us explore the alternative route of active thermal cloaking.

Active Thermal Cloaking with a large number of sources

Our strategy is to find sources for the heat equation (1) in a homogeneous medium that generate a cloaking temperature field $u_c(x,t)$ that cancels out a probing temperature field $u_i(x,t)$ inside a region Ω without perturbing the total temperature field outside Ω. By linearity of the heat equation the total temperature field $u_c(x,t) + u_i(x,t)$ vanishes inside Ω allowing us to hide e.g. an inclusion with zero temperature on its boundary (a homogeneous Dirichlet boundary condition). This total field is identical to the field $u_i(x,t)$ outside of Ω, making it impossible to detect the inclusion solely based on thermal measurements outside of Ω. Other cloaking temperature fields may be needed to deal with inclusions with different boundary conditions (e.g. homogenous Neumann data for a perfect insulator).
Fortunately, the Green identities show that a distribution of monopoles and dipoles supported on $\partial\Omega$ can provide the desired cloaking field[6]. This cloaking method inspired by [7] comes with two main drawbacks: (a) the incident field $u_i(x,t)$ needs to be known ahead of time and (b) the sources needed to generate the cloaking field completely surround the object, as shown in Figure 1(a-d).
To circumvent drawback (b), we consider the Fourier-Laplace transform $u(x,\omega)$ of $u(x,t)$ given by

$$u(x,\omega) = \int_0^\infty dt\ \exp[i\omega t]u(x,t), \tag{2}$$

with ω the angular frequency, that satisfies the Helmholtz equation

$$\Delta u(x,\omega) + (i\omega/\sigma)u(x;\omega) = -h(x,\omega)\ , \tag{3}$$

with a complex wavenumber k given by $k^2 = \imath\omega/\sigma$ and h the Fourier-Laplace transformed source.

Thanks to (3), we can achieve active exterior cloaking by generalizing the approach in [8,9] from real positive wavenumbers to complex wavenumbers and then take the inverse Fourier-Laplace transform to recover time domain sources for the heat equation that satisfy our requirements. The approach in [8,9] heavily relies on the Graf addition formula that essentially takes the many monopole and dipole sources surrounding the object and relocate them on a minimum of 3 points in 2D (and 4 in 3D, see [9]). At these points, one now has multipole sources that achieve active cloaking. A numerical example borrowed from [10] is shown in Figure 1(e) in the case of four multipole sources.

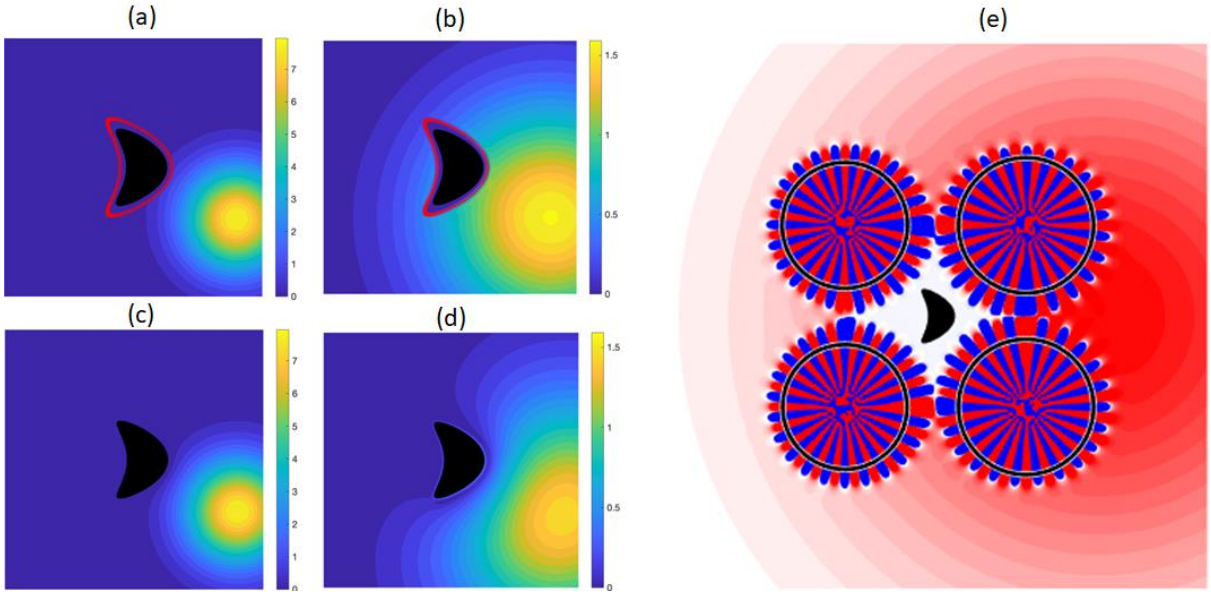

Figure 1 Numerical examples of active thermal cloaking routes for an object to hide having homogeneous Dirichlet boundary conditions. Images (a), (b) show time snapshots of the object when the cloak consisting of a large number of monopole and dipole sources is active and images (c), (d) the corresponding snapshots when the cloak is unactive (adapted from [6]). Image (e) corresponds to same object surrounded by only four multipolar sources (adapted from [10]) at a given complex wavenumber.

References

[1] Ji-Ping Huang Theoretical Thermotics Transformation Thermotics and Extended Theories for Thermal Metamaterials, 1st edition, Singapore, Springer 2021
[2] M.I. Hussein, M.J. Leamy, M. Ruzzene, *Applied Mechanics Reviews* **66**, 040802 (2014).
[3] S. Guenneau C. Amra, D. Veynante, *Optics Express* **20**, 8207–8218 (2012).
[4] R. Schittny, M. Kadic, S. Guenneau, M. Wegener, *Physical Review Letters* **110**, 195901 (2014).
[5] Q. Ji, X. Chen, J. Liang, V. Laude, S. Guenneau, G. Fang, M. Kadic, *International Journal of Heat and Mass Transfer* **169**, 120948 (2021).
[6] M. Cassier, T. DeGiovanni, S. Guenneau, F. Guevara Vasquez, *Proceeding of the Royal Society of London A* **477**, 20200941 (2021).
[7] D.A.B. Miller, *Optics Express* **14**, 12457-12466 (2006).
[8] F. Guevara Vasquez, G.W. Milton, D. Onofrei, *Wave Motion* **48**, 515-524 (2011).
[9] A.N. Norris, F.A. Amirkulova, W.J. Parnell, *Inverse Problems* **28**, 105002 (2012).
[10] M. Cassier, T. DeGiovanni, S. Guenneau, F. Guevara Vasquez, *Philosophical Transactions of the Royal Society A* **380**, 20220073 (2022).

PHONONICS 2023: 6th International Conference on Phononic Crystals/Metamaterials/Metasurfaces, Phonon Transport, and Topological Phononics
Manchester, England, June 12-16, 2023
PHONONICS-2023-0194

Roton-like Dispersion Relations in Designed Elastic Crystals

Martin Wegener[1]

[1] *Institute of Applied Physics, Karlsruhe Institute of Technology (KIT), 76128 Karlsruhe, Germany*
[2] *Institute of Nanotechnology, Karlsruhe Institute of Technology (KIT), 76128 Karlsruhe, Germany*
martin.wegener@kit.edu

Abstract: We review our work on mimicking the dispersion relation of rotons in liquid helium in elastic system using three different strategies, namely via periodic three-dimensional nonlocal metamaterials, three-dimensional chiral metamaterials, and three-dimensional monomode metamaterials.

The roton dispersion relation in liquid helium starts with frequency being proportional to wavenumber, followed by a maximum, a region of backward waves, a minimum, and a further increase of frequency versus wavenumber.

We start by briefly reviewing our work towards mimicking this dispersion relation in elastic and acoustic metamaterials [1,2] by using nonlocal interactions.

We emphasize in this talk more recent work on achieving similar roton-like dispersion relations by two different mechanisms, namely by chirality in the sense of chiral micropolar (Eringen) elasticity [3] and by back-folding of the soft mode in monomode metamaterials in the sense of Cauchy elasticity [4].

In all cases [1-4], roton-like behavior is achieved for the lowest band.

I thank all of the authors on the below references for their corresponding contributions. This research has been funded by the Deutsche Forschungsgemeinschaft (DFG, German Research Foundation) under Germany's Excellence Strategy via the Excellence Cluster “3D Matter Made to Order” (EXC-2082/1-390761711), which has also been supported by the Carl Zeiss Foundation through the “Carl-Zeiss-Foundation-Focus@HEiKA”, by the State of Baden-Württemberg, and by the Karlsruhe Institute of Technology (KIT). We further acknowledge support by the Helmholtz program “Materials Systems Engineering” (MSE) and by the Karlsruhe School of Optics & Photonics.

References

[1] Y. Chen, M. Kadic, and M. Wegener, Nature Commun. 12, 3278 (2021)
[2] J. A. Iglesias Martinez, M.F. Groß, Y. Chen, T. Frenzel, V. Laude, M. Kadic, and M. Wegener, Science Adv. 7, eabm2189 (2021).
[3] Y. Chen, J.L.G. Schneider, M. Groß, K. Wang, C. Wang, M. Kadic, and M. Wegener, submitted (2023)
[4] M. Groß, Y. Chen, J.L.G. Schneider, M. Kadic, and M. Wegener, in preparation (2023)

PHONONICS 2023: 6th International Conference on Phononic Crystals/Metamaterials/Metasurfaces, Phonon Transport, and Topological Phononics
Manchester, England, June 12-16, 2023
PHONONICS-2023-0223

Phononic crystals for elastic wave control

Richard Craster[1]

[1] *Department of Mathematics and Department of Mechanical Engineering, Imperial College London, London, U.K.,*
r.craster@imperial.ac.uk

Abstract: This talk will draw upon joint work with many collaborators and aims to give an overview of attempts at vibration control using ideas based upon classical ideas such as band-gaps and also around metamaterials. It will also draw on recent research around seismic met-amaterials, energy harvesting and rainbow trapping ideas that combine with topological wave physics.

Overview:

A continuing challenging in wave physics, and particularly for elastic vibration, is the broadband control of low frequency long wavelength signals and this challenge emerges naturally both at large scales for, say, seismic metamaterials and at smaller scales for, say, energy harvesting devices.
Classical ideas based around Bragg scattering, and constructive/ destructive interference to create bandgaps, create effective devices with the aim to obtain low frequency and very wide bandgaps.
These ideas will be illustrated in the extreme example of Ref. 1 where for an elastic wave system there is a zero-frequency bandgap, that is, the lowest edge of the bandgap is at zero. This then allows, at least in principle, for the very longest and most destructive waves to be mitigates and has application in urban environments; the most annoying noise and vibration tends to be that at lowest frequency.
Building upon these concepts we then introduce resonators to create the potential for sub-wavelength control with devices that are a similar scale, or smaller, that the incoming waves; frequency selection via grading as in Ref. 2 then allows us to either slow and "trap" waves at positions of our choosing, which then has implications for wave harvesters as in Ref. 3. The grading also has the convenience of allowing for mode conversion from surface Rayleigh waves into shear or compressional bulk waves with potential control over their directions too, see Ref. 5.
Finally, if time allows, these ideas of grading, band-gaps and concentrations of energy will be combined with topological edge states to create robust channels along which energy can be directed and then focussed as in Ref. 4.

References

[1] Y Achaoui, T Antonakakis, S Brûlé, RV Craster, S Enoch, S Guenneau, New Journal of Physics **19,** 063022, 2017 and US Patent WO2018073412A1

[2] A Colombi, D Colquitt, P Roux, S Guenneau, RV Craster, Scientific reports **6** (1), 27717, 2016

[3] JM De Ponti, A Colombi, R Ardito, F Braghin, A Corigliano, RV Craster, New Journal of Physics **22** (1), 013013, 2020

[4] B Ungureanu, MP Makwana, RV Craster, S Guenneau, Physical Review Applied **15** (1), 014057, 2021

[5] GJ Chaplain, JM De Ponti, A Colombi, R Fuentes-Dominguez, P Dryburg, D Pieris, RJ Smith, A Clare, M Clark, RV Craster, Nature Communications **11** (1), 1-6, 2020

PHONONICS 2023: 6th International Conference on Phononic Crystals/Metamaterials/Metasurfaces, Phonon Transport, and Topological Phononics
Manchester, England, June 12-16, 2023
PHONONICS-2023-0016

Drawing Dispersion Curves: Band Customization by Non-local Phononic Crystals

Arash Kazemi[1], Kshiteej J. Deshmukh[2], Fei Chen[1], Sharat Paul[1], Bolei Deng[3], Henry Chien Fu[1], Pai Wang[1*]

[1]Department of Mechanical Engineering, University of Utah, Salt Lake City UT, USA
[2]Department of Mathematics, University of Utah, Salt Lake City UT, USA
[3]Department of Mechanical Engineering, Massachusetts Institute of Technology, Cambridge MA, USA
** pai.wang@utah.edu*

Abstract: We demonstrate inverse design of phononic dispersion using non-local interactions on one-dimensional spring-mass chains. For both single-band and double-band cases, we can achieve any valid dispersion curves with analytical precision. We also plan to extend this design protocol to phononic crystals in two and three dimensions.

We report a new design methodology that uses non-local interactions to customize dispersion relations. First, we present an analytical protocol to solve the inverse problem, achieving any arbitrarily-defined single-band dispersion on mono-atomic non-local chains. Then, we use this design protocol to obtain dispersion curves with ordinary and higher-order critical points. Using time-domain simulations, we illustrate their unconventional wave dynamics, especially at the undulation point (a.k.a. stationary inflection point), where both the first and second derivatives of the dispersion curve vanish. This results in highly concentrated vibration energy since the wave mode is simultaneously non-propagating and non-spreading. Furthermore, we also investigate the diatomic non-local chain and develop the design protocol to customize its two dispersion bands [1]. In additional, we also plan to continue our study with experimental demonstrations as well as extend our method for two-dimensional and three-dimensional phononic crystals and acoustic metamaterials.

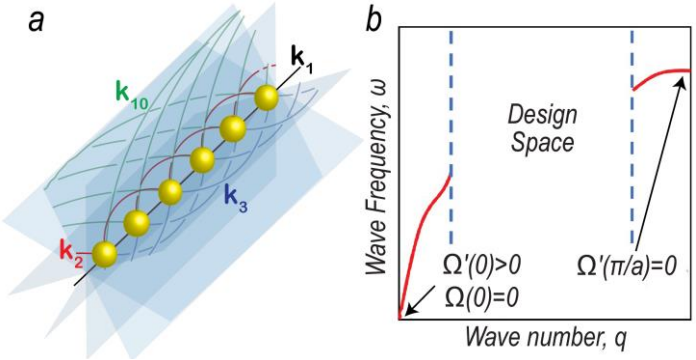

Figure 1 (a) A chain of identical masses. Each mass is connected to its nth-nearest neighbours with spring constant k_n. **(b)** The design space with fundamental constraints at the centre ($q = 0$) and edge ($q = \pi/a$) of the 1st Brillouin zone.

To sketch out the basic design, we start with a one-dimensional "mono-atomic" phonon chain of identical masses, m, and linear springs. A schematic of the model is depicted in Fig. 1(a). Each mass is connected with its two nearest neighbors by local interactions with the spring constant k1. In addition, each mass is also connected on both sides to its two *n*-th nearest neighbors with non-local interactions specified by the spring constants k_n, for $n = 2, 3, 4, ..., N$, where N is the longest-range non-local interaction in the system. Based on the Bloch theorem, we obtain the following dispersion relation:

$$\omega^2(q) = \frac{2}{m}\left(\sum_{n=1}^{N} k_n - \sum_{n=1}^{N} k_n \cos(nqa)\right),$$

where ω is the frequency, q is the wavenumber, and a is the spatial period of the lattice. For conventional chains with local springs k_1 only, Eq. (1) reduces to the following classical result:

$$\omega^2(q) = (4k_1/m)\sin^2(qa/2), \quad (2)$$

which is monotonic and reaches its maximum at the Brillouin zone boundary. The non-local interactions, on the other hand, may give rise to local minima and maxima at the interior of the Brillouin zone, as recently demonstrated by Chen et al. [2] and earlier by Farzbod & Leamy [3].

Since Eq. (2) takes the form of a Fourier series, we can use it to tailor the non-local interactions to achieve customized dispersion curves. Before the demonstration of customization procedures, it is necessary to understand all constraints in possible dispersion relations. Here, we consider the following physical and symmetry principles as fundamental assumptions:

- Passive with no energy input or output.
- Free-standing with no grounded springs.
- Time-reversal symmetric with no gyroscopic effect.
- Stable with a finite static stiffness.

Combining the above, we arrive at the requirements that, for any target dispersion relation $\Omega(q)$ defined on the nonnegative half of the first Brillouin zone ($q \in [0, \pi/a]$) to be valid, it needs to be a smooth curve with (See Fig. 1(b)):

$$\Omega(0) = 0, \quad 0 < \Omega'(0) < +\infty, \quad \text{and} \quad \Omega'(\pi/a) = 0. \quad (3)$$

Given an arbitrarily specified dispersion relation, $\Omega(q)$, satisfying Eqs. (3), we can design a non-local phononic crystal using the following protocol: First, we find the Fourier coefficients as

$$A_n = \frac{2a}{\pi} \int_0^{\pi/a} \Omega^2(q) \cos(nqa)\, dq, \quad n = 1, 2, ..., N. \quad (4)$$

Then, the design can be obtained by:

$$k_n/m = -A_n/2, \quad n = 1, 2, ..., N. \quad (5)$$

Fig. 2 shows results of this protocol with several examples. Since Eq. (5) shows all k_n's simply scale with m, we can set $m = 1$ for all cases. In each case, we compare the target dispersion with the actual one by examining the normalized root mean square deviation (NRMSD) between them. For each target curve, the stiffness design variables for the actual system are obtained using Eqs. (4) and (5). The total number of stiffness types is N=10 for Figs. 2(a)-2(d), N=20 for Figs. 2(e)-2(g), and N=25 for Fig. 2(h), respectively. The NRMSD is less than one percent in all cases.

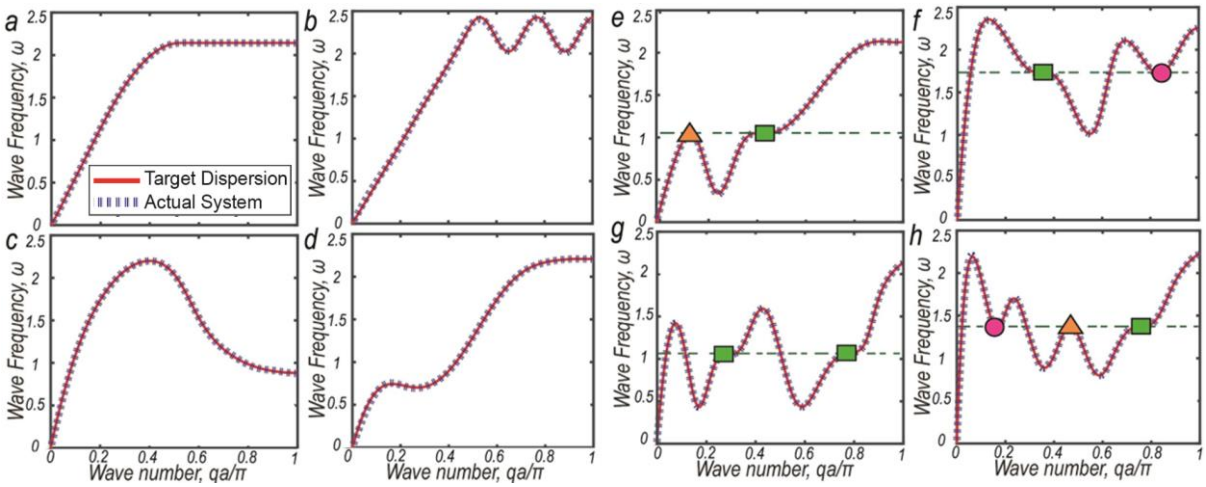

Figure 2 Customized dispersion curves with special features: **(a)** a flat top; **(b)-(d)** Non-monotonic behaviours at large, medium, and small wave number, q (i.e., at short, medium, and long wavelength as compared to lattice the unit cell size), respectively; **(e)-(f)** maxons (triangles), rotons (circles), and undulation points (squares) occurring at the same frequency.

References

[1] A. Kazemi, et al. *arXiv preprint* arXiv:**2302**.00591 (2023).
[2] Y. Chen, M. Kadic, and M. Wegener, *Nature Communications* **12**, 1 (2021).
[3] F. Farzbod and M. J. Leamy, *Journal of Vibration and Acoustics* **133,** 3 (2011).

PHONONICS 2023: 6th International Conference on Phononic Crystals/Metamaterials/Metasurfaces, Phonon Transport, and Topological Phononics
Manchester, England, June 12-16, 2023
PHONONICS-2023-0092

Acoustic Wave Steering in Disordered Networks by Rational Pruning

Anastasiia O. Krushynska[1], Martin van Hecke[2,3]

[1] Engineering and Technology Institute Groningen, Faculty of Science and Engineering, University of Groningen, Nijenborgh 4, Groningen 9747AG, the Netherlands
a.o.krushynska@rug.nl
[2]AMOLF, Science Park 104, 1098 XG Amsterdam, the Netherlands
[2]Huygens-Kamerlingh Onnes Lab, Leiden University, PO box 9504, 2300 RA Leiden, the Netherlands
mvhecke@gmail.com

Abstract: We propose rational pruning to implement acoustic wave steering in disordered networks and show that wave energy can be guided to different locations depending on the excitation frequency without changing the network architecture. This study opens a new route for the rational design of multi-frequency elastic metamaterials with programmable dynamics.

The ability to steer acoustic waves to desired locations is quintessential for many applications, including holography, focusing, imaging, data processing, computing, etc., and can be realized using rationally architected media – elastic metamaterials[1,2]. Most of the proposed metamaterials have a lattice architecture and achieve wave steering along pre-defined waveguiding paths, which consist of modified unit cells and connects an input to output(s)[3]. Other promising solutions are spatiotemporal metamaterials with non-periodic architecture that enable non-reciprocal features and control of scattered wave field[4]. In both cases, however, the locations of the input and outputs cannot be changed without modifying the metamaterial architecture, and the wave amplitude at the output(s) is governed by a metamaterial architecture and the mechanical behavior of constituent material(s)[5].

Here we propose a new concept for architecture-controlled wave steering inspired by rich functionalities of aperiodic, spatially textured designs[6] and the "allosteric" behavior of disordered networks when an excitation applied at one location yields a predefined response at a distant location[7].

We analyze the dynamics of randomly perturbed 2D triangular mass-spring lattices excited by a harmonic force at an input node (Fig. 1a). If the excitation frequency is chosen as a control parameter, can we achieve wave steering to several targets (outputs) with wave amplitude governed by the frequency without modifying the network architecture? If so, what are the limits on the number of outputs and frequencies for a network of a fixed size? What is the spatial and temporal spacing between the output locations and excitation frequencies?

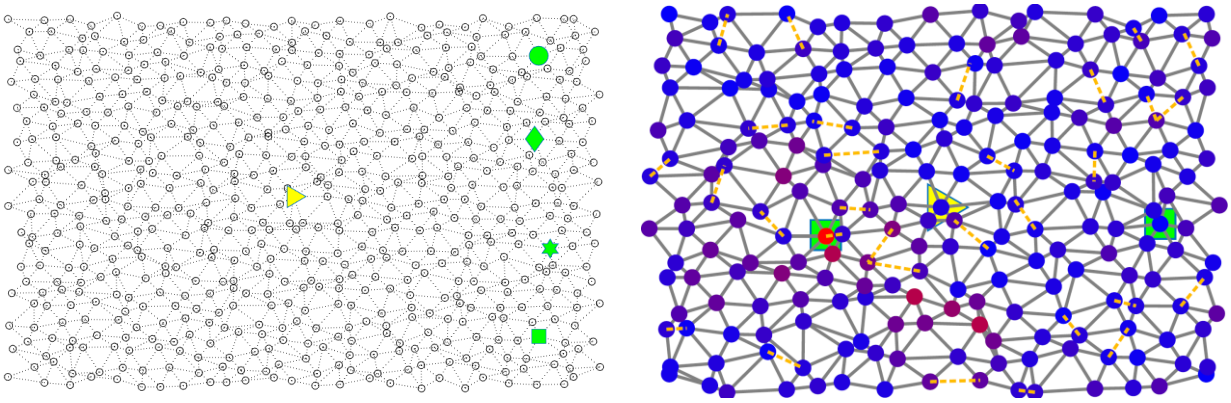

Figure 1 (a) Example of a perturbed (max. 35% displacement of nodes) triangular network of 25x 25 masses and 1776 springs with one (triangle) input and four (green symbols) outputs. **(b)** A rationally pruned network with 15x15 masses **(**pruned springs are shown in orange) excited on non-dimensional frequencies $f_1 = 1$ or $f_2 = 1.2$ directs the vibration energy towards output node 1 (square) or output node 2 (star). Colours of the node indicate their normalized amplitude (blue: 0, red: 1).

To answer these questions, we implemented a variation of the greedy pruning algorithm[8] that implies the targeted removal of certain springs, so that the vibration amplitudes at the outputs approach specified values on pre-defined excitation frequencies. We focused on a low-frequency range, where vibrational energy is homogeneously distributed throughout a network remaining below the mode localization threshold[9].

We have probed our pruning strategy for a range of network sizes, different numbers and positions of outputs, and different target amplitudes at outputs. For different combinations of these parameters, our strategy almost always produces network architecture, which supports multi-frequency wave steering, by pruning less than 10% of the total number of springs[9]. Interestingly, the spatial patterns of pruned springs reveal no waveguiding path connecting the input and outputs and no discernible correlations to, e.g., the outputs locations (see an example in Fig. 1b). The statistical analysis of the required number of the pruned springs shows that its distribution is well fitted by a lognormal distribution, irrespective of the system size, number of outputs, and the contrast in the values of the pre-scribed amplitudes. We also investigated the effects of the network parameters on the number of the pruned springs and found that this number increases with the contrast in the target amplitude values and the number of outputs, yet decreases with the network size. Surprisingly, it appeared that not the number of masses, but rather the linear system size controls the number of pruned springs. This suggests that larger systems can allow the integration of even more functionalities. Finally, our results are robust to excitation frequency variations and are valid for arbitrary locations of the outputs.

Therefore, we have shown that multi-frequency acoustic wave steering can be implemented by rationally pruning a small number of springs in randomly architected mass-spring networks that opens new avenues to the design of aperiodic acoustic metamaterials and exciting application possibilities, e.g., in acoustic acoustics be random networks.

References

[1] S. A. Cummer, J. Christensen, and A. Alù, *Nat. Rev. Mater.* **1**, 16001 (2016).
[2] S. Guenneau, A. Movchan, G. Pétursson, and S. A. Ramakrishna, *New J. Phys.* **9**, 399 (2007).
[3] A.O. Krushynska, N. Anerao, M.A. Badillo-Ávila, M. Stokroos and M. Acuautla, *Materials & Design* **205**, 109714 (2021).
[4] A.O. Krushynska, D. Torrent, A.M. Aragón, R. Ardito, ..., and O.B. Wright, *Nanophotonics* **12**(4), 659-686 (2023).
[5] A.O. Krushynska, A.S. Gliozzi, A. Fina, D. Krushinsky, et. al, *Adv. Funct. Mater.* **31**(30), 2103424 (2021).
[6] C. Coulais, E. Teomy, K. De Reus, Y. Shokef, and M. van Hecke, *Nature* **535** (7613), 529-532 (2016).
[7] J.W. Rocks, N. Pashine, I. Bischofberger, C.P. Goodrich, A.J. Liu and S.R. Nagel, *Proc. Nat. Acad. Sci. U.S.A.* **114**, 2520-2525 (2017).
[8] C.P. Goodrich, A.J. Liu, and S.R. Nagel, *Phys. Rev. Lett.* **114**, 225501 (2015).
[9] A.O. Krushynska and M. van Hecke, *arXiv preprint*, arXiv:2212.12274 (2022).

PHONONICS-2023-0013

Non-Hermitian Extended Topological Modes

Guancong Ma

[1]*Department of Physics, Hong Kong Baptist University, Kowloon Tong, Hong Kong, China*
phgcma@hkbu.edu.hk

Abstract: We use mechanical lattices with non-Hermitian active components to realize topological modes that are fully extended. Such modes occupy the entire bulk lattice while maintaining their topological characteristics. Furthermore, the wavefunctions of these modes can be flexibly tuned by adjusting the distributions of non-Hermiticity.

Since their first discovery, topological modes have always been localized modes bounded to edges or defects. This means that any attempt to leverage the desirable properties of topological modes, including robustness against perturbations and backscattering immunity, has a steep price to pay: such devices must base on a bulk lattice that occupies at least one more spatial dimension than the topological modes. This is obviously undesirable because it means the device must be large in size and costly to fabricate.

Here, we use active topological mechanical lattices to demonstrate that the non-Hermitian skin effect can completely delocalize an in-gap topological mode, even rendering it the only extended modes in the system[1]. In two-dimensional topological lattices, topological edge modes and even second-order topological corner modes can be converted to extended surface modes. The wavefunctions of the topological modes can even be engineered into a variety of shapes by controlling the non-Hermiticity distribution. The extended topological modes can also spatially and spectrally coexist with skin-localized bulk modes, realizing the inverted version of "bound state in a continuum." [2]

Acknowledgment. Supported the Hong Kong Research Grants Council (RFS2223-2S01, 12302420, 12300419, 12301822).

References

[1] W. Wang, X. Wang, G. Ma, *Nature* **608**, 50-55 (2022).
[2] W. Wang, X. Wang, G. Ma, *Phys. Rev. Lett.* **129**, 264301 (2022).

PHONONICS 2023: 6th International Conference on Phononic Crystals/Metamaterials/Metasurfaces, Phonon Transport, and Topological Phononics
Manchester, England, June 12-16, 2023
PHONONICS-2023-0147

Guided Waves in Glide-Reflection Symmetric Phononic Crystal Interfaces

Julio Andrés Iglesias Martínez[1], Nicolas Laforge[1], Muamer Kadic[1], Emil Prodan[2], Vincent Laude[1]

[1] *Université de Franche-Comté, CNRS, institut FEMTO-ST, Besançon, France,*
vincent.laude@femto-st.fr
[2] *Department of Physics, Yeshiva University, New York, USA*

Abstract: We consider a glide dislocation in a wide bandwidth phononic crystal and show that wide-bandwidth, single-mode, and symmetry-protected guided waves appear. The 2D Zak phase changes by π on either side of the interface, providing a topological invariant protected by glide-reflection symmetry at either the X or the Γ point of the first Brillouin zone.

We consider time-reflection symmetric (TRS) waveguides created by a glide dislocation in a two-dimensional (2D) phononic crystal. Because of the dislocations, these systems have only one periodicity (1D) left, but they still inherit the phononic band properties of the parent 2D crystal, hence constituting the bulk crystal from which the boundary, or interface, is created. The space group of a 1D periodic structure is also known as a frieze group. There are a total of 7 frieze groups, among which only the two groups p11g and p2mg possess a half-lattice glide-reflection symmetry (GRS). Recently, it has been shown that crystal interfaces belonging to these two frieze groups support a pair of non-interacting, or backscattering-free, guided waves with a smooth dispersion covering a large part of the 2D phononic band gap [1]. The band structure topology of those crystal interfaces is protected by the GRS. Glide-reflection symmetry belongs to nonsymmorphic symmetries, i.e. symmetries that do not leave a fixed point invariant inside the unit cell. Band inversion is obtained at the X point of the first Brillouin zone, i.e. at its edges. The crossing-point of the two guided bands is one example of a nodal point of the 1D band structure, similar to Dirac points in 2D and 3D crystals.

A demonstration experiment is performed with acoustic waves in water, at ultrasonic frequencies, and shows the continuous tuning of transmission as a function of the glide parameter. A square-lattice phononic crystal of steel rods in water is constructed with a total of 24 × 16 parallel rods aligned using perforated parallel plates. The rod diameter is d = 2 mm and the lattice constant is a = 2.22 mm (d/a = 0.9). The complete band gap extends from 0.28 MHz to 0.46 MHz. The experimental transmission is obtained based on the ultrasonic pulse-echo technique. The guided mode transmission covers most of the complete band gap when the frieze group of the interface is p2mg, in accordance with theory. For other glide parameter values, corresponding to frieze group p2 of lower symmetry, transmission is observed as well inside the complete band gap but within a reduced frequency range. A continously-tunable transmission filter is thus obtained. As a waveguide for transmission of information, the glide-reflection symmetric crystal waveguide offers wide bandwidth, single mode operation, and symmetry-protected backscattering immunity.

As a note, symmetry protection against backscattering of the guided waves is only achieved when the glide parameter $g = a/2$. The importance of glide-reflection symmetry is further verified by considering the oblique lattice instead of the square lattice, leading to the consideration of frieze group p11g. It is specifically found that inversion symmetry combined with the glide operation leads to a gapped spectrum, unlike GRS.

We also explore the resilience of the interface waves to disorder, a direct check of symmetry protection. It is observed numerically that they survive a position disorder of at least 5% of the lattice constant and an inclusion diameter disorder of 10%.

We further extend the theory of the glide-reflection symmetric phononic crystal interface in two different directions [2]. First, we show that the nodal point can be moved from the X point to the Γ point of the first Brillouin zone, by introducing a quarter-lattice-constant glide-reflection symmetry, when the 2D crystal unit cell is extended by a factor two along the interface direction (the extended lattice

constant $a_x = 2a$, with a the original lattice constant). The extended unit cell contains two different inclusions per unit cell, separated by a, such that taken separately they both lead to a similar complete phononic band gap range. Moving the nodal point to the Γ point, that is to a zero or integer value of the reciprocal lattice constant, may find applications for normal incidence excitation of the 1D waveguide. Second, we discuss the locality of the constraint of glide-reflection symmetric of the crystal interface and show that it can be deformed continuously to compensate for the glide dislocation away from the interface, while keeping in an approximate and local sense the topological properties of a buried glide-reflection symmetric interface.

The symmetry principles involved extend the existence of glide-reflection symmetric crystal waveguides to other material systems and lattices. We have specifically considered the cases of acoustic waves in a fluid with rigid inclusions and of vector elastic waves in a solid perforated with cylindrical holes or containing solid inclusions. By virtue of the well-established analogies between acoustic/elastic waves and optical/electromagnetic waves, the transposition to photonic crystals is also straightforward.

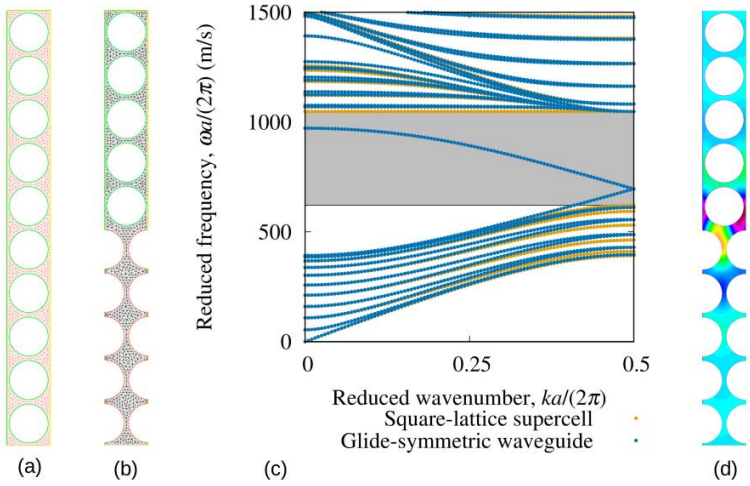

Fig. 1. (a) The finite element mesh (FEM) for a supercell with N = 10 unit-cells of a square-lattice sonic crystal of rigid cylinders in water is shown. The rod diameter to lattice constant is $d/a = 0.9$. (b) The FEM mesh of the glide-symmetric waveguide structure formed in the same crystal by shifting horizontally the 5 bottom rows by half a lattice constant ($g = a/2$). (c) The phononic band structure for $g = 0$ plotted with yellow dots shows a complete band gap (outlined gray region). The phononic band structure for $g = a/2$ plotted with blue dots shows a pair of guided waves with smooth dispersion (Bloch waves number N and $N + 1$). (d) The real part of the pressure distribution of the guided Bloch wave number $n = N + 1 = 11$ is displayed at $ka/(2\pi) = 0.1$, $\omega a/(2\pi) = 959$ m/s.

References

[1] Julio Andrés Iglesias Martínez, Nicolas Laforge, Muamer Kadic, and Vincent Laude, "Topological waves guided by a glide-reflection symmetric crystal interface," *Phys. Rev. B* **106**, 064304 (2022).
[2] Vincent Laude, Julio Andrés Iglesias Martínez, Nicolas Laforge, Muamer Kadic, and Emil Prodan, "Glide-reflection symmetric phononic crystal interface: variation on a theme," submitted (2023).

PHONONICS 2023: 6th International Conference on Phononic Crystals/Metamaterials/Metasurfaces, Phonon Transport, and Topological Phononics
Manchester, England, June 12-16, 2023
PHONONICS-2023-0137

From Effective Medium Theory to Acoustic Double-Zero-Index Materials

Keqiang Lyu[1], Changqing Xu[2], Mohamed Farhat[2], Guancong Ma[3], Yun Lai[4], Ying Wu[1,2]

[1] *Division of Physical Science and Engineering, King Abdullah University of Science and Technology, Saudi Arabia*
keqiang.lyu@kaust.edu.sa, ying.wu@kaust.edu.sa
[2] *Division of Computer, Electrical and Mathematical Science and Engineering, King Abdullah University of Science and Technology, Saudi Arabia*
changing.xu@kaust.edu.sa , mohamed.farhat@kaust.edu.sa
[3]*Department of Physics, Hong Kong Baptist University, Hong Kong, China*
phgcma@hkbu.edu.hk
[4]*Department of Physics, Nanjing University, China*
laiyun@nju.edu.cn

Abstract: A brief review on the effective medium theories is given followed by a demonstration of how the theories benefited the design of acoustic double-zero-index materials based on phononic crystals. The design principles and physical mechanisms are explained in detail. Several applications, including waveguiding and tunable transmission, will be demonstrated.

Double-zero-index material, with compressibility and mass density vanishing simultaneously, has attracted enormous attentions due to their unprecedented properties in controlling wave propagation. However, there is no naturally available materials that possesses such special combination of material parameters. To obtain a double-zero-index material, we need to strategically design artificial structures, whose effective medium gives rise to double zero compressibility and mass density. In the literature, a simple two-dimensional photonic crystal with a square array of aluminum cylinders were found to possess double zero permittivity and permeability at a frequency [1]. However, such design strategy cannot be directly transcribed to the airborne acoustics, even though the mathematical equations for acoustic and electromagnetic waves are equivalent. The reason is acoustic waves propagates much faster in any solid/liquid materials than in air and the impedance mismatch between air and other materials is super large. Despite some progresses in designing double-zero-index acoustic materials[2,3], most of them are subject to certain constrains. In addition, extending the two-dimensional problem to three dimensions is another challenging problem.

The fundamental framework for the study of double-zero-index material is the effective medium description. Thus, I will start with a brief review on the effective medium theories that we developed in the past for phononic crystals that can treat resonances. Basically, for cylindrical, spherical, and elliptical scatterers, the effective medium is derived from the coherent potential approximation [4], and analytic formula is explicitly obtained, whereas for arbitrarily shaped scatterers, semi-analytic approach based on field averaging [5] is needed to provide proper effective medium parameters. These theories not only give accurate descriptions on the effective medium parameters of the phononic crystal, but also offer guidance to the design routes of new double-zero-index materials.

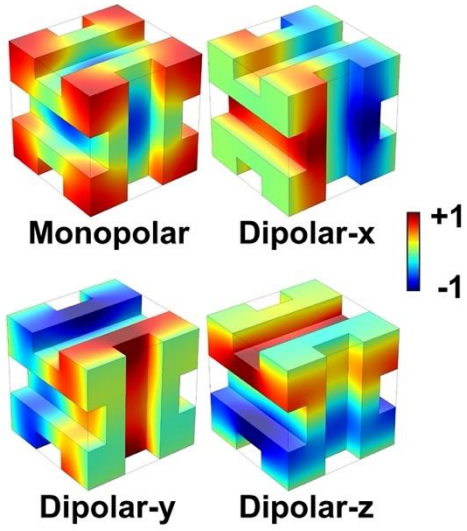

Figure 1 Pressure field distributions at the frequency where both effective mass density and effective compressibility are zero.

In the first example, I will show our design of the first three-dimensional acoustic double-zero-index material, which comprise square aluminum rods placed in a manner satisfying the glide symmetry [6]. In this design, the central air "cubic" can be viewed as a resonator and the passages connecting the neighbors provide interactions between the resonators. When the geometry is finely tuned, the monopolar and dipolar states

become degenerate at a particular frequency as shown in Fig. 1. The effective medium theory shows explicitly that the effective compressibility and effective mass density become zero at that frequency.

In the second example, a new design for the two-dimensional acoustic double-zero-index material will be presented. In this design, we judiciously combined the coiling-up structure [7] into the meta-atom to achieve desired monopolar and dipolar resonances. The advantage of a coiling-up space lies in its ability to effectively elongate the propagation distance, and therefore, equivalently reduced the effective wave speed of the meta-atom. By carefully tuning the size of the coiling-up structure, we obtain again a two-dimensional acoustic phononic crystals whose effective mass density and compressibility are vanishing simultaneously. An equivalent model is devised to describe the effective medium properties.

References

[1] X.Q. Huang, *et al Nat. Mater.* **10** 582 (2011)
[2] L. Y. Zheng, *et al Appl. Phys. Lett.* **104**, 161904 (2014).
[3] M. Dubois *et al*, *Nat. Commun.* **8**, 14871 (2017) .
[4] Y. Wu, J. Li, Z. Q. Zhang and C. T. Chan, *Phys. Rev. B* **74**, 085111 (2006).
[5] Y. Lai, Y. Wu, P. Sheng and Z. Q. Zhang, *Nat. Mater.* **10,** 620 (2011)
[6] C. Xu, *et al Phys. Rev. Lett.* **124,** 074501 (2020)
[7] M. Landi *et al Phys. Rev. Lett.* **120** 114301 (2018)

PHONONICS 2023: 6th International Conference on Phononic Crystals/Metamaterials/Metasurfaces, Phonon Transport, and Topological Phononics
Manchester, England, June 12-16, 2023
PHONONICS-2023-0137

Dissipation Driven Bloch Wave Degeneracies

A. Srikantha Phani[1]

[1] *Department of Mechanical Engineering, The University of British Columbia, Vancouver, CANADA, srikanth@mech.ubc.ca*

Abstract: Dissipation can have profound effect on the Bloch wave transmission. This seminar will examine Bloch wave degeneracies purely arising due to dissipation.

Bloch waves are central to understanding the wave phenomena associated with phononic crystals, acoustic and elastic metamaterials. Bloch spectrum, describing the dispersion branches and associated Bloch modes, can be viewed as a parameter dependent eigenvalue problem. The resulting eigenvalue problem becomes nonlinear when dissipation is included [1]. Further, Bloch waves can become degnerate with an associated trivial (a sign change in avoided crossings) or non-trivial geometric phase. This talk will address such degeneracies as non-Hermitian degeneracies associated with a geometric phase. The class of dissipation models that exhibit this degeneracy will be identified and sufficient conditions to observe them will be established. The necessity of a non-commutative and non-proportional dissipation model to observe non- Hermitian degeneracies (or exceptional points) is emphasized. Non-proportional dissipation is used to induce a non-Hermitian degeneracy in a local resonance sub-Bragg bandgap of a linear chain, without using negative damping. While Bloch waves are chosen to illustrate the influence of dissipation, the results readily extend to waves in non-periodic media as well as other wave and vibration transport problems. Implications of these degeneracies for sensing technologies will be discussed.

References

[1] A . S. Phani, 2022, Appl. Phys. Lett. **121**, 231701 (2022).

PHONONICS 2023: 6th International Conference on Phononic Crystals/Metamaterials/Metasurfaces, Phonon Transport, and Topological Phononics
Manchester, England, June 12-16, 2023
PHONONICS-2023-0158

Hypersonic Metamaterials Based on Architected Hybrid Colloids

Yu Cang[1,2], Rebecca Sainidou[3], Pascal Rembert[3], Krzysztof Matyjaszewski[4], Michael R. Bockstaller[5], Bartlomiej Graczykowski[6], George Fytas[1]
[1]Max Planck Institute for Polymer Research, Ackermannweg 10, 55128 Mainz, Germany
fytas@mpip-mainz.mpg.de
[2]School of Aerospace Engineering and Applied Mechanics, Tongji University, Zhangwu Road 100, Shanghai 200092, China
yucang@tongji.edu.cn
[3]Laboratoire Ondes et Milieux Complexes UMR CNRS 6294, UNIHAVRE, Normandie University, 75 rue Bellot, F-76600 Le Havre, France
sainidor@univ-lehavre.fr; rembertp@univ-lehavre.fr
[4]Chemistry Department, Carnegie Mellon University, 4400 Forbes Avenue, Pittsburgh, Pennsylvania 15213, United States
km3b@andrew.cmu.edu
[5]Department of Materials Science and Engineering, Carnegie Mellon University, 5000 Forbes Avenue, Pittsburgh, Pennsylvania 15213, United States
bockstaller@cmu.edu
[6]Faculty of Physics, Adam Mickiewicz University, Uniwersytetu Poznanskiego 2, Poznan 61-614, Poland.
bartlomiej.graczykowski@amu.edu.pl

Abstract: Soft material science offers unique ways of fabricating hypersonic phononic colloidal crystals via self-assembly with the introduction of polymer-grafted nanoparticles as platform for hybrid colloidal structures. The presence of the inorganic core and the tunable conformation of the grafted chains can intriguingly modulate the band diagram recorded by Brillouin light spectroscopy.

How phonons propagate in nanostructures determines the flow of elastic and thermal energy in dielectric materials. However, a reliable theoretical prediction of the phonon dispersion relation $\omega(q)$ (frequency vs. phonon wavenumber) requires experimental verification both near and far the Brillouin zone of the nanostructure. Control of the hypersonic band diagram goes beyond understanding high frequency sound propagation in isotropic media. Hybrid polymer-inorganic colloid based hypersonic structures (CS) present a solid platform for the experimental and theoretical study of $\omega(q)$ on the account of the controlled variation of the architecture, composition, periodicity and elastic contrast concurrently hosting vibration resonances. For transparent CS, the experimentally recorded $\omega(q)$ by Brillouin light spectroscopy revealed features that are commonly encountered in ordered metamaterials. These include a linear long-wavelength ($q \to 0$) collective response of the composite characterized by the effective medium speed of sound, $c_{\text{eff}} = \omega(q)/\, q$ and, at higher frequencies, the occurrence of forbidden frequency bands related either to the periodicity (Bragg gaps, BG) or to avoided-crossing effects (hybridization gaps, HG) usually arising from local resonances.[1-3] Note that for non-transparent structures access to $\omega(q)$ is indirect by pump-probe pico-acoustic techniques.[4,5]

The frequency response of close-packed CS, revealed important deviations from theoretical predictions using common assumptions such as non-overlapping, almost touching particles and perfect boundary conditions (PBC) across the solid/liquid interfaces (Fig. 1a).[6] An enhanced linear behavior (c_{eff}) and a blue-shifted HG is observed experimentally (Fig. 1c) as compared to the theoretical $\omega(q)$ of Fig. 1 that predicts in a quadrupolar-origin HG) resonance of the individual particles which occurs at $fd/c_{\text{eff}} = 0.40$ in Fig. 1a. Yet, the theory does not support the opening of periodicity-based BG, in contrast to the experimental $\omega(q)$ of fcc CS.

The potential of fabricating hypersonic colloidal crystals via self-assembly significantly advanced with the introduction of polymer-grafted nanoparticles (GNP) as platform for hybrid colloidal structures.[3] The core-to-core separation, d, is facilitated through control of the degree of polymerization, N, and grafting density, σ (number of chains/nm^2) of tethered chains at constant core radius, R_C (inset to Fig. 1b). The grafted-chain conformation (extended or Gaussian coil), the interpenetration of grafts on neighbouring GNPs (entanglements) is controlled by σ and N enabling the systematic testing of the theoretical $\omega(q)$. The experimentally recorded $\omega(q)$ of GNP solids composed of SiO_2 nanoparticles densely grafted

with PS (SiO_2-PS, σ=0.48 nm^{-2}, N=980) shown in Fig. 1c reveals a resonance-induced HG and, additionally, a localized band (empty squares), however, no BG is observed. Remarkably, the experimental dispersion for this GNP and the fcc PS/PDMS opal superimpose in the reduced band diagram in Fig. 1a implying a common origin of the avoided-crossing mechanism. [3,7]

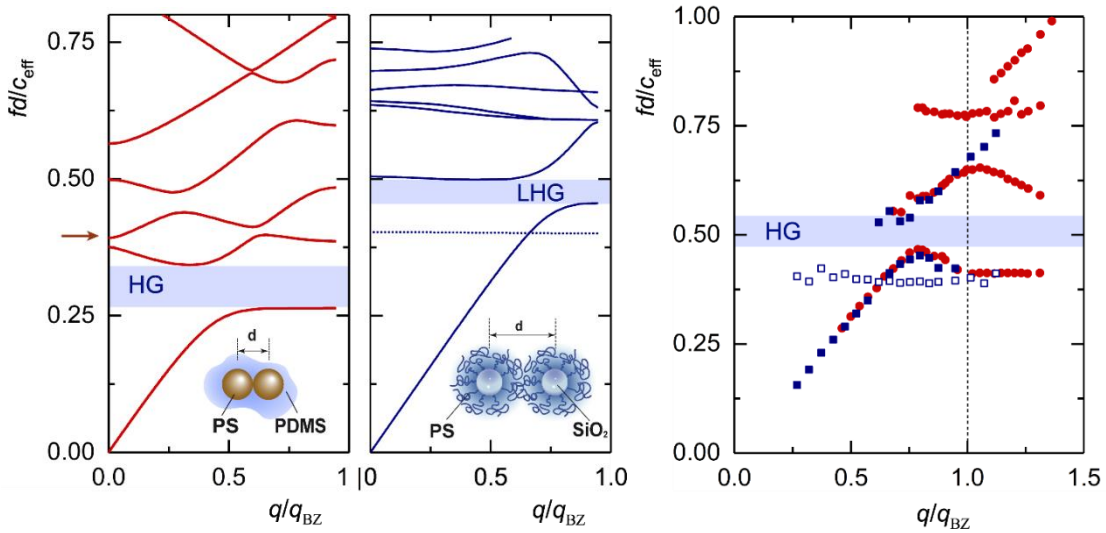

Figure 1 Calculated band structure along the [111] fcc high-symmetry direction for a) a polystyrene (PS) opal infiltrated in (fluid) PDMS. The horizontal red arrow indicates the position of the quadrupolar resonant frequency of the individual PS sphere in PDMS assuming PBC and b) SiO_2-PS GNP (N=980, σ=48nm^{-2}) assuming imperfect boundary conditions ($k_T = 0.021$ GPa nm^{-1}). Solid lines: longitudinal bands in (a) and non-degenerate bands including inactive bands in (b); dotted lines: quasi-flat (highly localized) band originating from dipole torsional modes. Shaded regions denote hybridization gaps of dipole-resonance origin (LHG for longitudinal modes; HG for all modes).c) a) Experimental dispersion plot for close-packed PS particles (diameter d=307nm) infiltrated in polydimethylsiloxane (PDMS) (red filled circles), and SiO_2-PS GNP (in b) assembly (square symbols, d=214 nm) with the empty symbols denoting the dispersionless, highly localized, rotational mode originating from dipole torsional modes of the individual particles; the wavenumber is normalized with respect to q_{BZ} along ΓM direction.

So far, the single report[3] on GNPs phononics focuses on the effect of N, i.e., the filling ratio for constant and high σ, i.e., extended graft conformation. However, grafting density σ is a second intriguing control parameter to tune the conformation of tethered chains and modulate $\omega(q)$ of GNP materials. Since the phonon wavelength in the vicinity of the HG is larger but close to the particle spacing, access to $\omega(q)$ can also index the conformation of the grafted chains. Architected SiO_2-PS assemblies with low (σ=0.08 nm^{-2}) and high (σ=0.53 nm^{-2}) and comparable N. While the structure of $\omega(q)$ is robust to these changes, unexpected quantitative differences in c_{eff} and the interfacial stiffness, k_{T}, are found between sparsely and densely GNP systems. Almost 30% higher c_{PS} than in bulk PS[8] and almost perfect boundary conditions (high k_{T}) are required to represent $\omega(q)$ of sparsely GNP. The interfacial stiffness k_{T} decreases with σ (overcrowding) at constant N much stronger than with N at constant σ. The distinctive features of GNP crystals provide new insights into the role of the molecular architecture on the interactions and phononic properties of GNP-based metamaterial systems.

References

1. T. Still, et al., *Phys. Rev. Lett.*, 2008**, 100**, 194301.
2. G. H. Zhu, et al., *Physical Review B*, 2013**, 88**, 144307.
3. E. Alonso-Redondo, et al., *Nat. Commun.*, 2015, **6**, 8309.
4. A. V. Akimov, et al., *Phys. Rev. Lett.*, 2008, **101**, 033902.
5. K. Rolle, et al., *Scientific Reports*, 2021, **11**,17174.
6. I. E. Psarobas, et. al., *Phys. Rev. B*, 2002, **65**, 064307.
7. Y. Cang, et al., *J. Phys. Chem. B*, 2022, **126**, 6575−6584.
8. J. Midya, et al., *Nano Lett.*, 2019, **19**, 2715.

Subwavelength Imaging of Flexural Waves Beyond the Diffraction Limit

H. Danawe, S. Tol

Department of Mechanical Engineering, University of Michigan
2350 Hayward Street, Ann Arbor, MI, 48109, U.S.A.,
danawe@umich.edu, stol@umich.edu

Abstract: Subwavelength imaging of elastic/acoustic waves in phononic crystals (PCs) has been enabled by two existing mechanisms that utilize the intense Bragg scattering in the first phonon band or negative effective properties (left-handed material) in the second (or higher) phonon band. However, both methods are limited to narrow frequency regions. This study presents a new approach for subwavelength imaging of flexural waves by exploiting the anisotropy of the PC lattice. The square-shaped equal frequency contours of PC (in the second phonon band) eliminate the need to match the wave vectors in PC and background material; hence, results in subwavelength imaging broadband frequency range. We numerically and experimentally demonstrated the proposed mechanism for high-resolution broadband imaging of flexural waves in plates. Furthermore, we extend the methodology to design a flat PC lens operating beyond the diffraction limit.

Ever since Veselago's discovery of the negative refraction phenomenon in left-handed materials (LHM) [1], architected materials enabling negative refraction of electromagnetic waves have attracted considerable attention. For the first time, Pendry[2] demonstrated a flat optical superlens with a double negative effective index and broke the diffraction limit resulting in super-resolution imaging of electromagnetic waves. Later, it was found that the flat superlens concept can also be realized using artificially engineered periodic structures called photonic crystals, which were further extended to phononic crystals (PCs) to enable negative refraction and subwavelength imaging of acoustic/elastic waves. There are two existing mechanisms for realizing subwavelength imaging in photonic/phononic crystals. The first mechanism exploits the first phonon band near the Bragg bandgap, where intense Bragg scattering results in convex equal frequency contours (EFCs) that enclose high symmetry points of the first Brillouin zone[3]. The image formation via the first phonon band was later attributed due to flat-face EFCs resulting in the self-collimation effect and complex near-field wave scattering effect. The second mechanism utilizes all-angle negative refraction (AANR) at a higher (typically second) phonon band (i.e., opposite directions of the wave vector and energy flow direction) due to a backward wave effect similar to LHM[4,5]. However, subwavelength imaging via both mechanisms is limited to a narrowband operation, which is at most 20% frequency range about a center frequency. In the first phonon band, negative refraction only occurs at frequencies close to the bandgap where the EFCs are convex. The

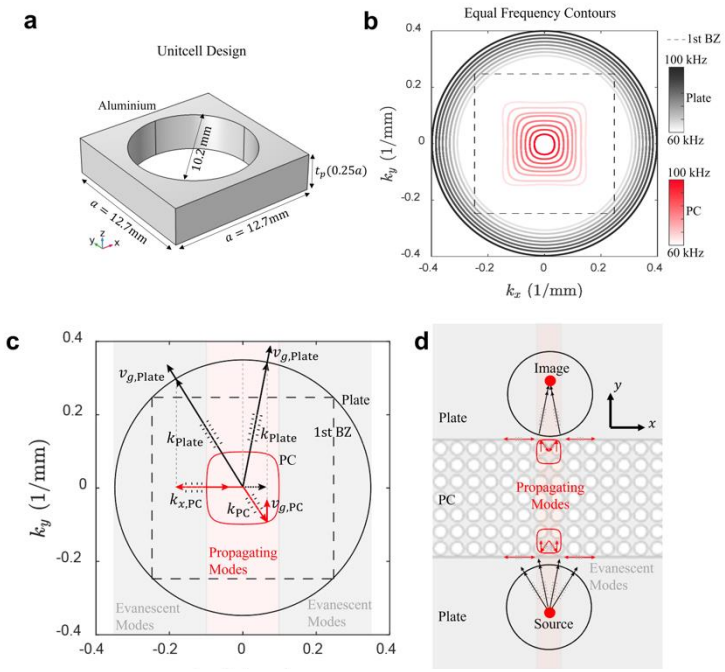

Figure 1 (a) Unit cell of phononic crystal (PC) made up of aluminium with central hole of diameter 10.2 mm and lattice constant (a) of 12.7 mm. The plate thickness is 0.25a (3.175 mm). **(b)** Equal frequency contours of the aluminum plate and phononic crystal plotted over the frequency range of 60 kHz to 100 kHz. **(c)** Wave vectors (k) and group velocity vectors (vg) for PC and plate plotted over EFCs for propagating waves and evanescent waves. **(d)** Schematic of negative refraction and subwavelength imaging due to flat EFCs of PC.

subwavelength imaging in the second band is limited to an even narrower range of frequencies at which the wave vectors in PC and background material are close to each other to support AANR.

In this work, we propose a new methodology for broadband subwavelength imaging of flexural elastic waves in the second phonon band[6], as depicted in Figure 1. As opposed to wavevector matching in circular EFCs, our PC design exploits anisotropy (i.e., the flat square-shaped EFCs in the second phonon band) of a square lattice to achieve subwavelength imaging over most of the second phonon band frequencies, which is validated experimentally at various frequencies ranging between 60 kHz to 100 kHz. It is shown that the proposed method expands the operation range of the subwavelength imaging phenomenon to a 50% frequency range at the central frequency. Furthermore, introducing a step-change design similar to our previous work[5], we achieve a super resolution of 0.4λ by the amplification of evanescent waves carrying the subwavelength information. This is only possible if the EFC of the PC is bigger than the EFC of the plate. The proposed lens design is shown in Figure 2, which is a step-change design with a plate thickness of 0.25*a* for the PC and 0.5*a* for the background plate. The EFCs of flexural (A_0) plate mode corresponding to this design at 45 kHz are depicted for plate and PC in Figure 2 (b). The EFC of PC still maintains its square shape, while the plate-EFC is circular but smaller than the PC-EFC. We numerically and experimentally demonstrate the image formation with frequency domain simulation at 45 kHz, and the steady state out-of-plane velocity amplitude in the image region is depicted in Figure 2 (c). The image formation takes place right at the top lens interface, which is peculiar to evanescent waves and can only form near-field images. The imaging resolution is again calculated using the FWHM measure, and the super-resolution of 0.4λ is obtained where λ (=33.87 mm) is the wavelength in an aluminum plate of thickness 0.5*a* at 45 kHz. Thus, the step-change design breaks the diffraction limit of 0.5λ. The resolution can be further improved by making the plate-EFCs further smaller by increasing its thickness to increase the contribution of evanescent waves in the image formation.

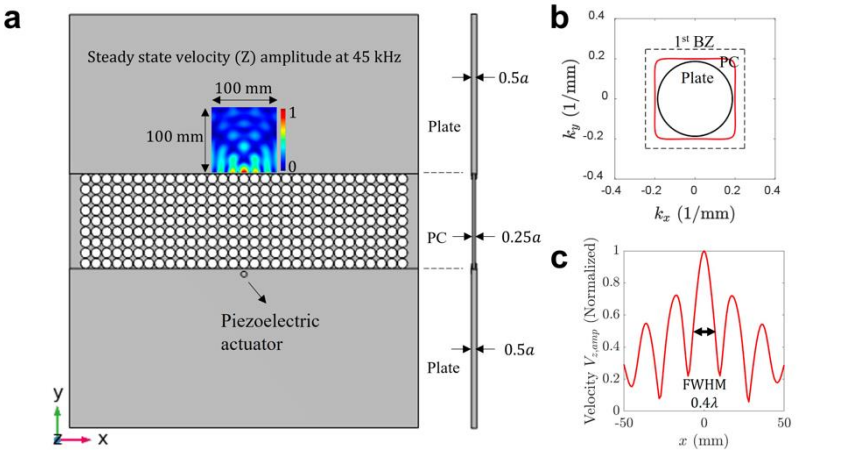

Figure 1 (a) Numerical model of phononic crystal flat lens with step change in plate thickness consisting of 9 x 31 unit cells embedded in an aluminum plate. A thickness mode piezoelectric actuator acts as a source of flexural waves placed at 0.5*a* distance away from the bottom lens interface. The plate thickness is 0.25*a* (3.175 mm) in PC region and 0.5*a* (6.35 mm) in the plate region. The normalized out-of-plane (Z) velocity amplitude in steady state is depicted in the image region of 100 x 100 mm at 45 kHz. **(b)** Equal frequency contours of PC and plate at 45 kHz for a step change in plate thickness from 0.5*a* in plate region to 0.25*a* in PC region. **(c)** Normalized (Z) velocity amplitude line plot along x-direction passing through highest intensity point (y_{max} = 0 mm) in the image region. The full width at half maximum (FWHM) is 0.4λ which is beyond the diffraction limit of 0.5λ resulting in super-resolution.

References

[1] V. G. Veselago, *Sov. Phys. Uspekhi*, **10**, 509–514 (1968).
[2] J. B. Pendry, *Phys. Rev. Lett.* **85**, 3966–3969 (2000).
[3] X. Zhang, and Z. Liu, *Appl. Phys. Lett.* **85**, 341–343 (2004).
[4] A. Sukhovich, L. Jing, and J. H. Page, *Phys. Rev. B* **77**, 014301 (2008).
[5] H. Danawe, and S. Tol, *J. Sound Vib.* **518**, 116552 (2022).
[6] H. Danawe, and S. Tol, *arXiv preprint arXiv: 2303.05923* (2023).

PHONONICS 2023: 6th International Conference on Phononic Crystals/Metamaterials/Metasurfaces, Phonon Transport, and Topological Phononics
Manchester, England, June 12-16, 2023
PHONONICS-2023-0022

Wave Propagation in a Phononic Material with Asymmetric Bilinear Stiffness

Elizabeth J. Smith, Kathryn H. Matlack

Department of Mechanical Science and Engineering, University of Illinois Urbana-Champaign, Urbana, IL, USA,
esmith19@illinois.edu

Abstract: This presentation discusses how bilinear asymmetric stiffness influences wave propagation in a phononic material. Numerical studies of the material show phase-reversal effects, attenuation of tensile strain, and cumulative displacement offsets. Bilinear stiffnesses are physically realized by fabricating samples with prescribed delaminations between stiff and soft layers.

Phononic materials exhibit several well studied wave propagation behaviors such as band gaps, negative refraction, and acoustic cloaking. Recently, phononics research has extended into the nonlinear regime, with the goal of augmenting phononic systems with the rich behavior of nonlinear dynamics[1]. Several methods have been developed to study the combined effects of nonlinear and phononic behavior[2–4] with potential applications such as mechanical sensing and blast mitigation. However, many nonlinear mechanisms such as bi-stable elements and granular media are difficult to extend to non-laboratory environments as they can be fragile and non-loadbearing structures. Layered media embedded with asymmetric bilinear stiffnesses are a promising approach to designing continuum nonlinear phononic materials, with both structural and dynamic capabilities. Waveform transformation has been studied in layered systems with bilinear asymmetric nonlinearity[5-6] and band gaps have also been studied in similar systems[7]. There is a need for a deeper understanding of the combined influence of waveform transformation and frequency dependence in phononic materials with asymmetric stiffness. Furthermore, physically realizing such asymmetrically stiff systems is vital to experimentally validate these concepts and extend them to higher dimensions.

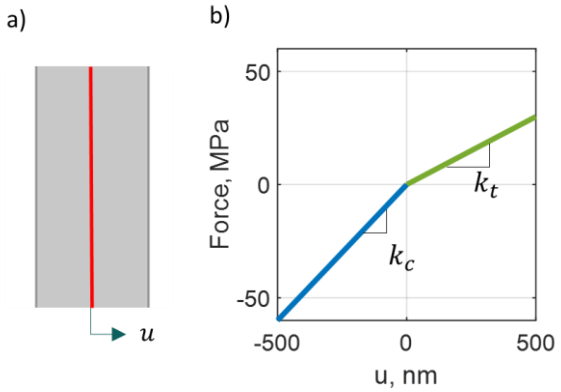

Figure 1 (a) The asymmetric spring layer is shown in red, with extension of the spring denoted by u. The linear elastic layers are shown in grey. (b) The force versus displacement relation for the asymmetric spring, where the tensile stiffness is denoted with slope k_c, and tensile stiffness, k_t.

To address these challenges, we study wave propagation in a time dependent finite element model of linear elastic layers coupled with asymmetric bilinear springs, where the spring's tensile stiffness is a fraction of its compressive stiffness (Figure 1). The band structure of the symmetric (linear) system are computed using Bloch wave analysis, and the nonlinear system is probed with frequencies across the band gaps to analyze the dispersion and energy transfer between frequencies. We characterize how the asymmetrically stiff layers change the propagation of waves through the system in relation to the underlying linear dispersion relation, including spatially cumulative displacement offset, attenuation of tensile strain, and phase-reversal effects. The asymmetrically stiff layers cause the system to be sensitive to the stress state of the system, and excitation waveforms are selected to exploit the bilinear stiffnesses to fundamentally change the shape of the propagating wave. We develop a relation between the system properties (stiffnesses, densities, length scales, and degree of asymmetry) and the observed wave propagation behaviors to provide a framework to engineer asymmetrically stiff phononic materials.

To experimentally probe the simulation results, we designed and fabricated a periodic phononic material containing asymmetrically-stiff layers embedded between elastic layers. This system draws inspiration from geomaterials, which have been shown to exhibit amplitude dependent resonance and harmonic generation, stemming from microcracks, pores, delamination, and material nonlinearity[8]. Unit

cells with bilinear stiffness were physically realized by prescribing delaminations between stiff and soft materials, such that the samples exhibit higher stiffness in compression than tension. Quasi-static experimental measurements confirmed that the delamination causes asymmetric stiffness behavior, where the asymmetry corresponds to the percent area of the non-bonded region. Measurements of wave propagation through a single delamination show a positive compressive offset in a propagating waveform through a delamination, if the amplitude of the waveform is sufficient to activate the mechanism of asymmetry (opening the delamination). Thus, we present a potential path forward to fabricate continuum, asymmetric materials where the material and delamination dimensions and locations can be engineered to obtain desired wave propagation behavior and control.

Acknowledgements
This research was carried out in part in the Advanced Materials Testing and Evaluation Laboratory, University of Illinois.

Research was sponsored by the Army Research Office and was accomplished under Grant Number W911NF-20-1-0250. The views and conclusions contained in this document are those of the authors and should not be interpreted as representing the official policies, either expressed or implied, of the Army Research Office or the U.S. Government. The U.S. Government is authorized to reproduce and distribute reprints for Government purposes not withstanding any copyright notation herein.

References
[1]G. U. Patil and K. H. Matlack, *Acta Mech.*, **233**(1), 1–46 (2022).
[2]Y. Xia, M. Ruzzene, and A. Erturk, *Appl. Phys. Lett.*, **114**(9), (2019).
[3]G. U. Patil and K. H. Matlack, *Phys. Rev. E*, **105**, 24201 (2022).
[4]E. Kim *et al.*, *Phys. Rev. E - Stat. Nonlinear, Soft Matter Phys.*, **92**(6),1–7 (2015).
[5]M. S. Kuznetsova, E. Pasternak, and A. V. Dyskin, *Nonlinear Process. Geophys.*, **24**(3), 455–460 (2017).
[6]V. A. Yastrebov, *Comptes Rendus Mécanique*, **350,** 1–26, (2022).
[7]Y. Wang, Z. Li, M. V Golub, G. Huang, W. Chen, and C. Zhang, *Math. Mech. Solids*, **27**(8), 1531–1545 *(2022).*
[8]M. C. Remillieux, T. J. Ulrich, H. E. Goodman, and J. A. Ten Cate, *J. Geophys. Res. Solid Earth*, **122**(11), 8892–8909, (2017).

PHONONICS 2023: 6th International Conference on Phononic Crystals/Metamaterials/Metasurfaces, Phonon Transport, and Topological Phononics
Manchester, England, June 12-16, 2023
PHONONICS-2023-0081

Tunable Mid Gap in Monoatomic-diatomic Convertible Phononic Crystal with Odd-even Alternating Nonlinearity

M.H. Bae[1], S.H. Kim[1], H.M. Seung[2], J.H. Oh[1]

[1] *Department of Mechanical Engineering, Ulsan National Institute of Science and Technology (UNIST), UNIST-gil 50, Eonyang-eup, Ulju-gun, Ulsan, 44919, South Korea,*
bmh8477@unist.ac.kr, ksh@0793@unist.ac.kr, joohwan.oh@unist.ac.kr
[2] *Intelligent Wave Engineering Team, Korea Research Institute of Standards and Science (KRISS), Gajeong-ro 267, Yuseong-gu, Daejeon, 34113, South Korea,*
shm@kriss.re.kr

Abstract: We proposes a novel monoatomic-diatomic convertible phononic crystal with odd-even alternating nonlinearity that exhibits a tunable mid gap. The nonlinearity-induced impedance mismatch between odd-even unit cells acts as a new periodic scatter, resulting in an amplitude-dependent mid gap. Tunable mid gap is investigated through analytical perturbation and validated via numerical simulations.

Metamaterials are a new type of material in mechanical engineering that can overcome physical limitations of conventional systems. They are artificially designed with specific building blocks called unit cells to have desired properties. In particular, since the metamaterials can exhibit extraordinary wave phenomena impossible in nature when the unit cells are responded to wavelength, metamaterial can achieve perfect wave attenuation, extreme transmission, or high-resolution imaging. In addition to these superb wave manipulations beyond conventional limits, one of the recent trends is to broaden or shift the range of operating frequencies to enhance performance or extend practical usability. Elastic metamaterial's bandgap, a frequency range where wave propagation is prohibited by engineering dispersion also has become tunable to reflect the various design strategies and meet increasing demands on advanced functionalities. Since the bandgap has already wide and active application including wave manipulations and vibration controls[1], tuning operating frequency of bandgap when the metamaterial is subjected to external conditions is highly expected to improve potential for design the efficient and practical mechanical systems[2].

Nonlinear metamaterials are a promising approach for achieving a tunable bandgap, which has attracted significant attention for its novel wave characteristics. The bandgap of nonlinear metamaterials can be shifted depending on the amplitude of the incident wave, which stems from the existing linear bandgap's Bragg gap and resonance gaps. A lot of literature on the nonlinear tunable bandgap has focused on high frequency with Bragg gap and low frequency with resonance gap. While the Bragg gap essentially has a broad band, the resonance gap has a narrow band. Hence, the nonlinear tunability in the mid frequency (the relatively lower frequency) has been truncated. To expand the practical use of the nonlinear tunability in the whole frequencies, we propose a novel monoatomic-diatomic convertible phononic crystal with odd-even alternating nonlinearity that exhibits a tunable mid gap. Figure.1 is scheme of our proposed metamaterial which provides nonlinearity with alternating elastic foundations. Under the low amplitude, the proposed nonlinear metamaterial can exhibit no mid gap alike linear monoatomic chain. As the incident amplitude increases, the propose nonlinear metamaterial can exhibit bandgap at mid frequency with folding of the 1st irreducible *Brillouin* zone. The mid frequency tunable bandgap is not originated from the local resonance but originated from the mismatched impedance between odd and

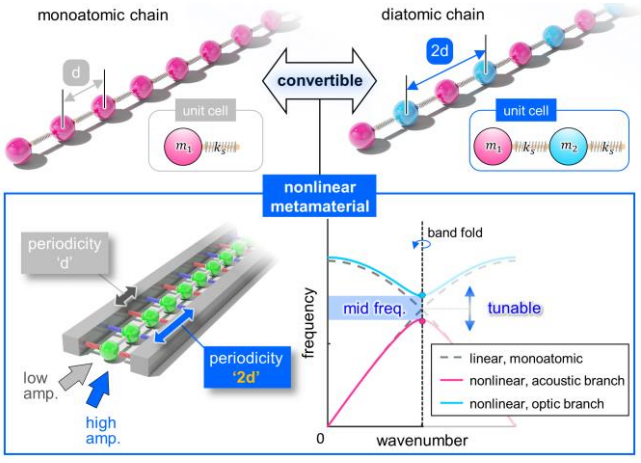

Figure 1 Scheme of tunable mid gap in monoatomic-diatomic convertible phononic crystal with odd-even alternating nonlinearity by elastic foundations.

even unit cells due to the different elastic foundations to act as a new periodic scatter for the wave with mid frequency. To enhance the amplitude-dependent behaviour of metamaterials, we design them with a feasible nonlinearity through geometric changes using elastic foundations commonly used for zero-frequency bandgap. By adding a quasi-zero stiffness effect, which depends on the amplitude, using symmetric elastic foundations made of non-stretched springs[3], we designed the phononic crystal which exhibit a tunable mid gap with the alternating nonlinearity.

Analytically, to capture the amplitude dependent tunable mid gap in our proposed metamaterial, we applied *Brillouin-Wigner* perturbation method. Actually, the equation of motion of our proposed metamaterial can be constructed as

$$\begin{cases} m\ddot{a}_n = -k_x(a_n - b_n) - k_x(a_n - b_{n-1}) - F_{y-x,a} \\ m\ddot{b}_n = -k_x(b_n - a_n) - k_x(b_n - a_{n+1}) - F_{y-x,b} \end{cases} \tag{1}$$

where m is mass, k_x denotes stiffness which link the masses, F_{y-x} denotes the odd-even alternating elastic foundation with nonlinear effect, and a_n, b_n express each displacement of odd-even unit cell. Since the widely used approach based on *Lindstedt-Poincaré* perturbation[4,5] cannot expect the shifted dispersion in our case (In the *Lindstedt-Poincaré* perturbation, the opening of the mid gap is not captured due to the identical shift is captured for the acoustic branch and optic branch), we applied the other perturbation method, *Brillouin-Wigner* perturbation. Before, applying the perturbation we converted eq. (1) with vector form as $H\psi = E\psi$ (where H is a 2 by 2 matrix of proposed metamaterial perturbed from the original matrix of unperturbed system H_0, ψ is a new eigenvector perturbed from the original eigenvector $\psi^{(0)}$, and E is a new eigenvalues also perturbed from $E^{(0)}$). By applying *Brillouin-Wigner* perturbation, we obtained the angular frequency for acoustic and optic branch as

$$\begin{cases} \omega_{aco}{}^2 = 2 - \sqrt{4\cos^2(qd) + \dfrac{9A_0{}^2(N_a - N_b)^2}{4}} + \dfrac{3A_0{}^2(N_a + N_b)}{2} \\ \omega_{opt}{}^2 = 2 + \sqrt{4\cos^2(qd) + \dfrac{9A_0{}^2(N_a - N_b)^2}{4}} + \dfrac{3A_0{}^2(N_a + N_b)}{2} \end{cases} \tag{2}$$

where q is wavenumber, d is the periodic length, A_0 is amplitude of incident wave, and N_a, N_b denote magnitude of nonlinearity in odd-even unit cells. This result is depicted in Figure 2. Furthermore, we validated the tunable mid gap in monoatomic-diatomic convertible phononic crystal with odd-even alternating nonlinearity through numerical simulations.

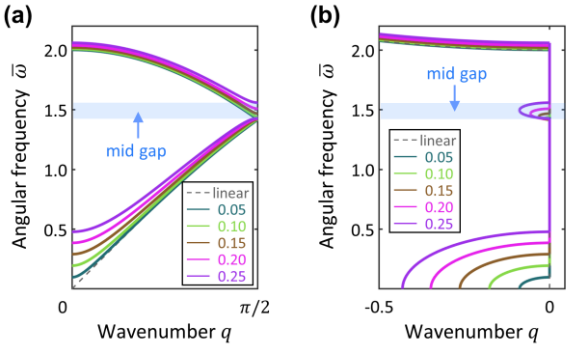

Figure 2 Captured tunable mid gap - **(a)** real dispersion branch and **(b)** imaginary dispersion branch.

Acknowledgements

This work was supported by the National Research Foundation of Korea (NRF) grant funded by the Korea government (No. 2021R1A4A1033224) and by the National Research Foundation of Korea (NRF) grant funded by the Korea government (No. 2022R1C1C2013024).

References

[1] M. H. Bae, W. Choi, J. M. Ha, M. Kim, and H. M. Seung, *Sci. Rep.* **12**, 1-13 (2022)
[2] M. F. Wang, Y. Z. Wang, B. Wu, W. Chen, and Y. S. Wang, *Appl. Mech. Rev.* **72**, 040801 (2020)
[3] M. H. Bae and J. H. Oh, *Mech. Syst. Signal Proc.* **170**, 108832 (2022)
[4] R. K. Narisetti, M. J. Leamy, and M. Ruzzene, *J. Vib. Acoust.* **132**, (2010)
[5] M. H. Bae and J. H. Oh, *J. Mech. Phys. Solids.* **139**, 103930 (2020)

PHONONICS 2023: 6th International Conference on Phononic Crystals/Metamaterials/Metasurfaces, Phonon Transport, and Topological Phononics
Manchester, England, June 12-16, 2023
PHONONICS-2023-0108

Nonlinear Propagation in 1D and 2D Acoustic Networks

I. Ioannou Sougleridis[1 2], O. Richoux[1] ,V. Achilleos[1],
G. Theocharis[1] , C. Desjouy[1] , D. J. Frantzeskakis[2]

[1] Laboratoire d'Acoustique de l'Université du Mans (LAUM), UMR 6613,
Institut d'Acoustique - Graduate School (IA-GS), CNRS, Le Mans Université, France
Ioannis.Ioannou_Sougleridis.Etu@univ-lemans.fr, olivier.richoux@univ-lemans.fr,
achilleos.vassos@univ-lemans.fr, georgios.theocharis@univ-lemans.fr, cyril.desjouy@univ-lemans.fr
[2] Department of Physics, National and Kapodistrian University of Athens,
Panepistimiopolis, Zografos, Athens 15784, Greece
dfrantz@phys.uoa.gr

Abstract: In this work we study the propagation of high-amplitude sound waves in acoustic networks. In particular, we experimentally demonstrate the formation of solitary waves in one dimensional periodic waveguides, despite the presence of nonlinear losses. Furthermore, for a two dimensional square network of connected waveguides, we show analytically and numerically the existence of anisotropic cylindrical solitary waves.

In this work we study the propagation of high-amplitude sound waves in air-filled acoustic networks composed of simply connected waveguides. In particular, we are interested in the interplay between nonlinearity, dispersion and dissipation in 1D and 2D periodic networks. One of the most intriguing phenomena in the presence of nonlinearity and dispersion is the formation and propagation of solitons, namely robust localized waves propagating undistorted in nonlinear dispersive media. First, we consider an 1D acoustic waveguide with periodically varying cross section [1]. The periodicity is employed in order to induce dispersion, while we incorporate nonlinear effects by using a high amplitude wave leading to an amplitude dependent correction of the sound celerity.

Our theoretical approach relies on an 1D effective partial differential equation (PDE) incorporating both the dispersive and nonlinear behaviour of the waveguide in the long-wavelength regime. Dispersion is modelled by a linearised Boussinesq equation, while for the nonlinearity we consider a Westervelt nonlinear term which is the most commonly used equation to model nonlinear effects in air-borne acoustics. Thus, the combination of dispersive terms with a Westervelt type nonlinear term leads to the following Boussinesq type equation, which allows to obtain exact analytical soliton solutions,

$$p_{tt} - c^2 p_{xx} - \beta_m p_{xxtt} - \beta_x p_{xxxx} - b\left(p^2\right)_{tt} = 0 , \quad (1)$$

where c, β_x, β_m and $b = \beta/\varrho_0 c_0^4$ are the effective speed of sound, the dispersive coefficients an nonlinear coefficient respectively.

We complement our analytical results with numerical simulations of the 2D compressible Navier Stokes equation using a time-dependant super-gaussian as a source as illustrated in Fig.(1) (a). The numerical simulations are found to be in good agreement with the theory regarding the soliton formation and propagation as illustrated in blue in Fig.(1) (b-d). On the other hand they unveil the generation of vortex pairs in the proximity of the change of cross section, due to the propagation of the acoustic soliton as illustrated in Fig. (1) (e). The generation and shedding of these vortices is well known to induce nonlinear dissipation in acoustics.

In order to verify our numerical and analytical results we perform experiments using balloon explosions to generate high amplitude acoustic waves inside the waveguide. The acoustic pressure is measured at different positions, as shown in black in Fig. (1) (b-d) for different positions x_i. The experimental results confirm the existence of solitons even in the presence of strong dissipation (linear and nonlinear). Finally, we investigated the soliton characteristics, amplitude/velocity and amplitude/halfwidth. The results were found to be in good agreement with corresponding theoretical and numerical predictions.

Following the results on soliton formation and propagation in 1D waveguide networks and metamaterials [1-2] we consider a square 2D network composed by simply connected waveguides of constant cross section as depicted in Fig.(2) (a). As in the 1D case the goal is to study high-amplitude sound waves in the acoustic network. To do so we extend our effective PDE approach in the 2D case, where we find that the dispersive coefficients are azimuthially dependent to take into account the anisotropy of the dispersion relation along different directions. In the long-wavelength limit we show that weak nonlinear and weak dispersive radially symmetric waves (rings) are modelled by a cylindrical Kortweg de Vries equation (cKdV),

$$p_R + pp_T + \beta(\theta)p_{TTT} + \frac{1}{2R}p = 0 \quad , \tag{2}$$

where $\beta(\theta)$ is the angle dependent dispersive coefficient. As the Eq. (1) in the 1D case, Eq. (2) supports soliton solutions, in this case ring type, that propagate in the acoustic network. To verify our analytical findings we perform numerical simulations, using a time dependent source condition in the form of a gaussian pulse (illustrated in Fig. 2(a)) at the center of a finite lattice of 101x101 size. In Figure (2) (b) we present the temporal profiles at different junction positions, along the horizontal axis, demonstrating the formation of soliton like structures with oscillating tails. The total field is illustrated in Figure (2) (c). In addition we find that the amplitude decay of long wavelength nonlinear pulses is captured by the amplitude decay of the CKdV soliton solutions provided by Ku et al [3].

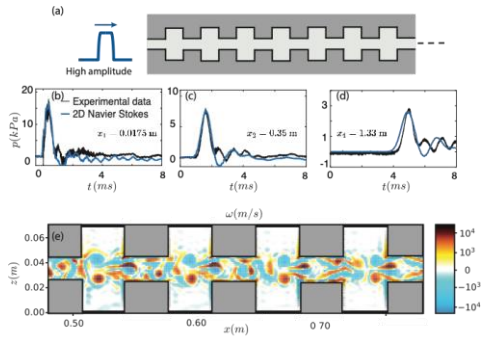

Figure 1 (a) An acoustic waveguide with periodic change of cross section. Illustrated in blue on the left is the high amplitude square pulse source. **(b)** Experimental and numerical temporal profiles in black and blue respectively at position x1. **(c-d)** Same as **(b)** at position x2 x3 respectively. **(e)** The vorticity field after the propagation of the pressure pulse.

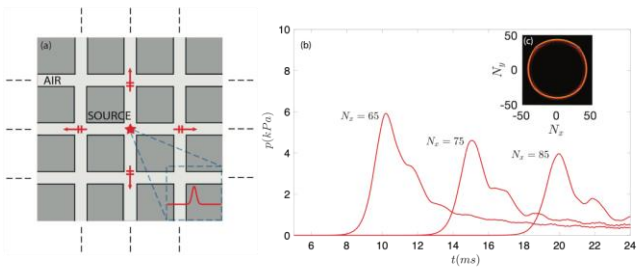

Figure 2 (a) A periodic network composed of simply connected waveguides of constant cross section. The red star corresponds to a gaussian source (illustrated in the blue rectangle) at the center of the network. **(b)** Temporal profiles of the pressure at the junctions $\boldsymbol{N_x}$= 65,75,85. **(c)** The total pressure field of the acoustic network.

References

[1]Achilleos, V., Richoux, O., Theocharis, G., & Frantzeskakis, D. J. (2015). Acoustic solitons in waveguides with Helmholtz resonators: Transmission line approach. *Physical Review E, 91*(2), 023204..

[2] Ioannou Sougleridis, I., Richoux, O., Achilleos, V., Theocharis, G., Desjouy, C., & Frantzeskakis, D. J. (2023). Acoustic solitons in a periodic waveguide: Theory and experiments. *Journal of Sound and Vibration*, *546*, 117433.

[3] Ku K. & Kuehl HH, Cylindrical and spherical Korteweg–de Vries solitary waves. The Physics of Fluids, 22,1343–1348 (1979).

PHONONICS 2023: 6th International Conference on Phononic Crystals/Metamaterials/Metasurfaces, Phonon Transport, and Topological Phononics
Manchester, England, June 12-16, 2023
PHONONICS-2023-0201

Hyperbolic Shear Elastodynamic Waves

Simon Yves[1], Emanuele Galiffi[1], Enrico Maria Renzi[1], Xiang Ni[1], Andrea Alù[1,2]

[1] Photonics Initiative, Advanced Science Research Center, City University of New York, 85 St. Nicholas Terrace, New York, NY 10031, USA
aalu@gc.cuny.edu
[2] Physics Program, Graduate Center, City University of New York, New York, NY 10016, USA

Abstract: We introduce and demonstrate hyperbolic elastodynamic shear waves in tailored metasurfaces. These waves support strong axial dispersion and loss redistribution, enabling broadband, directional, sub-diffractive propagation. We discuss physical insights into this phenomenon, bounds on the bandwidth and strength of these effects and their applications in elastodynamics and nano-optics.

Phonon polaritons in natural crystals have been shown to support a range of exciting applications for mid-infrared nanophotonics, including sub-diffractive imaging, enhanced light-matter interactions and topological trsnsitions [1]. Recently, we have shown that a nontrivial angle between non-degenerate dipolar phonon resonances in gallium oxide can support intriguing polaritonic phenomena, including axial dispersion, i.e., the rotation of the optical axis as a function of frequency, and loss redistribution caused by microscopic shear effects. The net result is that the hyperbolic axes of the resulting polaritons rotate with frequency, and that one branch of the hyperbolic polaritons results in much lower loss than in the more symmetric scenarios in the absence of shear. This new forms of phonon polaritons has been named hyperbolic shear polaritons [2-3].

So far these phenomena have been restricted to photonic platforms and specific mid-infrared frequencies, which are challenging to access. Even more importantly, they rely on limited geometries as a function of the availability in natural crystals. In this talk, we will discuss elastodynamic metasurfaces that translate these concepts to macroscopic 3D printed structures, and maximize these effects. We demonstrate giant axial dispersion and loss asymmetry of hyperbolic elastodynamic waves, reconfigurable by controlling the macroscopic shear phenomena in the metasurface design. We show extreme control of the elastic wave dispersion. Our work can support tunable, highly directional elastic wave propagation, new forms of nondestructive testing and can be translated onto nanophotonic metasurface platforms for nanoscale imaging.

References

[1] Hu, G. et al. Topological polaritons and photonic magic angles in twisted α-MoO3 bilayers. Nature 582, 209-213 (2020).
[2] Passler, N. C. et al. Hyperbolic shear polaritons in low-symmetry crystals. Nature 602, 595-600 (2022).
[3] Hu, G., Ma, W., Hu, D. et al. Real-space nanoimaging of hyperbolic shear polaritons in a monoclinic crystal. Nat. Nanotechnol. 18, 64–70 (2023).

PHONONICS 2023: 6th International Conference on Phononic Crystals/Metamaterials/Metasurfaces, Phonon Transport, and Topological Phononics
Manchester, England, June 12-16, 2023
PHONONICS-2023-0055

Auxeticity enables tuning of topological waveguiding in metamaterial plates

F. Bosia[1], G.Carta[2], M. Morvaridi[1], V.F. Dal Poggetto[3], A. S. Gliozzi[1], M.Miniaci[4], N. Pugno[3,5]

[1] Department of Applied Science and Technology, Politecnico di Torino, Corso Duca degli Abruzzi 24, Italy
federico.bosia@polito.it, antonio.gliozzi@polito.it
[2] Department of Mechanical, Chemical and Materials Engineering, University of Cagliari, Piazza d'Armi, 09123 Cagliari, Italy
giorgio.carta@unica.it , michele.brun@unica.it
[3] Laboratory for Bioinspired, Bionic, Nano, Meta Materials and Mechanics, Department of Civil, Environmental and Mechanical Engineering, University of Trento, Trento, 38123, Italy.
v.fonsecadalpoggetto@unitn.it, nicola.pugno@unitn.it
[4] CNRS, Univ. Lille, Ecole Centrale, ISEN, Univ. Valenciennes, IEMN - UMR 8520, Lille, France.
marco.miniaci@univ-lille.fr
[5] School of Engineering and Materials Science, Queen Mary University of London, London, E1 4NS, UK.

Abstract: Here, we discuss the possibility of controlling topologically protected states through the application of uniaxial deformation in an auxetic metasurface. The proposed structure can be simply realized in a thin slab applying oriented cuts in a hexagonal lattice, where degeneracy is removed and topological band gaps are opened by introducing a controlled variation in the cut lengths. Numerical simulations demonstrate the existence in the resulting auxetic structure of topologically protected scatter-free wave propagation at the interface between two sub-domains with modified cells, in distinct frequency ranges. Exploiting geometrical nonlinearity, the application of a uniaxial strain can then be used to close the topological band gaps or to modify their frequency range, i.e., to remove localization effects or to shift the frequency at which they occur. The spatial and temporal variation of the applied strain field can thus potentially be used for the dynamical tuning of metamaterial topological waveguiding properties, with application in mechanical devices for logic operations and computations.

Auxetic materials (i.e., materials with negative Poisson's ratio) exhibit the interesting and counter-intuitive property of expanding laterally when they are stretched longitudinally [1]. In previous work, we have shown both numerically and experimentally that a porous structure with hierarchical cuts can provide extremely negative Poisson's ratio values by activating kirigami-like behaviour [2]. In this work, we demonstrate that the proposed structure, shown in Fig. 1a, also demonstrates attractive dynamic, as well as static, properties.

The dispersion properties of an auxetic medium with cuts arranged in a hexagonal pattern, as shown in Fig.1a, illustrate the appearance of Dirac cones in two distinct frequency ranges. Perturbing the lengths on 3 of the 6 cuts in a unit cell allows the opening of band gaps in correspondence of broken Dirac cones. The topological properties of the system are quantitatively demonstrated by calculating the Berry curvature and the valley Chern number. Numerical simulations to show the occurrence of robust wave propagation at the interface between two sub-domains consisting of cells with different perturbations of the cut lengths (Fig.1b), including in the case of sharp corners. Additionally, the introduction of a uniform pre-strain, assuming weak material elastic nonlinearity and implementing geometrical nonlinearity, allows to modify the dispersion properties of the unit cells, either closing the band gap used for topological protection, or shifting it to higher frequencies, in the case of the two examined frequency ranges (Fig. 1c). Therefore, the presence of an externally applied uniaxial strain can eliminate the topologically protection of the interfacial wave (giving way to mode conversion) or shift it to a different frequency. Simulations also show the robustness of the proposed effect where, as a consequence of the application of a spatially non-uniform pre-strain, wave localization is lost in a finite region, but naturally reappears beyond it, where the pre-strain is absent (Fig.1d).

The presented numerical study demonstrates the possibility of creating dynamically reversibly tunable topological metamaterials applying pre-strains, exploiting their auxeticity and nonlinearity. This will potentially lead to the realization of proof-of-concept experiments, further extending the possibilities in the fast growing field of tunable metamaterials.

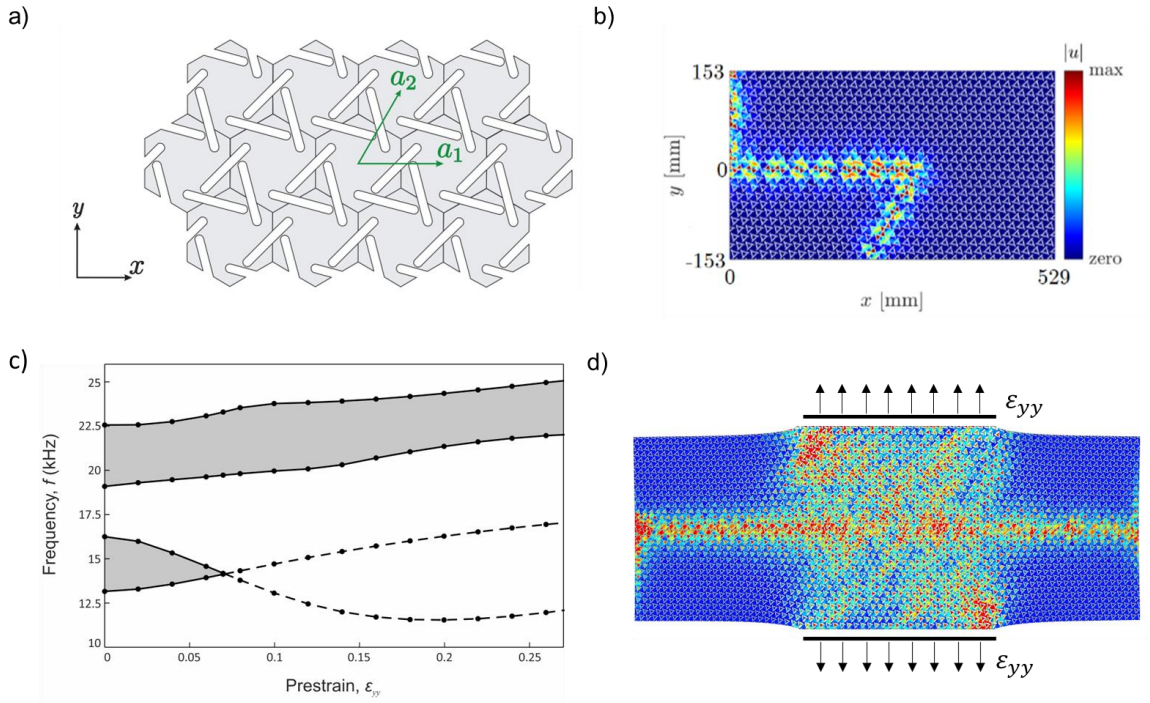

Figure 1: (a). Detail of the considered sample geometry, consisting of hexagonal auxetic unit cells A waveguiding interface can be created by perturbing cut lengths in adjacent cells **(b)**. Robust topologically protected waveguiding along such an interface, including a sharp corner. **(c)** Variation of the two band gap widths (shaded grey areas) for increasing applied uniaxial prestrain: the lower bandgap closes at ε_{yy}~0.07, while the higher one shifts to higher frequencies. **(d)** local modification of topologically protected waveguiding by applying a prestrain along a finite length of the considered sample. Wave amplitudes are represented in colour scale, from blue (zero) to red (max).

.

References

[1] R. H. Baughman, Avoiding the Shrink, Nature 425, 667 (2003).
[2] M. Morvaridi, G. Carta, F. Bosia, A. S. Gliozzi, N. M. Pugno, D. Misseroni, and M. Brun, Hierarchical Auxetic and Isotropic Porous Medium with Extremely Negative Poisson's Ratio, Extreme Mech Lett 48, 101405 (2021).

PHONONICS 2023: 6th International Conference on Phononic Crystals/Metamaterials/Metasurfaces, Phonon Transport, and Topological Phononics
Manchester, England, June 12-16, 2023
PHONONICS-2023-0023

Elastic Metasurface for Multi-Modes

Sung-Won Lee[1], Seung-Il Kim[2, 3], Hong-Min Seung[2, 3], and Joo-Hwan Oh[1]

[1]School of Mechanical Engineering, Ulsan National Institute of Science and Technology, UNIST-gil 50, Eonyang-eup, Ulju-gun, Ulsan 44919, South Korea
lsw6344@unist.ac.kr, joohwan.oh@unist.ac.kr
[2]Intelligent Wave Engineering Team, Korea Research Institute of Standards and Science, Daejeon, 34113, Republic of Korea
[3]Department of Precision Measurement, University of Science and Technology (UST), Daejeon, 34113, Republic of Korea
winone7367@kriss.re.kr, shm@kriss.or.kr

Abstract: The existence of both longitudinal and shear modes is the unique characteristic of elastics. Here, we propose a resonance-based metasurface unit cell which can control both elastic modes simultaneously and independently, by symmetric and rotational resonance. Finally, as a practical application, we suggest a metasurface which can selectively tailor the desired wave, fully reflecting the unwanted wave.

Existence of various modes such as longitudinal and shear waves is one of the unique characteristics that makes elastic wave different from acoustic or electromagnetic waves. Nonetheless, most of the previous elastic metasurfaces have considered only single mode incidence case since there has been no way to tailor the multi-modes simultaneously. To be specific, the effective mass and modulus should be tuned for the corresponding single wave, which infers that at least four effective parameters should be tuned independently for only two different wave modes. Here, we suggest a unit cell structure based on the design which can be deformed symmetrically and rotationally, so that the symmetric and rotational resonance can independently tune the longitudinal and shear waves, respectively.

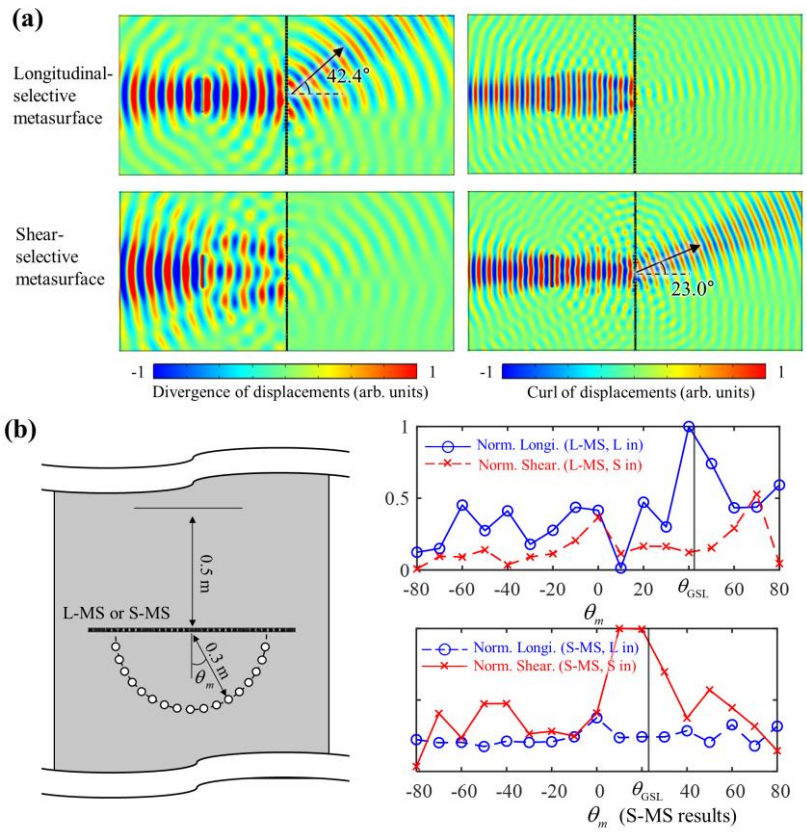

Figure 1. The longitudinal-selective and shear-selective metasurface (a) numerical studies results and (b) experimental results.

Finally, as a practical example, we design an elastic metasurface which can steer the desired wave with blocking the unwanted wave. i.e., the longitudinal-selective metasurface fully tailors longitudinal wave with full reflection of shear wave, while the shear-selective metasurface fully tailors the shear wave with full reflection of longitudinal wave. Both selective metasurfaces were validated numerically and experimentally. As can be seen in Figure. 1 (a), the corresponding waves are well-tailored according to the generalized Snell's law[1], while the undesired modes are fully reflected. Also, the experimental results show good agreement with the numerical study. Experimental results in Figure. 1 (b) shows the full transmission at the predicted angle by generalized Snell's law, while the undesired wave is suppressed at every angle.

References

[1] N. Yu, P. Genevet, M. Kats, F. Aieta, J. Tetienne, F. Capasso, and Z. Gaburro, *Science*, **334**, 333 (2011).

PHONONICS 2023: 6th International Conference on Phononic Crystals/Metamaterials/Metasurfaces, Phonon Transport, and Topological Phononics
Manchester, England, June 12-16, 2023
PHONONICS-2023-0039

Conformally Graded Metamaterials for Wave Attenuation

Charles Dorn[1], Dennis M. Kochmann[1]

[1] Department of Mechanical and Process Engineering, ETH Zurich, 8092 Zurich, Switzerland
dornch@ethz.ch, dmk@ethz.ch

Abstract: We present spatially graded metamaterials designed via conformal mappings as an effective means of elastic wave attenuation. Conformal maps involve only local scaling and rotation, which leads to metamaterials with approximately geometrically similar unit cells. We show that self-similarity leads to extreme wave attenuation capabilities, which we demonstrate in planar and curved meta-surfaces.

Periodic mechanical metamaterials with engineered bandgaps are an effective solution for vibration attenuation. Extensive research has focused on the inverse design of unit cells to achieve desirable bandgaps[1]. Alternatively, graded metamaterials with spatially varying unit cells offer a much larger design space, since the contents of the unit cells *and* how the unit cells vary in space can be designed. The enlarged design space of graded metamaterials allows for properties of different unit cells to be combined to achieve wave manipulation not possible with periodic architectures. For example, graded metamaterials achieve wide effective bandgaps spanning the bandgaps of constituent unit cells[2]. While the ability to combine unit cell properties using grading has been demonstrated, most existing work relies on intuitive designs; systematic design to take advantage of the vast design space of spatial grading remains an open problem.

In this work, we design spatially graded metamaterials using conformal mappings, which are mappings that involve local uniform scaling and rotation only. Assuming sufficiently dense unit cells, all unit cells of a conformally graded metamaterial are geometrically similar because each unit cell is only scaled and rotated by a conformal mapping.

Geometric similarity of unit cells allows for a greatly simplified framework for understanding wave propagation. In fact, the dispersion relations of a reference unit cell can be used to directly determine the dispersion relations of any geometrically similar unit cell. Let $\omega(\boldsymbol{k})$ be the dispersion relations of a reference unit cell, relating frequency ω and wave vector $\boldsymbol{k}$. The dispersion relations $\omega'(\boldsymbol{k}')$ of a scaled (by a factor of J) and rotated copy of the reference unit cell are determined from the reference unit's dispersion relations by

$$\omega'(\boldsymbol{k}') = J^{-1}\omega(\boldsymbol{k}), \tag{1}$$

where $\boldsymbol{k}'$ is the wave vector with respect to the scaled and rotated unit cell. Thus, the dispersion relations scale inversely with the unit cell size; the derivation will be outlined in the presentation.

To understand how to exploit this inverse frequency scaling relation, we view wave propagation from the perspective of ray theory, which we have recently developed for graded mechanical metamaterials[3] and is valid at high frequencies. There are two properties of ray solutions that we utilize. The first is that each ray is fixed at a certain frequency and the second is that each ray is associated with a particular mode. Combining these properties with Eq. (1), we can make a general observation: *high frequency waves cannot propagate along trajectories that see significant changes in unit cell size.* The properties of rays ensure that a ray is confined to a level set of its dispersion surface at the ray's fixed frequency ω_r. If that dispersion surface has a nonzero minimum frequency, it is always possible to scale that surface up or down such that it no longer intersects ω_r. This scaling argument, however, is not possible at low frequencies of dispersion surfaces emerging from the $\omega = 0$ limit.

We demonstrate that waves cannot propagate between small and large unit cells in the conformally graded truss lattice of Fig. 1a. Each unit cell consists of four beams along its edges and all unit cells are geometrically similar and approximated as squares. To exemplify the mechanism for wave attenuation, one dispersion surface of unit cell 1 is plotted in Fig. 1b, which is computed using a beam finite element (FE) model[4] (normalized by $\omega_0 = l^{-1}\sqrt{E/\rho}$, where l is the edge length and E and ρ are Young's

modulus and density). Consider a ray of frequency ω_r belonging to this mode that begins at unit cell 1 and propagates radially outward. We only need to consider this dispersion surface since the ray cannot switch between modes. Since the frequency of the ray is fixed, the wave vector of the ray lies on the ω_r level set of the dispersion surface. It is evident that this ray is forbidden in unit cell 2. This is because unit cell 2 is larger than unit cell 1 (with relative scaling factor $J > 1$), so by Eq. (1) its dispersion surface scales with J^{-1}. The scaling factor is large enough that the dispersion surface at unit cell 2 does not intersect ω_r, so propagation is forbidden.

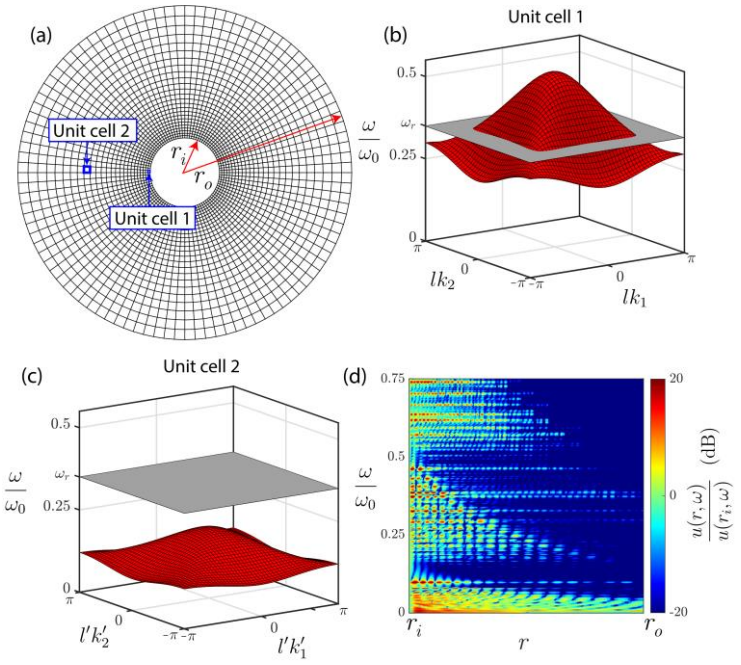

Figure 1 (a) Conformally graded truss lattice. One dispersion surface of unit cell 1 **(b)** and unit cell 2 **(c)**. **(d)** Displacement frequency response along a radial line from a FE simulation.

A similar scaling argument can be applied to all dispersion surfaces, except at low frequencies of those emerging from $\omega = 0$. Thus, this truss lattice acts as a *low-pass filter* of elastic waves since there is a sufficient scaling difference between unit cells at r_i and r_o. To demonstrate this, a transient finite element simulation was performed with broadband excitation applied along the inner radius r_i. Fig. 1d shows the frequency response along a radial line with respect to the displacement applied at r_i. Above a low-pass cutoff frequency of about $\omega = 0.05\omega_0$, all frequencies are attenuated before reaching r_o.

The design principle that large scaling differences in a conformally graded metamaterial attenuate waves can be exploited in a systematic design method. We develop an approach to design conformally graded meta-surfaces with a prescribed distribution of unit cell size. For example, Fig. 2 shows a 'conformal bump' with a region of large unit cells in the middle. Here, curvature is required to accommodate the large unit cells. Due to the unit cell scaling difference, the large units at the center are isolated from high frequency vibrations applied to the boundaries. The color map in Fig. 2 shows the maximum displacements during a transient finite element simulation where broadband excitation was applied to the lower left (red) edge, which demonstrates the isolation of the bump from incident waves.

Conformally graded metamaterials are shown to be a powerful tool for attenuating elastic waves, with the ability to achieve *low-pass* attenuation. A general and simple understanding of waves in such architectures is possible through a dispersion relation scaling argument since all unit cells are geometrically similar. This allows for systematic design of graded metamaterials for wave attenuation. Experimental validation on the truss lattice of Fig. 1a will also be presented, demonstrating the promise of conformal grading for vibration isolation applications.

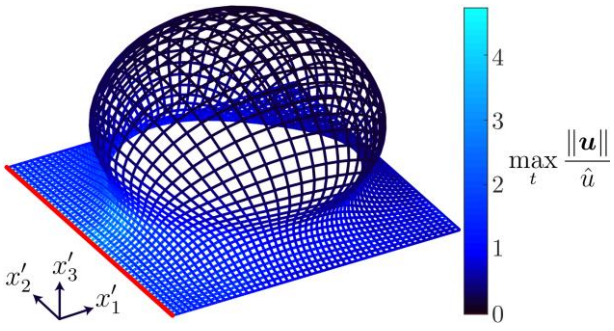

Figure 2 Conformally graded metamaterial surface. Color indicates displacement amplitude during a FE simulation.

References

[1] O. Sigmund and J.S. Jensen, *Phil. Trans. R. Soc. A*, **361**, 1001 (2003).
[2] G. Trainiti, J. Rimoli, and M. Ruzzene, *Int. J. Solids Struct.* **97**, 431 (2016).
[3] C. Dorn and D. Kochmann, *J. Mech. Phys. Solids*, **168**, 105049 (2022).
[4] A. Zelhofer and D. Kochmann, *Int. J. Solids Struct.*, **115**, 248-269 (2017).

PHONONICS 2023: 6th International Conference on Phononic Crystals/Metamaterials/Metasurfaces, Phonon Transport, and Topological Phononics
Manchester, England, June 12-16, 2023
PHONONICS-2023-0119

Design and Manufacturing of Monolithic Mechanical Metastructure with Ultrawide Bandgap for Low Frequency Vibration and Noise Control

Muhammad[1,2], John Kennedy[1], C. W. Lim[2]

[1] *Department of Mechanical, Manufacturing and Biomedical Engineering, Trinity College Dublin, Ireland, College Green, Dublin 02, Ireland*
Dr.Muhammad@tcd.ie, jkenned5@tcd.ie
[2] *Department of Architecture and Civil Engineering, City University of Hong Kong, 83 Tat, Che Avenue, Kowloon Tong, Kowloon, Hong Kong SAR*
bccwlim@cityu.edu.hk

Abstract: The all direction vibration and noise control by novel monolithic metastructures have received considerable research attention in the vibroacoustic community to solve multiple vibration and noise related engineering problems. This new class of acoustic metamaterial has grasped strong root in this research community for its versatile dynamic properties and wave manipulation characteristics exhibited by single unit cell structure. The advancements in numerical computation codes and advanced additive manufacturing technology provide other favorable avenues for breakthrough research in vibration and noise control technology. In that context, the present study proposes a novel 3-D monolithic mechanical metastructure with capability to induce ultrawide three-dimensional bandgap with relative bandwidth or gap-to-mid-gap ratio 171.5%. The bandgap is induced and discussed by principle of mode separation that utilizes the locally resonant global and local modes to open ultrawide bandgap. The proposed metastructure comprises of thin elastic beams connected orthogonally with rigid spherical masses. The axial compression mode by complete unit cell structure and the flexural stiffness of supporting elastic beams are manipulated to generate low frequency extremely wide bandgap. A monoatomic mass-spring chain analytical model is developed to obtain and compare the acoustic mode frequency responsible for initiating the bandgap with numerical wave dispersion study. The wave attenuation inside the bandgap frequencies are demonstrated by developing finite array model and performing numerical frequency response study through two different commercial FEA codes. The analytical and numerical findings are corroborated through experiment test on the 3-D printed prototype. An excellent agreement between numerical and experimental findings are obtained. The simple structural configuration, monolithic design and all direction wave control strategy may find potential industrial and infrastructural applications where all direction wave control is desirable.

The technological advancements of present and future technologies are relying on safe, sustainable, efficient and environmentally friendly technologies. Radically new industrial and infrastructural techniques, transportation and energy production sectors have substantially modified the urban and interurban vibrations and acoustic landscapes. Vibrations and noise control are among the essential and demanding field of research. Breakthrough technologies and novel smart approaches to cater these challenges are of utmost importance. The recent surge in metamaterial studies [1-4] and fascinating findings are testimony to the fact that the idea of metamaterial is no longer limited to pure theoretical concepts. In addition, the peculiar dynamic characteristics offered by these synthetic designs make it a potential candidate for vibration and noise control. These metamaterial findings are a prerequisite to advancements in computational approaches, improved numerical codes and additive manufacturing technology for manufacturing solid structures at any length that were once imagined unmanufacturable. When combined, this multi-disciplinary research provides a new platform for the design and application of novel metastructures to control vibration and noises over an ultrawide frequency range.

The present study is related to the novel design of monolithic 3D mechanical metastructure and to envisage the wave attenuation by the proposed structure over ultrawide frequency region. Further details about analytical modelling, numerical simulations and experimental setup can be found in Muhammad and Lim [5].

The opulent topology for the unit cell structure and schematic diagram for the finite array is shown in Figure 1. The lattice constant of the unit cell structure is a=50mm and all other geometric parameters are presented with reference to it. A detailed geometric parameters are discussed in Muhammad and Lim [5]. The proposed metastructure consists of two parts (i) rigid spherical masses supported by (ii) orthogonal thin elastic beams. This model can be replicated to one-dimensional monoatomic mass-spring chain. We calculated the acoustic mode frequency responsible for opening the bandgap. The analytical frequency obtained is . A comparison with numerical results showed percentage error of 8~9%. The numerical study is conducted by employing two different finite element code COMSOL Multiphysics 5.4® and ANSYS workbench R1 2020®. Further details about numerical and analytical model is given by Muhammad and Lim [5].

The numerical wave dispersion study revealed the presence of bandgap ranging from 1292.5 Hz to 16875 Hz corresponding to opening (global resonant mode) and closing (local resonant mode) bounding edges respectively. As shown in Figure 1, a finite array of supercell structure is constructed and frequency response study is performed. The harmonic excitation force is applied at the left edge and response in the form of displacement fields are recorded at the right end. The wave transmission curve showed presence of ultrawide bandgap covering broadband frequency region. The effect of material damping on the wave transmission curve is also taken into consideration. Material damping flattened the wave transmission curve and stretch the vibration attenuation region beyond the closing bounding edge [6, 7]. To corroborate the numerical findings, 3D printer OBJET30 Stratasys Ltd is used to manufacture the 3-D printed prototype, as shown in Figure 1. We performed low amplitude vibration test to envisage the real-time vibration attenuation over ultrawide frequency range. A good agreement between numerical and experimental results are observed although some discrepancy between reported results does exist that is explained in Muhammad and Lim [5].

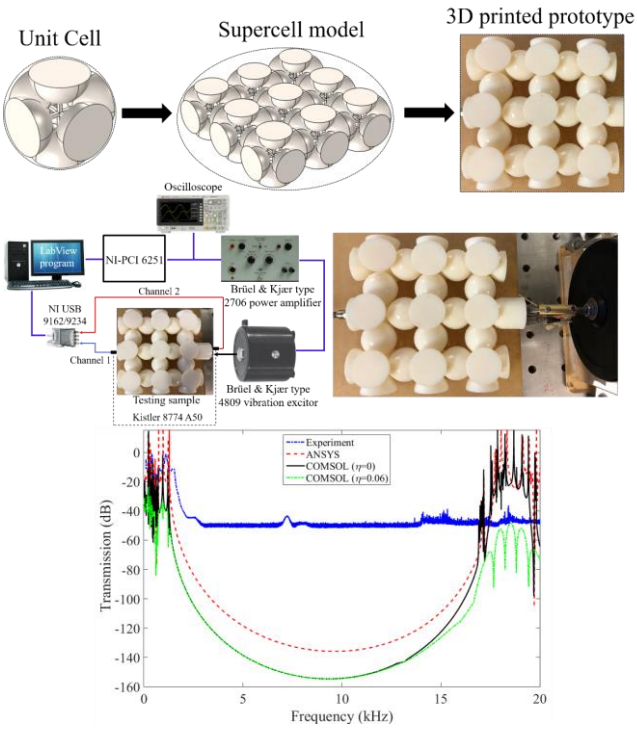

Figure 1. Schematic diagram for unit cell structure with finite supercell model. The real time 3D printed prototype is also shown. The experimental setup developed for performing low amplitude vibration test is presented. The numerical and experimental wave transmission curves revealed low frequency ultrawide vibration attenuation spread over broadband frequency range.

References

[1] Hussein, M. I., Leamy, M. J., and Ruzzene, M., 2014, *Applied Mechanics Reviews*, 66(4), p. 040802.
[2] Bertoldi, K., Vitelli, V., Christensen, J., and van Hecke, M., 2017, *Nature Reviews Materials*, 2(11), p. 17066.
[3] Nassar, H., Yousefzadeh, B., Fleury, R et al., *Nature Reviews Materials*, 5(9), pp. 667-685.
[4] Muhammad, and Lim, C. W., 2020, *Archives of Computational Methods in Engineering*, 29, 1137–1198.
[5] Muhammad, and Lim, C. W., 2021, *Archives of Civil and Mechanical Engineering*, 21, 52.
[6] Muhammad, and Lim, C. W., 2020, *Journal of Vibration and Acoustics*, 142(6), p. 061012.
[7] Muhammad, Lim, C. W., Li, J. T. H., and Zhao, Z., 2020, *Extreme Mechanics Letters*, 41, p. 100994.

PHONONICS 2023: 6th International Conference on Phononic Crystals/Metamaterials/Metasurfaces, Phonon Transport, and Topological Phononics
Manchester, England, June 12-16, 2023
PHONONICS-2023-0021

Tapered Resonator-Based Phononic Crystal: Avoided Level Crossings, Robust Self-Collimation, and Bi-Refringence

Debanik Das[1] , Chandriker K. Dass[2], Piyush J. Shah[2], Robert Bedford[2], and L.R. Ram-Mohan[3]

[1] Department of Physics, Worcester Polytechnic Institute, Worcester, Massachusetts 01609, USA,
ddas@wpi.edu,
[2] Air Force Research Laboratory, Materials and Manufacturing Directorate, Wright-Patterson Air Force Base, Dayton, Ohio 45433, USA
chandriker.k.dass.1@us.af.mil, piyush.shah.1.ctr@us.af.mil, robert.bedford@us.af.mil
[3]Departments of Physics, Electrical and Computer Engineering, and Mechanical Engineering, Worcester Polytechnic Institute,
Worcester, Massachusetts 01609, USA
lrram@wpi.edu

Abstract: In search of novel phononic crystals to effectively control the propagation of elastic waves, we use finite element method to investigate a new single-material phononic crystal (PnC) with unit cells containing tapered resonators which shows anomalous dispersion phenomena such as self-collimation and bi-refringence, phenomenon that is rare to find in a single-material PnC device.

The engineering of sound waves is a long-standing subject of research; around 20 BC, the Roman architect Vitruvius wrote about manipulating the acoustic properties of theaters, such as interference, echoes, and reverberation, by making the seats ascending and placing bronze vessels in appropriate locations of the theater to work as resonators. In recent times, following the theory of photonic crystals relevant to electromagnetic waves, phononic crystals (PnCs) are used to control elastic waves ranging from low frequency sound waves to high-frequency heat-conducting phonons. PnCs are designed by periodically arranging voids or inclusions in a base material where the base and inclusion materials have highly contrasting elastic parameters such as coefficients of the stiffness tensor and density. For both the electromagnetic wave and the elastic wave, conventional periodic crystals offer a finite bandgap originating from the Bragg scattering mechanism that has its root in discrete translational symmetry. In addition, exotic and anomalous physical phenomena such as negative refraction, bi-refringence, focusing, and collimation have been theoretically modeled and demonstrated. These properties have been associated with low-frequency locally resonant modes. Though the self-collimation effect has been previously studied extensively, most of the studies focus on the acoustic wave and airborne sounds. Hence, micro- and nanoscale applications at a frequency higher than MHz require innovative designs to tailor elastic wave propagation. Moreover, existing self-collimating device fabrications are limited by certain factors. Often many of the theoretically designed PnCs are hard to fabricate because of their complex geometries predicted by optimization techniques or combination of two or more highly contrasting materials. A new kind of PnC with unit cells having tapered resonators (TRs) is a promising candidate to solve these issues. The working principle of TR-based PnC has a similarity with an acoustic black hole (ABH)-based PnC. In the ABH-based PnCs, the central region that absorbs the elastic wave has ideally zero thickness. This restricts the structure for potential application as a finite thickness device, which can harvest the elastic energy and can host systems such as nitrogen- , silicon-, or germanium-vacancy defect centers. Although the applications of phononics in quantum information processing is mainly limited to highly confined phononic states, recent experimental progress has demonstrated the use of traveling phonons to create on-chip architecture for classical and quantum information processing. TR-based PnCs with dimension in the nm-range and frequency in the GHz-range have the potential to support these recent developments. The proposed device has a finite thickness everywhere and offers interesting wave dispersion phenomena such as zero group velocity, collimation, and bi-refringence. The circular TR (shieldlike structural unit) has a gradually increasing radial thickness profile with the highest thickness at the center. It is layered on the top of a hole-based conventional PnC. The specific structure starting with a narrow

wedge-like feature restricts the transfer of elastic wave energy between the thin Si plate and the TR. This results in an effective negative refractive index and leads to self-collimation and bi-refringence. In this talk we'll discuss the properties of this class of PnC and the applications of PnCs in quantum technologies.

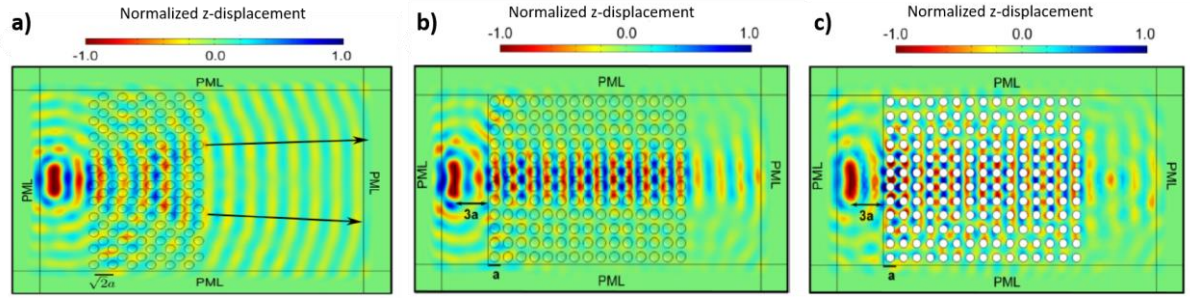

Figure 1 Normalized out-of-plane displacement of PnC for a **(a)** tapered resonator design showing bi-refringence and **(b)** self-collimation, and a **(c)** design without a tapered resonator on top showing uncollimated propagation[1].

References

[1] D. Das, C.K. Dass, P.J. Shah, R. Bedford, and L.R Ram-Mohan, *J. Appl. Phys.* **133(5)**, 055103 (2023).

PHONONICS 2023: 6th International Conference on Phononic Crystals/Metamaterials/Metasurfaces, Phonon Transport, and Topological Phononics
Manchester, England, June 12-16, 2023
PHONONICS-2023-0122

Breaking the symmetry: Do imperfect Phononic Crystals work?

Visnja Babacic[1], Marianna Sledzinska[2], Thomas Vasileiadis[1], Clivia M. Sotomayor Torres[2,3] and Bartlomiej Graczykowski [1]

[1] Faculty of Physics, Adam Mickiewicz University, Uniwersytetu Poznanskiego 2, 61-614 Poznan, Poland, visnja.babacic@amu.edu.pl, thomas.vasileiadis@amu.edu.pl, bartlomiej.graczykowski@amu.edu.pl
[2] Catalan Institute of Nanoscience and Nanotechnology (ICN2), CSIC and BIST, Campus UAB, Bellaterra, 08193, Barcelona, Spain
[3]ICREA, Pg. Lluís Companys 23, 08010 Barcelona, Spain
clivia.sotomayor@icn2.cat, marianna.sledzinska@icn2.cat,

Abstract: We investigate the effect of the broken symmetry on the propagation of GHz phonons in 2D Phononic Crystals. The mid-plane symmetry-breaking leads to a new band gap resulting from the avoided crossing. The perturbation of the translational symmetry affects mostly high-frequency bands, while the low-frequency Bragg gaps are preserved up to the highest level of the lattice disorder.

Phononic crystals (PnCs) are known to be sensitive to structural disorders leading to limited functionality of PnC-based devices. Translational disorder, surface/interface roughness, and shape/size defects of the periodic motifs are unavoidable obstacles for practical applications. Consequently, the dispersion relations of real PnCs may significantly differ from those calculated for designed ideal structures. Moreover, the calculation of the band structure for imperfect systems without possible simplifications, such as periodic boundary conditions, often ends up as an unfeasible computational problem. Thus, it is crucial to investigate experimentally the phonon propagation in PnCs of intended and controlled structural imperfections that may lead to decoherence, i.e., Brillouin zones or band gap vanishing, and in some cases, unforeseen benefits.

Here, we investigate the impact of two types of broken symmetry on the band structure of 2D solid-air PnCs fabricated by making a lattice of holes in 250 nm thick Si membranes. In pristine membranes, 1D confinement results in the appearance of the family of symmetric, antisymmetric, and shear horizontal Lamb waves [Figure 1 (a)]. Making an ordered pattern of holes leads to band folding at the X point of the first BZ.[1–3] This can lead to the opening of Bragg gaps, as illustrated in Figure 1 (a). On the other hand, in the case of randomly perturbed lattices, the phonon coherence gradually vanishes while the disorder increases. First, this leads to blurring of the BZ edge, vanishing of the zone folding, and, finally, the closing of the Bragg gaps. At a sufficient level of disorder, it ends with the phonon dispersion of a randomly porous membrane resembling that of an effective medium.

We fabricated solid-air PnCs by patterning a square lattice of holes in silicon-on-insulator (SOI) membranes by electron beam lithography (EBL) and reactive ion etching (RIE). Figure 1 (b) displays the scanning electron microscope (SEM) image of the PnC with an ordered lattice. Figure 1 (c) shows that the fabrication process leads to cone-like shaped holes rather than cylindrical ones. This results in broken mid-plane symmetry of PnCs. We then introduced different levels of translational in-plane disorder in the lattice. The SEM images of exemplary samples with in-plane translational disorder are displayed in Figure 1 (e), where η denotes the level of disorder.

To experimentally explore the modification of the dispersion relation in the considered PnCs caused by broken mid-plane and in-plane translational symmetry, we employed Brillouin light scattering (BLS). Moreover, we applied the finite element method (FEM) to obtain the theoretical dispersion relations of the non-perturbed structures. Our results have shown that the broken mid-plane symmetry leads to the opening of full band gaps due to the avoided crossing of quasi-symmetric and quasi-asymmetric branches.[4] Therefore, introducing asymmetry with respect to the middle plane of PnCs

leads to new possibilities and applications for these systems. The introduction of in-plane translational disorder modifies the phononic band structure of the PnCs. We show that increasing the disorder leads to reduced coherence, evidenced by the disappearance of peaks in the BLS spectra. Nevertheless, certain peaks remain, even for the highest level of disorder. More interestingly, the full band gap resulting from the avoided crossing, high-frequency band gap for in-plane modes, and partial Bragg gap remain robust to those imperfections. Thus, even the PnCs with high levels of in-plane disorder exhibit band gaps, confirming that extremely high precision in fabrication is not mandatory for certain applications. The only impact that the disorder has is on the width of these bandgaps. Our results provide new insights regarding the influence of imperfections on phononic band structure in the GHz range, relevant for applications in telecom devices, ultra-low temperature thermal transport and optomechanics.

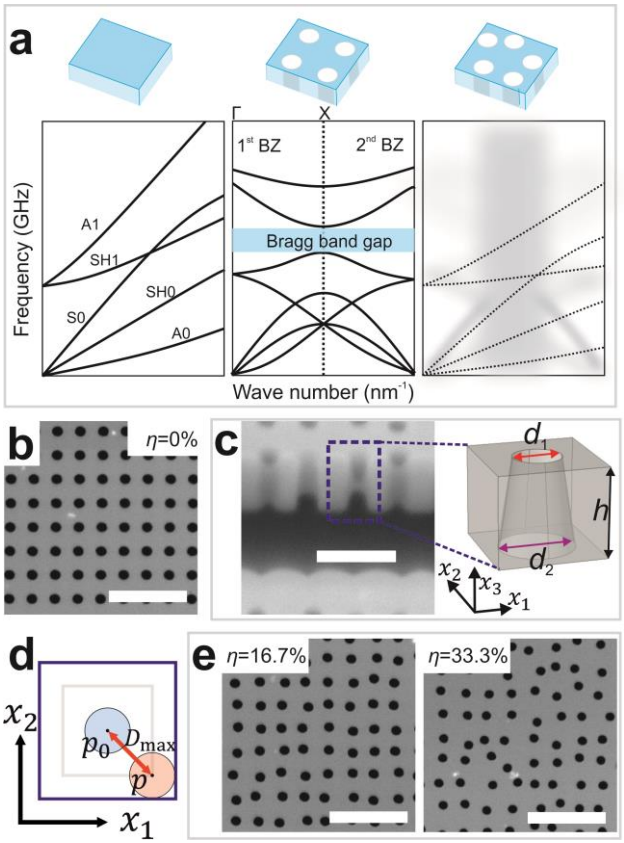

Figure 1 (a) Illustrative phonon dispersion curves for plane nanomembrane (left), ordered (center), and disordered 2D PnC (right). **(b)** SEM image of the ordered pattern of holes in 250 nm thick Si-membrane based PnC. The scale bar is 1 μm **(c)** Cross-section SEM image of an exemplary sample (left) and the corresponding unit cell schematics (right). Symbols d_1, d_2, and h denote diameters of upper and lower hole diameters and membrane thickness, respectively. The scale bar is 500 nm. **(d)** Schematic illustration of the unit cell top view being a square with a hole and of random displacements of holes in the x_1x_2 plane for disordered PnC. Symbols p_0, p, and D_{max} denote the hole position in the ordered lattice, the hole position after displacement, and the maximum allowed shift distance, respectively. **(e)** SEM images of exemplary disordered PnCs with indicated level of disorder, η. The scale bars are 1 μm.

References

[1] S. Alaie, D.F. Goettler, M. Su, Z.C. Leseman, C.M. Reinke, and I. El-Kady, *Nat. Commun*. **6**, 7228 (2015).
[2] J. Lim, H.-T. Wang, J. Tang, S.C. Andrews, H. So, J. Lee, D.H. Lee, T.P. Russell, and P. Yang, *ACS Nano* **10**, 124 (2016).
[3] C.M. Reinke, M.F. Su, B.L. Davis, B. Kim, M.I. Hussein, Z.C. Leseman, R.H. Olsson-III, and I. El-Kady, *AIP Adv*. **1**, 041403 (2011).
[4] Z. Hou and B.M. Assouar, *J. Phys. Appl. Phys*. **41**, 215102 (2008).

PHONONICS 2023: 6th International Conference on Phononic Crystals/Metamaterials/Metasurfaces, Phonon Transport, and Topological Phononics
Manchester, England, June 12-16, 2023
PHONONICS-2023-0145

Engineering phononic crystals – always finite and never perfectly periodic

Steffen Marburg[1], Felix Kronowetter[2]

[1] Chair of Vibroacoustics of Vehicles and Machines, Department of Engineering Physics and Computation, Technical University of Munich, Boltzmannstrasse 15, 85748 Garching, Germany, steffen.marburg@tum.de, felix.kronowetter@tum.de

Abstract:

Analysis of periodic structures has revealed many interesting material properties, which are hardly available in nature. Often, their analysis is limited to infinite and perfectly periodic systems. For phononic crystals, this includes perfectly periodic sound pressure distributions which are completely unrealistic in real applications. In this talk, the authors are discussing the interaction of mistuned meta-atoms and that they may couple in. Furthermore, the distribution of eigenvalues in the complex plane of a finite sonic crystal exhibits some interesting features, which are not (yet) fully understood by the authors. The results may help to understand how parameter variation and inaccuracies from one unit cell to the other may influence the performance of a sonic crystal as a tool for passive noise control.

Introduction

Acoustic metamaterials (AMMs)[1-7] break the rules of classic noise reduction, e.g. the dependence on mass and stiffness. AMMs usually consist of a perfectly infinite-periodic arrangement of meta-atoms. A notable property of AMMs is that they feature material properties that cannot be found in traditional materials, for example a negative effective mass density[8-10]. AMMs are mostly based on meta-atoms of complex shape, thus thermo-viscous losses need be considered, since they have a significant impact on the metamaterial performance[11-13]. Often, meta-atoms are subwavelength structures and are arranged close to each other. The analysis of AMMs in the reciprocal space leads to dispersion curves with corresponding band gaps, e.g. Ref. 7. By introducing uncertainties to AMMs we observe a significant change in the resulting band gaps, which are of reduce width[14].

We are always limited in space when designing real AMM applications and hence consider the AMM as finite-periodic arrangement of meta-atoms. Since meta-atoms behave like local resonators, they interact with propagating waves. Pressure coupling between individual meta-atoms occurs. Pressure coupling can lead to enhanced sound attenuation. Similar coupling effects are observed in either electro-magnetic metamaterials[15,16] or non-linear synchronization theory[17]. Studies of coupled meta-atoms exist for unit cell designs in the reciprocal space with periodic boundary conditions[18] or coupled resonators in waveguides[19].

Results

Here, we study the modal interaction of two C-shaped meta-atoms in an infinite 2d-domain. First, we run an eigenvalue analysis to identify two interacting high-Q modes. We denote them symmetric and antisymmetric cavity resonant modes, representing in- and anti-phase oscillation, respectively. Then, we investigate the influence of varying parameters on modal behavior and transmission spectrum (plane wave excitation). The results are mainly taken from more extended papers of the authors[20,21].

First, we vary the distance between the resonators. Starting from zero to twice the wavelength of their resonance frequency. We observe that the real and imaginary parts oscillate around the complex resonant frequency of the individual resonators. The crossing points of the real parts - or points of modal degeneracy - occur at periodic distances of half wavelength. Similar results are found for the imaginary part, but shifted by about a quarter wavelength compared to the real part. A transmission study shows that the highest sound attenuation occurs at the points of modal degeneracy.

Second, we introduce a detuning in one of the C-shapes. This is done by increasing the resonance frequency by five percent. As a result, the modes no longer cross in the real part, but the number of

crossing in the imaginary parts doubles. The state of degenerate modes is no longer realizable (except for the first crossing). We conclude that detuning weakens the modal coupling and hence leads to poorer sound attenuation properties compared to identical resonators. We now increase the radiation loss of the detuned C-shape by increasing its aperture width. Thus, the modal crossings of the real part are restored and we get degenerate modes again. We deduce that increased radiation loss stabilizes the system against detuning and increases modal coupling.

Third, we adjust the relative orientation of the apertures of the C-shapes. Starting from facing apertures and rotating them symmetric to 180 degrees. We compute two mappings in the rotation-distance plane. One for the difference of the real parts of the modes to identify modal crossings and one to analyze the transmission spectrum. The latter shows that transmission dips occur at locations of modal crossings (only where the symmetric mode dominates). Even regions of degeneracy form, enabling larger manufacturing tolerances. The authors find it quite interesting, that the maximum dip in the transmission spectrum it not at an orientation angle of 90 degrees but at a particular configuration dependent on orientation and distance.

Conclusion

We present an extensive study on the interaction of two meta-atoms. The two main findings are that we observe regions of modal degeneracy enabling larger manufacturing tolerances and that we can tune the system by changing parameters like distance, radiation loss and orientation. We even identify a best-case arrangement with maximum sound attenuation.

References

[1] S. Cummer, J. Christensen, and A. Alù, *Controlling sound with acoustic metamaterials*, Nature Rev. Mat., **1**, 16001 (2016).
[2] J. J. Wu, F. Ma, S. Zhang, and Liming Shen, *Application of Acoustic Metamaterials in Low-frequency Vibration and Noise Reduction*, Journal of Mechanical Engineering, **52**, 68-78 (2016)
[3] P. A. Deymier, *Acoustic Metamaterials and Phononic Crystals*, Springer, 2013.
[4] G. Ma and P. Sheng, *Acoustic metamaterials: From local resonances to broad horizons*, Science Adv., **2**, e1501595 (2016).
[5] F. Zangeneh-Nejad and R. Fleury, *Active times for acoustic metamaterials*, Reviews in Physics, **4**, 100031 (2019).
[6] A. Melnikov, Y. K. Chiang, L. Quan, S. Oberst, A. Alù, S. Marburg, and D. A. Powell, *Acoustic metaatom with experimentally verified maximum Willis coupling*, Nature Communications, **10**, 3148(2019).
[7] D. P. Elford, L. Chalmers, F. V. Kusmartsev, and G. M. Swallowe, *Matryoshka locally resonant sonic crystal*, The Journal of the Acoustical Society of America, **130**, 2746-2755 (2011).
[8] G. W. Milton and J. R. Willis, *On modifications of Newton's second law and linear continuum elastodynamics*, Proceedings of the Royal Society A: Mathematical, Physical and Engineering Sciences, **463**, 855-880 (2007).
[9] S. Yao, X. Zhou, and G. Hu., *Experimental study on negative effective mass in a 1D mass–spring system*, New Journal of Physics, 10, 43020 (2008).
[10] Z. Liu, X. Zhang, Y. Mao, Y. Y. Zhu, Z. Yang, C. T. Chan, and P. Sheng, *Locally Resonant Sonic Materials*, Science, **289**, 1734-1736 (2000).
[11] Y. K. Chiang, S. Oberst, A. Melnikov, L. Quan, S. Marburg, A. Alù, and D. A. Powell, *Reconfigurable Acoustic Metagrating for High-Efficiency Anomalous Reflection*, Physical Review Applied, **13**, 064067 (2020).
[12] V. Henríquez, P. Andersen, J. Jensen, P. Juhl, and J. Sánchez-Dehesa, *A Numerical Model of an Acoustic Metamaterial Using the Boundary Element Method Including Viscous and Thermal Losses*, J. of Comp. Acoustics, **25**, 1750006 (2017).
[13] V. C. Henríquez, V. M. García-Chocano, and J. Sánchez-Dehesa, *Viscothermal Losses in Double-Negative Acoustic Metamaterials*, Phys. Rev. Applied, **8**, 014029 (2017).
[14] F. Kronowetter, L. Moheit, M. Eser, K. K. Sepahvand, and S. Marburg, *Spectral Stochastic Infinite Element Method in Vibroacoustics*, Journal of Theoretical and Computational Acoustics, **28**, 2050009 (2020)
[15] D. A. Powell, M. Lapine, M. V. Gorkunov, I. V. Shadrivov, and Y. S. Kivshar, *Metamaterial tuning by manipulation of near-field interaction*, Phys. Rev. B, 82, 155128 (2010).
[16] D. A. Powell, K. Hannam, I. V. Shadrivov, and Y. S. Kivshar, *Near-field interaction of twisted split-ring resonators*, Phys. Rev. B, **83**, 235420 (2011).
[17] J. L. Fischer, R. Bader, and M. Abel, *Aeroacoustical coupling and synchronization of organ pipes*, The Journal of the Acoustical Society of America, **140**, 2344–2351 (2016).
[18] M. Krasikova, S. Krasikov, A. Melnikov, Y. Baloshin, S. Marburg, D. A. Powell, and A. Bogdanov, *Metahouse: Noise-Insulating Chamber Based on Periodic Structures*, Advanced Materials Technologies, **8**, 2200711 (2022).
[19] Y. Zhou, X. Fang, D. Li, T. Hao, and Y. Li, *Acoustic Multiband Double Negativity from Coupled Single-Negative Resonators*, Phys. Rev. Applied, **10**, 044006 (2018).
[20] L. Moheit, S. Anthis, J. Heinz, F. Kronowetter, and S. Marburg, *Analysis of scattering by finite sonic crystals in free field with infinite elements and normal modes*, Journal of Sound and Vibration, **476**, 115291 (2020).
[21] F. Kronowetter, L. Pretsch, Y. K. Chiang, A. Melnikov, S. Sepehrirahnama, S. Oberst, D. A. Powell, and S. Marburg, *Sound attenuation enhancement of acoustic meta-atoms via coupling*, submitted for publication 2023.

PHONONICS 2023: 6th International Conference on Phononic Crystals/Metamaterials/Metasurfaces, Phonon Transport, and Topological Phononics
Manchester, England, June 12-16, 2023
PHONONICS-2023-0111

Vibroacoustic Metamaterial Systems as Transformation Mechanisms: Towards Multi-Scale and Non-Periodicity

Sara E. Rodriguez[1], Emilio P. Calius[2], Andrew Hall[3], Raj Das[1]

[1] Aerospace Engineering and Aviation, RMIT University, Melbourne, Victoria 3083, Australia, S3761375@student.rmit.edu.au, raj.das@rmit.edu.au
[2] Architectured Materials Program, Computed Materiality, Auckland 0604, New Zealand emilio.calius@computedmatter.com
[3] Acoustics Research Centre, Mechanical Engineering, University of Auckland, Auckland 1001, New Zealand a.hall@auckland.ac.nz

Abstract: In metamaterials, unique behaviours emerge from the complexity of the internal architecture. Building on the concept of metamaterials as machines we discuss the functional abstraction of complex behaviours and the exploitation of the mechanics of non-periodic and heterogeneous meta-structures to achieve desired dynamic operations on an input vibroacoustic signal using a multiscale design approach.

Research in acoustic and mechanical metamaterials has achieved extreme, unprecedented properties by exploiting inhomogeneity in the form of periodic structures, enabled by advances in digital computation and manufacturing. The result has been a proliferation of metamaterials and, relatively recently, the emergence of non-periodic heterogeneous metamaterial systems, which we term metastructures.

Metamaterials as machines: This represents the beginnings of the evolution of metamaterials from just materials with unique properties towards systems capable of more complex, machine-like functions. In principle metamaterials can be based on any arrangement of unit cells or meta-atoms. Taking these building blocks as connected systems ensuring transmission and transformation of motions or forces either static or dynamic, these non-periodic metamaterials can be thought as mechanisms following the classical mechanical systems definition[1]. Moreover, this property of transforming static or dynamic forces and motions can be used to perform actions or functions, the classical concept of a simple machine[2,3].

A classification system: To better understand the essential features and relationships among this wide and growing variety of species within the field of mechanical metamaterials and metastructures, a classification scheme that focuses on functionality is needed. If both periodic and non-periodic metamaterials systems can be abstracted as mechanisms that produce desired outputs by performing specified transformations on given mechanical inputs, we can then propose an approach to functional classification and comparison based on these deformation and force transformations[7]. An example of this classification for quasi-static transformations is shown in Table 1 below. A similar classification for dynamic transformations is in preparation. Transformation-based approaches are prevalent in geometry processing, computer graphics and soft robotics.

Quasi-static transformations			
Homogeneous		**Non-homogeneous**	
Periodic	Non-periodic	Periodic	Non-periodic
Scaling: volume change **Uniaxial stretch:** no volume change **Linear shear** **Twist** (rotational shear) **Projection**	**Force transformations:** In the form of a tailored stress distribution but with uniform deformation	**Uniform bending:** Line to circle segment **Buckling-based** (modes) **Discrete:** • Monotonic • Non-monotonic	**Hybrid:** combined maps **Non-uniform twist** **Non-uniform bending** **Discrete** **Spatial filtering or steering**

Combining transformations: A generalized, machine-like metamaterial[4-6] can then be defined by the operations or transformations that it performs on static and dynamic inputs applied to the boundaries of a metamaterial domain, as illustrated in Figure 1. However, a machine, as we understand it, consists of multiple parts, each one with a targeted functionality. For mechanical metamaterials, different building blocks can be joined together to achieve a global transformation on the input that is the combination of multiple individual transformations. In this sense, an assembly or network of building blocks could form a "circuit" and one or more such circuits could constitute a machine.

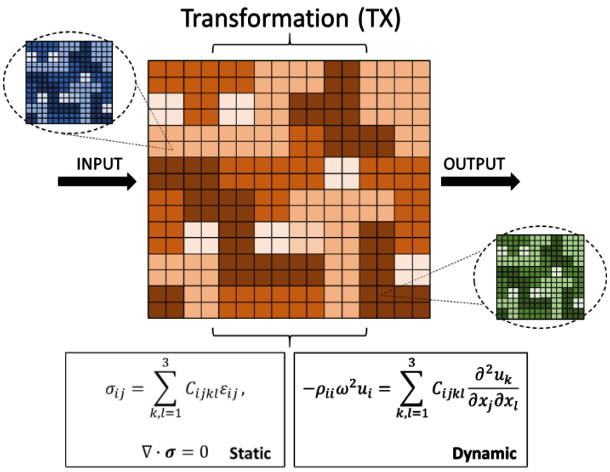

Figure 1. Conceptual illustration of a non-periodic, hierarchical metamaterial system as a transformation relationship.

How to construct meta-circuits: We can define each functional unit as that which produces a given transformation. The realization of metamaterial networks or circuits then depends on mungrating multiple building blocks with different topologies within a broader system, with all that implies of hrnessingin termcale mechanics, interface matching and other research questions. We can define

Case studies: Building on the concept of metamaterials as machines, two transformations are tackled as test cases, first static and then dynamic. The mechanical functionalities are expressed or encoded in terms of transformations that are performed by the metamaterial on incoming elastic waves. Using evolutionary optimization, new, irregular 2D pentamode metamaterials are being designed[8,9], which are defined by extreme values of the bulk-to-shear modulus ratio (B/G) ratio, and which provide the basis for an elastic cloak. Analog wave processing is an extension of the transformation approach to cloaking, with the transformation being a mathematical operation on a wave passing through the metamaterial. As such, the capabilities of multiscale, non-periodic metamaterials will be the basis for constructing targeted operations or transformations sequences, paving the way towards devices with novel dynamics.

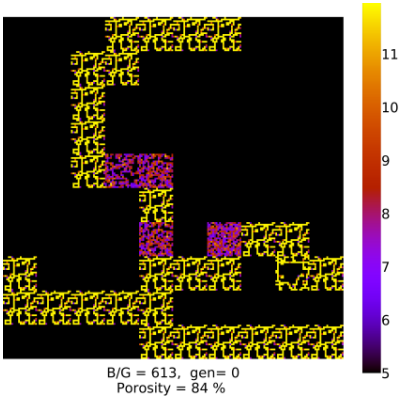

Figure 2. An example of a multiscale, irregular 2D metamaterial design.

References

[1] M. Z. Kolovsky, A. N. Evgrafov, Y. A. Semenov, A.V. Slousch, and L. Lilov, *Advanced theory of mechanisms and machines*: Springer Science & Business Media, 2012.
[2] J. Uicker, J. John, G.R. Pennock, and J.E. Shigley, *1.4 Terminology, Definitions, and Assumptions*, in *Theory of Machines and Mechanisms*, Oxford University Press, 2016.
[3] Harris, J., *Lexicon Technicum: Or, An Universal English Dictionary of Arts and Sciences: Explaining Not Only the Terms of Arts, But the Arts Themselves*. 1725: D. Brown.
[4] C. Coulais, E. Teomy , K. de Reus, Y. Shokef, M. van Hecke, *Nature*, **535**(7613):529-32, 2016
[5] A. Ion, D. Lindlbauer, P. Herholz, M. Alexa, P. Baudisch, in *Proceedings of the 2019 CHI Conference on Human Factors in Computing Systems*, Association for Computing Machinery: Glasgow, Scotland Uk. p. Paper 647, 2019.
[6] J. M. McCracken, B.R. Donovan, and T.J. White, *Advanced Materials*, **32**(20): p. 1906564, 2020.
[7] S. E. Rodriguez, E. P. Calius, A. Khatibi, A. Orifici, and R. Das, *Mechanical metamaterial systems as transformation mechanisms* in *Extreme Mechanics Letters, Available online March*, 2023
[8] S. E. Rodriguez, E. P. Calius, A. Khatibi, A. Orifici, and R. Das, *Evolutionary design of novel 2D pentamode metamaterials*, Article under review, 2023
[9] S. E. Rodriguez, E. P. Calius, A. Khatibi, A. Orifici, and R. Das, *Designing pentamodes with structural hierarchy: an evolutionary approach*, Article in preparation, 2023

PHONONICS 2023: 6th International Conference on Phononic Crystals/Metamaterials/Metasurfaces, Phonon Transport, and Topological Phononics
Manchester, England, June 12-16, 2023
PHONONICS-2023-0200

Dispersion Behaviour of a Non-Resonant Elastic Metamaterial

John D. Smith, Claudia L. Clarke

Physical Sciences Group, DSTL, Porton Down, Salisbury, Wiltshire, SP4 0JQ, UK
jdsmith@dstl.gov.uk, cclarke4@dstl.gov.uk

Abstract: Metamaterials are of great interest on account of their tunable material properties, arising from an internal microstructure, which can often be chosen to give a desired behaviour.

The behaviours of acoustic metamaterials are often derived via analogy with electromagnetic metamaterials, and typically described using Willis relations.

Here an elastic metamaterial consisting of a series of elastic plates interspaced by fluid is considered. It is found that the effective constitutive equations contain higher derivative terms than would normally be present in the Willis (or elastic) constitutive equations for an anisotropic material. This leads to behaviour that is highly dispersive due to an "emergent scale" associated with bending on the constituent plates. The existence of this scale is due to the boundary conditions on the plate-fluid interfaces and appears to be a purely elastic phenomena.

The metamaterial in this case has no resonant inclusions; nevertheless, the effective behaviour leads to broadband dispersion and is different from anisotropic elasticity. The dependence of the dispersion curves on the material properties of the constituents is examined and the connection with fractional derivative theories and rotons considered.

PHONONICS 2023: 6th International Conference on Phononic Crystals/Metamaterials/Metasurfaces, Phonon Transport, and Topological Phononics
Manchester, England, June 12-16, 2023
PHONONICS-2023-0072

Reinforcement Learning Guiding the Design Optimization of Graded Metamaterials for Energy Harvesting

Luca Rosafalco[1], Jacopo M. De Ponti[1], Luca Iorio[1], Richard V. Craster[3], Raffaele Ardito[1], Alberto Corigliano[1]

[1] Department of Civil and Environmental Engineering, Politecnico di Milano,
Piazza L. da Vinci, 32, 20133 Milano, Italy,
luca.rosafalco@polimi.it, jacopomaria.deponti@polimi.it, luca.iorio@polimi.it, raffaele.ardito@polimi.it, alberto.corigliano@polimi.it
[2] Department of Mathematics, Imperial College London,
180 Queen's Gate, South Kensington, London SW7 2AZ
r.craster@imperial.ac.uk

Abstract: We define a reinforcement learning approach to design optimised metamaterials for energy harvesting. The metamaterial is an elastic waveguide endowed with beam-like resonators subjected to a set of random vibrations; knowledge of the rainbow effect is exploited to reduce the variance of the optimisation procedure.

A graded metamaterial is a structure equipped with elements featuring a gentle variation of their resonant frequencies. The grading enables to modify in space the metamaterial dispersion properties by taking advantage of the creation of local band gaps. Specifically, propagating waves slow down as they come across resonator pairs with different frequencies, producing the so-called rainbow effect[1]; this mechanism can be exploited for energy harvesting[2] taking advantage from the elastic energy amplification in the resonators. While the effect of different grading laws has been investigated in the past[3], a Reinforcement Learning (RL) based approach is employed to optimise the grading for sake of energy harvesting[4]. The optimal design search is formalised as a Markov decision problem and solved via an actor-critic RL algorithm, namely the Proximal Policy Optimisation (PPO) algorithm.

Finite Element (FE) simulations are used to quantify the energy harvested for a particular resonator arrangement in case of a random excitation source. Specifically, we consider 128 possible realisations of the random excitation, each one with frequency content from 0.1 to 2 MHz. The frequency range is compatible with applications to microsystems. The waveguide is discretised through Euler-Bernoulli beam elements; the resonator pairs through equivalent lumped parameters accounting for the mechanical and piezoelectric components[5]. In particular, the effect of the attached circuit is simulated through mechanical quantities determined through a general impedance analysis[6].

The FE setting is the environment on which the RL agent operates by taking a discrete number of actions, each one modifying the grading rule. Specifically, resonant frequencies are changed by playing on the length of the resonator pairs. The agent decisions are guided by the harvested energy, here termed reward. In the starting configuration, all the resonator pairs have the same length.

Concerning the agent actions, it has been found that modifying one by one the length of the resonator pairs results in excessive computing time and does not produce any useful result. Indeed, a single action does not change the harvested energy as much, providing weak indications to possible design improvements. To solve the issue, we have constrained the design space using our knowledge of the rainbow-based effect, thus exploiting the physical understanding of the problem to reduce the variance of the optimization procedure. Specifically, we have allowed the RL agent to operate on the y-coordinate of the four points shown in Figure 1, and we have used their interpolation to set the lengths of the resonator pairs.

To judge the performance of the procedure, comparisons have been drawn between the RL-based optimised configuration and two linear grading configurations whose definition well agrees with the physical understanding of the problem. In particular, the two linear gradings take advantage of the rainbow effect, and employ resonator pairs with resonant frequencies in between 0.1 MHz and 2 MHz. The comparison has been carried out by considering how much the harvested energy has been increased with respect to a design featuring random resonator lengths.

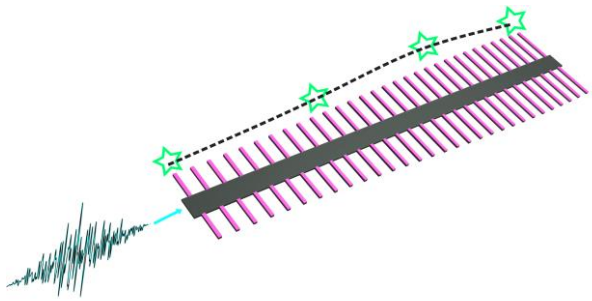

Figure 1 Optimised metamaterial geometry for a set of random vibrations. Resonator lengths are set according to the interpolation of four points (depicted as stars).

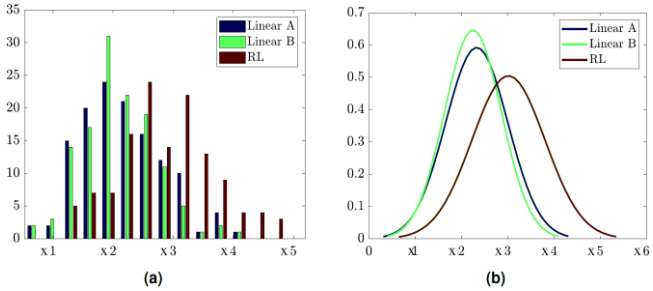

Figure 2 (a) Increase in the harvested energy with respect to a random resonator configuration. (b) Gaussian approximations of the obtained discrete distributions.

The procedure outcome is reported in Figure 2: on the left, the harvesting performance of the three configurations are compared for each of the 128 considered random excitations; on the right, a Gaussian approximation of the results is drawn, showing the increase amount of harvested energy in the RL configuration.

Contrary to the expectations, resonators pairs set by the RL agent have resonant frequencies within 0.55 MHz and 1.8 MHz, thus not covering the full frequency content of the random excitation. The reason behind is explained by Figure 3, reporting the dispersion relations (κ,f) and the resonance curves of the first and last resonators of RL configuration against the corresponding quantities obtained for resonator pairs with resonant frequency at 0.1 MHz and 2 MHz. Indeed, damping enlarges the range of frequencies with which each resonator interacts, justifying the RL decisions.

The current study shows that the RL-based procedure suggests useful insights of the physics of the system beyond being effective as design optimisation tool.

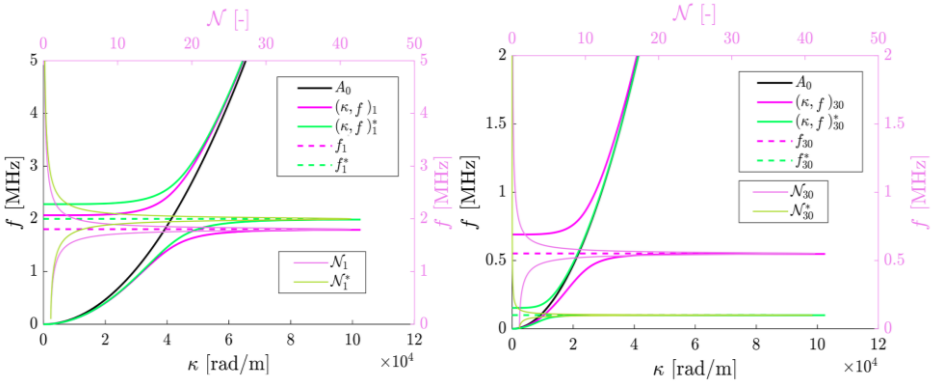

Figure 3 Dispersion relations and resonance curves of the first (*1*) and last (*30*) resonator pair of the RL configurations against the corresponding quantities obtained for two resonator pairs featuring 0.5 MHz and 2 MHZ as resonant frequencies.

References

[1] A. Colombi, D. Colquitt, P. Roux, S. Guenneau and R. V. Craster, A seismic metamaterial: The resonant metawedge. *Sci. Rep*. **6**, 27717 (2016).
[2] J. M. De Ponti, A. Colombi, R. Ardito, F. Braghin, A. Corigliano and R. V. Craster, Graded elastic metasurface for enhanced energy harvesting, *New J. Phys* **22**, 013013 (2020).
[3] M. Alshaqaq and A. Erturk, Graded multifunctional piezoelectric metasurfaces for wideband vibration attenuation and energy harvesting, *Smart Mater. Struct.* **30**, 015029 (2020).
[4] L. Rosafalco, J. M. De Ponti, L. Iorio, R. Ardito and A. Corigliano, Optimised graded metamaterials for mechanical energy confinement and amplification via reinforcement learning, *Eur. J. Mech. A Solids* **99**, 104947 (2023).
[5] B. Zhao, H. R. Thomsen, J. M. De Ponti, E. Riva, B. Van Damme, A. Bergamini, E. Chatzi and A. Colombi, A graded metamaterial for broadband and high-capability piezoelectric energy harvesting, *Energy Convers. Manag.* **269**, 116056 (2022).
[6] L. Liang and W.-H. Liao, Impedance modeling and analysis for piezoelectric energy harvesting systems, *IEEE ASME Trans. Mechatron.* **17**, 1145-1157 (2011).

PHONONICS 2023: 6th International Conference on Phononic Crystals/Metamaterials/Metasurfaces, Phonon Transport, and Topological Phononics
Manchester, England, June 12-16, 2023
PHONONICS-2023-0069

Acoustic Wave Scattering by a Lattice of Scatterers in a Soft Medium: Homogenisation Approach

Alex Skvortsov[1], Gyani Shankar Sharma[1], Ian MacGillivray[1], Nicole Kessissoglou[2]

[1] *Defence Science and Technology Group, Melbourne, VIC 3207, Australia,*
alexei.skvortsov, gyani.sharma, ian.macgillivray @defence.gov.au
[2] *School of Mechanical and Manufacturing Engineering, UNSW Sydney 2052, Australia*
n.kessissoglou@unsw.edu.au

Abstract: A simple design of an acoustic metamaterial for maritime applications comprises a grating of resonant scatterers embedded in a soft elastic matrix. We have developed analytical frameworks that employ homogenisation to determine the acoustic performance of soft media with voided or hard inclusions. To this end, we have translated some well-known analytical results from electrostatics, fluid dynamics, diffusion kinetics, and solid-state physics.

Acoustic metamaterials are engineered composite structures designed using distributions of resonant inclusions in a host material to exhibit favourable acoustic properties[1,2]. Due to tremendous progress in fabrication technology, acoustic metamaterials can be manufactured as subtle morphological structures that can exhibit a rich variety of acoustic properties which go beyond those of their bulk ingredients. Analytical modelling of acoustic metamaterials is often a challenging undertaking due to complexity of wave phenomena arising from multiple scattering, local resonances and resonance coupling. This necessities development of simplified models of acoustic metamaterials that are relatively easy to implement and computationally light to run.

One design of an acoustic metamaterial for maritime applications is a soft elastic medium embedded with a lattice of inclusions, employed as an external coating on marine vessels[3-5]. The main mechanism for sound attenuation by the coating arises from enhanced wave scattering and the associated strain field amplification near the inclusions at frequencies around local resonance of the inclusions. This behaviour facilitates conversion of sound waves to shear waves, which are efficiently absorbed due to high damping capacity of shear waves in rubber-like materials.

This work outlines the analytical capabilities developed by the authors to analyse the performance of acoustic coatings[6-12] Two homogenisation methods have been employed to investigate the acoustic performance of a grating of scatterers. These methods correspond to an effective medium approximation and an effective boundary approximation, as shown schematically in Fig. 1. Effective medium approximation involves modelling a layer of resonant inclusions as a layer of a homogeneous material with effective material parameters sandwiched between two layers of the host medium as shown in Fig. 1(a) For effective boundary approximation, each layer of scatterers in the direction of sound propagation is approximated as an effective boundary, as shown in Fig. 1(b). We conceptually map the sound scattering by the lattice to scattering by an inclusion in the centre of a rigid duct with a

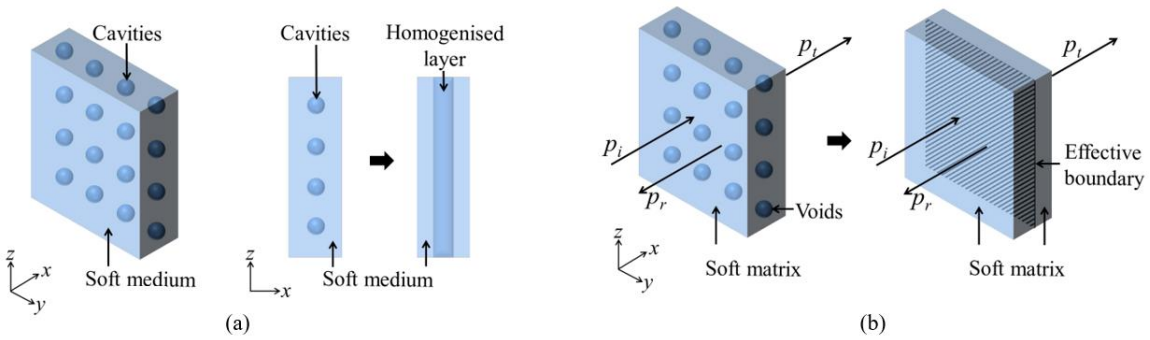

Figure 1 Schematic diagram showing (a) a layer of voids in a soft medium approximated as a homogenised layer with effective material and geometric properties, (b) a layer of voids in a soft medium approximated as an effective boundary. These figures are reproduced from Refs. 11 and 12.

cross section equal to the area of the unit cell. We then use the conventional transfer matrix method to calculate the reflection, transmission and absorption coefficients of a soft medium embedded with an arbitrary number of layers of inclusions Both methods take into account multiple scattering of waves by the inclusions, the resonance frequency of the inclusions, and resonance coupling between inclusions in proximity.

To demonstrate the effectiveness of each method, the sound coefficients of layers of scatterers obtained analytically are compared with numerical simulation as well as experimental results from the literature. Figure 2 presents the transmission coefficient of a coating comprising a soft medium embedded with one or four layers of spherical cavities and submerged in water. The cavities are arranged in a square lattice within each layer. The metamaterial is submerged in water and subject to a normally incident plane acoustic wave. The first trough in the transmission coefficient is due to monopole resonance of the cavities. The frequency of monopole resonance of the spheres is not significantly affected with additional layers of scatterers. However, the sound transmission reduces as the number of layers is increased arising from greater multiple scattering leading to generation and dissipation of shear waves. Excellent agreement between the analytical and numerical results across a broad frequency range with experimental results from Leroy et al, Ref. 5 can be observed. We believe our proposed methods will useful for targeted design and optimisation of the coating developed for maritime applications before proceeding with prototyping and experimental evaluation.

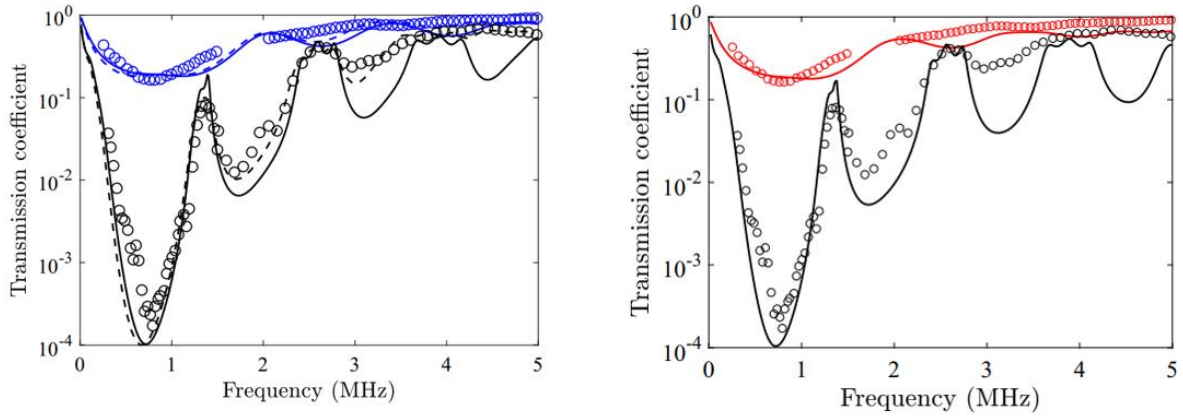

Figure 2 Left panel**:** Transmission coefficient of one layer (blue lines) and four layers (black lines) of spherical cavities embedded in a soft medium submerged in water, obtained analytically using the homogenisation approach (solid lines), the finite element method (dashed lines). Right panel: Transmission coefficient of one layer (red line) and four layers (black line) of spherical cavities embedded in a soft medium submerged in water, obtained analytically using the effective boundary approach (solid lines). Our analytical and numerical results are compared to experimental results from Leroy et al.,Ref 5 (circles). These figures are reproduced from Refs. 11 and 12.

References

[1]T. Brunet, J. Leng, and O. Mondain-Monval, *Science* **342**, 323 (2013)
[2]S. A. Cummer, J. Christensen, and A. Alù, *Nat. Rev. Mater.* **1**, 16001 (2016).
[3]D. C. Calvo, A. L. Thangawng, C. N. Layman Jr, R. Casalini, and S. F. Othman, *J. Acoust. Soc. Am.* **138**, 2537 (2015).
[4]P. Méresse, C. Audoly, C. Croënne, and A.-C. Hladky-Hennion, *C. R. - Mec.* **343**, 645 (2015).
[5]V. Leroy, A. Bretagne, M. Fink, H. Willaime, P. Tabeling, and A. Tourin, *Appl. Phys. Lett.* **95**, 171904 (2009).
[6]G. S. Sharma, A. Skvortsov, I. MacGillivray and N. Kessissoglou, *J. Acoust. Soc. Am.* **141**, 4694 (2017).
[7]G. S. Sharma, A. Skvortsov, I. MacGillivray and N. Kessissoglou, *Appl. Acoust.* **143**, 200 (2018).
[8]G. S. Sharma, A. Skvortsov, I. MacGillivray and N. Kessissoglou, *J. Sound Vib.* **443**, 652 (2019).
[9]G. S. Sharma, A. Skvortsov, I. MacGillivray and N. Kessissoglou, *Appl. Phys. Lett* **116**, 041602 (2020).
[10]A. Skvortsov, G. S. Sharma, I. MacGillivray, and N. Kessissoglou, *J. Acoust. Soc. Am.* **150**, 1448 (2021).
[11]G. S. Sharma, A. Skvortsov, I. MacGillivray and N. Kessissoglou, *Phys. Rev. B* **102**, 214308, (2020).
[12]A. Skvortsov, I. MacGillivray, G. S. Sharma, and N. Kessissoglou, *Phys. Rev. E* **99**, 063006 (2019).

PHONONICS 2023: 6th International Conference on Phononic Crystals/Metamaterials/Metasurfaces, Phonon Transport, and Topological Phononics
Manchester, England, June 12-16, 2023
PHONONICS-2023-0033

Hard-Magnetic Soft Elastic Metamaterials for Tunable Wave Manipulation

Quan Zhang[1], **Stephan Rudykh**[1]

[1] *School of Mathematical and Statistical Sciences, University of Galway, Ireland, quan.zhang@universityofgalway.ie, stephan.rudykh@universityofgalway.ie*

Abstract: The remote and reversible principle of actuation of *hard*-magnetic active elastomers (hMAEs) holds great potential for the design of robotics, actuators and sensors, and biomedical devices. Here, I propose to exploit the unique transformative ability of hMAEs integrated into the metamaterial design to develop novel tunable hard-magnetic soft elastic metamaterials with superior wave properties.

Elastic metamaterials draw their performance from neat microstructures, giving rise to topological phase transitions, extreme (and negative) effective parameters, and the bandgap (BG) phenomenon. The potential metamaterial applications range from vibration isolation and switching to subwavelength waveguiding and focusing, to the topological state of matter that enables elastic wave flows immune to backscattering losses. The metamaterial properties originate in their highly ordered microstructures that are fixed once designed and manufactured. Therefore, the active tunability of current metamaterials is limited.

Here, we put forward a novel design of magnetoactive elastic metamaterials, building on the rich physics offered by the unusual behavior of *hard*-magnetic active elastomers (hMAEs). Such active materials consist of a soft elastomer matrix embedded with hard-magnetic particles. Application of external magnetic fields generates micro torques on the embedded hard-magnetic particles. This microscopic effect leads to a macroscale response of the hMAE composite in the form of complex shape transformations[1,2]. The tunability of materials by a remote magnetic field – either through property modification or induced deformation – holds intriguing potential for designing metamaterials for manipulating elastic waves.

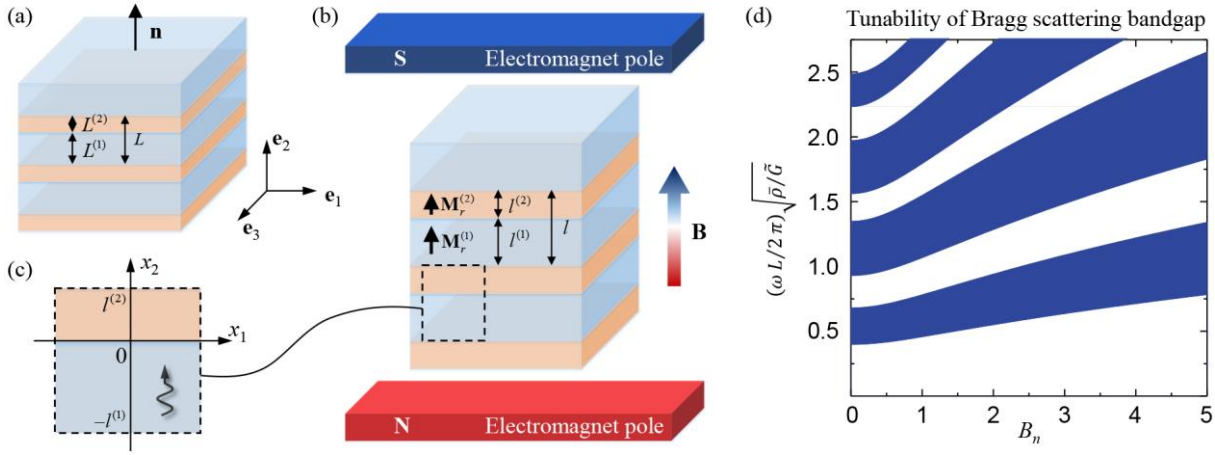

Figure 1 The hard-magnetic soft phononic crystals with bi-phasic layered microstructure in **(a)** the reference (undeformed) state and **(b)** the magnetic field induced deformed state. **(c)** The representative unit cell. **(d)** The evolution of the transverse wave BGs versus magnetic induction applied perpendicularly to the layers in the hard-magnetic soft laminates.

First, we analyze the magneto-mechanical behavior of periodic laminates made of hMAEs with intrinsic magnetization, as shown in Figure 1(a) and 1(b)[3]. We formulate an amended free-energy function for hMAEs and derive an explicit expression for the induced deformation of the hMAE laminate as a function of the applied magnetic field. Using the "small-on-large" framework, we investigate the small-amplitude shear waves propagating in the finitely deformed hMAE laminate activated by a magnetic field, see Figure 1(c). We discover that the remanent magnetization of the hMAE phases can cause compressive deformations (in the direction of the applied magnetic field), in contrast to the induced tensile deformation seen in previously studied soft-magnetic active laminates[4]. Additionally,

we derive dispersion relations for transverse elastic waves propagating in the direction perpendicular to the laminate layers. Our analytical findings demonstrate the tunability of the shear wave BGs with varying remanent magnetizations of the phases, and that the shear wave BGs can be remotely controlled by applying a magnetic field (Figure 1(d)).

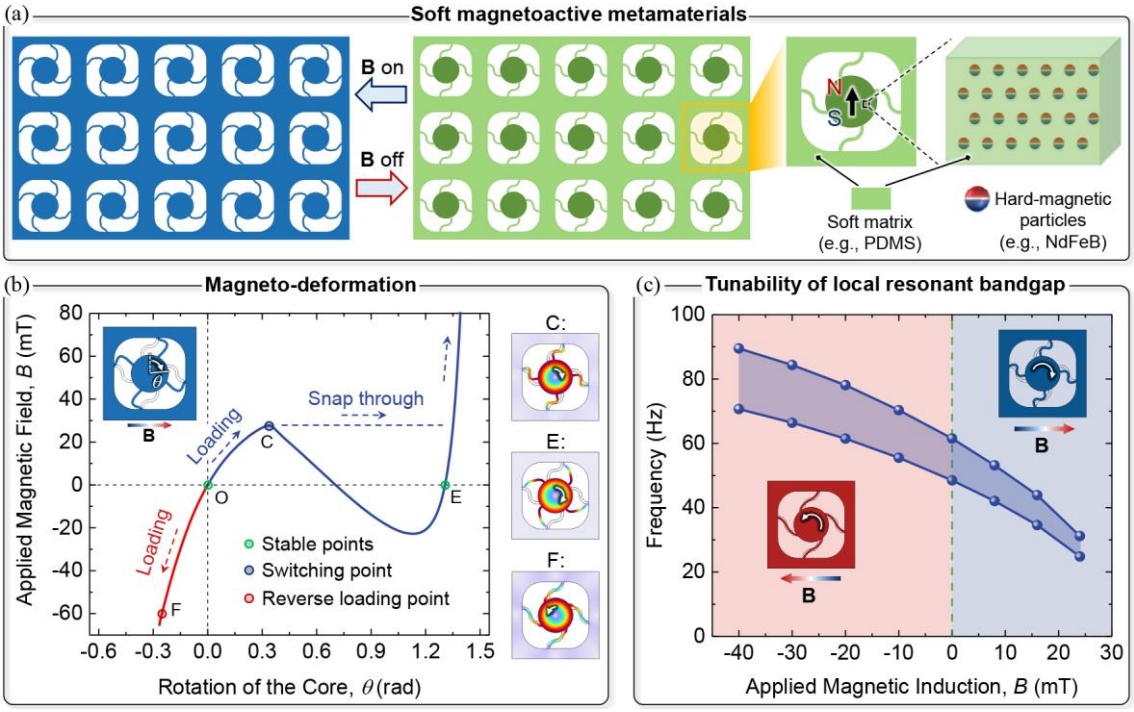

Figure 2 Magnetoactive elastic metamaterials with tunable local resonant BG. **(a)** Working principle of the magnetoactive elastic metamaterials. **(b)** Magnetic field-induced rotation of the resonator. **(c)** The evolution of the local resonant BG with respect to the applied magnetic field.

Next, we propose a novel magnetic field-induced asymmetric mechanical metamaterial, illustrated in Figure 2(a)[5], that incorporates hMAEs into the microstructural design combining snap-through, bistability, and local resonant effects. The metamaterial design consists of resonating units made out of hMAE, which are supported by highly deformable curved beams connected with an elastomeric matrix. Upon activation by a magnetic field, the resonating units enter an unstable regime characterized by dramatic configuration and stiffness variations, see Figure 2(b). These controlled transformations have a significant impact on elastic wave propagation. We demonstrate that the proposed magnetoactive metamaterial enables BG tunability over a broadband low-frequency range (see Figure 2(c)), thus, enabling remote and reversible control of the metamaterial performance. Additionally, the hMAE-based systems can incorporate polarity and chirality arising from the interaction between external magnetic fields and hMAE phases, resulting in unusual metamaterial behavior and potentially enabling elastic cloaking.

References

[1] Y. Kim, H. Yuk, R. Zhao, S. A. Chester, and X. Zhao, *Nature* **558**, 274 (2018).
[2] W. Hu, G. Z. Lum, M. Mastrangeli, and M. Sitti, *Nature* **554**, 81 (2018).
[3] Q. Zhang, and S. Rudykh, *Mech. Mater.* **169**, 104325 (2022).
[4] M. N. Karami, P. I. Galich, A. O. Krushynska, and S. Rudykh, *J. Appl. Mech.* **86**, 111001 (2019).
[5] Q. Zhang, A. V. Cherkasov, N. Arora, G. Hu, and S. Rudykh, *Extreme Mech. Lett.* **59**, 101957 (2023).

Wednesday 14th June

PHONONICS 2023: 6th International Conference on Phononic Crystals/Metamaterials/Metasurfaces, Phonon Transport, and Topological Phononics
Manchester, England, June 12-16, 2023
PHONONICS-2023-0120

Behavior of Thermal Phonons in Contrast to Photons

Masahiro Nomura

Institute of Industrial Science, The University of Tokyo, 4-6-1, Komaba, Meguroku, Tokyo, Japan
nomura@iis.u-tokyo.ac.jp

Abstract: Heat conduction control in a semiconductor membrane by nanostructuring will be discussed from the viewpoint of photonics. We classify the systems by similarity, difference, and hybridization of phonons and phonons, and explain characteristic thermal phonon transport in each system. Prospects of thermal phonon engineering will be also discussed.

Light propagation in ray optics and thermal phonon transport at the nanoscale are similar due to ballisticity. The characteristic propagation of light and mechanical vibrations in band-engineered periodic structures, i.e. photonic and phononic crystals, derives from the wave properties of electromagnetic and elastic waves [1]. Some recent work on the control of heat conduction by well-designed nanostructures are taken up to discuss how we can design nanostructures to control heat transport more effectively by considering the similarity and difference of photons and thermal phonons [2]. The ballistic behavior of phonons in their mean free path (MFP) allows advanced heat flux control such as directional heat flux and heat focusing. This thermal phonon behavior is similar to ray optics and is therefore named "Ray phononics" [3]. The selection of phonon *k*-vector direction by aligned nanoholes formed in a membrane results in the formation of directional heat flux. The directional heat flux is maintained within the MFP of thermal phonons. The interaction and hybridization of photons and phonons are also interesting and will lead to new functionality. Phonons can control the emission of a single photon from a quantum dot embedded in a high-Q optical micro/nanocavity [4, 5]. Regarding hybridization, phonons can travel faster by four orders of magnitude by shaking hands with photons; forming surface phonon polaritons (SPhPs). In addition, "phonon" scattering is strongly suppressed by the dressing of the electromagnetic wave, resulting in the enhancement of thermal conduction in thin dielectric membranes. This dramatic change in thermal energy transport property by SPhPs opens up new possibilities for thermal management in thin membranes [6]. The hydrodynamic behavior of phonons is an example of a different transport phenomenon that is a phenomenon rarely observed in optics. The collective behavior, which exists in electronic and phononic systems due to interaction, of phonons provides interesting thermal transport such as phonon Poiseuille flow [7] and second sound [8].

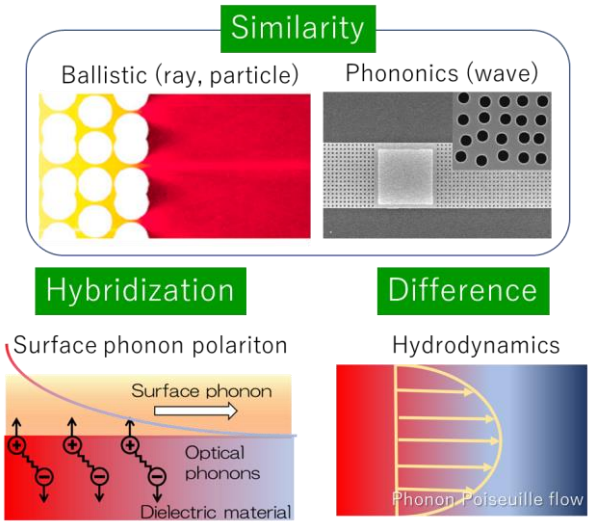

Figure 1. Discusses thermal phonon transport, categorizing photon and phonon similarities, differences, and hybridization.

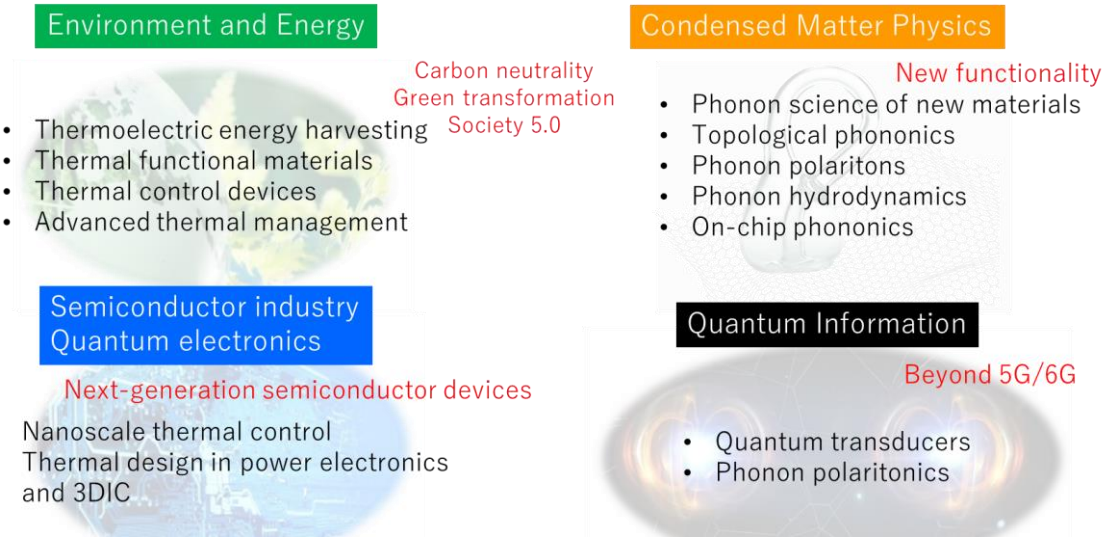

Figure 2. Prospects of phonon engineering applicable to a variety of fields: Environment & Energy, Semiconductor industry & Quantum electronics, Condensed Matter Physics, and Quantum information.

Acknowledgment
These results were obtained by collaborations with Drs. R. Anufriev, J. Ordonez-Miranda, L. Jalaberat, X. Huang, Y. Guo, J. Maire, and S. Volz.

References
[1] J. Ravichandran, *et al*., Nat. Mater., 13, **168** (2014).
[2] M. Nomura, *et al*., Mater. Today Phys. **22**, 100613 (2022). [Review]
[3] R. Anufriev and M. Nomura, Mater. Today Phys. 15, 100272 (2020).
[4] M. Nomura, Nat. Nanotechnol., **11**, 496 (2016).
[5] M. Nomura, *et al*., Nat. Phys. **6**, 279 (2010).
[6] Y. Wu, *et al*., Sci. Adv. 6, eabb4461 (2020).
[7] X. Huang, *et al*., Nat. Commun., accepted.
[8] S. Huberman, *et al*., Science., **364**, 375 (2019).

PHONONICS 2023: 6th International Conference on Phononic Crystals/Metamaterials/Metasurfaces, Phonon Transport, and Topological Phononics
Manchester, England, June 12-16, 2023
PHONONICS-2023-0124

Phonons and Nanomaterials, New Era

K. Termentzidis

CETHIL UMR5008, CNRS, INSA-Lyon,F-69621, 9 Rue de la Physique, 69100 Villeurbanne, France
Konstantinos.Termentzidis@insa-lyon.fr

Abstract: New thermal effects observed in semiconductor nanomaterials will be discussed here: phonon focusing, confinement, interference and percolation as well hydrodynamic heat transport. Using atomistic simulations, it is possible to obtain exotic thermal phenomena beyond Fourier, which in long-term they could be useful for thermal management applications.

The classic Fourier law relates the thermal conductivity with heat flux, the latter is proportional and in the same direction as the temperature gradient. While Fourier law describes well the most practical macroscopic problems, it fails when a temperature gradient imposed over a length scale comparable to or smaller than the phonon mean free path. The heat transfer through nanomaterials; both nanostructures and nanostructured materials with high density of internal or external surfaces and interfaces, at low temperatures, or during rapid processes diverges considerably from the Fourier law. Lately several new exotic phenomena are either measured or discovered by atomistic simulations; coherence effects, ballistic or quasi-ballistic heat transport, thermo-hydrodynamics, phonon tunneling, resonances etc. Here several such new thermal effects will be discussed: phonon focusing, confinement, interference and percolation effects as well hydrodynamic heat transport in nanostructures and nanostructured semiconductors combining crystalline and amorphous phases. The five paradigms will be analyzed briefly.

Nano-architectured composites can be used to obtain thermal anisotropy. One of them the phononic-like membranes beside the strong reduction of the heat transfer due to the porosity, they offer opportunities to create structures to **focus phonons**. The in-plane thermal conductivity of silicon phononic membranes with aligned and staggered lattices of holes has been investigated by micro time domain thermoreflectance and Monte Carlo simulations[1]. Thermal conductivities discrepancy of aligned and staggered lattice of identical porosities is observed, which arises from ballistic phonons that acquired directionality by propagating between the holes. The directionality effect strengthens when the temperature is decreased or when the diameter of the holes becomes close to the periodic pattern. Based on the **ballistic transport** at the nanoscale, thermal lens nanostructures have been proposed recently, in which the emitted phonons converge and create a hot spot of a few hundred nanometres. These results motivate the concept of ray-like heat manipulations at the nanoscale[2].

The concept of **phonon percolation** in a silica–gallium nitride nanocomposite has been proposed. A surprising enhancement of the thermal conductivity for crystalline volume fractions larger than 5% is found, which cannot be predicted by an effective medium approach. The behavior can instead be reproduced if an effective volume fraction twice larger than the real one is assumed, which translates into a percolation effect surprisingly stronger than the usual one. Such a scenario can be understood in terms of a phonon tunneling between crystalline nano-inclusions, enhanced further by the iso-orientation of all particles[3]. To go deeper in the subject, the effect on the vibrational properties of gradually interconnected nanoinclusions embedded in an amorphous matrix was studied, with nanoinclusion arrangement ranged from an aligned sphere array to an interconnected mesh of nanowires. Wave-packet simulations revealed that the interconnection of the nanoinclusions at constant volume fraction induces a strong increase of the mean free path of high frequency phonons, but does not affect the energy diffusivity. The observed enhancement of the effective thermal conductivity due to the existence of crystalline structural interconnections is dominated by the **ballistic transport of phonons**[4].

In the **thermal hydrodynamic transport**, the phonons flow collectively instead of diffusively, showing several similarities between phonons and fluids. In thermo-hydrodynamics, collective and coherent motion of phonons predominate heat transport. Interestingly the fluid hydrodynamic profile observed in a cylindrical pipe has been also observed in nanowires using Molecular Dynamics Simulations and Monte Carlo simulations[5]. Less heat flux is carried in the external layer of nanowires than in the center. The difference between the center and the surface is of the order of 50% and 30% with MD and MC simulations, respectively. This flux reduction close to the surface is related to the amorphous like phonon

density of states of the external atomic layers and flattened dispersion curves, thus lower phonon group velocities. To make a comparison between the atomistic simulations and the hydrodynamic heat equation, we used wave-packet propagation simulations and heat flux estimation via molecular dynamics[6]. We observe Poiseuille like heat flux profile, that cannot be described by a simple kinetic model such as the Fuchs-Sondheimer model. These results show that there is a heat flux depletion length of 1–2 nm away from the free surface.

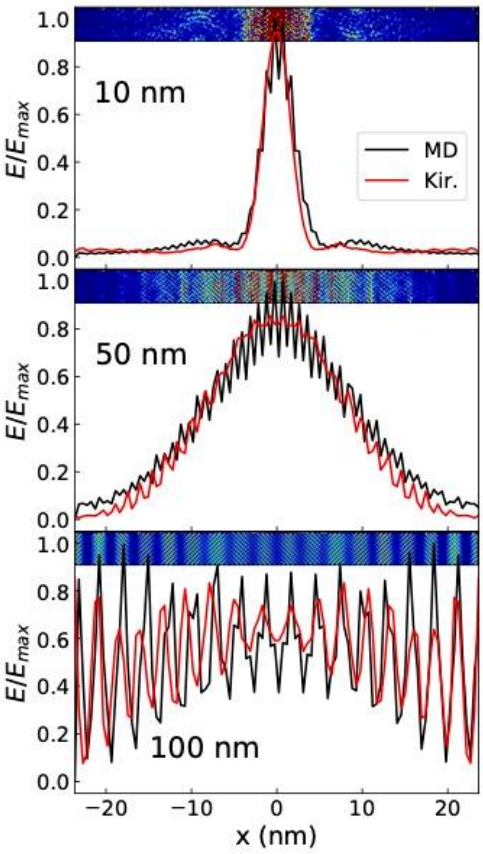

Figure Kinetic energy distribution along the x-axis at z=10, 50 and 100 nm distance from the slit, of the MD simulation (full black line) and the Kirchoff model in red. The upper insets for each distance, give an atomic representation of the kinetic energy (red-high, blue-low).

The **thermal rectification** is an effect in which the heat flux differs depending on the direction of the imposed temperature gradient. Several strategies based on nonlinear lattice models, asymmetric structures, interfaces between two materials or graded mass density have been proposed. Here asymmetric crystalline-core/amorphous-conical-shell nanowires have been studied and found that these nanostructures create a direction-dependent thermal conductivity due to variable axial and radial phonon propagation and confinement. The origin of this effect is related to the combination of a crystalline/amorphous interface parallel to the heat flux and the variable amount of amorphous coating (conical shell of the nanowire)[7].

Finally, **phonons diffraction and interference** patterns (Figure) are observed at the atomic scale, in systems containing crystalline silicon and nanometric obstacles as voids or amorphous-inclusions. The diffraction patterns caused by these nano-architectured systems of the same order as the phonon wavelengths are similar to the ones predicted by a simple Fresnel-Kirchhoff integral. These findings give evidence of the wave nature of phonons, and they can help to a better comprehension of the interaction of phonons with nanoobjects and at long term can be useful for intelligent thermal management and phonon frequency filtering at the nanoscale[8].

References

[1] M. Verdier, R. Anufriev, A. Ramiere, K. Termentzidis, and D. Lacroix, Phys. Rev. B 95, 205438 (2017)
[2] R. Anufriev, A. Ramiere, J. Maire and M. Nomura, Nat. Com 8, 15505 (2017)
[3] K. Termentzidis, V.M. Giordano, M. Katsikini, E. Paloura, G. Pernot, M. Verdier, D. Lacroix, I. Karakostas and J. Kioseoglou, Nanoscale 10, 21732 (2018)
[4] P. Desmarchelier, A. Carré, K. Termentzidis and A. Tanguy, Nanomaterials 11(8), 1982 (2021)
[5] M. Verdier, Y. Han, D. Lacroix, P.-O. Chapuis and K. Termentzidis, J. Phys.: Mater. 2, 015002 (2019)
[6] P. Desmarchelier, A. Beardo, F.X. Alvarez, A. Tanguy, and K. Termentzidis, Int. J. Heat Mass Transfer 194, 123003 (2022)
[7] P. Desmarchelier, A. Tanguy, and K. Termentzidis, Phys. Rev. B 103, 014202 (2021)
[8] P. Desmarchelier, E. Nikidis, Y. Nakamura, A. Tanguy, J. Kioseoglou, and K. Termentzidis, arXiv:2207.14064 (2022)

PHONONICS 2023: 6th International Conference on Phononic Crystals/Metamaterials/Metasurfaces, Phonon Transport, and Topological Phononics
Manchester, England, June 12-16, 2023
PHONONICS-2023-0125

Acoustic Phonon Tunneling Across a Vacuum Gap between Piezoelectric Crystals

Zhuoran Geng[1], Ilari. J. Maasilta[1]

[1] Nanoscience Center, Department of Physics, University of Jyväskylä, Survontie 9C, FI-40014 Jyväskylä, Finland,
maasilta@jyu.fi

Abstract: We present a review of our recent work on the phenomenon of piezoelectric acoustic phonon tunneling across a vacuum gap. We discuss the theoretical formulation based on anisotropic continuum elasticity theory, which can be used to solve the tunneling amplitude for any crystal symmetry and orientation, and demonstrate that complete, reflectionless tunneling is possible. In addition, we calculate the heat flux due to thermal phonons.

It has been known since the 70's [1,2] that acoustic waves can jump across vacuum gaps between two piezoelectric crystals mediated by the piezoelectrically generated evanescent electric fields that extend into vacuum. However, this effect that we call "piezoelectrically mediated acoustic phonon tunneling" is not widely known or studied fully. We have recently [3] generalized the formulation of this phenomenon in such a way that transmission and reflection amplitudes for the scattering of any incident bulk wave mode for any anisotropic crystallographic orientation can be solved, for the case of two parallel semi-infinite solids. The method takes advantage of the extended Stroh formalism [3] of continuum anisotropic elasticity for piezoelectrics, and thus takes fully into account the anisotropy of the slowness surfaces and mode conversions in the scattering problem.

In our numerical studies, we have observed cases where the incoming bulk wave can resonantly excite quasi-surface modes (or leaky gap-waves), enhancing the tunneled transmission coefficient to exactly one in some cases. Following that observation, we have analytically and numerically proven [4] that it is possible for acoustic waves to completely tunnel across a vacuum gap between two piezoelectric solids, with zero reflection amplitude. This is possible for gap widths smaller or equal than about the acoustic wavelength. We showed that such complete tunneling, with unity power transmittance, is possible only if just one transmitted partial bulk mode is excited, it being the same mode as the incident wave. We have also derived a strikingly simple resonance tunneling condition for the complete tunneling effect and checked its validity and range of applicability with numerical examples for arbitrarily rotated ZnO crystals. Mapping its occurrence over all possible crystal rotations, we find for ZnO a significantly large region of orientations, where complete tunneling is possible.

As a final example of the implications of piezoelectric acoustic phonon tunneling, we have also calculated its effect on thermal phonons, *i.e.* how much phonon heat flux can tunnel across the gap [5]. We find that the heat flux can be more than three orders of magnitude stronger than Planck's law for blackbody radiation when the gap width is smaller than the phonon characteristic thermal wavelength. We also show that while at room temperature the heat flux from acoustic phonon tunneling is still smaller than that from near-field radiative heat transfer enabled by surface phonon-polaritons, at temperatures below ~50 K it becomes dominant over all other mechanisms. In addition, it has a significant effect over large distances, allowing heat to tunnel across gaps ~ hundreds of nanometers wide at liquid helium temperatures. This means that with current nanofabrication techniques piezoelectrically mediated heat transfer (PEMHT) can be investigated experimentally.

References

[1] M. Balakirev and A. Gorchakov, *Fiz. Tverd. Tela (Leningrad)* **19**, 571 (1977) [*Sov. Phys. Solid State* **19**, 327 (1977)].
[2] M. Balakirev, S. Bogdanov, and A. Gorchakov, *Fiz. Tverd. Tela (Leningrad)* **20**, 587 (1978) [*Sov. Phys. Solid State*, **2**0, 338 (1978)].
[3] Z. Geng and I. J. Maasilta, *Phys. Rev. Res.* **4**, 033073 (2022).
[4] Z. Geng and I. J. Maasilta, arXiv:2209.08287.
[5] Z. Geng and I. J. Maasilta, arXiv:2303.05084.

PHONONICS 2023: 6th International Conference on Phononic Crystals/Metamaterials/Metasurfaces, Phonon Transport, and Topological Phononics
Manchester, England, June 12-16, 2023
PHONONICS-2023-0157

Determination of the In-plane Thermal Diffusivity Using Beam-Offset Frequency-Domain Thermoreflectance with a One-Dimensional Optical Heat Source

Kai Xu[1], Juan Sebastián Reparaz[1]
[1]Materials Science Institute of Barcelona, ICMAB-CSIC, Campus UAB, 08193 Bellaterra, Spain
kaixu@icmab.es, jsreparaz@icmab.es

Abstract: We present a novel contactless method to study in-plane heat transport based on beam-offset frequency-domain thermoreflectance using a 1D heat source. We show that the phase lag between the thermal excitation and response exhibits a linear dependence with their spatial offset. We apply this method to suspended films of Si and PDPP4T; bulk samples of Bi, Si, glass, HOPG; and several 2D materials.

The study of the thermal conductivity (or diffusivity) tensor (κ_{ij}) in bulk and low dimensional materials has gained considerable momentum in recent years. For example, in layered materials where the in-plane and out-of-plane components of the thermal conductivity exhibit strong anisotropy, or for the case of the "artificial anisotropy" induced by low dimensionality in the case of crystalline (or semi-crystalline) thin films. A large number of experimental methods to study the out-of-plane components of the thermal conductivity have been developed and successfully demonstrated using different methodologies, e.g., based on electrical or optical methods. On the other hand, the study of in-plane thermal transport is comparatively more challenging due to the lack of sensitivity to this component of most developed methods, among other reasons. Most experimental methods to study thermal anisotropy are based in achieving experimental sensitivity to in-plane thermal anisotropy, which has been demonstrated through different experimental configurations by several research groups. However, most of the developed methods suffer from the influence of the specific geometry of the heat source (actually its spatial energy distribution) on the acquired data, which originates from the rather small spatial offsets that can be set between the heat source and the probe. Typically, for zero-dimensional (0D) heat sources (approximated as focused Gaussian beams) large offsets cannot be achieved due to the rapid spatial decay of the thermal field.[1]

We demonstrate an original experimental approach with enhanced sensitivity to in-plane heat transport, which is based on using a 1D heat source with uniform power distribution along its long axis, but a point-like probe spot.[2,3] We show that the 1D geometry of the heat source leads to a slower spatial decay of the temperature field as compared to 0D heat sources, hence, allowing to probe the temperature field at relatively large spatial distances from the heat source. The present approach is based on measuring the phase lag between the thermal excitation and the thermal detection spot for different excitation frequencies of the heat source, hence, rendering the thermal diffusivity of the studied samples. In addition, one of its key advantages is that, for harmonic excitation sources, the phase lag (ϕ) between the thermal excitation (line-shaped heater) and the detection exhibits a linear relation with their in-plane spatial offset (Δx), where the slope, $\partial\phi(f)/\partial\Delta x$, is proportional to the thermal diffusivity of the sample for a given modulation frequency, f, of the heater. The linear relation between the phase lag and the spatial offset considerably simplifies the data analysis process, i.e., the thermal diffusivity (or thermal conductivity) of the samples is readily obtained through a linear fit of $\phi(\Delta x, f)$ through the following relation:

$$\partial^2\phi/(\partial\Delta x\partial f^{1/2}) = (\pi/D)^{1/2} \quad (1)$$

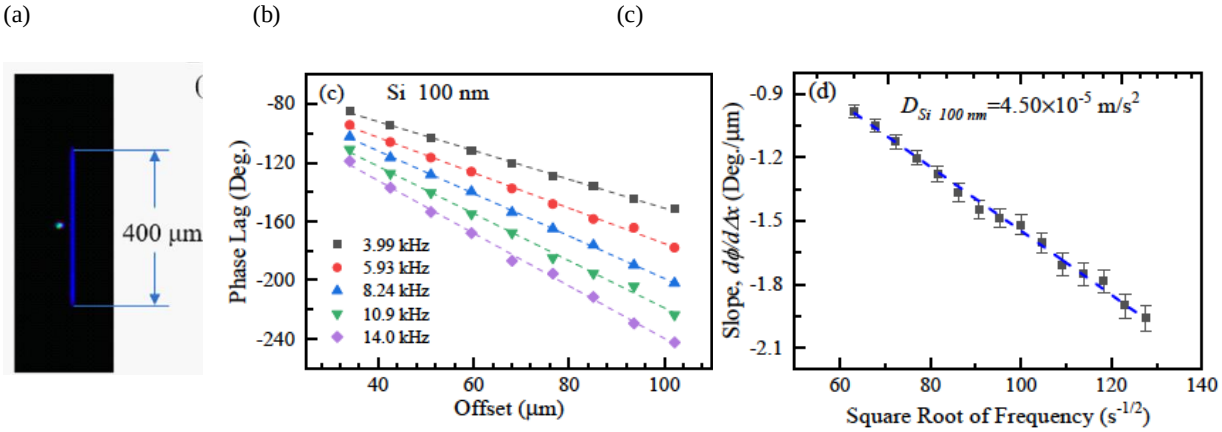

Figure 1 (a) Optical photograph of the line-shaped heat source (pump) as well as the spot-shaped probe. **(b)** Phase lag vs. offset for a 100 nm thick suspended Si thin film for different excitation frequencies between 4 kHz and 14 kHz. The dashed lines are linear fits to the data points. **(c)** Slopes obtained from fitting ϕ vs Δx for each excitation frequency.

Furthermore, the one-dimensional character of the heat source sets the frequency range of interest to f < 100 kHz, which allows the study of materials without the presence of a metallic transducer with almost no influence of the finite optical penetration depth of the pump and probe beams on the thermal phase lag.

In particular, we demonstrate the performance of the developed methodology to study materials with different heat flow geometries such as: (i) suspended Si and PDPP4T thin films with different thicknesses (2D sample; 1D heat flow), (ii) Bi bulk sample without metallic transducer (3D sample; 2D heat flow), (iii) Si and glass substrates with a 60 nm thick Au transducer (3D sample; 2D heat flow), and (iv) highly oriented pyrolytic graphite (HOPG) and several 2D materials such as: $NbSe_2$, VSe_2, $TiSe_2$, $TaSe_2$, TiS_2, NbS_2, TaS_2, $TaTe_4$, VTe_2, and $NbTe_2$ (3D samples; quasi-1D heat flow)

Figure 1 displays an example of the application of the present method to the case of a 100 nm thick suspended Si thin film. Figure 1(a) displays an optical photograph of the line-shaped pump (heater) and spot-shaped probe (thermometer) lasers. Figure 1(b) displays the phase lag (ϕ) between the heater and thermometer as a function of the excitation frequency of the heater and their spatial offset (Δx). As previously anticipated, the dependence of the phase lag with the spatial offset is linear for each excitation frequency. Moreover, as predicted by equation 1, the slopes, $\partial\phi/\partial\Delta x$, also exhibit a linear relation with $f^{1/2}$. Figure 1(c) displays the slopes, $\partial\phi/\partial\Delta x$, as obtained from the linear fits of ϕ versus Δx in Fig. 1b, for each excitation frequency. We compute the thermal diffusivity of the studied Si thin film from fitting the linear dependence in Fig. 1c as as D = 4.5x10^{-5} m^2/s, i.e., ≈50% of the Si bulk value and in good agreement with previous determinations

We think that the present method will provide new opportunities to study heat transport, specially for anisotropic materials, since it allows to obtain the in-plane components of the themal diffusivity tensor with enhanced sensitivity. Furthermore, its rather simple data analysis procedure makes it suitable for cases where numerical simulations cannot be conducted.

References

[1] Luis A. Pérez, Kai Xu, Markus R. Wagner, Bernhard Dörling, Aleksandr Perevedentsev, Alejandro R. Goñi, Mariano Campoy-Quiles, M. Isabel Alonso, and Juan Sebastián Reparaz, *Review of Scientific Instruments* **93**, 034902 (2022)
[2] Kai Xu, Jiali Guo, Grazia Raciti, Alejandro R. Goni, M. Isabel Alonso, Xavier Borrise, Ilaria Zardo, Mariano Campoy-Quiles, and Juan Sebastian Reparaz, Submitted to *International Journal of Heat and Mass Transfer* (2023)
[3] X. Qian, Z. Ding, J. Shin, A. J. Schmidt, and G. Chen, *Review of Scientific Instruments* **91**, 064903 (2020)

PHONONICS 2023: 6th International Conference on Phononic Crystals/Metamaterials/Metasurfaces, Phonon Transport, and Topological Phononics
Manchester, England, June 12-16, 2023
PHONONICS-2023-0193

Non-reciprocal amplification using Willis coupling

Jensen Li

Department of Physics, The Hong Kong University of Science and Technology, Kowloon, Hong Kong, China, jensenli@ust.hk

Abstract: While reciprocal Willis coupling generates asymmetric reflection, non-reciprocal Willis coupling is able to further achieve asymmetric and non-reciprocal transmission. We show the usage of non-reciprocal Willis coupling for amplified sensing and non-reciprocal communication in airborne acoustics by adopting active acoustic metamaterial atoms.

Willis coupling, as the analog picture of the bianisotropy in acoustics, resulting in asymmetric scattering properties[1,2,3,4]. Consequently, asymmetric reflections[1,2,3] or unidirectional zero reflections[4] have been achieved using Willis metamaterials. By designing asymmetric metamaterial structure with resonances, strong Willis coupling can be achieved, with possible extensions to different mechanical waves[5,6] . However, these Willis metamaterials are usually imposed by the constraints of passivity and reciprocity[7,8]. Here, we resort to active metamaterials to break these constraints[9,10], achieving non-reciprocal Willis coupling. Furthermore, using such a non-reciprocal Willis coupling, non-reciprocal transmission can be realized, allowing us to achieve novel applications such as amplified sensing and non-reciprocal communication.

Using our active metamaterials that implement a time-domain convolution by connecting microphones and speakers through a digital feedback circuit at each atom, we can realize the full and independent control of all constitutive parameters of the metamaterial in the stable working regime by programming[9,10]. Consequently, the transmission and reflection properties can be flexibly controlled. For a 1D metamaterial (along x direction) with a thickness L, the wave equation can be written as

$$\partial_x \begin{pmatrix} v \\ p \end{pmatrix} = \frac{i\omega}{c} \begin{pmatrix} \beta & i\tau \\ i\tau' & \rho \end{pmatrix} \begin{pmatrix} p \\ v \end{pmatrix}, \tag{1}$$

where p is the pressure, v is the velocity multiplied by the acoustic impedance of the air, and c is the sound speed in the air. For the constitutive parameters, β and ρ represent the dimensionless compressibility and density relative to air. τ and τ' are the Willis coupling terms, which can be decomposed into reciprocal τ_r and non-reciprocal components τ_{nr} by $\tau=\tau_r+\tau_{nr}$, and $\tau'=-\tau_r+\tau_{nr}$. With Eq. (1), we can obtain the relationship between scattering parameters and constitutive parameters with Padé's approximation[11]:

$$\begin{pmatrix} t_f & r_b \\ r_f & t_b \end{pmatrix} \cong \begin{pmatrix} 1+\frac{i\phi_0}{2}(\beta+\rho+2i\tau_{nr}) & \frac{i\phi_0}{2}(\beta-\rho-2i\tau_r) \\ \frac{i\phi_0}{2}(\beta-\rho+2i\tau_r) & 1+\frac{i\phi_0}{2}(\beta+\rho-2i\tau_{nr}) \end{pmatrix}, \tag{2}$$

where $\phi_0=\omega L/c$ is the phase that elapses across the air with the same thickness of the metamaterial L. When $\tau_r=0$ and $\beta=\rho$ (impedance matching condition), the reflection signals in both directions are zero ($r_f= r_b =0$), preventing the backscattering signals to the source. On the other hand, a non-zero τ_{nr} enables non-reciprocal transmission: $t_f \cong 1+i\phi_0 (i\tau_{nr}+\beta)$ and $t_b \cong 1+i\phi_0 (-i\tau_{nr}+\beta)$. By choosing a real τ_{nr}, the transmitted signal is amplified for one direction while suppressed for another direction, which forms the basis to obtain amplified sensing and non-reciprocal communications next.

We demonstrate the amplified sensing using a 1D active metamaterial with above-mentioned constitutive parameters. Figure 1(a) shows the schematic of setup for amplified sensing, where a sensor (black circle) is enclosed by the active and non-reciprocal metamaterial: 3 atoms with τ_{nr}=-0.09 (blue circles) on the left of sensor and 3 atoms with τ_{nr}=0.09 (green circles) on the right. When the metamaterial turns off, the |t| and |r| spectrum in Fig. 1(b) give the scattering properties of the sensor, absorbing power in free space. Now turning on the non-reciprocal metamterial, the scattering power remains the same as before (Fig. 1(c)), due to the zero reflections and non-reciprocal transmission

discussed in above. The solid lines in Fig. 1(b) and (c) are the same analytical results of the sensor, matching the scattering spectrum of two cases. However, comparing the detected signal at the sensor for the two cases, we obtain a 1.8-fold amplification at the designed frequency of 1.35 kHz when the metamaterial turns on (line), as shown in Fig. 1(d). Consequently, amplified sensing is achieved with the active and non-reciprocal metamaterials without modifying the scattering properties of sensor.

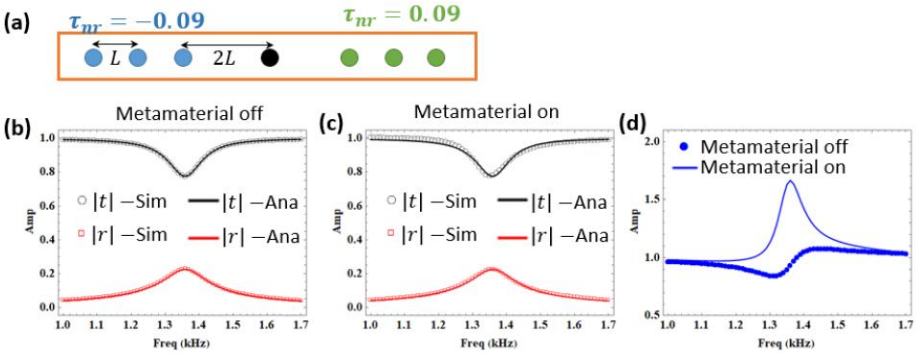

Fig. 1 (a) Amplified sensing with 3 non-reciprocal Willis atoms on the left (right) with $\tau_{nr} = -0.09\ (+0.09)$. The sensor is denoted in black color. (b) and (c) show the transmission and reflection coefficients stay the same disregarding whether the Willis atoms are on or off. (d) Detected signal at sensor is amplified at around 1.35 kHz when the metamaterial are turned on (line).

We further design a 2D ring of Willis atoms (Fig. 2(a)) for non-reciprocal communication, in which 24 active atoms form a circular metasurface with a radius of 15 cm. When we put a point source in the location A, the pressure field inside the metasurface (denoted by a black circle) is amplified, while the pressure field outside the metasurface is not affected by the metasurface. On the other hand, placing a point source in the location B, the pressure field inside the metasurface is not affected, while the pressure field outside the metasurface is suppressed, as non-reciprocal communication. We will also discuss experimental realizations of these non-reciprocal phenomena in the talk.

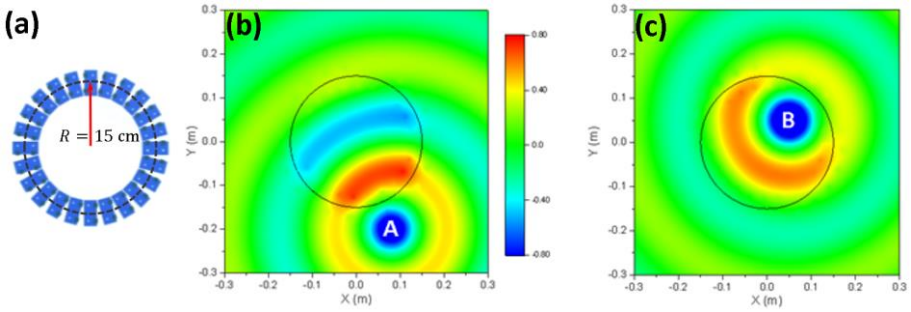

Fig. 2 Non-reciprocal communication. (a) 2D ring of Willis atoms. (b) Pressure field from a point source at A outside the ring. (c) Pressure field from a point source at B inside the ring.

We acknowledge support from RGC Hong Kong through project No. 16303019, AoE/P-502/20 and support from the Croucher Foundation.

References

[1] Muhlestein, M. B., Sieck, C. F., Wilson, P. S. and Haberman, M. R. *Nat. Commun.* **8**, 15625 (2017).
[2] Koo, S., Cho, C., Jeong, J. H. and Park, N. *Nat. Commun.* **7**, 13012 (2016).
[3] Liu, Y. et al. *Phys. Rev. X* **9**, 011040 (2019).
[4] Merkel, A., Romero-García, V., Groby, J. P., Li, J., and Christensen, *J. Phys. Rev. B* **98**, 201102(R) (2018).
[5] Meng, Y., Hao, Y., Guenneau, S., Wang, S., Li, J., and Christensen, *New J. Phys.* **23**, 073004 (2021).
[6] Hao, Y., Shen, Y. Groby, J. P., Li, J., *Wave Motion* **112**, 102931 (2022).
[7] Quan, L., Ra'di, Y., Sounas, D. L. and Alù, A. *Phys. Rev. Lett.* **120**, 254301(2018).
[8] Melnikov, A. et al. *Nat. Commun.* 10, 3148 (2019).
[9] Cho, C., Wen, X., Park, N., and Li, J. *Nat. Commun.* **11**, 251 (2020).
[10] Cho, C., Wen, X., Park, N., and Li, J. *Commun. Phys.* **4**, 82 (2021).
[11] Feng, T., Li, F., Tam, W. Y. and Li, *J. EPL (Europhy. Lett.)* **102**, 18003 (2013).

PHONONICS 2023: 6th International Conference on Phononic Crystals/Metamaterials/Metasurfaces, Phonon Transport, and Topological Phononics
Manchester, England, June 12-16, 2023
PHONONICS-2023-0159

Localization of Elastic Energy on Metasurfaces with Resonators

T. Deletang[1], A. Noual[2], R. Buisine[3], B. Djafari-Rouhani[3], Y. Pennec[3], L. Carpentier[3], and B. Bonello[1]

[1]*Sorbonne Université, Institut des Nanosciences de Paris (UMR CNRS 7588), 75005 Paris, France*
[2]*LPMR, Department of Physics, Faculty of Sciences, University Mohamed I, 60000 Oujda, Morocco.*
[3] *Université de Lille, Institut d'Electronique, de Microélectonique et de Nanotechnologie (UMR CNRS 8520), Département de Physique, 59650 Villeneuve d'Ascq, France*
thibault.deletang@insp.jussieu.fr, noualad@yahoo.fr, roman.buisine@iemn.fr, barham.djafari-rouhani@univ-lille.fr, yan.pennec@univ-lille.fr, laurent.carpentier2@univ-lille.fr, bernard.bonello@insp.jussieu.fr

Abstract: We present an experimental study of the localization of SAW after their propagation in a diffusive medium consisting of pillar-shaped mechanical resonators randomly distributed on a surface. The data are compared with numerical simulations. This study is the phononic part of a more global research on the co-localization of elastic and optical waves on random metasurfaces, with the main objective of enhancing the photon-phonon interaction.

We have investigated experimentally the propagation and the localization of Rayleigh waves in a metasurface consisting of an assembly of several thousand aluminum pillars arranged randomly on a 200 nm thick film, also made of aluminum, deposited on a semi-infinite silica substrate. Both the diameter and the height of the pillars are 300 nm. Depending on the samples, the filling ratio (ratio of the total section of the pillars to the surface of the sample) is between 7% and 9%. One of our goals being to study if the statistics has an influence on the efficiency of the localization, the positions of the centers of the pillars follow a Poisson, Gaussian or hyperuniform statistics, with the only constraint that there is no overlap between two neighboring pillars. The propagation and localization of SAW in the metasurface were recorded using an interferometric pump-probe experimental technique. This non-contact technique[1] consists in exciting a broadband surface elastic wave with a first ultrashort laser pulse and probing the resulting out-of-plane displacement of the surface with a second light pulse delayed with respect to the pump pulse, as a function of time and space. Given the light pulse duration (120 fs), pump spot diameter (~0.9 µm), physical and geometrical parameters of the aluminum film, SAW with spectral content extending up to ~2 GHz are excited. As for the spatial resolution, it is in principle limited by the size of the probe spot, i.e. ~0.9 µm as well, but it can be improved if signal deconvolution techniques are implemented.

As is the case for a cavity in a phononic crystal, the localization of elastic energy in a random metasurface results from interferences of the wave bouncing back and forth within the free surface surrounded by pillars. The "cavity" highlighted in the red rectangle in Fig. 1a is roughly rectangular in shape (~2×5µm^2) and interferences are expected to occur for elastic waves having a wavelength equal to its length. We have measured the displacement of the surface at a point of the cavity, as a function of time. The SAW are excited at a distance of about 5 µm from the left edge of the cavity (blue dot in Fig. 1a) and the signal is recorded in the center (red dot in Fig. 1a). The result is displayed in Fig. 1b where it can be seen that the wave front at 1.3 ns is followed by a series of oscillations, the more intense of which appearing at ~5 ns.

We then have recorded the cartography of displacements in the cavity at three different instants of a period of the oscillations. The result displayed in Fig. 1c clearly shows the stationary waves, which in this example lasts for approximately 2.5 ns.

It should be noted that the edges of the cavity not being perfectly defined, the spectral content of the localized waves may present several peaks at close frequencies, each having a different width, or equivalently, a different quality factor. For the same reason, the spectrum may vary according to the position of the acoustic source with respect to the cavity.

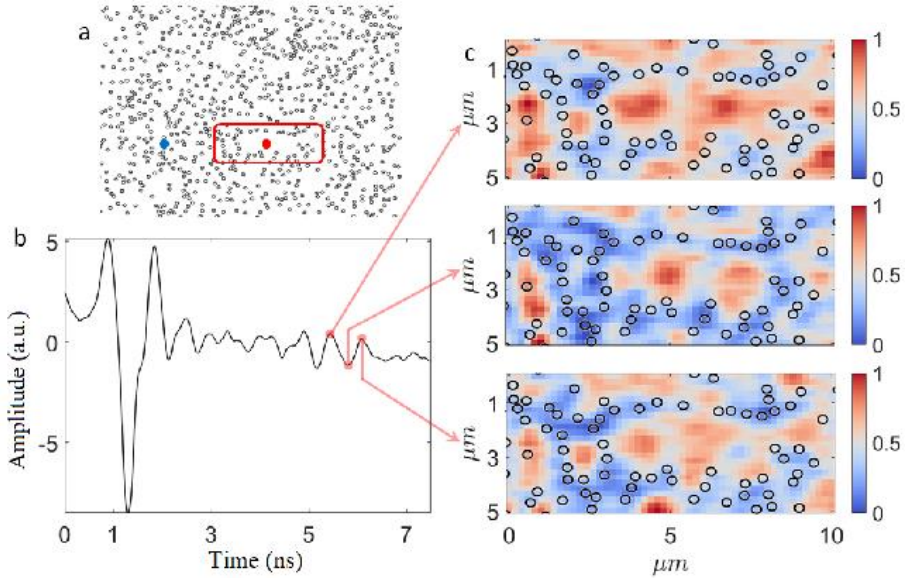

Figure 1: (a) Image of a sample with a Poisson statistic. The blue dot (resp. red) corresponds to the location of the pump (resp. probe) beam for the measurement of the time dependence of the normal displacement displayed in panel (b). The red rectangle delimits the area probed at the three moments marked by the red dots in panel (b) and displayed in panel (c).

This last point has been further investigated through numerical simulations using the finite element method (Comsol Multiphysics). The calculation of the transverse component of the displacement field in the time domain confirms the confinement over the duration of a few ns, of an oscillating mode in the cavity. The frequency analysis carried out at several points of the cavity shows a peak at the bending eigenfrequency of the cylindrical resonators which is superimposed on a broad peak of interferential origin related to the geometry and the dimensions of the cavity (Fig.2).

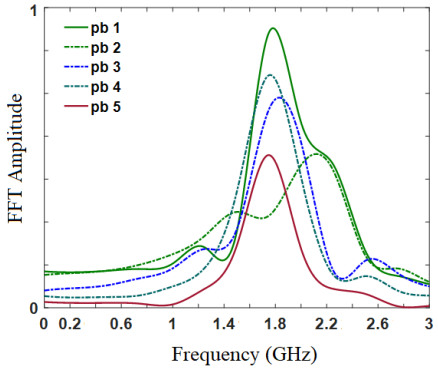

Figure 2: Fourier transform of the transverse component of the displacement field computed in five different points in the rectangular cavity shown in Fig. 1a. The calculation is made using a finite element method.

This work is supported by Agence Nationale de la Recherche under the project “RANDOM” (ANR-19-CE24-0014-04)

References

[1]T. Tachizaki, T. Muroya, O. Matsuda, Y. Sugawara, D.H. Hurley, and O.B. Wright, Rev. Sci. Instrum. **77**, 043713 (2006)
[2]Y. Jin, Y. Pennec, B. Bonello, H. Honarvar, L. Dobrzynski, B. Djafari-Rouhani, and M. I. Hussein, Rep. Prog. Phys. **84**, 086502 (2021)

PHONONICS 2023: 6th International Conference on Phononic Crystals/Metamaterials/Metasurfaces, Phonon Transport, and Topological Phononics
Manchester, England, June 12-16, 2023
PHONONICS-2023-0095

Focusing and Imaging of Flexural Lamb Waves by Pillared Metasurfaces

L. Carpentier[1], Y. Jin[2], W. Wang[2], J. Iglesias[3], A. Khelif[3], Y. Pennec[1], B. Bonello[4], B. Djafari Rouhani[1]

[1]*Université de Lille, CNRS, Centrale Lille, UPHF, Junia, UMR 8520 IEMN, F-59000 Lille, France*
[2]*School of Aerospace Engineering and Applied Mechanics,Tongji University, 200092 Shanghai, China*
[3]*Instiut FEMTO-ST, CNRS, University of Bourgogne Franche-Comté, 25030 Besançon, France*
[4]*Sorbonne Université, Institut des Nanosciences de Paris, UMR CNRS 7588, 75005 Paris, France*
Corresponding author, email: bahram.djafari-rouhani@univ-lille.fr

Abstract: We design metasurfaces made of an array of pillars on a plate for subwavelength focusing and imaging of flexural Lamb waves. The superposition of two pillar resonances allows to achieve a span of the transmission phases over a range of 2π. Two sets of metasurfaces are considered, cylindrical pillars with a gradient in their height or elliptic pillars with a gradient in their ellipticity parameter.

Metasurfaces are sub-wavelength thickness structures that allow an efficient control and manipulation of reflected and refracted waves. In this work, we are interested by the focusing and imaging of flexural waves propagating on a plate by using a metasurface constituted by an array of pillars with a gradient in their geometrical properties. A first structure is based on cylindrical pillars with a gradient in their heights. To avoid the difficulty of height variation in the microfabrication regime, a second solution is based on elliptical pillars where the ellipticity parameter is used to make the gradient in the metasurface. These designs allow to achieve sub-wavelength and broadband focusing functionalities and display a sufficient robustness with respect to disorder in the parameters or frequency fluctuations.

To achieve a span of the transmission phases in the array over a range of 2π, which is a requirement in the design of the metasurface, an essential feature will be to start with a pillar where two resonances (such as a bending and a compressional resonance) are superimposed. Indeed, the phase of the transmission coefficient through a line of identical pillars undergoes a variation of π when the frequency is swept around a resonance frequency. However, this phase variation can reach 2π if two resonances occur at the same frequency.

In our first theoretical design[1], the metasurface consists of an array of cylindrical pillars made of silicon over a silicon plate (Fig. 1(a). By chosing the initial parameters as: pillar diameter d=120μm, pillar height h=239μm, plate thickness e=145μm, period of the array a=150 μm, we obtain a superposition of the second bending and first compressional resonances of the pillar at 8.05MHz. A gradual change of the pillar height around the initial value allows to obtain a phase shift covering a range of 2π while keeping the level of transmission sufficiently high (Fig. 1(b)). Then, based on the generalized Snell law, the metasurface can be constructed from a set of pillars such as to satisfy for each pillar the phase shift condition for the desired functionality (Fig. 1(a)). Figure (1(c) shows an example of a sub-wavelength focusing of an incident A_0 Lamb mode at the frequency of 8.05 MHz (corresponding to a wavelength λ=423μm) at a focal length F=λ. Let us notice that this wavelength is 3.5 times larger than the thickness of the metasurface. The FWHM is in general dependent upon both the focal length F and the total length D of the metasurface. A comprehensive investigation of the FWHM as a function of these lengths show that the relevant parameter is the ratio F/D and the sub-wavelength focusing can be realized as long as F/D remains below 0.25-0.3. We have also checked the robustness of the focal length and FWHM with respect to a disorder in the geometrical parameters or to frequency fluctuations. A first experimental demonstration of the focusing functionality has been performed[2] with a sample fabricated by using 3D-printed polymer material in the mm range.

The second design is based on pillars of elliptic shape and identical height which are more convenient for fabrication at the nanoscale. The short axis of the ellipse, parallel to the metasurface, is fixed to

e_1= 20µm and the long axis e_2 is used as the parameter to make a gradient in the scattering properties of the pillars. For a value of e_2=50µm, the second bending and first compressional resonances of the pillar become in coincidence at 7.48 MHz, corresponding to a wavelength of the A_0 mode equal to λ=445µm. The other pillars in the metasurface are designed by varying e_2 around the initial value such as the phase shift of the transmission coefficient satisfies the value required by the generalized Snell law. Two examples of sub-wavelength focusing are presented in Fig. 2 for a normal A_0 incident wave, showing that the focal point can be chosen either along the axis or off-axis of the incident wave.

We project to design such a device for the focusing of a surface acoustic wave emitted by an electro-mechanical interdigitated component towards the entrance of an optomechanical nanobeam[4].

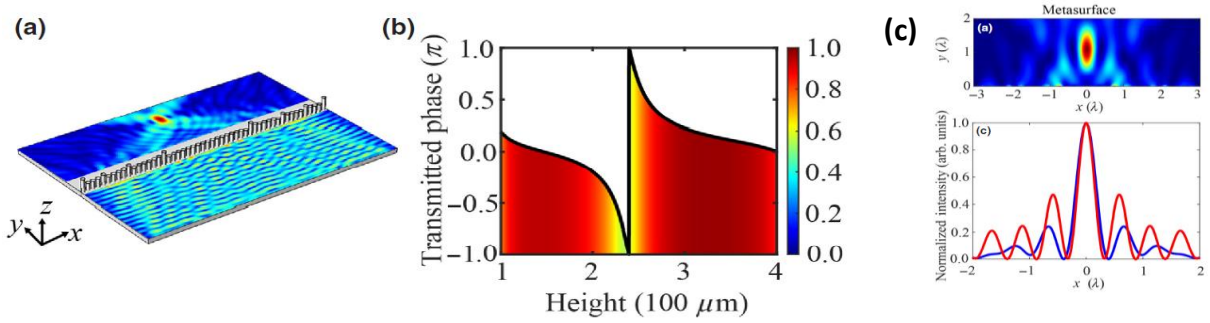

Figure 1 (a) Illustration of the gradient pillared metasurface for focusing effect. (b) Variation response of transmitted phase (black curve) and amplitude (color level) in a periodic array as a function of pillar height h in the unit cell[1]. (c) Intensity field of plane wave focusing[1].

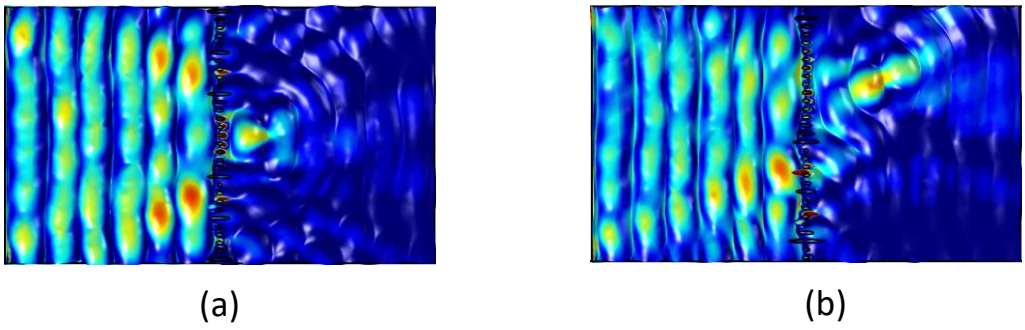

Figure 2 Focusing of an incident A_0 Lamb mode by a metasurface composed of elliptic pillars along the axis (a) or off-axis (b) of the incoming wave[3].

References

[1] Y. Jin, W. Wang, A. Khelif and B. Djafari Rouhani, *Phys. Rev. Appl.* **15**, 024005 (2021).
[2] W. Wang, J. Iglesias, Y. Jin, B. Djafari Rouhani and A. Khelif, *APL Mat.* 9, 051125 (2021).
[3] B. Djafari Rouhani, L. Carpentier and Y. Pennec, *IUS 2022 Symposium proceedings*, p. 2287.
[4]A. Korovin, Y. Pennec, M. Stocchi, D. Mencarelli, L. Pierantoni, T. Makkonene, J. Ahopelto and B. Djafari Rouhani, *J. Phys. D: Appl. Phys.* **52,** 32LT01 (2019).

PHONONICS 2023: 6th International Conference on Phononic Crystals/Metamaterials/Metasurfaces, Phonon Transport, and Topological Phononics
Manchester, England, June 12-16, 2023
PHONONICS-2023-0104

Tailoring Bound States in the Continuum by Circular Clusters of Scatterers

Marc Martí-Sabaté[1], Junfei Li[2], Steven Cummer[2], Bahram Djafari-Rouhani[3], Daniel Torrent[1*]

[1]Institut de Noves Tecnologies de la Imatge (INIT), Universitat Jaume I, 12071 Castelló de la Plana, Spain
[2] Department of Electrical and Computer Engineering,7 Duke University, Durham, North Carolina 27708, USA
[3]IEMN, University of Lille, Cité Scientifique, 59650 Villeneuve d'Ascq, France

Abstract: We study the localization of flexural and acoustic waves in highly symmetric clusters of scatterers placed atop a metasurface. We show that when the scatterers are placed regularly in the perimeter of a circumference, the quality factor diverges as the number of scatterers is larger than a few tenths. It is also found that in the continuous limit, that is to say, when the number of scatterers tends to infinite, the quality factor is also infinite so that the modes belong to the class of the so called bound states in the continuum or BICs. Numerical experiments are performed for two types of classical waves: elastic waves in thin elastic plates and acoustic waves trapped on a metasurface, and an experimental validation of the latter is also presented.

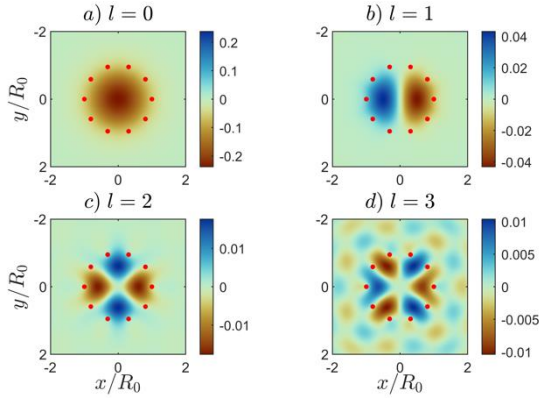

Figure 1 High quality resonances in circular clusters of scatterers

The realization of high-quality resonators is a challenging problem in all domains of physics devoted to the control and harness of classical waves, like photonics and acoustics. Bound states in the continuum (BICs) offer a route for the realization of a special class of resonant cavities, since although in principle these modes cannot couple to the free propagating waves, structures based on them can be used for the design of excellent resonators presenting extraordinarily high-quality factors. Also named quasi-bound states in the continuum or QBIcs, the efficient design of these cavities is of paramount importance in either photonics and acoustics.

In this work we focus on the problem of acoustic waves in two different structures. First, we consider the propagation of flexural waves in thin elastic plates, latter we study acoustic waves trapped atop a structured metasurface. The geometry analyzed for both systems is identical: clusters of scatterers regularly placed along the perimeter of a polygon, so that in the limit of a large number of scatterers the geometry diverges towards a perfect circular scatterer. It is shown that in this limit the structure forms a cavity which resonances have an infinite quality factor, obtaining therefore a perfect BIC. However, having a finite number of scatterers allows for a finite but extraordinarily high-quality factor, which is tunable with the number of scatterers in the cluster.

Numerical simulations and experimental realizations support our findings, showing that this work opens a path towards the design of easy-to-tailor acoustic cavities.

References

[1] Martí-Sabaté, M., Djafari-Rouhani, B., & Torrent, D. (2023). Bound states in the continuum in circular clusters of scatterers. Physical Review Research, 5(1), 013131.

PHONONICS 2023: 6th International Conference on Phononic Crystals/Metamaterials/Metasurfaces, Phonon Transport, and Topological Phononics
Manchester, England, June 12-16, 2023
PHONONICS-2023-0047

A Multiple Scattering Approach for Elastic Metasurfaces: from Quasi-Periodicity to Space-Time Modulation

X.Pu[1], A. Palermo[1], A. Marzani

[2] *Department of Civil, Chemical, Environmental and Materials Engineering, University of Bologna, 40033, Italy*
xingbo.pu2@unibo.it; antonio.palermo6@unibo.it; alessandro.marzani@unibo.it

Abstract: We present a general multiple scattering approach to investigate the dynamics of non-periodic, time-modulated elastic metasurfaces. We show how (time-invariant) quasi-periodic metasurfaces support the existence of localized surface edge modes. Conversely, when space-time modulation is introduced, one-way surface wave propagation is achieved.

Introduction

In the past two decades, the advent of so-called elastic metasurfaces, namely structured interfaces equipped with subwavelength mechanical resonators, has opened a new pathway toward the control of surface elastic waves. In fact, by exploiting the coupling between the propagating surface waves and the localized motion of the resonators, peculiar phenomena such as surface-to-bulk wave conversion[1], rainbow trapping[2], wave localization and rerouting have been demonstrated[3]. For linear elastic, time-invariant, and spatially periodic metasurfaces, several analytical formulations are available to predict the surface wave dispersive properties and compute the related elastic wavefields. Conversely, the dynamic response of a finite-size, non-periodic and/or time-modulated metasurface is typically investigated via numerical techniques (e.g. FEM) given the lack of analytical tools. Therefore, in this talk, we present and discuss a general analytical framework, based on the multiple scattering technique[5], to model the wave field along finite size, non-periodic and time-modulated elastic metasurfaces.

Methodology and Results

The proposed formulation combines: (i) a set of impedance operators able to describe the coupling between each modulated resonator and the elastic waveguide accounting for the multiple harmonics generated by the space-time material modulation; (ii) ad-hoc Green's functions to compute the scattered fields induced by the resonators vibrating on the waveguide; (iii) a multiple scattering scheme to couple the incident and scattered fields and obtain the total wavefield along and outside the resonators array. Exploiting this formulation, we first study the dynamics of quasi-periodic, linear-time invariant metasurfaces and show the existence of localized surface edge states[4] (see Fig. 1).

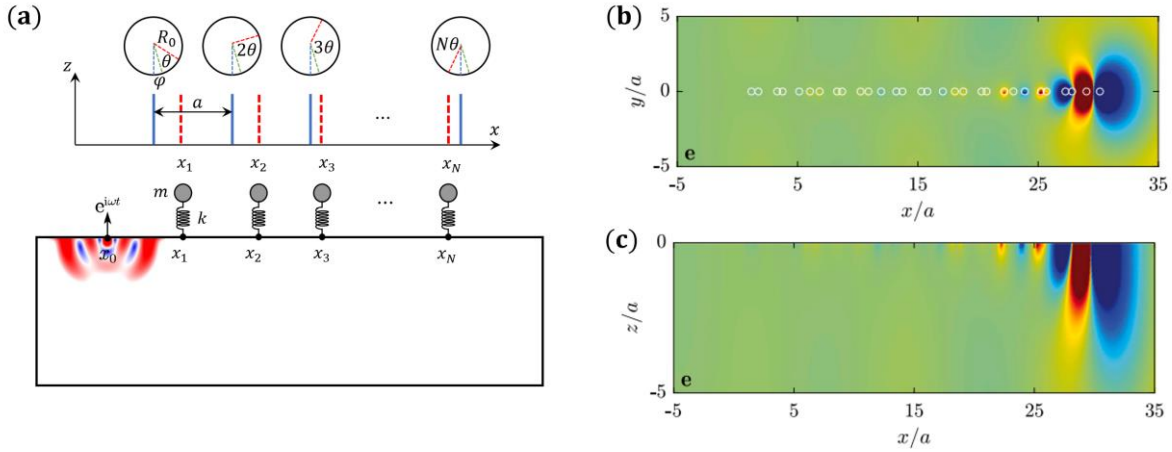

Figure 1 (a) Schematic of a finite-size metasurface where the resonators are located according to a quasi-periodic arrangement. **(b)** Plan view and **(c)** side-view of a localized surface-edge mode supported by a quasi-periodic metasurface (adapted from[4]).

Next, we use the formulation to model the response of a finite-size space-time modulated metasurfaces and show frequency conversion and one-way propagation of Rayleigh-like waves (see Fig. 2).

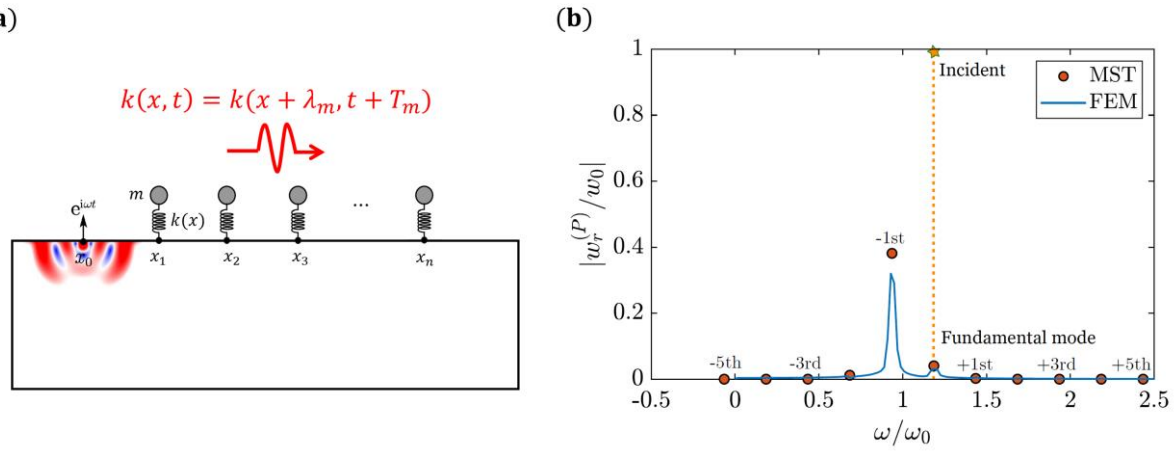

Figure 2 (a) Schematic of a finite-size time-modulated metasurface where the resonators spring is modulated in space-time according to a wave-like function. **(b)** Example of a wave field reflected by the metasurface where higher-order frequency components are evidenced (adapted from[5]).

Conclusions

In this work, we propose a multiple scattering formulation to model the interaction of a given incident field with an arbitrary non-periodic cluster of space-time-modulated resonators located at the surface of a given elastic waveguide. We anticipate the proposed formulation will serve as a computationally inexpensive tool to guide future experiments on space-time-modulated systems.

References

[1]Colquitt D., et al. Seismic metasurfaces: Sub-wavelength resonators and Rayleigh wave interaction, JMPS, 99, (2017).
[2]Colombi A., et al, A seismic metamaterial: The resonant metawedge, Sci. Rep., 6 ,1, (2016).
[3]Yabin, J., et al. "Physics of surface vibrational resonances: Pillared phononic crystals, metamaterials, and metasurfaces." Reports on Progress in Physics, 086502, (2021).
[4]Pu, X., Palermo, A., Marzani, A., Topological edge states of quasiperiodic elastic metasurfaces, MSSP,181, (2022).
[5]Pu, X., Palermo, A., Marzani, A., A multiple scattering formulation for elastic wave propagation in space-time modulated metamaterials, arXiv:2301.00874 (2023)

PHONONICS 2023: 6th International Conference on Phononic Crystals/Metamaterials/Metasurfaces, Phonon Transport, and Topological Phononics
Manchester, England, June 12-16, 2023
PHONONICS-2023-0006

Coupled Resonances Mechanisms to Broaden Low-Frequency Bandgaps in Acoustic Metamaterials

David Roca[1,2], Gastón Sal[1,2], Daniel Yago[1,2], Juan Cante[1,2], Javier Oliver[1,2], Mahmoud I. Hussein[3,4]

[1] *Physics Department, Aerospace division, Universitat Politècnica de Catalunya (ESEIAAT), Terrassa 08222, Spain*
[2] *Centre Internacional de Mètodes Numèrics en Enginyeria (CIMNE), Barcelona 08034, Spain*
droca@cimne.upc.edu, gsal@cimne.upc.edu, dyago@cimne.upc.edu, jcante@cimne.upc.edu, oliver@cimne.upc.edu
[3] *Smead Department of Aerospace Engineering Sciences, University of Colorado Boulder, Boulder 80303, USA*
[4] *Department of Physics, University of Colorado Boulder, Boulder 80303, USA*
mih@colorado.edu

Abstract: Novel acoustic metamaterials that exploit coupled resonances mechanisms are shown to exhibit a double-peak sound transmission loss response. Compared to conventional acoustic metamaterial solutions, these unique configurations offer enhanced sound attenuation over a broader range of frequencies, with potential applications in low-frequency noise insulation.

Noise insulation at low frequencies is a long-standing problem in acoustics that, in practical terms, still lacks an effective solution. In such frequency ranges, conventional acoustic insulation panels are restricted by the classical mass law, hence being forced to rely only on increasing their density or thickness to enhance the sound attenuation. With the advent of acoustic metamaterials, new pathways were opened to the possibility of obtaining huge levels of sound attenuation through resonance phenomena, thus breaking the mass law. This is due to acoustic metamaterials' ability to produce subwavelength frequency bandgaps, which in an acoustic context translates into intense levels of sound transmission loss (STL). However, current sound insulation panels based on acoustic metamaterials still face challenges due to the narrowband nature of the local resonance bandgaps (with an impact on the effective STL attenuation bandwidth) and the complex manufacturing processes involved.

To tackle both challenges, we propose innovative configurations of acoustic metasurfaces, which rely on coupled resonances mechanisms. Our aim is to make them suitable for mass production using currently established manufacturing technologies and emerging ones that are projected to expand rapidly in the near future. Studies based on spring-mass chains have exploited double-periodicity to show strong effects on local resonance bandgaps, where resonance coupling mechanisms take effect[1,2]. In the context of acoustic insulation, this concept manifests as double-peak STL responses that effectively broaden the frequency range of attenuation[3,4]. Figure 1 depicts different acoustic metamaterial unit-cell structures and their corresponding STL response. To establish a reference, the effective range of attenuation is defined here as the frequency region where the STL is 20 dB higher than the value obtained with a conventional panel of the same surface density. In the classical one-resonator case (Figure 1-a), a single narrowband STL peak is obtained. In contrast, an equivalent (i.e., same surface density) conventional two-resonator configuration (Figure 1-b) produces two STL peaks, but they are still narrowband and separated by sound transmission peaks. For an equivalent coupled two-resonator case (Figure 1-c) on the other hand, the two STL peaks are joined, producing as a result an extended effective range of attenuation.

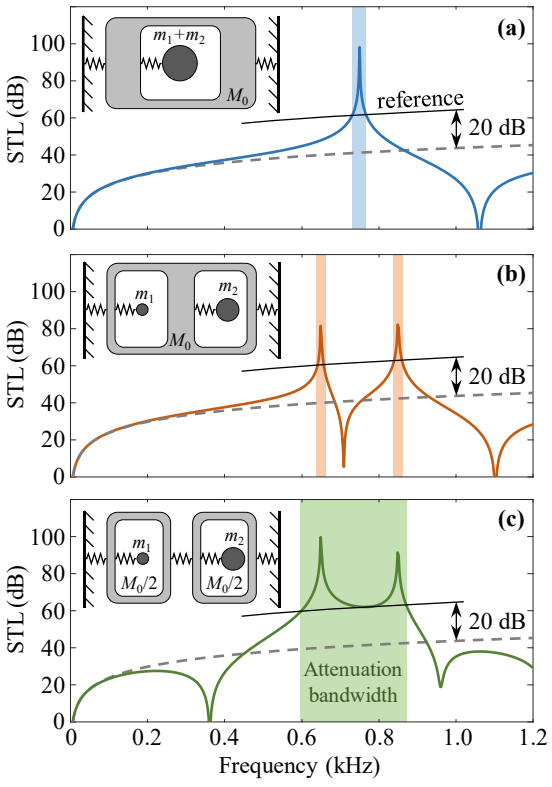

Figure 1 Different acoustic metamaterial configurations with their STL response: **(a)** Single resonator unit cell, **(b)** Double *uncoupled* resonators unit cell, **(c)** Double *coupled* resonators unit cell. Dashed lines correspond to conventional panel of the same surface density.

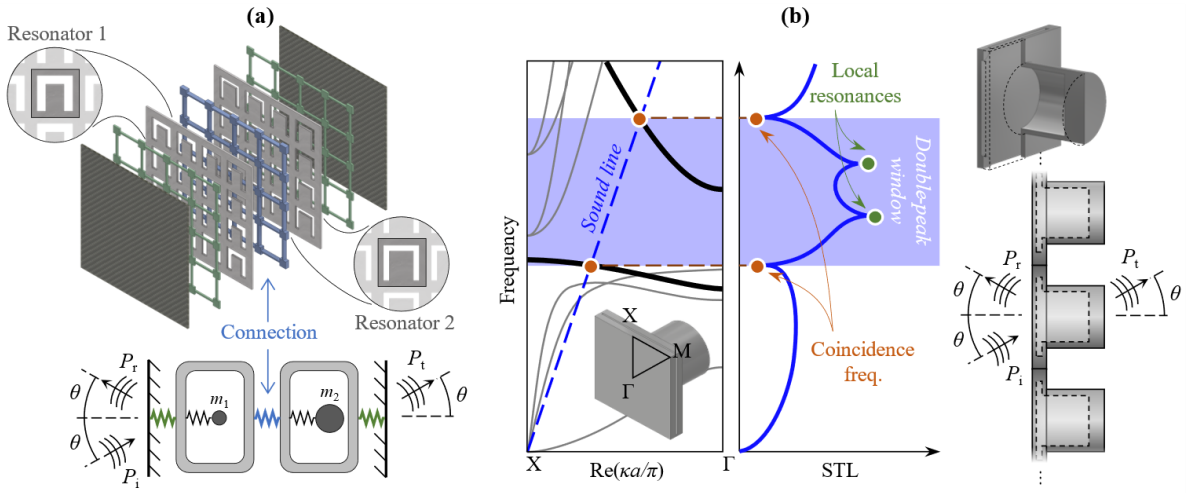

Figure 2 (a) Multiresonant layered acoustic metamaterial[3] (MLAM) panel compared to equivalent lumped spring-mass model. **(b)** Hollow pillar-hollow plate[4] (HP^2) configuration and depiction of the *coincidence-frequencies window* region where local resonance coupling is realized.

In Figure 2, two distinct mechanisms are proposed to show how the coupled resonances concept can be realized. The first one (Figure 2-a) consists of a multiresonant layered acoustic metamaterial[3] (MLAM) and is almost a direct translation of the lumped spring-mass model of Figure 1-c. The core structure is composed of two different resonant layers, each one with a specific hole pattern designed to trigger local resonances at the desired frequencies, separated by a connecting layer. The stiffness of this intermediate layer is key in order to guarantee a proper coupling of the STL peaks. In this regard, the necessary low stiffness values can be achieved either through the use of compliant materials (e.g., silicone rubber) or by increasing the layer's thickness (with the undesired impact on the overall panel thickness). The remaining layers do not play any significant role other than preventing sound from transmitting through the holes in the core layers. In the MLAM design, for a selected set of conventional materials, the geometrical features of each layer (e.g., cell size, thickness, etc.) can be conveniently adjusted to tackle and optimize the increased STL levels obtained over a target frequency range. As an example, combining a common plastic material with a silicone-rubber connecting layer, one can design an MLAM panel with surface density of 12 kg/m^2 and overall thickness below 30 mm capable of achieving 20 dB of additional sound attenuation in the whole range between 100 Hz and 500 Hz, compared to conventional panels of the same surface density.

The second mechanism (Figure 2-b) is based on a hollow pillar-hollow plate[4] (HP^2) panel. Unlike in the previous case, where the resonators need to be placed along the direction of acoustic transmission, here the resonating structures (pillars) are placed in the orthogonal plane. In the HP^2 configuration, the double-peak STL response is realized by placing two local resonance modes inside the frequency range defined by the coincidence-frequencies window (region bounded by two of the panel's coincidence frequencies). The parametric HP^2 design can also be adjusted to tackle different frequency ranges, with the added advantage that it can be built entirely of a single material.

To conclude, the combination of coupling mechanisms with local resonance phenomena represents a promising avenue for achieving enhanced acoustic attenuation over wider frequency ranges than previously achieved using conventional acoustic metamaterial designs. Our results suggest that exploiting this novel concept has the potential to establish a turning point in acoustic metamaterials technology, making it the ultimate solution for low-frequency noise insulation. This research opens up exciting new possibilities for applications in noise control and architectural acoustics in the construction and transport sectors, and may pave the way for further innovations in the field of acoustic metamaterials.

References

[1] Y. Gao and L. Wang, Journal of Applied Physics 127, 204901 (2020).
[2] A. Stein, M. Nouh, and T. Singh, *Journal of Sound and Vibration* **523**, 116716 (2022).
[3] D. Roca, J. Cante, O. Lloberas-Valls, T. Pàmies, and J. Oliver, *Extreme Mechanics Letters* **47**, 101368 (2021).
[4] D. Roca, and M. I. Hussein, *Physical Review Applied* **16**, 054018 (2021).

PHONONICS 2023: 6th International Conference on Phononic Crystals/Metamaterials/Metasurfaces, Phonon Transport, and Topological Phononics
Manchester, England, June 12-16, 2023
PHONONICS-2023-0074

Target scattering properties with correlated disorder

S. Kuznetsova[1], L.M. Garcia-Raffi[2], J.-P. Groby[1] V. Romero-García[2]

[1]Laboratoire d'Acoustique de l'Université du Mans, LAUM - UMR 6613 CNRS, Le Mans Université, Avenue Olivier Messiaen, 72085 LE MANS CEDEX 9, France
[2]Instituto Universitario de Matemática Pura y Aplicada (IUMPA), Universitat Politècnica de València, Camino de vera s/n, 46022, Valencia, Spain
svetlana.kuznetsova@univ-lemans.fr, vicente.romero@mat.upv.es

Abstract: We report a method to design 2D acoustic materials with prescribed scattering properties. We target information in reciprocal space to construct materials the structure factor of which matches the target scattering properties for a set of wavelengths. In this work the material is made of a distribution of rigid cylinders embedded in air.

I. Introduction

The ability to manipulate waves has long been one of the main goals in various areas of physics and engineering. Many-body scattering systems [1] and metamaterials [2] offer promising prospects to deal with this challenge due to their ability to be tuned and reconfigured. Properly designed highly disordered many-body systems have recently attracted attention as a tool for scattering manipulation. The introduction of local correlations between the positions of the scatterers constituting the disordered system allows to control the scattering of an incident radiation [3, 4, 5, 6]. In particular, stealth materials consist of multiple scatterers distributed in such a way as to completely suppress the scattering of the sample over a broadband frequency range [7, 8].

In this work, we develop a route to engineer 2D acoustic materials consisting of multiple rigid cylinders, which possess the desired scattering properties under the incidence of a plane wave. We characterize the scattering pattern of a set of scatterers under the approach of weak scattering by its structure factor. We validate this hypothesis calculating the scattered far-field amplitude using the multiple scattering theory that considers all scattering orders. We develop an optimization technique, which optimizes the positions of scatterers that lead to a chosen value of the structure factor over a given frequency range.

II. Hyperuniform materials

Figure 1(a) shows the spacial distribution of N = 100 cylinders with R0 = L/100 constructing a hyperuniform material. The structure factor, $S(\boldsymbol{G})$, is shown on Fig. 1(b). It is suppressed, $S(\boldsymbol{G}) = 0$ everywhere in the target region, $[0, \pi N/L]$, except the forward scattering (corresponding to $\boldsymbol{G} = (0, 0)$). The wave vector of the incident plane wave $\boldsymbol{k_0}$ and the scattered wave $\boldsymbol{k_s}$ are introduced following the von Laue formulation. According to this, the constructive interference takes place if $\boldsymbol{k_s}-\boldsymbol{k_0}=\boldsymbol{G}$ (see Fig. 1(c)). For elastic scattering $|\boldsymbol{k_0}|=|\boldsymbol{k_s}|$ and the possible vectors $\boldsymbol{k_s}$ form an Ewald circumference centered at the origin of the vector $\boldsymbol{k_0}$. In Fig. 1(d) the polar plot of the normalized scattered intensity is shown. For the dashed circle in Fig. 1(c) which fully lies in the $S(\boldsymbol{G})=0$ region the scattering is completely suppressed, while for the solid circle there is a strong backward scattering is exhibited corresponding to the part of the circle lying in the $S(\boldsymbol{G})\neq 0$ region.

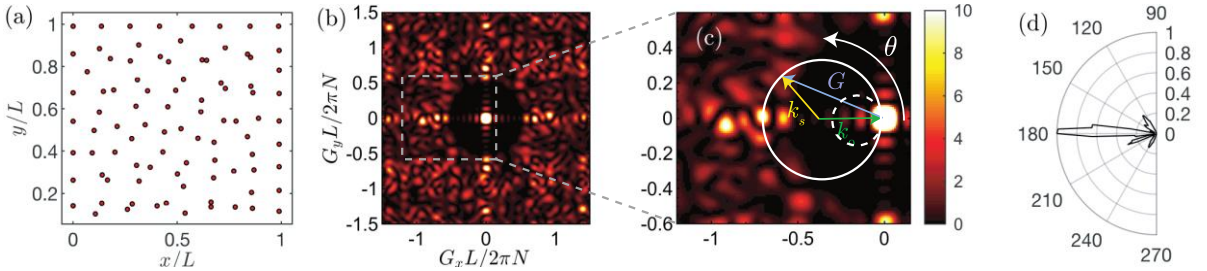

Figure 1. (a) spacial distribution of $N=100$ scatterers with $R_0=L/100$ composing a hyperuniform material, (b) corresponding structure factor, (c) zoomed region of the structure factor and the Ewald circumference, (d) normalized scattered intensity as a function of the scattering angle for the solid circle in (c).

III. Stealth materials

Figure 2(a) shows the distribution of scatterers for the designed stealth material with *N=64* scatterers obtained from the optimization method. The structure factor of the stealth material (Fig. 2(b)) exhibits an annular region of scattering suppression delimited by $|\boldsymbol{K_1}|$ and $|\boldsymbol{K_2}|$ shown by the circumferences in red continuous lines. For a given range of frequencies (a particular example is shown in Fig. 2(b)), the corresponding Ewald circumference (white continuous line) overlaps the scattering suppression area by its whitish area. This implies the total suppression of the back-scattering for all the scattering vectors $\boldsymbol{k_s}$ in the whitish area. Moreover, we can see that this scattering suppression mechanism is produced at any angle of incidence (another Ewald circumference with dashed white lines is depicted in Fig. 2(b) for another angle of incidence). The polar plot of the scattered intensity for this Ewald circumference is shown in Fig. 2(c) and it clearly matches the expected behavior from the structure factor, showing the back scattering suppression. Figure 2(d) illustrates the spatial distribution of the scattered pressure $|P_s^f|$ for a plane wave incident from the left. It also confirms the suppression of the back scattering.

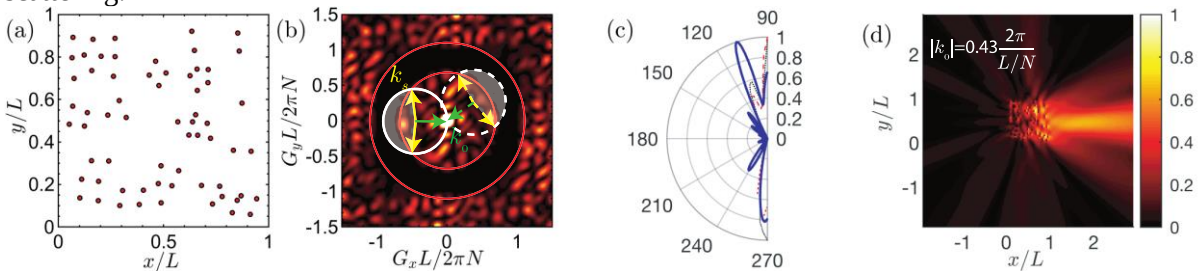

Figure 2: (a) Stealth material made of a distribution of *N*=64 cylinders. (b) Structure factor of a stealth material. (c) Polar plot of the scattered intensity calculated from the structure factor (black line) and from multiple scattering (blue line). (d) Map of the scattered pressure, $|P^f_s(\theta, \omega)|$, for the wavevector with $k_s = 0.43\ 2\pi N/L$ for the normal incidence.

IV. CONCLUSIONS

With the methodology shown in this work we demonstrate that distributions of sub-wavelength particles are good candidates to achieve target scattering properties for stealth materials with broadband and omnidirectional back scattering suppression. We have described the scattering properties of such systems by the structure factor in the framework of a single scattering approach and by the far-field scattered amplitude within the multiple scattering theory, validating this approach. Numerically optimizing the structure factor of the sample, we design the appropriate distributions of scatterers which, though counter intuitive, present the target scattering pattern.

V. ACKNOWLEDGEMENT

This work has been funded by the project HYPERMETA funded under the program Étoiles Motantes of the Région Pays de la Loire and by the ANR-RGC METARoom (ANR-18-CE08-0021) project. This publication is part of the R&D&I Project/Grant No. PID2020-112759GB-I00 funded by MCIN/AEI/10.13039/501100011033/.

References

[1] S.Torquato, *Random Heterogeneous Materials: Microstructure and macroscopic properties,* Springer, 2002.
[2] E. Chéron, J.-P. Groby, V. Pagneux , S. Félix , and V. Romero-García , *Experimental characterization of rigid-scatterer hyperuniform distributions for audible acoustics, PHYSICAL REVIEW B 106, 064206 (2022).*
[3] V. Romero-García and A.-C. Hladky-Hennion, *Fundamentals and Applications of Acoustic Metamaterials: From Seismic to Radio Frequency*, John Wiley & Sons Inc., ISTE, 2019.
[4] O.U. Uche, F.H. Stillinger and S. Torquato, "Constraints on collective density variables: Two dimensions," *Physical Review B,* vol. 70, p. 046122, 2004.
[5] S. Torquato,"Hyperuniformity and its generalizations,"*Physical Review E,*vol.94,p.022122,2016.
[6] E. Chéron, J.-P. Groby, V. Pagneux , S. Félix , and V. Romero-García, *Wave transport in stealth hyperuniform materials: The diffusive regime and beyond,* Appl. Phys. Lett., 121, 6, 061702, (2022)
[7] V.Romero-García,N.Lamothe, G.Theocharis, O.Richoux, and L.M.García-Raffi,"Stealth acoustic materials, *Physical Review Applied,* vol. 11, p. 054076, 2019.
[8] S. Kuznetsova and J. P. Groby and L. M. Garcia-Raffi and V. Romero-García, Stealth and equiluminous materials for scattering cancellation and wave diffusion, Waves in Random and Complex Media, 1-19, (2021)

Thursday 15th June

PHONONICS 2023: 6th International Conference on Phononic Crystals/Metamaterials/Metasurfaces, Phonon Transport, and Topological Phononics
Manchester, England, June 12-16, 2023
PHONONICS-2023-0207

Acoustic diffraction grating with space-time modulation

A. Maurel[1], K. Pham[2]

[1] Institut Langevin, ESPCI Paris, Université PSL, CNRS, 1 rue Jussieu, 75005 Paris, France, agnes.maurel@espci.fr
[2] IMSIA, CNRS, EDF, CEA, ENSTA Paris, Institut Polytechnique de Paris, 828 Bd des Maréchaux, 91732 Palaiseau, France kim.pham@ensta-paris.fr

We present a theoretical and numerical analysis of the diffraction of acoustic waves by space-time modulated gratings with rigid-type modulations. The numerical analysis is based on a multimodal method and is made possible by deriving the form of the modes which are exact, uncoupled, solutions of the problem in the unbounded regions, inside and outside the grating [1]. The dispersion of the modes is studied as a function of the ratio of the modulation speed to the speed of sound which shows that each spatial diffraction order is associated with a single temporal diffraction order. For a grating of finite extend, the solution is obtained as a superposition of these modes, which couple at the grating interfaces. For a single diffraction order (a condition which is fixed by a combination of low frequency regime and low modulation speed), a homogenized model is proposed which provides physical interpretation of the scattering properties of the grating [2].

References

[1] Pham, K., & Maurel, A. Diffraction grating with space-time modulation. *Journal of Computational Physics*, *469*, 111528 (2022).
[2] Pham, K., & Maurel, A. How space-time modulations modify spoof surface plasmons and scattering properties in acoustic metagratings, submitted (2023).

PHONONICS 2023: 6th International Conference on Phononic Crystals/Metamaterials/Metasurfaces, Phonon Transport, and Topological Phononics
Manchester, England, June 12-16, 2023
PHONONICS-2023-0224

Emergence of Willis Constitutive Coupling in Elastodynamic Heterogeneous Media

William J. Parnell, Philip A. Cotterill, David Nigro

Department of Mathematics, University of Manchester, Oxford Road, Manchester, M13 9PL, UK
William.Parnell@manchester.ac.uk

Electromagnetic bi-anisotropy finds an analogy in acoustic metamaterial science as Willis coupling. Its impact and emergence in the field of elastodynamic metamaterials is not as well understood however, given the coupling between compressional and shear waves. Here we discuss Willis coupling in heterogeneous elastic slabs embedded in an acoustic fluid. The microstructure of the slab comprises circular cylindrical voids and asymmetry is present via two neighbouring line arrays, each with a repeating void of differing radius. The slab matrix is considered soft, with Poisson ratio close to 1/2 so that the voids act as Giant Monopole Resonators and induce a strong dynamic response at low frequency. We show that the incorporation of Willis constitutive coupling ensures that a unique set of effective material properties can be assigned to the slab. This extends the work from the acoustics regime considered by Muhlestein et al [1] to the elastodynamic regime.

We also go further and consider the case when loss is included in the elastic substrate host medium via its shear modulus. We show that this induces strong directional-dependent absorption, whilst maintaining the physical restriction of reciprocity of course.

References

[1] Muhlestein MB, Sieck CF, Wilson PS, Haberman MR. Experimental evidence of Willis coupling in a one-dimensional effective material element. Nature communications. 2017 Jun 13;8(1):15625.

PHONONICS 2023: 6th International Conference on Phononic Crystals/Metamaterials/Metasurfaces, Phonon Transport, and Topological Phononics
Manchester, England, June 12-16, 2023
PHONONICS-2023-0053

Energy Transmission and Reflection at the Boundary of a Composite with Random Microgeometry

J. R. Willis

Department of Applied Mathematics and Theoretical Physics,
Cambridge University, Wilberforce Road, Cambridge CB3 0WA, UK
jrw1005@cam.ac.uk

Abstract: A plane wave incident on the boundary of a random composite generates a disturbance that depends on the realisation. The ensemble mean of the transmitted disturbance decays with distance but energy is conserved. Correct accounting requires calculation of the mean of the energy flux. This is illustrated for a simple model composite half-space.

The presentation is mostly based on recently published work[1]. A composite, which occupies $x_2 > 0$, has the special feature that its two component media have the same modulus $\mu_1 = \mu_2 = \mu$ but different densities ρ_1 and ρ_2. A plane wave impinges on the boundary $x_2 = 0$ from the adjoining homogeneous half-space $x_2 < 0$, which is assigned a modulus μ_3 and density ρ_3.

The system of equations that are employed to describe the physical system is derived from a variational structure into which trial fields can be substituted that generate equations that utilize only knowledge of the volume fractions and two-point probabilities for the distribution of its constituents. These equations could also be generated directly by invoking a version of the quasicrystalline approximation of Lax[2] but their derivation from a variational principle demonstrates a sense in which they are "optimal" relative to that amount of information on the composite.

The propagation of mean waves in a composite has been considered quite extensively in recent years, particularly for media with periodic microstructure, mostly motivated by interest in the dynamic response of metamaterials. For sufficiently low frequencies the theory of homogenization for effective constitutive response is applicable. The work reported here was initially motivated by the wish to gain some idea of how the boundary layer adjacent to any macroscopic interface, which is present even when the theory of homogenization is applicable, would mediate propagation into the composite when the frequency of the incident disturbance is increased. Even at low frequencies, however, the mean transmitted wave decays with distance of propagation and yet energy must be conserved. The answer is that, with increase of distance from the boundary, energy is transferred from the mean transmitted disturbance to that part of the disturbance whose mean is zero. There is, in fact, also a significant amount of energy associated with the mean-zero part of the reflected signal but this is independent of distance from the boundary because the lower half-space is uniform. The simple model system studied here permits a complete explicit solution. The crucial feature is that the correlation function for the composite is chosen to have the Debye exponential form as well as only density variation. The variational approximation then gives a mean disturbance composed from exactly two plane waves: an α-wave whose rate of decay tends to zero as frequency tends to zero (which standard low-frequency homogenisation would predict) and a β-wave whose decay length is always on the scale of the microstructure.

An illustrative result is provided in the figure. It is for a wave normally incident on the composite, at a normalised frequency of 3, at which both transmitted mean waves decay rapidly. The properties of the media are given in the caption. The fluxes of energy away from the interface $x_2 = 0$ are normalised to the incident energy flux. The α- and β-waves have comparable amplitudes and rates of decay. They interfere so that their resultant energy flux oscillates and energy is transferred into and out of the mean-zero disturbance to maintain a constant total. The reflected fluxes are also shown, as well as the total of the fluxes which is maintained at the value 1; the approximation conserves energy and minor deviation from 1 is attributed to computational inaccuracy.

The presentation will provide a brief outline of the method of calculation as well as additional results.

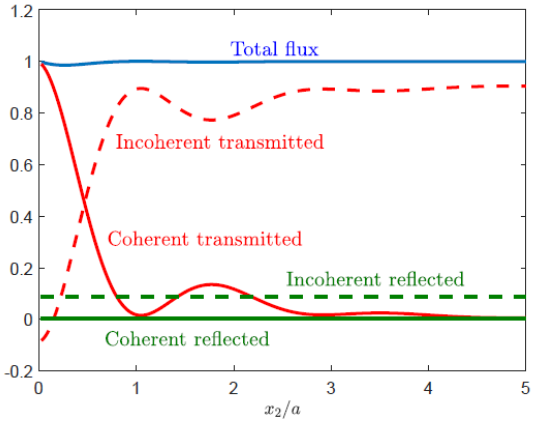

Figure 1. Coherent and incoherent energy fluxes transmitted in the composite, and coherent and incoherent reflected fluxes, normalized to incident flux. Composite has p_1= 0.5 and $\rho_2=5\rho_1$, homogeneous medium has $\mu_3=2\mu$ and $\rho_3=\rho_1$. Comparison medium has $\rho_0 = \langle\rho\rangle$. Normalized frequency $\omega a/c_1=3$.

References

[1] J.R. Willis, *Proc.R. Soc. A* **479,** 20220730 (2023).
[2] M. Lax, *Phys. Rev.* **85,** 621-629 (1952).

PHONONICS 2023: 6th International Conference on Phononic Crystals/Metamaterials/Metasurfaces, Phonon Transport, and Topological Phononics
Manchester, England, June 12-16, 2023
PHONONICS-2023-0190

Discrete One-dimensional Models for the Electromomentum Coupling

K. Muhafra[1] , Michael R. Haberman[2], G. Shmuel[1]

[1]Faculty of Mechanical Engineering, Technion–Israel Institute of Technology, Haifa 32000, Israel,

kevinmu@campus.technion.ac.il, meshmuel@technion.ac.il

[2] Walker Department of Mechanical Engineering, The University of Texas at Austin, Austin, Texas 78712-1591, haberman@utexas.edu

Abstract: By developing and applying a homogenization scheme for elastodynamics, Willis discovered that the linear momentum of composite materials is macroscopically coupled with their strain. Recent generalization of Willis' dynamic homogenization theory to the case of piezoelectric composites further revealed that their effective linear momentum is also coupled to the effective electric field. In this talk, we introduce the simplest possible model: a one-dimensional discrete model, that exhibits this so-called electromomentum coupling in sub-wavelength composites, in order to elucidate the physical origins of this coupling and illustrate its mechanism.

The response of materials is modeled by the coupling parameters between physical fields in germane constitutive equations. In the standard constitutive equations of elastic materials, the momentum is that coupled to the velocity, and the stress is coupled to the strain. By developing and applying a homogenization scheme for elastodynamics, Willis[1] discovered that the momentum and stress of composite materials are also macroscopically coupled with their strain and velocity, respectively. The Willis constitutive relations that arise from this dynamic homogenization procedure are nonlocal in space and time, namely, the response of a material point depends not only on the local fields at any instant in time, but also on neighboring points and their time history. The spatially local limit of the Willis equations, referred to as the Milton-Briane-Willis equations[2], is applicable when the wavelength is much larger than the microstructure, referred to as the metamaterial regime or when a single subwavelength element is analyzed.

The Willis couplings do not appear in the constitutive relations of the constituents, hence the resultant Willis materials are a type of metamaterial, whose behavior is fundamentally different from the behavior of their building blocks. Recently, Pernas-Salomon and Shmuel[3] generalized the theory of Willis to account for constituents that mechanically respond to non-mechanical stimuli, focusing on piezoelectric materials that respond to electric fields. The work demonstrated that the macroscopic linear momentum of piezoelectric composite is coupled to the electric field, and that electric displacement field is coupled to the velocity, a direct analogue to the Willis couplings. From a practical viewpoint, not only does the emergent electromomentum coupling constitute an additional degree of freedom to sense and generate elastic waves, it also opens up unique possibilities for the creation of tunable metamaterials using external electric fields.

The mechanism behind the local component of Willis-, piezoelectric-, and electromomentum effects is similar: it is the breaking some spatial symmetry in the material properties. While continuum models provide some insight to the origins of the electromomentum effect, they yield complicated expressions for the effective coupling coefficients which do not lend themselves to an intuitive understanding of this new material response. It is therefore advantageous to develop simpler, more intuitive models to provide a better understanding of the origins of this coupling and, in turn, enable more efficient design and fabrication of these materials. Similar models have previously been introduced to illustrate, understand, and design.

Willis coupling in elastic and acoustic metamaterials, but have yet to be developed to analyze the electromomentum coupling. Accordingly, here[4] we provide the simplest model that illustrates the mechanism of the electromomentum coupling and elucidates its physical origins.

To this end, we first introduce one-dimensional models for the Willis- and piezoelectric effects using systems of discrete masses, springs, and bound point charges. For the Willis effect, we introduce a model which is a generalization of the model that was introduced by Muhlestein et al[5]. The system we consider consists of three point masses that are connected by two linear springs. We analyze cases where the masses and springs differ and provide expressions for the effective stiffness, mass density per unit length, and Willis coefficients. Subsequently, we extend this lumped parameter model to consider bound charge in order to capture the piezoelectric effect. Piezoelectricity emerges from a simple system consisting of two different masses of opposite charge that are connected by a linear spring, reminiscent of the model introduced in the classic monograph of Auld. In contrast with the static analysis of Auld, we consider the inertia of the masses and hence also observe local resonances and Willis effects, which may be achieved using rationally designed metamaterials that display strong Willis- and piezoelectric couplings. The piezoelectric model serves as the building block in different assemblies with which we tailor effective material properties. Specifically, we show that by combining two building blocks that differ by their piezoelectric coefficient, we obtain an assembly whose effective response exhibits both the Willis- and electromomentum effects.

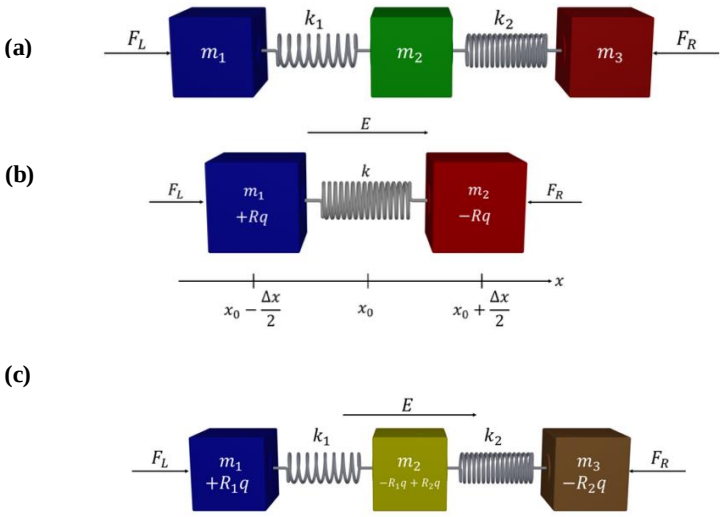

Figure 1. (a) Spring-mass models exhibiting Willis coupling owing combined mass-stiffness asymmetry. **(b)** Fundamental building block that exhibits the piezoelectric coupling owing to charge asymmetry. **(c)** Assembly of two building blocks from (b) with different stiffnesses, masses and point charges that yield both the electromomentum- and Willis couplings.

References

[1] J R Willis. *Variational principles for dynamic problems for inhomogeneous elastic media*. Wave Motion, (1981)

[2] G W Milton, M Briane, and J R Willis. *On cloaking for elasticity and physical equations with a transformation invariant form.* New J. Phys., (2006)

[3] René Pernas-Salomón and Gal Shmuel. *Symmetry breaking creates electro-momentum coupling in piezoelectric metamaterials.* J. Mech. Phys. Solids (2020)

[4] Michael B Muhlestein, Caleb F Sieck, Andrea Alù, and Michael R Haberman. *Reciprocity, passivity and causality in Willis materials*. Proc. R. Soc. London A Math. Phys. Eng. Sci., (2016)

[5] Muhafra, K., Haberman, R. M., Shmuel, G., *Discrete One-dimensional Models for the Electromomentum Coupling*, ArXiv

Strong Passive Willis Coupling

Phillip Brucks, Hussein Nassar*

Department of Mechanical and Aerospace Engineering, University of Missouri, Columbia, MO 65211, USA
**nassarh@missouri.edu*

Abstract: Willis elasticity is re-written as a particular case of micromorphic elasticity. This new insight allows to isolate three factors that are crucial to the emergence of strong passive Willis coupling: kinematic enrichment; inertial coupling; and resonance. As an application, the Willis materials that appear in transformation-based passive cloaking are resolved into mechanical lattices.

The peculiar version of elasticity theory here referred to as "Willis Elasticity" first appeared as an implicit byproduct of investigations carried by J. R. Willis in the early 1980's into the effective dynamic behavior of random composites.[1,2] It was not until 1996, it seems, that Willis recognized that the effective constitutive relations he had derived were unusually coupled. He wrote[3] "*It should be noted that the perturbation expansion demonstrates that, inevitably, the mean stress and mean momentum density are both coupled linearly to mean strain and mean velocity*". Formally, instead of the usual

$$\boldsymbol{\sigma} = \boldsymbol{C}\boldsymbol{e}, \qquad \boldsymbol{p} = \rho \boldsymbol{v}, \tag{1}$$

random composites turn out to be governed, on average, by two equations

$$\boldsymbol{\sigma} = \boldsymbol{C}\boldsymbol{e} + \boldsymbol{S}\boldsymbol{v}, \qquad \boldsymbol{p} = \rho \boldsymbol{v} + \boldsymbol{S}^{\dagger}\boldsymbol{e}, \tag{2}$$

coupled by what is now called a "Willis coupling" tensor $\mathbf{S}$. In the two cases therein investigated, namely weakly heterogeneous composites and dilute suspensions, Willis notes that the coupling vanishes $\mathbf{S} \to \mathbf{0}$ in the limit of low frequencies $\omega \to 0$. What was unclear, and remains so to a certain extent, is whether there are circumstances where there would be a significant coupling even for low frequencies. This question became more pressing when it was discovered by Milton, Briane and Willis that materials described by Willis elasticity can be used for elastodynamic cloaking purposes.[4] In that setup, we are faced with the inverse problem: the desired Willis coupling is known; but the underlying microstructure that would exhibit it in its effective response is not.

More recently, it was demonstrated that laminates whose properties are modulated in time in a periodic progressive fashion obey a form of Willis elasticity that is non-reciprocal.[5] The time modulation induces a bias in propagated frequencies that is similar to a Doppler effect and whose magnitude is proportional to the depth and frequency of the modulation. In the constitutive equations, the bias takes the form of a strong Willis coupling. That said, this version of Willis elasticity, being non-reciprocal, is different from the one originally proposed by Willis and is not useful for passive cloaking applications.

In this work, we propose a purely mechanical, passive, and reciprocal, mean to achieve a strong Willis coupling. The starting point is the balance equations for an abstract micromorphic medium here written in a simplified 1D setting:

$$(\kappa u' + \beta\phi)' = -\omega^2 \rho u, \qquad (\alpha\phi)' - \xi\phi - \beta u' = -\omega^2 I\phi, \tag{3}$$

where ω is angular frequency, $(k, \alpha, \beta, \xi, \rho, I)$ are constitutive properties, u is displacement and ϕ is a scalar kinematic enrichment. This, somewhat standard albeit simplified, formulation ignores an inertial coupling J with which the equations become

$$(\kappa u' + \beta\phi)' = -\omega^2(\rho u + J\phi), \qquad (\alpha\phi)' - \xi\phi - \beta u' = -\omega^2(I\phi + Ju). \tag{4}$$

The assumption $J = 0$ is often, if not always, implicitly admitted in the classics[6,7] and amounts to identifying the center of mass of the microcontinuum with its centroid. Solving the latter equation for ϕ and substituting back in the former equation leads to

$$\left[\left(\kappa + \beta g_\beta\right)u' - \omega^2 \beta g_J u\right]' = -\omega^2\left[\left(\rho - \omega^2 J g_J\right)u + J g_\beta u'\right], \tag{5}$$

where the operator $g_p : q \mapsto g \star (pq)$ denotes a convolution product with g being the Green kernel of the differential operator $\phi \mapsto \alpha\phi' - \xi\phi + \omega^2\, I\phi$ (under suitable boundary conditions). Low and behold, Equation (5) is the motion equation of a Willis medium with a Willis coupling operator equal to $-\omega^2 \beta g_J$. This coupling would vanish in the limit $\omega \to 0$ except under resonance conditions for which g explodes.

To summarize, the presence of a strong Willis coupling necessitates three crucial ingredients

1. a kinematic enrichment in the form of extra degrees of freedom (e.g., micro-rotation, micro-stretch, etc.),
2. an inertial coupling between the velocities associated with the displacement and the kinematic enrichment,
3. frequencies that are close to the natural frequencies of the kinematic enrichment.

This recast of Willis elasticity into a sub-class of micromorphic elasticity is advantageous because, as it turns out, equation (4) is far easier to handle from an inverse design perspective than equation (5). In the talk, we describe how the above three conditions can be realized simultaneously in 2D mechanical lattices and provide architectures that realize a strong passive Willis coupling. As an application, the Willis materials that appear in harmonic 2D transformation-based passive cloaking are resolved into mechanical lattices and the first simulations that demonstrate cloaking with microstructurally resolved Willis materials are presented.

References

[1] Willis, J. R. A polarization approach to the scattering of elastic waves-I. Scattering by a single inclusion. *J Mech Phys Solids* **28**, 287–305 (1980).
[2] Willis, J. R. A polarization approach to the scattering of elastic waves-II. Multiple scattering. *J Mech Phys Solids* **28**, 307–327 (1980).
[3] Willis, J. R. Dynamics of composites. in *Continuum Micromechanics* (ed. Suquet, P.) 265–290 (Springer-Verlag New York, Inc., 1997).
[4] Milton, G. W., Briane, M. & Willis, J. R. On cloaking for elasticity and physical equations with a transformation invariant form. *New J Phys* **8**, 248–267 (2006).
[5] Nassar, H., Xu, X. C., Norris, A. N. & Huang, G. L. Modulated phononic crystals: Non-reciprocal wave propagation and Willis materials. *J Mech Phys Solids* **101**, 10–29 (2017).
[6] Mindlin, R. D. Micro-structure in linear elasticity. *Arch Ration Mech Anal* **16**, 51–78 (1964).
[7] Eringen, A. C. *Microcontinuum field theories I: Foundations and solids*. (Springer, 1999).

Wave asymptotics in two-dimensional periodic media

Raphael Assier[1], Andrey Shanin[2], Andrey Korolkov[2], Oleg Makarov[2]

[1] *Department of Mathematics, University of Manchester, Oxford Road, Manchester, M13 9PL, UK*
raphael.assier@manchester.ac.uk
[2] *Department of Physics (Acoustics Division), Moscow State University, Leninskie Gory, 119992 Moscow, Russia*

Abstract: We propose a technique to estimate the far-field asymptotic behaviour of Green's functions tailored to a two-dimensional doubly-periodic media. It is based on a double integral representation and multidimensional complex analysis.

In this talk we will investigate how some recent work [1] on the asymptotic evaluation of double Fourier integrals using multidimensional complex analysis can be adapted to two-dimensional periodic media, and hence to phononics.

The work [1] is concerned with wave fields, satisfying the Helmholtz equation with wavenumber k, given by integrals of the form

$$u(\boldsymbol{x};k) \;=\; \iint_{\mathbb{R}^2} F(\boldsymbol{\xi};k)\, e^{-i\boldsymbol{x}\cdot\boldsymbol{\xi}}\, \mathrm{d}\boldsymbol{\xi} \tag{1}$$

that occur when u is the solution to a diffraction problem in an homogeneous media. The function F here is understood as a holomorphic function of the two complex variables $\boldsymbol{\xi}=(\xi_1,\xi_2)\in\mathbb{C}^2$. For the integral (1) to be well defined, the wave number k has to be assumed to have a small imaginary part $\varkappa=\mathrm{Im}[k]>0$ say. As $\varkappa\to 0$, the singularities of F hit the real plane and the integral needs to be rewritten as

$$u(\boldsymbol{x};k) \;=\; \iint_{\boldsymbol{\Gamma}} F(\boldsymbol{\xi};k)\, e^{-i\boldsymbol{x}\cdot\boldsymbol{\xi}}\, \mathrm{d}\boldsymbol{\xi}, \tag{2}$$

where $\boldsymbol{\Gamma}$ can be interpreted as an indentation of the initial surface of integration that was $\mathbb{R}^2$. A precise description of how $\boldsymbol{\Gamma}$ can and should bypass the singularities of F in $\mathbb{C}^2$ has been given in [1] and we classified specific singularity configurations that lead to a non-exponentially-decaying far-field wave component of u as $r=|\boldsymbol{x}|\to\infty$.

With this talk, we will consider doubly periodic media with vector periods $\boldsymbol{d}$ and $\boldsymbol{\ell}$ and a unit cell S that contains the origin and can also include some scatterers for instance. We will be interested in evaluating the tailored Green's function of this media. Namely we consider a point source located at a point $\boldsymbol{r}_s$ of the unit cell. For $\boldsymbol{r}$ within the unit cell we denote this function $U(\boldsymbol{r},\boldsymbol{r}_s;k)$. We will show that this function can be written everywhere in the media as a double integral similar to (1). Namely, for any $\boldsymbol{m}=(m_1,m_2)\in\mathbb{Z}^2$ and any $\boldsymbol{r}\in S$, we have

$$U(\boldsymbol{r}+m_1\boldsymbol{d}+m_2\boldsymbol{\ell},\boldsymbol{r}_s;k) \;=\; \iint_{[-\pi,\pi]^2} L(\boldsymbol{r},\boldsymbol{r}_s;\boldsymbol{\xi},k)e^{-i\boldsymbol{m}\cdot\boldsymbol{\xi}}\mathrm{d}\boldsymbol{\xi}, \tag{3}$$

where L can be shown to be a holomorphic function of the two complex variables $\boldsymbol{\xi}=(\xi_1,\xi_2)\in\mathbb{C}^2$ that is singularity free on $[-\pi,\pi]^2$ as long as $\varkappa=\mathrm{Im}[k]>0$.

As $\varkappa \to 0$, the singularities of L hit the real plane and the integral (3) has to be rewritten as

$$U(\boldsymbol{r}+m_1\boldsymbol{d}+m_2\boldsymbol{\ell},\boldsymbol{r}_s;k) \;=\; \iint_{\boldsymbol{\Gamma}} L(\boldsymbol{r},\boldsymbol{r}_s;\boldsymbol{\xi},k)e^{-i\boldsymbol{m}\cdot\boldsymbol{\xi}}\mathrm{d}\boldsymbol{\xi}, \tag{4}$$

where $\boldsymbol{\Gamma}$ can be seen as an indentation in $\mathbb{C}^2$ of $[-\pi,\pi]^2$ that by passes the singularities of L. As we did in [1], we will discuss how certain configurations of these singularities lead to some far-field asymptotics of U as $|\boldsymbol{m}| \to \infty$.

If time permits, we will discuss how a similar approach can be taken for time-dependent problems.

Bibliography

[1] R C Assier, A V Shanin, and A I Korolkov. A contribution to the mathematical theory of diffraction: a note on double Fourier integrals. *The Quarterly Journal of Mechanics and Applied Mathematics*, 76(1):1–47, 2022.

Bi-orthogonality Relations in the Waveguide Theory

Sergey V. Sorokin[1], Lasse S. Ledet[2]

[1] *Department of Materials and Production, Aalborg University, Fibigerstraede 16, Aalborg, Denmark, svs@mp.aau.dk*
[2] *GRUNDFOS Holding A/S, Poul Due Jensens vej 7, Bjerringbro, Denmark lledet@grundfos.com*

Abstract: Reciprocity and bi-orthogonality relations are very useful but, unfortunately, still underestimated tools to solve a broad range of wave propagation problems in a surprisingly simple way. In this talk, we summarize advances in formulation and application of these relations. The underlying ideas and technicalities are presented in full detail in recent papers [1-2].

1. Bi-orthogonality relation and non-symmetric waveguides

So far, bi-orthogonality relations have been derived for analytical models of symmetric waveguides. As soon as the waveguide becomes non-symmetric the obvious 'twin-pairing' of right and left going waves, which are essential constituents of a bi-orthogonality relation, vanishes. First, we claim that the bi-orthogonality relation, which readily provides an analytical solution of a forcing problem for symmetric waveguides, also exists and possesses the same property for non-symmetric waveguides. Second, we claim that, even more intriguingly, the bi-orthogonality relation emerges from a simple factorisation of the linear combination of dispersion equations written for two distinct wavenumbers. As an example, we consider an infinitely long thin elastic plate with heavy fluid loading produced by a layer, which occupies the strip $0 < y < H$ (incompressible fluid, uniform flow parallel to plate with the speed U), in the plane strain formulation. The plate has thickness h, its material has Young's module E, Poisson ratio ν and density ρ_{plate}. The fluid's density is ρ_{fl}. At the bottom, the layer of fluid is bounded by a rigid baffle. We choose dependence of all functions upon the axial coordinate as $\exp(-i\omega t)$, where $k = k_{dim}$. Then it is a straightforward matter to derive the dispersion equation:

$$D(k,\Omega) = k^4 - \Omega^2 - \rho(\Omega - ku)^2 \frac{\coth(k\eta)}{k} = 0$$

This transcendental equation involves three purely real parameters $\rho = \frac{\rho_{fluid}}{\rho_{plate}}$, $\eta = \frac{H}{h}$, $u = \frac{U}{c}$. Thus, $D(k,\Omega)$ is real on real *k*-axis for any real Ω. Then, as known from the theory of complex functions, the condition $D^*(k,\Omega) = D(k^*,\Omega)$ is held (asterisk designates a complex conjugate), and, therefore, it may have only purely real and complex conjugate roots for any real Ω. Another important property of this dispersion equation is that, as soon as $u \neq 0$, the wavenumber $-k$ ceases to be a root of the dispersion equation, if the wavenumber k is, and so the obvious relation between left- and right-going waves vanishes. Physically, it simply means that the wave propagation downstream differs from the wave propagation upstream. The bi-orthogonality relation is readily obtained as:

$$\frac{D(k_A,\Omega) - D(k_B,\Omega)}{k_A + k_B} = \frac{k_A\left[D(k_A,\Omega) - D(k_B,\Omega)\right]}{k_A^2 - k_B^2} - \frac{k_B\left[D(k_B,\Omega) - D(k_A,\Omega)\right]}{k_B^2 - k_A^2} = 0$$

In scaled physical variables ($A \leftrightarrow B$, $k_A \neq k_B$), it reads:

$$-Q_A(x)w_B(x) + M_B(x)\beta_A(x) + \rho u w_A(x)\phi_B(x,\eta) + \rho\int_0^\eta v_x^A(x,y)\phi_B(x,y)dy + R_{AB}(x) = 0$$

This relation is held at any station along the waveguide. The 'residual function' of the axial coordinate is introduced as an indefinite integral:

$$R_{AB}(x) = \rho u \int \left[v_x^A(x,\eta) w_B(x) - v_x^B(x,\eta) w_A(x) \right] dx .$$

Equating bi-orthogonality relations for A, B and B, A to each other (each of these equals zero individually) yields the orthogonality relation, which is simply a linear combination of two bi-orthogonality relations. We note that the classical derivation of the bi-orthogonality relation from the orthogonality one heavily relies on the waveguide's symmetry and, therefore, is not applicable for the case in hand. In contrast, the derivation from the dispersion relation is equally valid for waveguides of both types.

2. Bi-orthogonality relation and periodic waveguides

Addressing properties of periodic continuous waveguides, it should be noted that bi-orthogonality relations have been heuristically employed by D. Mead. He introduced the Class A and Class B frequencies and modes for a single system element (a symmetric periodicity cell), which is 'free' or 'locked' (in terms of the boundary conditions). These eigenfrequencies coincide with the boundaries between pass- and stop-bands, and eigenmodes represent standing waves in an infinite waveguide at these frequencies. Thus, the finite element modal analysis of free vibrations is available as a simple and convenient tool to predict properties of periodic waveguides of arbitrary complexity and hence, in a broader prospective, to design and optimize performance of metamaterials. In contrast to a segment of the uniform waveguide, the Class A/A and Class B/B eigenfrequencies of a unit symmetric periodicity cell are different.

In [2], we demonstrate application of these properties to identify frequency-wise positions of band gaps from a finite element modal analysis, see details in this reference. For clarity, we begin with the dispersion diagram obtained by the conventional WFEM. As conventional for studies of wave propagation in periodic systems, it presents the frequency-dependence of propagation constants (Bloch's parameters) after post-processing of 'raw' FEM output data. However, the same results can be obtained using modal analysis. To distinguish between distinct partial, or modal, stop bands and to identify the full ones, it is necessary to distribute the full set of eigenfrequencies into the individual modal families (subsets) belonging to each branch of the dispersion diagram. Thus, an inspection of eigenmodes constitutes an integral part of the analysis of periodic waveguides. The identification of modal families should be conducted with keeping track of both the sequential order of a given eigenfrequency within its family, and the Class of boundary conditions, for which it is obtained. Once the modes are clustered into their families, the positions of stop bands are governed by the intermittency of 'Class A' and 'Class B' ones at the ends of each partial stop band. This is immediately verified from WFEM solution. By visual inspection of eigenmodes, it is fairly straightforward to pair Class A and B eigenfrequencies into their modal families. As the complexity of mode shapes increases, it becomes more difficult to visually pair eigenmodes and clustering algorithms are needed.

Developing good and robust modal clustering algorithms for periodic waveguides are challenging as the eigenmodes are 'polluted' and thus no longer consists of pure sinusoidal shapes as is the case for the homogeneous waveguide. Therefore, more advanced techniques than spatial Fourier transforms are needed. A combination of spatial Fourier transforms, quarter wavelength shifts and utilisation of the Modal Assurance Criterion (MAC) may help to identify the various modal clusters or, alternatively, use of more 'exotic' techniques based on, for example, machine learning, may be explored. However, this constitutes a topic for future research.

3. Concluding remarks

The on-going research encompasses formulation of algorithms for keeping track of 'high-order' modes in periodic waveguides and extension of proposed methodologies to 2D and 3D waveguides.

References

[1] S.V. Sorokin, and L.S. Ledet, *Wave Motion* **112**, 102928 (2022).
[2] S.V. Sorokin, P.H. Broberg, M.T. Steffensen, and L. S. Ledet, *Int. J. Mech. Sci.* **227**, 107444 (2022).

Waves in Time-Dependent Systems

J. B. Pendry

Department of Physics, The Blackett Laboratory,
Imperial College London, Prince Consort Road,
London SW7 2AZ, UK
j.pendry@imperial.ac.uk

Abstract: Spatial structure as in photonic crystals and metamaterials strongly influences wave propagation. Now interest has turned to structure which changes in time on a scale comparable to the period of incident waves. Many phenomena are revealed such as new amplification mechanisms, quantum effects including models for Hawking radiation, conservation laws applying to photon/phonon number, and more.

More details are to be had in the following papers

References

[1] JB Pendry, E Galiffi, PA Huidobro, *Gain mechanism in time-dependent media*, *Optica* **8** (5), 636-637 (2021).
[2] JB Pendry, E Galiffi, PA Huidobro, *Photon conservation in trans-luminal metamaterials*, *Optica* **9,** 724-30 (2022).
[3] R Tirole, S Vezzoli, E Galiffi, I Robertson, D Maurice, B Tilmann, SA Maier, John B. Pendry, Riccardo Sapienza, *Double-slit time diffraction at optical frequencies*, *arXiv*: 2206.04362 (2022).
[4] Simon A. R. Horsley and John B. Pendry, *Time varying gratings model Hawking radiation, arXiv:* 2302.04066 (2023).

PHONONICS 2023: 6th International Conference on Phononic Crystals/Metamaterials/Metasurfaces, Phonon Transport, and Topological Phononics
Manchester, England, June 12-16, 2023
PHONONICS-2023-0037

Underwater Acoustic Absorption by Using Impedance-Matched Composites*

Ping Sheng

Department of Physics, HKUST, and Institute for Advanced Study, HKUST
Clear Water Bay, Kowloon, Hong Kong, China
sheng@ust.hk

An ideal underwater absorber should be (1) thin in thickness, (2) high in absorption performance, and (3) having an absorption spectrum that has a broad frequency range. How to satisfy these three requirements simultaneously? In this talk, I show that by using a *structured* tungsten-polyurethane composite that is impedance-matched to water while simultaneously having a much slower longitudinal sound speed, we have theoretically designed, and experimentally realized, an underwater acoustic absorber exhibiting high absorption from 4 to 20 kHz, measured in a 5.6 m×3.6 m water pool with the time-domain approach. The broadband functionality is achieved by optimally engineering the distribution of the Fabry-Perot resonances, based on an integration scheme, to attain impedance matching over a broad frequency range. The average thickness of the integrated absorber, 8.9 mm, is in the deep subwavelength regime (~λ/42 at 4 kHz) and close to the causal minimum thickness of 8.2 mm that is evaluated from the simulated absorption spectrum. The structured composite represents a new type of acoustic metamaterials that has high acoustic energy density and promises broad underwater applications.

*Collaborators: Sichao Qu, Nan Gao, Alain Tinel, Bruno Morvan, Vicente Romero-García, and Jean-Philippe Groby.

PHONONICS 2023: 6th International Conference on Phononic Crystals/Metamaterials/Metasurfaces, Phonon Transport, and Topological Phononics
Manchester, England, June 12-16, 2023
PHONONICS-2023-0008

Phase Nonreciprocity in a Periodic Material with a Nonlinear Asymmetric Unit Cell

Ali Kogani[1], Behrooz Yousefzadeh[2]

[1&2] *Department of Mechanical, Industrial and Aerospace Engineering, Concordia University, Montreal, QC, Canada*
[1]*ali.kogani@concordia.ca*

Abstract: This work explores nonreciprocal vibration transmission in a discrete model of a nonlinear periodic material consisting of eight asymmetric unit cells. Focusing on the frequency-preserving response (weak nonlinearity), we identify response regimes characterized by a nonreciprocal phase shift in vibration transmissibility (phase nonreciprocity). We hope this response characteristic enables new functionalities for nonlinear periodic materials.

Reciprocity is an important property of linear time-invariant systems. Despite its practical applications[1,2], it also limits the control over vibration transmission and wave propagation in mechanical systems. Avoiding reciprocity allows more opportunities for control of wave transmission[3]. Passive nonreciprocity can be achieved by a nonlinear local relationship between restoring force and deformation in a system with broken mirror symmetry. A nonreciprocal response is normally associated with different transmitted wave amplitudes along opposite direction. In this work, however, we focus on identifying response regimes characterized by a nonreciprocal phase change: when there is a phase shift between the left-to-right and right-to-left transmission [4]. We do this for the weakly nonlinear steady-state response of nonlinear lattice to harmonic external excitation; i.e. the frequency-preserving regime.

We consider a periodic system containing eight asymmetric unit cells, shown in Fig. 1, inspired by an experimental model of beams and magnets[5]. Each unit cell consists of two masses M_1 and $M_2 = \mu M_1$, and each mass is grounded with a nonlinear spring $k_g = 1 + k_n x^2$ and a linear damper ζ_g. The external excitation is a harmonic force with frequency ω_f and amplitude P. The equations of motion for this system can be written as

$$\begin{aligned} \ddot{x}_{2i-1} + 2k_c x_{2i-1} - k_c(x_{2i-2} + x_{2i}) + x_{2i-1} + k_n x_{2i-1}^3 + 2\zeta_g \dot{x}_{2i-1} &= F_{2i-1}\cos\omega_f t \\ \mu\ddot{x}_{2i} + 2k_c x_{2i} - k_c(x_{2i-1} + x_{2i+1}) + x_{2i} + k_n x_{2i}^3 + 2\zeta_g \dot{x}_{2i} &= F_{2i}\cos\omega_f t \end{aligned} \quad (1)$$

The subscripts $i = 1, \dots, 8$ denote the counter of unit cells.

Testing for reciprocity requires two different configurations: (i) the forward configuration with $F_1 = P$ and $F_{16} = 0$, in which the measured output is $x_{16}^F(t)$; (ii) the backward configuration with $F_1 = 0$ and $F_{16} = P$, where the output is the displacement of the first mass, $x_1^B(t)$. The system is reciprocal if and only if $x_{16}^F(t)$=$x_1^B(t)$.

To quantify the degree of nonreciprocity in the response, we define the reciprocity bias as

$$R = \frac{1}{T}\int_0^T (x_{16}^F(t) - x_1^B(t))^2 dt \quad (2)$$

where $T = 2\pi/\omega_f$ is the period of excitation. $R = 0$ corresponds to a reciprocal response.

When the excitation amplitude is not very high, the steady-state response of the system remains predominantly harmonic. It is therefore reasonable to start with a harmonic approximation:

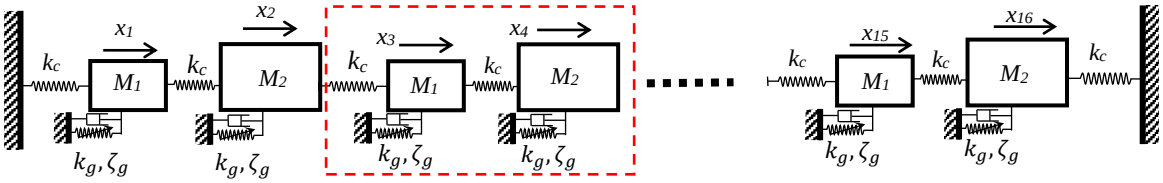

Figure 1. Schematic of the finite periodic structure. The red dashed box shows the unit cell, which consist of two linearly coupled oscillators with different masses. $k_c = 1, k_g = 1 + x_j^2, \zeta_g = 0.02,\ M_2 = 2M_1$

$$x_j^k(t) = |X_j^k| \cos(\omega_f t + \phi_j^k) \quad (3)$$

The subscripts $j = 1, \ldots, 16$ refer to each degree of freedom. The superscript k is F for *forward* configuration and B for the *backward*. We define output norms as $N^F = |X_{16}^F|^2$ and $N^B = |X_1^B|^2$ to quantify the output.

Fig. 2 shows different output amplitudes for the forward and backward configurations as a function of forcing frequency for the nonlinear asymmetric system, where the response is clearly nonreciprocal near the primary resonances of the system. Fig. 3(a) shows the corresponding reciprocity bias. The red circle markers in Fig. 3 correspond to anti-resonances of the system where the output mass is not moving, and R is nearly zero. At frequencies indicated by the blue diamond markers the reciprocity bias has a relatively large value even though $N^F = N^B$. The large reciprocity bias occurs because $\phi^F \neq \phi^B$; i.e. phase nonreciprocity. Fig. 3 (b) and (c) show the time-domain response of the system for points corresponding to red circles (anti-resonance) and blue diamonds (phase nonreciprocity).

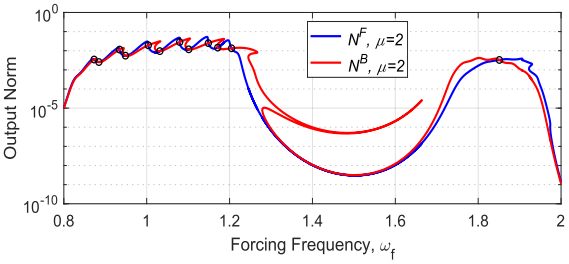

Figure 2. Output norms (5) at P=0.2 for asymmetric system ($\mu = 2$). The circle markers denote the points at which N^F and N^B intersect.

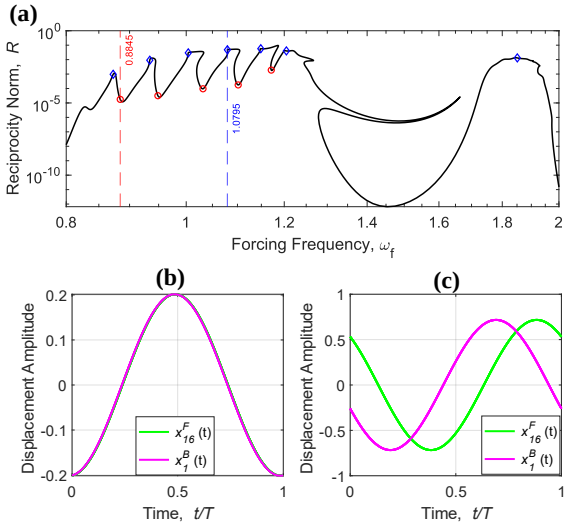

Figure 3. Nonreciprocal dynamics (a) The reciprocity norm. (b) Time-domain response at $\omega_f = 0.88$ (c) Time-domain response at $\omega_f = 1.079$

To analyze different aspects of phase nonreciprocity in our system, we compute the locus of phase nonreciprocity by implementing a constraint as $N^F = N^B$ and allowing the symmetry-breaking parameter to change. Using this approach, Fig. 4 shows the locus of phase nonreciprocity for the point indicated in Fig. 3 (a) at $\omega_f = 1.079$. Panel (a) shows that the normalized reciprocity bias defined as $R/(N^F + N^B)$ increases with μ. The reciprocity bias is normalized to eliminate the influence of response amplitude. Panel (b) shows the changes of $\Delta\phi$ along the locus of phase nonreciprocity. As expected, both R and $\Delta\phi$ become zero as μ approaches 1 because the system is mirror-symmetric and reciprocal at $\mu = 1$. The results in Fig. 5 imply that the degree of nonreciprocity may saturate at high values of μ along this locus: $\Delta\phi$ seems to approach π.

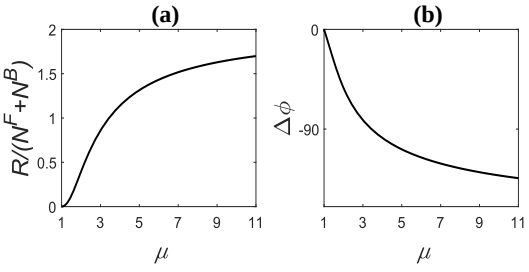

Figure 4. Phase nonreciprocity at $P = 0.2$ as a function of μ. (a) The normalized reciprocity bias. (b) The output phase difference, $\Delta\phi = \phi^F - \phi^B$

In summary, we presented a computational analysis of nonreciprocal vibration transmission in a periodic material model. Focusing on the frequency-preserving response regime, we identified operating conditions characterized by nonreciprocal phase shifts (nonreciprocity in the transmitted phase, but not the amplitude). As expected, both the reciprocity bias and nonreciprocal phase shift increase with the degree of asymmetry in the system.

References

1. Ewins, D. J. *Modal testing: theory, practice and application*. (John Wiley & Sons, 2009).
2. Junger, M. C. & Feit, D. *Sound, Structures, and Their Interaction*. (MIT Press, 1986).
3. Nassar, H. *et al.* Nonreciprocity in acoustic and elastic materials. *Nat Rev Mater* **5**, 667–685 (2020).
4. Yousefzadeh, B. Computation of nonreciprocal dynamics in nonlinear materials. *Journal of Computational Dynamics* (2022).
5. Kimura, M. & Hikihara, T. Experimental manipulation of intrinsic localized modes in macro-mechanical system. *Nonlinear Theory and Its Applications, IEICE* **3**, 233–245 (2012).

PHONONICS 2023: 6th International Conference on Phononic Crystals/Metamaterials/Metasurfaces, Phonon Transport, and Topological Phononics
Manchester, England, June 12-16, 2023
PHONONICS-2023-0079

Contact Stiffness Evaluation and Wave Response Study of Engineered Contact-Based Nonlinear Phononic Material

Md Kamruzzaman[1], Ganesh U. Patil[1], Kathryn H. Matlack[1]

[1] Department of Mechanical Science and Engineering, University of Illinois Urbana-Champaign, Urbana, IL 61801, USA,
mdk6@illinois.edu, gupatil2@illinois.edu, kmatlack@illinois.edu

Abstract: Nonlinear wave propagation in phononic materials exhibits promising features with diverse potential to control wave propagation effectively and efficiently. The present study aims to investigate the nonlinear wave behaviors of contact-based phononic material with engineered wavy surfaces. The study can facilitate manufacturing modern application devices with advanced wave propagation features.

Phononic materials, made by the periodic arrangement of unit cells, have many unique wave behaviors, such as band gaps[1] and negative refraction[2], which are not possible in conventional materials. These unique features that control waves through engineered materials lead the way for advanced applications, e.g., seismic isolation[3] and flow stabilization[4]. The incorporation and modeling of nonlinearity in phononic materials enables enriched behavior such as second harmonic generation[5], energy transfer between frequencies[6], solitary wave generation[6], and nonreciprocal wave characteristics[7]. Therefore, incorporating nonlinearity in phononic material can open diverse capabilities for controlling wave propagation. Among the different forms of nonlinearity that can cause nonlinear wave responses, such as contact nonlinearity[5], material nonlinearity[8], and geometric nonlinearity[9], contact nonlinearity is a realizable and tunable source of nonlinearity[1,6-7], but thus far studies have been mostly limited to Hertzian contacts and rough contact nonlinearity.

In this pursuit, the present study characterizes the contact nonlinearity of *engineered* contact interfaces and explores how this nonlinearity changes the wave propagation in phononic materials comprised of these engineered contact interfaces. Specifically, the study consists of two parts: (1) an experimental and numerical study of the contact nonlinearity that arises from the contact between a flat surface and a sinusoidal wavy surface where the interface is approximated as a nonlinear spring, and (2) finite element simulations to characterize the nonlinear wave behaviors in phononic materials containing periodic arrangements of these nonlinear springs.

For the characterization of contact stiffness, wavy against flat and wavy against wavy surface cases are considered under various pre-compression. Two methods, Digital Image Correlation (DIC) and nonlinear ultrasound are used. In the DIC test, subsequent images of the contact interface under different loads that are taken using a high-speed camera with a microscope for enhanced resolution, are compared to the reference unloaded image to capture the displacement field of the contact region. This enables measuring the contact stiffness directly from the load-displacement curve. On the contrary, the ultrasound test uses a high-frequency excitation at the contact interface and measures the resulting reflected wave, and the stiffness of the contact interface is evaluated using an analytical model[10] that correlates the stiffness to the reflection coefficient with other material and acoustic properties. The finite element method is also used in parallel to characterize the force-displacement relation of smooth wavy surfaces to draw meaningful comparisons between the experimental and finite element results.

The second part focuses on the finite element investigation of the nonlinear wave response of phononic material with the nonlinear stiffness-precompression results found in the first part. For this, the contact interfaces are modeled as thin elastic layers with the hybrid experimental-analytical force-displacement model[10]. Two cases are considered: the weakly nonlinear regime and the strongly nonlinear regime. In the first case, the excitation amplitude is much lower than the initial displacement caused by the precompression, and no separation between layers occurs, whereas in the latter case, the excitation causes separation between layers. The study will enable us to explore the effects of engineered wavy contact-induced nonlinearity on wave behaviors in phononic materials.

Initial results found by ultrasound test show a different power law relation between the stiffness and precompression for engineered contact interfaces compared to the flat case. The finite element results, although different, also exhibits different nonlinear force-displacement relation that also depends on the curvature of the contact surface topography. These results suggest that the experimentally-derived parameters may be strongly related to surface roughness of the engineered surfaces. While DIC gives a straightforward way of stiffness measurement, the ultrasound technique can probe the effects of various parameters, such as frequency, and contact parameters, in the stiffness measurement, which could be helpful in understanding the effects of these parameters on wave propagation characteristics. The results of DIC and ultrasound tests could also be useful for developing an improved contact stiffness model.

Both the weakly and strongly nonlinear analysis are expected to exhibit nonlinear wave behavior, such as new frequency generation and solitary wave generation, with unprecedented characteristics due to the distinct contact nonlinearity and the associated stiffness values. This study will help explore the capabilities of nonlinear wave propagation, and the results could be useful in pioneering advanced wave propagation-controlled applications.

References

[1] G. U. Patil and K. H. Matlack, *Wave Motion*, **105**, 102763 (2021).
[2] A. Sukhovich, L. Jing, and J. H. Page, *Physical Review B*, **77**(1), 014301 (2008).
[3] Y. Yan, Z. Cheng, F. Menq, Y. L. Mo, Y. Tang, and Z. Shi, *Smart Materials and Structures*, **24**(7), 075006 (2015).
[4] M. I. Hussein, S. Biringen, O. R. Bilal, and A. Kucala, *Proc. R. Soc. A*, **471**, 20140928 (2015).
[5] V. J. Sánchez-Morcillo, I. Pérez-Arjona, V. Romero-García, V. Tournat, and V. E. Gusev, *Physical Review E*, **88**(4), 043203 (2013).
[6] G. U. Patil and K. H. Matlack, *Physical Review E*, **105**(2), 024201 (2022).
[7] G. U. Patil, S. Cui, and K. H. Matlack, *Extreme Mechanics Letters*, **55**, 101821 (2022).
[8] K. L. Manktelow, M. J. Leamy, and M. Ruzzene, *Journal of the Mechanics and Physics of Solids*, **61**(12), 2433–2453 (2013).
[9] R. Khajehtourian and M. I. Hussein, *AIP Advances*, **4**(12), 124308 (2014).
[10] S. Biwa, S. Nakajima, and N. Ohno, *Journal of Applied Mechanics*, **71**(4), 508–515 (2004).

PHONONICS 2023: 6th International Conference on Phononic Crystals/Metamaterials/Metasurfaces, Phonon Transport, and Topological Phononics
Manchester, England, June 12-16, 2023
PHONONICS-2023-0103

Non-Linear Waves in Bistable Mechanical Metamaterials and Transition Waves

Apostolos Paliovaios[1,2], Vassos Achilleos[1], Georgios Theocharis[1], Vincent Tournat[1], Nikolaos Stefanou[2]

[1] Laboratoire d'Acoustique de l'Université du Mans (LAUM), UMR 6613, Institut d'Acoustique - Graduate School (IA-GS), CNRS, Le Mans Université, France
apostolos.paliovaios.etu@univ-lemans.fr, achilleos.vassos@univ-lemans.fr, georgios.theocharis@univ-lemans.fr, vincent.tournat@univ-lemans.fr
[2] Section of Condensed Matter Physics, National and Kapodistrian University of Athens, University Campus, GR-157 84 Athens, Greece
nstefan@phys.uoa.gr

Abstract: The main goal of this work is to generate transition waves in bistable mechanical metamaterials using spatio-temporal modulations. To that aim, we first show how to generate moving nonlinear waves (discrete breathers) in such a system and then investigate how counter-propagating breathers trigger transition waves at arbitrarily chosen positions. The case of driven-damped lattices is also discussed.

Flexible mechanical metamaterials (FlexMMs) can be defined as artificial, architected structures possessing the ability to deform substantially, repeatedly and reversibly. The study of this class of metamaterials has recently emerged and has attracted considerable attention because of the potential applications as well as conceptual advances[1]. Among the different FlexMMs we focus on those which can host nonlinear waves[2] and especially transition waves[3].

Thanks to the advanced manufacturing techniques which have been developed during the last decade, nonlinear FlexMMs can be designed in order to support different phenomena. The dynamics of FlexMMs are most commonly modeled using lattice models which consist of an inter-site term for the interaction between the elements and an on-site term which is associated with forces acting on every element.

Specifically, in our work we consider a system of *N* bistable elements of mass *m*. The bistability of each element arises because of the existence of two bistable states (see Fig.1). Every element interacts linearly with its nearest neighbors while the on-site potential, because of the existence of the buckling beams, is of polynomial form[3,4]. As a result, the displacement of every element of the system under consideration, neglecting the effect of losses, is described by the following Klein-Gordon equation

$$m\frac{d^2u_n}{dt^2} = G(u_{n+1} + u_{n-1} - 2u_n) - V_0(u_n - {u_n}^2 + \beta {u_n}^3)\,, \quad (1)$$

where G is the strength of the linear inter-site potential and V_0 the strength of the bistable potential.

It is known that systems described by Klein-Gordon equations can host time-periodic and localized in space nonlinear waves, the so-called discrete breathers[5]. Discrete breathers can be either standing or moving. We can obtain standing breathers with a given frequency, determined in advance, by solving numerically the next set of equations

$$Y[T_{br};\, Y(0)] - Y(0) = 0\,, Y(t) = [u_1, \ldots, u_N, v_1, \ldots, v_N]^T, \quad (2)$$

where T_{br} is the period of the breather and $Y(t)$ is a state vector in which the first N components are the displacements of the elements and the next N components are the velocities of the elements.

Then, we are able to produce moving breathers with different velocities by appropriately perturbing the standing ones.

The first goal of this work is to generate transition waves from the inter such breathers. Specifically, we investigate under which conditions the collision of moving breathers can trigger a transition wave. We

show that the outcome of the breather collisions strongly depends on their phase at the collision point, the relative phase between them at the moment of the collision, and their energy. By fine-tuning these relevant parameters we are able to produce transition waves at prescribed positions as shown in Fig.2. Moreover, by taking advantage of the collision properties, we demonstrate that more than one transition wave can be triggered in the same lattice at different points and instants.

In regards to realistic mechanical systems, such as the FlexMM that we consider, losses are present. In particular, strong losses modify the phenomenology and thus can not be ignored. To counterbalance their effect, achieving a non-decaying propagation of discrete breathers, we study systematically the case where the structure (FlexMM) is uniformly driven.

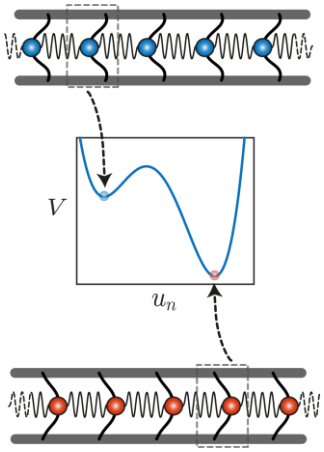

Figure 1 Schematic representation of a lattice with bistable elements. Every element consists of a mass connected with buckling beams giving rise to a bistable potential. On the top/bottom the first/second equilibrium point and the corresponding position in the bistable potential.

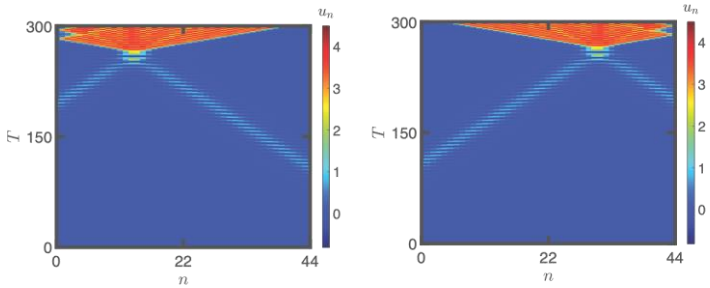

Figure 2 Transition waves generated at different lattice points after the collision of counter-propagating breathers.

References

[1] K. Bertoldi, V. Vitelli, J. Christensen, and M. Van Hecke, *Nature Reviews Materials* **2**, 1 (2017).
[2] B. Deng, J. Raney, K. Bertoldi, and V. Tournat, *Journal of Applied Physics* **130**, 040901 (2021).
[3] J.R. Raney, N. Nadkarni, C. Daraio, D.M. Kochmann, J.A. Lewis, and K. Bertoldi, *Proceedings of the National Academy of Sciences* **113**, 9722 (2016).
[4] M. Hwang and A. F. Arrieta, *Scientific reports* **8**, 1 (2018).
[5] S. Flach and A. V. Gorbach, Physics Reports **467**, 1 (2008).

PHONONICS 2023: 6th International Conference on Phononic Crystals/Metamaterials/Metasurfaces, Phonon Transport, and Topological Phononics
Manchester, England, June 12-16, 2023
PHONONICS-2023-0015

Asymmetric Elastic Metasurface between Different Media

S. V. Jang[1], S. W. Lee[1], J. H. Oh[1]

[1] School of Mechanical Engineering, Ulsan National Institute of Science and Technology, UNIST-gil 50, Ulju-gun, Ulsan, 44919, South Korea,
svjang@unist.ac.kr, lsw6344@unist.ac.kr, joohwan.oh@unist.ac.kr

Abstract: Elastic metasurface has been studied to manipulate refracted wave with high transmission. However, most of previous research is limited to the case of identical media across the metasurface even though various applications of wave refraction occur between different media. In this study, we propose asymmetric metasurface consisting of geometrically asymmetric units for wave manipulation between different media. It is proven that the proposed metasurface can manipulate wavefront under high transmission in single layer by theoretical and numerical analysis.

Metasurface, an artificially designed layer which consists of several unit cells, has advantages in that it occupies smaller volume compared to metamaterials. By introducing artificial surface made of sub-wavelength units, metasurface can transfer the incident wave energy across the interface and to manipulate the direction of the transmitted wave. The main key in metasurface is to design the units to provide full transmission and desired phase shifts so that wave manipulations are possible via generalized Snell's law.

Despite of the active researches, however, Lee et al. recently reported that the existing symmetric metasurface cannot be used between different media[1]. It was shown that if metasurface is placed between different materials, wave manipulation and high transmission cannot be achieved simultaneously with the existing metasurfaces. Accordingly, only the limited approaches have been made for the metasurface between different media, such as introducing two metasurfaces or sacrificing full transmission, etc. This limitation is essentially critical in elastic waves where almost all applications involve multiple materials, unlike in acoustics or electromagnetics.

In this presentation, we will show the way to break this limit and achieve wave manipulation between two different materials. The key idea is the asymmetry – we found that if metasurface is designed to have asymmetric configuration, it is possible to achieve the full transmission and desired phase shift simultaneously between two different media. In addition, we will propose an actual asymmetric elastic metasurface to show that the wave manipulation between two different mediums is indeed possible with various numerical supports.

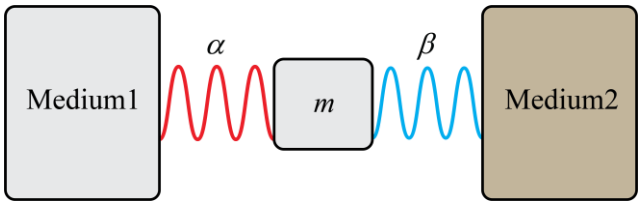

Figure 1 The mass-spring model for unit cell. The letter *m* means a mass, the letter α and β are spring constants.

Firstly, we will present why the previous researches cannot be applied to the case when the metasurface is installed between different materials. We adopt mass-spring model to analyze the phenomena between different media, as following figure 1. Under the zero reflection condition, we can describe the transmission coefficients for symmetric and asymmetric case with the transfer matrix method[2] as

For the case of symmetric mass-spring unit cell,

$$T = \pm i\sqrt{Z_1 / Z_2}. \tag{1}$$

For the case of asymmetric mass-spring unit cell,

$$T = |T|\cos\phi + |T|\sin\phi,\ |T| = \sqrt{Z_1 / Z_2},\ \text{and}\ \phi = \sin^{-1}\left(-\omega m_{eff} / \sqrt{Z_1 Z_2}\right). \tag{2}$$

Here, T is the transmission coefficient, $|T|$ is its magnitude, ϕ is its phase and Z is the mechanical impedance of each medium. The subscript 1 and 2 is the medium in front and behind of unit cells respectively. To manipulate waves with metasurface, it is essential to achieve various phase shifts[3]. Unfortunately, with the existing symmetric system, the phases of refraction coefficient are fixed as $\pi / 2$ or $3\pi / 2$ as shown in Eq. (1). On the other hand, various phase shifts are possible when asymmetric unit cells are adopted, indicating that asymmetric metasurface can manipulate waves between two different materials.

In addition to theoretical approach, actual asymmetric metasurface is designed and numerically verified. Through the 1-D wave simulation, we designed each metasurface units which satisfies the full transmission condition and the desired phase shifts simultaneously. For numerical analysis, we consider two cases: one is the case of different materials, aluminum-to-copper, and the other is the case of different thickness, 1mm thick aluminum-to-3mm thick aluminum. Note that in elastic waves, different thickness also makes different mechanical impedance for the longitudinal wave. The results of 2-D wave simulation are shown in figure 2. For both cases, the direction of refracted wave is well-matched with the predicted direction under full transmission. We can find that the proposed asymmetric metasurface can manipulate wavefront and transmit most of energy from incident wave in the case of different media which are even different materials or different thickness.

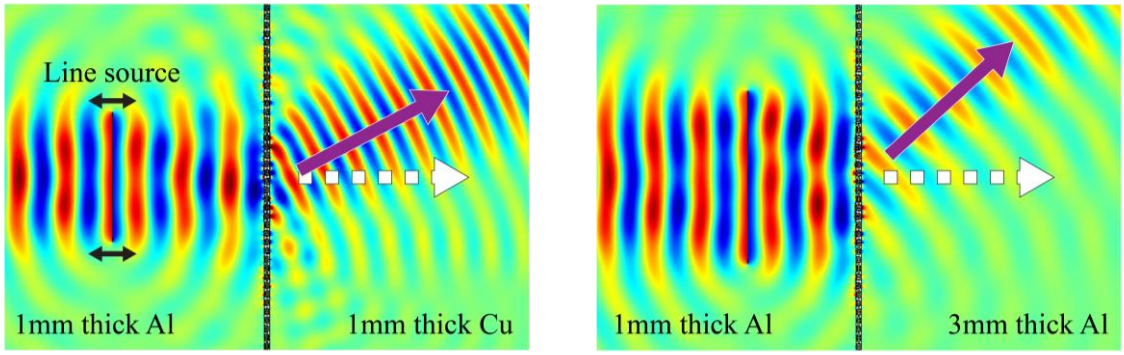

Figure 2 The results of 2-D incidence simulation in the case of **(a)** Aluminium-to-Copper **(b)** thickness 1mm-to-3mm Aluminium. The purple arrow is the intended direction from generalized Snell's law, and the white dashed arrow is the direction of natural refraction.

In this work, asymmetric metasurface is verified by theoretical and numerical analysis. Compared to the previous symmetric metasurface, the proposed metasurface can manipulate the refracted wave and satisfy full transmission condition simultaneously. Using this asymmetric metasurface, the various applications are possible such as beam focusing, bending, and space cloaking between different media. So, we expect that this asymmetric metasurface can be used for various industrial fields such as medical ultrasonics and nondestructive testing where wave transmits from one material to the other different material or even different thickness material.

Acknowledgement: This work was supported by the Center for Advanced Meta-Materials (CAMM) funded by the Ministry of Science, ICT and Future Planning as Global Frontier Project (CAMM-2014M3A6B3063711), by the National Research Foundation of Korea (NRF) grants funded by the Korean government (No. 2020R1A2C4002383 and 2021R1A4A1033224).

References

[1] S. W. Lee, Y. J. Shin, H. W. Park, H. M. Seung, and J. H. Oh, *Phys. Rev. Appl.* **16**, 064013 (2021).
[2] H. Lee, J. K. Lee, H. M. Seung, and Y. Y. Kim, *J. Mech. Phys. Solids* **112**, 577 (2018).
[3] N. Yu, P. Genevet, M. A. Kats, F. Aieta, J. P. Tetienne, F. Capasso, and Z. Gaburro, *Science* **334**, 333 (2011)

PHONONICS 2023: 6th International Conference on Phononic Crystals/Metamaterials/Metasurfaces, Phonon Transport, and Topological Phononics
Manchester, England, June 12-16, 2023
PHONONICS-2023-0151

Fluid-like Elastic Metasurface

Ye-Jeong Shin[1], Hong-Min Seung[2, 3], and Joo-Hwan Oh[1]

[1]Department of Mechanical Engineering, Ulsan National Institute of Science and Technology, UNIST-gil 50, Eonyang-eup, Ulju-gun, Ulsan 44919, South Korea
yjshin0920@unist.ac.kr, joohwan.oh@unist.ac.kr
[2]Intelligent Wave Engineering Team, Korea Research Institute of Standards and Science, Daejeon, 34113, Republic of Korea
[3]Department of Precision Measurement, University of Science and Technology (UST), Daejeon, 34113, Republic of Korea
shm@kriss.or.kr

Abstract: Elastic mode coupling limits wave manipulation. Our proposed fluid-like elastic metasurfaces decouple longitudinal and shear waves and only reflect longitudinal (or shear); mimicking fluidic boundaries (hard- and soft-wall). The designed metasurfaces are validated numerically and experimentally, and the opposite phase shift characteristics of two types of metasurfaces will suggest further study.

Elastic waves are distinct from acoustic or electromagnetic waves due to their complex mode coupling properties. Elastic waves have longitudinal and shear modes, and their intricate coupling has posed challenges in manipulation of elastic waves. These complicated issues are a major obstacle to the design and application of elastic wave devices.

Recently, elastic metasurfaces, which are thin periodic artificial structures with subwavelength unit cells, offer solutions for mode manipulation by providing new physics that cannot be observed in nature. Su et al.[1] presented metasurfaces that split the shear and longitudinal wave modes into different directions by modulating the phase change of the shear wave. Kim et al.[2] proposed a reflection-type metasurface that totally converts an incident longitudinal wave to a shear wave at broad incidence angles, and the refraction-type transmodal metasurface was also realized by Lee et al.[3] More recently, Zheng et al.[4] suggested a nonresonant elastic metasurface that perfectly split longitudinal waves with shear waves, achieving selective wave mode control. Also, Li et al.[5] designed a piezoelectric-based meta-boundary that realizing total mode conversions from longitudinal to shear waves in programmable way. However, previous attempts focused on suppressing shear waves or total mode conversion, while the coupling between longitudinal and shear waves still existed. The physical barrier between acoustic and elastic waves is still concrete, and the challenge to decouple each elastic wave mode remains one of the biggest challenges in wave physics.

In this work, we present the first realization of decoupling between elastic wave modes by using the elastic metasurface. Due to the coupling, if longitudinal (or shear) wave mode obliquely incident to the surface, the generation of both wave modes is inevitable in general boundary conditions. However, by using our metasurface, the coupling is eliminated so that only longitudinal (or shear) wave mode is reflected for the incident longitudinal (or shear) wave, for all incidence angle – the elastic surface becomes similar to the fluidic surface in acoustics. In addition, we realized the acoustic hard-wall-like (case 1) and soft-wall-like (case 2) metasurfaces in an elastic medium. To support our idea, we provide not only theoretical investigations but also numerical results and experimental realization of the proposed fluid-like elastic metasurface.

In order to achieve the fluid-like elastic metasurface, we must find the key condition for decoupling elastic wave modes. So, we focused on elastic boundary condition and adopted 'mixed boundary condition' that mixed fixed and free boundary conditions. The fact that shear and longitudinal wave is decoupled in mixed boundary condition is well known in elastic wave theory.[6] However, since it is presented only in theory, realizing and implementing it as an elastic metasurface is the core idea of our study. Generally, the elastic metasurface is composed of unit cells, and it provides a phase shift for reflected waves.[7] So, we should derive the phase shift required to achieve the mixed boundary condition and we performed an analytical investigation about obliquely incident of elastic wave with various angles. As a result, it was found that the hard-wall-like case is satisfied if the unit cell provides out-of-phase for the longitudinal wave and soft-wall-like case can be achieved with unit cell

having out-of-phase for the shear wave. Also, it is revealed that reflected wave in case 1 and case 2 have out-of-phase each other.

A simple strip-type structure is selected as unit cell, and the size-optimization is conducted to achieve the desired phase shift for each case, using the length (l) and width (w) of the strip as parameters. The designed parameters from the optimization were l = 12.7 mm and w = 0.5 mm for the hard-wall-like case, and l = 2.9 mm and w = 1.5 mm for the soft-wall-like case.

Based on designed unit cell, numerical validation is performed; the 650 units are modeled at the right side of aluminum plate with the 1 mm thickness and 20 cm line source actuates at the target frequency of 100kHz. Figure 1(a) shows the simulation results. For both longitudinal and shear incident case, modes are decoupled, and only incident mode is reflected (Compared to free boundary case, the no mode conversion is evident.). Also, experiments for all cases are conducted and Figure 1(b) demonstrates that the experimental results are fit well with numerical result. In addition, opposite phase characteristic of case 1 and case 2 is proven as shown in below plots of Figure 1(b).

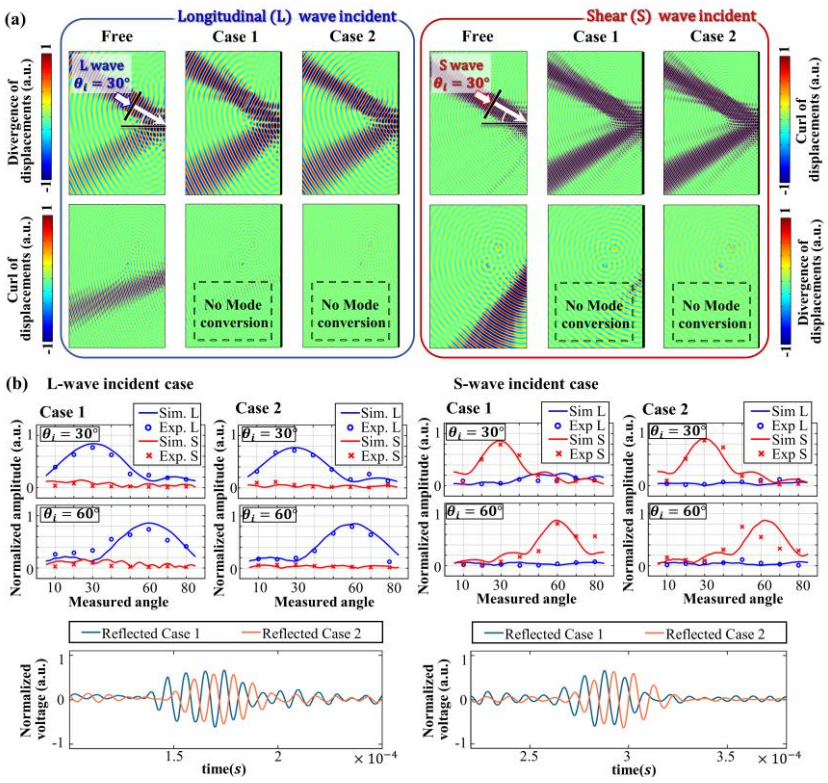

Figure 1 The hard-wall-like (case 1) and soft-wall-like (case 2) fluid-like elastic metasurfaces **(a)** numerical and **(b)** experimental results in various incident angle (θ_i).

In the presentation, fluid-like elastic metasurfaces that decouple the wave mode in all incident angle will be introduced. Considering that the coupling between the longitudinal and shear wave has been critical problem in elastic wave manipulation application, we believe that our proposed metasurfaces can present remarkable ability in mode control and open the new way in elastic wave device.

Acknowledgements
This work was supported by the Center for Advanced MetaMaterials (CAMM) funded by the Ministry of Science, ICT and Future Planning as a Global Frontier Project (No. CAMM2014M3A6B3063711) and by the National Research Foundation of Korea (NRF) grants funded by the Korean government (No. 2021R1A4A1033224).

References
[1] X. Su, Z. Lu, and A. N. Norris, J. *Appl. Phys.* **123**(9), 091701 (2018).
[2] M. S. Kim, W. R. Lee, Y. Y. Kim, and J. H. Oh, *Appl. Phys. Lett.* **112**(24), 241905 (2018).
[3] S. W. Lee, H. M. Seung, W. Choi, M. Kim, and J. H. Oh, *Appl. Phys. Lett.* **117**(21), 213502 (2020).
[4] M. Zheng, C. I. Park, X. Liu, R. Zhu, G. Hu, and Y. Y. Kim, *Appl. Phys. Lett.* **116**(17), 171903 (2020).
[5] X. P. Li, Y. Y. Chen, X. Zhang, and G. L. Huang, *Extreme Mech. Lett.* **39**, 100837 (2020).
[6] K. F. Graff, Wave Motion in Elastic Solids (Dover, New York, 1975).
[7] B. Assouar, B. Liang, Y. Wu, Y. Li, J. C. Cheng, and Y. Jing, *Nat. Rev. Mater.* **3**(12), 460 (2018).
[8] Y. J. Shin, H. M. Seung, and J. H. Oh, *Appl. Phys. Lett.* **122**(10), 101701 (2023).

PHONONICS 2023: 6th International Conference on Phononic Crystals/Metamaterials/Metasurfaces, Phonon Transport, and Topological Phononics
Manchester, England, June 12-16, 2023
PHONONICS-2023-0020

Controlling Thermal Transport with Pillar-Based Phononic Crystals

T. A. S. Korkiamäki[1], T. A. Puurtinen[1], T. Loippo[1], I. J. Maasilta[1]

[1] Nanoscience Center, Department of Physics, University of Jyväskylä, P. O. Box 35, FI-40014 University of Jyväskylä, Finland,
tatu.a.s.korkiamaki@jyu.fi, maasilta@jyu.fi

Abstract: We have fabricated Al pillar-based phononic crystals and measured their thermal conductance at sub-Kelvin temperatures. The results show a reduction in thermal conductance of up to an order of magnitude compared to a clean membrane. However, we also observe a trend which we attribute to a breakdown of coherence. The observations are supported by coherent and incoherent simulations.

For some time now, phononic crystals (PnCs) have been used to control thermal conductance in insulating and semiconducting materials[1,2]. The mechanisms by which PnCs work can be generally divided into two categories: (i) one where incoherent, diffusive, particle-like scattering dominates, and (ii) another where the coherent, wave-like scattering is operational. A large majority of earlier thermal conduction studies, including our own[3], has concentrated on geometries where a membrane is perforated by a periodic array of holes. Much less studied are 2D pillar-based PnCs, where the lattice is formed by a periodic array of pillars instead of holes. For such PnCs, the phonon spectrum can also include localized resonances which cannot carry heat. To our knowledge, all previous experimental observations of thermal conductance reduction using pillar-based PnCs have been attributed to incoherent effects[2].

In this work, we have fabricated and measured the thermal conductance of four pillar-based PnCs with different lattice constants ranging from 300 nm to 5 µm. The samples consist of cylindrical-shaped superconducting aluminium pillars on a 300 nm thick suspended SiN membrane, with a pillar height of 300 nm, and a filling factor of 0.65. The measurements were conducted at temperatures below 1 K, with the help of a SINIS-SNS (superconductor-insulator-normal metal) heater-thermometer setup fabricated onto the sample (Fig. 1).

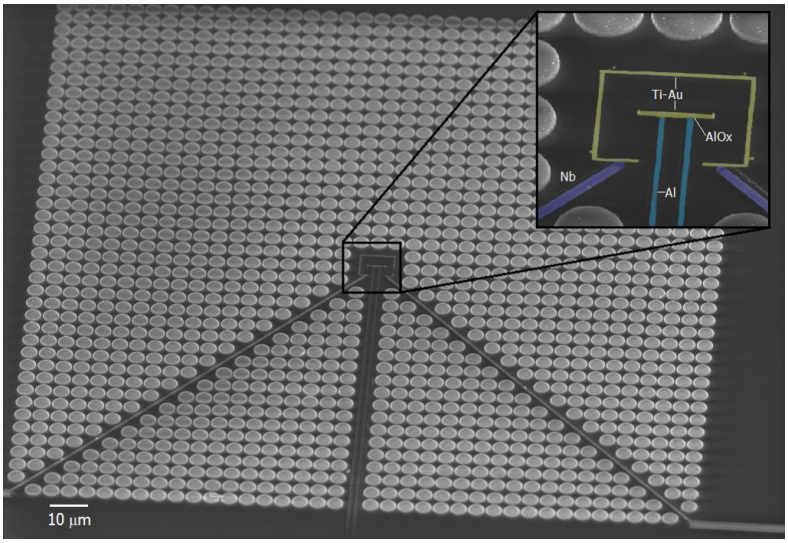

Figure 1 A 5 µm period Al pillar PnC, with the heater-thermometer structure highlighted in the zoom-in.

We observed a significant reduction in thermal conductance compared to an unaltered membrane, close to an order of magnitude for the 1 µm period PnC. To our knowledge, this is the largest experimentally observed reduction achieved with a pillar-based PnC. Coherent theory finite element method (FEM) simulations were used to compute the phonon dispersion relations and calculate the thermal conductance of all the PnCs. For the two smaller period (0.3 µm and 1 µm) structures, the simulations

qualitatively match the experimental data, yielding a similar power law for the temperature dependence. The thermal conductance reduction thus appears to originate from the coherent mechanism of group velocity reduction[3] induced by the hybridization of the pillar phonon modes with the plate modes.

However, with the larger periods (3 μm and 5μm), the thermal conductance begins to rise as a function of the period, in contrast to our coherent theory simulations, which predict that the conductance should decrease monotonically. We have actually seen a similar turning of the trend for the hole-based PnC before[4]. To explore an alternative mechanism for the conductance reduction, we also employed Monte Carlo simulations for our sample geometry to calculate the conductance in the incoherent, diffusive surface scattering limit. The incoherent simulations predict that the conductance increases as a function of the period, providing an explanation for the observed increasing trend for the larger period samples. Thus, we interpret that a breakdown in coherence takes place around a crossover period of ~1 μm, caused by the surface and sidewall roughness of the Al pillars, which is significantly higher than the SiN surface roughness. Fabrication techniques to reduce the sidewall roughness are in development.

References

[1] M. Maldovan, *Phys. Rev. Lett.* **110**, 025902 (2013).
[2] M. Nomura et al., *Mater. Today Phys*., **22**, 100613 (2022).
[3] N. Zen et al., *Nat. Commun.* **5**, 3435 (2014).
[4] Y. Tian et al, *Phys. Rew. Applied* **12**, 014008 (2019).

PHONONICS 2023: 6th International Conference on Phononic Crystals/Metamaterials/Metasurfaces, Phonon Transport, and Topological Phononics
Manchester, England, June 12-16, 2023
PHONONICS-2023-0029

Characterization of biphasic architectured media towards ultrasound monitoring applications

M. Gattin[1], N. Bochud[1], G. Rosi[1], Q. Grossman[2], D. Ruffoni[2], and S. Naili[1]

1. *Univ Paris Est Creteil, Univ Gustave Eiffel, CNRS, UMR 8208, MSME, F-94010 Créteil, France*
max.gattin@u-pec.fr, nicolas.bochud@u-pec.fr, giuseppe.rosi@u-pec.fr, naili@u-pec.fr
2. *Mechanics of Biological and Bioinspired Materials Laboratory, Department of Aerospace and Mechanical Engineering, University of Liège, Quartier Polytech 1, Allée de la Découverte 9, B-4000 Liège, Belgium*
quentin.grossman@uliege.be, druffoni@uliege.be

Abstract: Multi-material additive manufacturing is receiving growing attention in the field of acoustics, in particular for the design of micro-architectured periodic media used to obtain programmable ultrasonic responses. In this context, there is a need to develop wave propagation models to predict and optimize the impact of both the material properties and the spatial arrangement of the printed constituents. This work aims to investigate the transmission of longitudinal ultrasonic waves through periodic biphasic media that display viscoelastic constituent material properties. Thereby, we apply Bloch-Floquet analysis to unravel the relative contributions of viscoelasticity and periodicity on ultrasonic signatures, such as dispersion, attenuation, and bandgap characteristics. The impact of the finite size of such structures is also assessed by comparing the results from Bloch-Floquet analysis to those obtained using a transfer matrix formalism. The modelling outcomes, expressed in terms of frequency-dependent phase velocity and attenuation, are finally compared with experiments carried out on 3D-printed samples, which exhibit a 1D or 2D periodicity at a few hundred of micrometres length-scale. Altogether, the results provide insights into the modelling characteristics that must be accounted for to accurately predict the complex acoustic behaviour of periodic media in the ultrasonic regime.

Biological tissues are inherently heterogeneous materials with a multiscale hierarchical organization[1], whose singular properties are extremely difficult to replicate. From a mechanical viewpoint, their outstanding properties at the tissue scale are hypothesized to result from the combination of two main factors[2]: (i) the contribution of multiple constituent materials (soft and rigid) and (ii) the presence of a structural organization (periodic microstructure, functional gradients of mechanical properties, etc.). In this context, the rational design of architectured orthopaedic implants possessing an acoustic signature linked to their microstructure could open the way towards the ultrasound monitoring of their integration to the surrounding biological environment. To this end, it is necessary to have a precise knowledge of the acoustic properties of the constitutive media, as well as to accurately model the effect of the microstructure on the ultrasonic signatures.

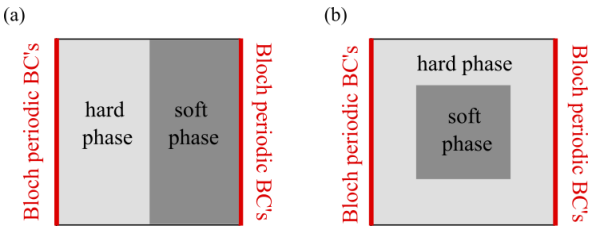

Figure 1: Schematic representation of biphasic (a) 1D unit cell, and (b) 2D unit cell.

In this work, we investigate the capability of multi-material 3D printing (*polyjet* technology) to design micro-architectured periodic media with programmable ultrasonic responses in a controlled laboratory environment. Our study focuses on simplified periodic structures made of 1D or 2D unit cells (see Fig. 1) to disentangle the roles played by viscoelasticity, finite size nature of the sample, and periodicity on the modelled ultrasonic responses. In a former study by our group[3], the viscoelastic properties of the constituent materials (soft and hard phases) were shown to exhibit dispersive losses, which could be described using a frequency power law

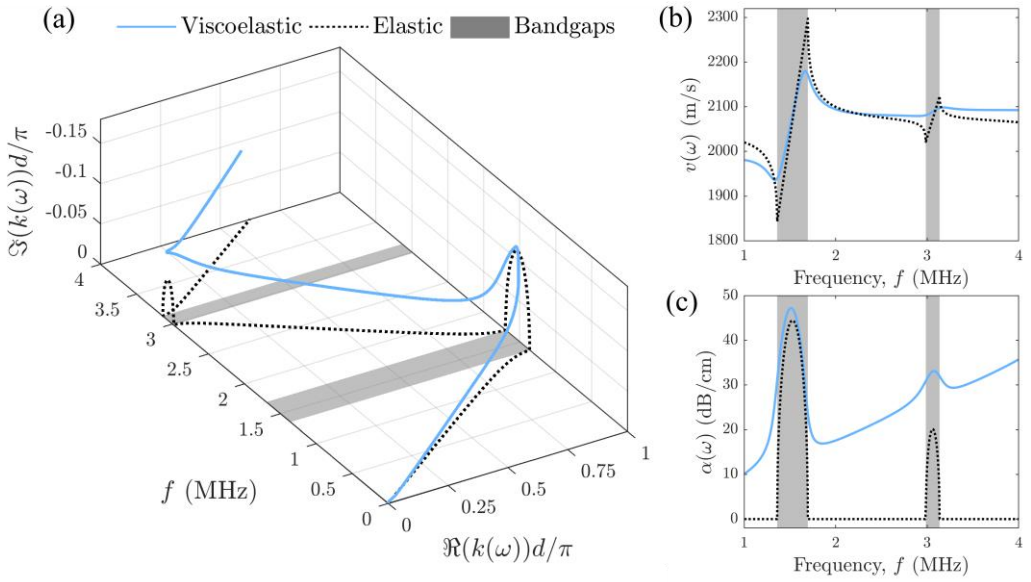

Figure 2: Normalized dispersion curve for an infinite 1D-periodic medium, displayed for the pure elastic (dotted black lines) and viscoelastic (continuous light blue lines) cases: (a) Complex Bloch wave number $k(\omega)$ as a function of the frequency f in the first Brillouin zone; (b) phase velocity $v(\omega)$; and (c) attenuation $\alpha(\omega)$. The light grey areas display the positions and widths of the bandgaps for the elastic case.

model[4]. The reported properties are here used to feed models of the transmission of longitudinal ultrasound waves through periodic biphasic samples. Applying Bloch-Floquet analysis to a 677 µm-thick 1D unit cell with either elastic or viscoelastic constituent materials allows recovering the dispersion curves and the corresponding phase velocities and attenuations depicted in Fig. 2, which underline the significant differences between the pure elastic and viscoelastic cases[5]. The impact of the finite size nature of these structures is then assessed by using a modelling approach based on the transfer matrix formalism. To serve as an example, Fig. 3 shows the comparison between the frequency-dependent phase velocities and attenuations derived from both modelling approaches, as well as an experimental validation for a 3D-printed sample consisting of 12 replicated 1D unit cells. As Bloch-Floquet analysis is valid for an infinite medium only, it fails in accurately capturing the variations of the ultrasonic characteristics when the number of unit cells is low. Similar evidences, which are not shown here for the sake of conciseness, were also observed for measurements performed on samples made of 2D unit cells. Altogether, the reported findings provide a basis for future research towards the development of ultrasound monitoring techniques for periodic biomaterials with more complex geometric topologies, such as scaffolds used in orthopaedic applications.

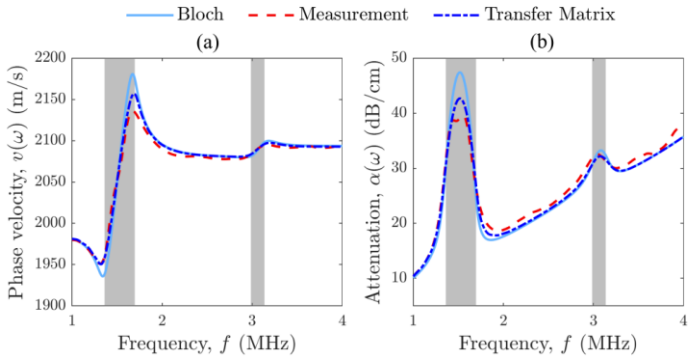

Figure 3: Ultrasound characteristics obtained using Bloch-Floquet analysis (continuous light blue lines), the transfer matrix formalism (dotted blue lines), and measurements (dashed red lines): (a) Phase velocity $v(\omega)$ and (b) attenuation $\alpha(\omega)$.

References

[1] P. Fratzl and R. Weinkamer, *Prog. Mater. Sci.*, **52(8)**, 1263–1334 (2007).
[2] A. A. Zadpoor, *Biomater. Sci.*, ***8*(1)**, 18–38 (2020).
[3] M. Gattin, N. Bochud, G. Rosi, Q. Grossman, D. Ruffoni, and S. Naili, *J. Acoust. Soc. Am.*, ***152*(3)**, 1901–1912 (2022)
[4] T. L. Szabo and J. Wu, J., *J. Acoust. Soc. Am.*, **107(5)**, 2437–2446 (2000).
[5] M. Gattin, N. Bochud, G. Rosi, Q. Grossman, D. Ruffoni, and S. Naili, *Ultrasonics*, **131**, 106951 (2023).

PHONONICS 2023: 6th International Conference on Phononic Crystals/Metamaterials/Metasurfaces, Phonon Transport, and Topological Phononics
Manchester, England, June 12-16, 2023
PHONONICS-2023-0057

Design and characterization of Snell Lenses with Gradient Index Phononic Crystals

Paolo H. Beoletto[1], Fabio Nistri[1], Antonio S. Gliozzi[1], Federico Bosia[1]

[1] DISAT, Politecnico di Torino, Italy,
paolo.beoletto@polito.it, fabio.nistri@polito.it, antonio.gliozzi@polito.it, federico.bosia@polito.it

Abstract: Gradient index phononic crystals allow to manipulate the phase profile of elastic waves and control their propagation. A detailed design procedure for elastic gradient index lenses is proposed, together with a proof that the mathematical model behind it is coherent with the Snell law, that correlates the position of an object and its image.

Manipulating the phase profile of an elastic wave allows to have full control on the spatial distribution of the mechanical energy. Mechanical metamaterials can be used to have a spatially changing refractive index, to design a gradient index phononic crystal. The idea is to create a monochromatic lens that is composed by a series of lines of cells whose refractive index changes in the direction perpendicular to the propagation: the lines are divided by partitions[1] that avoid the crosstalk between them and make them independent channels where the wave propagates with different wavevector. The phase profile at the lens end is produced by the spatial distribution of the refractive index in each line that induces a specific phase delay. Figure 1 shows an example of converging lens that has been designed following these criteria: the parameter that has been used to tune the refractive index is the filling factor, *i.e.* the normalised space occupied by the cross hole in the primitive cell, as reported in figure 2. In this research we present the detailed procedure that allows to obtain the array of cells with correct filling factor that induces the desired phase profile in the propagation direction.

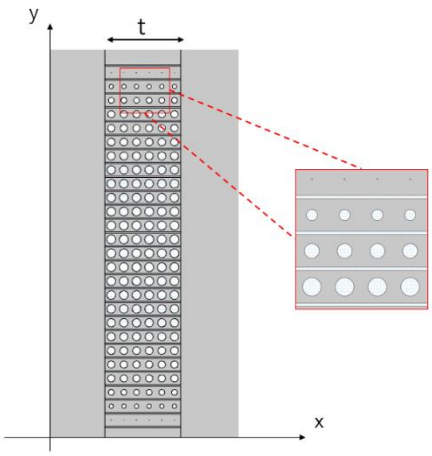

1. Partitioned GRadient INdex lens.

Primitive cell's dimensions and hole pattern can be chosen at will, with the only requirement of being able to isolate a flexural branch of the dispersion curves at the working frequency of the lens. On the contrary, array dimensions and filling factor of each cell are determined by this design procedure. The first step consists in obtaining the relation between the refractive index n at given frequency and the filling factor F. To do that, the dispersion curves of a set of cells with different filling factors are calculated with solid mechanics simulations on Comsol and the function n(F) is obtained with polynomial fitting. The number of cells in the propagation direction x is imposed by the width W that grants a phase delay of 2π between the line with minimum and maximum filling factor. The filling factor of the cells of each line is imposed in order to match the desired phase profile $\phi(y)$ at lens end. The refractive index profile is given by:

$$n(y) = \frac{\phi(y)}{k_0 W}$$

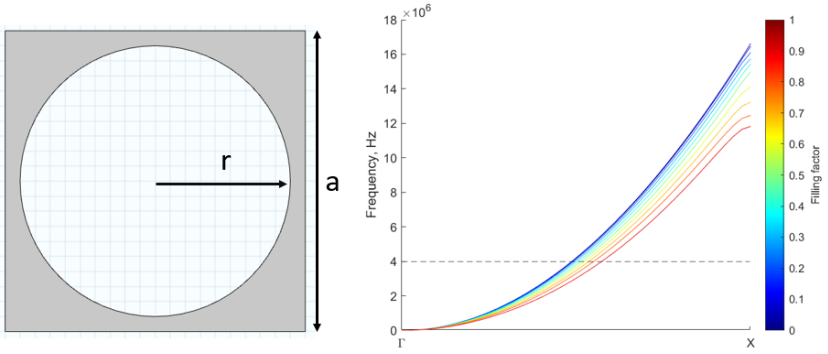

2. Effect of the filling factor $\boldsymbol{F = \frac{2r}{a}}$ on out-of-plane flexural mode $\boldsymbol{A_0}$.

The final step consists in inverting the function $n(F)$ obtained by the initial fitting of the data of the dispersion curves: this way the final design with the filling factor of each cell is determined. In order to design a lens that is able to focus an incoming plane wave, the desired phase profile needs to compensate the post-lens phase delay to have constructive interference at the focal point:

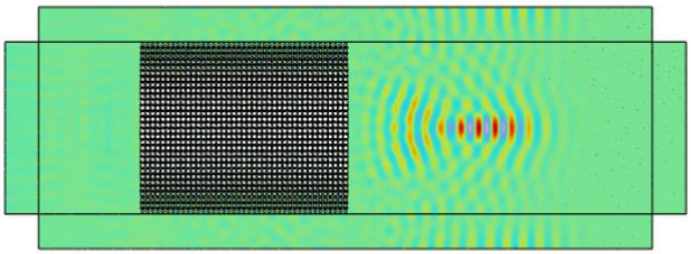

3. Snapshot of time domain simulation of a lens with focal point $\boldsymbol{f = 3mm}$ on a silicon plate, focusing a gaussian pulse centered at $\boldsymbol{1MHz}$.

$$\phi_P(y) = k_0\sqrt{y^2 + f^2}$$

$$n(y) = n_{max} - \frac{\sqrt{y^2 + f^2}}{W}$$

When considering a plane wave, the phase profile at the input of the lens remains constant. However, in general, this is not the case: a point-like source located at a distance d_o on the central axis ($y = 0$) induces a phase profile:

$$\phi_{in} = k_0\sqrt{y^2 + d_o^2}$$

For different paths of the wave propagating from $(-d_o, 0)$ to a point $(d_i, 0)$, the phase delay depends only on y, *i.e.* the position where the wave impinges the lens:

$$\phi_{tot} = \phi_{in}(y) + \Delta\phi(y) + \phi_P(y)$$

$$\phi_{tot}(y) = k_0\sqrt{y^2 + d_o^2} + \phi_0 - k_0\sqrt{y^2 + f^2} + k_0\sqrt{y^2 + d_i^2}$$

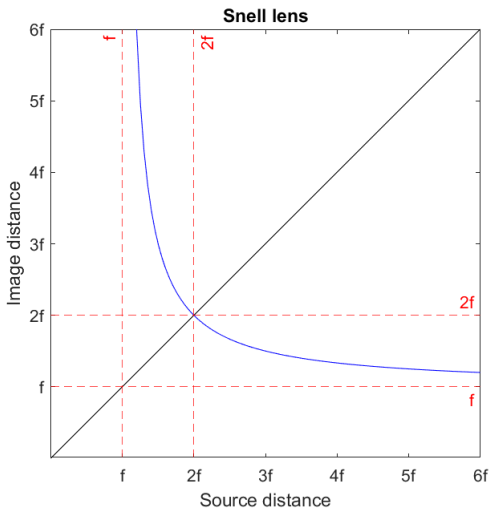

4. Bijective relation between source and image position in a Snell lens.

Imposing the paraxial approximation ($d_o, d_i, f \gg y$), *i.e.* limiting the model to small angles of propagation, allows to simplify the previous formula to the first order:

$$\phi_{tot}(y) = \phi_0 + k_0 y^2 \left(\frac{1}{\mathrm{d_o}} + \frac{1}{\mathrm{d_i}} - \frac{1}{\mathrm{f}}\right)$$

This formula is equivalent to the description of Snell lenses in Fourier Optics, where imaging conditions are obtained at a distance d_i for a given source location d_o, when constructive interference occurs and the phase ϕ_{tot} becomes independent of the acoustic path (i.e., independent of y). This condition is defined by the Snell law:

$$\frac{1}{\mathrm{d_o}} + \frac{1}{\mathrm{d_i}} - \frac{1}{\mathrm{f}} = 0 \qquad d_i = \frac{d_o f}{d_o - f}$$

In summary, this mathematical model of gradient index phononic crystals provides a powerful tool for designing lenses that conform to Snell's law, expanding the range of possibilities from focusing plane waves to imaging point-like sources. By achieving full control over the phase profile of the propagating wave, a bijective relation between the object location and its image can be established, mapping the pre-lens plane to the post-lens one. This opens up exciting opportunities for applications in the field of non-destructive testing[2,3].

References

[1] J Hyun, M Kim, and W Choi, *Scientific Reports* 10.1 (2020).
[2] M Miniaci, AS Gliozzi, B Morvan, A Krushynska, F Bosia, M Scalerandi, and NM Pugno, *Physical Review Letters* (2017).
[3] M Miniaci, A Krushynska, AS Gliozzi, N Kherraz, F Bosia, and NM Pugno, *Physical Review Applied*, (2018).

PHONONICS 2023: 6th International Conference on Phononic Crystals/Metamaterials/Metasurfaces, Phonon Transport, and Topological Phononics
Manchester, England, June 12-16, 2023
PHONONICS-2023-0090

Metamaterial-based barriers for railway-generated ground borne vibration

F. Nistri[1], R.M. Cosentini[2], V. F. Dal Poggetto[3], Paul Charkaluk [5], Nicola Pugno[3,6], M. Miniaci[4], A. Gliozzi[1], F. Bosia[1]

[1] DISAT, Politecnico di Torino, C.so Duca degli Abruzzi, Torino, Italy, fabio.nistri@polito.it, antonio.gliozzi@polito.it, federico.bosia@polito.it
[2] DISEG, Politecnico di Torino, C.so Duca degli Abruzzi, Torino, Italy
[3] Laboratory for Bioinspired, Bionic, Nano, Meta Materials & Mechanics, Department of Civil, Environmental and Mechanical Engineering, University of Trento, Trento, 38123 Italy
[4]CNRS, Centrale Lille, ISEN, Univ. Lille, Univ. Valenciennes, UMR 8520 - IEMN, Villeneuve-D'Ascq, 60069, France
[5]Phononic Vibes s.r.l., Via Simone Schiaffino 11, 20158, Milano, Italy
[6]School of Engineering and Materials Science, Queen Mary University of London, London, 4NS, United Kingdom

Abstract: This study evaluates the effectiveness of using elastic metamaterials to attenuate ground-borne vibrations caused by trains. A lab-scale model with resonating structures is proposed, and numerical simulations and experimental modal analysis are conducted to assess the influence of parameters like metamaterial structure. The study aims to find optimized solutions for efficient designs that can mitigate ground-borne vibrations in the low-frequency range.

This study aims to assess the effectiveness of a new MM-based design used in a trench barrier configuration[1,2] through experimental and numerical tests. Performance evaluations were conducted on a lab-scale model, requiring rescaling of sample sizes and frequency ranges. Samples with dimensions of around 10 and 3 mm thickness were used, necessitating a shift in frequency range from tens of Hz to 0.1-5 kHz. The investigation focused on an axisymmetric case where waves were directed normally onto the barrier, with propagation considered only in the soil, excluding surface modes from analysis. Although not entirely representative of real-world conditions, these experiments provided valuable insights into soil-structure interaction, numerical model validation, and the effectiveness of the proposed solution in mitigating ground-borne vibrations. A scaled model comprising resonating structures originating from two main metamaterial designs is proposed (Fig. 1a). The resonating metamaterial barrier designs are considered together with a cylindrical encasement (also shown in Fig.1a) to couple the structures to the soil, while allowing the resonators to freely vibrate. The influence of various parameters is evaluated: metamaterial type, size, thickness, and material (polymeric or metal). Numerical Finite Element Analysis is used to develop a suitable design, analysing mode shapes and frequencies of the resonating structures with and without the surrounding case. Metamaterial resonator structures were fabricated in polymeric material (PLA), or in steel. Typical specimens were 126 mm in diameter and 10 mm in thickness (polymer) or 3 mm in thickness (steel). The cylindrical case was (30 + 30) mm in thickness. Samples with and without case were experimentally tested exciting in a single point at the bottom using a linear sweep over a frequency range from 0.1 to 5 kHz. Whereas the acquisition was performed scanning the top surface with a Doppler laser vibrometer (Fig. 1b). FE models of the plates and plates within the case were developed and validated through experimental tests (Figs 1c-d). Comparison between the tests w/ and w/o case proved the presence of structural attenuation in the transmission spectra of the resonator-case in correspondence with the resonating frequencies of the resonator. Tests for the evaluation of the performance of meta-resonators in contact with the soil were performed by adopting a "sandwich" experimental setup, in which the resonating plate/case was placed between the two soil samples, prepared as described above. The entire system was encased in the modified oedometer cell to provide lateral confinement. At the bottom of the soil, a piezo buzzer element was placed as an excitation source (Fig. 2a). The adopted input signal was a sweep (duration of 2 s) with a frequency spectrum ranging from 0.1 to 5 kHz. Results (Fig. 2b) showed attenuation regions emerge in different specific frequency ranges for all MM designs. To verify if these attenuation ranges coincide with the resonances of the plates' structures, the FRF compari-

son plot between the resonant plate and resonant plate/case shown was used. For the CR geometry there is a relatively good match between the central attenuation range in the out- and in-soil configuration, whereas the other two frequency attenuation ranges do not appear in the in-soil results (Fig. 2b, above). For the FLC geometry, there is a partial coincidence between two regions of attenuation in- and out of-soil (Fig. 2b, below).

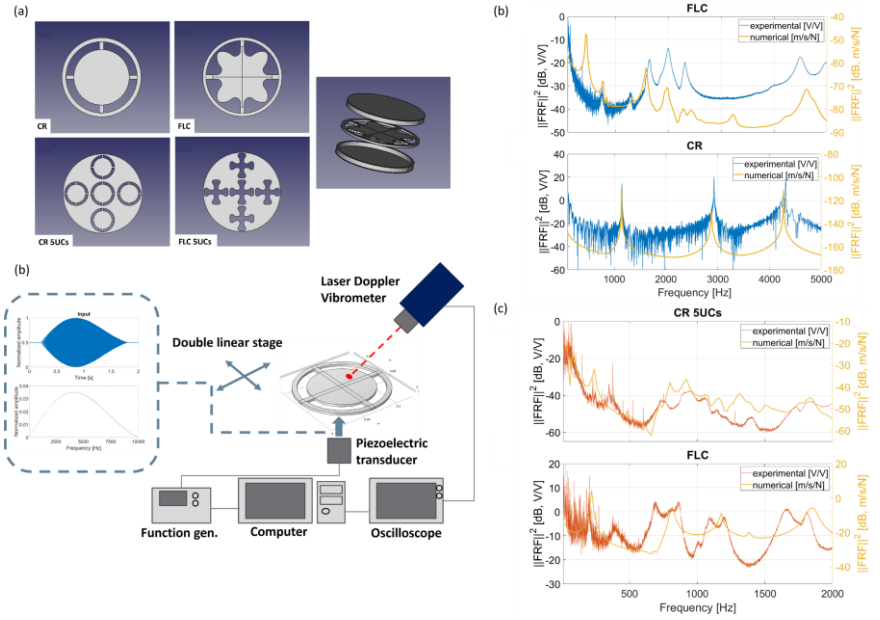

Figure 1 (a) Different designs of the resonant structures and exploded view of the in-case configuration. **(b)** schematic of the experimental setup and inset of the input function used in time and frequency domain. **(c-d)** comparison between experimentally and numerically calculated FRF function for the free resonant plate and the in case plate above and below, respectively.

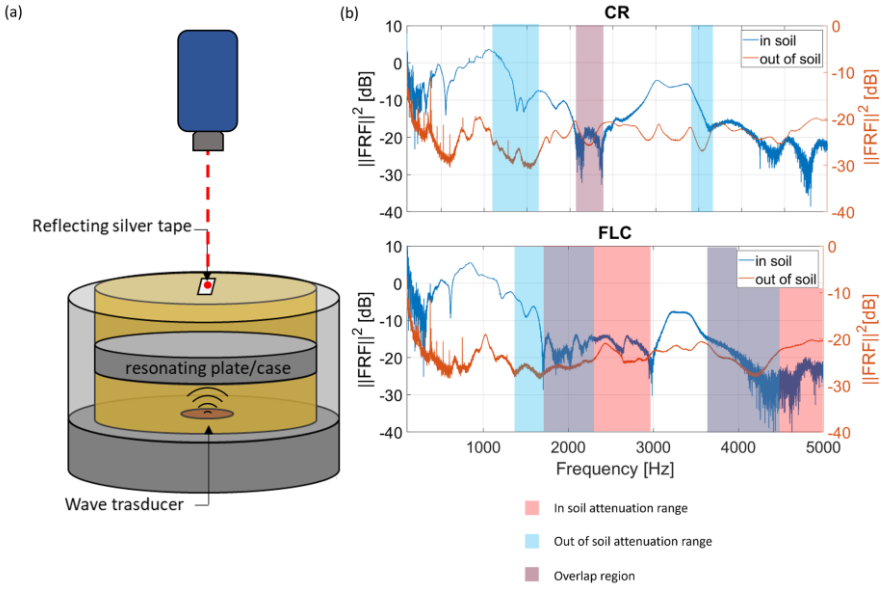

Figure 2 (a) schematic of the "sandwich" experimental setup. **(b)** comparison between the in-soil and out-of-soil FRF function for the resonant plate/case setup of the CR and FLC polymeric design.

References

[1] A. Dickmans et al.: Efficacy of a sheet pile wall as a wave barrier for railway induced ground vibration. Soil Dynamics and Earthquake Engineering. 55-69 (2016)
[2] P. Coulier et al.: Experimental and numerical evaluation of the effectiveness of a stiff wave barrier in the soil. Soil Dynamics and Earthquake Engineering. 238-253 (2015)

PHONONICS 2023: 6th International Conference on Phononic Crystals/Metamaterials/Metasurfaces, Phonon Transport, and Topological Phononics
Manchester, England, June 12-16, 2023
PHONONICS-2023-0105

Elastic Hyperbolic Strips

Nicholas H. Patino[1], Luca Lomazzi[2], Luca De Beni[1], Massimo Ruzzene[1]

[1] *Paul M. Rady Mechanical Engineering, University of Colorado, Boulder, CO, USA,*
[2] *Dipartimento di Meccanica, Politecnico di Milano, Milano, Italy,*

nicholas.patino@colorado.edu, luca.lomazzi@polimi.it, luca.debeni@colorado.edu, massimo.ruzzene@colorado.edu

Abstract: Elastic hyperbolic strips leverage the high density of localized modes which characterize circular elastic hyperbolic lattices, while presenting themselves as useful engineering structures. A conformal mapping gives rise to hyperbolic strips and provides the versatility to accommodate any direction or path, as well as produce an infinite extension in bulk geometry designs through simple rotations and translations of the generating space. The result is a practical engineering structure which not only inherits a high density of boundary modes, but also a notable number of center-localized modes, which could be of interest for a variety of engineering applications. As such, elastic hyperbolic strips open the door to a new class of elastic hyperbolic metamaterials with waveguiding capabilities that rely on the ability to localize vibrations at edges or to the interior of structural assemblies.

The hyperbolic plane, a 2D space of constant negative curvature, accommodates an infinite number of regular tessellations in contrast to the Euclidean plane which supports but three. Such a rich design space sets the stage for a large new class of elastic metamaterials, characterized by a high density of localized modes of vibration: an attractive property for vibration isolation applications. Heretofore, hyperbolic geometry has provided a useful paradigm for quantum and classical particle interactions and transport in curved spaces, with explorations ranging from topological states of matter to classical diffusion[1,2]. In tandem, recent advances in their theoretical framework has supported our understanding of their physical properties[3], spanning all areas of wave physics, including elastic wave propagation which up until recently has been largely unexplored.

Elastic hyperbolic lattices are rotationally symmetric beam coupled networks defined by a hyperbolic tessellation. These lattices boast a high density of modes localized at their boundary and exhibit edge-confined wave propagation robust to defects[4]. Upon pulse excitation at the boundary, it has been observed that an elastic hyperbolic lattice will guide wave energy around its edge rather than through its bulk, protecting the bulk media from unwanted vibrations. Fig. 2 shows this phenomenon empirically for a 7-fold symmetric triangular elastic hyperbolic lattice through snapshots in time.

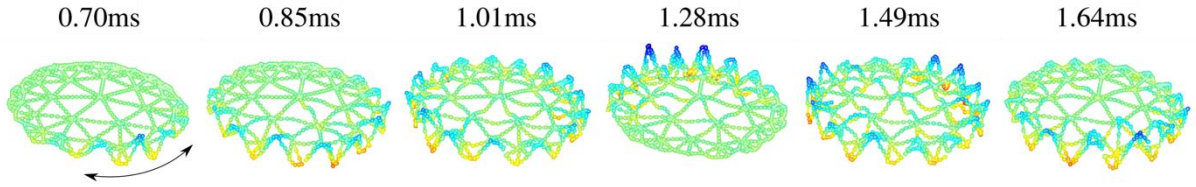

Figure 1 Measurement of the time evolution of a boundary-dominated wave in an elastic hyperbolic lattice. The lattice is excited by a short pulse centered at 10 kHz through a piezoelectric transducer attached to an edge node. Counter-rotating waves travel along on the lattice boundary.

Though a useful proof of concept, these hyperbolic lattices have limited interest in terms of application. However, these lattices form the basis for the generation of a class of hyperbolic 2D strips through conformal mapping. The result is a conformal, strip-like waveguide which inherits all the possible tiling geometries of its parent lattice as well as the versatility to accommodate any specified path. This extension gives rise to many designs of potential engineering interest, including 2D periodic configurations that can be analyzed in the framework of Bloch's Theorem to estimate dispersion properties for example.

The hyperbolic strips are created by a conformal mapping of the Poincaré disk, whereby two critical points of a holomorphic function (z=-1 and z=1) define canonical points of the transformation from

which a principle "stretching" direction is defined, as seen in Figure 2a. The general mapping is given by,

$$f(z) = w = \frac{2}{\pi} \ln\left(\frac{1+z}{1-z}\right) \quad (1)$$

where z is a complex point in the Poincaré disk, and w is a complex point in the hyperbolic strip. The result of this mapping with the canonical fixed points is shown in Figure 2b.

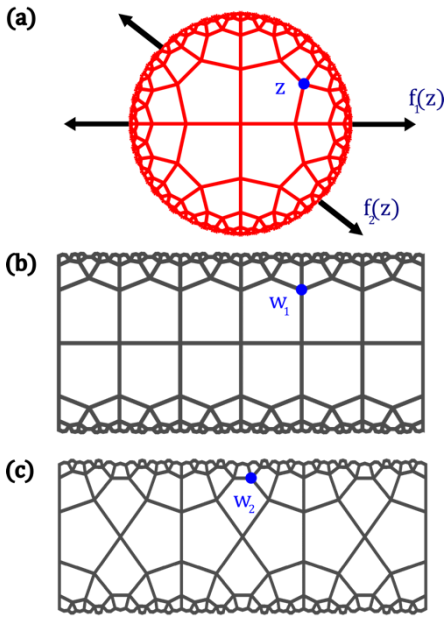

Figure 2 (a) Conformal mapping of a {5,4} hyperbolic lattice in the Poincaré disk to **(b)** a hyperbolic strip and to **(c)** another hyperbolic strip by an isometric rotation of the fixed points.

This hyperbolic strip, like the generating hyperbolic lattice, is characterized by a high density of modes localized at the boundary, as illustrated in the normalized integrated density of states of Figure 3a. An example of a boundary mode is shown in Figure 3b. At the same time, the strip supports center-localized modes, also exemplified by Figure 3b. Unlike in the generating hyperbolic lattices, center-localized vibrations in the strips can travel in space, creating a waveguide with both center and boundary-localized wave transport. The hyperbolic strip paired with a set of additional conformal mappings then allows us to generalize the path followed by the strip. Such a versatile geometry allows for a greater number of waveguiding applications than their generating hyperbolic lattices, which take on only circular geometries.

We can explore numerous conformal mappings of the hyperbolic strip to investigate the properties associated with new geometries and configurations from the same generating lattice. An example is shown in Figure 2c, where the fixed points of the transformation in Figure 2a are no longer at canonical positions of z=-1 and z=1, but at a -π/4 rotation of such points. These alternative mappings produce different types of localized modes in different frequency ranges, with different densities, opening a plethora of possibilities for waveguiding.

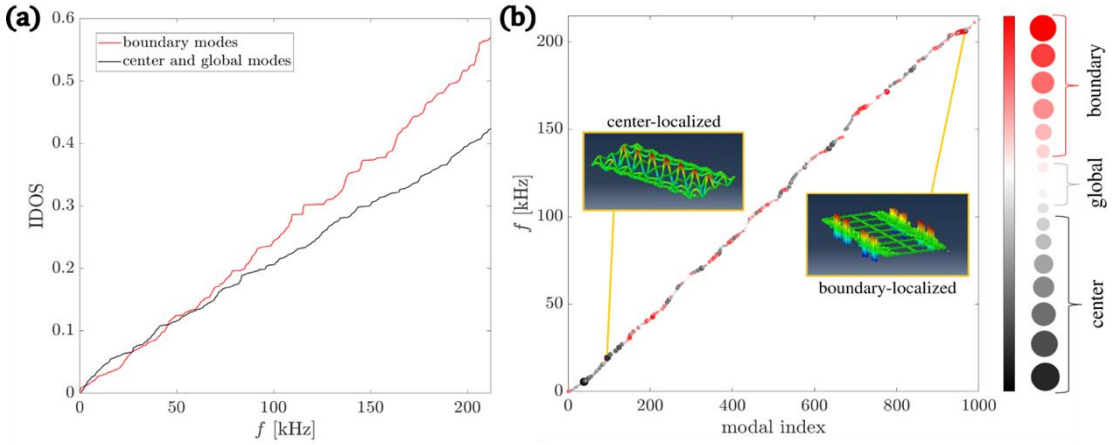

Figure 3 (a) Integrated density of states of the {5,4} hyperbolic strip (refer to Figure 2b). **(b)** Spectrum of {5,4} strip with modal points colored and scaled based on location of average displacement field and degree of localization respectively.

References

[1] W. Zhang, H. Yuan, N. Sun, H. Sun, and X. Zhang, *Nature Communications*, ***13***, 2937 (2022)
[2] S.K. Baek, S.D. Yi, and B.J. Kim. *Physical Review E*, **77**(2), 022104 (2008).
[3] I. Boettcher, A.V. Gorshkov, A.J. Kollár, J. Maciejko, Steven Rayan, and Ronny Thomale. *Physical Review B*, **105**(12), 125118 (2022).
[4] N.H. Patino, C. Rasmussen, M Ruzzene. *SPIE Photonics West Proceedings*, **12431**, 5 (2023).

PHONONICS 2023: 6th International Conference on Phononic Crystals/Metamaterials/Metasurfaces, Phonon Transport, and Topological Phononics
Manchester, England, June 12-16, 2023
PHONONICS-2023-0170

Silicon Based Suspended Thermometry Device Fabrication for Phonon *Ballistic and Coherent* Regimes Study

J. Canosa Diaz[1], H. Ikzibane[1], B. Brisuda[2], C. Polanco Garcia[3], L. Saminadayar[2], N. Mingo[3], O. Bourgeois[2], E. Dubois[1] and J.-F. Robillard[1]

[1] *Univ. Lille, CNRS, Centrale Lille, Junia, Univ. Polytechnique Hauts-de-France, UMR 8520 – IEMN – Institut d'Electronique de Microélectronique et de Nanotechnologie, F-59000 Lille, France*
jon.canosa-diaz@junia.com, emmanuel.dubois@iemn.fr, jean-francois.robillard@iemn.fr
[2] *Institut NEEL, CNRS-Université Grenoble Alpes, 25 avenue des Martyrs, 38042 Grenoble, France*
boris.brisuda@neel.cnrs.fr, laurent.saminadayar@neel.cnrs.fr, olivier.bourgeois@neel.cnrs.fr
[3] *Université Grenoble Alpes, CEA, LITEN, 17 rue des Martyrs, 38054 Grenoble, France*
carlos-andres.polanco-garcia@cea.fr, natalio.mingo@cea.fr

Abstract: This works addresses the current experimental gap in thermal transport regimes and phonon transport at low temperatures and small scales. We have fabricated a (SOI based) suspended thermal sensor platform functional from room-T down to 20 mK. The device will be used for the study phonon transport across several Si-based samples like phononic crystals, metamaterials and nanowires.

The aim of this project is to learn more about the different thermal transport regimes and investigate the behavior of phonons transport at very low temperatures (down to 20 mK) in nanoscale materials. Under these conditions, the mean free path (Λ) and dominant wavelength (λ_{DOM}) of phonons become comparable to or greater than the sample's size, leading to a variety of interesting phenomena, such as phonon interferometric effects[1], thermal rectification, and quantization of thermal transport[2].

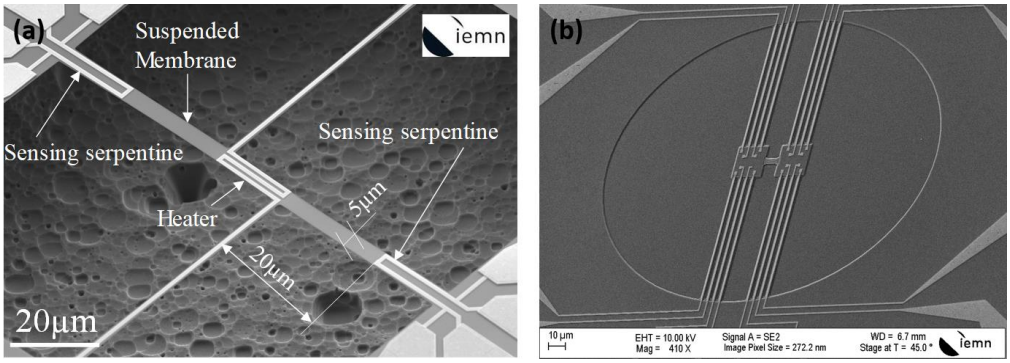

Figure 1 (a) Example of a silicon based suspended device fabricated at our laboratory and **(b)** New design of the suspended thermal device.

Suspended thermal devices have already been developed on previous works at the IEMN[3]. The first step in our project has been the adaptation of this processes towards the fabrication of a different design of suspended systems[4], produced from silicon-on-insulator (SOI) wafers by means of micro-/nano-fabrication techniques, mainly based on e-beam lithography and reactive ion etching (RIE). These devices possess a double reservoir configuration, each one with an externally controlled thermometer and a heater, allowing for the inversion of the thermal current across a sample. The sensing is done using the precise superconducting NbN material, with a goal of achieving sensitivities up to zeptowatts (10-21 W).

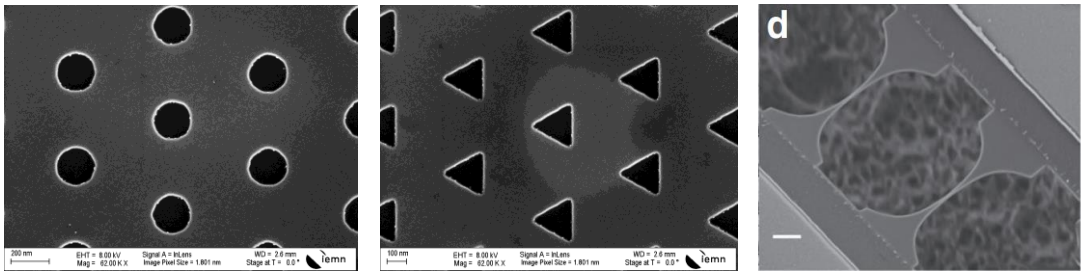

Figure 2 Display of the patters etched into the silicon membranes and image of the nanowires to be fabricated.

We will be fabricating different kinds of samples, such as nanowires and patterned membranes, in between the sensing platform for the study of the desired phenomena. The project is done in collaboration with CEA-LITEN (Grenoble) for theoretical simulations and Institut Néel (Grenoble) for sample fabrication and low-temperature measurements on a dilution refrigerator. Our poster will present the scientific and technological challenges associated with this work, showing the recently fully finished devices and the future perspectives on sample characterization.

References

[1] N. Zen, T. Puurtinen, T. Isotalo et al, Nature Communications **5**, 3435 (2014).
[2] K. Schwab, E. Henriksen, J. Worlock et al., *Nature* **404**, 974 (2000).
[3] M. Haras et al., *IEEE Electron Device Lett.* **37**, 1358 (2016).
[4] A. Tavakoli, *Nature Communications* **9**, 4287 (2018).

PHONONICS 2023: 6th International Conference on Phononic Crystals/Metamaterials/Metasurfaces, Phonon Transport, and Topological Phononics
Manchester, England, June 12-16, 2023
PHONONICS-2023-0024

Metapile: Resonator Impregnated Pile Towards Enhanced Passive Vibration Control

Rishab Das[1], Arnab Banerjee[2], Bappaditya Manna[3]

[1]Indian Institute of Technology, Delhi; cez208310@civil.iitd.ac.in
[2]Indian Institute of Technology, Delhi; abanerjee@civil.iitd.ac.in
[3] Indian Institute of Technology, Delhi; bmanna@civil.iitd.ac.in

Abstract: Mono-pile foundations are often used in soft soils in order to support heavy mega-structures, whereby often these deep footings may undergo dynamic excitation due to many causes like earthquake, wind or wave loads acting on the superstructure, blasting, and unbalanced machines, etc. A comprehensive analytical study is performed to study the dynamics of the mono-pile system embedded in cohesion-less soil. The soil is considered homogeneous and visco-elastic in nature and is analytically modelled using complex springs. Considering the N number of the elements of the pile, the final global stiffness matrix is obtained by using the theories of the spectral element matrix method. Further, statically condensing the intermediate internal nodes of the global stiffness matrix results in a smaller sub matrix, containing the nodes experiencing the external translation and rotation, and the stiffness and damping functions (impedance functions) of the embedded piles are determined. Proper plots showing the variation of the real and imaginary parts of these impedance functions with the dimensionless frequency parameter are obtained. The plots obtained from this study are validated by that provided by [1]. Further, a novel approach of the resonator-impregnated pile is proposed within this study..

Mono-pile foundations are often used in soft soils in order to support heavy mega-structures, whereby often these deep footings may undergo dynamic excitation due to many causes like earthquakes, wind or wave loads acting on the superstructure, blasting, unbalanced machines, etc. A comprehensive analytical study is performed to study the dynamics of the mono-pile system embedded in cohesion-less soil utilizing the concept of Spectral Element Method (SEM). The soil is considered homogeneous and visco-elastic in nature and is analytically modeled using complex springs. The derived dynamic stiffness matrix obtained makes it easier to construct the closed-form equation for the dynamic stiffness and damping coefficients of the pile.

A novel paradigm for "metapile: resonator impregnated pile" is proposed in the study, which is designed and analyzed to improve the capacity to withstand dynamic harmonic loads. The dynamic response of the pile is found to significantly diminish when the excitation frequency of the harmonic loading approaches the natural frequency of the resonator. The stiffness and damping of the pile at the resonant frequency become infinite, allowing for the observation of this meta response. Also, a comparative analysis of several performance improvement methods for a conventional pile under dynamic loading circumstances is carried out. Increasing the mass density of the pile, adding lumped masses on a regular basis to the pile body, and adding periodic resonators are a few performance improvement approaches taken into consideration Figure 1. Proper plots showing the variation of the real and imaginary parts of these impedance functions with the dimensionless frequency parameter are obtained. The plots obtained from this study are validated by that provided by [1]. Furthermore, the variations in the stiffness and damping plots after incorporating the resonator are illustrated in the attached Figures 2, Figures 3 and Figures 4.

The solid lines in the plot refer to the real part of the stiffness parameter, while the dotted line represents the imaginary part of the stiffness parameters. The difference in variation of the stiffness can be observed for all four different cases. The variation of parameters are almost similar for the spring-mass system and lumped mass system; however, for the spring-mass system, there's a sudden increase in the stiffness near the natural frequency of the resonator imposed on the pile. Whenever the external frequency coincides with the natural frequency of the spring mass, local resonance leads to the increased stiffness and also a significant decrease in deflection.

[1] Milos Novak. "Effect of soil on structural response to wind and earthquake". In: Earthquake Engineering & Structural Dynamics 3.1 (1974), pp. 79–96.

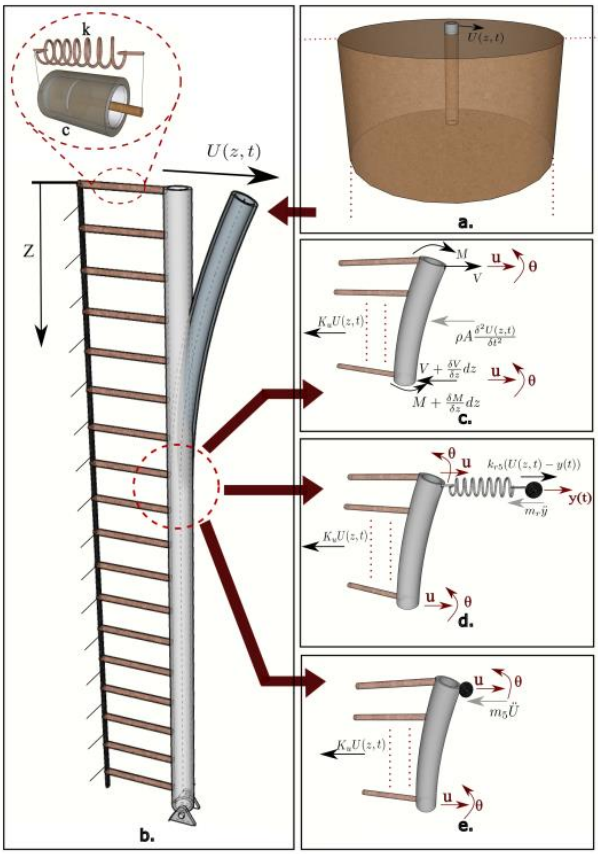

Figure 1: Free-body diagram of the (b) pile linked with visco-elastic springs; (c) pile with added mass linked with visco-elastic springs; (d) pile with resonator linked with visco-elastic springs; (d) pile with lumped mass linked with visco-elastic springs.

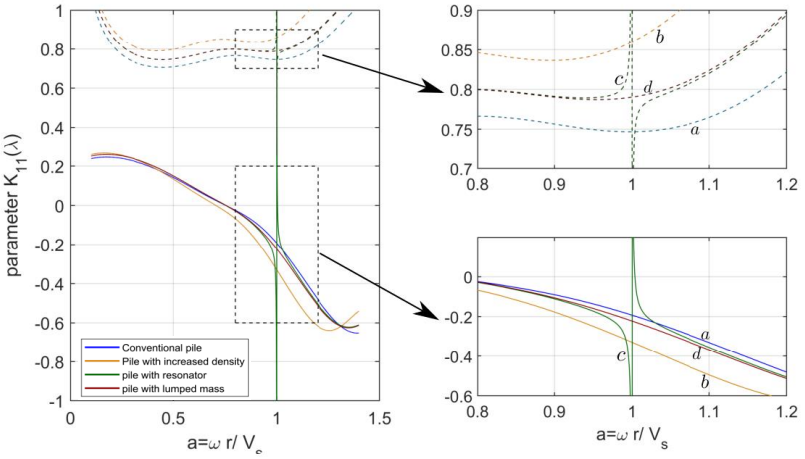

Figure 2: Variations in the dynamic horizontal stiffness and damping values of the pile.

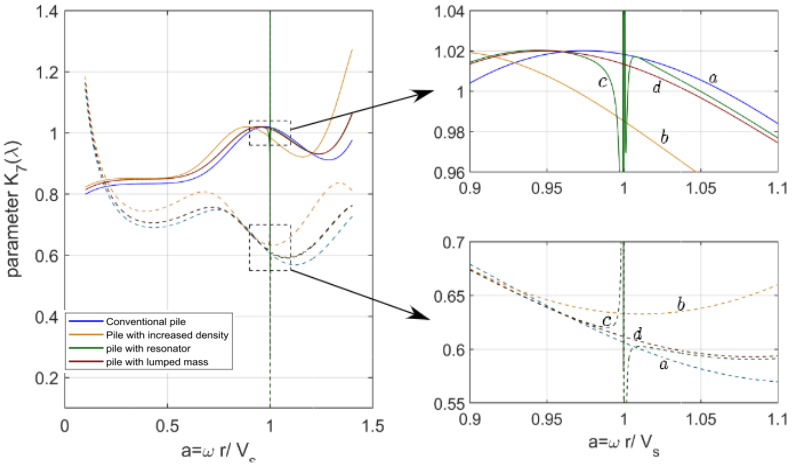

Figure 3: Variations in the dynamic rotational stiffness and damping values of the pile.

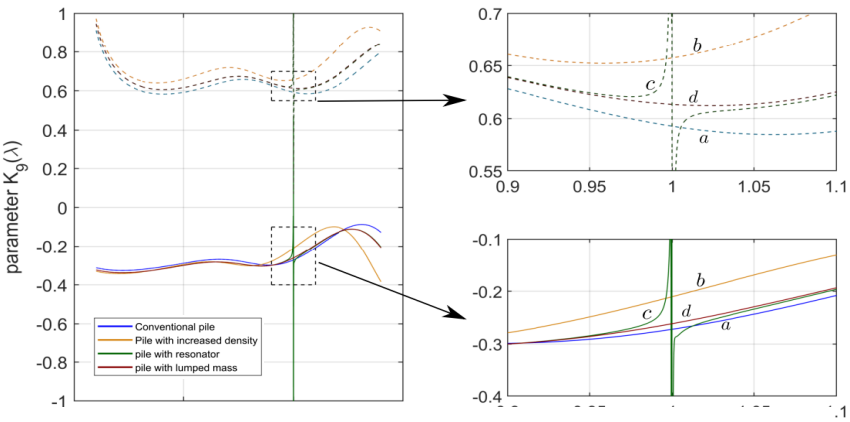

Figure 4: Variations in the dynamic cross rotational stiffness and damping values of the pile.

PHONONICS 2023: 6th International Conference on Phononic Crystals/Metamaterials/Metasurfaces, Phonon Transport, and Topological Phononics
Manchester, England, June 12-16, 2023
PHONONICS-2023-0027

Acoustic attenuation bands using graded metamaterials

A. I. Adham[1], V. Sorokin[1], B. Mace[1], A. Hall[1]

[1] *Acoustics Research Centre, Department of Mechanical and Mechatronics Engineering, The University of Auckland, Private Bag 92019, Auckland 1142, New Zealand*
**Email: aalg195@aucklanduni.ac.nz*

Abstract: We present a method to construct low-vibration transmission regions utilising graded resonators without restrictions on their dynamic characteristics and positions. The wave approach is used to model the system. The bandwidth of the attenuation bands, location and magnitude of vibration suppression is controlled by tuning and optimally positioning the resonators.

The system (Figure 1) consists of a uniform rod with N attached resonators, and the wave approach is used to analyse the system. Regarding vibration suppression magnitude and bandwidth, the performance of graded resonators is compared to that of conventional, periodic, and identical resonators. The method presented here can be applied to other structures, such as beams. The reflection, r, and transmission, t, coefficients of a damped resonator attached to a rod can be calculated by considering the continuity of displacement and force equilibrium at the point of connection to the structure [1]. They can be written as

$$r = \frac{1}{\frac{2i}{\Phi\beta}\left(\frac{1+2i\xi\beta-\beta^2}{1+2i\xi\beta}\right)-1} \quad ; \quad t = 1 + r \tag{1}$$

where time-harmonic motion at frequency ω is assumed, $\beta = \omega/\omega_r$ is the frequency ratio, $\omega_r = \sqrt{k_r/m_r}$ is the resonator's natural frequency, k_r and m_r are the stiffness and mass of the resonator, respectively, $\Phi = m_r\omega_r/(\rho_g A c_g)$, ρ_g is the density of the rod, A is the cross-section area, c_g is the wave speed, and ξ is the resonator's damping ratio. Generally, a finite rod with multiple segments, N resonators, and a length L can be analysed by considering the n^{th} segment. As shown in Figure 1, the n^{th} rod segment can be modelled as subject to two external forces and bounded by two discontinuities at either end. The discontinuities are represented by their r and t. The negative-going wave amplitude, $w^-_{n,(1,2)}$, at each end node is a result of the excitation, the reflection of the incident wave, $w^+_{n,(1,2)}$, on the node within the segment, and the transmission of the incident wave on the node from the adjacent segment. The wave amplitudes are related to each other by

$$w^+_{n,1} - r_{n,1}\, w^-_{n,1} - t_{n,1}\, w^+_{n-1,2} = \frac{\Gamma_{n,1}}{ikL_n} \quad ; \quad w^-_{n,2} - r_{n,2}\, w^+_{n,2} - t_{n,2}\, w^-_{n+1,1} = \frac{\Gamma_{n,2}}{ikL_n} \tag{2}$$

$$w^+_{n,2} - w^+_{n,1}\, e^{-ikL_n} = 0 \quad ; \quad w^-_{n,1} - w^-_{n,2}\, e^{-ikL_n} = 0 \tag{3}$$

where kL is the non-dimensional spatial frequency, $L_n = (\alpha_n - \alpha_{n-1})L$, α_n and α_{n-1} are the relative positions of the discontinuities at each end of the rod segment, $\Gamma_{n,(1,2)} = F_{n,(1,2)}/(EA/L)$, and E is the rod's elastic modulus. For a finite rod with multiple segments, Equations (2) through (3) can be applied to each segment to create a system of equations in which the number of unknowns equals the number of equations. Solving the system of equations yields analytical formulations for the wave amplitudes, allowing the displacement at any point to be calculated. The displacement at any point in the n^{th} segment is

$$u(\zeta_n) = w^+_{n,1} e^{-ikL_n\zeta_n} + w^-_{n,1} e^{ikL_n\zeta_n} \tag{4}$$

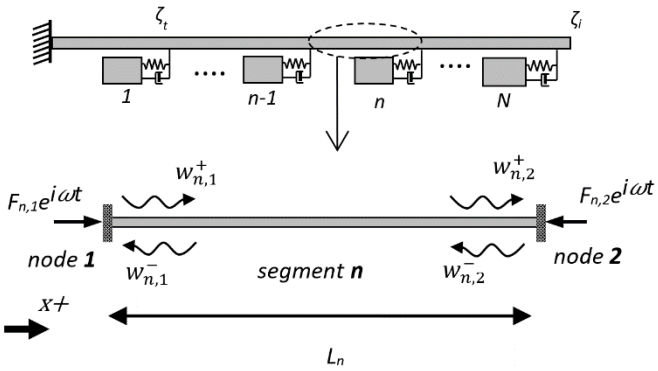

Figure 1 A rod with multiple resonators and the n^{th} segment

where ζ_n is the relative position on segment n. The transmissibility (TR), Equation (5), of the graded metamaterial rod is defined as the ratio of displacement at the point of observation ζ_t to that of excitation ζ_i, which can be any two points in the system. Attenuation bands (ABs) are those for which TR < 1. An AB can be created by targeting a peak in the TR with a resonator, see Figure 2, and then systematically targeting the bounds of the AB by other resonators. The bandwidth of the AB can be increased by increasing the mass of the resonator(s). The resonance effect outside the ABs can be reduced by regulating the damping of the resonators, and the magnitude of vibration attenuation inside the ABs can be increased by optimising the positions of the resonators.

$$TR = \left| \frac{u(\zeta_t)^2}{u(\zeta_i)^2} \right| \tag{5}$$

Notice that the resonators' properties can vary independently, allowing for flexible and effective use. Figure 2 (left) shows an AB constructed with two resonators which can be further widened by adding resonators targeting the ABs bound frequencies. Figure 2 (right) compares conventional and graded metamaterial rods, where the latter outperforms the former. The first two graded resonators target 3π, and the other two target 3.3π. The TR dips in the graphs emerge as the deformation shape of the structure changes with the introduction of resonators, so $TR \rightarrow -\infty$ at the frequencies of the dips. Since the magnitude and phase of the waves are determined at any point in the structure, the resonance frequencies of the graded metamaterial rod can be found by following the phase-closure principle [2].

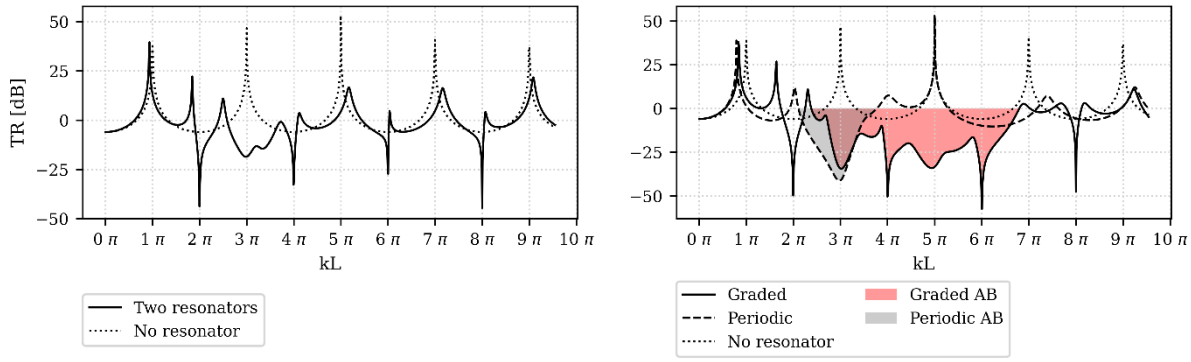

Figure 2 Left: AB created with two resonators tuned to kL = {3π, 3.3π}, α = {0.2, 0.5}, ξ = 0.05, and Φ = 1/2 for both resonators. Right: Four periodic resonators tuned to kL = 3π and four graded resonators where two tuned to kL = 3π and two tuned to kL = 5π, $\alpha_{periodic}$ = {0.2, 0.4, 0.6, 0.8} and α_{graded} = {0.15, 0.21, 0.37, 0.5}. ξ = 0.05, and Φ = 1 for both type of resonators. $\zeta_i = 0$, $\zeta_t = 1/2$ for both plots.

References

[1] BR Mace. *Journal of Sound and Vibration*, **97** (2) 237–246, (1984)
[2] D.J. Mead. *Journal of Sound and Vibration* **171** (5) 695-702 (1994)

PHONONICS 2023: 6th International Conference on Phononic Crystals/Metamaterials/Metasurfaces, Phonon Transport, and Topological Phononics
Manchester, England, June 12-16, 2023
PHONONICS-2023-0028

Weight Reduction Strategies for Underwater Acoustic Cloaking

Sebastiano Cominelli[1], Davide E. Quadrelli[1], Gabriele Cazzulani[1], Francesco Braghin[1]

[1] *Department of Mechanical Engineering, Politecnico di Milano, Via La Masa, 1, 20156 Milano, Italy,*
sebastiano.cominelli@polimi.it, davideenrico.quadrelli@polimi.it, gabriele.cazzulani@polimi.it, francesco.braghin@polimi.it

Abstract: Cloaking is a challenging application of metamaterials since high anisotropy on a broadband frequency range is needed. On top of that, underwater acoustic cloaking shall also consider balance of hydrostatic forces and weight if the buoyancy of the surrounded target is required. In this work, we show some techniques for improving buoyancy and investigate the consequent performance trade-off.

Transformation acoustics (TA) has been the quintessential tool to design cloaks since 2006[1]. This method consists in applying a deformation to the space coordinates such that an acoustic target is mapped into a smaller one. The resulting changes in the Helmholtz equation are interpreted as modifications of the physical properties of the cloak. In this way, an acoustic target covered with such a device has an overall acoustic response equivalent to a smaller object to which is mapped; such that it is concealed with respect to SONAR localization techniques.

The physical realization of such devices implies adopting the use of anisotropic inertial properties (inertial cloak IC) and/or anisotropic elastic properties (pentamode PM cloak)[2]. In typical underwater applications of such devices, i.e., making submarines undetectable, the overall mass plays an important role, since the vehicle equipped with the cloak should be neutrally buoyant. Pure PM cloaking has been recently successfully demonstrated in underwater environment, and it is often regarded as the most interesting option for practical purposes, not requiring working fluids and avoiding infinite mass requirements. Nonetheless, even if PM cloaks have limited mass, TA still requires that the inertia of the device is the same of the equivalent virtual volume of water, so that the weight of the cloak is by itself equal to the overall buoyancy thrust. This implies that the vehicle-cloak pair cannot be buoyant, and that a buoyant submarine cannot be perfectly acoustically invisible.

To work around this issue, in this work we compare two alternative strategies that are illustrated in Figure 1. In the middle, it is shown a target of radius R_i surrounded by a grey region with boundaries $\partial\Xi^{\pm}$. A perfect cloak makes the acoustic target equivalent to the bubble shown on top left of Figure 1, such that the *Total Scattering Cross Section* (TSCS) is null. This solution suffers from the problem explained above and is not of practical use.

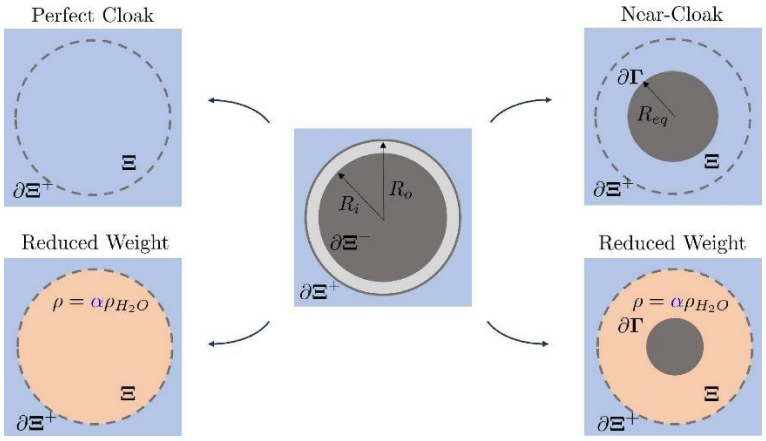

Figure 1: we propose two strategies for reducing the weight of the cloak with respect to the perfect one (top left): either increase the size of the virtual obstacle (top right) or scale down the density (bottom left); a combination of them can be also applied (bottom right).

A popular method consists in choosing an equivalent radius R_{eq} not infinitesimal with respect to the characteristic wavelengths of interest (near cloak). In this way, the acoustic performance degrades, but the cloak becomes lighter. By changing R_{eq}, one can obtain the following relationships

$$\hat{T} = \frac{T_{av}}{T_{unclk}} = \left(\frac{R_{eq}}{R_i}\right)^{d}, \qquad \hat{P} = \frac{P_{sc}}{P_{sc,unclk}} = \left(\frac{R_{eq}}{R_i}\right)^{d-1}, \tag{1}$$

where T_{unclk} and T_{av} are the thrusts before and after the application of the cloak, and $P_{sc,unclk}$ and P_{sc} are estimates of the corresponding total scattered powers. By this simple analysis, is not possible to have T_{av}/T_{unclk} tending to one and simultaneously reducing the scattered power. So other techniques shall be considered.

The strategy we propose consists in rescaling inertia and stiffness properties of an arbitrary factor α: ($\rho = \alpha\rho_{H_2O}$ and $\kappa = \alpha\kappa_{H_2O}$). In this way, the sound speed distribution in the cloak is conserved and, if α is chosen smaller than the unity, the overall mass is reduced; this allows the cloak to work in the same way throughout its thickness, even if the pressure intensity is scaled accordingly. As a drawback, the acoustic impedance changes in accordance with the formula $Z = c\rho = \alpha Z_{H_2O}$. So, this results in a decrease of the concealing performance of the devices[3].

Figure 2 quantifies the increase of TSCS for different values of α between 0.01 and 0.5, where α is chosen constant throughout the thickness. We show that the spikes that appear in the plot are in correspondence of the resonance modes of the cloak. Moreover, two values of $\beta = R_o/R_i$ are chosen to quantify the TSCS reduction obtained with by a near-cloak. Finally, the trade-off is even improved by allowing α to vary with space. In particular, the impedance mismatch is reduced on the outer radius, so less scattering is shown, consider Figure 2 for a comparison with the performance given by constant α.

Both strategies can be combines to obtain the best compromise between acoustic performance and buoyancy requirements, as illustrated in Figure 3. The diagram shows design parameters when the conditions about scattering reduction and buoyancy are met such that $\hat{T} < 1$ and $\hat{P} < 1$.

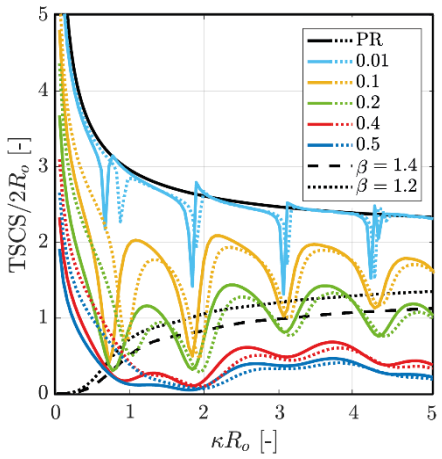

Figure 2: considering a perfect cloak, the figure shows the increase of the target strength by changing the rescaling coefficient $\hat{\alpha}$ between 0.5 and 0.01 space constant (solid) and varying (dotted). The performance is compared with two near-cloaks defined by the parameter β chosen between 1.2 and 1.4. In all cases, the resulting cloaks tends to perform as a larger target of size $\partial\Xi^{+}$ (black solid line).

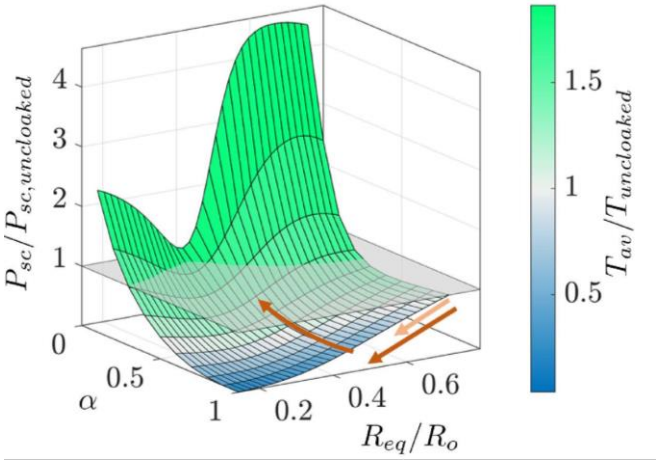

Figure 3: total scattering power for an incident pressure wave such that $kRo = 1.7$. By varying α and R_{eq}/R_o, the performance of the cloak is affected. The colour scale refers to the hydrodynamics available thrust normalized with respect to the uncloaked target. The light and the dark arrows indicate respectively the effect of choosing a near-cloak or a reduced-weight strategy.

References

1. Pendry, John B., David Schurig, and David R. Smith. "Controlling electromagnetic fields." Science 312.5781 (2006).
2. Norris, Andrew N. "Acoustic cloaking theory" Proceedings of the Royal Society A 464.2097 (2008).
3. Quadrelli, Davide Enrico, et al. "Experimental validation of a broadband pentamode elliptical-shaped cloak for underwater acoustics." Extreme Mechanics Letters 101526 (2021).

PHONONICS 2023: 6th International Conference on Phononic Crystals/Metamaterials/Metasurfaces, Phonon Transport, and Topological Phononics
Manchester, England, June 12-16, 2023
PHONONICS-2023-0042

Full Ultrasound Transmission in the Metal-Water-Metal System using Elastic Metamaterials

Gihyun Kim[1], Jeseung Lee[1], Jae Heung Cho[1], Minwoo Kweun[2], Yoon Young Kim[1]

[1] *Department of Mechanical Engineering, Seoul National University, 1 Gwanak-Ro, Gwanak-Gu, Seoul 08826, Republic of Korea*
[2] *Department of Applied Nano Mechanics, Korea Institute of Machinery & Materials, 156 Gajeongbuk-Ro, Yuseong-Gu, Daejeon 34103, Republic of Korea*
gikim@snu.ac.kr, enda95@snu.ac.kr, jjhstarcjswo@snu.ac.kr, jmkweun@kimm.re.kr, yykim@snu.ac.kr

Abstract: We propose a non-locally resonant elastic metamaterial with X-shaped microstructures to achieve full ultrasound penetration through a highly impedance-mismatched barrier. Our proposition is validated through numerical simulations and ultrasound experiments. It can be applied to medical ultrasound or ultrasonic non-destructive testing.

I. Introduction

Reflected waves generated from a highly impedance-mismatched barrier cause a significant reduction in the transmission of ultrasound through the barrier. This issue of low transmission through the barrier has limited the range of applications of ultrasonic equipment. One of the general methods to address the issue is the use of the Fabry-Pérot resonance (FPR). However, it has a limitation in that full penetration is realized only when the product of the frequency and the barrier thickness has a specific value[1]. Alternatively, the use of a complementary metamaterial (CMM) can theoretically eliminate the barrier and allow full ultrasound penetration without any reflection[2]. However, the implementation of CMMs requires extremely sensitive locally resonant structures, making their experimental application impractical[3]. In recent years, research has been actively conducted on using non-resonant metamaterials for elastic ultrasonic wave control to circumvent the limitations of resonant metamaterials[4,5]. In this study, we investigate the feasibility of applying non-locally resonant elastic metamaterials for full ultrasound penetration through a barrier. Our investigation shows that full ultrasound penetration through highly impedance-mismatched barriers can be achieved by utilizing non-resonant elastic metamaterials with X-shaped microstructures. The performance of the proposed metamaterials is verified through finite element method (FEM) simulations and ultrasound experiments.

II. Theory and Physical Interpretation

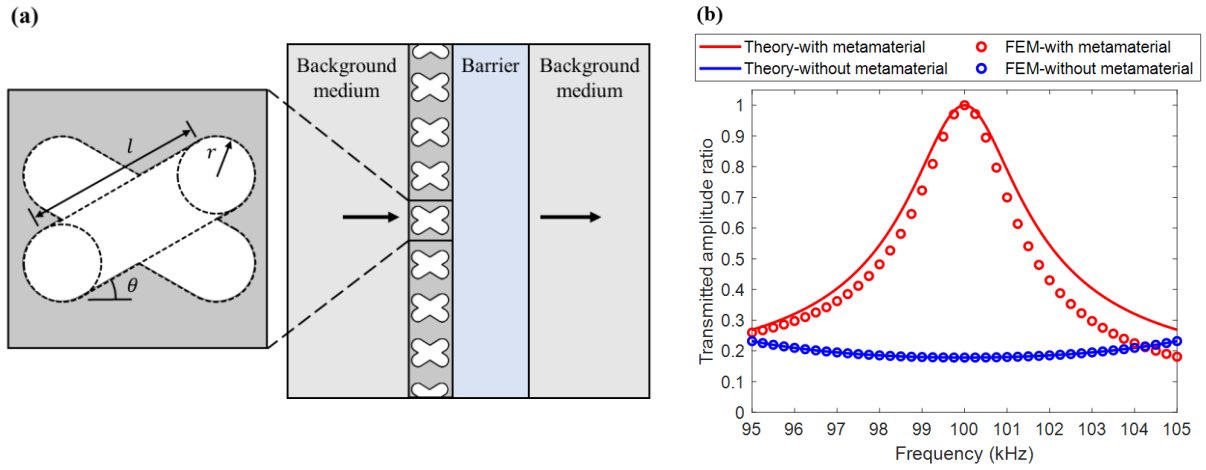

Figure 1 (a) The non-locally resonant elastic metamaterial with X-shaped microstructures. (b) Theoretical (line) and numerical (circle) transmission spectra without (blue) and with (red) the proposed metamaterial.

We consider the propagation of an ultrasonic longitudinal wave through a fluid barrier (water, characteristic impedance of $1.49\text{x}10^6$ kg·m^{-2}·s^{-1}) with a thickness of 33.75 mm sandwiched by solid media (aluminum, characteristic impedance of $1.66\text{x}10^7$ kg·m^{-2}·s^{-1}). The metamaterial has an X-shaped microstructure characterized by three geometric parameters: length (l), width (r), and angle (θ), as shown in Figure 1(a). In Figure 1(b), we present a comparison of transmission spectra with and without the

proposed metamaterial. The results indicate that, in the absence of the metamaterial, the transmitted amplitude ratio at a frequency of 100 kHz is only about 0.17. However, when the metamaterial layer is inserted in front of the barrier, the transmitted amplitude ratio increases to unity (1). To determine the material properties required for the metamaterial to enable full penetration through the barrier, we conducted a wave analysis by using a transfer matrix approach. As a result, we derived the impedance and phase-matching conditions that the material properties of the metamaterial should satisfy. The conditions are expressed as

$$Z_L = Z_B \text{ and } k_L \cdot d_L + k_B \cdot d_B = n\pi \ (n\text{: integers}) \quad (1)$$

where Z_L and Z_B denote the characteristic impedance of the metamaterial and barrier, respectively. k_L and k_B denote the wavenumber of the wave propagates in the metamaterial and barrier, respectively. d_L and d_B denote the thickness of the metamaterial and barrier. From those conditions, the physical properties of metamaterial for full ultrasound penetration can be expressed as

$$\rho = Z_B(n\pi - k_B \cdot d_B)\omega^{-1} \cdot d_L^{-1} \text{ and } C_{11} = Z_B \cdot d_L \cdot \omega(n\pi - k_B \cdot d_B)^{-1} \ (n\text{: integers}) \quad (2)$$

where ρ and C_{11} represent the density and longitudinal stiffness, respectively, of the metamaterial.

III. Numerical and Experimental Results

We designed a metamaterial with an X-shaped micro-structure with a unit cell size of 7mm. The geometric parameters of the metamaterial were determined via a gradient-based optimization technique, considering a normal incidence case at a frequency of 100 kHz. The values of optimized parameters are l = 4.868 mm, r = 2.088 mm, and θ=29.854°. To experimentally validate our finding, we fabricated the designed metamaterial with 21 unit cells and conducted ultrasound experiments, as shown in Figure 2(a). The experimental result in Figure 2(b) shows that the use of the metamaterial increased the maximum magnitude of the transmitted wave signal 2.73 times. Despite the decrease in transmission efficiency attributed to the use of a finite-sized source, both FEM and experimental results were in good agreement. It suggests that the realization of the metamaterial for full ultrasound penetration is now feasible.

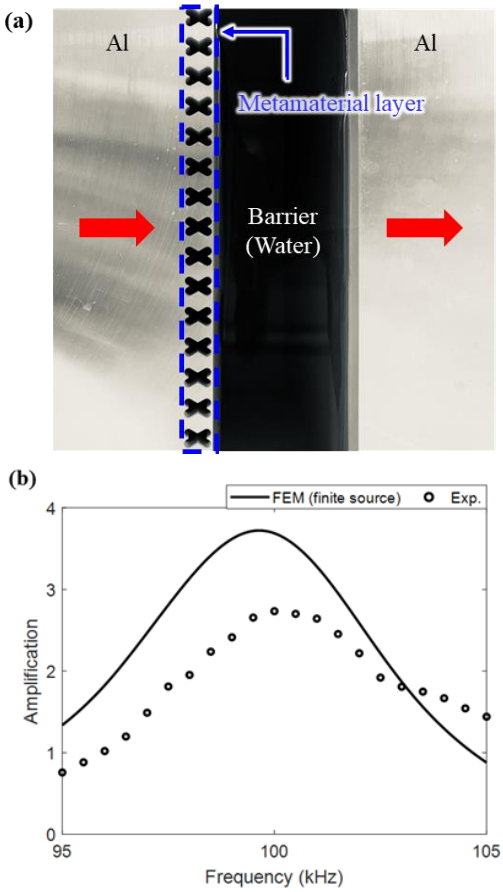

Figure 2 (a) Schematic of experimental setup (b) FEM using finite length of source and experimental frequency responses of transmitted displacement amplification.

IV. Conclusion

This paper presented a novel approach to overcoming the issue of low transmission through the barrier. We demonstrated that full ultrasound penetration through the barrier can be achieved by the insertion of the proposed elastic metamaterial in front of the barrier. Our approach offers a solution to the enhancement of ultrasonic transmission through the barrier by designing non-locally resonant metamaterials with tailored material properties and thickness, even for challenging barriers such as fluids. These findings have far-reaching implications for various applications of ultrasonic wave technology.

References

[1] A. Perot and C. Fabry, *Astrophys. J.* **9**, 87 (1899).
[2] K. Kobayashi, *J. Phys. Condens. Matter* **18**, 3703 (2006).
[3] C. I. Park, C. Piao, H. Lee, Y. Y. Kim, *Int. J. Mech. Sci.* **206**, 106619 (2022).
[4] J. Lee, M. Kweun, W. Lee, C. I. Park,, Y. Y. Kim, *Extreme Mech. Lett.* **51**, 101606 (2022).
[5] J. Lee, J. Park, C. W. Park, S. H. Cho, Y. Y. Kim, *Int. J. Mech. Sci.* **232**, 107655 (2022).

PHONONICS 2023: 6th International Conference on Phononic Crystals/Metamaterials/Metasurfaces, Phonon Transport, and Topological Phononics
Manchester, England, June 12-16, 2023
PHONONICS-2023-0056

Multi-Objective Design Optimization of a Metamaterial-Based Interface

Ana C. A. Vasconcelos[1], Alejandro M. Aragon[2], Dingena L. Schott[1], Jovana Jovanova[1]

[1] Department of Maritime and Transport Technology, Delft University of Technology, Mekelweg 5, 2628 CD Delft, The Netherlands,
a.c.azevedovasconcelos@tudelft.nl, d.l.schott@tudelft.nl, j.jovanova@tudelft.nl
[2] Department of Precision and Microsystems Engineering, Delft University of Technology, Mekelweg 5, 2628 CD Delft, The Netherlands,
a.m.aragon@tudelft.nl

Abstract: Elastic metamaterials have been mostly designed to control structural vibration for a specific frequency range. However, the stresses developed due to the wave propagation are not commonly consider in their design phase. This work proposes a multi-objective design optimization of a metamaterial-based interface to tune its dynamic characteristics, while keeping stresses below the allowed value.

Elastic metamaterials (EMMs) have drawn attention of researchers because of their unique wave control abilities, since they can be designed for steering incident waves at specific directions or to attenuate waves for specific frequency ranges (band gaps)[1]. Such unique features have instigated the development of EMM designs for protecting structures against dynamic loadings[2]; which can range from small applications, for instance, precision machines under external excitations, to large cases, such as fracture caused by a traffic collision.

The iterative design process of such EMMs usually consists of obtaining the dispersion relation (for a resonant unit cell with Bloch-Floquet periodic boundary conditions) or the transmission loss (for a finite structure formed by such unit cells) of different pre-defined resonant geometries until obtaining the band gap at the desired frequency ranges, which can be an extremely time-consuming approach. Besides, the EMM structural integrity during the impact wave propagation is normally not considered into the design process. Therefore, the desired functionality may not be guaranteed under real-time operation.

To overcome the identified limitations of EMM design process, we propose a design optimization through a multi-objective genetic algorithm to tune the EMMs band gaps while keeping the stresses under the allowed level. Instead of calculating the dispersion relation, here we adopt the effective mass density approach, whereby band gaps are identified at frequency ranges where the resonator moves out-of-phase in relation to the applied excitation. These ranges have shown to be associated to negative mass density values[3], which are used to define the first fitness function. Regarding to the EMM mechanical resistance, stresses are calculated by an equivalent static analysis; the dynamic load is replaced by a static load with magnitude equals to the maximum impact force multiplied by a dynamic load factor. Then, the second fitness function is defined as a ratio of maximum von Mises stress to yield stress of the EMM design. Through such optimization, the metamaterial can be used for vibration suppression and noise control of structures undergoing high amplitude impact loads.

References

[1] M. Kadic, G. W. Milton, M. van Hecke and M. Wegener, *Nature Reviews Physics*, **1(3)**, 198–210 (2019).
[2] M. H. Khan, L. Bing, and K. T. Tan, *International Journal of Impact Engineering* **118**, 50–59 (2018).
[3] H. H. Huang, C. T. Sun and G. L. Huang, *International Journal of Engineering Science*, **47(4)**, 610–617 (2009).

PHONONICS 2023: 6th International Conference on Phononic Crystals/Metamaterials/Metasurfaces, Phonon Transport, and Topological Phononics
Manchester, England, June 12-16, 2023
PHONONICS-2023-0057

Data Driven Geometric Design of Biomimetic Minimal Surface Metamaterial for Elastic to Acoustic Band Gaps

Daniel Saatchi[1,2] , Il-Kwon Oh[1,2]

[1] National Creative Research Initiative for Functionally Antagonistic Nano-Engineering, Republic of Korea
[2] Department of Mechanical Engineering, KAIST, Daejeon, Republic of Korea
d.saatchi@kaist.ac.kr, ikoh@kaist.ac.kr

Abstract: Biomimetic minimal surface metamaterials have computational design parameters that can change the geometry of unit cell surfaces, affecting the modes, band gap, and frequencies within the acoustic band structure. The power of data science and data analytics enables the customizable data-driven design of triply periodic minimal surface metamaterials observed in the structures of biological living organisms for versatile wave manipulation applications.

Minimal surface metamaterials are an emerging type of metamaterials that are designed or inspired by the biological structures that are discovered in nature by collecting microscopic image databases, such as Schwarz minimal surface in the shell of weevil beetle's exoskeleton[1] or the hard shell of Echinoidea species living in ocean[2]. Day by day, researchers are discovering more potential applications of minimal surfaces. Triply Periodic Minimal Surfaces (TPMS) have interesting properties that can be customized by adjusting various design parameters, such as the geometrical factors of surfaces and the volume fraction of unit cells. TPMS reportedly have versatile potential applications, such as thermal engineering[3], biomedical developments[4], wave manipulation applications in acoustic metamaterials[5], and phononic crystals[6,7]. The power of data science and data analytics has enabled the customizable data-driven geometric design of TPMS metamaterials. TPMS parameters affect the modes, bandgap, and frequencies in the acoustic band structure, making these metamaterials interesting for acoustic applications. Typically, TPMS has a trigonometric mathematical relationship for its geometry. For instance, the equation for the Schwarz Primitive TPMS in this research is presented in Equation (1).

$$cos(x) + cos(y) + cos(z) = t \tag{1}$$

The parameter *'t'* in Equation (1) changes the surface geometry, gantry, and volume fraction (VF) of the unit cell. The corresponding VFs are measured using computer-aided design software for the corresponding parameter *'t'*. This parameter not only changes both the elastic and acoustic band structures at different frequencies, but also has an inverse relationship with the formation of complete acoustic and elastic band gaps, as shown in Figure 1. The acoustic complete band gap (CBG) appears when the VF increases from 27% in Figure 1a to VF=50%, and it widens as the VF increases to VF=59% shown in Figure 1d. In contrast, the elastic CBG begins to narrow when the VF increases from 27% in Figure 1e to 38% in Figure 1f, where it disappears after the elastic inception point. Furthermore, the elastic partial band gaps (PBG) in the band structure begin to overlap with each other shown in Figure 1g.

These patterns are interesting because sweeping over the parameter *'t'* not only changes the volume fraction, but also causes the elastic and acoustic CBGs to widen or narrow inversely prior to the inception points, and to appear or disappear after the elastic or acoustic inception points.. Another interesting factor about inception points is that they are not identical but define a transitional inception range (TIR) for elastic-to-acoustic band gap conversion. For example, as is apparent from the extracted data from VF=38% to VF=50%, no elastic CBG or acoustic CBG exists. However, the elastic CBG began widening below TIR, and the acoustic CBG began widening above CBG. Lastly, another phenomenon that is attracting attention is the size of the gantry of the unit cell, which changes with the parameter *'t'*. The gantry surface area increases with VF and decreases with a decrease in VF. The elastic CBG appears at a small gantry, while the acoustic CBG happens at a larger gantry.

PHONONICS 2023: 6th International Conference on Phononic Crystals/Metamaterials/Metasurfaces, Phonon Transport, and Topological Phononics
Manchester, England, June 12-16, 2023
PHONONICS-2023-0057

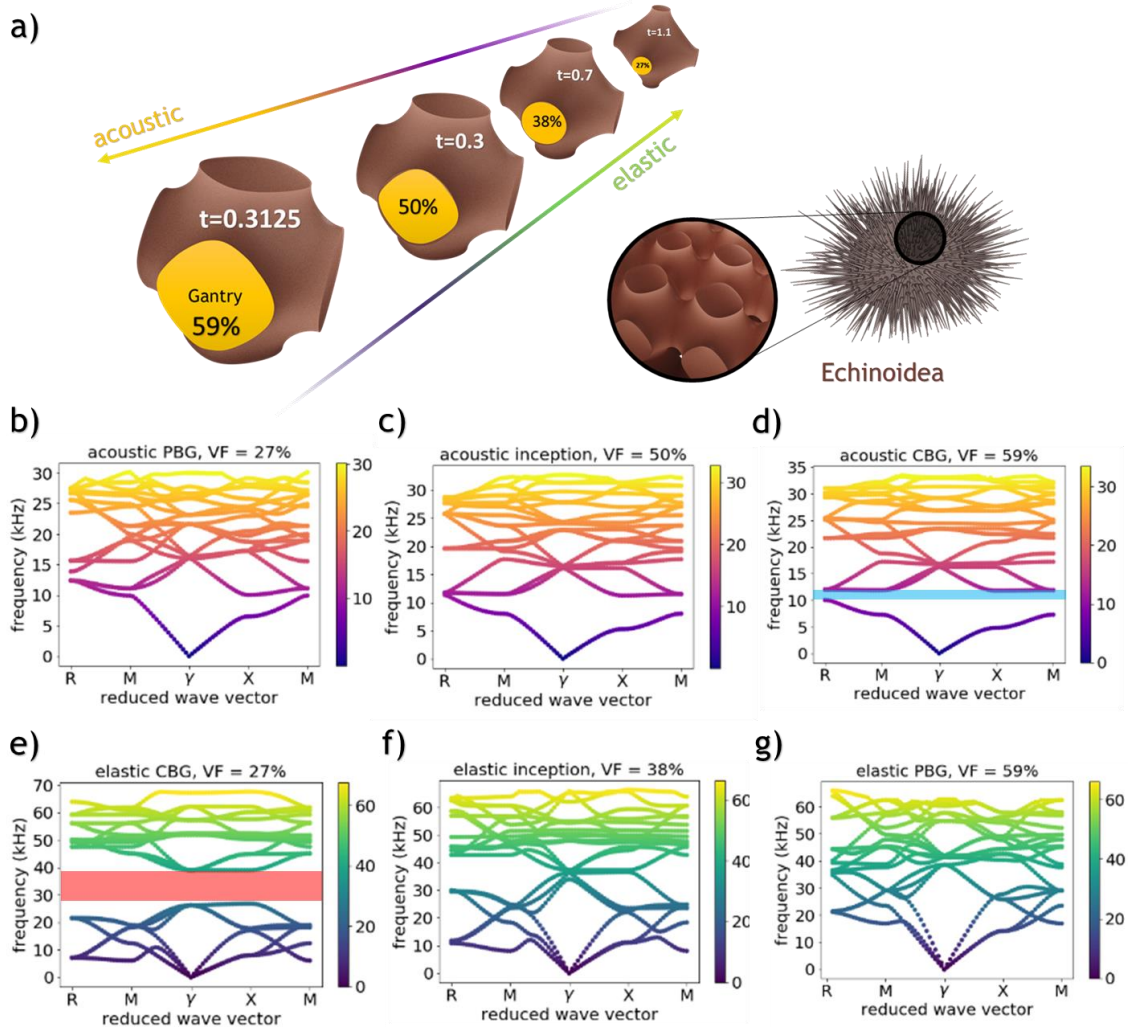

Figure 1 shows the schematics of **(a)** Schwarz-P TPMS unit cells (a=20mm) that exists in the structure of Echinoidea, where the volume fraction (VF) of the unit cell changes with parameter *'t'*. **(b)** Acoustic partial band gap (PBG) with VF=27%. **(c)** Acoustic inception point and appearance of the complete band gap (CBG). **(d)** Widening of acoustic CBG at VF=59%. **(e)** Elastic complete band gap (CBG) at VF=27%. **(f)** Elastic inception point and disappearance of elastic CBG at VF=38%. **(g)** Elastic PBG at VF=59%

References

[1] Galusha, J. W., Richey, L. R., Gardner, J. S., Cha, J. N., and Bartl, M. H. Discovery of a diamond-based photonic crystal structure in beetle scales. Physical Review E, vol. 77, no. 5, 050904, (2008).
[2] M. Lai, A. N. Kulak, D. Law, Z. Zhang, F. C. Meldrum, and D. J. Riley, Chemical communications, (34), 3547-3549 (2007).
[3] Z. A. Qureshi, S. A. B. Al-Omari, E. Elnajjar, O. Al-Ketan, and R. A. Al-Rub, International Journal of Thermal Sciences, 173, 107361 (2022).
[4] E. F. Lehder, I. A. Ashcroft, R. D. Wildman, L. A. Ruiz-Cantu, and I. Maskery, Biomechanics and Modeling in Mechanobiology, 20, 2085-2096 (2021)
[5] Abueidda, D.W., Jasiuk, I., Sobh, N.A. Acoustic band gaps and elastic stiffness of PMMA cellular solids based on triply periodic minimal surfaces. Materials & Design 145, 20-27 (2018).
[6] Chen, Y., Yao, H., Wang, L. Acoustic band gaps of three-dimensional periodic polymer cellular solids with cubic symmetry. Journal of Applied Physics 114, 043521 (2013).
[7] Saatchi, D., Oh, IK. "Implementation of Triply Poly Minimal Surfaces in Design of Phononic Crystals and Acoustic Metamaterials." Proceedings of the ASME 2021 International Mechanical Engineering Congress and Exposition, vol. 1, 72624 (2021).

PHONONICS 2023: 6th International Conference on Phononic Crystals/Metamaterials/Metasurfaces, Phonon Transport, and Topological Phononics
Manchester, England, June 12-16, 2023
PHONONICS-2023-0142

Vibration Control of Beams under the Action of Moving Loads using Inertial Amplifier

Susmita Panda[1], Arnab Banerjee[1], Bappaditya Manna[1]

[1] *Department of Civil Engineering, Indian Institute of Technology, Delhi, India,*
Susmita.Panda@civil.iitd.ac.in , abanerjee@iitd.ac.in, bmanna@iitd.ac.in

Abstract: The vibrations induced under the action of moving wheel loads on bridges, can detrimentally lead to fastener loosening, structural failures that weren't intended, excessive wear, and frequent, expensive maintenance. Hence an attempt has been made in this paper to suppress vibrations of beams under the action of moving loads using metamaterial-inspired inertial amplifiers. Results show that proposed IA designs are capable of reducing the induced vibration due to the passage of moving loads under optimal parameters due to their inherent mass amplification characteristics.

Vibration control of bridges has been a topic of interest in the field of civil engineering for several decades, with a significant amount of research being conducted in this area. Passive techniques such as dampers and isolators[1-3] have been used traditionally to control vibrations in bridges. Dampers are devices that absorb vibration energy, while isolators reduce the transfer of vibration from the ground to the structure. These techniques have proven to be effective in reducing the effects of vibrations, but they have limitations such as high cost, maintenance requirements, and limited performance under extreme loading conditions.

With regard to this problem, inertial amplifiers have recently been explored as a potential technique for the vibration control of bridges. Inertial amplifiers use the principle of mass amplification to reduce the response of structures to dynamic loads. They consist of a mass attached to the structure, which amplifies the dynamic response of the mass, thereby reducing the response of the structure. Inertial amplifiers can be designed to operate in a variety of modes, including tuned mass dampers, tuned mass absorbers, and inertial vibration absorbers. The design of the amplifier depends on the specific requirements of the application.

One advantage of using inertial amplifiers for vibration control is that they are passive, meaning they do not require external power or control systems. Additionally, they are relatively simple and inexpensive to implement compared to other active control techniques.

A simplified mathematical model as shown in Figure 1 is considered for the present study, where the bridge is idealized as a simply-supported beam with an IA system subjected to moving wheel loads. A series of concentrated forces have been considered to represent the wheel loads of a train situated at equal distances. The governing equation of the beam (attached inertial amplifier) under the action of moving concentrated loads can be expressed as follows:

$$M_b \frac{\partial^2 Y_b(x,t)}{\partial t^2} + C_b \frac{\partial Y_b(x,t)}{\partial x} + EI \frac{\partial^4 Y_b(x,t)}{\partial x^4} = F_V(x,t) + F_T(x,t) \quad (1)$$

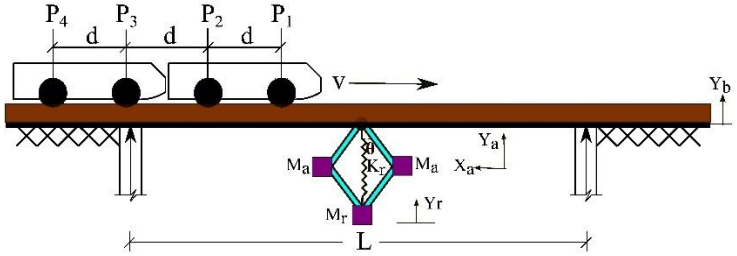

Figure 1 Illustration of a simply-supported beam with attached IA under the action of a series of moving loads.

Where M_b, C_b represents the mass per unit length and damping of the beam, respectively; the bending rigidity is denoted by EI; Q_b is the vertical displacement of the beam at time t at position x.

The force F_V induced under the action of N sequential moving loads P_n can be written as:

$$F_V(x,t) = \sum_{n=1}^{N} \delta\big(x - (vt - d_n)\big).P_n.H(t - t_n) \tag{2}$$

where d_n is the distance between adjacent wheel axles; t_n is the time taken by the n^{th} moving load to reach the left end of the beam; δ is the Dirac delta function; $H(t\text{-}t_n) = H_0(t\text{-}t_n) - H_0(t\text{-}t_n\text{-}L/v)$ defines the position function with H_0 being the Heaviside function to judge whether the moving loads still act on the beam.

For the novel inertial system, the forces can be expressed as

$$F_T = K_r(Y_b - Y_t) + \left(\frac{M_a}{2\tan^2(\theta)}\left(\ddot{Y}_b - \ddot{Y}_t\right) + \frac{M_a}{2}\left(\ddot{Y}_b + \ddot{Y}_t\right)\right) \tag{3}$$

The vertical displacement of the beam can be expressed as the linear combination of modes, using the mode decomposition method as

$$Q_b(x,t) = \sum_{j=1}^{\infty} Y_{bj}(t)\phi_j(x) = \sum_{j=1}^{\infty} Y_{bj}(t)\sin\frac{j\pi x}{L} \tag{4}$$

in which $Y_{bj}(t)$ is the generalized coordinate and $\varphi_j(x)$ is the mode shape/deflected shape of the beam corresponding to the j^{th} mode of the beam. Implementing orthogonality of modes and integrating the entire equation along the span of the beam from 0 to L, we get

$$\frac{\partial^2 Y_{bj}(x,t)}{\partial t^2} + 2\zeta_b\omega_{bj}\frac{\partial Y_{bj}(x,t)}{\partial t} + \omega_{bj}^2\frac{\partial^4 Y_{bj}(x,t)}{\partial x^4} = \frac{\int_0^L \left[F_{Vj}(t) + F_{Tj}(t)\right]\phi_j\,dx}{\int_0^L M_b\,\phi_j^2 dx} \tag{5}$$

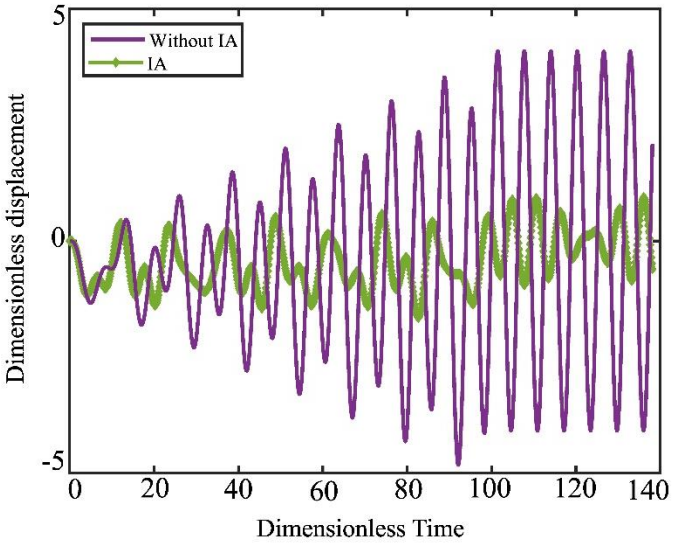

Figure 2 Mid-point displacement of the undamped beam (ζ=0) under the action of (N=8 loads) situated at 25mt moving at speed of 288 Km/h with and without IA.

The optimum parameters of IA are:

Mass ratio = 0.04, Frequency ratio = 0.79 at Θ = 7 degrees.

Using the optimum values of IA, the resulting displacement under the action of N=8 car units has been evaluated using (5) and plotted respectively. It can be clearly noticed in Figure 2 that the mid-point displacement of the beam is greatly reduced by 71%.

In conclusion, inertial amplifiers have shown potential as a technique for vibration control of bridges, particularly in reducing vibrations induced by moving loads. However, further research is necessary to fully understand their effectiveness and limitations in various loading conditions and to optimize their design for specific applications.

References

[1] D. Kwon, H. C., Kim, M. C., & Lee, I. W, Vibration control of bridges under moving loads. *Computers & structures*, 66(4), 473-480. (1998).
[2] Debnath, N., Deb, S. K., & Dutta, A, Multi-modal vibration control of truss bridges with tuned mass dampers under general loading. *Journal of Vibration and Control*, *22(20)*, 4121-4140. (2016).
[3] Chen, Z., Han, Z., Zhai, W., & Yang, J. TMD design for seismic vibration control of high-pier bridges in Sichuan–Tibet Railway and its influence on running trains. *Vehicle system dynamics*, 57(2), 207-225. (2019)

PHONONICS 2023: 6th International Conference on Phononic Crystals/Metamaterials/Metasurfaces, Phonon Transport, and Topological Phononics
Manchester, England, June 12-16, 2023
PHONONICS-2023-0143

Flexural wave propagation of Metamaterial inspired Rigid Elastic metastrcutures

Somya R. Patro[1] , Arnab Banerjee[1], G. V. Ramana[1]

[1] Department of Civil Engineering, Indian Institution of Technology Delhi, New Delhi, India, cez198252@iitd.ac.in, abanerjee@iitd.ac.in, ramana@iitd.ac.in

Abstract: Flexural wave attenuation characteristics of rigid elastic metastrcutures has been studied. Each unit cell comprises of combination of rigid elements and elastic Euler Bernoulli beams. The force displacement relationship between rigid and elastic elements are formulated using Spectral element method and the wave propagation study between each unit cell is done using Bloch Floquet theorem.

In recent years, flexural beams periodically attached local resonators has engrossed researchers from the decades for controlling the vibration in structures[1-3]. Their unique physics properties such as the band gap characteristics of elastic wave possess extensive potential application value in vibration and noise reduction[4,5]. At present, the band gap formation mechanisms can be mainly divided into Bragg scattering (BS) mechanism[6] and local resonance (LS) mechanism[7]. BS bandgap is formed because of the destructive interference and standing wave formation while the wavelength is multiple of the periodicity. Consequently, the wavelength corresponding to the central frequency of the lowest Bragg scattering band gap is about two times of the lattice constant, which is almost difficult to achieve in engineering applications. In order to overcome the application limitation of Bragg scattering band gap in the low-frequency vibration and sound control, the concept of locally resonant periodic structure has been developed which provide low frequency bandgaps due to the simultaneous out of phase motion of multiple resonating units, making dynamic effective mass or effective stiffness of the structure negative in a specific band of the excitation frequency. This lower frequency vibration isolation can be achieved by designing resonators with lower natural frequency, i.e., having heavier mass or lower stiffness. However, lower stiffness and heavier mass are difficult to achieve from a stability perspective. Therefore, researchers are inclined toward designing vibration isolators that can work well in lower frequency ranges without increasing their static mass.

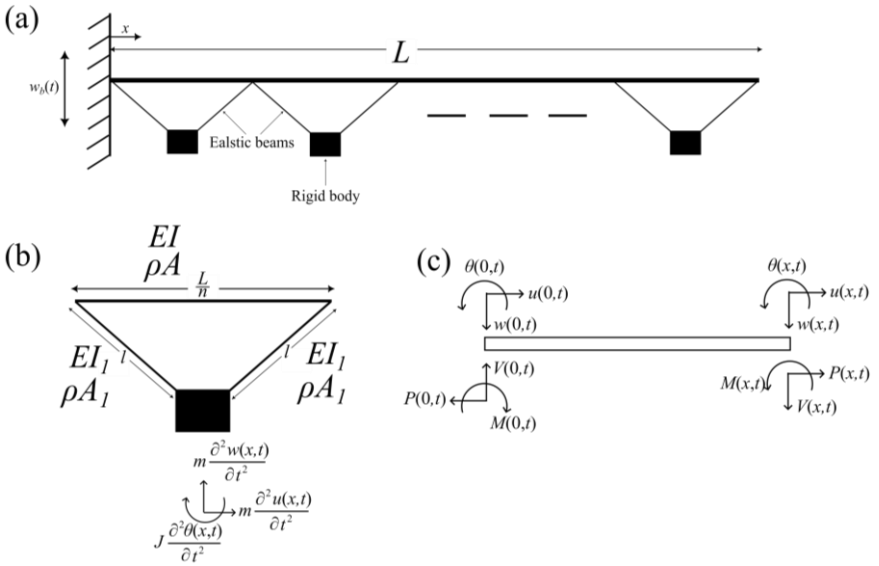

Figure 1 Schematic diagram of the proposed metastructure: **(a)** Infinite periodic structure, **(b)** Unit cell model, **(c)** Free body diagram of a single element.

The need of wider bandwidth has driven the research towards the merging of several bandgaps originated from the different physics, such as use of inertia[8], inertial amplifier[9], periodic resonators[10,11,3,12], negative stiffness[13], etc. The band structure characteristic in infinitely long beam incorporating non-linearity[14], linear variation in mass and stiffness[15,16], geometric variation in beam[17], etc. has been explored in the past. However, no study in the field of wave propagation through the combination of elastic beams and rigid masses considering the finite dimension was reported. Generally to create destructive interference, the varying beam thickness is used, which actually increases the rigidity of beams[18]. If the beams are connected with rigid body, then sudden change of mass, length, and rotary inertia can be observed

which can be used to tailor the dispersion relation. This has motivated us to explore the wave propagation through rigid elastic metastructures.

In this paper, Flexural wave attenuation characteristics of rigid elastic metastrcutures has been studied. Each unit cell comprises of combination of rigid elements and elastic Euler Bernoulli beams. The force displacement relationship between rigid and elastic elements are formulated using Spectral element method. The obtained spectral element matrix has been converted into transfer matrix to obtain the dispersion relationship of one-dimensional periodic structures can be obtained very efficiently by evaluating logarithms of eigenvalues of the transfer matrix of the representative cell using the Bloch Floquet theorem. Both Bragg band and local resonance band is observed due to the periodic interference of the coupled rigid elastic body The proposed model gives a stop band in a frequency range lower than the equivalent classical spring mass resonator. The antiresonance phenomenon in the proposed model facilitates this occurrence of a lower frequency stop band. Future investigation can be carried out to realize the system in practice by developing a system in combination of elastic beam connected with rigid body with mass ratio, length ratio, and rotary inertia as per required band structure.

References

[1] G. Failla, R. Santoro, A. Burlon, and A. F. Russillo, "An exact approach to the dynamics of locally-resonant beams," *Mech. Res. Commun.*, vol. 103, p. 103460, 2020.
[2] A. Dwivedi, A. Banerjee, S. Adhikari, and B. Bhattacharya, "Bandgap merging with double-negative metabeam," *Mech. Res. Commun.*, vol. 122, p. 103889, 2022.
[3] Y. Li, X. Li, and J. Ding, "Broadband low-frequency flexural wave attenuation in beam-type metastructures with double-sides inertial amplified resonators," *J. Vib. Control*, p. 10775463221126930, 2022.
[4] F. Simon, "Long elastic open neck acoustic resonator for low frequency absorption," *J. Sound Vib.*, vol. 421, pp. 1–16, 2018.
[5] A. Banerjee, "Influence of the torsional vibration of the periodically attached perpendicular beam resonator on the flexural band of a Euler-Bernoulli beam," *Phys. Lett. A*, vol. 384, no. 29, p. 126757, 2020.
[6] S. C. Barman, S. Boral, and T. Sahoo, "Bragg scattering of flexural-gravity waves by a series of polynyas in the context of blocking dynamics," *Phys. Fluids*, vol. 35, no. 1, p. 016601, 2023.
[7] R. Santoro, M. Mazzeo, and G. Failla, "A computational framework for uncertain locally resonant metamaterial structures," *Mech. Syst. Signal Process.*, vol. 190, p. 110094, 2023.
[8] Ozmutlu, A., Ebrahimian, M., and Todorovska, M. I., 2018, "Wave Propagation in Buildings as Periodic Structures: Timoshenko Beam With Rigid Floor Slabs Model," J. Eng. Mech., 144(4), p. 04018010.
[9] Frandsen, N. M., Bilal, O. R., Jensen, J. S., and Hussein, M. I., 2016, "Inertial Amplification of Continuous Structures: Large Band Gaps From Small Masses," J. Appl. Phys., 119(12), p. 124902.
[10] Yu, D., Wen, J., Shen, H., Xiao, Y., and Wen, X., 2012, "Propagation of Flexural Wave in Periodic Beam on Elastic Foundations," Phys. Lett. A, 376(4), pp. 626–630.
[11] Xiao, Y., Wen, J., and Wen, X., 2012, "Broadband Locally Resonant Beams Containing Multiple Periodic Arrays of Attached Resonators," Phys. Lett. A, 376(16), pp. 1384–1390.
[12] Banerjee, A., 2020, "Non-Dimensional Analysis of the Elastic Beam Having Periodic Linear Spring Mass Resonators," Meccanica, 55(5), pp. 1181–1191.
[13] Wang, T., Sheng, M.-P., and Qin, Q.-H., 2016, "Multi-Flexural Band Gaps in an Euler–Bernoulli Beam With Lateral Local Resonators," Phys. Lett. A, 380(4), pp. 525–529.
[14] Sugino, C., and Erturk, A., 2018, "Analysis of Multifunctional Piezoelectric Metastructures for Low-Frequency Bandgap Formation and Energy Harvesting," J. Phys. D: Appl. Phys., 51(21), p. 215103.
[15] Banerjee, A., 2021, "Flexural Waves in Graded Metabeam Lattice," Phys. Lett. A, 388, p. 127057.
[16] Hu, G., Austin, A. C., Sorokin, V., and Tang, L., 2021, "Metamaterial Beam With Graded Local Resonators for Broadband Vibration Suppression," Mech. Syst. Signal Process., 146, p. 106982.
[17] Gopalakrishnan, S., and Doyle, J., 1994, "Wave Propagation in Connected Waveguides of Varying Cross-Section," J. Sound Vib., 175(3), pp. 347–363.
[18] Lee, S.-K., Mace, B., and Brennan, M., 2007, "Wave Propagation, Reflection and Transmission in Non-uniform One-Dimensional Waveguides," J. Sound Vib., 304(1–2), pp. 31–49.

PHONONICS 2023: 6th International Conference on Phononic Crystals/Metamaterials/Metasurfaces, Phonon Transport, and Topological Phononics
Manchester, England, June 12-16, 2023
PHONONICS-2023-0148

Vibration attenuation in a mass in mass frictional metamaterial: An analytical investigation

Muskaan Sethi[1], Arnab Banerjee[1], Bappaditya Manna[1]

[1] Department of Civil Engineering, IIT Delhi, India,
muskaansethi1106@gmail.com, abanerjee@civil.iitd.ac.in, bmanna@civil.iitd.ac.in

Abstract: This paper presents a mass in mass frictional metamaterial unit cell for vibration attenuation study. A linear complementary problem (LCP) approach is employed along with Euler's discretization scheme to form a time domain solver to investigate the dynamics of frictional systems. A phase portrait has been plotted to depict the attenuation zone for the proposed metamaterial unit cell.

A mass in mass frictional metamaterial unit cell is considered as shown in Figure 1. Coulomb's law of friction is employed at the interface of the two masses in contact. According to Coulomb's friction law, three states are possible for the two contacting bodies. The mathematical form of Coulomb's friction law is expressed as[2]:

$$|\lambda_T| < \mu\lambda_N \Longrightarrow \dot{g_T} = 0 \rightarrow \text{sticking} \tag{1a}$$

$$\lambda_T = \mu\lambda_N \Longrightarrow \dot{g_T} < 0 \rightarrow \text{backward slipping} \tag{1b}$$

$$\lambda_T = -\mu\lambda_N \Longrightarrow \dot{g_T} > 0 \rightarrow \text{forward slipping} \tag{1c}$$

where λ_T and λ_N represents the tangential friction force and normal reaction force respectively. μ represents the coefficient of friction and $\dot{g_T}$ is the tangential relative velocity between two contact points.

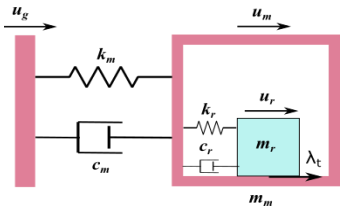

Figure 1 A mass in mass frictional metamaterial unit cell

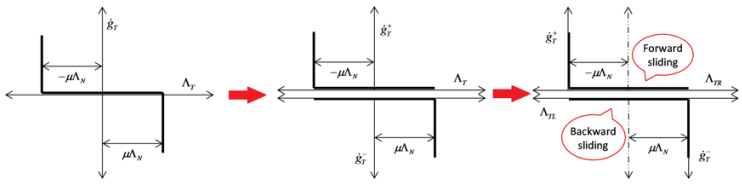

Figure 2 Coordinate transformation to obtain LCP equation from Coulomb's friction law

The complementary form of Eq 1 can be written by applying co-ordinate transformation as shown in Figure 2, which is expressed as:

$$\lambda_{TR}^{T}\dot{g_T^+} = 0 \tag{2a}$$

$$\lambda_{TL}^{T}\dot{g_T^-} = 0 \tag{2b}$$

where,

$$\lambda_{TR} = \mu\lambda_N + \lambda_T \tag{3a}$$

$$\lambda_{TL} = \mu\lambda_N - \lambda_T \tag{3b}$$

$$\dot{g_T} = \dot{g_T}^+ - \dot{g_T}^- \tag{3c}$$

The dynamic equation of motion for a system is expressed as[3]:

$$M\ddot{u} - h - W_N\lambda_N - W_T\lambda_T = 0 \tag{4}$$

Applying Euler's discretization to Equation 4, we get:

$$M\Delta q - h\Delta t - W_N\Lambda_N - W_T\Lambda_T = 0 \tag{5a}$$

$$\Delta q = M^{-1}h\Delta t + M^{-1}W_N\Lambda_N + M^{-1}W_T\Lambda_T \tag{5b}$$

$$\Delta u = (q + \Delta q)\Delta t \tag{5c}$$

where $q = \dot{u}$ and $\Lambda_i = \lambda_i t$. Applying Taylor series expansion yields:

$$g_N^e = g_N + \Delta g_N(u,t) = g_N + \underbrace{\frac{\partial g_N}{\partial u}}_{w_N^T}\Delta u + \underbrace{\frac{\partial g_N}{\partial t}}_{\widetilde{\omega}_N}\Delta t \tag{6a}$$

$$\dot{g_T}^e = \dot{g_T} + \Delta \dot{g_T}(u,\dot{u},t) = \dot{g_T} + \underbrace{\frac{\partial \dot{g_T}}{\partial \dot{u}}}_{w_T^T}\Delta q + \underbrace{\frac{\partial \dot{g_T}}{\partial u}}_{\dot{w}_T^T}\Delta u + \underbrace{\frac{\partial \dot{g_T}}{\partial t}}_{\dot{\widetilde{\omega}}_T}\Delta t \tag{6b}$$

Substituting Eq 5 into Eq 6a and Eq 6b, the final LCP equation takes the form:

$$\begin{bmatrix} g_N^e \\ \dot{g_T^+}\Delta t \\ \Lambda_{TL}\Delta t \end{bmatrix} = \begin{bmatrix} G_{NN} - \mu G_{NT} & G_{NT} & 0 \\ G_{TN} - \mu G_{TT} & G_{TT} & I \\ 2\mu & -I & 0 \end{bmatrix} \begin{bmatrix} \Lambda_N \Delta t \\ \Lambda_{TR}\Delta t \\ \dot{g_T^-}\Delta t \end{bmatrix} + \begin{bmatrix} C_N \\ C_T\Delta t \\ 0 \end{bmatrix} \tag{7}$$

where $G_{NX} = W_N^T M^{-1} W_X$, $G_{TX} = \left(W_T^T + \dot{W}_T^T \Delta t\right) M^{-1} W_X$, $C_N = W_N^T (q + M^{-1} h \Delta t)\Delta t + \widetilde{\omega}_N \Delta t + g_N$, $C_T = \left(G_T h \Delta t + \dot{W}_T^T q \Delta t + \dot{\widetilde{\omega}}_T \Delta t + \dot{g_T}\right)$ and $X \in \{N, T\}$.

The above equations are simplified using non-dimensional quantities corresponding to the various physical quantities. Thus, the above equations are used to build a solver in MATLAB.

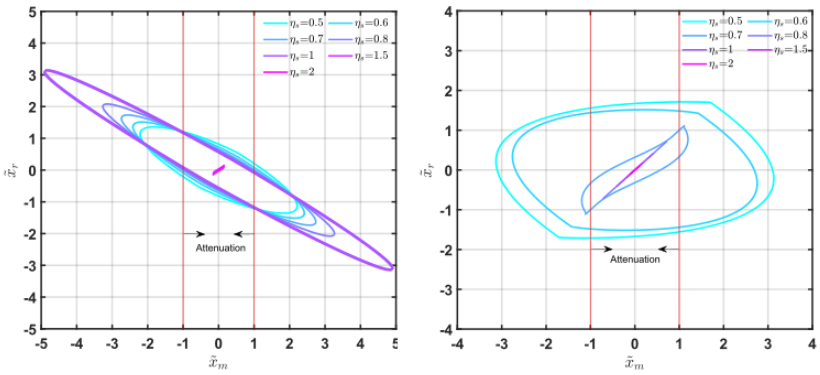

Figure 3 Phase portrait depicting attenuation zone

Figure 3 illustrates the phase portrait of inner and outer mass for non-dimensional maximum frictional force ($\mu\widetilde{\lambda_N}$) equal to 0.3 and 1.0. It can be noticed that the maximum value of $\frac{\widetilde{x_m}}{\theta \eta_s}$, which primarily denotes the transmittance, decreases with an increase in the value of η_s after some threshold value[1]. For example, while the $\mu\widetilde{\lambda_N} = 0.3$, the response increases upto $\eta_s = 1$ and after that the response decreases. On the other hand, amplitude of the motion always shows a declining nature with increasing η_s, once $\mu\widetilde{\lambda_N} = 1$. A transition from out of phase motion, when the phase portrait primarily lie in second and fourth quadrant, to in phase motion, when phase portrait lies in first and third quadrant, can be observed with the increasing η_s. For higher value of η_s, the vibration response in outer mass reduces significantly, which forms the attenuation band gap in the transmittance spectrum. For higher value of η_s primarily the motion is in phase and often inner and outer masses stick to each other, this increases the mass of the system and contributes towards attenuation.

References

[1]Banerjee, M. Sethi, and B. Manna. *Vibration transmission through the frictional mass-in-mass metamaterial: An analytical investigation.* International Journal of Non-Linear Mechanics, page 104035 (2022)

[2]F. Pfeiffer and C. Glocker. *Multibody dynamics with unilateral contacts*. John Wiley & Sons (1996).

[3]R. Leine, D. Van Campen, and C. H. Glocker. *Nonlinear dynamics and modeling of various wooden toys with impact and friction*. Journal of vibration and control, 9(1-2):25–78 (2003)

PHONONICS 2023: 6th International Conference on Phononic Crystals/Metamaterials/Metasurfaces, Phonon Transport, and Topological Phononics
Manchester, England, June 12-16, 2023
PHONONICS-2023-0198

Mathematical Model for Layered Acoustic Materials with Random Particulate Microstructure

Paulo S. Piva[1], Kevish K. Napal[1], Artur L. Gower[1]

[1] *Department of Mechanical Engineering, University of Sheffield, Sheffield, South Yorkshire, UK,*
pspiva1@sheffield.ac.uk, k.k.napal@sheffield.ac.uk, a.l.gower@sheffield.ac.uk

Abstract: Many acoustic metamaterials are composed by layered media, and for the case where the microstructure is made of a random particulate, there is no simple model to deal with the layers. We propose an extension of the quasi-crystalline approximation that leads to clear and simple models, which separate the influence of random microstructure from its material geometry and outward layers.

Introduction

The theoretical framework behind the design of an acoustic material ranges from the fundamental description of sound waves in complex media, heuristic mathematical modelling, and the development of numerical methods. The combination of those three leads to accurate predictions of the acoustic response of complex media, inspiring the design of metamaterials[1].

Layered acoustic metamaterials have been considered in recent literature[2] not just because of its known mathematical description, but also for being easy to test and manufacture. One type of layered media for which a mathematical framework has not been established is the random microstructure case, even though Willis[3] have solved the problem for a half-space.

In this paper, we present an approach to describe pressure waves in layered media with random particulate microstructure. The mathematical modelling takes into account multiple scattering, and it is based on an extension of the Quasi-Crystalline Approximation[4] (QCA), which provides a correction to the problem of canonical scattering by layered media. The model has a compatible numerical method in literature[5], that provides a solution to quantify the average acoustic behaviour for a broad range of frequencies.

General Strategy

We consider the scattering problem of a half-space with different homogeneous acoustic properties for the regions $x < 0$ and $x > 0$, where we defined $\mathbf{r} := (x, y, z)$ in 3D. We fill the region of the half-space $x > \delta$ with a random complex material, and study the scattering problem by an incoming wave from the region $x < 0$, as illustrated in Figure 1 on the left.

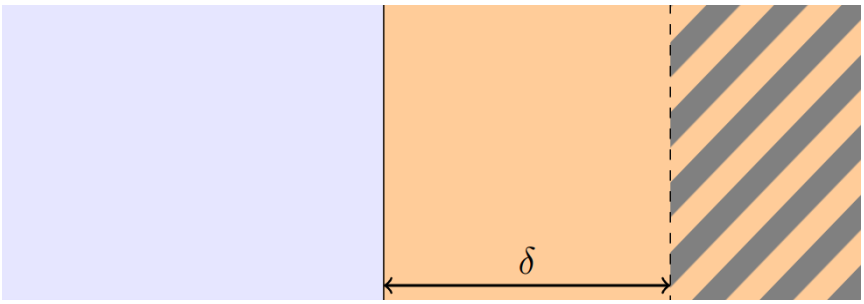

Figure 1 Half-space composed by two different homogeneous acoustic media. The medium on the right is filled with random particulate material on the striped area.

The microstructure of the region $x > \delta$ denoted by σ, which is a random variable for all possible positions and acoustic properties of the small scatterers composing the particulate. For an incoming plane wave, the pressure field is given by

$$u(\mathbf{r}) = \begin{cases} \exp(ikx) + C\exp(-ikx) + \varepsilon_1(\mathbf{r}), & x < 0 \\ A\exp(ik_0 x) + B\exp(-ik_0 x) + \varepsilon_2(\mathbf{r}), & 0 < x < \delta \end{cases} \tag{1}$$

$\varepsilon_{\cdot}(\mathbf{r})$, where represents the non-planar contribution from the random material, is the k

$\varepsilon_{\cdot}(\mathbf{r})$ wavenumber of the region , and is the wavenumber of the region k
k_0 $0 < \delta < x$.

We introduce the particulate scattering operator

$$T_\sigma A := B \tag{2}$$

, that depends on σ. We also attribute a probability distribution for each configuration *p*(σ), for which the average of eq. (1) becomes

$$\langle u(\mathbf{r})\rangle = \begin{cases} \exp(ikx) + \langle C\rangle\exp(-ikx), & x < 0 \\ \langle A\rangle\exp(ik_0 x) + \langle T_\sigma A\rangle\exp(-ik_0 x), & 0 < x < \delta \end{cases} \tag{3}$$

, where $\langle\varepsilon_{\cdot}(\mathbf{r})\rangle = 0$ by construction. Finally, we consider the following approximation in eq. (3)

$$\langle T_\sigma A\rangle \approx \langle T_\sigma\rangle\langle A\rangle \tag{4}$$

, which decouples the microstructure from the boundary effects at $x = 0$, and the problem can be solved with appropriate transmission boundary conditions (TBC).

Application for spherical particles microstructure

We have used the strategy described by Gower and Kristensson[4] to model the operator T_σ for spherical sound-penetrable particles, randomly distributed in any material shape. We also perform an average over self-interaction terms from the multiple scattering pattern, which leads to eq. (4) after performing the full ensemble average. This procedure was found to be equivalent to QCA[4] for a wide range of probability distributions *p*(σ).

The numerical solution for the approach is based on the solution of a dispersion equation depending only on the microstructure and overall symmetry of the medium, which computes all possible modes to be excited by the incident wave. Then, a combination of TBC for the layers, and generalized ensemble boundary conditions[5] determine the amplitude of each excited mode.

An example of the full numerical solution for a sound wave scattered by an infinite cylinder filled with small spherical scatterers (compared with the cylinder radius) is shown in Figure 2 on the left. The incident wave is a plane wave coming from the left with an amplitude of 1, and its wavevector is orthogonal to the boundary of the cylinder. The cylinder has a sound speed and density two times higher than the outside medium, while the spherical scatterers have a small sound speed and density compared with their host medium.

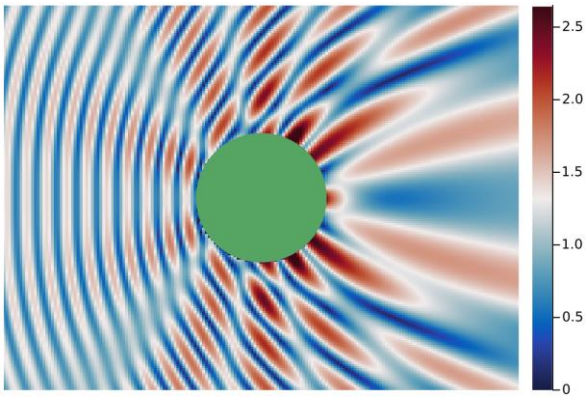

Figure 2 Numerical simulation for the absolute value of the average scattered field due to multiple scattering of small quasi-Dirichlet spherical scatterers inside an infinite homogeneous cylinder (in green). The particles occupy 5% of the volume of the cylinder.

Further work to be considered is the extension of the model for thermal and shear waves, which can be considered by accounting for their coupling with the pressure wave on the surface of all scatterers involved in the problem.

References

[1] Gorishnyy, Taras, Martin Maldovan, Chaitanya Ullal, and Edwin Thomas, *Sound ideas*, Physics World 18, no. 12 (2005).
[2] Mikhail V. Golub *et al.*, *Design and Manufacturing of the Multi-Layered Metamaterial Plate with Interfacial Crack-like Voids and Experimental-Theoretical Study of the Guided Wave Propagation*, Acoustics 2023, 5(1), 122-135 (2023).
[3] J. R. Wills, *Transmission and reflection at the boundary of a random two-component composite*, Proc. of the Royal Soc. A, Vol. 476, Issue 2235 (2020).
[4] Vasundara V. Varadan and Vijay K. Varadan, *The quasicrystalline approximation and multiple scattering of waves in random media*, The Journal of the Acoustical Society of America 77, S3 (1985).

PHONONICS 2023: 6th International Conference on Phononic Crystals/Metamaterials/Metasurfaces, Phonon Transport, and Topological Phononics
Manchester, England, June 12-16, 2023
PHONONICS-2023-0112

Automated design of multiscale mechanical metamaterials

Sara E. Rodriguez[1], Raj Das[1], Emilio P. Calius[2]

[1] *Aerospace Engineering and Aviation, RMIT University, Melbourne, Victoria 3083, Australia, S3761375 @student.rmit.edu.au, raj.das@rmit.edu.au*
[2] *Architectured Materials Program, Computed Materiality, Auckland 0604, New Zealand emilio.calius@computedmatter.com*

Abstract: Non-periodic and topologically heterogeneous metamaterials promise novel capabilities but their complexity makes design challenging. We introduce an evolutionary design framework and present a case study in which new, irregular 2D pentamode architectures are generated. Extreme bulk-to-shear modulus ratios, well above 10^4, are obtained without the point-like connections of the classic pentamode.

While the complexity of metamaterial mesostructures can be almost limitless in theory, in practice metamaterials have tended to be based on periodic structures with a homogeneous topology and materiality. Periodicity and homogeneity limit the number of variables, making the design problem more tractable, but the reduced number of degrees of freedom inevitably constrains the range of functionality that can be achieved, and this is particularly evident when combinations of multiple extrema are sought[1-5].

Discarding the bonds of periodicity and topological uniformity, and varying its constituent mechanical properties, all contribute to considerable expansions of the mechanical metamaterial system design space. However, the concomitant growth in design complexity is a major hurdle, with structure-to-property maps typically being complex hyper-dimensional functions with multiple local optima.

Therefore, the design of non-periodic, multi-material metamaterial structures is critically dependent upon automated design and computing capabilities[6]. Current approaches to metamaterial design automation typically involve the application of computational intelligence techniques that are based on black-box machine learning, whose training presents an expensive and difficult challenge.

Here we present a metaheuristic inverse design approach, using a sequential evolutionary framework to generate designs for multiscale, multi-material metamaterial systems in a 2D square domain. This global domain is discretized into $n \times n$ subdomains or voxels, and each voxel is assigned individual mechanical properties. The Covariance Matrix Adaptation Evolutionary Strategy (CMA-ES) is used to move and reshape a multivariate Gaussian distribution of voxel properties over this n^2-dimensional design space to generate populations of candidates[7]. Voxels whose mechanical properties fall below a certain threshold are considered voids. Although this framework is based on a black-box evolutionary algorithm, the mechanics are incorporated through a finite element model of the structural domain together with the definition of objective functions. Using this model, the evolutionary fitness of the entire population in each generation is evaluated simultaneously using parallel processing[8].

Once mesoscale property distributions have been obtained, the next step in the sequence is to generate structures within each voxel whose effective properties closely match the values established at the mesoscale step. The process takes advantage of the direct encoding of structures at both the mesoscale domain and microscale voxel levels. To accomplish this, voxels are themselves discretized into $m \times m$ tiles, CMA-ES is used to generate a pool of microstructure candidates by optimizing the L2 norm of the effective elastic moduli differences, with selection through a boundary matching process to ensure continuity between adjacent voxels[9]. The selection process is still under development to optimize performance.

This design framework is being tested through a case study on the design of new, irregular 2D pentamode metamaterials. Pentamode metamaterials, which are defined by extreme values of the bulk-to-shear modulus ratio (B/G) ratio, are a particularly interesting test case, not only because of their unique properties but also because they may offer a path to realization of any physically possible stiffness matrix.

The B/G ratios for a range of $n = 10$ designs produced by this evolutionary framework are given in Figure 1. Large B/G ratios, mostly well above our 10^4 target, have been obtained without the point-like connections of the classic pentamode diamond-type lattice. In contrast, the minimum size of connections in the designs shown here is 1/10 of the unit domain size. Figure 1 also shows how evolutionary algorithm parameters such as the population size λ directly affects the sampling of the solution space; with increasing λ the algorithm is more likely to find higher values of B/G and tends to reach the target in fewer generations[8].

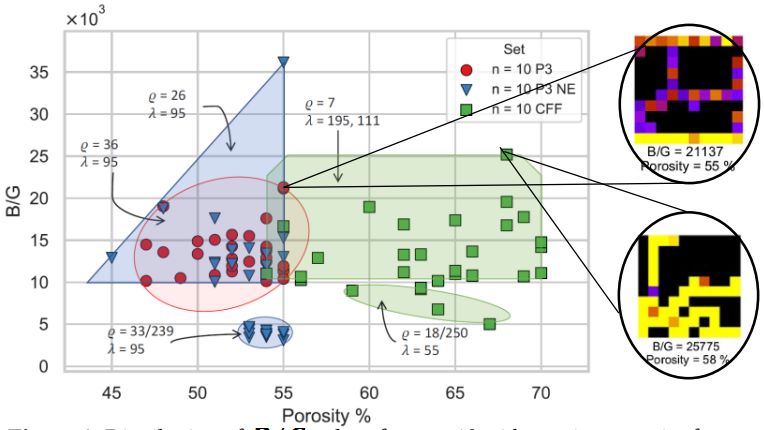

Figure 1. Distribution of B/G values for $n = 10$ with varying porosity for multiple sets of 30 independent evolutionary runs. The scatter plots are grouped by the three major run sets, the population size **λ**, and the number of generations **ϱ** needed to obtain that design solution[8].

Initial results from the voxel microstructure design step are given in Figure 2. Note their regular patterns, the relatively low number of generations need to obtain these solutions and the variety of porosity values.

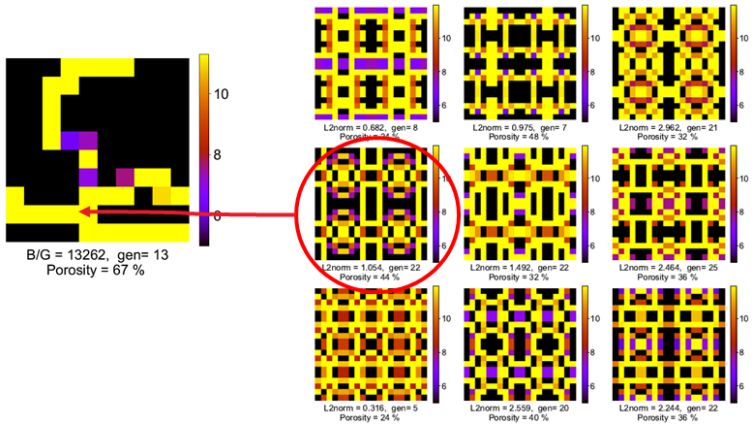

Figure 2. Microstructure optimisation results for a single voxel in the global domain with $m = 20$ and a population **λ** = 195. Nine candidates are shown out of 30 runs of the evolutionary process. The variations in their porosity are driven by different initial normal distributions. The colour bars show the variation of the elastic modulus as a power of 10, i.e. ($10^{✗}$) Pa[9].

References

[1] J. Wang, W. W. Chen, D. Da, M. Fuge, and R. Rai, *Computer Methods in Applied Mechanics and Engineering*, **vol. 396**, pp. 115060, 2022.
[2] J. Panetta, Q. Zhou, L. Malomo, N. Pietroni, P. Cignoni, and D. Zorin, *ACM Trans. Graph.*, **vol. 34** (4), pp. Article 135, 2015.
[3] D. C. Tozoni, J. Dumas, Z. Jiang, J. Panetta, D. Panozzo, and D. Zorin, *ACM Trans. Graph.*, vol. 39 (4), pp. Article 101, 2020
[4] J. Deng, C. B. W. Pedersen, and W. Chen, *Frontiers of Mechanical Engineering*, vol. 14 (2), pp. 129-140, 2019.
[5] Z. Du, and H. A. Kim, In *2018 AIAA/ASCE/AHS/ASC Structures*, Structural Dynamics, and Materials Conference: American Institute of Aeronautics and Astronautics, 2018.
[6] S. Kumar, S. Tan, L. Zheng, *npj Computational Materials*. **6**(1): p. 7, 2020.
[7] N. Hansen, *The CMA evolution strategy: A tutorial*, *arXiv preprint arXiv:1604.00772*, 2016
[8] S. E. Rodriguez, E. P. Calius, A. Khatibi, A. Orifici, and R. Das, *Evolutionary design of novel 2D pentamode metamaterials*, Article under review, 2023
[9] S. E. Rodriguez, E. P. Calius, A. Khatibi, A. Orifici, and R. Das, *Designing pentamodes with structural hierarchy: an evolutionary approach*, Article in preparation, 2023

PHONONICS 2023: 6th International Conference on Phononic Crystals/Metamaterials/Metasurfaces, Phonon Transport, and Topological Phononics
Manchester, England, June 12-16, 2023
PHONONICS-2023-0060

Thermal Rectification using Asymmetrically Perforated Graphene

Markos Poulos[1], Konstantinos Termentzidis[1,2]

[1] *University of Lyon, INSA de Lyon, CETHIL UMR5008, Villeurbanne, 69100, FRANCE, markos.poulos@insa-lyon.fr*
[2] *University of Lyon, CNRS, INSA de Lyon, CETHIL UMR5008, Villeurbanne, 69100, FRANCE konstantinos.termentzidis@insa-lyon.fr*

Abstract: Non-Equilibrium Molecular Dynamics simulations were performed to study thermal rectification effects in perforated graphene monolayers with various geometrical pore parameters. Rectification ratios of the order of 6% have been found.

Controlling the flow of energy carriers has always been of fundamental importance in technological applications. Managing the flow of electric current had been traditionally done by means of electrical conductors and insulators, while the invention of the p-n junction and consequently of the solid-state diodes, transistors and integrated circuits has triggered the technological boom of the last century. The continuous miniaturization and high integration density of micro/nanodevices inevitably results in high heat flux densities, creation of hotspots and consequently to mechanical failure. Therefore, efficient strategies for thermal management at the nanoscale are indispensable for the further technological development of high-power nanodevices. It is well known that heat flow, as opposed to electrical current, is not easily controlled and manipulated. Thermal conductors and insulators have been extensively used as the sole means to control heat currents, but still efficient thermal diodes are not yet fully developed. Various strategies for understanding the principles of thermal diodes at the nanoscale and building them have been recently proposed[1-3]. In this work, we have studied the use of asymmetrically perforated graphene monolayers as a potential candidate that can lead to thermal rectification.

Graphene has captured the interest of the scientific community since its discovery and first isolation due to its exceptional mechanical, electrical, and thermal properties. Thermal transport at the nanoscale presents some peculiarities, as it is not accurately described by macroscopic transfer laws, which mainly describe diffusive transfer. This is a direct consequence of the fact that the heat carriers, mainly phonons, have mean free paths and wavelengths of the same order of magnitude as the characteristic geometrical dimensions of the system under study (ballistic effect), while also hydrodynamic behaviour has been observed in both 1D and 2D structures[4,5]. By creating a nanopore mesh on the one side of a Graphene Monolayer Sheet (GMLS), we create an asymmetry in the structure and phonon distribution, which results in higher heat flow in the direction from the perforated to the pristine side (see figure 1), than the opposite direction.

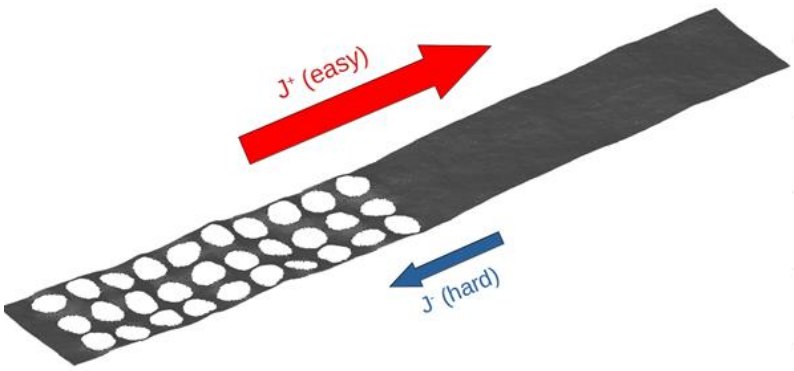

Figure 1 An example of an asymmetrically perforated nanoporous GMLS. The flow of heat is easier from the nanoporous to the pristine region.

In our study we have used Non-Equilibrium Molecular Dynamics simulations to study the presence of thermal rectification in asymmetrically perforated Graphene Monolayers with varying lengths, pore necks and diameters, porosities and porous-to-pristine region ratios. We have found a thermal rectification ratio of the order of 6%. We have also found that the rectification ratio increases by increasing the total system size, by increasing porosity and by decreasing the percentage of the perforated region compared to the pristine one. Although the exact mechanisms responsible for thermal rectification are not clear yet, we can attribute these findings to

the mismatch between the phonon distributions of the two regions created by the perforation. Some of the heat carrying phonons in the pristine side do not match with existing modes in the perforated side, while most of the phonon modes in the perforated side match with modes in the pristine one. This leads to an effective thermal barrier with preferential directionality for phonons flowing from the pristine to the perforated side. These findings shall further contribute to the understanding of the mechanisms of thermal rectification and, by consequence, to potentially optimize the performance of thermal diodes.

References

[1] P. Desmarchelier, A. Tanguy and K. Termentzidis, *Phys. Rev. B* **103**, 014202 (2021).
[2] H. Wang, S. Hu, K. Takahashi, X. Zhang, *Nat Commun* **8**, 15843 (2017).
[3] X-K Chen, M. Pang, T. Chen, D. Du and K-Q Chen, *ACS Appl. Mater. Interfaces* **12**, 15517 (2020).
[4] P. Desmarchelier, A. Beardo, F. X. Alvarez, A. Tanguy and K. Termentzidis, *Int. J. Heat Mass Transf.* **194**, 123003 (2022)
[5] S. Lee, D. Broido, K. Esfarjani and G. Chen, *Nat Commun* **6**, 6290 (2015)

PHONONICS 2023: 6th International Conference on Phononic Crystals/Metamaterials/Metasurfaces, Phonon Transport, and Topological Phononics
Manchester, England, June 12-16, 2023
PHONONICS-2023-0065

Phonon Transport in Defected Bi-Layer Graphene Nano-ribbons

Temitope Boriwaye[1], Jihong Ma[1,2,3,*]

[1] Materials Science Program, University of Vermont, Burlington, Vermont 05405, USA
[3] Department of Mechanical Engineering, University of Vermont, Burlington, Vermont 05405, USA
[4]Department of Physics, University of Vermont, Burlington, Vermont 05405, USA
[*]Corresponding Author: Jihong.Ma@uvm.edu

Abstract: Although it has been experimentally characterized that grain boundaries commonly exist in graphene, the studies of the impact of these grain boundaries are sporadic. In this study, we use non-equilibrium molecular dynamics simulations to investigate the influence of grain boundaries in one of the layers of bi-layer graphene nanoribbons. We demonstrate that, despite being coupled with a pristine graphene nanoribbon, the reduction in thermal conductivity due to the grain boundary is still prominent.

As a high-performance material possessing ultra-high thermal and electrical conductivities, as well as excellent mechanical stabilities, graphene and its derivatives have been commonly considered as promising candidates for various semiconducting applications. For example, by growing graphene on copper damascene structures with foundry's back-end compatible process as the capping layer on wafers, an improvement in the electromigration has been achieved through the graphene capping layer on the copper line [1] With chemical functionalization, graphene has also been proven to enhance adsorbate transport, promoting efficient electromigration [2].

In addition to electromigration, high mechanical stability, and good thermal and electrical performances are also desirable in next-generation interconnects, which allow efficient spread of energy along and across thin films and substrates. Graphene and its derivatives, such as bi-layer graphene and graphene nanoribbons are highly suitable for these applications.

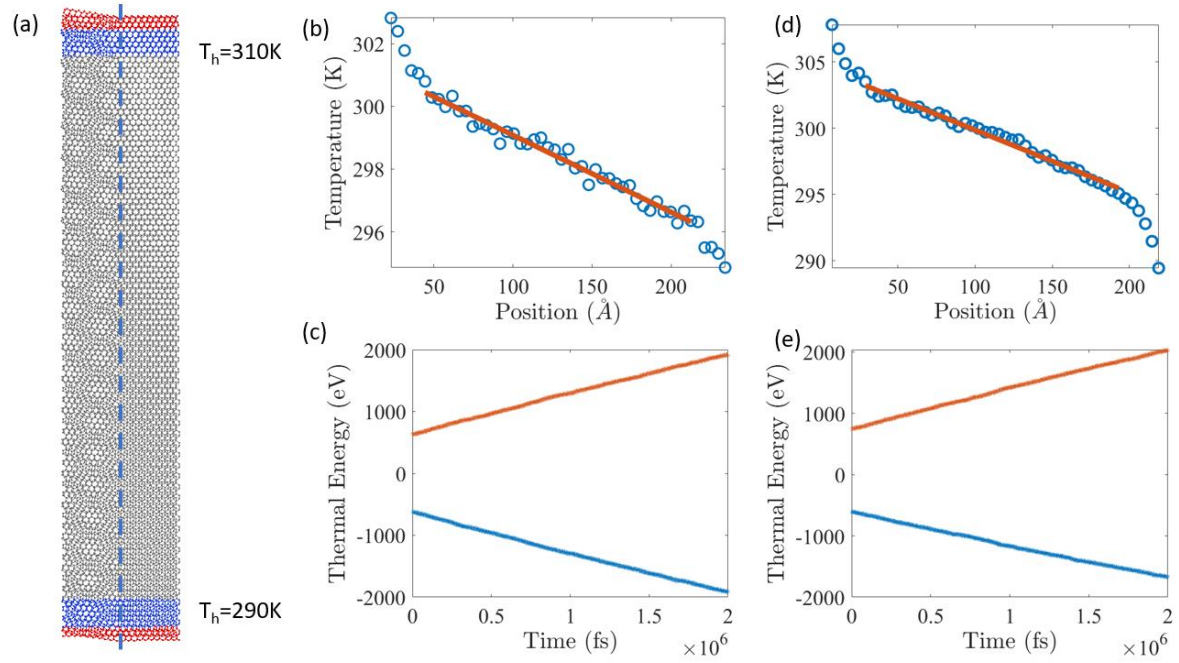

Figure 1 (a) A bi-layer graphene nanoribbon with defected top and pristine bottom layers. Red and blue regions denote the fixed ends and heat reservoirs, respectively. The dashed line denote the line of grain boundaries. (b) and (d): Temperature profiles of the (b) pristine and (d) defected bi-layer graphene nanoribbons. (c) and (e): Thermal energies of the hot and cold reservoirs of the (c) pristine and (e) defected bi-layer graphene nanoribbons.

Despite being investigated for decades since their first discovery, limitations on their applications persist. For example, not until recently, the influence of grain boundaries in monolayer graphene on thermal transport has been understood from an atomistic point of view [3]. Like monolayer graphene, bi-layer graphene also presents a zero bandgap, behaving like a semimetal. Recently, researchers have achieved the fractional quantum Hall effect tuned by an electric field in bi-layer graphene [4]. Moreover, the additional layer induces an extra dimension of tunability. One famous example would be the achievement of superconductivity in twisted bi-layer graphene with a "magic" angle [5], *i.e.*, the Moire pattern.

In this study, we delve into the study of the influence of grain boundaries in one of the two layers of bi-layer graphene nanoribbons, as shown in **Fig. 1(a)**. The grain boundary is formed by a line of periodic 5-7 Stone-Wale defects, which have been shown to present magic stability [6]. An energy optimization reveals that on one side of the grain boundary, the bi-layer graphene still maintains an A-B stacking pattern, while on the other side, a Moire pattern forms.

We then applied the non-equilibrium molecular dynamics simulations to investigate the thermal transport properties along the grain boundaries. Temperature profiles and heat flux calculations show that, compared to pristine bi-layer graphene nanoribbons with the same dimensions, the one with a grain boundary in one of the layers possesses a much lower thermal conductivity. A reduction of 50% in thermal conductivity has been demonstrated.

In conclusion, our molecular dynamics simulations reveal a significant decrease in the thermal conductivity of bi-layer graphene nanoribbons due to the existence of grain boundary, despite having one layer maintaining its pristine form. More details on the phonon analysis of graphene with various sizes and densities of defects are presented in Ref [6].

The authors would like to acknowledge the Semiconductor Research Corporation Contract 2023-PK-3181 for the support of this research.

References

[1] Hung, Y. T., Huang, J. Z., Chang, H. H., Huang, K. P., Lee, O. H., Chiu, W. L., ... & Wu, C. I. (2021, May). Electromigration Improvement by Graphene on Cu Wire for Next Generation VLSI. In *2021 International Conference on Electronics Packaging (ICEP)* (pp. 103-104). IEEE.
[2] Solenov, D., & Velizhanin, K. A. (2012). Adsorbate transport on graphene by electromigration. *Physical Review Letters*, *109*(9), 095504.
[3] Tong, Z., Pecchia, A., Yam, C., Dumitrică, T., & Frauenheim, T. (2021). Phononic thermal transport along graphene grain boundaries: a hidden vulnerability. *Advanced Science*, *8*(18), 2101624.
[4] Kou, A., Feldman, B. E., Levin, A. J., Halperin, B. I., Watanabe, K., Taniguchi, T., & Yacoby, A. (2014). Electron-hole asymmetric integer and fractional quantum Hall effect in bilayer graphene. *Science*, *345*(6192), 55-57.
[5] Cao, Y., Fatemi, V., Demir, A., Fang, S., Tomarken, S. L., Luo, J. Y., ... & Jarillo-Herrero, P. (2018). Correlated insulator behaviour at half-filling in magic-angle graphene superlattices. *Nature*, *556*(7699), 80-84.
[6] Yin, H., Shi, X., He, C., Martinez-Canales, M., Li, J., Pickard, C. J., ... & Zhong, J. (2019). Stone-Wales graphene: A two-dimensional carbon semimetal with magic stability. *Physical Review B*, *99*(4), 041405.
[7] Boriwaye, T. & Ma, J. Phonon Transport in Defected Bi-Layer Graphene Nanoribbons. In Manuscript.

PHONONICS 2023: 6th International Conference on Phononic Crystals/Metamaterials/Metasurfaces, Phonon Transport, and Topological Phononics
Manchester, England, June 12-16, 2023
PHONONICS-2023-0209

Propagation Characteristics of Narrowband Thermal Phonons under Atomic-scale Local Resonance Conditions

Albert Beardo[1], Paul Desmarchelier[2], Chia-Nien Tsai[3], Prajit Rawte[3], Konstantinos Termentzidis[2], and Mahmoud I. Hussein[3]

[1] Department of Physics, JILA and STROBE NSF Science and Technology Centre, University of Colorado and NIST, Boulder, Colorado 80309, USA
albert.beardo@colorado.edu
[2] University of Lyon, CNRS, INSA Lyon, CETHIL, UMR5008, Villeurbane, 69621, France
paul.desmarchelier@insa-lyon.fr, konstantinos.termentzidis@insa-lyon.fr
[3] Smead Department of Aerospace Engineering Sciences, University of Colorado Boulder, Boulder 80303, USA
chianien.tsai@colorado.edu, prajit.rawte@colorado.edu, mih@colorado.edu

Abstract: We investigate the impact of local resonances on thermal phonon propagation in silicon nanostructures at room temperature. Simulating narrowband wave packet propagation, we demonstrate atomic-scale phonon localization explicitly in the space-time domain. Our study sheds light on the interplay between thermal and acoustical properties at the nanoscale and provides insights into the fundamental propagation properties of thermal phonons under local resonance conditions.

Thermal energy conduction in nanostructures involves various atomic-scale phonon mechanisms with a complex interplay between wavelike and particle behavior. While reducing the dimensionality or introducing obstacles to the heat flow in nanostructures can reduce thermal conductivity[1], it can also limit the figure of merit, *ZT*, and the resulting thermoelectric power by affecting the transport of electrons. To address this issue, an alternative strategy is to introduce resonating substructures to the nanosystem to form a *nanophononic metamaterial* (NPM)[2]. These substructures can create standing phonon waves that couple with the in-plane propagating phonons and modify the dispersion relations, reducing the average phonon group velocities, creating mode localizations, and ultimately decreasing the lattice thermal conductivity–all without affecting the electronic properties[3]. In this work, we use narrowband wave-packet excitations to investigate the impact of local resonances on the phonon transport in NPMs at room temperature, and compare with corresponding nanostructures without the local resonances.

In Figure 1. we show the anharmonic phonon dispersion curves for a uniform silicon membrane and an NPM in the form of a nanopillared membrane with the same membrane thickness, both obtained using equilibrium molecular dynamics (MD) simulations and spectral energy density (SED) calculations. We can see that the phonon dispersion relation in the membrane fundamentally changes due to the introduction of the nanopillars. The NPM local resonances, or *vibrons*, which appear as horizontal lines in the dispersion diagram indicate a coupling with the underlying phonon dispersion curves associated with the membrane. This demonstrates the resonance hybridization effect at certain frequencies in the NPM phonon band structure, causing reductions in the group velocities of the heat-carrying modes and phonon mode localizations[1-4]. To further investigate these coherent effects in the NPM, we simulate a narrowband wave-packet propagation[5] around a resonant frequency $\omega = 0.45$ THz and two non-resonant frequencies $\omega = 0.35$ THz and 0.65 THz as shown in Figure 1b and compare it with a similar set of frequencies in the uniform membrane as shown in Figure 1a. The wave packet is excited by perturbing the atoms within a thin vertical layer of the membrane in both systems after establishing equilibrium in the systems at room temperature. The force is polarized in the transversal direction relative to the membrane orientation. After the perturbation, the kinetic energy distribution in the system is monitored to study the propagation of energy as a function of frequency in both systems. In Figures 1a and 1b, we illustrate the propagation of the kinetic energy of the wave packets in both systems. In the absence of nanopillars, for all excitation frequencies, the wave packet propagates at a well-defined velocity in good agreement with the group velocity $(\mathrm{d}\omega/\mathrm{d}k)$ determined by the dispersion relation. In the NPM at the non-resonant frequencies $\omega = 0.35$ THz and 0.6 THz, we obtain the same kind of wave-packet propagation with a well-defined velocity as observed in the uniform membrane. On the other hand, the wave-packet excited at the resonant frequency $\omega = 0.45$ THz is not able to propagate and experiences strong phonon localization effects. This indicates a strong coupling with the standing waves in the nanopillars which prevents the transfer of energy at those specific frequencies through the NPM. This is a

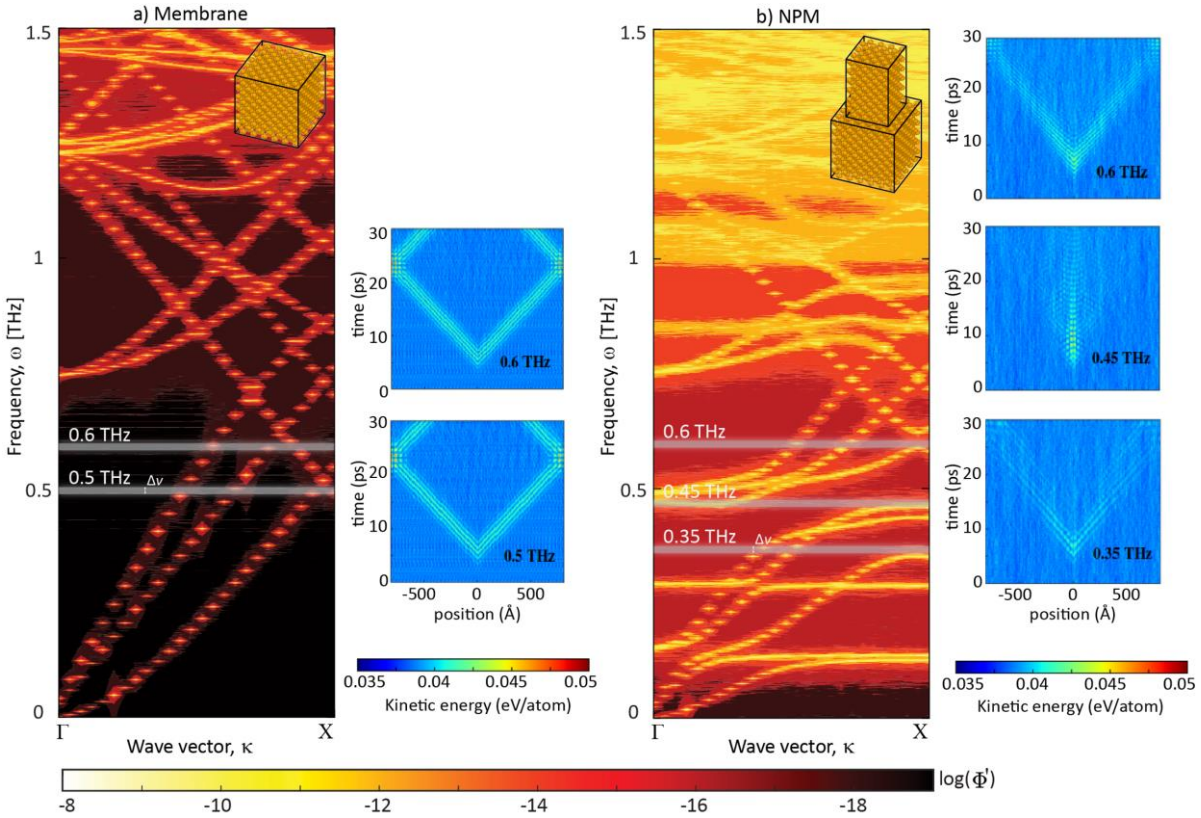

Figure 1. SED phonon dispersion of **(a)** a uniform membrane and **(b)** a membrane-based NPM indicating the effects of anharmonicities on the phonon band structure. The grey lines indicate the frequencies used to simulate a narrowband wave-packet propagation along the membrane and the NPM. The plot of position vs time demonstrates the propagation of kinetic energy of wave-packets at different frequencies along the membrane and the NPM.

consequence of the flattening of the dispersion bands around the resonant frequency in the NPM. This is the first direct demonstration of deterministic phonon localization induced by local resonances at the atomic scale in a system nominally under thermal equilibrium. It is notable that this form of localization is distinct from the well-known Anderson localization mechanism induced by disorder.

Both the localization and velocity reduction hinder the efficient heat conduction in the NPM when compared to the uniform membrane. In the present study, we also calculate the thermal conductivity using the Green-Kubo method and compute the work performed by the external force in the NPM in comparison to the uniform membrane. This emphasizes the role of local resonances in modifying the thermodynamic behaviour of NPMs.

In conclusion, we have computationally demonstrated the presence of phonon localization effects due to wave-packet excitations in an NPM at room temperature. By controlling the wave-packet frequency, we distinguished the role of the local resonances on the thermal energy propagation from other effects also influencing the total lattice thermal conductivity such as phonon-boundary scattering. These observations open up exciting new possibilities for experiments to further unlock and potential of atomic-scale local resonances.

References

[1] D. Li, Y.Wu, P. Kim, L. Shi, P. Yang, and A. Majumdar, *Appl. Phys. Lett.*, **83**, (14), 2934-2936, (2003).
[2] B.L. Davis and M.I. Hussein, *Phys. Rev. Lett.*, **112**, 055505, (2014).
[3] B.T. Spann, J.C. Weber, M.D. Brubakera, T.E. Harveya, L. Yang, H. Honarvar, C.-N. Tsai, A.C. Treglia, M. Lee, M.I. Hussein, and K.A. Bertness, *Adv. Mat.*, 2209779, in press (2023).
[3] H. Honarvar and M.I. Hussein, *Phys. Rev. B*, **97**, 195413, (2018).
[4] H. Honarvar and M.I. Hussein, *Phys. Rev. B*, **93**, 081412, (2016).
[5] A. Tlili, V.M. Giordano, Y.M. Beltukov, P. Desmarchelier, S. Merabia, and A. Tanguy, *Nanoscale*, **11**, 21502-21512, (2019).

PHONONICS 2023: 6th International Conference on Phononic Crystals/Metamaterials/Metasurfaces, Phonon Transport, and Topological Phononics
Manchester, England, June 12-16, 2023
PHONONICS-2023-0083

Sensing 6G Communication Ultra-high Frequency Radio Waves via Phononic Crystal

N.J.Kim[1], Y.J.Shin[1], S.W.Lee[1], H.W.Park[1], M.H.Bae[1], J.H.Oh[1]

[1] *Department of Mechanical Engineering, Ulsan National Institute of Science and Technology, UNIST-gil 50, Eonyang-eup, Ulju-gun, Ulsan 44919, Korea*
njk5261@unist.ac.kr, yjshin0920@unist.ac.kr, lsw6344@unist.ac.kr, ghddnsi@unist.ac.kr, bmh8477@unist.ac.kr, joohwan.oh@unist.ac.kr

Abstract: Ultra-high frequency band should be used for the future 6G communication. However, the existing SAW and BAW filters have limitations because they have to be designed with very small size for the ultra-high frequencies. Here, based on defect phononic crystal, we propose a novel acoustic/elastic wave filter to sense the ultra-high frequency wave while maintaining the thickness of the filter.

In everyday life, mobile communication technology has been tremendous advanced and now advancing toward 6G. However, with the current 5G technology, it is impossible to achieve high speed communication with giant data transmission yet. Although the 5G technology supports both frequency ranges below 6GHz and above 24GHz, the current 5G is only activated below 6GHz due to the lack of technology dealing with high-frequency band. Unfortunately, the frequency range below 6GHz is now almost reached saturation that no more additional communication within this frequency range is possible. Accordingly, there is a rapidly growing need of utilizing the unexplored frequency band, ultra-high frequency band for the future communication technology 5G or 6G[1]. In order to actually implement various future technologies such as telemedicine, autonomous driving and ultra-realistic metaverse, as well as responding to the rapidly increasing traffic usage, 6G communication should use the unexplored band, ultra-high-frequency terahertz band, with a proper technology allowing the usage of this unexplored frequency range.

Among various technical issues that hinder the usage of the unexplored high frequency range, we'd like to focus on the issue related to the frequency filter. Before explaining the technical issue, let us introduce the frequency filter first. To perform mobile data communication, an acoustic/elastic wave-based frequency filter is built in each mobile phone. The main purpose of the filter is to extract the authorized radio signals from various radio signals generated from base stations. This elastic wave-based filter is a type of band pass filter for selecting a specific frequency signal, which temporarily converts electromagnetic wave signals into mechanical vibrations and converts them back into electromagnetic waves through piezoelectric devices and filter them as shown in Figure 1. Surface Acoustic Wave (SAW) filter and a Bulk Acoustic Wave (BAW) filter are the most widely used to sensing the specific radio wave signal. As shown in Figure 2(a), the SAW filter induces a specific wavelength waveguide according to the interval between the cathodes and anodes alternately disposed on the piezoelectric device. Then, as shown in Figure 2(b), the BAW filter generates vibration of a specific frequency using *Fabry–Pérot* resonance according to the thickness of the piezoelectric device disposed between electrodes.

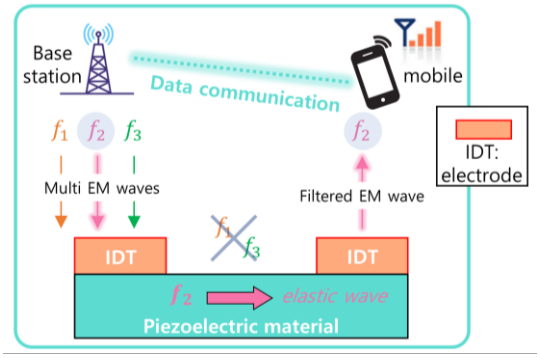

Figure 1 Acoustic/Elastic wave-based frequency filter for mobile communication

Figure 2 A schematic diagram of (a) a SAW filter (b) a BAW filter (c) Size of BAW filter getting smaller in response to higher frequencies

Unfortunately, the frequency filter is facing

technical barrier these days. As the frequency band of communication gradually increases, the wavelength becomes extremely small so that previous methods of SAW and BAW filters are almost impossible to be applied. The SAW filter has difficulty in extremely fine arrangement of electrodes for short wavelengths. Also, the BAW filter also should be designed with extremely thin structure for the shorter wavelength, as shown in Figure 2 (c)[2]. Accordingly, one can easily expect the difficulties in the extremely high precision and the over cost in manufacturing for sensing ultra-high frequency radio wave with elastic wave-based filter.

In this study, we propose a new elastic wave filter that can be applied to ultra-high frequencies, thereby presenting a solution to ultra-high frequency sensing, one of the expected technical challenges to achieve the future 6G communication. While the BAW filter uses *Fabry–Pérot* resonance to pass waves only when the thickness of the filter matches half the wavelength. Under the constant thickness of BAW filter, using the harmonics such as 2nd, 3rd, 4th can be considered instead of the 1st resonance in order to exhibit resonance at the higher frequency. However, the magnitude of the higher harmonic response was negligible compared to the 1st resonance. Here, we propose to apply the principle of defected phononic crystal that can achieve the local focusing of wave energy to extremely amplify the response of higher harmonic resonance. Defected phononic crystal has a flat branch inside the bandgap on the dispersion relation and wave energies are highly focused when a different type of defect is imposed inside a phononic crystal[3,4]. Hence, to implement sensing the high-frequency wave with higher order of *Fabry–Pérot* resonant motion, we additionally designed and placed a periodic lattice around the existing BAW filter depending on the bandgap corresponding to the frequency were the high-order resonance occurs. As such, in this study, we propose an elastic metamaterial-based filter that amplifies the response of higher-order modes with defected phononic crystals while maintaining the thickness of filter, which is expected to be suitable for future communication 6G.

Acknowledgements
This work was supported by the National Research Foundation of Korea (NRF) grant funded by the Korea government (No. 2021R1A4A1033224) and by the National Research Foundation of Korea (NRF) grant funded by the Korea government (No. 2022R1C1C2013024).

References
[1] C. E. Shannon, *The Bell system technical journal*, **27**, 379-423 (1948).
[2] I. El-Kady, R. H. Olsson III, and J. G. Fleming, *Appl. Phys. Lett.* **92**, 233504 (2008).
[3] M. H. Bae, W. Choi, J. M. Ha, M. Kim, and H. M. Seung, *Sci. Rep.* **12**, 3993 (2022).
[4] H. W. Park, H. M. Seung, W. Choi, M. Kim, and J. H. Oh, *Sci. Rep.* **12**, 9714 (2022).

PHONONICS 2023: 6th International Conference on Phononic Crystals/Metamaterials/Metasurfaces, Phonon Transport, and Topological Phononics
Manchester, England, June 12-16, 2023
PHONONICS-2023-0101

Apertures for Generating Spatial Superoscillations of Coherent Acoustic Phonons

Monty E. Clark, Keith A. Benedict, Khouloud Sellami, Andrey V. Akimov, James Bailey, Richard P Campion, and Anthony J. Kent

University of Nottingham, NG7 2RD Nottingham, UK,
monty.clark@nottingham.ac.uk, keith.benedict@nottingham.ac.uk, khouloud.sellami@nottingham.ac.uk, andrey.akimov@nottingham.ac.uk, james.bailey@nottingham.ac.uk, richard.campion@nottingham.ac.uk, anthony.kent@exmail.nottingham.ac.uk

Abstract: In this presentation we discuss the approaches we have taken to design superresolving devices for phonons by exciting an opto-acoustic transducer with a spatially modulated femtosecond-pulsed light beam.

Superoscillation is an interference effect whereby, in specific regions, functions can oscillate faster than their fastest Fourier component. This can be exploited to achieve superresolution, where the diffraction limit may be broken, as has been demonstrated in optical imaging[1].
Our objective was to design an array of standard apertures (holes, discs, annuli) in an optically opaque mask such that the overall diffraction pattern obtained by illuminating the mask with light of a given wavelength generates a superoscillating optical field at the opto-acoustic transducer thereby generating a superoscillating acoustic strain field. Our route to solving the inverse problem of finding the required positions for the apertures in the mask was by aiming to generate a far-field pattern within the broad class of superoscillations constructed by Aharonov[2] with well-characterized Fourier components. A simulation of the acoustic superoscillations generated by a grating pattern, Figure 1(a), is shown in Figure 1(b).
In the pump-probe experiments, gold shadow masks corresponding to the aperture designs were fabricated by optical lithography on the surface of a 5 GHz Ga(Al)As superlattice transducer, Figure 1(c). Where the pump light fell on gold it was reflected leaving a spatially modulated light intensity distribution on the transducer. The spatial distribution of the 5 GHz phonon signal intensity on the opposite side of the 450 micron-thick GaAs substrate was measured using a scanning probe beam, Figure 1(d).
Further work is being done to generalise the solving process by using overlap integrals to resolve both aperture widths and offsets.

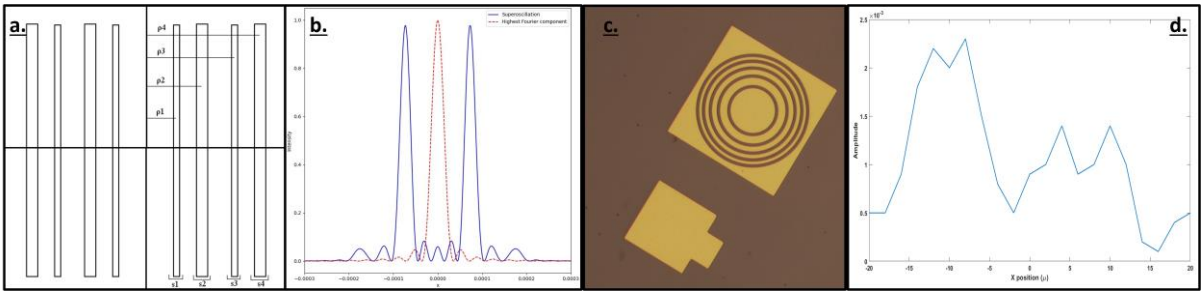

Figure 1: (a) Designs for a diffraction grating superoscillating aperture array. **(b)** Simulated results in natural units for the design in **(a)** with a phonon wavelength of approximately 1µm. The orange dashed line shows the simulated intensity distribution of a single slit compared to the solid blue line of the superoscillating aperture array. As can be seen there are features smaller than the highest Fourier component, a superoscillation. **(c)** A gold shadow mask for the opto-acoustic transducer in the shape of the superoscillating concentric annuli aperture array described by Torlado di Francia[3], examined by Cox et al[1] and produced by us using optical lithography. **(d)** Results from an initial investigation of the design in **(c).** Due to noise and acoustic anisotropy, it is difficult to resolve the superoscillation.

References

[1] I. J. Cox., C. J. R. Sheppard, and T. Wilson. *JOSA* **72**, (no. 9), 1287-1291 (1982)
[2] Y. Aharonov, F. Colombo, I. Sabadini, T. Shushi, D. C. Struppa, and J. Tollaksen, *Proceedings of the Royal Society A*, 477(2249), p.20210020 (2021)
[3] G. Toraldo di Francia, *Atti della Fondazione "Giorgio Ronchi"* **7**, 366-372 (1952)

PHONONICS 2023: 6th International Conference on Phononic Crystals/Metamaterials/Metasurfaces, Phonon Transport, and Topological Phononics
Manchester, England, June 12-16, 2023
PHONONICS-2023-0210

Design of 3D Printable Phononic Subsurfaces based on Locally Resonant Elastic Metamaterials

Adam R. Harris[1,2], Thomas Calascione[1], John A.N. Farnsworth[1], Mahmoud I. Hussein[1,2,3]

[1] *Department of Aerospace Engineering Sciences, University of Colorado Boulder, Boulder, CO 80303, USA*
[2] *Materials Science and Engineering, University of Colorado Boulder, Boulder, CO 80303, USA*
[3] *Department of Physics, University of Colorado Boulder, Boulder, CO 80302, USA*
adam.harris@colorado.edu, thomas.calascione@colorado.edu,
john.farnsworth@colorado.edu, mih@colorado

Abstract: Phononic materials such as phononic crystals and locally resonant elastic metamaterials have become increasingly relevant over the past few decades for their applications in a broad range of disciplines, from seismic wave protection to ultrasound imaging. An intriguing application that emerged in recent years is the use of phononic materials for passive flow control through the notion of a *phononic subsurface* (PSub)[1]. A PSub can be designed to intervene with flow instabilities in a desired manner, enabling favorable effects such as reduction of skin-friction drag. Here, a 3D-printable model of an elastic metamaterial-based PSub is proposed and its dynamical characteristics relevant for flow control are provided.

A PSub is an elastic structure that *passively* interacts with a flow via controlled small vibrations at the fluid-structure interface[1]. A PSub may comprise several unit cells with carefully tuned dispersion properties and finite-structure truncation characteristics. Nominally, this structure is oriented to enable elastic wave propagation in the wall-normal direction as demonstrated in Fig. 1. Excitations stemming from flow instabilities will excite the PSub structure; meanwhile the structure is designed to resonate out of phase with these excitations causing their attenuation by destructive interferences. This in turn may delay or prevent the flow's transition to turbulence and reduce skin-friction drag. Alternatively, a PSub can be designed to constructively interfere with the flow and generate destabilization, which is useful for other functions such as the delay or prevention of flow separation or the enhancement of chemical mixing or wall heat transfer. The design of the PSub may be done offline following a set of theoretical considerations.

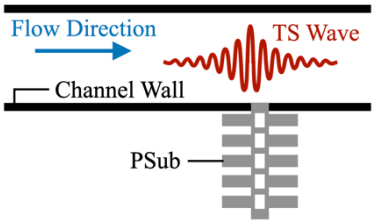

Figure 1 2D schematic of a MM-based PSub installed to a flow channel. The top surface of the PSub replaces a section of the channel's bottom wall allowing elastic waves within the PSub to couple with unstable Tollmien-Schlichting (TS) waves in the flow.

PSubs have previously been configured to utilize either Bragg-scattering[1,2] or local resonance[3] considering that each has unique dispersion and frequency response characteristics, including tunable band gaps and resonant structural frequencies. A design limitation for phononic-crystal-based PSubs is their long length which prohibits its practical implementation. This can be addressed via a coiled phononic-crystal design or through the use of an elastic metamaterial (MM). A key advantage of MM-based PSubs is the ability to tune their properties within the elastic subwavelength regime.

Varying the material parameters of the PSub such as density, elasticity constants, and damping properties in addition to manipulating the geometry of the PSub's unit cell gives the designer the ability to "program" the PSub for operation at any desired frequency or range of frequencies.

In Fig. 2, a 1D discrete mass-in-mass MM unit cell is shown in (a) and a corresponding 3D realization is demonstrated in (b). The 3D unit cell is constructed entirely from ABS polymer and employs horizontal pillars to mimic the resonator masses in the discrete

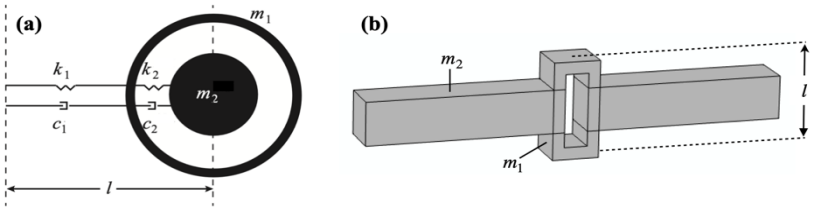

Figure 2 Metamaterial unit-cells of the **(a)** discrete 1D lumped-parameter model where m, k, and c are the mass, stiffness, and damping, respectively, and **(b)** equivalent 3D elastic model. In both models, m_1 is the chained mass while m_2 is the resonator mass.

model, while a hollow central column mimics the chained mass in the discrete model. Five unit cells of the form shown in Fig. 2(b) are stacked on top of each other to create the complete PSub (Fig. 3). Due to the dominance and tunability of local resonance in the frequency response of the structure, the PSub performance may be dictated primarily by adjusting the dimensions of the resonator pillars in the 3D model while leaving the dimensions of the central hollow column constant.

The response characteristics of the PSub model were obtained using COMSOL[4] and are shown in Fig. 4. These include the unit-cell dispersion, followed by the frequency and phase response functions when a harmonic point force is applied on the top of the PSub and a fixed boundary condition is prescribed at the bottom. The displacement amplitude and phase are measured at the same position on the PSub where the harmonic force is applied. Note that the displacement amplitude is normalized by the maximum displacement amplitude at this point. The fourth plot shows the performance metric (PM), which is the product of the normalized displacement amplitude and the displacement phase. Negative PM regions reveal flow instability wave frequencies where stabilization by the PSub will occur, while positive regions correspond to destabilization.

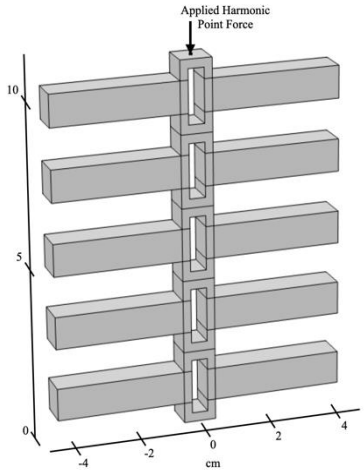

Figure 3 3D MM-based PSub consisting of 5 unit cells. Each unit-cell length is 2.25 cm, the width is 9 cm measured from resonator ends, and the thickness is 1 cm everywhere.

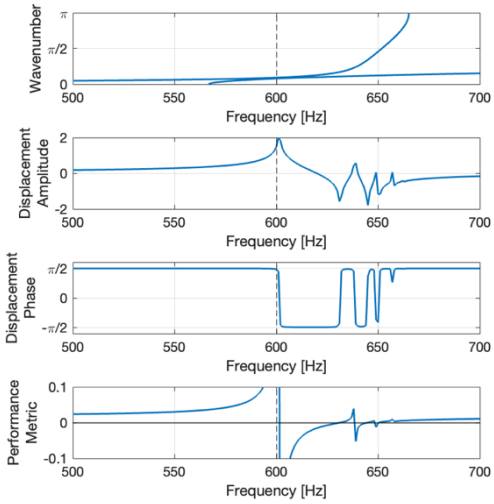

Figure 4 Plots of dispersion, displacement amplitude, displacement phase, and performance metric for the MM-based PSub tuned to control an instability with a frequency near 600 Hz.

In practice, PSubs are tuned to a target resonant frequency that matches the known frequency of an instability in the flow. Here, our PSub is tuned to a flow instability frequency of 600 Hz and yields a negative PM region spanning approximately 600-630 Hz. While this negative PM region is rather narrow, this design demonstrates the ability to produce a resonant frequency anywhere from 250 to 5000 Hz based on the tuning of the resonator pillars. This implies that the proposed PSub design layout could be used to target flow instabilities anywhere within this frequency range.

References

[1] M.I. Hussein, S. Biringen, O.R. Bilal, and A. Kucala, *Proc. R. Soc. A* **471**: 20140928 (2015).
[2] C.J. Barnes, C.L. Willey, K. Rosenberg, A. Medina, and A.T. Juhl, AIAA Scitech 2021 Forum, AIAA 2021–1454 (2021).
[3] A. Kianfar, M.I. Hussein, arXiv:2302.14330 (2023).
[4] COMSOL Multiphysics Structural Mechanics Module, COMSOL Inc., Burlington, MA USA.

PHONONICS 2023: 6th International Conference on Phononic Crystals/Metamaterials/Metasurfaces, Phonon Transport, and Topological Phononics
Manchester, England, June 12-16, 2023
PHONONICS-2023-0211

Phononic Dispersion Coupling as Flowmeter

S. Hales Swift[1], Ihab F. El-Kady[1]

[1] *Photonic and Phononic Microsystems Department, Sandia National Laboratories, Albuquerque, NM, USA, shswift@sandia.gov, ielkady@sandia.gov*

Abstract: Flow sensors are common features on the exterior of flight vehicles; however, for vehicles that face reentry or other harsh flight environments, a simple pitot tube may not survive with uninterrupted functionality. We present a method to employ interior sensors to the problem of detecting flow velocity in harsh environments by examining the excitation of A0 modes of an instrumented test plate.

Sensors to detect airspeed are ubiquitous on flight vehicles. These often take the form of pitot tubes, the forward pointing protrusions seen on aircraft ranging from CESNAs to the SR-71 Blackbird. However, there is not one on the space shuttle or other vehicles that face the environments associated with reentry because they aren't suited to those conditions. It would obviously be beneficial to have a means of measuring airspeed in flight for these vehicles as the popularity of these sensors in other flight contexts has confirmed their usefulness, but how can this best be accomplished?

One approach which has been examined recently at Sandia National Laboratories is to use the structure itself, and its relationship to the excitation produced by passing flow, as a means of measuring the velocity. As a preliminary numerical example of how this can be done, consider a 3-mm steel plate. The 1-D dispersion can be calculated in the usual way be applying Bloch-Floquet boundary conditions and calculating the associated eigenfunctions (modes) and eigenfrequencies as a function of wavenumber. The dispersion relations for the first ten modes are shown for k between 0 and 10,000 in Figure 1. The phase speed, important for coupling between the flow and the Lamb modes of the plate, is given by $v_p=\omega/k$. Conveniently, the A0 mode can travel at any velocity between 0 and roughly 2,890 m/s, which takes care of the possibilities between roughly Mach 0 and Mach 8.4. Also, very conveniently, it is the only mode with sufficiently low frequency and low phase velocity to couple with the flow at lower speeds with the only mode with comparable frequency coverage, the S0 mode, exhibiting a phase speed greater than 5,000 m/s at low frequencies.

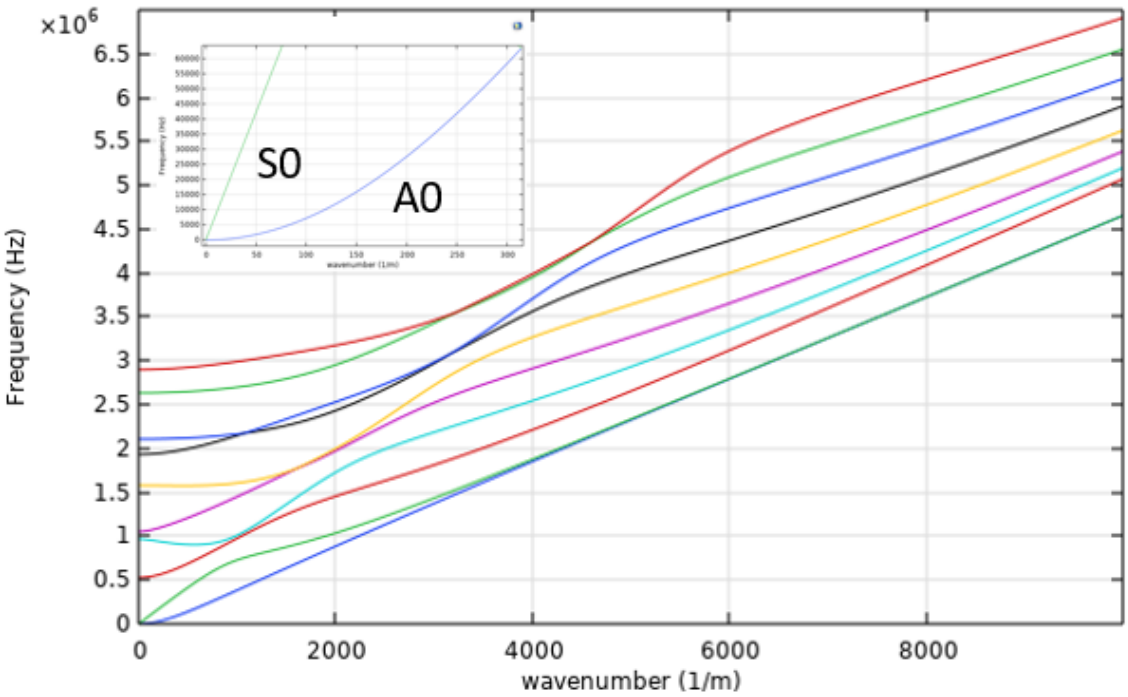

Figure 1: Phononic dispersion relations of a 3-mm steel plate for k between 0 and 10,000. (Inset) detailed look at the A0 and S0 modes.

The relationship between phase velocity and frequency is shown in Figure 2 for velocities from zero to around 1200 m/s and the corresponding frequencies between 0 and around 60000 Hz.

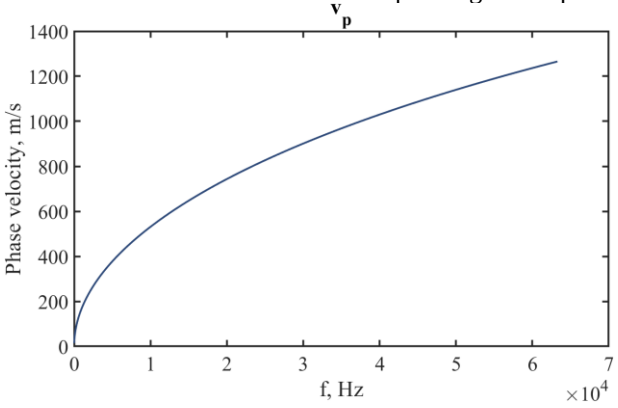

Figure 2: Phase velocity is shown for the A0 mode of a 3-mm thick plate as a function of frequency.

To provide a preliminary proof of concept for this approach, we simulate a plate with 2-m length and 3-mm thickness in COMSOL. Low-reflecting boundary conditions were applied at the left and right ends of the plate to minimize reflections. A boundary load was applied along the upper surface of the plate at each of the designated frequencies with phase designed to duplicate the coherent convection of turbulent pressure fluctuations at the stipulated flow rate. If acoustic fluctuations were present traveling in the downstream direction they would be expected to travel at the convective velocity plus the acoustic velocity relative to the plate. Both acoustic and turbulent pressure fluctuations can impose boundary loads and thus can be considered using this approach.

Taking a sampling of frequencies between 4,000 Hz and 17,000 Hz, spaced by thousands, the vertical motion of the plate, as represented by an integration over the vertical displacement, and is shown in Figure 3. The response peaks near the A0 phase speed for each frequency. This then provides the basis for a velocity inversion procedure in which the frequency response of the plate can be used to estimate velocity. Although low-reflecting boundary conditions were used in this model, provided an appropriate range of frequencies are utilized peculiar boundary conditions on the plate should not necessarily be a problem as long as the response of the structure is appropriately calibrated. The balance between A0 and S0 modes (available if sensing is performed using an array using wavenumber spectra) can additionally be used as a proxy estimate of the coherence of the excitation and thus provide additional information about the external flow.

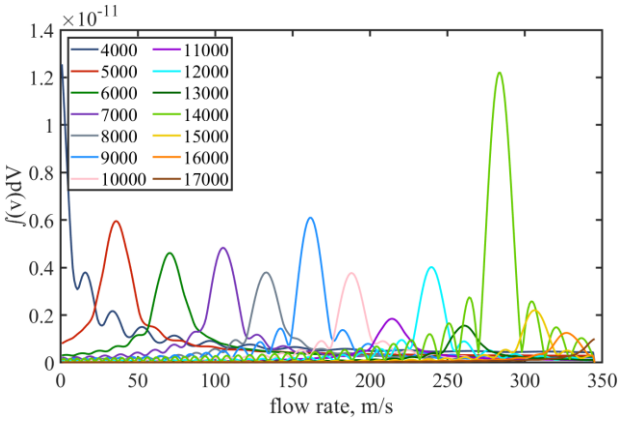

Figure 3: The response of a plate with to convecting boundary loads at frequencies between 4000 and 17000 Hz is shown for convective velocities between0 and 350 m/s. Low absorbing boundary conditions were used with a plate of 2 m.

Sandia National Laboratories is a multimission laboratory managed and operated by National Technology and Energy Solutions of Sandia, LLC, a wholly owned subsidiary of Honeywell International, Inc., for the U.S. Department of Energy's National Nuclear Security Administration under contract DE-NA0003525.

PHONONICS 2023: 6th International Conference on Phononic Crystals/Metamaterials/Metasurfaces, Phonon Transport, and Topological Phononics
Manchester, England, June 12-16, 2023
PHONONICS-2023-0094

Flat Band Induced Topological Tamm States in One-Dimensional Comb-like Structures

S. Khattou[1], Y. Rezzouk[1], M. Amrani[1], M. El Ghafiani[1], E. H. El Boudouti[1], A. Talbi[2], Y. Jin[3], B. Djafari-Rouhani[2]

[1]LPMR, Département de Physique, Faculté des Sciences, Université Mohammed I, Oujda, Morocco
[2]CNRS – Univ. Lille - UPHF - Ecole Centrale – JUNIA, UMR 8520 -IEMN - F-59000 Lille, France
[3]School of Aerospace Engineering and Applied Mechanics, Tongji University, 200092 Shanghai, China
corresponding author: bahram.djafari-rouhani@univ-lille.fr

Abstract: We study Tamm interface states at the boundary of two 1D phononic or photonic crystals consisting of comb-like structures. We propose a new mechanism of band inversion symmetry, at the origin of the topological nature of the interface modes, which is based on the existence of flat bands. The demonstrations are based on the Zak phases of the bulk bands or the phase of the reflection coefficients.

Interface states at the boundary of two phononic crystals (PnCs), also called acoustic Tamm states, have been studied in several structures. In particular, in one-dimensional PnCs consisting of superlattices[1], pillars on a beam[2] or comb-like structures as shown in Fig. 1(a)[3], some papers have demonstrated the topological nature of the interface modes by using the well-known Su-Schrieffer-Heeger (SSH) model where each unit cell is composed of two different resonators. The existence of the interface mode is insured by a mechanism of band inversion symmetry around a common gap of two topologically different crystals. This gap is opened in the vicinity of a Dirac cone when the two resonators are identical.

The objective of this work is to propose a different mechanism of symmetry inversion induced by the existence of a flat band, namely around a frequency where the width of a passband decreases until zero before increasing again. In the proposed structure (Fig. 1(a)), each PnC is constituted by a periodic array of stubs of length d'_1 with a period d_1. We chose the latter as the unit of length. Figure 1(b) displays (in dimensionless frequency $\Omega = \omega d_1/v$ where v is the velocity of sound in air) the band structure of the PnC as a function of d_1. The limits of the passbands are highlighted by bold lines where pink and cyan colors indicate the symmetric or antisymmetric character of the band edge modes, respectively. Also, the Zak phase of each bulk band is directly related to the above symmetries and can take the values of 0 or π depending on whether the edge modes of a given band have the same or a different symmetry. These bulk bands are respectively hatched with gray or dark cyan colors according to the value 0 or π of the Zak phase. In Fig. 1(b), one can observe that at the points labeled 1 and 2, the passbands close and reopen which is a signature of a flat band at the corresponding geometrical parameters and frequency. These flat bands originate from the local resonances of the stubs in the PC. Since the edge modes of two bands in the vicinity of a flat band have the same symmetry, one can easily select around a flat band two PnCs with different periods exhibiting a common band gap such that the band edges of their lower passbands have two different symmetries. Such a gap necessarily supports a topological interface mode. All the conclusions about the possibility of existence of interface states based on the symmetry argument for different configurations in Fig. 1(a) is summarized in Table 1. As an illustration, we plot in Fig. 1(c) the transmission coefficient for a finite PnC made of two connected PnCs (PnC1-PnC3) (with d_1=0.2 and d_1=1 respectively) versus Ω. One can see that the interface state (labeled T) appears as a transmission peak inside the common bandgap (gray area) at the dimensionless frequency Ω = 1.18.

Although we focused our attention on phononic PnCs, similar demonstrations can be easily extended to other comb-like structures such as photonic[4] or plasmonic metal-insulator-metal waveguides[5] with attached stubs. In particular, a simple experimental proof of the above behaviors can be realized by using coaxial cables working in the radio-frequency range (around 100 MHz)[4]. An illustration is given in Fig. 1(d) when we plot the transmission coefficient for a finite PC made of PC1-PC3, each one being composed of N = 2 stubs. The stubs have the same lengths as in Fig. 1(c), but in meter. Blue and green dashed lines represent the theoretical results without and with loss, respectively, while open

circles give the experimental measurements. The interface state appears as a Fano resonance in the common bandgap around 117 MHz. The experiment reproduces well the theoretical result with loss.

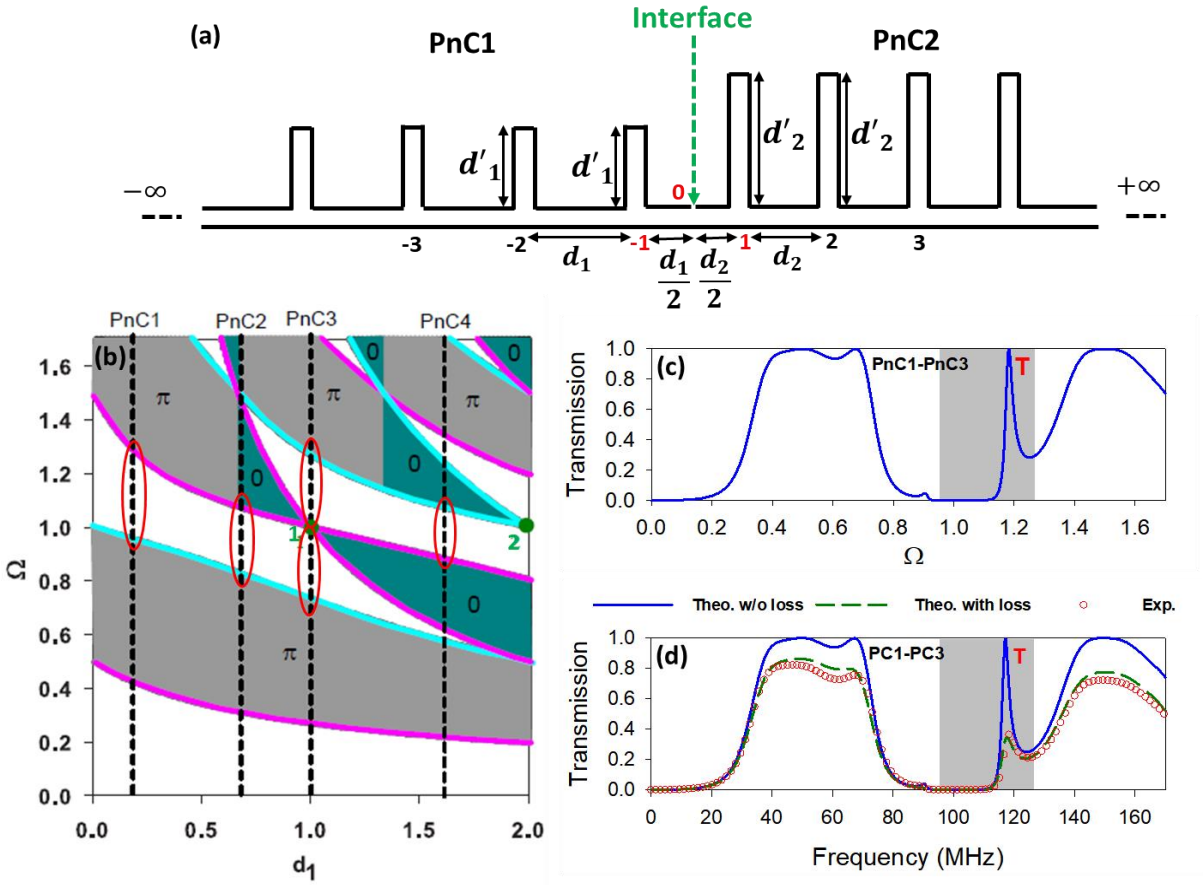

Figure 1: (a) Interface between two PnCs (PnC1 and PnC2), each composed of a unit cell made of a stub of length $\mathbf{d'_i}$ and period $\mathbf{d_i}$ (i = 1, 2). (b) Band structure (in dimensionless units) as a function of $\mathbf{d_1}$. The green dots 1 and 2 indicate the band crossing points where the bands close and reopen. Pink and cyan colors indicate the symmetric or antisymmetric character of the band edge modes, respectively. The bands with π and 0 Zak phases are indicated by gray and dark cyan colors, respectively. The large circles indicate the gap of each PnC. (c) Transmission coefficient for a finite PnC made of PnC1-PnC3, each one being composed of N = 2 stubs. (d) Transmission coefficient for a finite photonic crystal (PC) made of PC1-PC3, each one being composed of N = 2 stubs, with an experimental validation in the radiofrequency domain. Blue and green dashed lines represent the theoretical results without and with loss, respectively, while open circles give the experimental measurements. Gray area indicates the common gap. The symbol T refers to the Tamm state.

PnCs	PnC1/PnC2	PnC1/PnC3	PnC1/PnC4	PnC2/PnC3	PnC2/PnC4	PnC3/PnC4
Common gap	No	Yes	Yes	Yes	Yes	Yes

Table 1 Presence or no of topological interface states for the interface configurations constructed from the 4 PCs in Fig. 1(b)

Acknowledgments: The work of BDR is supported by HORIZON-CL4-2022-RESILIENCE-01-10 project No. 101091968 MAGNIFIC and by the CHIST-ERA ERA-NET project MUSICIAN.

References

[1] M. Esmann, F. R. Lamberti, P. Senellart, I. Favero, O. Krebs, L. Lanco, C. Gomez Carbonell, A. Lemaître, and N. D. Lanzillotti-Kimura, *Phys. Rev. B* **97**, 155422 (2018).
[2] Y. Jin, W. Wang, Z. Wen, D. Torrent, and B. Djafari-Rouhani, *Extreme Mech. Lett.* **39**, 100777 (2020).
[3] S. Khattou, Y. Rezzouk, M. Amrani, M. El Ghafiani, E. H. El Boudouti, A. Talbi, B. Djafari-Rouhani, *Crystals* **12**, 1685 (2022).
[4] S. Khattou, Y. Rezzouk, M. Amrani, M. El Ghafiani, E. H. El Boudouti, A. Talbi, A. Akjouj, B. Djafari-Rouhani., *Phys. Rev. B* **107**, 125405 (2023).
[5] Y. Rezzouk, M. Amrani, S. Khattou, E. H. El Boudouti, B. Djafari-Rouhani, *J. Opt. Soc. Am. B* **39**, 600-610 (2022).

PHONONICS 2023: 6th International Conference on Phononic Crystals/Metamaterials/Metasurfaces, Phonon Transport, and Topological Phononics
Manchester, England, June 12-16, 2023
PHONONICS-2023-0136

Tailoring Valley Displacement in Valley Topological Mechanical Honeycomb Lattice

Myung-Joon Lee[1], Il-Kwon Oh[1]

[1] Department of Mechanical Engineering
Korea Advanced Institute of Science and Technology (KAIST)
291 Daehak-ro, Yuseong-gu, Daejeon, 34141, Republic of Korea
audwns410@kaist.ac.kr, ikoh@kaist.ac.kr

Abstract: The locations of the valleys should be tailored to ensure efficient valley protection on arbitrarily oriented bent waveguides. We design a modified valley topological mechanical honeycomb lattice that can be used for valley displacement, and analyze the relationship between the parameters of the lattice and valley displacement. The efficiency of valley protection in the valley-displaced lattice is analyzed and verified through simulations.

Topological phase has proven its worth in wave control, which ensures the robustness of propagation against sharp turns or disorders in waveguides. In the field of mechanics, the valley topological phase, amongst two-dimensional topological phases, has captured special attention as it can be induced by passive and simple, so manufacturable, geometry. Valley topological phase has been realized in megahertz region for on-chip elastic wave manipulation[1] and in gigahertz region for the utilization in quantum computing[2], and has been adopted for various applications including topological acoustic delay lines[3], directional antennas[4], and elastic mode separation[5].

The sufficiency of simple geometry for the valley topological phase stems from how valleys can emerge in an energy band diagram. The symmetry of the reciprocal space such as C_6 or C_{3v} in a honeycomb lattice ensures the degeneracy with linear dispersion in the energy band diagram, and the degeneracy is replaced by valleys and bandgap at the same location when the degeneracy is lifted by C_3 preserving symmetry breaking[1-5]. In brief, a single degree of freedom breaking the symmetry of the lattice is sufficient for the emergence of the valley topological phase.

While utilization of the symmetry for the valley phase has made the phase easily accessible, it also has restricted the scope of the valley topological phase to the ones in which the valleys are located exactly on the high symmetric points, namely K and K' (Figure 1). These valley topological phases serve robust propagation for the zigzag boundary waveguide as projection images of inequivalent valleys onto the zigzag boundary are distinct[1-5]. Though for the armchair boundary waveguide, inequivalent valleys are mixed totally and the valley topological phase loses its worth of robustness as inequivalent valleys are projected on the same location. Valleys should be displaced from the high symmetric points for the valley phase to serve robust propagation for the armchair boundary.

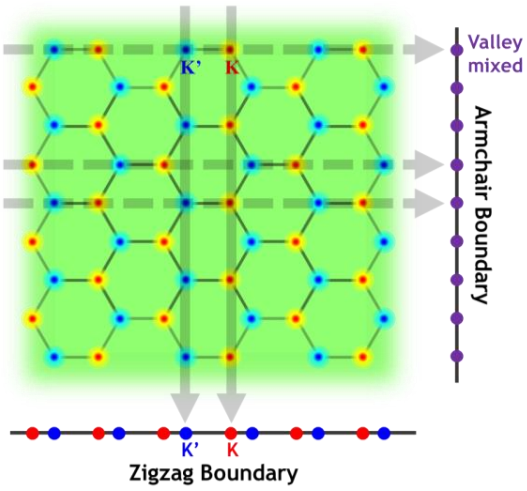

Figure 1 Projection images of the inequivalent valleys K and K' onto zigzag and armchair boundary, when the valleys are located exactly on high symmetric points.

Phononic crystals possessing valley phase which is preserved for both zigzag and armchair boundary might be able to be designed[6,7]. However, generally speaking, the boundary always exists in which inequivalent valleys are mixed nearly perfectly as long as the structure supporting the valley phase is passive. Therefore, the location of the valleys should be tailored according to the boundaries of the waveguide for effective valley protection. Though valley topological phases which are not originated from symmetry and the locations of valleys are displaced from high symmetric

points have been reported, they focus on the emergence of the valley topological phase itself[6] or have physically unrealizable parameters[7]. How the location of valleys can be tailored or displaced from the high symmetric points with realizable parameters has not been studied so far to the best of our knowledge.

The present work studies the relationship between the model parameters and valley displacement in the valley topological mechanical honeycomb lattice. The conventional model in a honeycomb lattice for the valley topological phase always preserves C_3 symmetry, prohibiting the valley displacement from high symmetric points. We break this constraint and set the model parameters related to this constraint breaking. Thanks to the simplicity and abstractness of the lattice model, calculations can be done analytically while the same principle or technique can be adopted to design the elastic model of the same analog. Feasibility of the valley protection is also studied for valley displaced topological phase exploiting the Berry curvature and valley Chern number. Simulations show that the valley phase preserved for both zigzag and armchair boundaries can be designed by tailoring the valley displacement (Figure 2).

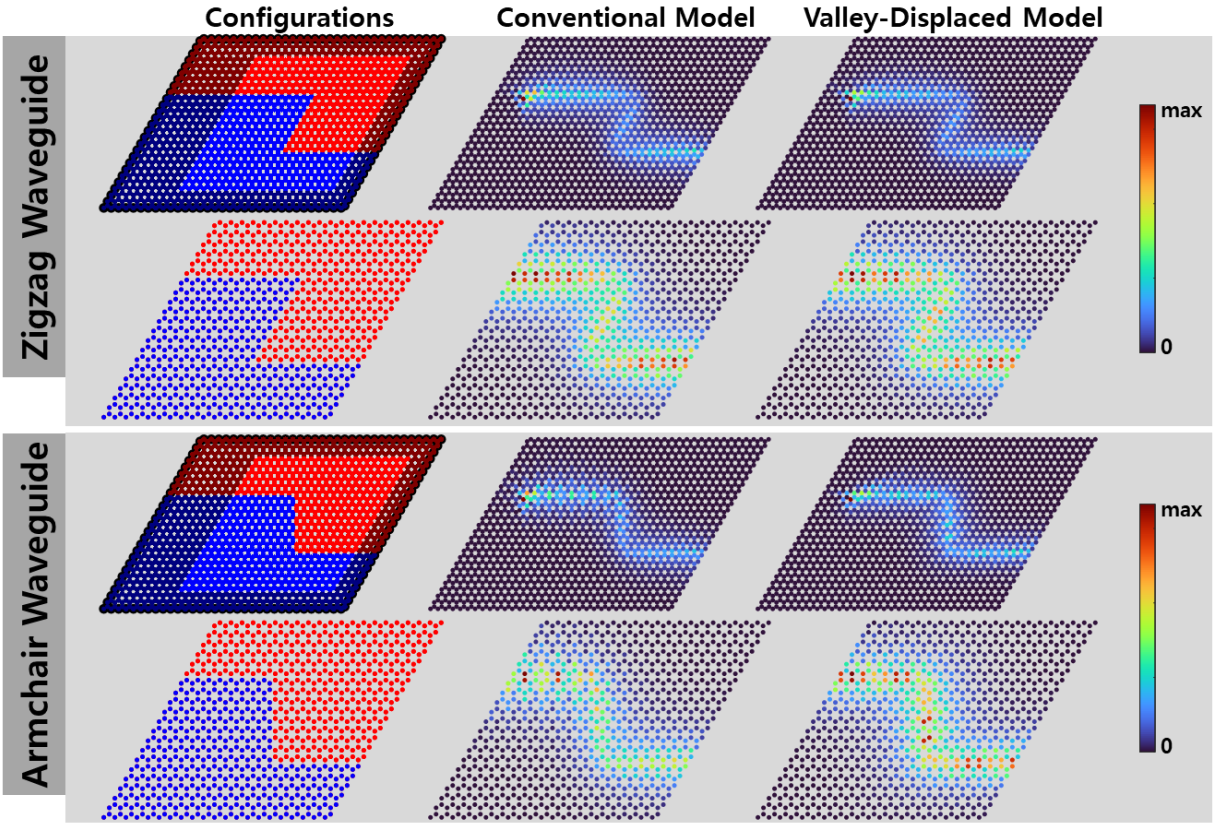

Figure 2 Wave propagation along zigzag and armchair bent waveguide generated by conventional valley topological lattice and valley-displaced valley topological lattice.

References

[1] M. Yan, J. Lu, F. Li, W. Deng, X. Huang, J. Ma, and Z. Liu, *Nat. Mater.* **17**, 993-998 (2018).
[2] Q. Zhang, D. Lee, L. Zheng, X. Ma, S. I. Meyer, L. He, H. Ye, Z. Gong, B. Zhen, K. Lai, and A. T. C. Johnson, *Nat. Electron.* **5**, 157-163 (2022).
[3] Z. Zhang, Y. Tian, Y. Cheng, Q. Wei, X. Liu, and J. Christensen, *Phys. Rev. Appl.* **9**, 034032 (2018).
[4] Z. Zhang, Y. Tian, Y. Wang, S. Gao, Y. Cheng, X. Liu, and J. Christensen, *Adv. Mater.* **30**(36), 1803229 (2018).
[5] M.-J. Lee and I.-K. Oh, *Commun. Phys.* **5**(1), 17 (2022).
[6] S. Li and J. Yang, Phys. Rev. Appl. **15**, 014058 (2021).
[7] H. Qu, X. Liu, and G. Hu, *Appl. Phys. Lett.* **119**, 051903 (2021).

Harmonics dispersion relation: Inner makings of a time evolving strongly nonlinear wave

Mahmoud I. Hussein[1,2], **Romik Khajehtourian**[3]

[1]*Ann and H.J. Smead Dept. of Aerospace Engineering Sciences, University of Colorado Boulder, Boulder, Colorado 80303,*
[2]*Dept. of Physics, University of Colorado Boulder, Boulder, Colorado 80302,*
[3]*Dept. of Mechanical and Process Engineering, ETH-Zürich, Zürich 8092, Switzerland.*
mih@colorado.edu, rkh@ethz.ch

Abstract: An unbalanced nonlinear wave distorts acutely as it travels and appears to ultimately fully lose its original shape. Inherent to this distortion is an intricate mechanism of harmonic generation manifesting in intensive time-varying exchange of energy between the harmonics that matches the wave's ongoing nonlinear evolution in space and time. We present a general theory for the dispersion of these generated harmonics as they emerge, develop, and mature[1]. Specifically, the harmonics dispersion relation−derived by the theory−provides direct and exact analytical prediction of the collective nonlinear harmonics spectrum in the frequency-wave-number domain, and does so without prior knowledge of the spatial-temporal solution. Despite its time-independence, the new relation is shown to be applicable at any temporal state of evolution of the nonlinear wave as long as the wave is balanced or has not yet reached its breaking point.

Wave motion lies at the heart of many disciplines in the physical sciences and engineering. For example, problems and applications involving light, sound, heat, or fluid flow are all likely to involve wave dynamics at some level. While the key tenets of the theory of linear waves are fairly established, nonlinear wave motion remains a complex, often mysterious, object—particularly when the nonlinearity is strong. For example, an unbalanced nonlinear wave will distort severely as it travels causing it to fully lose its original waveform, and in many instances the final outcome is onset of breaking instability. This distortion is caused by a complex mechanism of harmonic generation whereby energy is continuously exchanged between the harmonics.

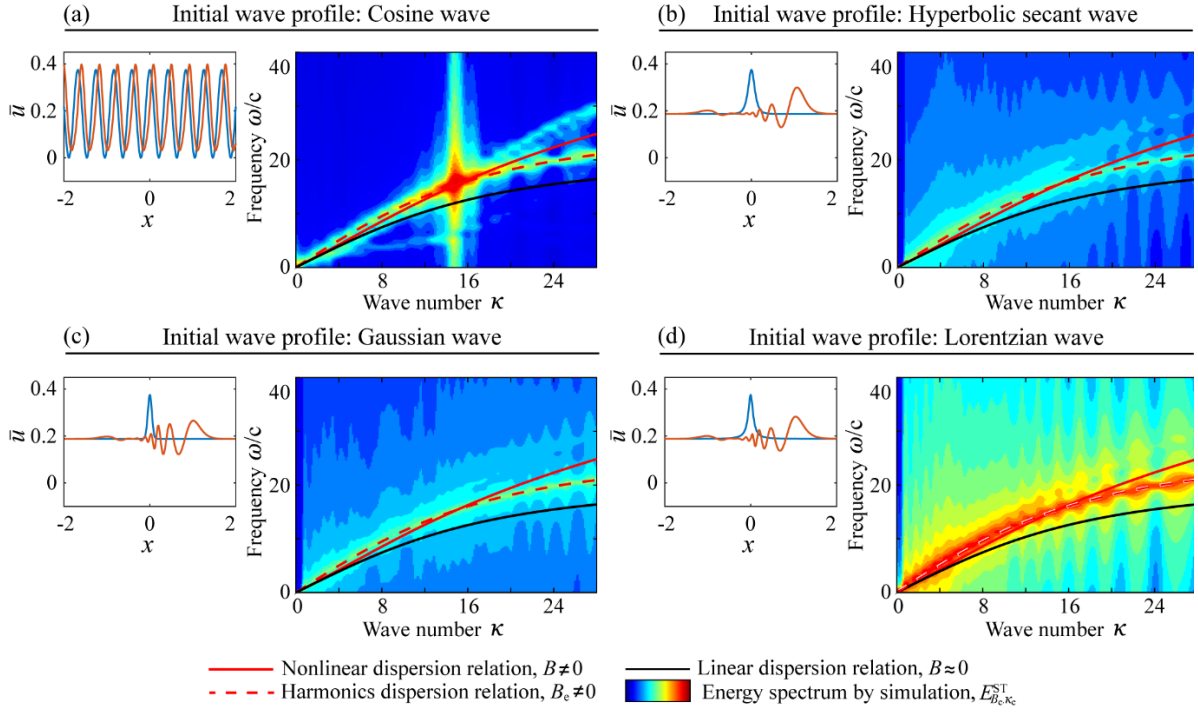

Figure 1 Exact prediction of the dispersion of the generated harmonics in a strongly nonlinear wave by the harmonics dispersion relation for a wave that is initially in a form described by the following function: (a)

cosine, (b) hyperbolic secant, (c) Gaussian, and (d) Lorentzian. In the left inset in each case, both the initial and evolved waveform is shown demonstrating severe distortion in the (b)-(d) cases.

The developed theory produces two relations. The first is a *general nonlinear dispersion relation* that is derived as a function of the wave amplitude and wavenumber. This relation provides an exact instantaneous prediction of the frequency for a given wavenumber (or vice versa) for a given amplitude at any instant during the evolution of a strongly nonlinear wave[2]. Furthermore, the relation predicts the frequency of the fundamental harmonic of the evolved wave for a given initial wavenumber and amplitude of the wave signal. The second is the *harmonics dispersion relation*, which predicts the full dispersion spectrum of all generated harmonics of the evolved wave for a given initial wavenumber and amplitude of the wave signal[1]. The two relations are analytically related in that they both predict the fundamental harmonic.

The theory is generally applicable to models described by arbitrary nonlinear elastic constitutive relations and any of the Seth-Hill family of finite-strain measures, such as Green-Lagrange or Hencky strain for example. Regardless of the strength of the nonlinearity, it is shown to hold irrespective of the spatial form of the initial wave profile (see Fig. 1), intensity of the wave amplitude, and the level of dispersion in the linear limit[1]. We will demonstrate the application of the theory to nonlinear elastic waves in a thick (linearly dispersive) homogeneous rod, and an extension will be provided for an approximate prediction of the nonlinear dispersion in rods with a periodic array of property modulation (phononic crystal; see Fig. 2a)[3] or intrinsic resonators (elastic metamaterial; see Fig. 2b)[4].

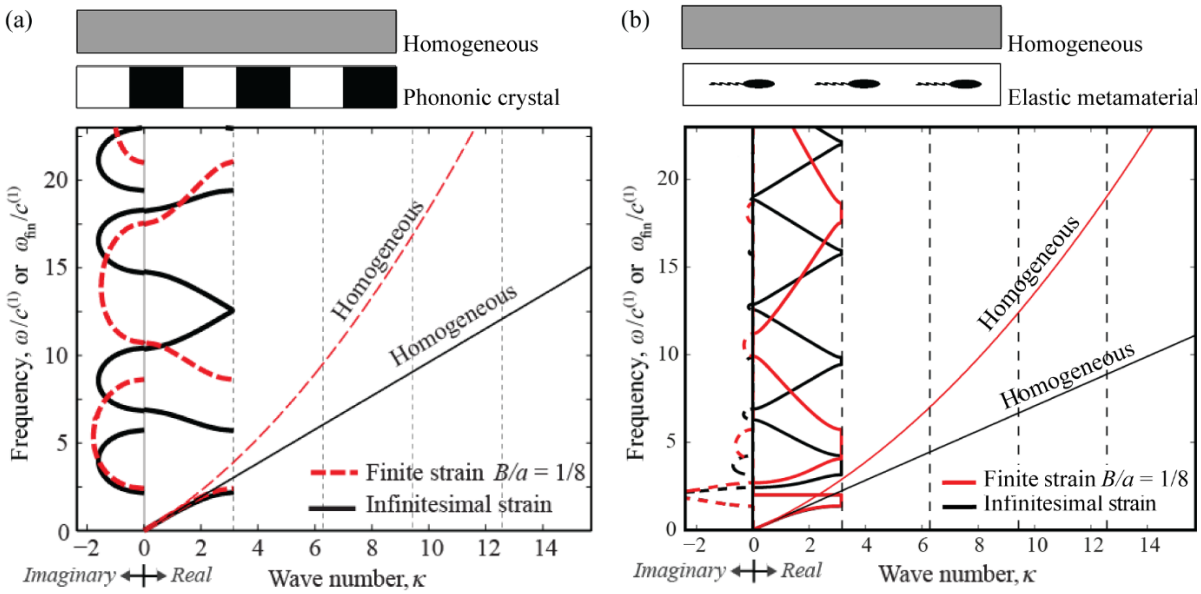

Figure 2 Approximate complex dispersion relation of a nonlinear (a) phononic crystal[3] and (b) elastic metamaterial[4] under a relatively high wave amplitude of one-eighth of the unit cell length. Analysis of the amplitude range of validity is given in Ref. [3]. In each case, the linear dispersion relation and the equivalent nonlinear dispersion relation for a corresponding homogenized media is provided for comparison.

References

[1] R. Khajehtourian, M.I. Hussein, *Sci. Adv.* **7**, eabl3695 (2021).
[2] M.H. Abedinnasab and M.I. Hussein, *Wave Motion* **50**, 374-388 (2013).
[3] M.I. Hussein and R. Khajehtourian, *Proc. R. Soc. A* **474**, 20180173 (2018).
[4] R. Khajehtourian, M.I. Hussein, *AIP Adv.* **4**, 124308 (2014).

PHONONICS 2023: 6th International Conference on Phononic Crystals/Metamaterials/Metasurfaces, Phonon Transport, and Topological Phononics
Manchester, England, June 12-16, 2023
PHONONICS-2023-0098

A Perturbation Approach for Interfaced Transmission Between Linear and Nonlinear Monatomic Lattices

Lezheng Fang[1], Michael J. Leamy[1]

[1]*George W. Woodruff School of Engineering, Georgia Institute of Technology, Atlanta GA 30332, USA, lezheng.fang@gatech.edu, michael.leamy@me.gatech.edu*

Abstract: We present a multiple scales approach for studying wave transmission through spatial and temporal interfaces between linear and nonlinear periodic structures. The approach predicts higher harmonic generation at the interfaces together with spatial and temporal self-interaction in the back-scattered and transmitted wave fields. We document strong agreement between the multiple scales predictions and results from numerical simulations.

Introduction

The study of wave propagation in periodic structures has been an active area of research for decades, with applications to phononic crystals and elastic/acoustic metamaterials. More recently, the behavior of weakly nonlinear waves in periodic structures has received significant attention as a means to accomplish passive wave control, amplitude-based tunability, extra-harmonic generation, and wave mode conversion. Perturbation approaches, a class of semi-analytical methods, approximate the solutions to weakly nonlinear systems by asymptotically expanding the governing equations, leading to linear sub-problems whose solutions can be found in a hierarchical manner. While existing perturbation approaches have accurately captured nonlinear behavior such as dispersion shifting, extra-harmonic generation, and invariant waves [1], sparse attention has been paid to interfaced periodic structures, especially those interfacing linear and nonlinear media which appears often in practical applications. In this talk, we present a multiple scales approach for investigating the effects of spatial and temporal interfaces between linear and weakly nonlinear monatomic chains.

System Description

We investigate wave propagation from a linear to a weakly nonlinear monatomic chain in two types of interfaces, spatial and temporal. To simplify the problem, the masses and linear stiffness in both chains are assumed to be the same.

As depicted in Fig. 1a, a linear semi-infinite chain is coupled with a weakly nonlinear semi-infinite chain at $j = 0$, which defines a *spatial interface*. The incident wave arrives from $j = -\infty$. The blue and yellow masses mark the termination points of each semi-infinite domain, and their equations of motion inform the interface conditions,

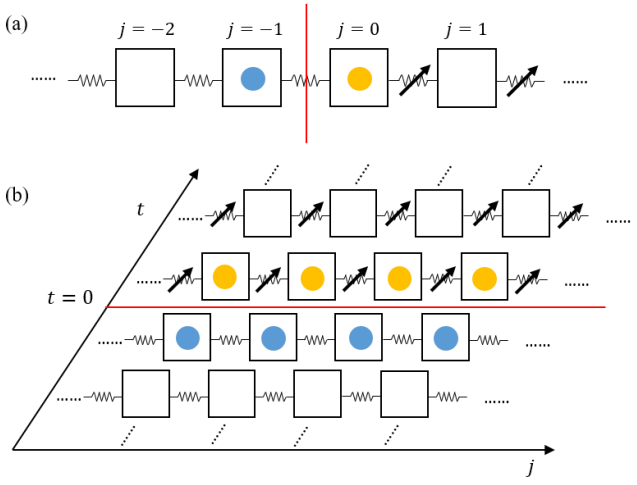

Figure 1 A schematic of (a) a spatially-interfaced monatomic chain (b) a temporally-interfaced monatomic chain. The spring with oblique arrow indicates nonlinearity.

$$m\ddot{u}_{-1} + k_1(2u_{-1} - u_0 - u_{-2}) = 0, \tag{1}$$

$$m\ddot{u}_0 + k_1(2u_0 - u_{-1} - u_1) + \epsilon k_3(u_0 - u_1)^3 = 0, \tag{2}$$

where u_j denotes the displacement of the j^{th} mass, and k_1 and k_3 are the linear and cubic stiffness coefficients. A small parameter, ϵ, serves as a bookkeeping device in the perturbation analysis.

In contrast, in Fig. 1b we depict a *temporal interface* between the linear and nonlinear chains. At $t < 0$, a propagating plane wave exists in the entire domain of the linear monatomic chain. At $t = 0$, the nonlinearity ϵk_3 emerges in all springs, introducing a temporal interface. Again, the blue and yellow masses mark the termination points of each domain. Temporal interfaces, wittingly or unwittingly, are often introduced in the simulation of nonlinear media.

Analysis Approach

As per the multiple scales procedure we expand time ($t = T_0 + \epsilon T_1 + \epsilon^2 T_2 + O(\epsilon^3)$) and the response quantity ($u_j = u_j^{(0)} + \epsilon u_j^{(1)} + \epsilon^2 u_j^{(2)} + O(\epsilon^3)$). We apply the expansions to both the nonlinear domain and the interface conditions. At each perturbation order, we first analyze the nonlinear domain where expansion generates a forcing term as a function of solutions from previous orders. Upon removing the secular terms, we derive the particular solutions accordingly. Deviating from previous perturbation approaches which proceed to the next order and consider only particular solutions [1], we also introduce homogeneous solutions in order to satisfy the interface conditions. These additional homogeneous solutions obey nonlinearly-corrected dispersion relationships similar to the zeroth-order homogenous solution. We carry both the particular solutions and the interface-informed homogeneous solutions to the next order. In this study, we truncate the expansion at the second order and reconstitute sub-problem results to form the complete solution.

Results

The perturbation analysis yields two groups of results: the multi-harmonic solutions and the dispersion corrections. Typically, a spatial interface generates extra-harmonics with integer multiples of the fundamental frequency, and dispersion corrections on wavenumber. A temporal interface generates integer multiples of the fundamental wavenumber, and dispersion corrections on frequency. In Fig. 2, we present a set of the perturbation predictions, together with numerical verification, depicting the transmitted waves in the nonlinear domain following a spatial interface. The three simulations are conducted at the same frequency and with increasing amplitudes. In each figure, we capture the spatial evolution of the fundamental and third frequency. The first-order perturbation results (red curves) predict a sinusoidal self-interaction pattern in the third harmonic. The second-order results (yellow curves) reveal a similar self-interaction pattern in the fundamental harmonic, which is of opposite phase to the third harmonic interaction pattern, indicating an energy exchange in space between the two harmonics. Additionally, the numerical results illustrate a trend of increasing wavelength of the self-interaction envelope from Fig. 2a to 2c, which can only be captured by extending the perturbation analysis to the second order. At much higher frequencies (not shown), the spatial interface generates evanescent higher harmonics, inducing self-interaction patterns localized near the interface. The temporal interface, however, will only generates propagative harmonics, though the higher wavenumber may exceed the first Brillouin zone, introducing intricate propagation patterns.

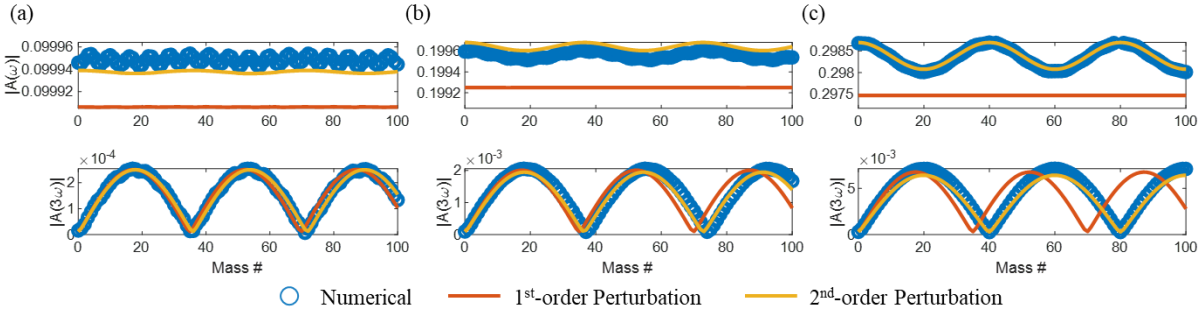

Figure 2 The propagation pattern of the transmitted waves from a spatial interface.

Conclusions

We propose a multiple scales approach capable of analyzing interface problems between linear and nonlinear monatomic chains. We expand the interface conditions and integrate homoegeneous solutions in both back-scattered and transmitted waves at each order. The reconsituted results indicate higher harmonic generaiton and intricate self-interaction in both transmitted and backscattered waves. We verify the findings using numerical simulations and find strong agreement, particularly for second-order analysis.

References

[1] M. D. Fronk and M. J. Leamy, Higher-order dispersion stability, and waveform invariance in nonlinear monoatomic and diatomic systems, J. Vibr. Acoust. 139, 051003 (2017).

PHONONICS 2023: 6th International Conference on Phononic Crystals/Metamaterials/Metasurfaces, Phonon Transport, and Topological Phononics
Manchester, England, June 12-16, 2023
PHONONICS-2023-0030

Effective Dynamics for Low-Amplitude Transient Elastic Waves in a 1D Periodic Array of Non-Linear Interfaces

C. Bellis[1], B. Lombard[1], M. Touboul[2], R. Assier[3]

[1] LMA, AMU-CNRS-ECM, Marseille, France,
bellis@lma.cnrs-mrs.fr, lombard@lma.cnrs-mrs.fr
[2] Department of Mathematics, Imperial College London, London, UK
m.touboul@imperial.ac.uk
[3] Department of Mathematics, University of Manchester, Manchester, UK
Raphael.assier@manchester.ac.uk

Abstract: We study the propagation of 1D elastic waves through a periodic array of interfaces with nonlinear transmission conditions, which describe an imperfect contact. The asymptotic developments are carried out at order 1. The properties of the obtained nonlinear hyperbolic system are studied, in particular the existence of a shock time. Full field and effective simulations are successfully compared.

This article focuses on the time-domain propagation of elastic waves through a 1D periodic medium that contains non-linear imperfect interfaces, i.e. interfaces exhibiting a discontinuity in displacement and stress governed by a non-linear constitutive relation. The array considered is generated by a cell repeated periodically. The imperfect interfaces are characterized by a linear dynamics but a non-linear elasticity law. The latter is not specified at first and only key theoretical assumptions are required. We investigate transient waves with both low-amplitude and long-wavelength, and aim at deriving homogenized models that describe their effective motion. To do so, the two-scale asymptotic homogenization method is deployed, up to the first-order. An effective model is obtained for the leading zeroth-order contribution to the microstructured wavefield. It amounts to a wave equation with a non-linear constitutive stress-strain relation that is inherited from the behavior of the imperfect interfaces at the microscale. The next first-order corrector term is then shown to be expressed in terms of a cell function and the solution of a linear elastic wave equation. Without further hypothesis, the constitutive relation and the source term of the latter depend non-linearly on the zeroth-order field, as does the cell function. Combining these zeroth- and first-order models leads to an approximation of both the macroscopic behavior of the microstructured wavefield and its small-scale fluctuations. Finally, particularizing for a prototypical non-linear interface law and in the cases of a homogeneous periodic cell and a bilaminated one, the behavior of the obtained models are then illustrated on a set of numerical examples and compared with full-field simulations (Figure 1). Both the influence of the dominant wavelength and of the wavefield amplitude are investigated numerically.

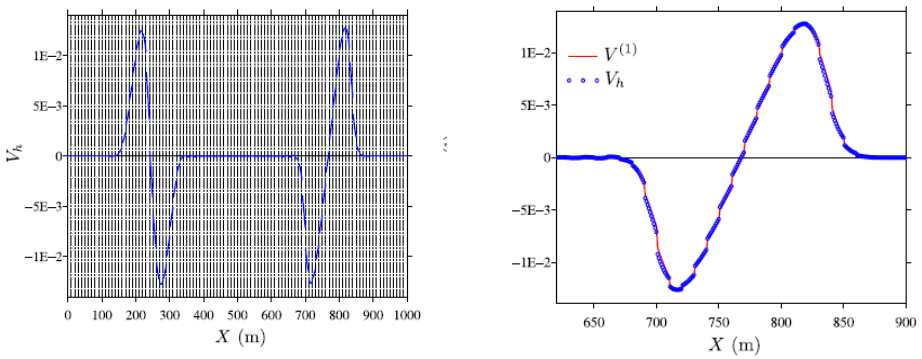

Figure 1 Snapshot of the field in the microstructured medium (left). Comparison between the effective field and the direct field (right). Issued from [1].

References

[1] C. Bellis, B. Lombard, M. Touboul and R. Assier, *J. Mech. Phys. Solids* **149**, 104321 (2021).

PHONONICS 2023: 6th International Conference on Phononic Crystals/Metamaterials/Metasurfaces, Phonon Transport, and Topological Phononics
Manchester, England, June 12-16, 2023
PHONONICS-2023-0152

Nonlinear wave propagation through phononic materials with rough contact interfaces

Ganesh U. Patil, Kathryn H. Matlack

Department of Mechanical Science and Engineering, University of Illinois Urbana-Champaign, Urbana, IL, USA,
kmatlack@illinois.edu

Abstract: This presentation discusses nonlinear wave responses due to periodic nonlinear interfaces embedded in a continuum. The nonlinearity arises from deformation of micron-sized asperities on the contacting surfaces, that manifests as either a nonlinear pressure-displacement relation upon normal deformation or a hysteretic nonlinearity due to friction upon shear deformation. Finite element modeling is used to characterize nonlinear wave responses such as stegoton propagation and eigenstrain generation that could enable fast energy propagation at high amplitudes and ultrasonic-controlled surface reconfigurability, respectively.

Periodic architected materials can control mechanical wave propagation in novel ways. For example, band gaps, negative refraction, or topologically protected modes confined to boundaries or interfaces can be supported. While substantial work has explored these concepts in the linear regime, introducing nonlinearity in the building blocks or constituents leads to a richer variety of nonlinear wave responses not supported in the linear domain[1], such as amplitude-dependent properties, wave mixing, transition waves, solitary waves, and supratransmission. While these properties have been studied in both continuous and discrete systems separately, relatively little has been explored in terms of discrete nonlinearity embedded in a continuous system. This presentation discusses recent research on nonlinear periodic media with discrete nonlinear interfaces, in terms of both longitudinal and shear wave propagation.

We study a system based on nonlinear building blocks that are discrete rough contact interfaces arranged periodically in a continuum. In terms of longitudinal wave propagation (i.e. displacement normal to the interface), rough contacts have a nonlinear dependence of pressure on longitudinal displacement, due to deformation of micron-sized asperities on the contacting surfaces. Time-dependent finite element models combined with experimentally informed reduced order models of the nonlinear response of the contacts are used to study the weakly and strongly nonlinear wave responses in systems with different arrangements of rough contacts. The weakly nonlinear regime occurs when this system is pre-compressed to a higher stress than the stress induced by the propagating wave, such that the surfaces remain in contact throughout the wave excitation. The strongly nonlinear regime occurs when the stress induced by the propagating wave is high enough to cause complete separation of contacting interfaces during wave propagation – in this case only a portion of the wave is transmitted. Results demonstrate longitudinal wave responses such as energy transfer to higher harmonics and resonances of the system, as well as a special type of solitary wave termed “stegotons”, all of which are modulated by their underlying band structure[2]. In addition, we numerically show how this system can be used to realize multi-frequency non-reciprocal wave propagation based on the concept of wave mixing in nonlinear media[3].

Finally, our recent work has explored shear wave propagation through this system of periodic rough contacts that includes friction. The roughness of contacting surfaces results in a structural instability that causes the contacts to switch between stick, and slip regimes - giving rise to strong nonlinearity. Due to the presence of friction, the contacts also exhibit hysteretic or “memory-dependent” nonlinearity that is experimentally measured. Numerical results will be discussed that demonstrate that as an ultrasonic shear wave propagates through a single frictional interface, a shear-polarized “eigenstrain” is generated, akin to a residual strain in the system, and effective band gaps that are strongly amplitude-dependent. These results may have engineering applications as mechanisms for precision surface reconfigurability and programmable switch-like functionalities[4].

Acknowledgements
This work was supported in part by the Army Research Office under Grant Number W911NF-20-1-0250, and by the National Science Foundation under Award No. 2047041.

References

1. Patil, G. U. & Matlack, K. H. Review of exploiting nonlinearity in phononic materials to enable nonlinear wave responses. *Acta Mech.* **233(1)**, 1-46 (2022).
2. Patil, G. U. & Matlack, K. H. Strongly nonlinear wave dynamics of continuum phononic materials with periodic rough contacts. *Phys. Rev. E* **105(2)**, 024201 (2022).
3. Patil, G. U., Cui, S. & Matlack, K. H. Leveraging nonlinear wave mixing in rough contacts-based phononic diodes for tunable nonreciprocal waves. *Extrem. Mech. Lett.* **55**, 101821 (2022).
4. Patil G. U., Fantetti, A., Matlack, K. H., Mechanics of wave-induced friction in periodic interfaces for programmable and tunable shear wave responses, (*under review*).

Mechanical Multi-level Memory

Jack E. Pechac, Michael J. Frazier

Department of Mechanical and Aerospace Engineering, University of California, San Diego, CA 92093, USA, mjfrazier@ucsd.edu

Abstract: In this presentation, we couple a multi-stable metamaterial to an elastic foundation to realize a mechanical system within which the position of a transition wavefront can be precisely controlled and remotely determined. We exploit these mechanisms for mechanical multi-level memory which may find application, e.g., in soft robots as a flexible alternative to current rigid memory technologies.

(Multi-)ferroics are crystalline materials whose unit cells notably exhibit multiple, energetically-equivalent stable configurations (i.e., phases, states) distinguished by one or more order parameters and, possibly, unique physical properties. Within a given sample, each stable configuration may appear simultaneously, organized into regions of uniform phase (i.e., domains) separated by an interface (i.e., domain wall). Under the influence of a conjugate field, the domain wall moves, constituting a transition wave that transforms the local configuration in its path. The manipulation of domains and domain walls is critical to developing functionality and, therefore, remains an active area of research in condensed matter physics. In this presentation, we propose a metamaterial design for mechanical multi-level (i.e., high-density) memory functionality. The concept may find utility in soft robotics and the emerging paradigm of physical reservoir computing.

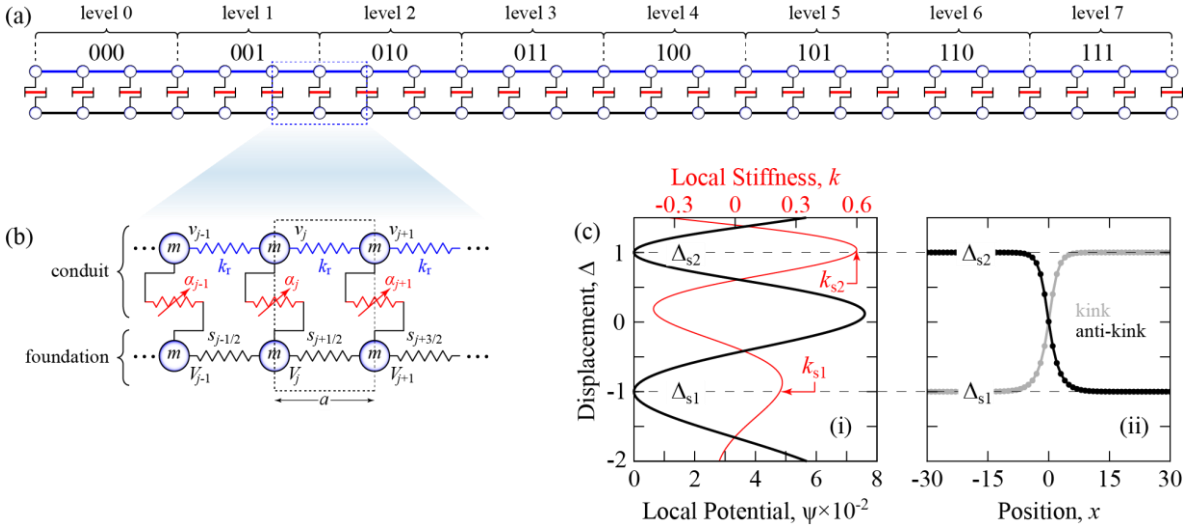

Figure 1 Mechanical Multi-level Memory. **(a)** Schematic of the mechanical (8-bit) memory device comprising 8 levels of J unit cells, including a defect cell. Each level is assigned a binary-encoded value from 000 to 111. **(b)** Detail of three unit cells. **(c) (i)** The non-convex on-site potential (black) and corresponding local stiffness (red) supporting the formation of **(ii)** transition wavefronts separating domains in configuration, Δ_{si}, and on-site stiffness, k_{si}.

Figure 1a displays a representative mechanical multi-level memory device, comprising two discrete chains distinguished by periodic and uniform inter-site coupling, $s_{j+1/2}$ and k_r, respectively. The two chains are connected locally through a non-linear spring adhering to the non-convex potential, $\psi(\Delta_j)$, $\Delta_j = v_j - V_j$, providing for the formation of transition waves. As discussed below, wave motion will be (effectively) confined the substructure (i.e., the conduit) comprising the uniform chain and non-linear springs. The periodic chain is labeled the foundation. The corresponding non-dimensional governing equations (with viscous damping, η) of an arbitrary site j are derived as

$$\ddot{v}_j + \eta\dot{v}_j + \left(2v_j - v_{j+1} - v_{j-1}\right) + \alpha_j \frac{\partial\psi(\Delta_j)}{\partial v_j} = 0, \tag{1a}$$

$$\ddot{V}_j + \eta\dot{V}_j + s_{j+1/2}(V_j - V_{j+1}) + s_{j-1/2}(V_j - V_{j-1}) + \alpha_j \frac{\partial\psi(\Delta_j)}{\partial V_j} = 0, \quad (1b)$$

where $\alpha_j = (1+\gamma j)[1+\beta\delta_{Ij}]$ is a positive scalar responsible for effecting (i) the on-site potential gradient as prescribed by $\gamma = (-\infty, \infty)$ and (ii) the nature and distribution of "soft" point defects (i.e., unit cells storing anomalous deformation energy) as controlled by $\beta \in (-1, \infty)$ and the Kronecker delta, δ_{Ij}, $I = \{j|(j/J) \in \mathcal{N}\}$ with $J \in \mathcal{N}$.

In order to elicit the desired functionality, the system adheres to certain design requirements. For one, $\psi(\Delta_j)$ possesses $n \geq 2$ degenerate ground states, $\Delta_j = \{\Delta_{s1}, \Delta_{s2}, \ldots, \Delta_{sn}\}$, supporting the formation of a (anti-)kink wave profile, yet, is asymmetric such that the linearized on-site stiffness about each ground state, $k_{si} = \psi''(\Delta_{si})$, is unique (Fig. 1b.i). For another, the α_j vary monotonically across the device except at p periodically-distributed defect sites collected in I, where, for $\beta < 0$ ($\beta > 0$), α_j is less (greater) than $\alpha_{j\pm1}$ in order to create a locally attractive (repulsive) potential suitable for immobilizing transition waves. The monotonic variation otherwise supports the uni-directional propagation of both kink and anti-kink modes, permitting phase reversals. The soft defects divide the system into $p+1$ levels of J unit cells, each of which may be assigned an m-bit binary value where $m = \lfloor \log_2(p+1) \rfloor$ (Fig. 1a). Finally, although the foundation is pliable, proper function requires $s_{j+1/2}$ to be, effectively, rigid in comparison to k_r and k_{si}, i.e., $\min(s_{j+1/2}) \gg \max(k_r, k_{si})$. This condition ensures that, upon the application of a boundary displacement, the inhomogeneous strain field that arises in the foundation is, effectively, transferred to the conduit while the reciprocal is not permitted. Thus, the dynamics of the conduit to be treated in isolation at low frequencies.

Consider, for example, the case in which $\gamma, \beta < 0$ such that α_j progressively reduces the on-site potential and establishes an energy well at defect sites. A transition wave initialized at the left boundary of the conduit will propagate to the right until entering and, with the aid of dissipative effects, becoming pinned (i.e., immobilized) within the potential well of a soft defect. However, as we will discuss, the strain transferred to the conduit may de-pinn and mobilize the wave, even if only to become pinned again at a subsequent defect site; thus, the wavefront is re-positioned. The wavefront divides the conduit into two regions homogeneous in either configuration Δ_{s1} or Δ_{s2}. The current memory state is interpreted as the number of consecutive levels (enumerated in binary) in the configuration arbitrarily designated as the "ON" phase; the opposing configuration fittingly labeled the "OFF" phase. Thus, repositioning the wavefront alters the memory state. The system is the mechanical analogue of an electronic CTF memory cell, where the configurations, Δ_{si}, are likened to two electric charge states; J cells and defect sites are, respectively, likened to floating gates and isolators; mechanical load likened to voltage. Altogether, controlling and reading the defect-stabilized position of the domain wall enables a multi-level memory functionality.

PHONONICS 2023: 6th International Conference on Phononic Crystals/Metamaterials/Metasurfaces, Phonon Transport, and Topological Phononics
Manchester, England, June 12-16, 2023
PHONONICS-2023-0004

Origami-based Metamaterial: A New Type of Versatile Mechanical Waveguide

Hiromi Yasuda[1,2], Yasuhiro Miyazawa[1], Panayotis Kevrekidis[3], Jinkyu Yang[1,4]

[1] *Aeronautics and Astronautics, University of Washington, Seattle, WA, USA*
yasuda.hiromi@jaxa.jp, ymyzw@uw.edu, jkyang@aa.washington.edu
[2] *Japan Aerospace Exploration Agency, Aviation Technology Directorate, Japan*
[3] *Department of Mathematics and Statistics, University of Massachusetts, Amherst, MA, USA*
yasuda.hiromi@jaxa.jp, ymyzw@uw.edu, jkyang@aa.washington.edu
kevrekid@umass.edu
[4] *Mechanical Engineering, Seoul National University, Seoul, Republic of Korea*

Abstract: In this talk, we will demonstrate how origami can be used as a design principle to realize a new type of mechanical metamaterials. Specifically, we will start with showing the feasibility of forming reconfigurable origami tessellations with tailorable mechanical properties. Then, we will demonstrate an origami-based waveguide with (i) topological edge states in the linear regime, and (ii) counter-intuitive impact mitigation in the nonlinear regime.

Origami is an ancient art of paper folding. It is only recently that origami has received significant interest from the scientific community. This is due to its richness in mathematics and physics, as well as its potential for engineering applications, such as deployable solar panels, sails, space habitat structures, biomedical devices (e.g., stents), and leisure and sport equipment. It is not surprising that the origami principle has been exploited as a design method for constructing mechanical metamaterials. However, previous studies on origami-based metamaterials focused mainly on their kinematics and static/quasi-static properties, e.g., negative Poisson`s ratios, anisotropic stiffness, and multi-stability.

In this presentation, we show how origami can be used as a versatile design method for building mechanical metamaterials with desired wave dynamic properties. Specifically, we present our recent work on origami-based metamaterials composed of volumetric origami [1, 2] (see Fig. 1(a) for examples), and demonstrate that these platforms can serve as an ideal testbed to form a variety of linear and nonlinear mechanical waves. We start with linear wave dynamics observable in origami-based metamaterials. One example is the formation of topological edge states by using a chain of twisted origami tubes. By using sophisticated fabrication methods, we can construct chiral origami unit cells called Kresling origami, which can exhibit tailored stiffness and stability characteristics (see the right panel of Fig. 1(a) for the prototype). We alter the chirality of the composing unit cells to realize a diatomic chain and validate the formation of topological edge states by computations and experiments. The feasibility of in-situ topological state transfer between the two ends is also explored by using the same system [3].

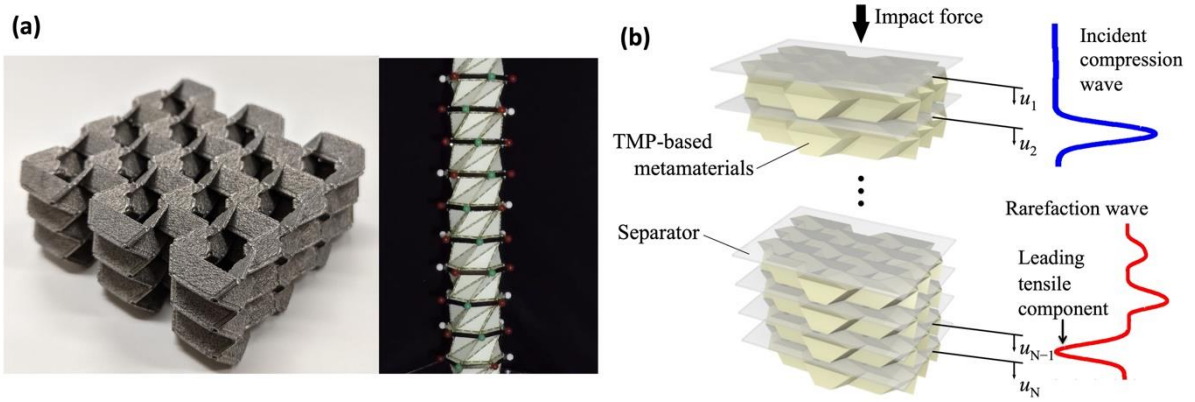

Figure 1 Graphical illustrations of a cluster of origami-based metamaterials. (a) Prototypes fabricated by (left) metallic 3D printer (material used: AlSi10Mg) and (b) laser cutter (art paper). (b) Conversion of compressive waves to rarefaction waves for efficient impact mitigation [4].

Next, we show the unique nonlinear wave dynamics that can be witnessed in the setting of origami-based metamaterials. The advantage of origami structures over other types of architected materials is that they can be tailored to exhibit desired properties by altering crease patterns. For our study, we systematically designed the origami cells to have strain softening behavior in compression, while showing strain stiffening behavior in tension. In this case, given a strong external impact condition, we can observe that the origami-based system can create a tensile solitary wave, which overtakes the initial compressive wave. This implies that upon a compressive impact applied to one side of a structure, the other side of the structure will feel tension instead of compression. The discovery of such counter-intuitive wave dynamics (i.e., the discovery of mechanical rarefaction waves [4, 5], see also Fig. 1(b)) can be useful for impact mitigation in an efficient and tunable manner. This is just one example among numerous unique nonlinear wave dynamics that can be found in the platform of origami-based metamaterials.

Our recent work has also identified other promising opportunities enabled by the origami-based metamaterials, e.g., mechanical memory and logic devices [1], wave filters [2], imaging devices [6], 2D topological waveguiding [7], and others. We envision that the principle of origami can provide us with a powerful tool to design and fabricate novel metamaterials with unique linear and nonlinear wave dynamics.

References

[1] H. Yasuda, T. Tachi, M. Lee, J. Yang, *Nature Communications* 8: 962 (2017).
[2] H. Yasuda, J. Yang, *Journal of International Association for Shell and Spatial Structures* 58(4): 287 (2017).
[3] Y. Miyazawa, C. Chen, T. S. Gormley, G. Yin, R. Chaunsali, G. Theocharis, J. Yang, *Communications Materials* 3, 62 (2022).
[4] H. Yasuda, C. Chong, E.G. Charalampidis, P.G. Kevrekidis, J. Yang, *Physical Review E* 93: 043004 (2016).
[5] H. Yasuda, Y. Miyazawa, E.G. Charalampidis, C. Chong, P.G. Kevrekidis, J. Yang, *Science Advances* 5, eaau2835 (2019).
[6] R. Zhu, H. Yasuda, G. Huang, J. Yang, *Scientific Reports* 8:483 (2018).
[7] Y. Wu, R. Chaunsali, H. Yasuda, K. Yu, J. Yang, *Scientific Reports* 8:112 (2018).

PHONONICS 2023: 6th International Conference on Phononic Crystals/Metamaterials/Metasurfaces, Phonon Transport, and Topological Phononics
Manchester, England, June 12-16, 2023
PHONONICS-2023-0067

Acoustogalvanic Effect in Dirac Materials

Habib Rostami[1]

[1] *Department of Physics, University of Bath, Claverton Down, Bath BA2 7AY, United*
hr745@bath.ac.uk

Abstract: Acoustogalvanic refers to a sound-induced nonlinear current in Dirac materials with the unique coupling of Dirac electrons to acoustic phonons in terms of a time-reversal preserving pseudo-gauge field. We investigate longitudinal and transverse sound-induced rectification currents in both two- and three-dimensional Dirac materials such as graphene and topological Weyl semimetal.

Light-matter interaction is usually understood in terms of the minimal coupling, where the gauge field of light A shifts the quasiparticle momentum **p** as **p** + e**A(r,t)**. On the other hand, in Dirac materials, it is possible to introduce fictitious gauge fields via lattice defor- mation that couple differently to quasiparticles of opposite chirality or valley index $\chi = \pm$, i.e., $\mathbf{p} \rightarrow \mathbf{p} + e\mathbf{A}_\chi$. Here $\mathbf{A}_\chi = \chi\mathbf{A}$ is the fictitious (or pseudo-) gauge field which preserve the time reversal symmetry.

The strain-induced gauge field was first introduced in carbon nanotube, which is one- dimensional (1D) chiral fermionic system, by C. Kane and E. Mele[1]. Similar analogy was built in two dimensional (2D) systems such as graphene[2-4] and transition metal dichalcogenides[5]. Very recently, the idea was generalized to the case of three- dimensional (3D) chiral fermions realized in Weyl and Dirac semimetals, where the fictitious gauge field is also known as the axial gauge field. Although axial (pseudo) gauge field are predicted to be ubiquitous in chiral fermion systems and even metamaterials, its experimental realization in solids is only confirmed in 2D via the local density of states spectroscopy of pseudo-Landau levels induced by the pseudomagnetic field $\mathbf{B}_\chi = \nabla \times \mathbf{A}_\chi$ in graphene. The majority of studies was focused on effects of static strains on physical properties of chiral materials. However, dynamical strain in these systems is not extensively explored.

Among the most immediate consequences of time-dependent strains is the appearance of the pseudoelectric field $\mathbf{E}_\chi = -\partial_t \mathbf{A}_\chi$. In a previous study we show that such a field can be generated by a propagating lattice deformation that we interpret as a pseudo-electromagnetic (P-EM) wave. The latter is nothing else as a high-intense ultrasound wave (acoustic phonon), which could be readily used in experiments. Linear response to a pseudoelectric field does not allow for a net electric current since electrons with different chirality flow in opposite directions. Therefore, drawing on the similarity with the photogalvanic effect, where a direct current is generated in response to the real EM wave (light), we predict that a rectified electric current will also emerge in the second-order response to the P-EM wave (sound). We use the term acoustogalvanic (AG) effect for this novel phenomenon.

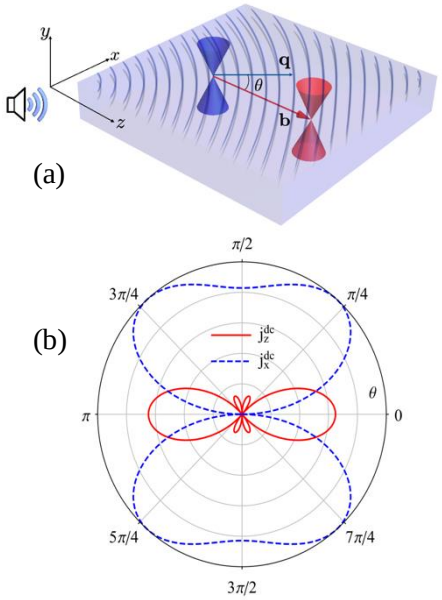

Figure 1 (a) Dirac material slab with chiral shift vector **b** is directed along the z axis and the sound wave vector **q** forms an angle θ with **b**. (b) Sound-induced rectified current components versus polarization angle θ.

The second-order rectification AG current in response to acoustic phonon displacement filed $\boldsymbol{u}(\Omega, \boldsymbol{Q})$ with frequency Ω and wavevector $\boldsymbol{Q}$ formally reads

$$j_a^{\mathrm{AG}} = \chi^{(2)}_{abc} u_b(\Omega, \boldsymbol{Q}) u_c(-\Omega, -\boldsymbol{Q}). \qquad (1)$$

We utilized Boltzmann kinetic theory and evaluated second-order nonlinear response to P-EM waves in 3D Weyl and Dirac materials[6] such as Cd_3As_2. We calculate and analyzed the sound-induced rectification current in terms of sound frequency, electronic relaxation time, and sound intensity and polarization direction. Unlike the conventional piezoelectric, flexoelectric, and acoustoelectric effects, the acoustogalvanic one is nonlinear in the displacement field u and

scales differently with the strain gradient ~ $\nabla(\nabla u)^2$. Moreover, the longitudinal acoustogalvanic response reveals quadratic scaling with the relaxation time, i.e., $\propto \tau^2$, which contrasts with the photogalvanic conductivity that scales linearly with τ. The schematic setup and the numerical result in Weyl semimetal is shown in Figure 1.

We further investigate the effect in graphene which host two-dimensional Dirac electrons[7]. Using a diagrammatic scheme and Green's function method. The study examines the impact of sound-induced pseudogauge fields on both uniform and spatially dispersive currents in response to copropagating and counterpropagating sound waves. We find that in addition to the longitudinal acoustoelectric current, a transverse charge current is also generated, flowing perpendicular to the sound propagation direction. This transverse current arises from the interplay of transverse and longitudinal gauge field components and has an anisotropic directional profile, with a highly anisotropic transverse component of $j_T \sim \sin(6\theta)$ resulting from the threefold symmetry of the hexagonal lattice of graphene. The longitudinal uniform current is almost isotropic in its directional profile, but both the longitudinal and transverse parts of the dispersive current are predicted to be strongly anisotropic, with a directional dependence of ~ $\sin^2(3\theta)$ or $\cos^2(3\theta)$. Finally, we highlight that in an independent experimental study where the sound-induced Hall voltage is measured[8], and it nicely confirm the validity of our theoretical predication in graphene. The schematic setup and the numerical results in graphene are shown in Figure 2.

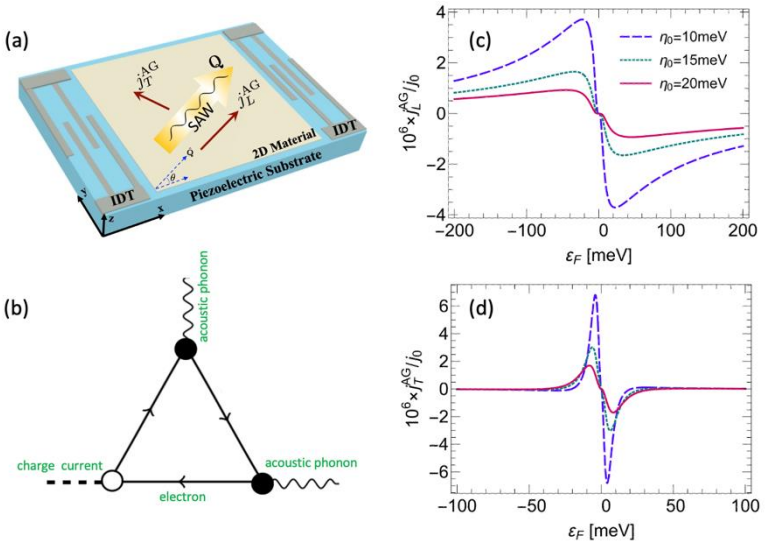

Figure 2 depicts the experimental setup used to generate acoustogalvanic (AG) currents due to the second-order response to the pseudogauge potential induced by a surface acoustic wave (SAW) propagating in a 2D hexagonal Dirac material placed on a piezoelectric substrate. Electric signals are converted into SAW with frequency Ω using interdigital transducers (IDTs), which propagate along $\boldsymbol{Q}$. In this figure, $\boldsymbol{j_L^{AG}}$ and $\boldsymbol{j_T^{AG}}$ represent the longitudinal and transverse AG currents, respectively, while θ is the angle obtained by the phonon wave vector with the x direction (zigzag orientation on the hexagonal lattice). The Feynman diagrams for the acoustogalvanic response function in 2D hexagonal Dirac materials are shown in (b). The longitudinal and transverse components of the AG current in 2D hexagonal Dirac materials, such as graphene, depend on various factors. In (c) and (d), we see the longitudinal and transverse components of the uniform AG current, respectively.

Acknowledgment
I acknowledge P. O. Sukhachov, P. Bhalla, and G. Vignale for collaboration in separate studies of acoustogalvanic effect in 3D and 2D Dirac materials. This work was supported by Nordita and the Swedish Research Council (VR 2018-04252).

References
[1]C. L. Kane and E. J. Mele, Phys. Rev. Lett. **78**, 1932 (1997).
[2]H. Suzuura and T. Ando, Phys. Rev. B **65**, 235412 (2002).
[3]M. I. Katsnelson and K. S. Novoselov, Solid State Commun. **143**, 3 (2007).
[4]M. A. H. Vozmediano, M. I. Katsnelson, and F. Guinea, Phys. Rep. **496**, 109 (2010).
[5]H. Rostami, R. Roldán, E. Cappelluti, R. Asgari, F Guinea, Phys. Rev. B **92** , 195402 (2015).
[6] P. O. Sukhachov and H. Rostami, Phys. Rev. Lett. **124**, 126602 (2020)
[7] P. Bhalla, G. Vignale, and H. Rostami, Phys. Rev. B **105**, 125407 (2022).
[8] P. Zhao, C. H. Sharma, R. Liang, C. Glasenapp, L. Mourokh, V. M. Kovalev, P. Huber, M. Prada, L. Tiemann, and R. H. Blick, Phys. Rev. Lett. **128**, 256601 (2022).

Friday 16th June

PHONONICS 2023: 6th International Conference on Phononic Crystals/Metamaterials/Metasurfaces, Phonon Transport, and Topological Phononics
Manchester, England, June 12-16, 2023
PHONONICS-2023-0173

Non-reciprocal Sound Scattering with Spatiotemporally Modulated Acoustic Metasurfaces

Janghoon Kang, Michael R. Haberman

Walker Department of Mechanical Engineering, The University of Texas at Austin
204 E. Dean Keeton Street, Austin, Texas 78712-1591, USA
jh3010.kang@utexas.edu, haberman@utexas.edu

Abstract: This work employs a semi-analytical model to investigate acoustic scattering from a geometrically flat surface with spatiotemporally modulated input impedance. The modulation frequency and depth are varied in order to demonstrate regimes of acoustic diffusion or nonreciprocal scattering. Investigation of the scattering amplitudes as a function of frequency and wavenumber enables simple interpretation of the transition between these scattering regimes.

Introduction. Spatiotemporal modulation of material properties has been used in unbounded electromagnetic and acoustic domains to provide enhanced control of propagating waves via non-reciprocity[1]. Modulated material stiffness was recently analyzed in the context of vibrating finite-length Euler beams using a semi-analytical modal expansion technique that includes modulation harmonics to show that losses are required to observe nonreciprocal vibrational motion[2]. We have recently employed a similar modal expansion method to show that spatiotemporally modulated surface admittance at the boundary of an acoustic domain improves the performance of sound diffusers by altering the direction of scattered diffraction modes via the introduction of modulation harmonics for all diffracted orders[3]. That work showed that the far field scattering pattern depends on the direction of spatiotemporal modulation, which indicates the possibility of generating highly nonreciprocal reflective acoustic metasurfaces (AMS) by tuning the spatiotemporal modulation of the input acoustic admittance. We therefore considered the case of a flat reflecting surface having admittance that can be modulated in the form of a travelling wave with the modulation frequency ω_m and the amplitude Y_m, i.e. $Y(x,t) = Y_0(x) + j\mathrm{Y}_m \cos(\omega_m t \pm k_m x)$ and identified parameter combinations the enable diffusive or non-reciprocal sound scattering.

Parametric Study. A parametric study on a wide range of the modulation frequency and admittance. We note that the spatial wavenumber of the modulation is fixed with the predetermined length of one period, Λ, which we fix as L, where L is the length of one unit cell of the scattering surface. A parametric study show that some modulation parameter pairs generate a high degree of non-reciprocity, while others do not. The case of $c_m/c_0 = 0.92$ and $\mathrm{Y}_m = 1.97$ yields the strongly non-reciprocal scattering response shown in Fig. 1. The far-field scattered directivity response for this case is determined using the semi-analytical model and the resultant scattering amplitudes within the sonic cone shown in Fig. 2(a). The directivity plot in Fig. 1(a) shows that the response changes significantly depending on the direction of spatial modulation. These results demonstrate that

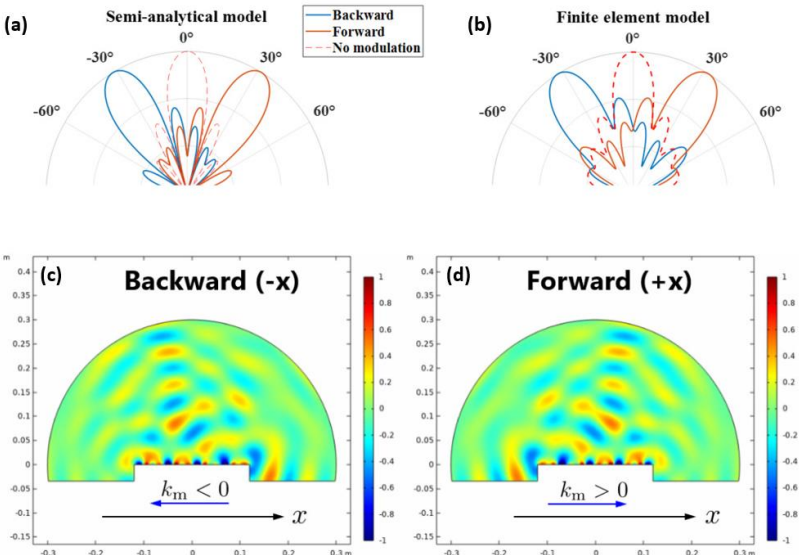

Figure 1: The far-field scattering pattern of a normally incident plane wave for different modulation directions using modulation parameters found in a parametric study to induce strongly non-reciprocal scattering. The predictions using the semi-analytical model and a time-domain finite element model are shown in (a) and (b), respectively. Panels (c) and (d) show the near-field of the scattered sound for two different modulation directions calculated using FEM.

the symmetric (flat) geometry of the surface enables the use of spatiotemporal modulation and a specific set of modulation parameters to produce a high degree of nonreciprocal scattering. The plot of the magnitude of the scattering amplitudes provided in Fig. 2(a) shows that for the case considered here, the sound energy is concentrated in the direction of the mode of $n = 1$ and $p = 1$ and that when the direction of modulation reverses, sound is scattered primarily in the direction of the $n = -1$ and $p = -1$ mode, leading to strongly nonreciprocal scattering. The iso-frequency curves (i.e. slowness contours) and the dispersion diagram in Figs. 2(c) and (b), respectively, shows a convenient representation to interpret how the spatiotemporal modulation leads the control of backscattered sound energy and mode selection for propagating or evanescent modes. Finally, we have compared the far-field response predicted using the semi-analytical model with the results obtained using time-domain finite element model using Comsol Multiphysics with the same geometry and modulation function. These results are shown in Fig. 1(b)-(d). Modulated surface admittance was realized using an impedance boundary condition defined with the same modulation function used to generate the scattered field predictions provided in Fig. 1(a).

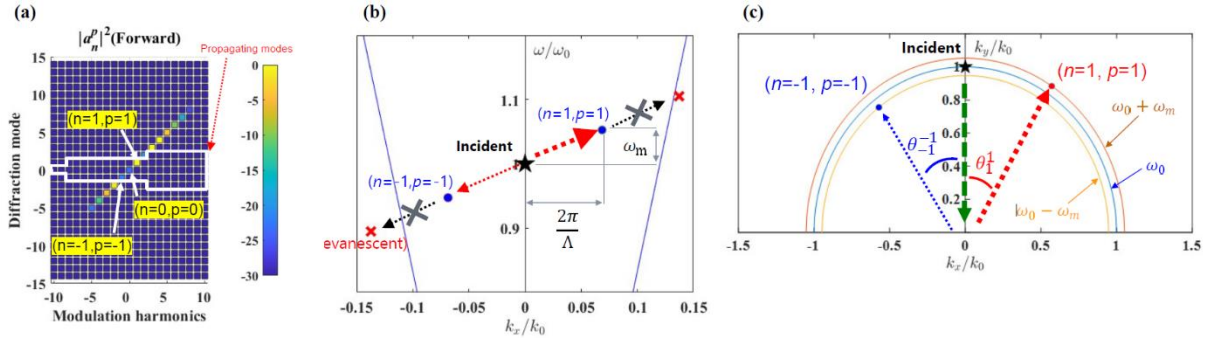

Figure 2: (a) Magnitudes of the scattering amplitudes for different diffraction orders, n, and modulation harmonics, p, for the case shown in Fig. 1. (b) Identification of propagating and evanescent modes depending on the wavenumber of the scattered sound in the x-direction and the direction-dependent shifted frequencies. (c) Propagating scattered plane wave modes shown on a slowness surface (wavenumber space). Concentric half-circles represent iso-frequency contours in wavenumber-space for the incident and frequency-modulated scattered fields with the diffracted order-modulation frequency pairs (p, n) = (-1, -1) and (p, n) = (1, 1) shown on the isofrequency contours.

Conclusions. A previously-developed semi-analytical model to predict the performance of a spatiotemporally modulated sound diffuser was employed in this work to show that flat surfaces with spatiotemporal modulation of the input impedance can be used to generate nonreciprocal scattering behaviour. This was explored by investigating the frequency-wavenumber shifting of the scattering amplitudes due to time and space modulation of the surface response. Continuity of momentum at the AMS-fluid interface imposes the scattering of energy into directions associated with diffraction orders and frequencies that are shifted away from the incident wave frequency by integer multiples of the modulation frequency. We have shown that the diversification of propagating modes can be used to improve diffusion performance or to generate a nonreciprocal sound scattering depending on the selection of the appropriate modulation parameters. We have selected a representative nonreciprocal scattering case by performing a parametric study of the modulation parameters and evaluating the performance with a nonreciprocity metric. The far-field responses obtained from the semi-analytical model and finite element model clearly show that the scattered sound field becomes asymmetric when modulated and that the direction of scattered field asymmetry is controlled by the modulation direction.

References

[1] H. Nassar, B. Yousefzadeh, R. Fleury, M. Ruzzene, A. Alù, C. Daraio, A.N. Norris, G. Huang, M.R. Haberman, "Nonreciprocity in acoustic and elastic materials," Nat. Rev. Mat. **5**, 667-685 (2020).
[2] B.M. Goldsberry, S.P. Wallen, M.R. Haberman, "Nonreciprocal vibrations of finite elastic structures with spatiotemporally modulated material properties," Phys. Rev. B **102**, 014312, (2020).
[3] J. Kang and M.R. Haberman, "Sound diffusion with spatiotemporally modulated acoustic metasurfaces," Appl. Phys. Lett. **121**, 181703 (2022).

PHONONICS 2023: 6th International Conference on Phononic Crystals/Metamaterials/Metasurfaces, Phonon Transport, and Topological Phononics
Manchester, England, June 12-16, 2023
PHONONICS-2023-0129

Shannon Entropy as a Characterization Tool in Acoustics

José Sánchez-Dehesa

Department of Electronic Engineering, Universitat Politècnica de Valencia, Camino de vera s.n. (building 7F), ES-46020 Valencia, Spain,
jsdehesa@upv.es

Abstract: We introduce Shannon entropy as a tool to characterize the spreading of acoustic modes. Here, it is employed to study the acoustic analog of the resonant Zener tunneling observed in graded acoustic superlattices. It is shown that the two acoustic levels involved in the phenomenon maximize their Shannon entropy at the critical gradient where the levels anticross.

The Shannon entropy formula has been applied to a large variety of interdisciplinary fields since his introduction in 1948[1]. For example, it has opened new avenues of interpretation of well-known physical phenomena in crystallography and atomic physics[2]. Here, we introduce the acoustic version of the Shannon entropy to describe acoustic effects where localization plays a fundamental role. There are already several indicators of the spatial spreading of an eigenmode, among others the inverse participation ratio (IPR)[3]. However, we believe that Shannon entropy is a good alternative to IPR since it is a global concept, coupling information and complexity from wave phenomena to virtually any discipline in science. Here, Shannon entropy is employed to study the dynamics of the Zener-like effect occurring in graded acoustic superlattices[4]. This will be done by analyzing the avoided crossing occurring between acoustic levels belonging to different minibands in ultrasonic superlattices. In what follows, we introduce the Shannon entropy formula adapted to acoustics and applied to the case of a multilayer of water cavities and metamaterial slabs, a structure equivalent to that studied in Ref. 4.

In atomic physics, the Shannon entropy has been defined as $S_\rho = -\int \rho(\mathbf{r}) \ln \rho(\mathbf{r}) d\mathbf{r}$, where $\rho(\mathbf{r})=|\psi(\mathbf{r})|^2$ is the probability density distribution of a given electronic state. For classical fields, however, there is no equivalent magnitude having an interpretation of a probability distribution. To overcome this issue we have exploited the analogy between electronic states in quantum mechanics and acoustic levels in material structures. Slabs of solid material in the air sustain acoustic vibrations that can be considered as the eigenmodes of their associated wave equations, with the boundary conditions imposed by the material interfaces. These eigenmodes have a certain lifetime and can be considered the quantum counterparts of the atomic levels. From the analogy with atomic systems, we introduce the following probability distribution function[5]:

$$P(\boldsymbol{r}) = |u(\mathbf{r})|^2 / \int |u(\mathbf{r})|^2 d\mathbf{r}, \quad (1)$$

with $u(\mathbf{r})$ being the displacement field, which will play in acoustics the same role as the electronic density distribution in quantum mechanics. Let us stress that the velocity or the pressure fields can be equally employed to define P(r) since they are related quantities in linear acoustic. Therefore, Shannon's information entropy is defined by:

$$S_u = -\int P(r) \ln P(r) dr, \quad (2)$$

The quantity S_u provides an information measure of the spatial spreading of the acoustic level, hence yielding uncertainty in the field localization. Like the Shannon entropy, S_u increases with increasing uncertainty (i.e., spreading of the field state).

Let us consider structures like that schematically depicted in Figure 1, consisting of a multilayer made of *m* coupled cavities, Wm, enclosed by m + 1 slabs, Am. In addition, we consider that the slabs Am are made of a metamaterial (sonic crystal) with homogeneous parameters ρ_A and c_A, respectively, mass density and sound speed. Analogous structures made of water cavities enclosed by Plexiglas slabs have been employed to observe acoustic Bloch oscillations and Zener tunneling (ZT).[4]

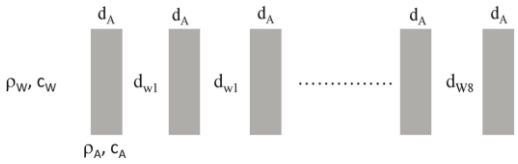

Figure 1 Scheme of the multilayered structures considered in this study, consisting of eight cavities, Wm, separated by nine homogenized sonic crystal slabs, Am, embedded in an inviscid fluid with acoustic parameters ρ_W and c_W

To observe the resonant ZT effect, we break the translational symmetry by introducing a gradient $\Delta(1/d_W)$ in the thicknesses, d_W, of the water cavities. Figure 2 displays the frequency and Shannon entropy, respectively, of the levels involved in the avoided crossing, a feature describing the ZT. Figure 2A shows that the frequency of u_2 (red dashed line) is always higher than that of u_1 (blue line), although both frequencies approach each other near the critical thickness gradient. Figure 2B shows that the entropy of the modes exhibits different behaviors, strongly correlated with the gradient values. For small gradients (i.e., for values much lower than the critical) the entropy S_{u2} is smaller than S_{u1}. This behavior indicates that the sound in the mode u_2 is more localized than in u_1. For increasing values of the gradient, both modes show a similar trend, increasing their entropy up to the region between 10.02% and 10.06%, where the modes strongly mix up and the slope of their entropy abruptly changes from positive to negative at the critical gradient value (10.04%). This interpretation is further supported by the calculated lifetimes of the acoustic modes shown in Fig. 2C and the results of the modes' amplitude shown in Fig. 3. Figure 3 (middle panel) shows that at the critical gradient (10.04%), the modes resulting from the interaction are the bonding and antibonding combinations of the non-interacting modes. Then, their corresponding displacement fields (wavefunctions) show maximum spreading and the Shannon entropy have maximum values.

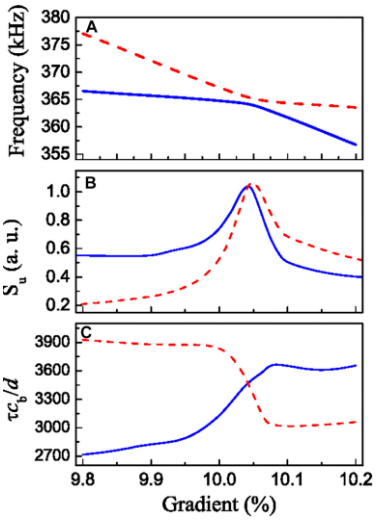

Figure 2 Frequency (A), Shannon entropy (B), and lifetime (C) of the two interacting acoustic modes, u_1, and u_2, near the avoided crossing region for the acoustic structure described in Figure 1

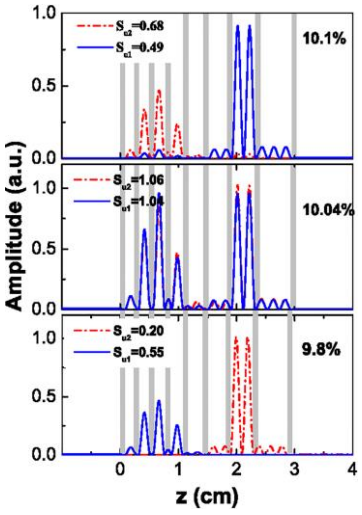

Figure 3 Amplitude (in arb. units) of the acoustic modes u_1 (blue line) and u_2 (red line) calculated for three values of the thickness gradient. The value 10.04% corresponds to the critical gradient where the avoided crossing occurs.

Work supported by grant PID2020-112759GB-I00 funded by MCIN/AEI/10.13039/501100011033.

References

[1] C. E. Shannon. A mathematical theory of communication. *Bell Syst Tech J* **27**, 379–656 (1948).

[2] R. González-Férez, J. S. Dehesa. Shannon entropy as an indicator of atomic avoided crossings in strong parallel magnetic and electric fields. Phys Rev Lett. **91**, 11301 (2003).

[3] D. J. Thouless DJ. Electrons in disordered systems and the theory of localization. *Phys Rep* 13, 93-142 (1974).

[4] H. Sanchis-Alepuz, Y. A. Kosevich, J. Sánchez-Dehesa. Acoustic analog of electronic Bloch oscillations and resonant Zener tunneling in ultrasonic superlattices. *Phys Rev. Lett.* **98**, 134301 (2007).

[5] J. Sánchez-Dehesa and R. Arias-González. Characterization of avoided crossings in acoustic superlattices: The Shannon entropy in acoustics. *Front. Phys.* **10**, 971171 (2022).

PHONONICS 2023: 6th International Conference on Phononic Crystals/Metamaterials/Metasurfaces, Phonon Transport, and Topological Phononics
Manchester, England, June 12-16, 2023
PHONONICS-2023-0167

Nonlocally-Resonant Elastic Metamaterials

Aleksi Bossart[1] , Romain Fleury[1]

[1]École Polytechnique Fédérale de Lausanne, 1015 Lausanne, Switzerland,
aleksi.bossart@epfl.ch, romain.fleury@epfl.ch

Abstract: Here, we show how to leverage nonlocal resonances -delocalized zero-energy modes with nontrivial wavevectors- to induce anomalous dispersion cones in architected phononic media. The presence of such cones induces many hallmark properties of metamaterials, such as negative refraction, band gaps, slow sound and subwavelength character, albeit without suffering from the same bandwidth limitations. We explain how to control and even inversely design key properties of anomalous cones, namely their shapes, positions and overall number.

To date, the vast majority of architected materials leverage either Bragg interference (in phononic crystals) or local resonances (in traditional metamaterials). Here, inspired by interlaced wire media[1,2], we introduce a third class, which we call *nonlocally-resonant metamaterials*. The prototypical dispersion of a locally-resonant metamaterial is shown in Fig.1(ab): the overlap of negative-property bands leads to a subwavelength but narrow branch with negative group velocity. Nonlocally-resonant metamaterials rely on an entirely different concept: the essential ingredient is a zero-energy mode that extends over the entire lattice. In a band diagram, this translates into an intersection with the zero-frequency axis at a particular wavevector k_R (see Fig.1(c)); by continuity, an anomalous cone nucleates from k_R. This leads to broad ranges of negative group velocity and gap-inducing hybridization with other branches, among other unusual wave properties. In the realm of elasticity, this zero-mode translates into a nontrivial, sample-spanning mechanism; we show a concrete example in Fig.1(d). In Ref.[3], we introduce the theory of nonlocally-resonant metamaterials and study the associated wave phenomena using full-wave simulations and experiments. In particular, we 3D-printed a flexible metamaterial, in which we directly observed the signature of two nonlocal resonances at the K and K' points using laser Doppler vibrometry (Fig.1(ef)).

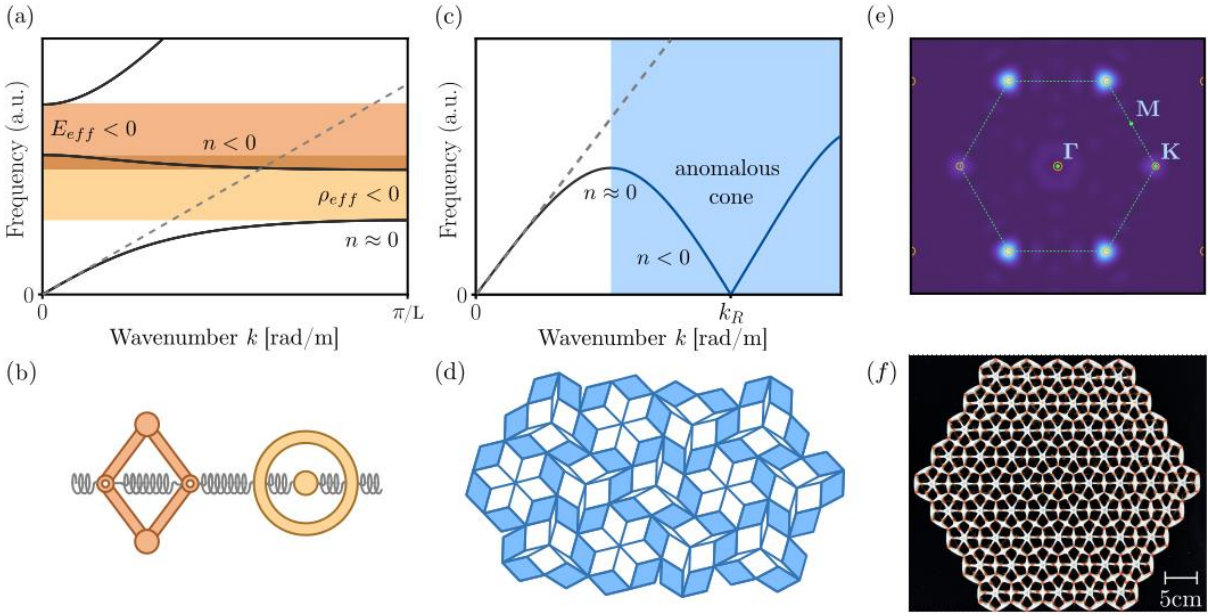

Figure 1 Contrasting the concepts of locally-resonant **(ab)** and nonlocally-resonant metamaterials **(cd)**. **(a)** Band structure of a 1D chain with a negative compressibility range (orange) and a negative density range (yellow). **(b)** Geometry of the locally-resonant chain. **(c)** Dispersion of a nonlocally-resonant metamaterial, with the anomalous cone highlighted in blue. **(d)** Zero-energy deformation mode responsible for the anomalous cone. Experimental realisation of nonlocally-resonant metamaterial **(ef)**. (e) Spatial Fourier transform of in-plane velocity at 106Hz. **(f)** 3D-printed nonlocally-resonant flexible metamaterial.

To provide backing for our bandwidth claim, we pick one of the hallmark properties of metamaterials, namely negative refraction, and conduct a series of full-wave simulations in which we compare non-locally-resonant and locally-resonant metamaterials. In Fig.2(a-e), we see that the nonlocally-resonant metamaterial provides negative refraction over a relative bandwidth of 48%, without distorting the beam profile. In contrast, considering a representative locally-resonant metamaterial with the geometry reported in Ref.[4], negative refraction occurs over a 0.33% relative bandwidth. The locally-resonant metamaterial is also less subwavelength; the resulting increase in metamaterial granularity leads to more distorted outgoing beam profile (see S.I of Ref.[3]).

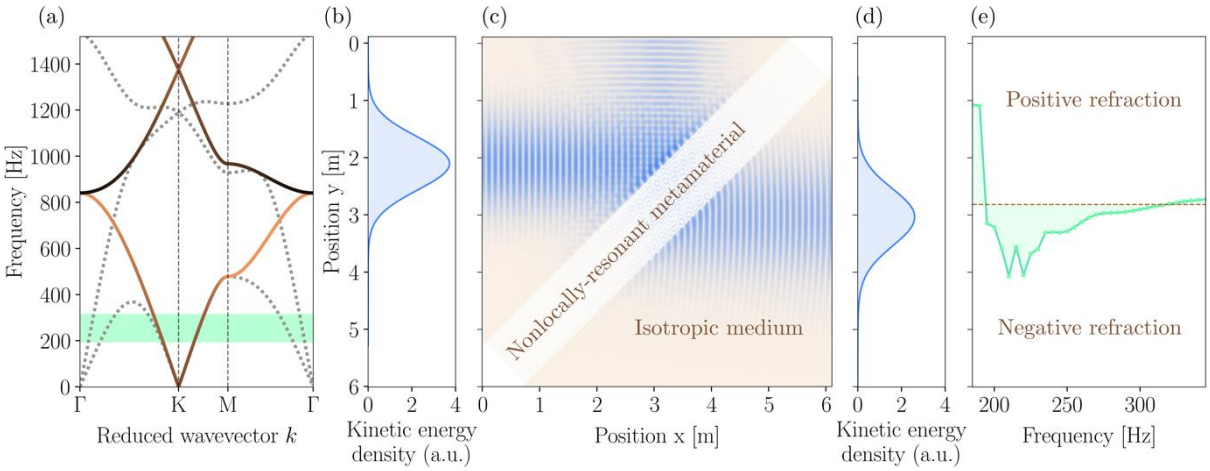

Figure 2 Bandwidth of negative refraction. (a) Band structure corresponding to our 3D-printed geometry (dashed lines) and pinned version (solid line). The frequency range of negative refraction for a single choice of isotropic medium is indicated in green. (b) Profile of a monochromatic gaussian beam. (c) Frequency-domain finite-element simulation with the aforementioned beam imposed on the left side, and perfectly-matched layers on all sides (not shown). (d) Profile of the beam on the right edge, after having been refracted twice. (e) Position of beam center for varying frequencies, with a dashed line indicating the transition from positive to negative refraction.

Nonlocal resonances extend the metamaterial toolbox with anomalous cones whose shape, number and position can be designed using a directed graph theory[5]. There, we use directed graphs to encode the quasistatic deformations of the zero-modes using minimal ingredients, without having to consider dynamical aspects. It also allows for a combinatorial approach to design in which we can combine building blocks with known kinematics to reach target deformation patterns. Finally, it allows for inverse design of geometries exhibiting anomalous dispersion cones at target locations in k-space. Such cones drastically impact wave propagation, leading to broadband wave properties such as band gaps, slow sound and negative refraction at an extremely subwavelength scale.

References

[1] W.-J. Chen, B. Hou, Z.-Q. Zhang, J. B. Pendry, and C. T. Chan, *Nat Commun*, **vol. 9**, no. 1, p. 2086 (2018)
[2] D. Sakhno, E. Koreshin, and P. A. Belov, *Phys. Rev. B*, **vol. 104**, no. 10, p. L100304 (2021)
[3] A. Bossart and R. Fleury *arXiv (under review in PRL)*, http://arxiv.org/abs/2209.02618. (2022)
[4] Y.-F. Wang, Y.-S. Wang, and C. Zhang *J. Acoust. Soc. Am.*, **vol. 139**, no. 6, pp. 3311–3319 (2016)
[5] A. Bossart, D. M. J. Dykstra, J. van der Laan, and C. Coulais *Proc. Natl. Acad. Sci. U.S.A.*, **vol. 118**, no. 21, p. e2018610118, (2021)
[6] Y. Chen, M. Kadic, and M. Wegener *Nat. Commun.*, **vol.12**, no. 1, p. 3278, (2021)
[7] K. Bertoldi, V. Vitelli, J. Christensen, and M. van Hecke, *Nat Rev Mater*, **vol. 2**, no.11, p. 17066 (2017)
[8] K. D. Hammonds, M. T. Dove, A. P. Giddy, V. Heine, and B. Winkler, *American Mineralogist*, **vol. 81**, no. 9–10, pp. 1057–1079 (1996)

PHONONICS 2023: 6th International Conference on Phononic Crystals/Metamaterials/Metasurfaces, Phonon Transport, and Topological Phononics
Manchester, England, June 12-16, 2023
PHONONICS-2023-0154

On the Nature of Boundaries and Interfaces in Metamaterials and Phononic Crystals

Ankit Srivastava[1]

[1] *Mechanical Materials and Aerospace Engineering, Illinois Institute of Technology, 10 West 32nd St., John T. Rettaliata Engineering Center, Room 243*
Chicago, IL 60616-3793
asriva13@iit.edu

Abstract: In this talk, we discuss the problem of determining appropriate conditions at the interfaces and boundaries of metamaterials and phononic crystals. We show that the proposed solutions fall under two categories – augmenting the boundary/interface conditions through the use of additional relations, and smearing out the boundary/interface so that it cannot be considered sharp anymore. In either case, we show that the solution involves the use of additional parameters – in some scenarios these parameters may be thought of simply as fitting parameters but in others they behave as material properties which appropriately satisfy such principles as causality and passivity.

In this talk, we consider the problem of determining the nature of the boundaries and interfaces involving metamaterials and phononic crystals. The problem appears when one tries to join two distinct heterogeneous media (or a heterogeneous media and a homogeneous media) and describe the wave physics based upon overall (metamaterial) property descriptions. We note that this problem appears naturally in other areas of physics, especially peridynamics, and is connected to the general problem of determining the appropriate boundary/interface conditions in materials which can exhibit nonlocal behavior. In such media, especially in the presence of nonlocality, material behavior near a boundary or an interface is markedly different from the behavior in the bulk and, as such, leads to additional complications when joining such media to other media. The practical implication of this is that even if one creates an appropriate method of assigning properties to the bulk of a heterogeneous media (such as in metamaterials), it still does not solve the problem of joining at an interface or understanding its dynamics near the boundaries. The purpose of this talk is to succinctly describe this problem and lay out some approaches (both old and new) towards solving it.

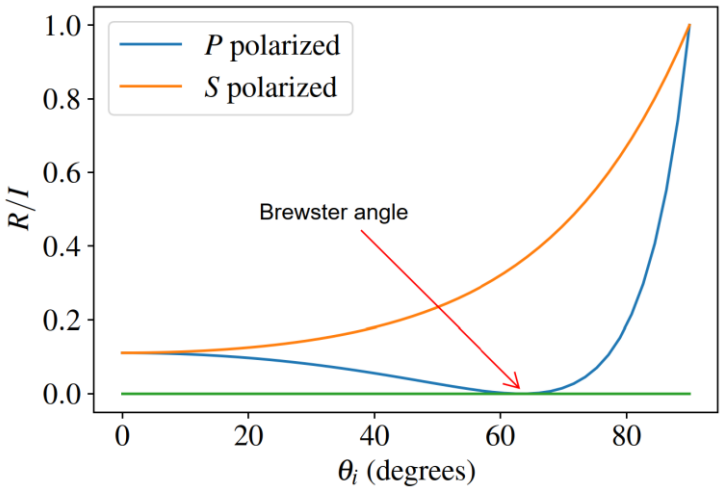

Figure 1: Reflection coefficient of P/S waves as a function of incidence angle. The Brewster angle is indicated.

The early origins of this problem are charted to the mid-1800s with the discovery of the Brewster angle anomaly in real materials such as glass and diamond. In his landmark paper in the early 19th century, Fresnel considered the problem of reflection and transmission of light at an interface between two media and arrived at what are now known as the much celebrated Fresnel equations. These equations, and the subsequent experimental studies carried out to verify their predictions, form some of the first forays into understanding the nature of the interface which exists between two media. This question - what is the nature of the interface between two media? - has again assumed modern importance with the advent of the field of metamaterials. While the early history of metamaterials concerned itself largely with the question of assigning appropriate material properties to infinitely repeating heterogeneous structures, of late, the question of finite samples of metamaterials has been gaining research interest. This is only natural since any prac-

tical application of metamaterials necessarily requires its finite samples and not its hypothetical infinite incarnation. With finite samples, however, comes the natural question of interfaces and boundaries, and of how to consider them in a consistent manner. Fresnel derived the reflection and transmission coefficients of light which is polarized parallel to the plane of the interface (P-polarized) and of light which is polarized perpendicular (S-polarized) to the plane of the interface. Brewster angle is defined as the angle of incidence where unpolarized light is reflected as perfectly S-polarized light (since the P-polarized part of the light is perfectly transmitted). Experiments were carried out by Jules Jamin in the mid 19th century to verify the predictions from Fresnel equations and found that the experimental results differed from these predictions near the Brewster angle.

The early proposed solutions to this discrepancy fell into two categories which both amount to arming oneself with a set of fitting parameters in order to account for the deviations from locality near the Brewster angle. In one case, the fitting parameters are physically understood to represent an interface (or a boundary) which ceases to be sharp in the homogenized context and in the other case, the interface is physically understood to exhibit modified interface conditions. Thus, to properly account for finite material specimens in appropriate nonlocal regimes, either the interface was to be understood as non-sharp or the interface conditions were to be understood as non-conventional.

A similar categorization of solutions appears to have taken shape in modern metamaterials research where transition layers (similar to those originally proposed by Drude; Drude transition layers) appear to have gained popularity in electromagnetic metamaterials whereas “extra” continuity conditions emerge naturally in elastic/acoustic micromorphic theories and other homogenization schemes where nonlocality is implicitly subsumed in extra variables (in an interesting modern parallel to the classical nonlocal vs hidden variables schemes). Other techniques proposed include satisfying interface conditions in a variational sense or through a process of optimization. The goal of this talk, therefore, is to provide a vantage point from which to examine the various approaches towards attending to the problem of boundaries and interfaces in modern metamaterials research.

PHONONICS 2023: 6th International Conference on Phononic Crystals/Metamaterials/Metasurfaces, Phonon Transport, and Topological Phononics
Manchester, England, June 12-16, 2023
PHONONICS-2023-0192

Propagation of Elastic Waves in Randomly Distributed Pillars on Metamaterial Phononic Plate

Yan Pennec[1], Laurent Carpentier[1], Runcheng Cai[1,2], Yabin Jin[2], Adnane Noual[3], Bahram Djafari-Rouhani[1], Thibault Deletang[4], and Bernard Bonello[4]

[1]IEMN, UMR 8520 CNRS, Université de Lille, F-59000 Lille, France
[2] School of Aerospace Engineering and Applied Mechanics, Tongji University, 200092 Shanghai, China
[3]LPMR, Département de Physique, Faculté des Sciences, Université Mohamed Premier, 60000 Oujda, Morocco
[4]UPMC Univ Paris 06, UMR CNRS 7588, INSP, 75005, Paris, France
Corresponding author: yan.pennec@univ-lille.fr

Abstract: We theoretically investigate the interaction between an array of sub-wavelength pillars on a substrate or a plate. FEM simulations allows to calculate the resonant modes of a finite chain of N pillars with linear, bent or random distributions and demonstrate the propagation along the chain. Then, using a mass-spring model of pillars on a plate, the propagation and confinement of 2D elastic waves are studied analytically by multiple scattering method.

Pillared phononic crystals and meta-materials are an emerging class of artificial structures consisting of pillars standing on a substrate or a plate[1, 2]. In most cases, in the low frequency regime, pillars of sub-wavelength dimensions are considered as single entities, resonating independently from their close neighbors.

In this work, we first use the finite element method to study the eigen-modes of a pair or a chain of N pillars on a substrate and demonstrate that the coupling between pillars occurs essentially through their compressional resonances. The pillars and the substrate are respectively made of aluminum and silicon. The height of the pillars is 1µm with a diameter of 200nm, assuming that the fundamental eigen resonances of the pillar-on-plate are frequency independents of each other. The coupling between the pillars manifests itself in the lifting of the degeneracy of the compressional resonances and the spreading of the corresponding eigenmodes over the pillars. In contrast, the bending resonances remain at the same frequency and do not contribute to the coupling. In the case of a chain of pillars, we calculate the eigen-modes using the super cell presented in Fig. a, applying periodic boundaries along the directions x and y. We first consider a distance of l = 50 nm between the cylinders and increase the number N of pillars constituting the chain (Fig. b). One can see that the number of eigenmodes is equal to the number of pillars and their frequencies spread over a passband ranging from 1.1 to 1.2 GHz when N increases. This property thus offers a new opportunity to propagate the surface acoustic waves along the chain, by coupling the compressional modes whose frequency can be tuned with the geometrical parameters of the pillars. Fig. c represents the evolution of the eigenvalues of a chain constituted by five pillars as a function of pillar separation and the corresponding eigenmodes are presented in the inset. Moreover, one can follow the evolution of the width of the pass band for 5 pillars and how it decreases when the inter-pillar distance (l) increases. Furthermore, we shall discuss how the excitation of the compressional resonance in one pillar can be transmitted through a linear chain, possibly in presence of zigzag, defects or disorder along the chain.

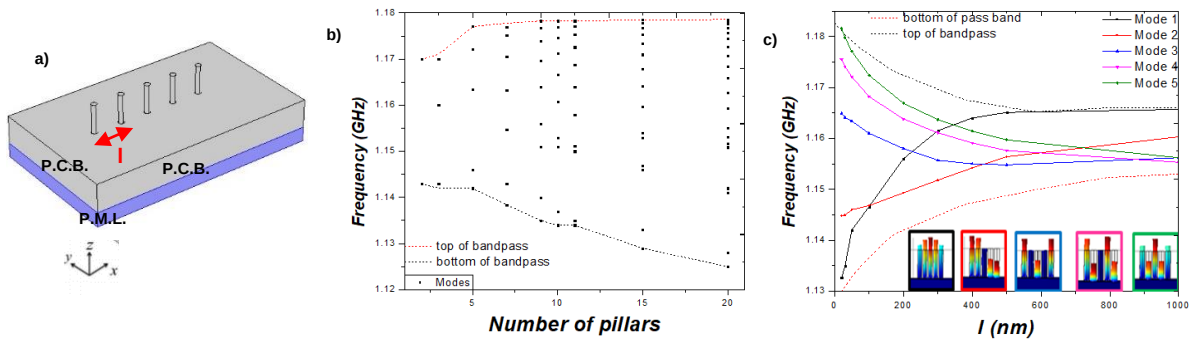

Fig. (a) 3D-schematic view of the elementary unit cell for the eigen-modes calculation of a linear chain of pillars. (b) Evolution of the eigen-modes as a function of the number of pillars separated by 50 nm from each other. (c) Evolution of the compressional eigen-modes as a function of the distance *l* between the pillars for a chain of 5 pillars.

Another outcome of this work is to calculate the scattering of a surface acoustic wave by a 2D array of pillars and evaluate how the scattered wave deviates from a sum of waves emitted by individual pillars. To perform this analysis on a statistical basis, we develop an analytical calculation based on the Green function formalism[3]. We aim to study the opportunities of propagation and confinement of elastic waves in the case of periodic, hyperuniform and random distributions. The disorder in position will be introduced with the help of the Poisson's law, playing with the variance parameter. The results obtained with the multiple scattering method are compared with those of the numerical finite element method, considering both a half infinite silicon substrate and a thin membrane.

The dual confinement of photonic and phononic waves can be achieved in a same structure, managing the random distribution of the scatterers. Such co-localization and control of elastic wave in the hypersonic range and electromagnetic ones in the 1.55 µm wavelength range offers new opportunities of application in the telecommunication area.

Acknowledgements

This work was supported by the French National Research Agency ANR as part of the project "RANdom", ANR-19-CE24-0014.

References

[1] Y. Jin, Y. Pennec, B. Bonello, H. Honarvar, L. Dobrzynski, B. Djafari-Rouhani and M. Hussein, Physics of surface vibrational resonances: Pillared phononic crystals, metamaterials, and metasurfaces, *Reports on Progress in Physics*, 2021

[2] M. Lott, P. Roux, L. Seydoux, B. Tallon, A. Pelat, S. Skipetrov, and A. Colombi. "Localized Modes on a Metasurface through Multi-Wave Interactions." *Physical Review Materials* 4, no. 6 (June 29, 2020): 065203.

[3] D. Torrent, D. Mayou, J. Sanchez-Dehesa, *Phys. Rev.* B 87, 115143 (2013).

PHONONICS 2023: 6th International Conference on Phononic Crystals/Metamaterials/Metasurfaces, Phonon Transport, and Topological Phononics
Manchester, England, June 12-16, 2023
PHONONICS-2023-0050

Design of Metamaterials for Acoustic Stealth Using Optimization Tools

L. Roux[1], C. Croënne[2], M. Pouille[2], C. Audoly[1], A.-C. Hladky[2]

[1] *Naval Group Research, 199 Avenue Pierre-Gilles de Gennes, 83190 Ollioules, France,*
laetitia.roux@naval-group.com, christian.audoly@wanadoo.fr
[2] *Univ. Lille, CNRS, Centrale Lille, Univ. Polytechnique Hauts-de-France, Junia, UMR 8520 - IEMN, 59000 Lille, France,*
charles.croenne@isen.fr, monique.pouille@isen.fr, anne-christine.hladky@isen.fr

Abstract: For underwater acoustic stealth, submerged vehicles have to be coated with absorbing materials. In this work, an optimization tool is used for the design of such metamaterial coatings, in order to get a low anechoism coefficient over a broad frequency range. The optimized panel made of a specific arrangement of homogeneous layers has been fabricated and experimentally tested in a water tank.

For navies and naval industries, underwater sound has always been a crucial matter. Therefore, submerged vehicles are coated in order to make them less detectable. If transmission T and reflection R coefficients of the structure placed between two semi-infinite fluid media are often quantities of interest, specific quantities are introduced for underwater applications, such as the anechoic coefficient C_A, related to active detection. In that case, an acoustic wave is sent in the underwater environment and the detection of potential reflected waves informs on the presence and location of an obstacle. For underwater applications, the performance of the coating is evaluated using the coefficient C_A. It corresponds to the reflection coefficient when the structure is fixed on a perfectly rigid plate. Provided some assumptions, the coefficient C_A is related to the transmission T and reflection R coefficients[1].

In this presentation, optimization tools are used for the design of an anechoic panel, of a given thickness, made of different layers of only two different materials: stainless steel and a specific polyurethane rubber. This configuration is referred as the 1D-solution. First, normal incidence is considered. The optimization process[2], based on a genetic algorithm, is performed to search for the most efficient layer arrangement, taking into account both manufacturing and water tank testing limitations. The maximum length of the medium is set to 4 cm, consisting of 40 layers. The target frequency range for a low anechoic coefficient is [3 kHz − 25 kHz].

A bi-objective function is implemented in order to minimise the anechoic coefficient C_A over the given frequency range: (1) The first objective function aims to minimise the Root Mean Square (RMS) of the anechoic coefficient, referred to as $|C_A|$. (2) The second objective function aims at lowering the values of the coefficient that are higher than $|C_A|$, referred as σ_{CA}. The best layer arrangements are classically obtained following the Pareto front of the whole set of calculated solutions. The corresponding solutions are presented on Figure 1.a, They are sorted according to $|C_A|$ increasing.

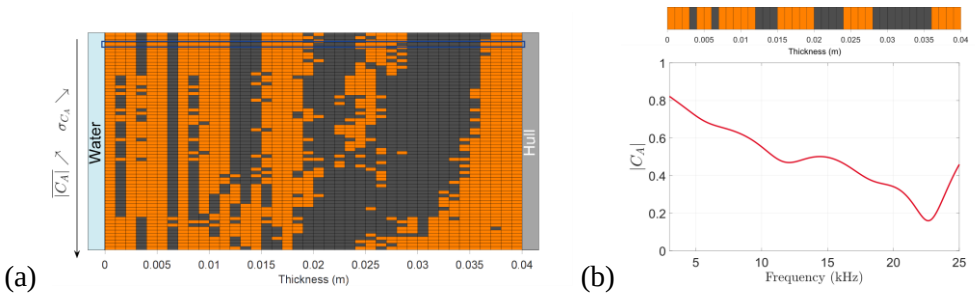

Figure 1 (a) Layer arrangement for all the solutions of the Pareto front. The orange color represents polyurethane while the dark grey color corresponds to stainless steel (b) Top: Theoretical layer arrangement and thicknesses (in meters) of the manufactured panel. In the anechoic configuration, Face 2 is on the hull and the incident plane wave arrives on Face 1. Bottom: theoretical C_A of the selected panel.

On Figure 1.a, x = 0 corresponds to the water/medium interface and x = 0.04 m to the face placed on the rigid surface (hull). It shows that some patterns are similar. One layer arrangement is selected for fabrication and measurements in a water tank: the design is presented in Figure 1.b as well as the corresponding numerical anechoic coefficient. The picture of the panel is presented on the left of Figure 2.

The 3-point method is used to measure the panel[3]. The reflection and transmission coefficients are derived for each side of the panel. On Figure 2, they are compared with the results from the numerical model. There is a good overall consistency between experimental and numerical results.

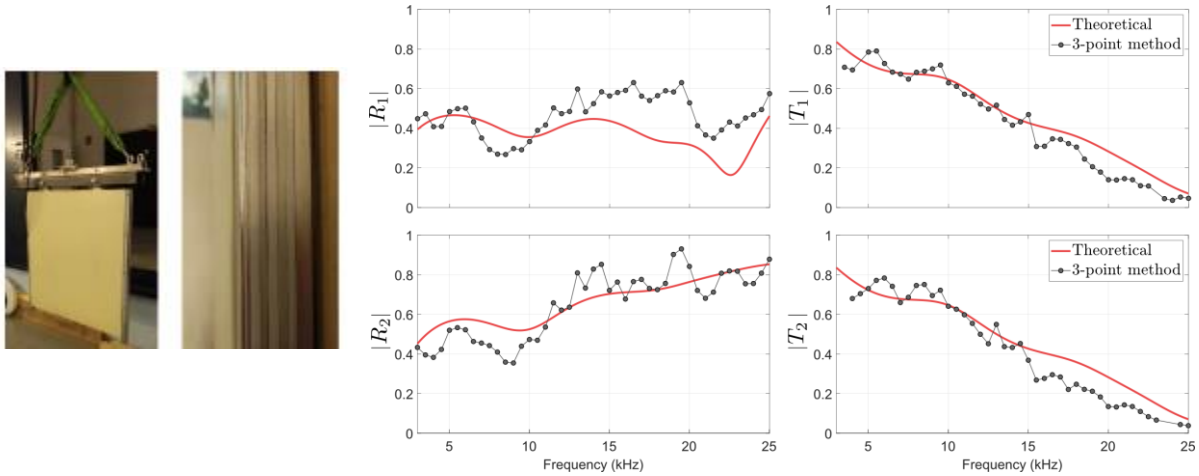

Figure 2: Left :picture of the panel, Right : Reflection and transmission coefficients of the multilayered medium obtained by insonification of Face 1 (R_1 and T_1) and) of Face 2 (R_2 and T_2).

The optimisation method has then been extended to layers containing various inclusions. Figure 3 presents the 14 considered unit cells. Two of them are homogeneous, made of either polyurethane or steel, whereas the others consist in a polyurethane matrix containing a steel inclusion. This configuration is referred to as the 2D-solution. A database is built, containing the effective properties of each unit for each frequency[4]. The same optimization algorithm has been run for the 2D-solution, considering the same material properties and total length as for the 1D-solution. It is observed (although not shown here) that the arrangements are similar: where a thin or thick steel layer is obtained for the 1D-solution within the given total length, a small or large steel inclusion, respectively, is obtained for the 2D-solution. However, the 2D-solution provides a much lower anechoic coefficient at higher frequencies (out of the given frequency range of interest), thanks to various resonances that can be tuned such as to be nicely spread in the frequency range of study.
The design of an anechoic coating using optimization tools can greatly help improving the broadband acoustic performance, by using multilayered media or media with macro inclusions, as well as their combination (i.e. media with both macro-inclusions and uniform layers). The optimization process could also be performed for other objective functions, as well as oblique incidence cases.

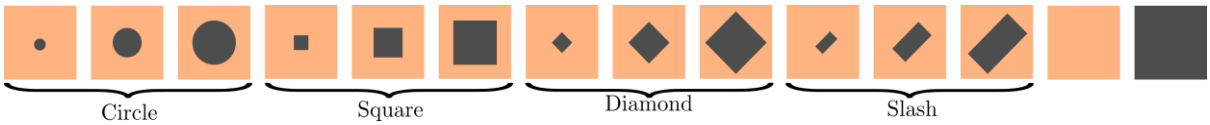

Figure 3 : Schematic diagram of the unit cells composing the database.

References

[1] C. Audoly, C., and C. Giangreco, Journal of Wave-Material Interaction 5(1), 55–72, (1991)
[2] Deb, K., and Goel, T. (Zurich, Switzerland, 7-9 March 2001) in Proceedings of the First International Conference on Evolutionary Multi-Criterion Optimization. Elitist genetic algorithm, variant of NSGA-II is used through the MATLAB Global Optimization Toolbox.
[3] L. Roux, M. Pouille, C. Audoly and A.C. Hladky, Journal of the Acoustical Society of America 147(2), 1104–1112 (2020)
[4] L. Roux, C. Croënne, C. Audoly and A.C. Hladky-Hennion, Journal of Applied Physics 127(22), 450 225102, (2020)

PHONONICS 2023: 6th International Conference on Phononic Crystals/Metamaterials/Metasurfaces, Phonon Transport, and Topological Phononics
Manchester, England, June 12-16, 2023
PHONONICS-2023-0225

Spherical aberration in a 2D sound delivery system

Chinmay Rajguru, Gianluca Memoli

[1] *AURORA Project, School of Engineering and Informatics, University of Sussex, Brighton (UK)*
c.rajguru@sussex.ac.uk; g.memoli@sussex.ac.uk

Abstract: 3D sound underpins immersive experiences and traditionally requires headphones or multiple speakers. In this study, metamaterial lenses turn a single speaker into a 2D sound delivery system, delivering sound at variable locations and distances. We evaluate the performance of this system, using acoustic measurements, highlighting its possibilities and limitations in preparation for a user study.

An increasing number of studies highlight the key role that accurate 3D sound delivery has in successful immersive virtual experiences (IVEs) across the reality continuum[1,2]: if visuals are what capture our attention first, sound is essential for the "feeling of being there"[3]. Current methods to achieve 3D sound, however, either limit interpersonal interaction (headphones), require a significant amount of space and electricity (speaker arrays), or fail to pass high quality sound (parametric speakers have limited bandwidth and fail with higher volumes[5]). In this work, we present a 2D sound projector based on acoustic metamaterials. We build on recent results, where noise-cancelling metamaterial panels have been used to build a speaker cabinet[6] and a metamaterial super-lens has been used to collimate the emission of a standard speaker, replicating the precision of a parametric speaker at much lower frequencies[7]. Crucially, we exploit the fact that that some key result for visible light (like the thin-lens equation) are applicable to sound, when metamaterial lenses are involved[8], to build a mechanized telescope. We evaluate the performance of our device by microphone measurements, in preparation for a classical sound localization experiment: a user study where a tone is delivered around a stationary participant and the listener is asked where they perceive the sound to come from.

Experimental set-up

We designed the source by inserting a low-cost car speaker into a metamaterial cabinet. The system was tested first in a professional studio[5] and then in an open area outdoor (equivalent to an anechoic setup), to make sure that its emission had the same characteristics of a standard source (ISO 6926:2016), at least in the range of frequencies used for our experiments (5000-6000 Hz). We augmented the source mounting in front of it a system of two converging metamaterial lenses (focal lengths F1 = 63 ± 1 mm and F2 = 48 ± 1 mm), whose relative distance was controlled using a linear actuator[6]. We purposefully selected the room for the experiment to be a standard large room ($T_{20} \leq 0.6$ seconds at 5000 Hz, before treatment), to avoid that perception effects in hemi-anechoic rooms[9] might affect the user study. A chair for the participants was set in the middle of the room and the source was mounted on a turntable facing it (PC-controlled with a precision of 1°) at the distance of 2.62 m from the users (see Figure 1). A group of panels lined with standard absorbers (insertion loss: 10 dB at 5-6 kHz) was used to line up the walls behind the chair, thus avoiding direct back-reflections, which could influence measurements and future user studies. The system was calibrated so that it was possible to select 13 delivery locations (see Figure 1) by remotely changing the angle of the turntable and the distance between the lenses.

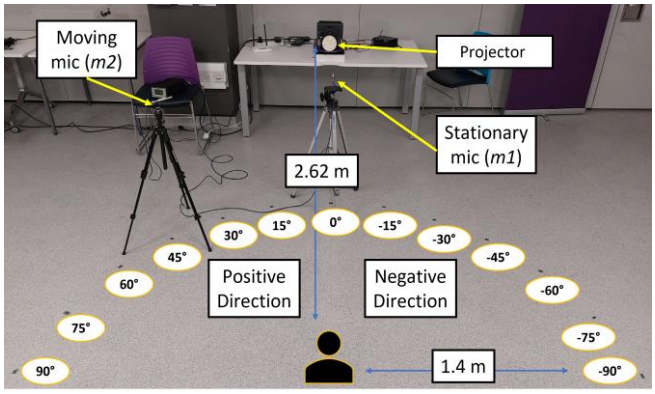

Figure 1. The experimental set-up used for this study, highlighting the position of the projector relative to the users and how the measurements were taken.

Measurements were taken using two nominally identical microphones (1/2 in., model Norsonic, type 1201/30323), connected to a digital scope through a 2-channel B&K NEXUS 2690-0S2 conditioning amplifier.

Microphone measurements

The shape of the focus at different delivery locations was determined by measuring the sound pressure level along the line that connects the speaker, the lenses, and the delivery point, and then perpendicularly to it at two focusing positions (0° and 90° in Figure 2), with fixed frequency tones (5500 Hz). For each measurement, one of the microphones was fixed at the delivery point and the other moving.

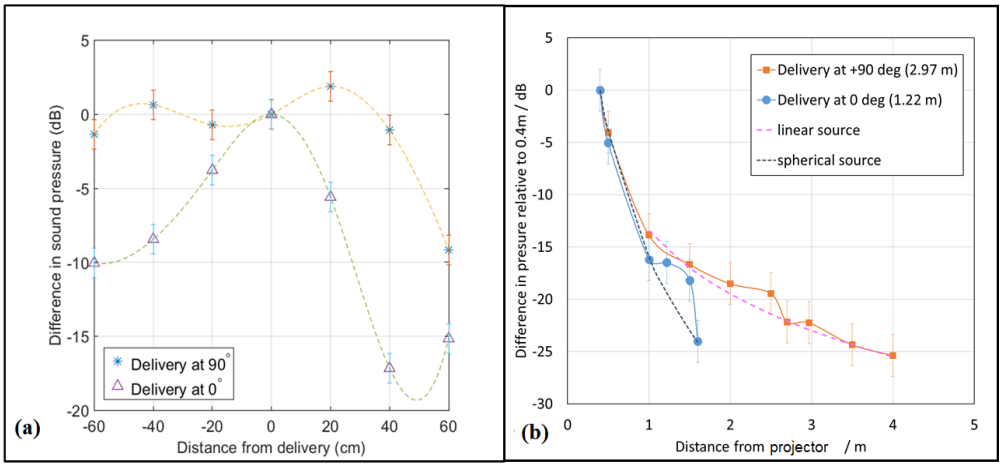

Figure 2. Two-microphone measurements taken in this study, at the delivery positions of 0° and 90° in Figure 1: (a) perpendicular to the line of propagation and (b) along the line of propagation.

Figure 2a shows the results for the “width" of the focus i.e., the sound pressure level measured perpendicularly (in 20 cm steps) and normalized with the value on the axis at the delivery point. In line with what is expected from the thin lens equation[8], the lateral dimension of the focus increases as the distance of the audio spot from the projector increases. Delivery is therefore “sharp" at 0°, where the sound pressure level decreases by 6~dB at 20 cm from the delivery position while this is no longer true at 90°, where the -6~dB line is 50 cm to the side of the delivery point (expected value: 48~cm).

Figure 2b shows the results for the “length" of the focus. When the delivery point is 0° (1.22 m), the sound pressure level follows the trend of a spherical source when the distance increases (i.e., it decreases by 12 dB when the distance is doubled). The focal zone (of maximum length 40 cm) can be clearly seen superimposed on this trend, with the maximum effectively measured at the delivery point: when the delivery is at 0° the audio spot can therefore be imagined as a circle of radius 20 cm.

When the delivery point moves at 90° (2.97 m from the projector), however, the focal area becomes “much less sharp" and elongates for more than 1 m in the direction of propagation (between 2.0 m and 3.5 m in Figure 2b). In addition, not only the sound pressure level seems to decrease much less with the distance, following the trend of a linear source (i.e., it decreases by 6 dB when the distance is doubled), but the maximum sound-pressure level (SPL) is no longer at the delivery point.

Since humans can clearly perceive a change in sound intensity[9] only if it is greater than 3 dB, it is therefore expected that, as the angle of delivery increases, it will be more difficult for the participants of future user studies to determine where the sound is being delivered, as shown by a preliminary user study (19 participants). A similar deformation of the focal region, getting worse when the distance from the lens increases, is described in optics with the term ``spherical aberration''. In optics, this is due to the fact that peripheral rays (in ray optics) do not converge in the same place as the ones passing near the axis. Understanding how to correct this effect will be the subject of future studies.

References

[1] C. Rajguru, M. Obrist and G. Memoli, *Front. Psychol.*, vol. 11, p. 2714 (2020).
[2] I. de Villiers Bosman, O. Buruk, K. Jørgensen and J. Hamari, *Behaviour & Information Technology*, pp. 1-35 (2023).
[3] F. Hruby, *Journal of Cartography and Geographic Information*, vol. 69, no. 1, pp. 19-28 (2019).
[4] J. Reis, in Proceedings of the International Computer Music Conference (2016).
[5] J. Kuutti, J. Leiwo and R. E. Sepponen, *Technologies*, vol. 2, no. 1, pp. 31-53 (2014).
[6] L. Chisari, M. Di Cola, P. Martignon, G. Memoli, in Proceedings of Euronoise 2021 (2021).
[7] L. Chisari, E. Ricciardi and G. Memoli, in AES ENGINEERING BRIEFS 2022 (2022).
[8] G. Memoli, L. Chisari, J. Eccles, M. Caleap, B. Drinkwater and S. Subramanian, in Proceedings of CHI 2019 (2019).
[9] Jin Yong Jeon, Pyoung Jik Lee, Jin You, Jian Kang, *JASA* vol. 127(3), pp.1357—1366 (2010)

Tunable Nonlinear Magnetic Lattices as a Platform for Controlling Waves

Osama R. Bilal

Department of Mechanical Engineering, University of Connecticut, Storrs, Connecticut 06269, USA

osama.bilal@uconn.edu,

Abstract: In this work, we study the self-assembly of free-floating magnetic lattices in one and two-dimensions. By harnessing the interplay between the unit cells and their coupling with the boundaries, we engineer the nonlinear potentials of the metamaterial to demonstrate intriguing phenomena such as amplitude dependent response, non-reciprocity, and topological solitons.

Metamaterials can be defined as repeating geometric patterns in space, creating artificial lattices. Such lattices can be utilized as platforms to realize peculiar static and dynamic behavior (such as negative effective mass density, negative effective dynamical stiffness, and negative effective Poisson's ratio). These geometric patterns are usually fixed once the metamaterials are fabricated. While many theoretical and numerical studies of tunable metamaterials exist, realization of experimental platforms remain limited because of challenges in manufacturability, the destructive nature of reprogramming, and inherent nonlinearities. A valid path for functional tunability of matter is external stimuli, e.g., either static or dynamic load, which can effectively induce an external field to tune the materials. This, however, can translate to large shape change in the material with the potential rise of instabilities, phase transitions, degradation, and geometric frustration. This can hinder our ability to utilize programmable materials[1,2].

In this line of work, we realize metamaterials with programmable dynamical characteristics by combining analytical, numerical, and experimental analyses, to utilize tunable nonlinear magnetic lattices to[3-6]. We create our lattices by confining self-aligned, free-floating disks of embedded permanent magnets in a range of symmetries within a fixed boundary and a pre-engineered magnetic field. The magnetic repulsive forces between the boundary magnets and the free-floating disks cause the disks to self-align and rest within their surrounding magnetic potential wells. Each disk or group of disks can act as a single building block, or a unit cell, of the lattice. These unit cells repeat in space, forming a one-dimensional or two-dimensional metamaterial with unique wave propagation characteristics. We design the geometry of the confining boundary, disk symmetry, and number of embedded magnets within each disk such that the tuning of the boundary's magnetic field controls the assembly of the disks. The relative positions and orientation angles between the disks define the corresponding metamaterial phase (ordered, quasi-ordered or random) and its stability conditions (mono-stable or multi-stable). By changing the boundary geometry, number of disks, their symmetry, and therefore the resulting magnetic couplings within the unit cell, the transmittable frequencies through the metamaterial can be programmed.

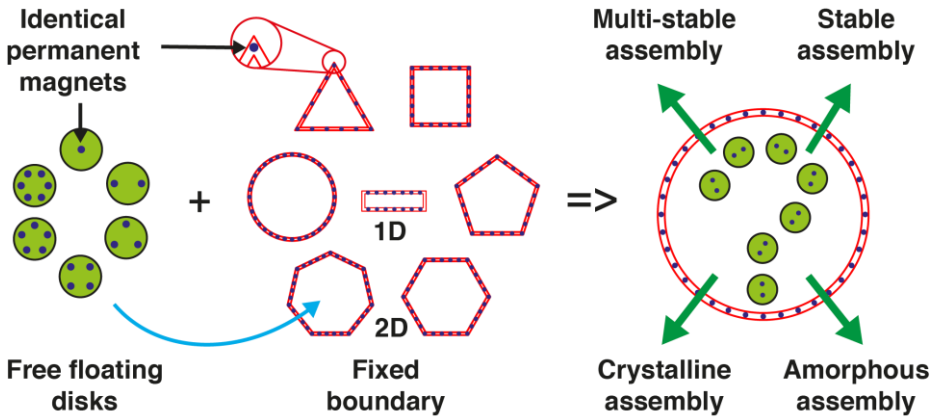

Figure 1: Schematic representation of the different symmetries of the disks confined within boundaries with embedded magnets of different shapes, resulting in a variety of lattice types and properties.

Figure 2 shows a few examples of the possible ordered lattices (crystalline), semi-ordered lattices (quasi-crystalline) or random (amorphous) assemblies that can self-assemble within the different boundaries.

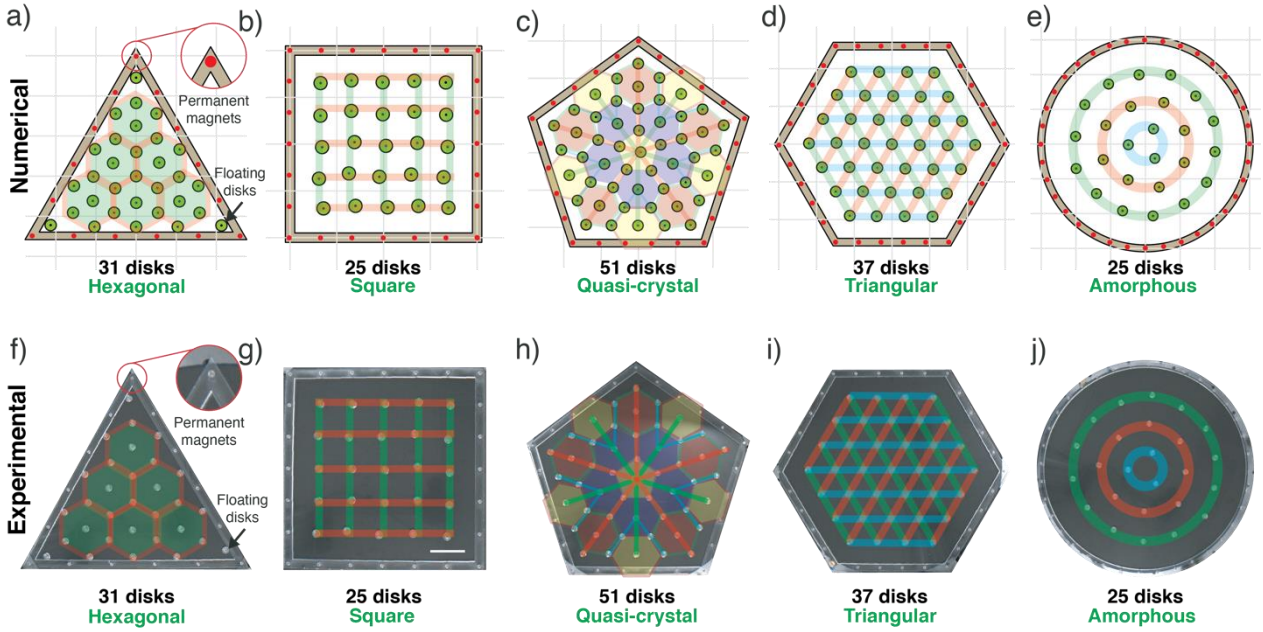

Figure 2: Example of numerical (top) and experimental (bottom) self-assembled lattices within two-dimensional magnetic boundaries with highly ordered, semi-ordered and random configurations.

The proposed platform can be utilized to engineer self-assembled metamaterials capable of manipulating low-frequency waves, within a relatively small volume, while utilizing negligible mass. Moreover, the nonlinear potentials between the disks and their boundaries can be harnessed to demonstrate phenomena with no linear parallel such as amplitude dependent response, bifurcation, chaos, non-reciprocity, and solitons. In addition, the self-assembling nature of the disks can be key in creating re-programmable materials with exceptional properties.

References

[1] Deng, Bolei, et al. *Proc. Natl. Acad. Sci. U.S.A.* 117.49 (2020): 31002-31009.
[2] Li, Jian, Nitesh Arora, and Stephan Rudykh. *Curr. Opin. Solid State Mater. Sci.* 25.2 (2021): 100898.
[3] Watkins, Audrey A., and Osama R. Bilal. *Front. Mater.* (2020): 410.
[4] Watkins, Audrey A., Austin Eichelberg, and Osama R. Bilal. *Phys Rev. B* 104.14 (2021): L140101.
[5] Norouzi, Ehsan, Audrey A. Watkins, and Osama R. Bilal. *Phys Rev. E* 104.4 (2021): 044902.
[6] Watkins, Audrey A., Austin Eichelberg, and Osama R. Bilal. *Phys. Rev. Applied* 17.2 (2022): 024036.

PHONONICS 2023: 6th International Conference on Phononic Crystals/Metamaterials/Metasurfaces, Phonon Transport, and Topological Phononics
Manchester, England, June 12-16, 2023
PHONONICS-2023-0176

Sound Attenuation by Pancake structures and Acoustic Black Holes in Linear and Nonlinear regimes

Olga Umnova[1], Daniel Brooke[1], Philippe Leclaire[2], Thomas Dupont[3]

[1] *University of Salford, Manchester, England, UK*
o.umnova@salford.ac.uk,
d.c.brooke@salford.ac.uk

[2] *DRIVE – ISAT Universitie de Bourgogne, Nevers, France*

Philippe.Leclaire@u-bourgogne.fr

[3] *Department of Mechanical Engineering, École de Technologie Supérieure, Montréal, Québec, Canada*

Thomas.Dupont@etsmtl.ca

Abstract: In this work two types of metamaterials – pancake absorbers for sound absorption in narrow bands and Acoustic Black Hole absorbers for broadband sound attenuation are studied theoretically and experimentally in linear and nonlinear regimes. It is shown that the effect of nonliearity is stronger for pancake absorbers leading to deterioration of their performance at high amplitude of incident sound.

In this work two types of metamaterials have been modelled, built and are tested with focus on low frequency airborne sound absorption in linear and nonlinear regimes[1, 2]. The Pancake absorbers (Figure 1, a) are made up of a series of piled up flat cavities, separated by thin walls and traversed by a perforation at their centre. The Acoustic Black Hole (ABH) absorbers (Figure 1, b) consist of thin metallic circular plates, each with a central perforation, separated by annular air cavities. Radius of the perforation in each plate is gradually decreasing with the distance from the plate to the front surface, forming a central channel with a staircase radius profile[3].

A model for the effective properties of the pancake absorber is developed and compared with experimental data. By changing its geometry, the structure can be tuned to achieve the absorption in the narrow bands. The model is used to derive simple formulae for the frequency and the peak value of the absorption coefficient at the lowest frequency resonance, depending on the geometrical parameters of the structure. Optimum design of the pancake structure allows to obtain nearly perfect absorption at the desired frequency. Flow resistivity measurements at low flow rates show that the periodic set of cavities does not modify resistivity significantly when compared to a simple perforated cylinder with same thickness. As flow rate increases, the flow resistivity grows linearly according to Forchheimer's law and has a significant dependence on the absorber thickness. It is shown, that the Forchheimer's nonlinearity is very strong which leads to a relatively low nonlinearity threshold. A model is developed accounting for the linear growth of flow resistivity with particle velocity amplitude in the central perforation. It is used to predict sound absorption coefficient and is compared with the measurements at high amplitudes of the incident wave. Nonlinear properties of the pancake absorbers are investigated experimentally using sine wave excitation around the resonance frequency with the amplitude of the incident wave up to 250 Pa.

ABHs are first studied in the linear regime. A semi-analytical equivalent fluid model accounting for the variations of both the effective density and compressibility of air inside this channel is developed, which incorporates the staircase variations of the perforation radius with distance and assumes motionless plates.

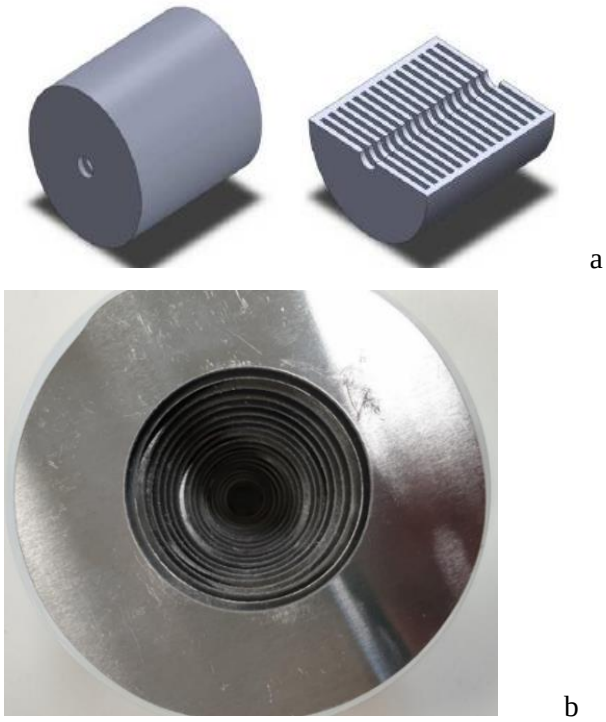

a

b

Figure 1. Pancake absorber[1] (a) and front view of the ABH absorber (b)

The viscous and thermal losses inside the side cavities and the central channel are accounted for using a well-established Johnson-Champoux-Allard-Lafarge model. It is shown that high absorption coefficient values are achieved in a wide range of frequencies starting from a few hundred Hz or less. At low frequencies, the resonances along the length of the structure, i.e. global resonances, are responsible for sound attenuation. At higher frequencies, the resonances of the lateral cavities, i.e. local resonances, play a major role. The upper boundary of the frequency range of high sound absorption is determined by the resonance frequency of the front annular plate. The model is validated against impedance tube measurements on five samples of different geometry (length ranging from 6 cm to 10 cm) and FEM models. Finally, the attenuation properties of the ABH are studied in the nonlinear regime – in specially designed impedance tube and in a shock tube. In the latter the amplitudes of the incident acoustic pulses up to 40kPa were achieved. It is shown that the nonlinearity of ABHs is weaker than that of the pancake absorbers and they remain relatively efficient even when the amplitude of the incident wave is very high.

References

1. T. Dupont, P. Leclaire, R. Panneton, O. Umnova, A microstructure material design for low frequency sound absorption, Applied Acoustics **136**, 86-93, (2018).
2. D.C.Brooke, O.Umnova, P.Leclaire, T. Dupont, Acoustic metamaterial for low frequency sound absorption in linear and nonlinear regimes. Journal of Sound and Vibration **485**, 115585 (2020)
3. O.Umnova, D.C. Brooke, P.Leclaire, T. Dupont, Multiple resonances in lossy acoustic black holes – theory and experiment. Journal of Sound and Vibration **543**, 117377 (2023)

Optical generation and detection of GHz compression/dilatation and shear acoustic waves in transparent medium with two-dimensional metallic grating structure

Osamu Matsuda[1], Kouji Momiyama[1], Motonobu Tomoda[1], Gwenaëlle Vaudel[2], and Vitalyi Gusev[3]

[1] *Division of Applied Physics, Faculty of Engineering, Hokkaido University, Sapporo 060-8628, Japan,*
omatsuda@eng.hokudai.ac.jp, koji-m-87@eis.hokudai.ac.jp, mtomoda@eng.hokudai.ac.jp
[2] *Institut des Molécules et Matériaux du Mans, UMR 6283 CNRS, Le Mans Université, Avenue Olivier Messiaen, 72085 Le Mans, France*
gwenalle.vaudel@univ-lemans.fr
[3]*Laboratoire d'Acoustique de l'Université du Mans, UMR 6613 CNRS, Le Mans Université, Avenue Olivier Messiaen, 72085 Le Mans, France*
vitali.goussev@univ-lemans.fr

Abstract: Picosecond laser ultrasonics measurement is done on a sample consisting of a fused silica substrate and a two-dimensional metallic grating opto-acoustic transducer. It is demonstrated that shear acoustic waves as well as the compression/dilatation acoustic waves in GHz frequency region can be optically generated and detected in the fused silica substrate with appropriate optical configuration.

Absorption of short light pulses (pump light) of picosecond temporal width in a medium may generate acoustic waves therein up to THz frequency region. The propagating acoustic waves can be monitored by delayed light pulses (probe light) as the modulation of optical reflectivity (transient optical reflectivity change) through photoelastic effect. The technique is called picosecond laser ultrasonics and is used to evaluate structural, elastic, and optical properties of the medium.[1]

Application of picosecond laser ultrasonics to transparent medium with an opaque thin film formed on the surface as an opto-acoustic transducer results in a transient reflectivity change showing a long-lasting oscillation, known as Brillouin oscillation. This is caused by the interference between the probe light reflected at the sample surface and that scattered by the propagating acoustic waves. For the probe light normal incident to the sample surface and the acoustic wave propagating perpendicular to the surface (the latter usually happens for the acoustic waves generated by the film opto-acoustic transducer), the oscillation frequency f is given as $f=2nv/\lambda$, where v is the sound velocity, n the refractive index of the transparent medium, and λ the probe light wavelength in vacuum. The Brillouin oscillation frequency is typically in the range from 10 GHz to 100 GHz. From the Brillouin oscillation frequency, one may extract v if the refractive index n is known, and vice versa, but it is not straightforward to get v and n simultaneously. One way for this is getting the Brillouin oscillation frequencies at several different probe light incident angles to the sample surface.[2,3] However, maintaining necessary accuracy among the measurements for several different incident angles is not an easy task.

This difficulty can be avoided by using a grating structure, e.g. periodic array of metallic rods, instead of a thin film as the opto-acoustic transducer on the transparent medium. The pump light irradiation on such grating structure may generate acoustic waves in several different directions in addition to the direction normal to the surface because of the diffraction of generated acoustic waves by the grating. The probe light is also diffracted by the grating structure and propagates in several different directions in the transparent medium. These diffractions make a single measurement effectively equivalent to the set of measurement with various probe light incident angles. The measurement for the fused silica glass plate with Au grating of submicron periods has demonstrated the simultaneous determination of compression/dilatation sound velocity v and refractive index n through measurements with a fixed probe light incident angle (normal incident in this case).[4]

A metallic film optoacoustic transducer on isotropic medium irradiated by pump light pulse may generate only compression/dilatation acoustic waves because of the symmetry of the system. However, it is preferable to monitor the shear acoustic waves as well, for the completeness of the evaluation of the

material's elastic properties. The grating opto-acoustic transducer can emit shear acoustic waves in oblique direction to surface normal because of its symmetry breaking. The generation and detection of shear acoustic waves in the fused silica glass plate with Al grating of submicron periods has been reported.[5] The polarization of the generated shear acoustic waves, i.e., the direction of their mechanical displacement vectors, is parallel to the plane which is perpendicular to the grating rods. The detection of such shear acoustic waves is only possible with the specific optical configuration conditions: 1) in the scattering of light by the acoustic wave, the wave vectors of probe light before and after the scattering must not be parallel with the acoustic wave vector, and 2) the plane, defined by the probe light wave vectors before and after the scattering, must not be parallel to the polarization of the shear acoustic waves to be monitored. These conditions are fulfilled for the probe light incident obliquely to the sample surface when its wave vector is not in the plane perpendicular to the grating rod.

In this paper, a fused silica plate with two-dimensional Al grating is investigated with picosecond laser ultrasonics measurement, to observe shear acoustic waves with simpler optical configuration than one in the measurement mentioned above. The grating consists of Al square islands (200×200 nm^2) with 50 nm thickness. They are periodically arranged in a square lattice with the period a=380 nm. The edges of the square islands are aligned to the unit cell vectors which defines the x and y axes of the sample coordinate. The z axis is taken along the depth direction of the sample. Measurement is done with a typical picosecond ultrasonics setup using a Ti-sapphire mode lock laser generating the light pulses of temporal width 100 fs, central wavelength 830 nm, and repetition frequency 80 MHz. The fundamental light is used for the pump, whereas the frequency doubled 415 nm wavelength light is used for the probe. The probe light is obliquely incident on the sample from the grating side with the wavevector (k_x, k_y, k_z>0). The reflected/diffracted light wave vector is expressed as ($k_x+m_xG_x$, $k_y+m_yG_y$, k_z'<0), where $G_x=G_y=2\pi/a$ are the components of unit reciprocal lattice vectors and m_x, m_y are the diffraction orders along x and y axes, respectively. We took a particular incident angle which allows the diffracted probe light at $m_x=m_y=-1$ to be anti-parallel to the incident probe light. This choice of incident angle simplifies the optical setup. Even though the probe light incident to and diffracted from the sample are anti-parallel, the probe light incident to and scattered by the acoustic waves may fulfill the above-mentioned conditions for the shear acoustic wave detection with the appropriate diffraction(s) along x and/or y axes by the two-dimensional metallic grating. Figure 1 shows the Fourier spectra of the obtained transient reflectivity taken with linearly polarized probe light. In the frequency range 35-42 GHz, several Brillouin oscillation peaks are observed at the theoretically calculated frequencies for the compression/dilatation acoustic waves (red symbols). By choosing an appropriate polarization of the incident probe light, we observe a peak around 25 GHz which agrees well with the theoretically calculated frequency for the shear acoustic wave (green symbol). The observed frequency corresponds to the scattering of the (diffracted) probe light at $m_x=0$, $m_y=-1$, $k_z>0$ to $m_x=m_y=-1$, $k_z<0$, and those equivalent to this. The peaks in the frequency region below 22 GHz have no corresponding theoretical values: they are the vibrational modes of Al structure itself. In this way, we confirmed that the two-dimensional grating structure is capable to monitor compression/dilatation and shear acoustic waves as Brillouin oscillations in the picosecond laser ultrasonics measurement. This would form a basis for evaluating more complicated anisotropic and/or inhomogeneous materials.

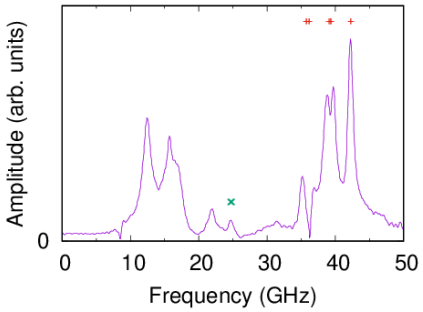

Figure 1 Fourier spectra of the transient reflectivity data obtained for two-dimensional Al grating/SiO_2 sample. Red + and green x symbols indicate the calculated Brillouin oscillation frequency for the compression/dilatation and shear acoustic waves, respectively.

References

[1] C. Thomsen, H. T. Grahn, H. J. Maris, and J. Tauc, *Phys. Rev. B* **34**, 4129-4138 (1986).
[2] A. M. Lomonosov, A. Ayouch, P. Ruello, G. Vaudel, M. R. Baklanov, P. Verdonck, L. Zhao, and V. E. Gusev, *ACS Nano* **6**, 1410-1415 (2012).
[3] M. Tomoda, O. Matsuda, and O. B. Wright, *Appl. Phys. Lett.* **90**, 041114-1-4 (2007).
[4] O. Matsuda, T. Pezeril, I. Chaban, K. Fujita, and V. Gusev, *Phys. Rev. B* **97**, 064301-1-11 (2018).
[5] O. Matsuda, K. Tsutsui, G. Vaudel, T. Pezeril, K. Fujita, and V. Gusev, *Phys. Rev. B* **101**, 224307-1-9 (2020).

PHONONICS 2023: 6th International Conference on Phononic Crystals/Metamaterials/Metasurfaces, Phonon Transport, and Topological Phononics
Manchester, England, June 12-16, 2023
PHONONICS-2023-0077

Multiscale Mechanical Study of Marine Seashells and Implications in the Design of Bioinspired Structures for Advanced Vibration Control

Y. Liu[1], M. Lott[1], S.F. Seyyedizadeh[1], I. Corvaglia[1], G. Greco[2], V. F. Dal Poggetto[2], A.S. Gliozzi[1], R. Mussat Sartor[3], N. Nurra[3], C. Vitale-Brovarone[1], N. M. Pugno[2,4], F. Bosia[1], M. Tortello[1]

[1]Dipartimento di Scienza Applicata e Tecnologia (DISAT), Politecnico di Torino, 10129 Torino, Italy, yuxuan.liu@polito.it, martin.lott@polito.it, seyedehfatemeh.seyyedizadeh@unito.it, ilaria.corvaglia@polito.it, antonio.gliozzi@polito.it, chiara.vitalebrovarone@polito.it, federico.bosia@polito.it, mauro.tortello@polito.it
[2]Laboratory for BioiBionspired, Bionic, Nano, Meta, Materials & Mechanics, Dipartimento di Ingegneria Civile, Ambientale e Meccanica, Università di Trento, 38123 Trento, Italy gabriele.greco-2@unitn.it, v.fonsecadalpoggetto@unitn.it, nicola.pugno@unitn.it
[3]Dipartimento Scienze della Vita e Biologia dei Sistemi (DBIOS), Università degli Studi di Torino, 10123 Torino, Italy rocco.mussat@unito.it, nicola.nurra@unito.it
[4]School of Engineering and Materials Science, Queen Mary University of London, London, United Kingdom

Abstract: We present a combined experimental and numerical study of two seashells belonging to the Turritellidae family, featuring a helicoconic shape with hierarchical spiral elements and show that these characteristics may also be linked to their vibration attenuation behavior. Implications in the design of bioinspired metamaterials and phononic structures are also expected.

Over millions of years of evolutionary process, biological systems have developed mechanical, optical, and thermal properties that aid their fitness by helping them to solve specific needs. Regarding the mechanical properties, an intense research activity has been carried out so far dealing with the remarkable quasi-static properties of many natural systems[1]. On the other hand, the dynamic mechanical properties of biological systems are, up to now, less explored, although some noticeable examples can be found[2,3]. Marine shells are designed by nature to ensure mechanical protection from predators and shelter for mollusks living inside them. A huge amount of work has been done to study the multiscale mechanical properties of their complex microstructure and to draw inspiration for the design of impact-resistant biomimetic materials. While the microstructure in shells plays a fundamental role in impact attenuation, their overall shape, however, determines their modal characteristics and vibration damping capabilities. These can, at least partially, be related to the main function of the shell. Here, we focus[4] on two shells belonging to the Turritellidae family, namely the *Turritella terebra* (Linnaeus, 1758) and the *Turritellinella tricarinata* (Brocchi, 1814) which feature a characteristic helicoconic shape with additional second-order spirals on the surface, as it can be seen in Figure 1a). By applying a combined numerical and experimental procedure at the micro and macro scale, we investigate the complex architecture of the shells and determine global mechanical properties studying their modal response and vibration properties. The μCT scan and the subsequent use of a specific software for the elaboration of the recorded images allowed to characterize the geometry of the shell that could be imported in a finite element software. The electron microscope was employed to directly observe the microstructure of the shells, and the Atomic Force Microscopy allowed to obtain the spatial distribution of the Young's modulus at the nanoscale along with the topographic characterization of the polished surface of the samples. The obtained results were supported by further instrumented nanoindentation experiments.

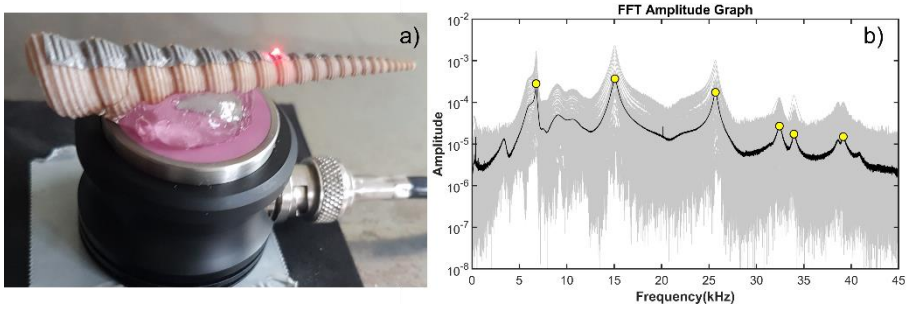

Figure 1 a) *Turritella terebra* sample mounted on the transducer during ultrasonic excitation experiments. **b)** Gray lines are the frequency spectra recorded along the longitudinal axis of the shell while the black line represents their average. Yellow symbols represent the resonance frequencies.

Resonant Ultrasound Spectroscopy (RUS) was performed to characterize the vibrational properties of the overall structure of the samples and to retrieve, via numerical Finite Element Analysis (FEA), the mechanical properties of the samples from the experimental results and to further investigate their vibration attenuation capabilities. Figure 1a) shows the experimental setup for the ultrasound measurements, while panel b) reports the resonance frequency spectra recorded along the longitudinal axis of the shell. By using Comsol Multiphysics, FEA was performed on the shell geometry to match the simulated eigenfrequencies with the experimental ones, thus determining the global mechanical properties i.e., Young's modulus and the Poisson's ratio.

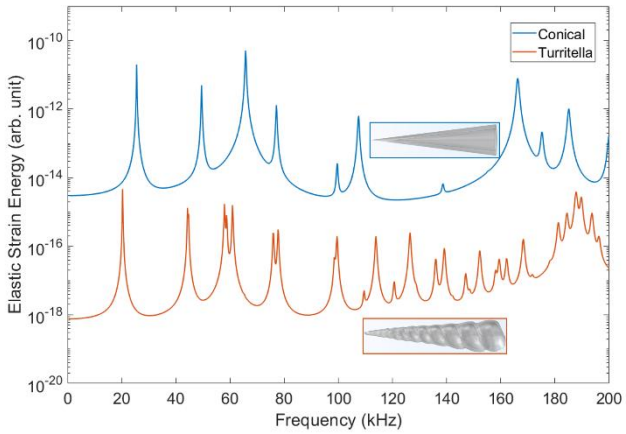

Figure 2 Calculated elastic strain energy spectrum for a Turritellinella tricarinata sample (red) and for an ideal, conical shell (blue) with the same mass and length as the Turritella. The loss factor, in both cases, is equal to $\mathbf{5 \times 10^{-3}}$.

Then, the dynamic response of the complex structure of the *Turritella* was calculated and compared to that of a simplified, purely conical, shell (Figure 2). It was shown that, in addition to the same vibration modes as the ideal conical one, the real shell features a much richer spectral behavior, deriving from the greater structural complexity, particularly from the helicoconic structure. This could also be related to improved attenuation capabilities of the structure under impacts. Then, the contribution of the smaller spirals (second order of hierarchy) to the dynamic behavior of the structure was investigated along with hypothetical higher-order hierarchy levels. Indeed, it is known that many natural systems that are efficient in impact attenuation feature hierarchical, interfacial, porous and composite architecture. In the dynamical analysis reported here, we have shown that some of these characteristics play a significant role in the rich frequency response of the shells. Thus, these effects can be analyzed in view of the design of efficient impact resistant or vibration damping bioinspired phononic structures.

The method presented here could be implemented in a systematic manner for the characterization of other biological structures of interest for their vibration behavior, focusing on hierarchical features, allowing to gain further insight into their evolutionary development, and to draw inspiration for other bioinspired designs. Some examples in this regard are under investigation and will also be presented.

References

[1] U.G.K. Wegst, H. Bai, E. Saiz, A.P. Tomsia, R.O. Ritchie, *Nat Mater.*, **14**, 23 (2015).
[2] B.S. Lazarus, A. Velasco-Hogan, T. Gómez-del Río, M.A. Meyers, I. Jasiuk, *J Mater Res Technol.*, **9**, 15705 (2020)
[3] F. Bosia, V. Dal Poggetto, A.S. Gliozzi, G. Greco, M. Lott, M. Miniaci, et al., *Matter* **5**, 3311 (2022)
[4] Y. Liu, M. Lott, S.F. Seyyedizadeh, I. Corvaglia, G. Greco, V. F. Dal Poggetto et al., *arXiv:2301.12747*.

PHONONICS 2023: 6th International Conference on Phononic Crystals/Metamaterials/Metasurfaces, Phonon Transport, and Topological Phononics
Manchester, England, June 12-16, 2023
PHONONICS-2023-0222

Discrete Helmholtz equation on a square lattice with corners

Anastasia Kisil[1]

[1] *Department of Mathematics,The University of Manchester, Oxford Rd, M13 9PL*
anastasia.kisil@manchester.ac.uk

Abstract: In this talk we are interested in solving the discrete Helmholtz equation on a square lattice with two perpendicular semi-infinite boundary conditions. The interaction of the two boundary forms an interesting multiple scattering problem which leads to a new equation to solve. This is a generalisation of the classical Wiener-Hopf equation, now in two variables and with three unknown function. A solution method for this type of equation will be presented by defining an underlining manifold that links the two variables. Next the analyticity regions of unknown functions is extended and that allows to simplify the problem. As the result the problem is fully solvable in terms of Cauchy type integrals which is surprising since this is not always possible for such complicated type of problems. Some toy examples are presented to illustrate the method.

There has been increased interest in lattices due to the unusual properties that they possess especially in the context of metamaterials. In the majority of mathematical literature, lattices are considered to be infinitely periodic in all directions (away from some local defect). Typically this allows the asymptotic problem to be reduce to the study of an individual repeated component, which is a significant simplification. However, it is know that infinite boundaries of the domain have a profound effect on wave propagation[1,2] . We are interested in situations where the periodicity of the material extends in some directions but there are boundaries in other directions (forming edges and corners). In this situation many of the existing methods of studying lattices are not applicable. New methods have to be developed which is the subject of this talk. The aim is to develop some of the techniques that were introduced in the context of random walks in order to solve the lattice motivated equation[3].

References

[1] M.J. Nieves, G.S. Mishuris, and L.I. Slepyan, Transient wave in a transformable periodic flexural structure, International Journal of Solids and Structures 112 (2017),185–208

[2] A. V. Shanin and A. I. Korolkov, Sommerfeld-type integrals for discrete diffraction problems, Wave Motion 97 (2020), 102606.

[3] G. Fayolle, R. Iasnogorodski, and V. Malyshev, Random walks in the quarter plane, Second, Probability Theory and Stochastic Modelling, vol. 40, Springer, Cham, 2017.

PHONONICS 2023: 6th International Conference on Phononic Crystals/Metamaterials/Metasurfaces, Phonon Transport, and Topological Phononics
Manchester, England, June 12-16, 2023
PHONONICS-2023-0169

Wave Dispersion in Monocoupled System with Inertial Amplifier and Embedded Resonator

Abhigna S. Bhatt[1], Arnab Banerjee[1]

[1] *Department of Civil Engineering, Institution of Technology Delhi, Delhi, India,*
Abhigna.sandipkumar.bhatt@civil.iitd.ac.in, abanerjee@iitd.ac.in

Abstract: In this paper, the monocoupled system consisting of inertial amplifier with resonator embedded masses has been developed. Further, the wave dispersion study consisting of attenuation characteristics of non-propagating waves has been explored in detail. The rationale behind peak in attenuation level due to resonance in embedded resonator has been observed using inhouse software for animating the wave dispersion in periodic monocoupled system.

A monocoupled system consists of unit cells that are periodically linked at a single node and have just one degree of freedom[1]. When a vibration is given at one end to the periodic system, a wave either propagates or attenuates, which can be obtained from the dispersion relation. The wave dispersion is the relation between temporal frequency and spatial wavenumber of propagating wave. Moreover, the dispersion relation also demonstrates the features of attenuating waves.

The representative unit cell has been developed by combining the inertial amplifier mechanism and embedded resonator with monoatomic chain as base. The said unit cell and its periodic chain has been demonstrated in Figure 1. The unit cell is coupled with neighboring unit cell at mass *M* and a degree of freedom in x direction as given in Figure 1 (a). The inertial mass m_a is connected to base mass *M* with rigid massless links and both masses are embedded with resonators of mass and stiffness respectively m_2, k_2 and m_1, k_1. The degrees of freedom corresponding to all the eight masses is shown in Figure 1 (b).

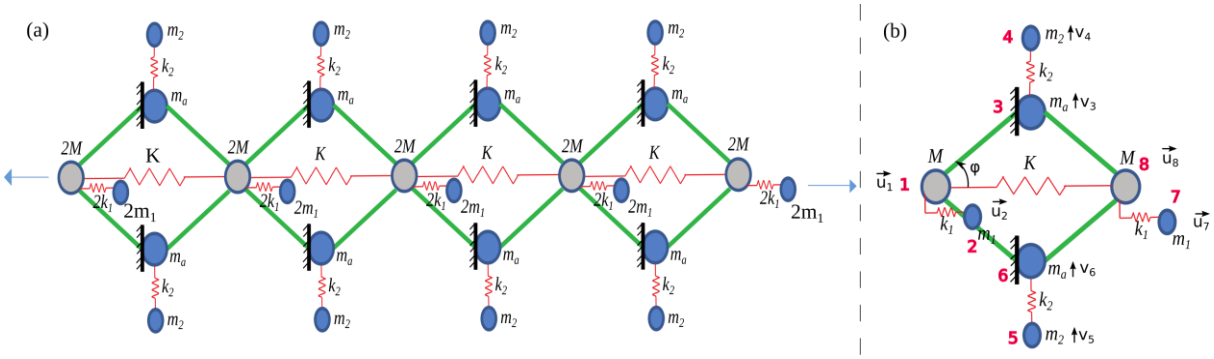

Figure 1 (a) Periodically connected infinite chain of monocoupled system with inertial amplifier and embedded resonators. **(b)** The representative unit cell with degrees of freedom defined at each node.

Dispersion Relation

The dispersion relation can be obtained by applying Bloch Floquet equation to the transfer matrix. Further the transfer matrix can be obtained from the dynamic stiffness matrix of the representative unit cell by matrix manipulation. The mass matrix, stiffness matrix and the continuity equations has been determined to obtain the dynamic stiffness matrix. The dynamic stiffness matrix is a function of temporal frequency ω and comparing it with Bloch Floquet equation (which is function of spatial frequency μ) will produce dispersion relation equation as[2]:

$$\cos(\mu) = 1 - F(\omega^2) \tag{1}$$

The poles of $F(\omega^2)$ shows the location of peaks in attenuation band and the zeros demonstrates the location of band boundaries. Moreover, the real wave number (μ) between *0* to π, confirms the propagation however, the imaginary value of wave number (μ) depicts the level of attenuation of the wave.

Results and Discussions

The dispersion relation of the developed representative unit cell has been obtained for the example case and the sensitivity of attenuation level with embedded resonator has been shown in Figure (2).

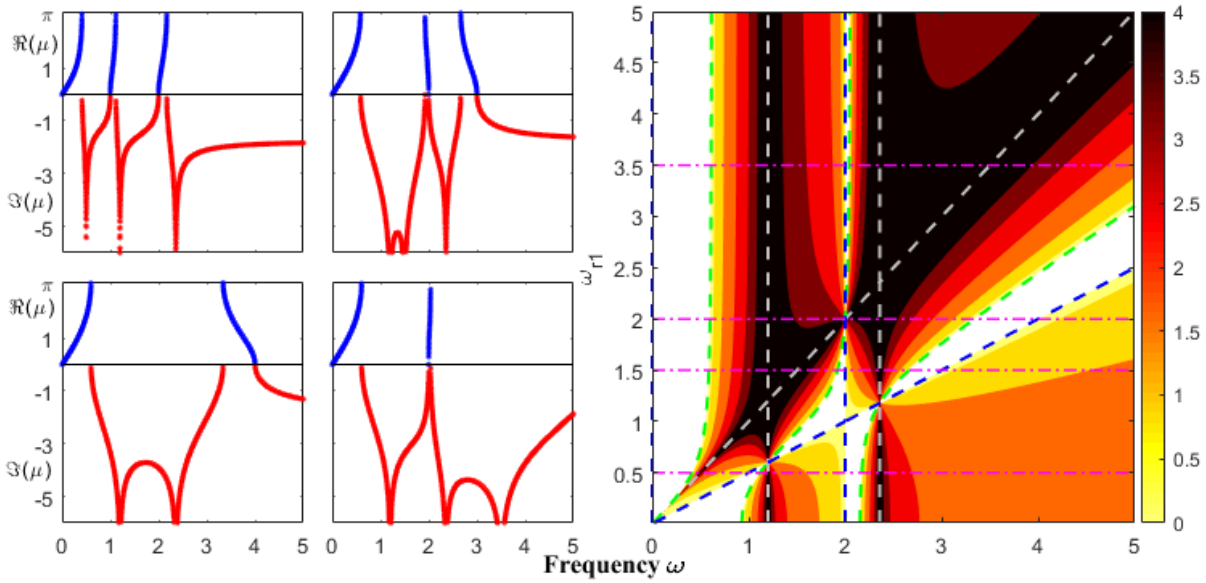

Figure 2 Plots with the values of governing parameters $m_a=1$; $m_1=3$, $m_2=0.25$, $\varphi=45$; $k_2=1$ and varying $\omega_{r1} = (k_1/m_1)^{0.5}$ from 0 to 5. The contour plot for frequency ω varying from 0 to 5 versus ω_{r1} is shown in (e). In this figure (e) the roots and poles of dispersion equations. The (a), (b), (c) and (d) figures demonstrates the dispersion relation for the system at sections drawn by dash-dot lines at ω_{r1}= 0.5, 1.5, 2 and 3.5 respectively.

Figure (2) (e) demonstrates the contour of attenuation level with varying natural frequency of embedded resonator in base chain keeping the other parameters to be constant. In the contour darker the shade, higher the attenuation level. The dashed line in dark color shows the peak in attenuation and the dashed line at the boundaries shows the band boundaries. The colorless area in the contour is the propagation band of the unit cell. Figure (2) (a-d) demonstrates dispersion relation at the sections given in contour plot, which confirms the existence of double peaks in attenuation band. The double peaks in attenuation band gives a wide bandgap of high attenuation level.

The in-house code has also been developed to visualize wave propagation in developed periodic system. Fast Fourier transform and inverse Fourier transform have been used to develop the code. In the animation a continuous wave of particular frequency is given at one end and its dispersion is observed. In case of attenuation the embedded resonators resonate and absorb the given energy. However, in propagation their vibrations respective to base mass are minimum. The animations are given in the following links.

Propagation:
https://drive.google.com/file/d/1kZbRMPSYMZz-DClRcfTEYG87scsBDrt7/view?usp=share_link
Attenuation:
https://drive.google.com/file/d/10PJryuUJI-70JovQup_UPZiiPZLMD5SF/view?usp=share_link

References

[1] Mead, Denys J. "Wave propagation and natural modes in periodic systems: I. Mono-coupled systems." Journal of Sound and Vibration 40.1 (1975).
[2] Bhatt, Abhigna, Arnab Banerjee, and Sondipon Adhikari. "Closed-form solutions for attenuation peaks and band boundaries of general monocoupled systems." Journal of Sound and Vibration 541 (2022).

PHONONICS 2023: 6th International Conference on Phononic Crystals/Metamaterials/Metasurfaces, Phonon Transport, and Topological Phononics
Manchester, England, June 12-16, 2023
PHONONICS-2023-0046

High-frequency Homogenization of Dispersive Media

Marie Touboul[1], Benjamin Vial[1], Raphaël Assier[2], Sébastien Guenneau[3], Richard Craster[1]

[1] *Department of Mathematics, Imperial College London, Huxley Building, Queen's Gate, London SW7 2AZ, UK*
m.touboul@imperial.ac.uk, b.vial@imperial.ac.uk, r.craster@imperial.ac.uk
[2] *Department of Mathematics, University of Manchester, Oxford Road, Manchester, M13 9PL, UK*
raphael.assier@manchester.ac.uk
[3] *The Blackett Laboratory, Department of Physics, Imperial College London, London, SW7 2AZ, UK*
s.guenneau@imperial.ac.uk

Abstract: The high-frequency homogenization method is used to study dispersive media for which the properties of the material depend on the frequency (Lorentz or Drude type). Effective properties are obtained near a given point of the dispersion diagram and the method is validated thanks to comparison with finite element method simulations.

Configuration under study

Classically, dynamic homogenization is understood as a low-frequency approximation to wave propagation in heterogeneous media. A particularly successful approach is the two-scale asymptotic expansion method and the notion of slow and fast variable[1]. The idea of high-frequency homogenization (HFH), introduced in[2], is to use similar asymptotic methods to approximate how the dispersion relation and the media behave near a given point that satisfies the dispersion relation. In the present work, we extend the HFH method to the case of dispersive media where the properties of the material depend on the frequency.

More precisely, we consider the Helmholtz equation in a doubly periodic structure on a square lattice. The physical properties (permittivity or permeability in electromagnetism, or effective elastic parameters arising from high-contrasts in elasticity, for example) may depend in some constituents of the unit cell on the frequency, following a Lorentz (or Drude) model:

$$a(\boldsymbol{x},\omega) = a_0\left(1 - \sum_{p=1}^{N} \frac{\omega_p^2}{\omega(\omega + \mathrm{i}\gamma_p) - \omega_{D,p}^2}\right) \tag{1}$$

with a being the physical parameter that depends on the space variable $\boldsymbol{x}$ and the frequency ω, ω_p the plasmon frequency, γ_p a damping coefficient, and $\omega_{D,p}$ the Lorentz resonant frequency (we recover the Drude model if the latter vanishes). These models are especially relevant to describe wave propagation in metals and dielectrics throughout the visible spectrum[3].

High-frequency homogenization methodology

The starting point of HFH is to pick a wavenumber and Ω_0 one of the eigenvalues satisfying the dispersion relation at this point. Then, following the two-scale expansion technique, an ansatz is assumed for both the wave field and the frequency near this solution of the dispersion relation:

$$u_\delta(\boldsymbol{x}) = \sum_{j\geq 0} \delta^j u_j(\boldsymbol{x}, \boldsymbol{\xi}) \text{ and } \omega^2 = \sum_{\ell \geq 0} \delta^\ell \Omega_\ell^2 \tag{2}$$

with $\boldsymbol{x}$ the slow variable, $\boldsymbol{\xi}$ the fast variable, and δ the small parameter of the HFH method. Upon an expansion of the frequency-dependent parameters in (1), we extend this methodology to the case of dispersive media.

Results

We obtain the approximations of band diagrams such as the ones describing effective negative-n materials[4], or metals in dielectrics[5], together with information on the nature of the effective equation for the wavefields.

More precisely, we first consider the case of high-symmetry points of the Irreducible Brillouin Zone for which Ω_0 is a single eigenvalue, i.e., for which branches of the dispersion diagram do not intersect. In that case, we write the zeroth order wavefield as

$$u_0(\boldsymbol{x}, \boldsymbol{\xi}) = f_0(\boldsymbol{x}) \mathcal{U}_0(\boldsymbol{\xi}, \Omega_0) \tag{3}$$

where U_0 is the eigenfunction associated to Ω_0 and f_0 the large-scale modulation function that has to be found. In this case, we assume that Ω_1 is zero, and we get an approximation for Ω_2 together with an effective equation for f_0:

$$T_{ij} \frac{\partial^2 f_0}{\partial x_i \partial x_j} + \Omega_2^2 f_0 = 0 \tag{4}$$

with index summation assumed for repeated indices and where the effective tensor $\boldsymbol{T}$ depends on the mean value of the eigenfunction, and on the physical and geometrical parameters of the media. We therefore get a quadratic approximation of the dispersion relation and an effective equation that allow to get a zeroth-order approximation of the wavefield.

The exact dispersion diagrams, which require to solve a non-linear eigenvalue problem at any point of the diagram, are computed thanks to Finite Elements Methods, and compared to the approximations obtained for the dispersion relation, see Figure 1 for square metallic rods in a dielectric in TM polarization[5]. Source point simulations are also performed to compare wave propagation in the microstructured media and in the effective media characterized by equation (4). An analysis of the effective tensor is also conducted in order to understand the nature of wave propagation depending on the choices of the physical components.

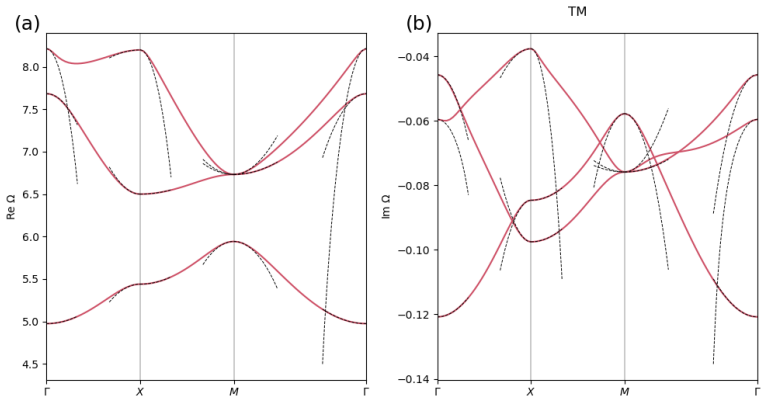

Figure 1 Imaginary and real parts of dispersion diagrams for a periodic material made of square rods of metals in a dielectric [3]. Plain red lines are the exact diagram, dotted black lines are the approximations from HFH near the high symmetry points.

The same methodology is also applied for repeated eigenvalues, and for points which are not high-symmetry points. In those cases, the zeroth-order wavefield is again characterized by an effective equation, but the approximation for the frequency is linear and no longer quadratic.

The occurrence of accumulation points in the dispersion diagram, for which the classical approximation obtained by assuming that the wavefield writes as in equation (3) fails, is also discussed analytically.

References

[1] A. Bensoussan, J.-L. Lions, G. Papanicolaou, *Asymptotic Analysis for Periodic Structures*, AMS Chelsea Publishing (2011).
[2] R. V. Craster, J. Kaplunov, A. V. Pichugin. *Proceedings of the Royal Society A: Mathematical, Physical and Engineering Sciences, The Royal Society*, **466**, 2341-2362 (2010).
[3] A. Moroz. *Physical Review Letters*, **83**, 5274, (1999).
[4] J. Li, L. Zhou, C. T. Chan, P. Sheng. *Physical Review Letters, American Physical Society*, **90**, 083901 (2003).
[5] Y. Brûlé, B. Gralak, G. Demésy. *Journal of the Optical Society of America B*, **33** (2016).

PHONONICS 2023: 6th International Conference on Phononic Crystals/Metamaterials/Metasurfaces, Phonon Transport, and Topological Phononics
Manchester, England, June 12-16, 2023
PHONONICS-2023-0078

Modeling and optimization of discrete phononic lattices

Benjamin Vial[1], Richard V. Craster[1]

[1] *Department of Mathematics, Imperial College London, London SW7 2AZ, UK,*
b.vial@imperial.ac.uk, r.craster@imperial.ac.uk

Abstract: In this talk, we present the modeling of discrete phononic lattices made of masses connected with elastic beams. A versatile implementation of the model with automatic differentiation makes it suitable for optimizing the lattice parameters using gradient based techniques, allowing for instance to maximize bangaps.

The propagation of elastic waves in lattice structures is strongly dependent of the micro-structural geometry, allowing the design of metamaterials that can completely block mechanical waves of certain frequencies, or manipulate those waves to engineer desired effects such as focusing or attenuation[1]. Besides from more sophisticated numerical techniques such as the finite element method, discrete network models such as the one proposed here can be used to quickly determine the band gaps, a method that is easily implemented on a computer for analysis of complicated structures.

We have implemented a general-purpose code that is able to treat truss (with only translational degrees of freedom) or frame (with added rotational degrees of freedom) structures. Each node in the lattice is defined by its coordinates and the mass m lumped at this node, with an additional polar moment of inertia J in the case of frames. Nodes are linked with elastic beams with axial stiffness k, and bending stiffness d in the case of frames. Applying Newton's second law for each node in the lattice and using Bloch's theorem, one obtain an eigenvalue problem of the form:

$$[\sigma(\mathbf{k}) - \omega^2 \mathrm{M}]\, \mathrm{u}(\mathbf{k}) = 0 \tag{1}$$

where eigenvectors u contain the Fourier coefficients of the displacement (and rotation in the case of frames) field at each node, ω is the frequency and $\boldsymbol{k}$ the wavevector. The mass matrix M is diagonal and easily obtained, whilst assembling the stiffness matrix σ requires to find connections between the nodes, a task that is entirely automated by our code. One typically solve this problem by fixing $\boldsymbol{k}$ and solving for ω, obtaining the dispersion relation. In addition, a similar methodology can be applied to study finite lattices eigenmodes and their response to harmonic excitation.

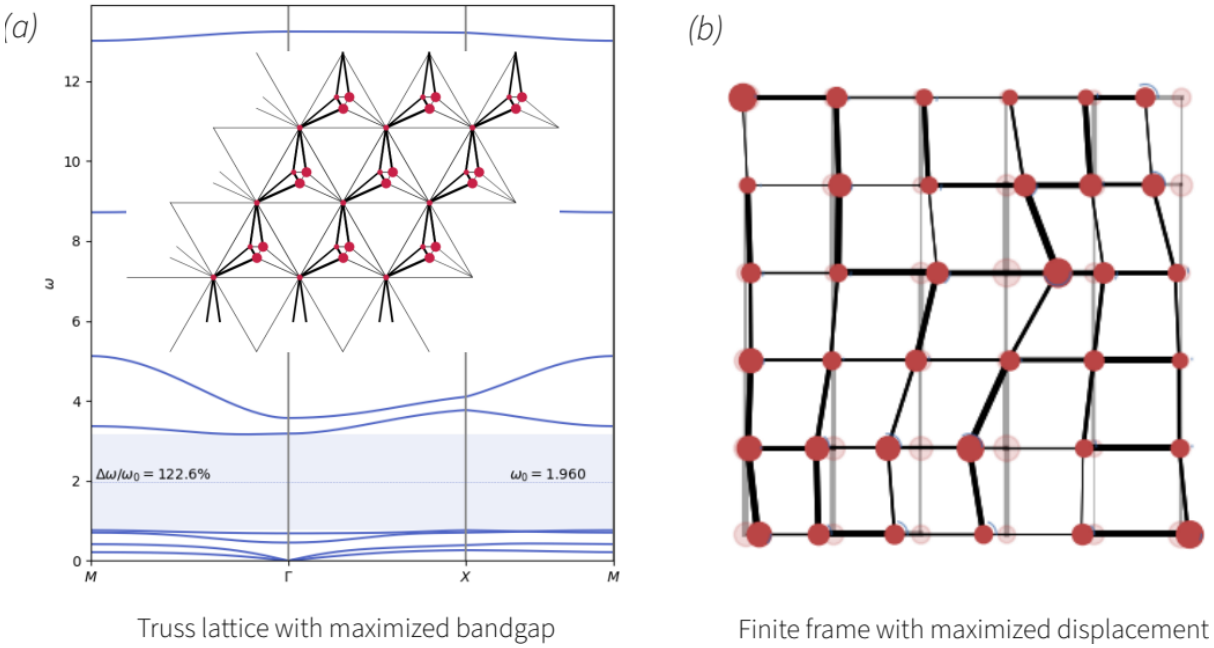

Figure 1 Optimization of truss and frame structures. (a) The design of a triangular truss lattice with inner complex resonator that maximizes the relative bandgap between the 4th and 5th eigenvalues. (b) Finite frame structure excited with a force on the x-axis at the bottom left corner. The objective is to maximize the displacement at the top right node.

An additional feature of our implementation is that it is endowed with automatic differentiation[2] (AD). At the core of an AD programming framework is gradient-aware elementary functions, which allow the software developer to implement only the forward simulation and compose the elementary building blocks to produce more complex code with gradient support with a few extra modifications of the underlying code. For instance in the lattice problem we are interested herein, one can obtain efficiently the sensitivity of eigenvalues with respect to the parameters of the nodes and beams.

We leverage this capability for inverse design of phononic crystals with desired properties, where the process is automated by an optimization algorithm[3] to attain specific objective under prescribed constraints. As an example, we have designed a triangular truss structure that would maximize the relative bandgap between the 4th and 5th bands, where the design variables are the beams stiffness and the masses of the nodes (see Fig. 1(a)). For finite structures, an application is to maximize the displacement at a given node for a prescribed excitation (see Fig. 1(b)).

Our approach can be used for the dispersion engineering of elastic waves in periodic lattices to obtain exotic effects that can be used to manipulate the localization of energy by using metamaterials with optimized microstructures.

References

[1] P. G. Martinsson and A.B. Movchan, *Quarterly Journal of Mechanics and Applied Mathematics, **56**(1),* 45–64 (2003).
[2] G. Corliss, C. Faure, A. Griewank, L. Hascoet and U. Naumann. *Automatic Differentiation of Algorithms: From Simulation to Optimization.* Springer Science & Business Media (2013).
[3] K. A. Svanberg, *SIAM J. Optim.* **12**, 555–573 (2002).

PHONONICS 2023: 6th International Conference on Phononic Crystals/Metamaterials/Metasurfaces, Phonon Transport, and Topological Phononics
Manchester, England, June 12-16, 2023
PHONONICS-2023-0049

Joining the Dots to Understand the Spectral Convergence of Finite-Sized Acoustic Metamaterials

H. Ammari[1], B. Davies[2], E. O. Hiltunen[3]

[1] Department of Mathematics, ETH Zurich, Zurich, Switzerland.
habib.ammari@sam.math.ethz.ch
[2] Department of Mathematics, Imperial College London, London, UK.
bryn.davies@imperial.ac.uk
[2] Department of Mathematics, Yale University, New Haven, USA.
erik.hiltunen@yale.edu

Abstract: We prove that the spectra of periodic arrays high-contrast acoustic resonators which have been truncated converge to the spectrum of the original unbounded structure, as the truncation size increases. Asymptotic analyses in terms of the material contrast are used as the starting point to obtain results for both propagating Bloch modes and localised defect modes.

A ubiquitous workflow in wave physics is to use analyses of unbounded periodic metamaterials to predict the behaviour of finite-sized, truncated versions. This is motivated by the fact that, while finite-sized samples can be realised in the laboratory, modelling periodic structures is often far more convenient and efficient (e.g. Floquet-Bloch analysis for characterising spectra). While this strategy is well known to give excellent prediction of most features, a rigorous convergence theory is yet to be established in general.

We consider locally resonant acoustic metamaterials and study how the spectrum of finite-sized (truncated) metamaterials converge to that of their infinite counterparts. The metamaterials we study are composed of repeating high-contrast material inclusions which experience resonance in a deeply subwavelength regime, often known as *Minnaert resonance*[1]. Within this regime, the resonators act as very strong scatterers of sound so can be used for a variety of subwavelength manipulation applications[2].

A crucial difference between an unbounded periodic metamaterial and its truncated counterpart is the occurrence of edge effects. While it is reasonable to expect that the two structures will present similar wave scattering properties away from the edges, they will behave very differently near to the ends of the finite-sized array. Several aspects of these edge effects have been studied extensively in the literature[3], such as the tendency for waves of specific frequencies to be localised to the edges[4,5] and the extent to which Bloch waves are excited[6,7]. In this work, we focus on understanding how these edge effects influence the convergence of the spectrum of the truncated operator to the original periodic operator.

Consider a high-contrast acoustic metamaterial given by a single bounded material inclusion B that is repeated in a $d \in \{1,2,3\}$ dimensional lattice to give the full metamaterial where $D = \bigcup_{n\in\mathbb{Z}^d} B + n$. Then, we will study solutions to a scalar resonance problem $\Delta u + \frac{\omega^2}{v^2}u = 0$ in $\mathbb{R}^3\backslash\partial D$ with transmission conditions on the boundary of the resonators: $u|_+ - u|_- = 0$ and $\delta \frac{\partial u}{\partial v}\Big|_+ - \frac{\partial u}{\partial v}\Big|_- = 0$ on $\mathbb{R}^3\backslash\partial D$. We also assume that u satisfies the appropriate radiation condition in the far field (which depends on the dimension of the lattice). The crucial parameter in this system is the contrast parameter δ which describes the ratio of the density of the materials inside and outside the resonators. We will assume that δ is small and it will serve as the asymptotic parameter for our analysis. For example, the famous case of air bubbles in water has $\delta \approx 10^{-3}$.

We are interested in characterising *subwavelength* solutions, which we define as being non-trivial solutions for which $\omega \to 0$ as $\delta \to 0$. This formulation lends itself to asymptotic analysis. It turns out that the set of such subwavelength eigenfrequencies ω for which the Helmholtz problem has a non-trivial solution is given by the eigenvalues of the *generalized capacitance matrix*. For a review of this approach see Ammari et al.[2] and references within.

The modes for which a convergence theory can be formulated most conveniently are *defect modes*. These are localised solutions u that can exist when the periodic structure is perturbed and whose

amplitude decays exponentially as a function of the distance from the defect. Since their amplitude decays quickly, they only interact minimally with the edges in a large finite-sized array. Further, a defect mode typically corresponds to a pure-point eigenvalue in the spectrum of the unbounded operator, so the convergence can be quantified in terms of the distance between this eigenvalue and the corresponding eigenvalue of the truncated operator. In a recent work, we proved that any defect mode that is due to a compact perturbation of the unbounded periodic structure has a sequence of modes of the truncated structures whose eigenfrequencies converge to its eigenfrequency[8]. This convergence is shown numerically in Fig. 1. It is notable that the rate of convergence depends on the dimension of the lattice d. When $d = 3$ (i.e. is equal to the dimension of the three-dimensional space in which the metamaterial is embedded) the convergence is exponential. This is consistent with previous studies of one-dimensional[9] and two-dimensional[10] differential systems. Conversely, when $d < 3$, the convergence is only algebraic, due to coupling with the far field in this case[8].

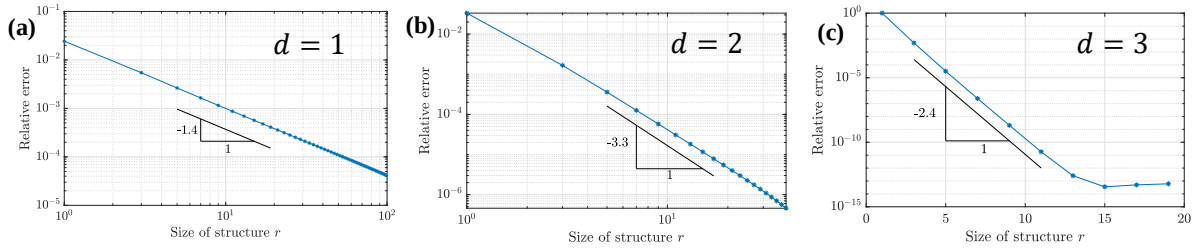

Figure 1 Convergence of the eigenfrequencies of defect modes in truncated high-contrast metamaterials. When the dimension of the lattice is 1 or 2, as in **(a)** and **(b)**, we observe algebraic convergence. Conversely, exponential convergence is observed in **(c)** when the dimension of the lattice is equal to that of the space in which it is embedded (which is 3, in this case).

The Bloch mode part of the spectrum is harder to characterise, since the discrete set of eigenvalues of the truncated structure is a qualitatively different object to the spectral bands of the unbounded structure. There are two main ideas for approximating the spectrum of the truncated structure. The first is to use a Floquet transform to derive an approximate Bloch parameter and the second is to compare the spectra using the density of states[11,12]. Fig. 2(a) compares the continuous first spectral band of the unbounded structure with the discrete resonances of the finite structure, with approximated Bloch parameters. There is close agreement between the two curves. In a forthcoming work, we prove this convergence[13], which we observe numerically (in Fig. 2(b)) to be linear as a function of the structure size.

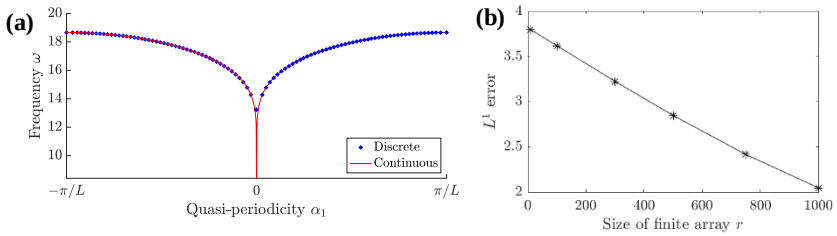

Figure 2 Convergence of the Bloch eigenfrequencies in truncated high-contrast metamaterials. **(a)** Approximate Bloch parameters can be computed for the modes in the truncated system, allowing for comparison with continuous spectral bands. **(b)** The convergence of the density of states is linear as a function of the size of the truncated array.

References

[1] M. Minnaert. *Philos. Mag.*, **16**, 235–248 (1933).
[2] H. Ammari, B. Davies, E.O. Hiltunen, H. Lee, S. Yu, *Wave Interaction with Subwavelength Resonators*. In M. Chiappini and V. Vespri, *Applied Mathematical Problems in Geophysics. Lecture Notes in Mathematics*, vol 2308. Springer, Cham (2022).
[3] N. L. Hills and S. N. Karp, *Commun. Pure Appl. Math.*, **18**, 203–233 (1965).
[4] C. M. Linton, R. Porter, and I. Thompson, *SIAM J. Appl. Math.*, **67**, 1233–1258 (2007).
[5] E. D. Vinogradova, K. Kobayashi, and T. Eizawa, *Wave Motion*, **86**, 44–62 (2019).
[6] I. Thompson and R. I. Brougham, *Q. J. Mech. Appl. Math.*, **71**, 1–24 (2018).
[7] N. Tymis and I. Thompson, *Q. J. Mech. Appl. Math.*, **67**, 469–503 (2014).
[8] H. Ammari, B. Davies, and E.O. Hiltunen, *arXiv preprint arXiv:2301.03402v2*, (2023).
[9] J. Lin and F. Santosa, *SIAM J. Appl. Math.*, **73**, 1002–1019 (2013).
[10] J. Lin and F. Santosa, *SIAM J. Math. Anal.*, **47**, 1458–1488 (2015).
[11] E. Eisenberg, A. Baram, and M. Baer, *J. Phys. A*, **28**, L433 (1995).
[12] O. Narayan and B.S. Shastry, *J. Phys. A*, **54**, 175201 (2021).
[13] H. Ammari, B. Davies, and E.O. Hiltunen, *In preparation*, (2023).

Frequency Spectrum of Sturmian Quasiperiodic Tilings

M. Lázaro[1], A. Niemczynowicz[2], P. Siemaszko[2], L. M. García-Raffi[1]

[1] *Instituto de Matemática Pura y Aplicada, Universitat Politècnica de València, , Camí de Vera s/n, 46022 València. Spain*
malana@upv.es, lmgarcia@mat.upv.es
[2] *Department University of Warmia and Mazury in Olsztyn, Faculty of Mathematics and Computer Science, Żołnierska str.14, 10-561 Olsztyn. Poland*
aga.niemczynowicz@gmail.com, artur@uwm.edu.pl

Abstract: In this work quasiperiodic structures generated by Sturmian aperiodic sequences are under investigation. The concept of Sturmian bulk spectrum is introduced and the observed self-similarity properties analyzed. This research is carried out in the context of structural dynamics and wave propagation and allows the application to mechanical engineering of concepts that until now have been applied in other fields.

Quasiperiodic systems based on Sturmian patterns are recursively defined using a generation parameter $0 < \alpha \leq 1$ given by its continued fraction $\alpha = [0; a_1, \dots, a_n, \dots]$, where $a_k > 0$ are positive integer numbers. Sturmian tilings are generated recursively by a words concatenation. Consider two segments (tiles) of lengths A and B. We define the following sequence of words with the alphabet $\{A, B\}$

$$\mathcal{W}_n = \mathcal{W}_{n-1}^{a_n} \mathcal{W}_{n-2} \quad , \quad \mathcal{W}_{-1} = A, \quad \mathcal{W}_0 = B \tag{1}$$

where both the exponent and the product must be understood as concatenations, for instance $A^3B^2A = AAABBA$. From the definition given above, if α is a rational number the Sturmian word $\mathcal{W}_n$ is properly the last iteration and strictly the infinite word arises as the periodic concatenation of W_n. Otherwise, if α is irrational, then it is known that the sequence $\{a_n\}$ becomes infinite and the associated Sturmian word has a pattern purely quasiperiodic. For numerical purposes, irrational numbers must be approximated by rationals approximants. Each one of the words emerging from the recursive sequence (1) will be named Sturmian blocks. The last block of a sequence $\{\mathcal{W}_k\}_{k\geq 1}$ for $k = n$ is said to be the Sturmian block associated to the approximant $\alpha = [0; a_1, \dots, a_n]$, and for them we will use the notation $\mathcal{W}(\alpha) = \mathcal{W}_n$.

Consider a 1D dynamical system that we are going to build it via the concatenation of different elements as for instance masses, springs, rods, elastic supports, beams.... All of these elements have mechanical, inertial and geometrical properties in the context of elastic waves. One of the parameters of the system above (mass or spring constant,...), that we call generically Θ, can vary but takin g only two values among the binary set $\{\theta_A, \theta_B\}$. The rest of parameters remain constant from element to element along the block. In Fig. 1 are shown three different examples covering discrete lattices, continuous rods and flexural beams.

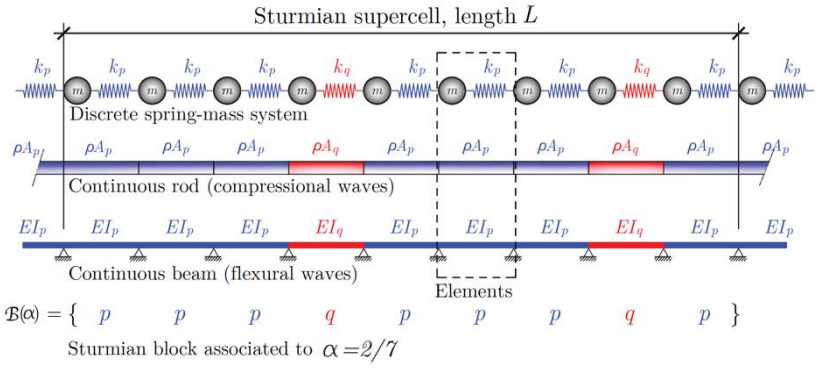

Figure 1 . Three simple examples of how we can build a dynamical systems based on Sturmian blocks correspondint to number α = 2/7 = [0; 3, 2]. Above: a discrete spring-mass system. Middle: a continuous rod (axial waves), changing the mass per unit of length. Bottom: a continuous beam (flexural waves) using the sectional stiffness

It is well-known that one of the most relevant properties of wave propagation in periodic media is the emergence of bandgaps in the frequency spectrum. A proper design of the unit cell can result in optimized location of bandgaps or passbands. On other side, quasiperiodic media, like for example Fibonacci sequence–based systems, exhibit self-similarity of the spectrum [1, 2, 3]. Here we want to study the spectral properties of one-dimensional quasiperiodic systems formed by structural elements whose

distribution is associated to a Sturmian word. The proposed method allows to relate a value of the generating parameter α ∈ [0, 1] with a system. By sweeping out the values of such generating parameter, we can form a family of structures with specific properties as for instance can be the dispersion relations or the distribution of resonances. Then we seek to relate this generating parameter α to the admitted frequencies in the system by means of the so–called bulk spectrum. The transfer matrix method (TMM) is an analytical method suitable for the study of one–dimensional wave propagation. Denoting $\boldsymbol{T}_j$ the transfer matrix between nodes $j-1$ and j, the relationship between the state vectors at the two ends of the unit cell can be written as

$$\boldsymbol{u}_N = (\boldsymbol{T}_N \cdot \cdots \cdot \boldsymbol{T}_1) \cdot \boldsymbol{u}_0 = \boldsymbol{T}(\alpha) \cdot \boldsymbol{u}_0 \tag{2}$$

The above expression holds for any one-dimensional dynamic model, regardless of the algorithm used for its construction. In the Sturmian case each block emerges from concatenation of previous blocks according to the rule (1). If we consider the transfer matrix associated to the kth Sturmian block $\mathcal{W}_k$, $\boldsymbol{T}_k$ we can stablish the recursion

$$\boldsymbol{T}_k = \boldsymbol{T}_{k-2} \cdot \boldsymbol{T}_{k-1}^{a_k} \qquad 1 \le k \le n \quad , \quad \boldsymbol{T}_{-1} = \boldsymbol{T}_A, \qquad \boldsymbol{T}_0 = \boldsymbol{T}_B \tag{3}$$

The TM of the unit cell is then $\boldsymbol{T}(\alpha) = \boldsymbol{T}_n$ and relates the state variables $\boldsymbol{u}_0$ and $\boldsymbol{u}_N$ yielding $\boldsymbol{u}_N = \boldsymbol{T}(\alpha)\boldsymbol{u}_0$. Applying the Bloch theorem to the supercell we know that $\boldsymbol{u}_N = e^{i\kappa L}\boldsymbol{u}_0$. Thus, Eq. (3) can be written then as the linear eigenvalue problem $[\boldsymbol{T}(\alpha) - \lambda\, \boldsymbol{I}]\boldsymbol{u}_0 = 0$, where the parameter is $\lambda = e^{i\kappa L}$

The fact that the supercell is made up of single elements with different parameters leads to heterogeneity and therefore to the appearance of passbands and stopbands. Projection on a vertical line of the whole set of admitted frequencies leads to a simplified representation of passbands and stopbands, resulting a vertical line in pieces that can be associated to the number α, generator of the chain. The graphical representation that arises from the repetition of the process over the entire interval $0 \le \alpha \le 1$ gives rise to a figure like that of fig. 2. We call this representation the Sturmian bulk spectrum. The fractal nature emerges for each portion of the graph. This nature can be justified mathematically using Chebyshev polynomials, as shown in Ref. [4]. The procedure can be extended to other one-dimensional wave guides like rods and beams

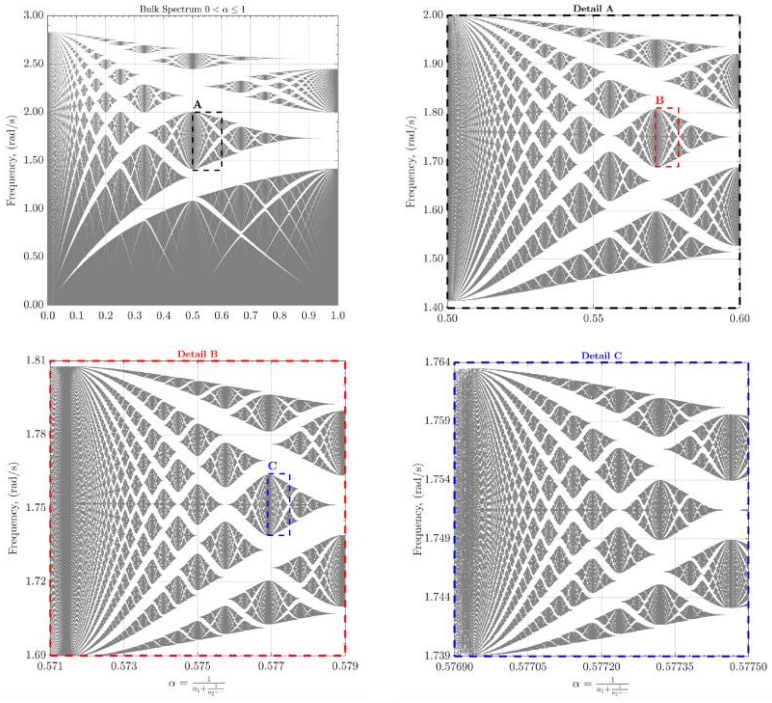

Figure 2 . Sturmian bulk spectrum of a spring-mass system with quasiperiodic distribution of rigidities . Top-left: bulk spectrum for the whole range of generator parameter $0 \le \alpha \le 1$. Top-right, bottom-right and bottom-left: details A, B and C to visualize the selfsimilar structure of the bulk spectrum.

References

[1] E. Maciá, *Aperiodic Structures in Condensed Matter. Fundamentals and Applications*. Boca Raton: Taylor & Francis, (2009).
[2] V. Velasco and J. Zárate, "Elastic waves in quasiperiodic structures," *Prog. Surf. Sci.*, **67 (1)**, pp. 383 – 402, (2001).
[3] D. Huang, G. Gumbs, and M. Kolar, "Localization in a one-dimensional Thue-Morse chain," *Phys. Rev. B*, **46**, pp. 11 479–11 486, (1992).
[4] M. Lázaro, A. Niemczynowicz, A. Siemaszko, and L. Garcia-Raffi, "Elastodynamical properties of Sturmian structured media," *Journal of Sound and Vibration*, **517**, 116539, (2022).

PHONONICS 2023: 6th International Conference on Phononic Crystals/Metamaterials/Metasurfaces, Phonon Transport, and Topological Phononics
Manchester, England, June 12-16, 2023
PHONONICS-2023-0116

Negative refraction in canonical quasicrystalline-generated phononic metamaterials

Z. Chen[1], L. Morini[1], M. Gei[2]

[1] *School of Engineering, Cardiff University, 14-17 The Parade, CF243AA Cardiff, UK*
chenz51@cardiff.ac.uk, morinil@cardiff.ac.uk
[2] *Department of Engineering and Architecture, University of Trieste, Via A. Valerio 6/1, 34127 Trieste, Italy*
massimiliano.gei@dia.units.it

Abstract: A class of two-phase periodic laminates with quasicrystalline-generated fundamental cells is introduced. For specific ratios between the geometrical and constitutive parameters of the two constituent phases (*canonical ratios*), the Floquet-Bloch spectrum of this particular type of laminate is periodic. We show how this unique property can be used to obtain negative refraction of an antiplane wave incident at the interface with an elastic substrate.

Canonical quasicrystalline-generated laminates

We introduce a class of two-dimensional, two-phase quasicrystalline-generated laminates with layering direction parallel to the axis y (see Fig. 1/(A)). Each laminate of this family is composed of a repeated elementary cell F_i where the two basic components, A and B, are arranged in series according to the standard Fibonacci sequence, which is based on the substitution rule $A \rightarrow AB$, $B \rightarrow A$. The repetition of the fundamental cells assures global periodicity along axis x and the possibility of applying the Floquet-Bloch technique in order to study harmonic wave propagation in these systems.

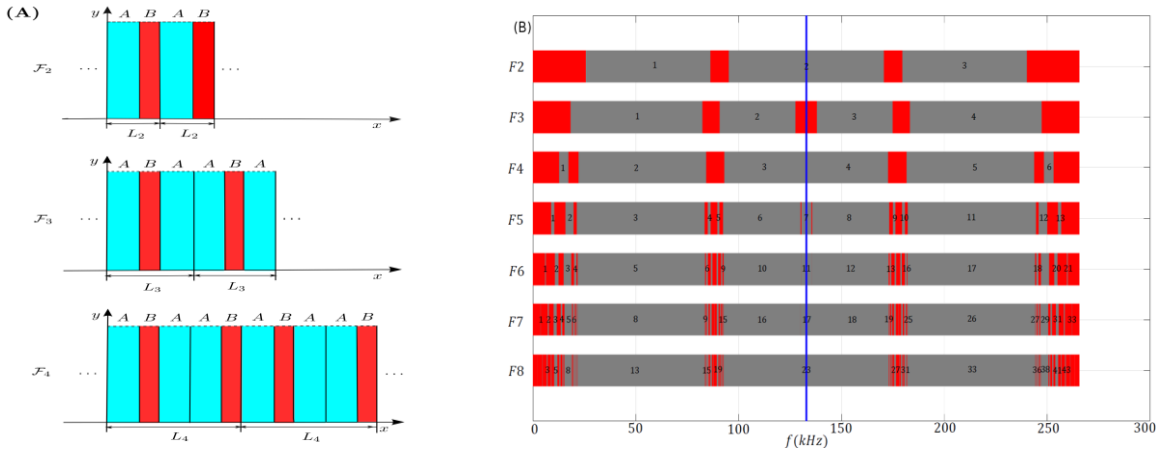

Figure 1 (A): Two-dimensional laminates assembled according to F_2, F_3 and F_4 Fibonacci cells. **(B)**: Diagram reporting, in the grey zones, the number N_i^f of real solutions K_y of the dispersion relations for cells F_2 to F_8 as a function of the frequency. Transition zones are highlighted in red.

The dispersion relation for Floquet-Bloch harmonic antiplane waves propagating in Fibonacci laminates as those illustrated in Fig. 1/(A) assumes the form

$$\cos(K_x L_i) = \text{tr}\, \boldsymbol{M}_i(f, K_y)/2, \tag{1}$$

where $\boldsymbol{M}_i$ is the transmission matrix of the ith-order cell F_i, L_i is the total length of the cell, $f = \omega/2\pi$ is the wave frequency, K_x and K_y are the components of the wave vector directed along x and y axis, respectively. $\boldsymbol{M}_i$ is unimodular, i.e. $\det \boldsymbol{M}_i = 1$, and follows the recursion rule $\boldsymbol{M}_{i+1} = \boldsymbol{M}_{i-1}\boldsymbol{M}_i$, with $\boldsymbol{M}_0 = \boldsymbol{M}_B$ and $\boldsymbol{M}_1 = \boldsymbol{M}_A$ [1]. Assuming a given wave frequency f, for any real value of K_x we found a finite number $N_i{}^f$ of real and an infinite number of imaginary solutions K_y of the dispersion relation (1) [2]. The numerical solution of (1), obtained for a determinate set of frequencies by varying K_x along the intervals $0 \leq K_x \leq m\pi/L_i$, $m \in \mathbb{N}$ (*Brillouin zones*), shows that: i) assuming given values of f and K_x, $N_i{}^f$ increases for high order Fibonacci cells F_i [1]; ii) if f belongs to some particular frequency ranges, $N_i{}^f$

depends on the value of K_x and we have $N_i{}^f = t - 1$ for $0 \leq K_x \leq \underline{K}_x$ and $N_i{}^f = t$ for $K_x \leq \underline{K}_x \leq m\pi/L_i$. We denote these frequency ranges as *transition zones*. The t-th transition zone is that where $N_i{}^f$ switches from $t - 1$ to t. An example of transition zone layout for laminates designed according to cells F_2 to F_8 is reported in Fig. 1/(B) as a function of the frequency. We note that they are disposed according to a self-similar pattern. The analysis of the dispersion curves obtained assuming $K_y = 0$ (transverse wave propagation in the laminate) reveals that for any cell F_i, the position of pass bands coincide with that of transition zones. In this specific case, the transfer matrix $\boldsymbol{M}_i$ and the dispersion relation (1) becomes identical to those previously defined by the authors for quasicrystalline-generated structural waveguides[3]. Consequently, the self similarity is governed by a local scaling whose factor is analogous to that used to characterize the spectrum of this family of waveguides. By observing Fig. 1/(B), we also note that for any cell F_i, the arrangement of the transition zones is periodic. This is achieved for rational values of the ratio $\beta = c_A h_B / c_B h_A$, where h_A and h_B are the thicknesses of phases A and B, c_A and c_B the shear wave speed in materials A and B, respectively. We denote β as *canonical ratio*, and the laminates characterized by $\beta \in \mathbb{Q}$ as *canonical laminates*[4, 5] (for the case shown in Fig.1/(B), $\beta = 2$).

Negative refraction using canonical quasicrystalline laminates

We now use the canonical quasicrystalline laminates to obtain negative refraction of an antiplane wave across an interface with an elastic substrate (schematic of the problem reported in Fig.2/(A)). For each value of K_x corresponding to a given frequency and an arbitrary angle of incidence in the interval $0 \leq \theta \leq \pi/2$, we have $N_i{}^f$ real solutions of the dispersion relation (1). These real solutions correspond to propagating modes transmitted at the interface. In order to have only one single negatively refracted mode (*pure negative refraction*), the incident wave frequency should belong to the interval $f^{min} \leq f \leq f^{max}$ where f^{min} depends on the constitutive parameter of the substrate, and f^{max} is the high est frequency of the second transition zone. Remembering the spectrum analysis reported in the first section, we can calculate f^{max} for any Fibonacci cell F_i. By using the obtained analytical scaling factors[5] together with the associated scaling relationships and the condition of periodicity by $\beta \in \mathbb{Q}$, we can design canonical laminates providing pure negative refraction in several ranges of frequencies considering different elastic substrates. The results illustrated in Fig.2/(B) for a PMMA-steel laminate bonded to a polyethylene substrate show that, by considering the same angle of incidence ($\theta = 20^\circ$) high-order Fibonacci cells yield single negatively refracted modes at lower frequencies with respect to standard two-phase periodic laminates (represented by cell F_2).

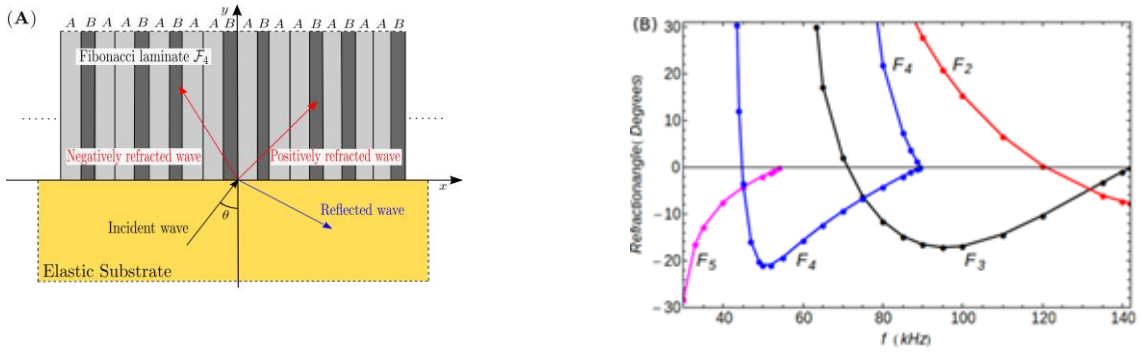

Figure 1 (A): Schematic of a problem of an antiplane wave approaching at the interface between an elastic substrate and a Fibonacci laminate F_4. **(B)**: Angles of refraction corresponding to an incident angle $\theta = 20^\circ$, plotted versus the frequency for cells F_2 to F_8.

References

[1] L. Morini, Y. Eyzat, Y. and M. Gei, *J. Mech. Phys. Solids*, **124**, 282-298 (2019) .
[2] J.R. Willis, *J. Mech. Phys. Solids*, **97**, 10-18 (2016).
[3] L. Morini and M. Gei, *J. Mech. Phys. Solids* **119**, 83-103, (2018).
[4] Z. Chen, L. Morini and M. Gei, *Eur. J. Mech. A - Solids*, 104577, (2022) in press.
[5] Z. Chen, L. Morini and M. Gei, *Phil. Trans. R. Soc. A*, **380**, 20210401, (2022).

PHONONICS 2023: 6th International Conference on Phononic Crystals/Metamaterials/Metasurfaces, Phonon Transport, and Topological Phononics
Manchester, England, June 12-16, 2023
PHONONICS-2023-0121

The Topological Valley Edge State of the Archimedean Tilings Phononic Crystal

Yu-Jui Liang[1], Pei-Ju Guo[2], De-Han Jhu[1], Lien-Wen Chen[2]

[1] *Department of Aeronautics and Astronautics, National Cheng Kung University, No. 1, University Rd., East Dist., Tainan City 701, Taiwan*
yliang@gs.ncku.edu.tw, P46111135@gs.ncku.edu.tw
[2] *Department of Mechanical Engineering, National Cheng Kung University, No. 1, University Rd., East Dist., Tainan City 701, Taiwan*
myps50824@gmail.com, chenlw@mail.ncku.edu.tw

Abstract: In recent years, the research of topological insulators (TIs) has been involved in various engineering fields, such as electromagnetic wave, sound waves, and elastic wave, etc. In this work, Archimedean (3,4,6,4) tilings phononic crystal is considered to study the TIs on longitudinal wave and sound wave based on quantum valley hall effect (QVHE) theory. The spatial inversion symmetry of the structure is destroyed by changing the lattice parameters for obtaining two inequivalent structures, which are used to design five propagation paths including perfect, Z-shape, disorder, defect 1 and defect 2. Through two topologically distinct interfaces, we prove that the proposed structures possess not only high transmission but also strong wave propagation where the defects and immune backscattering can be neglected.

The research of lossless transmission has been received much attention during the past decade. Topological insulators (TIs) have a special surface state called topologically protected edge state. Many researchers have been studied TIs and achieved significant progress in simulations and experiments in recent years. Fei-Fei Li et al. [1] employed the cut-and-glue technique to design a TI with dislocation. They predicted theoretically and experimentally robust light-trapping into a cavity mode in a 2D photonic crystal. Fei Gao et al. [2] experimentally demonstrated valley-polarized kink states with polarization multiplexing in valley photonic crystals, which was designed from a spin-compatible four-band model. Zhiwang Zhang et al. [3] demonstrated that the helical edge states hosted by the topological antenna was excited or out-coupled in a highly directional fashion to provide sophisticated acoustic duplex communication. Mou Yan et al. [4] proposed a valley topological structure fabricated on silicon chips by using a micromanufacturing technology. The TIs structure can be freely adjusted elastic waves at mode in a 2D photonic crystal. Jiuyang Lu et al. [5] proposed a unique bilayer design of sonic crystals that allowed wave propagates alternately in the upper and lower layers of the structures, or only in the upper (lower) layer. Xiujuan Zhang et al. [6] proposed a higher-order TIs by using tunable two-dimensional sonic crystals. The TIs in the bulk and edges were triggered independently by tuning the geometry of the sonic crystals. From those work mentioned above, breaking the symmetry of structures may form the topologically protected edge states to control the wave propagation within the structures. Therefore, a highly symmetrical Archimedean(3,4,6,4) tilings phononic crystal is investigated in this work. The topologically protected edge states are created based on the quantum valley hall effect (QVHE) by breaking the spatial inversion symmetry of the structure. Finite element method will be applied for the verification of wave propagation in the proposed structures.

The Archimedean(3,4,6,4) tilings periodic structure is shown in Figure 1(a). The unit cell of the periodic structure consists of six steel cylinders with the air background as shown in Figure 1(b). The density and sound velocity of air and steel are $\rho_a = 1.2\ \mathrm{kg/m^3}$, $\rho_s = 7800\ \mathrm{kg/m^3}$, $c_a = 343\ \mathrm{m/s}\ (20°\mathrm{C})$ and $c_s = 6100\ \mathrm{m/s}$, respectively. The geometrical parameters as shown in Figure 1(b) where the cylinder radius of r = 16 mm, the distance between the center of circle of d = 40 mm, and the lattice constant $a_0 = d(1+\sqrt{3}) \approx 109.28$ mm are selected in this work. The dispersion relations of the proposed model are shown in Figure 2. To create the topologically protected edge states, a new parameter *f* is used to control the size of the steel rod as shown in Figure 3 where r_a and r_b are equal to r(1+f) and r(1-f), respectively. Here we consider the geometry of the structure as the upper triangle and the lower triangle. The circle radius in the upper triangle is equal to $r_a(r_b)$ as well as the circle radius in the lower triangle $r_b(r_a)$, and we define it as type I(II) crystal. Figure 4 shows the dis-

persion relations of f = 0.1 and f = 0.2. More discussions regarding the band structures and observations will be discussed in the conference.
In this work, the supercell method and the full wave simulations for 5 different propagation paths including perfect, Z-shape, disorder, defect 1 and defect 2 will be more discussed in the upcoming conference to demonstrate the high transmission at the edge mode frequency and verify the proposed structures having robust wave propagation where defects and immune backscattering can be neglected. Therefore, the proposed design structure has high potential to become novel acoustic devices such as waveguides, signal splitters, and filters in the acoustic applications.

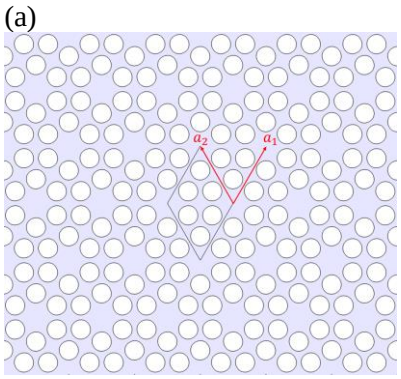

Figure 1 Schematics of Archimedean (3,4,6,4) tilings phononic crystal. **(a)** Periodic structure, and **(b)** unit cell.

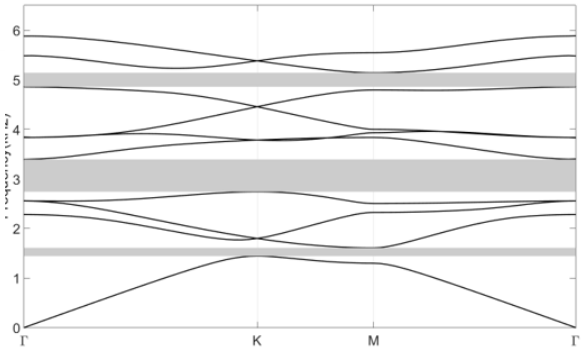

Figure 2 Band structures of Archimedean (3,4,6,4) tilings phononic crystal.

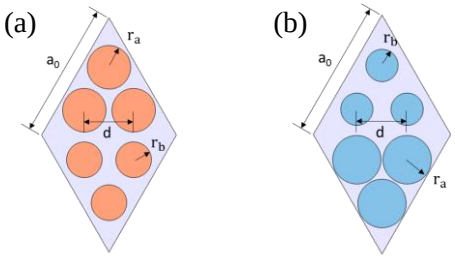

Figure 3 Unit cell of **(a)** f = 0.1 **(b)** f = 0.2

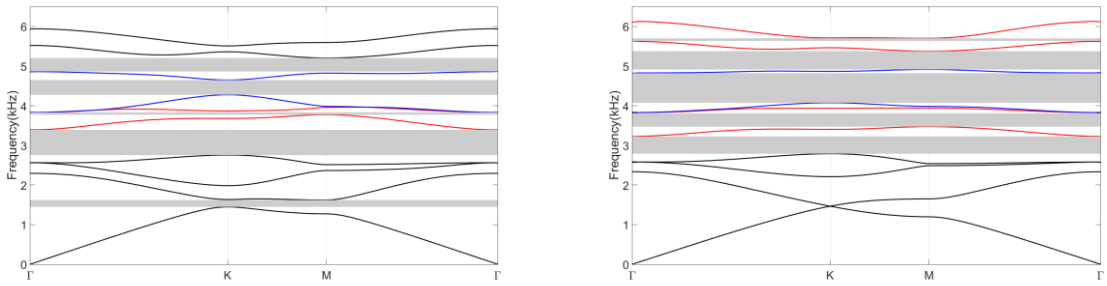

Figure 4. Band structure of Archimedean(3,4,6,4) tilings crystal **(a)** f = 0.1 and **(b)** f = 0.2.

References

[1] F.-F. Li et al., Topological light-trapping on a dislocation, *Nature Communications*, vol. 9, no. 1, p. 2462, (2018).
[2] F. Gao et al., Topologically protected refraction of robust kink states in valley photonic crystals, *Nature Physics*, vol. 14, p. 140, (2017).
[3] Z. Zhang et al., Directional Acoustic Antennas Based on Valley-Hall Topological Insulators, *Advanced Materials*, vol. 30, no. 36, p. 1803229, (2018)
[4] M. Yan et al., On-chip valley topological materials for elastic wave manipulation, *Nature Materials*, vol. 17, no. 11, pp. 993-998, (2018)
[5] J. Lu et al., Valley Topological Phases in Bilayer Sonic Crystals, *Phys. Rev. Lett.*, vol. 120, no. 11, p. 116802, (2018)
[6] X. Zhang et al., Second-order topology and multidimensional topological transitions in sonic crystals, *Nature Physics*, vol. 15, no. 6, pp. 582-588, (2019)

PHONONICS 2023: 6th International Conference on Phononic Crystals/Metamaterials/Metasurfaces, Phonon Transport, and Topological Phononics
Manchester, England, June 12-16, 2023
PHONONICS-2023-0212

Principles Underlying 2-D Phononic Pseudocrystal Isolators

S. Hales Swift[1], Ihab F. El-Kady[1], Rick A. Kellogg[2]

[1] Photonic and Phononic Microsystems Department, Sandia National Laboratories, Albuquerque, NM, USA, shswift@sandia.gov, ielkady@sandia.gov
[2] Mechanisms V – Advanced and Stockpile Systems Department, Sandia National Laboratories, Albuquerque, NM, USA
rakello@sandia.gov

Abstract: A family of phononic pseudocrystal interposers was recently developed at Sandia National Laboratories for wideband isolation applications. The self-similarity underlying the family of designs highlighted in this work may limit mode conversion within the interposer region enabling suppression ranges larger than those predicted by an adiabatic translation of the bandgap.

Vibration isolators are designed, by definition, to suppress the transmission of vibration into or out of some identified region. The capabilities in terms of frequency range and suppression depth of isolator designs tend to be constrained by available real estate—the amount of space available, the size of selected unit cells, the numbers of such cells required to achieve meaningful suppression, and the frequency ranges affected by a given unit cell—and manufacturability. Consequently, for such space-constrained circumstances, designs which enable wideband isolation with adequate depth and relatively modest space requirements are valuable.

A family of phononic pseudocrystal interposers was recently developed at Sandia National Laboratories that offers extended suppression ranges while retaining a relatively small footprint. The concept originally developed in response to a need to provide wideband vibration isolation at Megahertz frequencies that fit into an approximately annular region. While phononic crystals were an early contender, an adiabatic bandgap expansion concept was instead explored that involved taking an existing 2-D unit cell and allowing it to grow radially between the inner and outer annular boundaries. Under the adiabatic bandgap expansion concept it was assumed that we would change the whole size gradually enough that the waves would not be effected by discontinuous changes in the local properties; indeed, the filling fraction is kept constant in the radial direction within the interposer region. The cell was then allowed to grow by an equal ratio in each row in the radial direction. Consequently, exact symmetry was maintained within each row in the circumferential direction while in the radial direction translational symmetry was replaced by self-similarity. For this reason, the basic building blocks of the pseudocrystal are called “pseudounit” cells because the array of holes is not fully symmetric as is the case in a true crystal, but instead self-similar. A related approach taken with 1-D, effectively non-self-similar, pseudocrystal materials suggested that the dispersion of the local unit cell (effectively, a sort of pseudocell) was usable for predicting vibration suppression and reflection properties [1, 2]. We assumed that the typical phononic crystal requirement of at least 5 similar unit cells for meaningful suppression held for pseudocrystals also; however, wedefined similarity in our case as cells exhibiting overlapping bandgaps and mutual scaled self-similarity rather than identity as is conventional for pure phononic crystals.

An underlying pseudounit cell which exhibited a ratio of 1.334 between its upper and lower bandgap edge frequencies was chosen and expanded at a geometric growth ratio of 1.05 to ensure sufficient radial overlap of bandgaps to ensure good suppression. If we were relying solely on expanding the existing total bandgap, we would expect to need log(10)/log(1.05)=47.2 pseudocells in the radial direction plus an additional four 4 pseudocells at the beginning and end in order to be ensured of having efficacy at the extreme frequencies. Thus, we would expect to need roughly 55 pseudocells. However, in the course of building up the numerical experimentation to determine the insertion loss resulting from the interposer, we found that examples with far fewer cells were more than adequate.Consider, for example, the 28-radial-hole case shown below. It’s performance went substantially beyond the desired factor of 10 ratio between the upper and lower 20+ dB-suppression frequencies, achieving a factor of greater than 36 for the longitudinal mode considered, and posing substantial computational challenges

for calculating exactly how far the suppression range went. While the reasons for this better-than - expected performance continue to be clarified, an important component of their performance appears to be due to the self-similar unit pseudocell geometry and the annular pattern.

The geometry of the annular configuration limits the possible propagation angles of waves which reach the center, which in effect limits the relevant portion of the 2-D dispersion potentially opening up additional bandgaps. In the circumferential direction all cells and holes are equal, while in the radial direction all holes are scaled versions of their neighbors. In a regular phononic crystal, only those mode conversions are allowed which appear in the phononic dispersion relations[1]. The local phononic dispersion relations (associated to the square cell approximation of the phononic pseudocell) are also scaled with the pseudocell size; consequently, we can infer that the set of allowable mode conversions also scales. When this scaling process moves the dispersion branch upon which a mode is propagating into a range that excludes its frequency, it can be expected to evanesce and, because of the adiabatic rate of growth, is unlikely to find an appropriate mode onto which to project for continued propagation. Because of this, as the dispersion is scaled in frequency due to the underlying pseudocell being scaled in size, the family eventually excludes many of the frequencies that it supported at the outer edge of the interposer. Consequently, it appears that a geometrically growing phononic pseudocrystal can exhibit large suppression ranges that are not present as total bandgaps in any of the underlying unit pseudocells. This additional formation mechanism appears poised to inaugurate a new class of phononic materials, many characteristic examples of which exhibit exceptionally wide suppression bands while requiring less real estate than is required by conventional phononic crystals. Additionally, 1-D Bloch-Floquet analysis of a strip of the interposer shows large numbers of flat bands with intervening gaps similar to results seen in 1-D pseudocrystals.

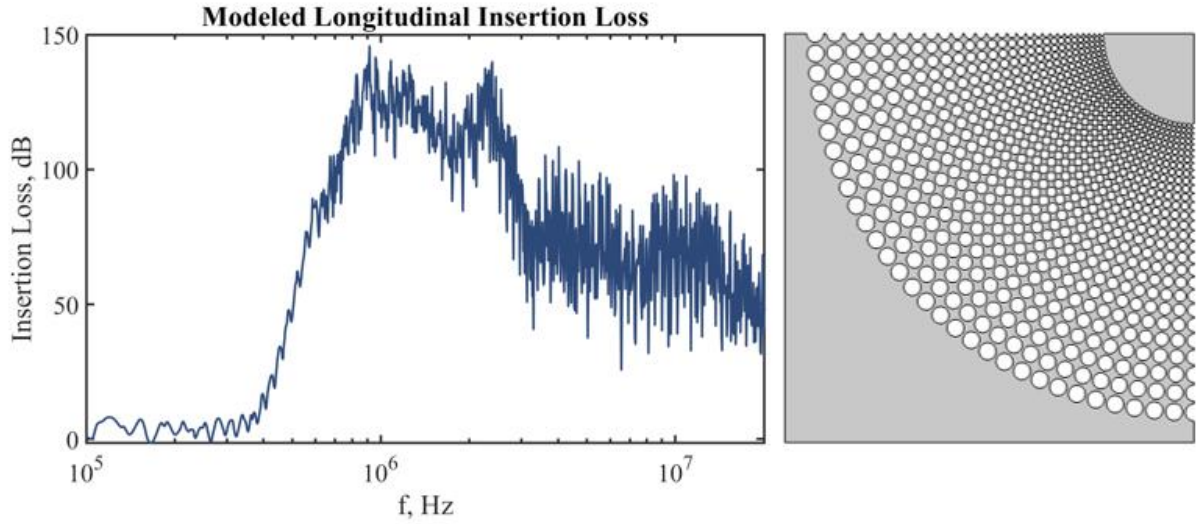

Figure 1:(left) Insertion loss for longitudinal waves associated with the phononic pseudocrystal interposer shown to the right. (right) A 2-D phononic pseudocrystal with 28 unit cells and a growth rate of ~1.05. A quarter view is shown and was used for the calculations.

Sandia National Laboratories is a multimission laboratory managed and operated by National Technology and Energy Solutions of Sandia, LLC, a wholly owned subsidiary of Honeywell International, Inc., for the U.S. Department of Energy's National Nuclear Security Administration under contract DE-NA0003525.

References

[1]Z. Tian, L. Yu, *Nat. Sci. Rep.*, **7**, 40004 (2017).
[2]V. Romero-García, R. Picó, A. Cebrecos, V. J. Sánchez-Morcillo, K. Staliunas, *Appl. Phys. Lett.* **102**, 91906 (2013).
[3]T. Ding, A. Song, C. Sun, Y. Xiang, F.-Z. Xuan, *J. Appl. Phys.* **132**, 225103 (2022).

PHONONICS 2023: 6th International Conference on Phononic Crystals/Metamaterials/Metasurfaces, Phonon Transport, and Topological Phononics
Manchester, England, June 12-16, 2023
PHONONICS-2023-0075

Broad-angle Coherent Perfect Absorption-Lasing in two-dimensional non-Hermitian Phononic Crystals

Changqing Xu[1], Ying Wu[2]

School of Physics and Technology, Nanjing Normal University, Nanjing 210023, China
changqing.xu@nnu.edu.cn
Division of Computer, Electrical and Mathematical Science and Engineering, King Abdullah University of Science and Technology (KAUST), Thuwal 23955-6900, Saudi Arabia
ying.wu@kaust.edu.sa

Abstract: Coherent perfect absorption-lasing (CPAL) has been intensively studied for normal and small angle wave incidence. Here, we report a two-dimensional non-Hermitian phononic crystal for broad-angle CPAL. The synergy of a nonsymmorphic glide symmetry of the lattice, gain-loss modulation and an optimization of unit cell induces a parity-time phase transition in the band structure along the Brillouin zone boundary. The transition points, i.e., the exceptional points, form a slab-like contour, with nearly zero dispersion in both real and imaginary parts of the band structure. Such dispersionless band structure significantly enhances the range of incident angle for CPAL.

PHONONICS 2023: 6th International Conference on Phononic Crystals/Metamaterials/Metasurfaces, Phonon Transport, and Topological Phononics
Manchester, England, June 12-16, 2023
PHONONICS-2023-0082

Piezoelectrically Mediated Acoustic Phonon Heat Transfer Across a Vacuum Gap

Zhuoran Geng[1], Ilari. J. Maasilta[1]

[1] *Nanoscience Center, Department of Physics, University of Jyväskylä, Survontie 9C Jyväskylä, Finland, zhgeng@jyu.fi, maasilta@jyu.fi*

Abstract: Acoustic phonons can "tunnel" across a vacuum gap with the aid of piezoelectricity, enabling them to transmit a much stronger heat flux than blackbody radiation. We investigate this phenomenon experimentally, demonstrating a significant heat transfer between two suspended microscopic beams at sub-Kelvin temperatures.

Acoustic phonons are particle-like quanta of solid vibrations and can be excited thermally. As a first thought, it appears that phonons cannot traverse a vacuum gap separating two media since they do not exist in the vacuum. However, potential mechanisms, such as the van der Waals force and the electrostatic force [1,2], have been proposed, which could facilitate coupling at nanometer-scale gap widths, enabling the transfer of heat carried by phonons between the two solids. Nevertheless, these studies have also shown that the effect of such heat transfer diminishes rapidly with an increase of the vacuum gap, contributing significantly only when gap widths are less than 1 nm at room temperature. Although current state-of-the-art nanotechnology has made it possible to access nanometer-scale gaps, no concrete experimental demonstration of heat transfer facilitated by acoustic phonon tunneling has been presented to our knowledge.

This study focuses on another, relatively unexplored mechanism of acoustic phonon tunneling that utilizes piezoelectricity. When a thermally excited acoustic phonon hits a free surface of a piezoelectric solid, it generates a decaying evanescent electric field that penetrates the vacuum. This electric field interacts with the lattice deformations of the second piezoelectric solid placed within the phonon wavelength, resulting in the transfer of heat through the vacuum. The emitted heat flux J_γ from the solid $\gamma = 1,2$ at temperature T_γ across a vacuum gap with width d can be expressed as

$$J_\gamma(T_\gamma, d) = \sum_\alpha \int \frac{d^3k}{(2\pi)^3} \hbar\omega_\alpha(\boldsymbol{k}) n(\omega_\alpha, T_\gamma) \hat{\boldsymbol{n}}_\gamma \cdot \frac{\partial \omega_\alpha}{\partial \boldsymbol{k}} \Theta\left(\hat{\boldsymbol{n}}_\gamma \cdot \frac{\partial \omega_\alpha}{\partial \boldsymbol{k}}\right) \mathcal{T}_\alpha(\theta, \varphi, k, d), \quad (1)$$

where $n(\omega_\alpha, T_\gamma)$ is the Bose-Einstein distribution describing the thermal occupation of the phonon modes of energy $\hbar\omega_\alpha(\boldsymbol{k})$, and $\hat{\boldsymbol{n}}_\gamma$is the outward unit normal of the vacuum-solid interface. The power transmittance $\mathcal{T}_\alpha$ of mode α contains the essential physics of the piezoelectrically mediated acoustic wave tunneling phenomenon, and takes the form [3,4]

$$\mathcal{T}_\alpha(\theta, \varphi, k, d) = \frac{2Re\left[r_V^{(2)}\right]\left|t_{\alpha\to V}^{(1)}\right|^2 e^{-2kd\sin\theta}}{\left|1 - r_V^{(1)} r_V^{(2)} e^{-2kd\sin\theta}\right|^2}, \quad (2)$$

in which $t^{(\gamma)}$ and $r^{(\gamma)}$ are the single surface transmission and reflection coefficients derived in Ref.[3] for the plane-plane geometry.

Our numerical studies have demonstrated that while the heat flux from acoustic phonon tunneling is still smaller than that from near-field radiative heat transfer enabled by surface phonon-polaritons at room temperature, it becomes dominant over other mechanisms and has a significant effect over a much larger distances at low temperatures, allowing heat to tunnel across gaps ~ hundreds of nanometers wide at liquid helium temperatures [5].

In order to experimentally demonstrate this phenomenon, we conducted two sets of measurements at sub-Kelvin temperatures, using microscopic devices comprised of two closely spaced suspended beams. The first set of measurements qualitatively shows the increased heat transfer achieved by using devices made from piezoelectric AlN compared to non-piezoelectric SiN devices. In the second set of

measurements, we quantitatively determine the transferred power and compare the results to theoretical estimations.

The experimental thermal model is depicted in Figure 1, where each beam is equipped with a superconducting junction heater and thermometer for localized heating and temperature sensing. In order to obtain the tunneled power P_t, we adopt the temperature-dependent expression $P_\gamma = K_\gamma(T_\gamma^{n_\gamma} - T_{sub}^{n_\gamma})$ for the conducted power flow from each beam to the substrate, and experimentally determine the beam specific parameters K_γ and n_γ. Using those parameters, an expression for the tunneled power reads as

$$P_t = K_R\left(T_R^{n_R} - T_{sub}^{n_R}\right) - e_R \tag{3}$$

in which T_R and T_{sub} are the results from measuring the temperatures of the receiver beam ($\gamma = R$) and the substrate while applying heating on emitter beam ($\gamma = E$), whereas K_R, n_R and e_R are determined by the additional supplementary measurement.

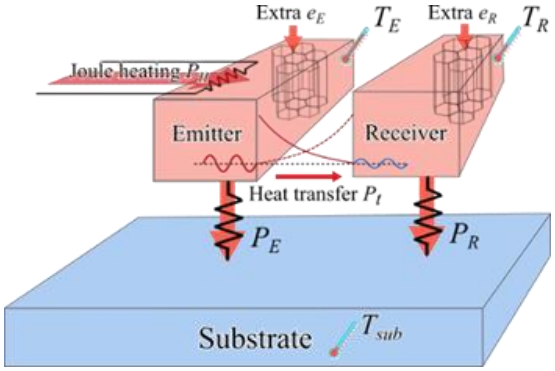

Figure 1 The schematic of the thermal model for the device used in the experiment.

We observe a clear difference in the transferred power between two AlN devices with a different gap width, and such a difference can be observed over the whole measured temperature range, implying that the underlying heat transfer mechanism depends strongly on the vacuum gap width. These observations are qualitatively in agreement with the theory described above, in which the transferred heat depends exponentially on the vacuum gap width. In contrast, two measured SiN devices show roughly the same transferred powers, which is considerably lower than that of the AlN devices. There is no clear gap width dependence for the SiN devices. This is likely due to SiN being non-piezoelectric and incapable of enabling acoustic phonon tunneling. As a result, comparing the results for SiN and AlN devices leads to the conclusion that piezoelectrically mediated acoustic phonon tunneling is present.

However, there is big quantitative discrepancy between the experimental results and the theoretical estimations, which could be due to several reasons. The first and most obvious reason is the violation of the plane-plane geometry assumption that was made in the theoretical modeling. The suspended AlN beam has a thickness that is much smaller than the other two dimensions, making it a 2D-like structure. Additionally, at the lowest temperatures, the thermal wavelengths of the phonons can be longer than the thickness of the beam, leading to inaccurate estimations of tunneled power. On the other hand, the possible presence of the piezoelectric acoustic gap waves [6] may also contribute to enhanced heat transfer. Related research on acoustic phonon tunneling between two non-piezoelectric solids suggests that Rayleigh surface waves can contribute, with this contribution being of a similar magnitude as that from the bulk wave tunneling [1,2].

References

[1] J. B. Pendry, K. Sasihithlu, and R. V. Craster, *Phys. Rev. B* **94**. 075414 (2016).
[2] A. I. Volokitin, *J. Phys. Condens. Matter* **32**, 215001 (2020).
[3] Z. Geng and I. J. Maasilta, *Phys. Rev. Res.* **4**, 033073 (2022).
[4] Z. Geng and I. J. Maasilta, *Complete Tunneling of Acoustic Waves between Closely Spaced Piezoelectric Crystals*, arXiv:2209.08287.
[5] Z. Geng and I. J. Maasilta, *Heat transfer across a vacuum gap induced by piezoelectrically mediated acoustic phonon tunneling*, arXiv:2303.05084.
[6] A. N. Darinskii and M. Weihnacht, *IEEE Trans. Ultrason. Ferroelectr. Freq. Control* **53**, 412 (2006).

PHONONICS 2023: 6th International Conference on Phononic Crystals/Metamaterials/Metasurfaces, Phonon Transport, and Topological Phononics
Manchester, England, June 12-16, 2023
PHONONICS-2023-0174

Universal Behavior of Highly-Confined Heat Flow in Semiconductor Nanosystems: from nanomeshes to metalattices

Brendan McBennett[1], Albert Beardo[1], Emma Nelson[1], Begoña Abad[1], Travis Frazer[1], Amitava Adak[1], Yuka Esashi[1], Baowen Li[2,3], Henry Kapteyn[1], Margaret Murnane[1], Joshua Knobloch[1]

1 Department of Physics, JILA, and STROBE NSF Science and Technology Center, University of Colorado and NIST, Boulder, Colorado 80309

2 Department of Materials Science and Engineering, Southern University of Science and Technology, Shenzhen, PR China

3 Paul M. Rady Department of Mechanical Engineering and Department of Physics, University of Colorado, Boulder, CO 80309, USA

Abstract: We use extreme ultraviolet beams to study phonon transport dynamics in a 3D silicon phononic crystal, and observe two orders of magnitude reduction on the thermal conductivity relative to bulk. To explain this behavior, we develop a predictive theory wherein thermal conduction separates into a geometric permeability component and an intrinsic viscous contribution, arising from a universal effect of nanoscale confinement on phonon flow. Using experiments and atomistic simulations, we show that our theory applies to a general set of highly-confined silicon nanosystems, from metalattices, nanomeshes, porous nanowires to nanowire networks.

Under highly confined conditions, phonons are usually assumed to travel between boundaries without internal collisions. Accordingly, ray-like propagation of ballistic phonons is predicted in silicon nanostructures [1]. This contrasts with recent Molecular Dynamics (MD) studies in systems such as nanowires, which show thermal energy flow profiles reminiscent of hydrodynamics [2]. These observations indicate the existence of a significant amount of phonon-phonon scattering and momentum diffusion at length scales much smaller than most of the bulk phonon MFPs. Moreover, the relevance of phonon coherent behavior to describe heat transport in complex structures at elevated temperatures is still under debate. These contradictions illustrate the lack of consensus on a unified description of heat transport in nanostructured semiconductors, especially at the smallest length scales and in emerging 3D phononic crystals.

In this work, we study highly-confined heat flow in a 3D silicon phononic crystal "metalattice" at room temperature using time-resolved extreme ultraviolet scatterometry [3]. The metalattice periodicity is 36 nm, far below the average phonon mean free path in bulk silicon. We model the system as an effective media obeying a Fourier relation with a conductivity reduced by two orders of magnitude with respect to the bulk. To explain this and a broad set of similar measurements on highly-confined silicon nanosystems—including metalattices, nanomeshes, porous nanowires and nanowire networks—we develop a predictive theory of heat flow in nanostructured silicon with dimensions far below the bulk phonon MFP [3]. Through an analogy to the hydrodynamics of rare gases in porous media, we decompose the thermal conductivity into permeability and viscosity components, where the former accounts for nanoscale geometry effects and the latter captures the intrinsic effect of nanoscale confinement on the phonon population. By comparing a broad set of experimental data with MD simulations, we uncover a universal relationship between viscosity and porosity, which yields a general analytical expression for thermal conductivity in highly-confined silicon nanosystems. In contrast to the ballistic interpretation, this result suggests a modified phase space for phonon-phonon interactions in nanostructured silicon with respect to the bulk.

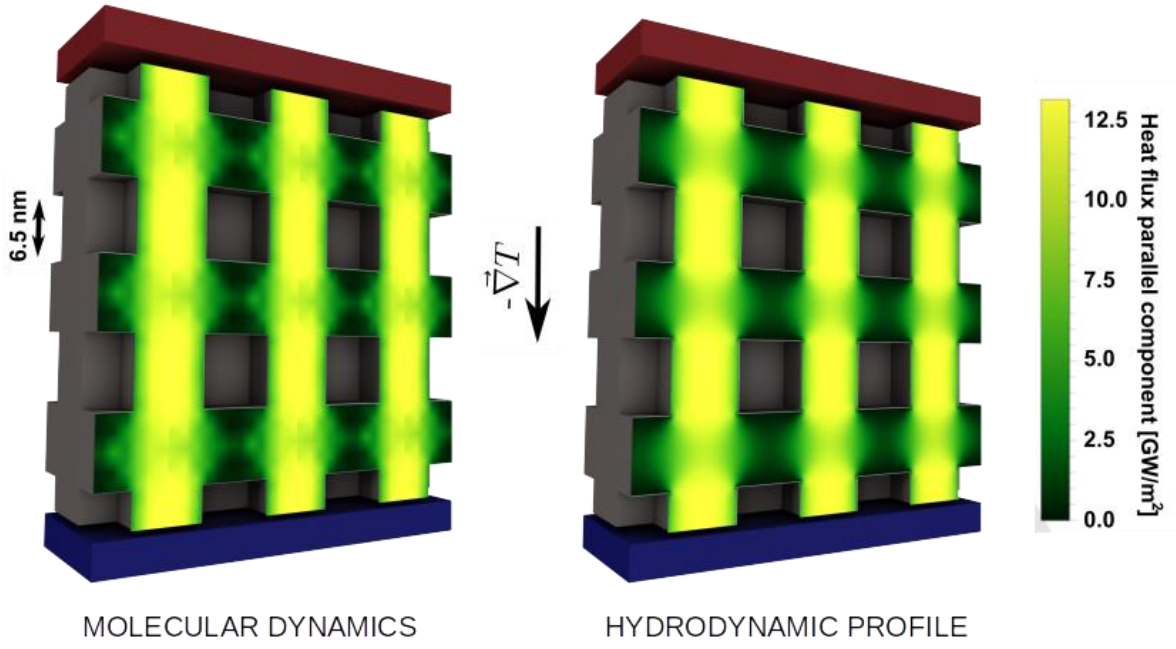

Figure: Heat flux profile obtained from non-equilibrium Molecular Dynamics simulations (left) and the hydrodynamic heat equation (right). The resemblance between the two profiles, and the lack of ballistic or ray-like phonon transport features in MD, motivate the use of hydrodynamic transport theory to describe the thermal energy transfer in 3D phononic crystals.

Furthermore, we microscopically justify the use of hydrodynamic transport analogies to model nanoscale phonon transport by quantifying the heat flux distribution in a 3D metalattice using non-equilibrium MD simulations, as shown in the Figure. We obtain Poiseuille-like profiles between the pores, and we do not observe shadowing effects behind the pores as predicted by the ballistic description. Therefore, the MD profiles can be reproduced using hydrodynamic mesoscopic modeling [4], which suggests collective evolution of the phonon distribution rather than independent phonon evolution of the distinct phonon modes.

In conclusion, we measured the thermal conductivity of a 3D silicon nanophononic crystal and we developed a predictive theory using analogies with hydrodynamic transport in porous media. This approach unifies the modeling of our measurements and a broad variety of similar experiments and atomistic simulations in other 2D and 3D nanostructured silicon systems with characteristic length scales much smaller than the average
bulk mean free path.

References

1 R. Anufriev, et al. Heat guiding and focusing using ballistic phonon transport in phononic nanostructures- *Nature Communications* 8, 15505 (2017)
2 Desmarchelier, et al. Atomistic evidence of hydrodynamic heat transfer in nanowires. *International Journal of Heat and Mass Transfer* 194, 123003 (2022)
3 B. McBennett, et al. Universal behavior of highly-confined heat flow in semiconductor nanosystems: from nanomeshes to metalattices. *Nano Letters* doi/10.1021/acs.nanolett.2c04419 (2023)
4 L. Sendra, et al., Derivation of a hydrodynamic heat equation from the phonon Boltzmann equation for general semiconductors. *Phys. Rev. B* 103, L140301 (2021)

PHONONICS 2023: 6th International Conference on Phononic Crystals/Metamaterials/Metasurfaces, Phonon Transport, and Topological Phononics
Manchester, England, June 12-16, 2023
PHONONICS-2023-0117

Net heat current at zero mean temperature gradient

Jose Ordonez-Miranda[1,2], Roman Anufriev[2] , Masahiro Nomura[2,1], Sebastian Volz[1,2]

[1] *LIMMS, CNRS-IIS UMI 2820, The University of Tokyo, Tokyo 153-8505, Japan*
[2] *Institute of Industrial Science, The University of Tokyo, Tokyo 153-8505, Japan*

Abstract: The existence of a net thermal current of conductive thermal waves is demonstrated even in the absence of a mean temperature gradient. This effect, which we call thermoelectric shuttling, is generated by the temperature dependence of the thermal conductivity of materials excited with a thermal excitation periodically modulated in time.

The existence of a net thermal current of conductive thermal waves is demonstrated even in the absence of a mean temperature gradient. This effect, which we call thermoelectric shuttling, is generated by the temperature dependence of the thermal conductivity of materials excited with a thermal excitation periodically modulated in time (Fig. 1(a)). We show that this modulation gives rise to a thermal current superimposed on the one generated by the mean temperature gradient, which enhances heat transport when the thermal conductivity increases with temperature. By contrast, if the thermal conductivity decreases as temperature increases, the thermal wave heat current inverts its direction and reduces the total heat flux. The reported shutting effect is sensitive to the amplitude of the periodic thermal excitation (Fig. 1(b)), which can facilitate its observation and application to harvest energy from the temperature variations of the environment [1].

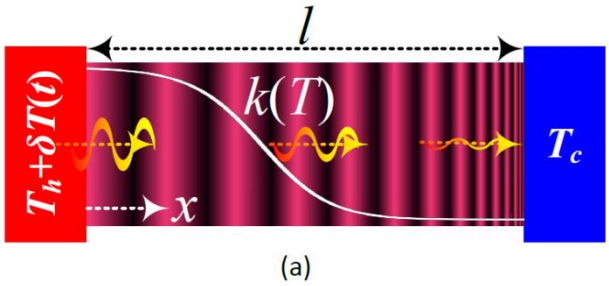

(a)

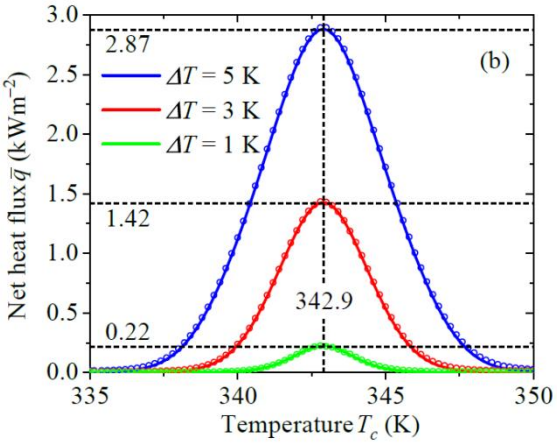

Figure 1: (a) Scheme of a phase-change material supporting the heat conduction between two thermal baths due to their temperature difference $\delta T = \Delta T \cos(\omega t)$ periodically modulated in time *t*. (b) Average (net) heat flux as a function of the temperature $T_h = T_c$, for three amplitudes of the periodic excitation.

References

[1] J. Ordonez-Miranda, R. Anufriev, M. Nomura, S. Volz, Phys. Rev. B 106 (2022) L100102.

PHONONICS 2023: 6th International Conference on Phononic Crystals/Metamaterials/Metasurfaces, Phonon Transport, and Topological Phononics
Manchester, England, June 12-16, 2023
PHONONICS-2023-0185

Three-dimensions auxetic metamaterials with tunable ferroelectric properties for guiding elastic waves

Mohamed Roshdy[1],Tian Chen[2], Serge Nakhmanson[3], Osama R. Bilal[1]

[1] *Department of Mechanical Engineering, University of Connecticut, Storrs, 06269, CT, USA.*
[2] *Department of Mechanical Engineering, University of Houston, Houston, 77004, Tx, USA.*
[3] *Department of Material Science and Engineering, University of Connecticut, Storrs, 06269, CT, USA.*

Mohamed.roshdy@uconn.edu, tianchen@uh.edu , serge.nakhmanson@uconn.edu,osama.bilal@uconn.edu

Abstract: We investigate the static and dynamic properties of three-dimensional, dynamically tunable ferroelectric metamaterials. The considered designs have effective Poisson's ratios varying from positive to negative. We study the dynamics of the proposed designs and explore various methods to tune their transmission characteristics, such as external mechanical loads, poling effects, or a combination of both. The potential of these metamaterials is demonstrated through multiplexing and guiding elastic waves at different frequencies. Our findings could have significant implications for the development of advanced and multifunctional acoustic devices.

Metamaterials are man-made materials that can be created with unique and exceptional properties, such as effective negative Poisson's ratio, mass density, and Young's modulus[1,2]. These metamaterials have potential applications in a wide range of areas, including controlling acoustic, elastic, and thermal waves, as well as cloaking[3-7]. Typically, the properties of metamaterials are fixed once they are fabricated, but a growing trend in research involves designing metamaterials that can be dynamically tuned, offering even more potential applications and integration into devices. Tunability can be achieved through mechanical[8,9], thermal[10], electrical[11], or magnetic stimulus[12]. While some research has explored the use of piezoelectric metamaterials[13,14], the potential for tuning metamaterials using ferroelectric poling effects remains largely unexplored. This work explores different tuning methods, such as poling effects, mechanical deformations, and combination of both[15] (Figure 1).

The metamaterial is made of polyvinylidene fluoride (PVDF) in its intermediate un-polar phase (β-phase), which is a ferroelectric non-polar polymer that can be converted to piezoelectric poled material through electric poling. We study the effect of elastic stiffness change on the properties of the considered metamaterials. Such change occurs as a result of electrical poling of β-PVDF. That transitions the material into a polar and piezoelectric phase. It is worth noting that, due to the negative value of piezoelectric constant d_{33} for PVDF, the material undergoes softening rather than stiffening.

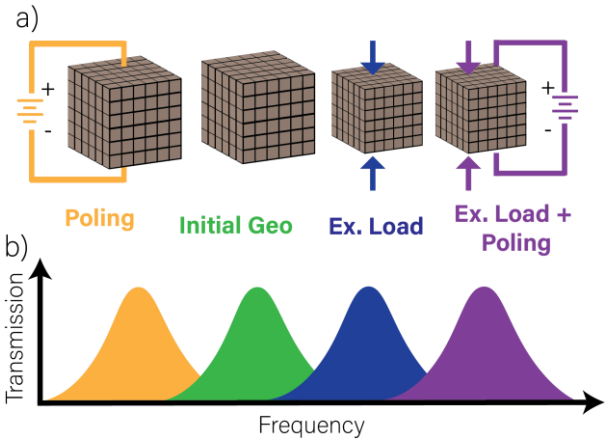

Figure 1 Concept: (a) Applying external tuning method including electrical poling, mechanical loads, and combination of both. (b) Changing the position of transmission peaks of elastic waves through the metamaterial via proposed tuning techniques.

We start our analysis by calculating the dispersion curves for different unit cell designs with different effective Poisson's ratios. Through dispersion analysis, we identify the frequency ranges of interest, where waves do not propagate (i.e., band gaps). We then electrically pole the underlying material (i.e., PVDF) and recalculate the dispersion curves. We observe a significant change in the dispersion curves due to poling. To verify our unit cell analysis, we consider two finite structures (poled and unpoled), each consisting of 5 x 5 x 5-unit cells. We excite each structure at its corner in all directions and measure the transmitted

wave at the opposite corner. We sweep through a range of excitation frequencies from 1 Hz to 12 MHz. By examining the frequency response functions (FRFs) of the finite structures, we can confirm the band gap frequency ranges where the waves are attenuated and prevented from propagating.

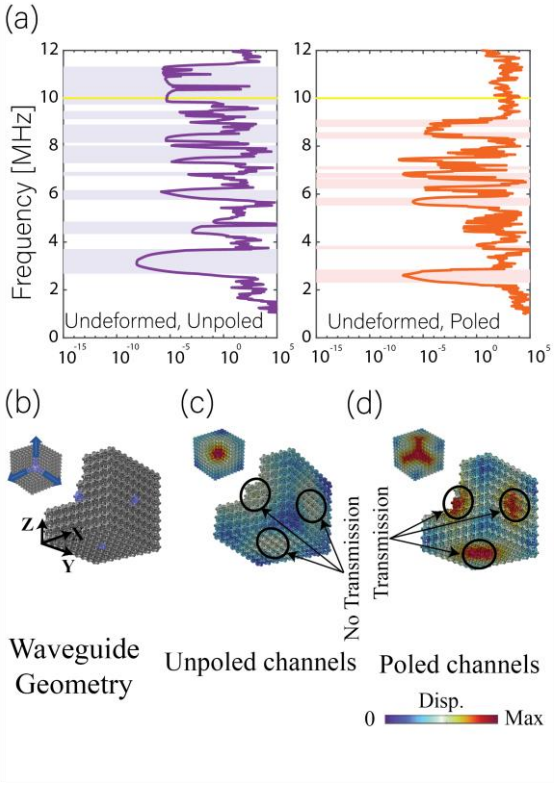

Figure 2 3D waveguide: (a) Frequency response function (FRF) for a structure composed of 5x5x5 negative Poisson's ration unit cells. (b) Three-dimensional waveguide composed of 9x9x9 negative Poisson's ratio unit cells. Exciting the center of the waveguide at 10.1 MHz of (c) the un-poled channels, and (d) the poled channel.

We employ the simulated frequency response functions (FRFs) as a guide for designing a tunable 3D waveguide that can control the propagation of elastic waves. Figure 2 depicts a structure made up of a 9 x 9 x 9 grid with repeated unit cells (Figure 2b). The metamaterial's waveguide path can be modified by poling three right angle channels that connect between the structure's center to its side faces. We excite a homogeneous cube at the center of the structure, while the measuring points are the center of side faces. At a frequency of 10.1 MHz, which is a stop band frequency in the unpoled material and a pass band frequency in the poled material (Fig. 2a). The wave only propagates through the poled channels (Fig. 2d), while it attenuates elsewhere (i.e., the unpoled material) (Fig. 2c).

In summary, we consider the tunability of ferroelectric auxetic metamaterials through electrical poling, external loading and the effect of both methods on the change of metamaterials' dynamics. We employ these findings to design a 3D wave guide that can control the propagation of elastic waves in all directions. These findings can be implanted in different applications including acoustic devises.

References

[1] J. Christensen, M. Kadic, O. Kraft, M. Wegener, *MRS Commun.* 5 (2015) 453.
[2] K. Bertoldi, V. Vitelli, J. Christensen, M. Van Hecke, *Nat. Rev. Mater.* 2 (2017) 1.
[3] M.M. Sigalas, *J. Sound Vib.* 158 (1992) 377.
[4] H. Huang, C. Sun, *New J. Phys.* 11 (2009) 013003.
[5] O.R. Bilal, C.H. Yee, J. Rys, C. Schumacher, C. Daraio, *Appl. Phys. Lett.* 118 (2021) 091901.
[6] A.A. Watkins, O.R. Bilal, *Front. Mater.* 7 (2020) 606877.
[7] P. Wang, F. Casadei, S. Shan, J.C. Weaver, K. Bertoldi, *Phys. Rev. Lett.* 113 (2014) 014301.
[8] B. Nguyen, X. Zhuang, H. Park, T. Rabczuk, *J. Appl. Phys.* 125 (2019) 095106.
[9] M. Kheybari, C. Daraio, O.R. Bilal, *Appl. Phys. Lett.* 121 (2022) 081702.
[10] Q. Zhang, K. Zhang, G. Hu, *Sci. Rep.* 6 (2016) 1.
[11] X. Zhou, C. Chen, *Physica B* 431 (2013) 23.
[12] O.R. Bilal, A. Foehr, C. Daraio, *Adv. Mater.* 29 (2017a) 1700628.
[13] Z. Hou, F. Wu, Y. Liu, *Solid State Commun.* 130 (2004) 745.
[14] J.O. Vasseur, A.-C. Hladky-Hennion, B. Djafari-Rouhani, F. Duval, B. Dubus, Y. Pennec, P. Deymier, *J. Appl. Phys.* 101 (2007) 114904.
[15] Roshdy, M. Chen, T., Nakhmanson, S. and Bilal O.R., *Extreme Mech. Lett.* 59 (2023): 101966.

PHONONICS 2023: 6th International Conference on Phononic Crystals/Metamaterials/Metasurfaces, Phonon Transport, and Topological Phononics
Manchester, England, June 12-16, 2023
PHONONICS-2023-0172

Latent Symmetries in Acoustic Systems

Malte Röntgen[1], Christian V. Morfonios[2], Peter Schmelcher[3], Vincent Pagneux[4]

[1] *Laboratoire d'Acoustique de l'Université du Mans,*
Unite Mixte de Recherche 6613, Centre National de la Recherche Scientifique, Avenue O. Messiaen, F-72085 Le Mans Cedex 9, France,
malte.rontgen@univ-lemans.fr
[2] *Zentrum für optische Quantentechnologien, Universität Hamburg, Luruper Chaussee 149, 22761 Hamburg, Germany,*
cmorfoni@physnet.uni-hamburg.de
[3] *Zentrum für optische Quantentechnologien, Universität Hamburg, Luruper Chaussee 149, 22761 Hamburg, Germany*
and
The Hamburg Centre for Ultrafast Imaging, Universität Hamburg, Luruper Chaussee 149, 22761 Hamburg, Germany
pscmelc@physnet.uni-hamburg.de
[4] *Laboratoire d'Acoustique de l'Université du Mans,*
Unite Mixte de Recherche 6613, Centre National de la Recherche Scientifique, Avenue O. Messiaen, F-72085 Le Mans Cedex 9, France,
vincent.pagneux@univ-lemans.fr

Abstract: Due to their strong impact on its behavior, symmetries are a common theme in the treatment of any physical system. For instance, the eigenmodes of a reflection-symmetric system necessarily have definite parity. In this talk, I will show that there is also another possibility: Asymmetric waveguide networks which, facilitated by a so-called latent symmetry, feature parity in all their eigenmodes.

PHONONICS 2023: 6th International Conference on Phononic Crystals/Metamaterials/Metasurfaces, Phonon Transport, and Topological Phononics
Manchester, England, June 12-16, 2023
PHONONICS-2023-0186

Dynamically Tunable Metamaterial for Controlling Airborne Sound in *Real-time*

Melanie Keogh[1], Majid Kheybari[1], Osama R. Bilal[1]

[1] *Department of Mechanical Engineering, University of Connecticut, Storrs, Connecticut 06269, USA*

melanie.keogh@uconn.edu, majid.kheybari@uconn.edu, osama.bilal@uconn.edu

Abstract: In this work, we study a tunable metamaterial composed of asymmetric pillars that can manipulate acoustic waves based on their angular orientation. The proposed metamaterial can produce different attenuation frequency regions (i.e., band gaps) that can be altered in real-time by means of active control. We characterize our metamaterials numerically and experimentally for different unit cells in both 1 and 2D configurations.

Metamaterials are artificially engineered materials that have properties not commonly found in nature, such as negative effective mass[1] and stiffness[2]. These materials are composed of assemblies of multiple elements arranged in repeating patterns. In addition to the properties provided by the base material itself, the consideration of the repeated geometric pattern adds new unique properties. Depending on a metamaterial's arrangement, orientation, scale, and geometry, it can be utilized to manipulate waves via absorption, enhancement, bending, or blocking of waves. Unlike passive metamaterials, which have properties that cannot be altered after they are manufactured, active metamaterials can utilize an external stimulus to manipulate their properties.[3] While the majority of the literature is focused on passive metamaterials, incorporating additional control methods via active components can open the door to more potential applications[3,4]. Overall, the versatility and tunability of active metamaterials make them a fascinating area of research.

Our metamaterial is composed of an array of asymmetric 3D pillars that are repeated in the x and the y-directions. The pillars are treated as rigid scatterers that interact with the sound wave propagating in the surrounding air. Each pillar has the ability to rotate in the xy-plane with a given angle Θ (Figure 1). Due to the asymmetry in the pillar geometry, the dispersion curves of the unit cell differ depending on their phase angle Θ (Figure 1). In other words, we align all the pillars in our metamaterials at a certain angle Θ, allowing the waves to propagate through the metamaterials at a given frequency ω. Then, we can program our metamaterials to change the angular orientation of the pillars and block the sound waves from propagating on-the-fly.

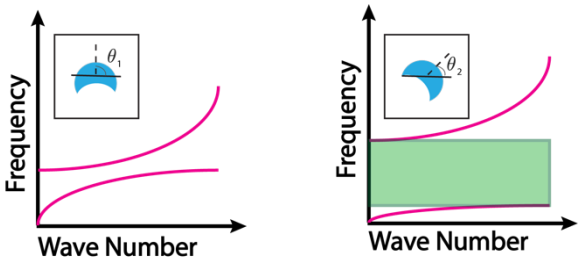

Figure 1 Dispersion curves of the same metamaterial unit cell with two different pillar angular orientation Θ.

We start our analysis by calculating the dispersion curves of two unit-cells composed of the same pillar, but with different angular orientations (Θ = 0 and 90°). When the pillars are oriented at Θ = 0°, three wide band gaps exist within the frequency spectrum between 0 and 14 kHz. At Θ = 90° no band gaps are present within the same frequency range (Figure 2-left). To validate our infinite unit cell model, we numerically simulate the sound transmission in a finite array of 11 unit-cells. We excite one end of the array with a chirp signal and measure the total acoustic pressure at the other end of the array. We normalize the output signal by the input amplitude to calculate the transmission within the metamaterial (Figure 2-middle). At Θ = 0°, the predicted band gap frequency ranges show clear attenuation, which is in agreement with the dispersion curves. At Θ = 90°, there are no band gaps present. To further verify our analysis, we experimentally characterize the sound transmission through an array of 11 unit-cells. We excite the sound waves using an arbitrary function wave generator and a loudspeaker to measure the acoustic pressure using two microphones at both ends of the sample. The experimentally measured transmission shows very good agreement with the numerical simulations, particularly at the band gap regions (Figure 2-right).

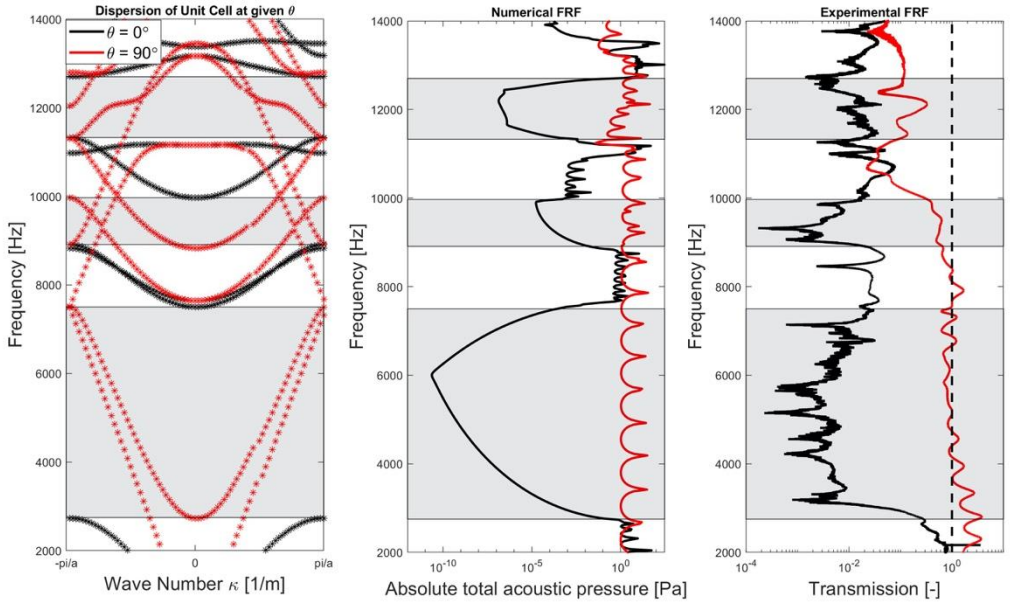

Figure 2 Dispersion curves (left), numerical transmission (middle), and experimental transmission (right) of the same unit cell with two different pillar orientation Θ.

To visualize the wave transmission through the material, we plot the acoustic pressure at the same frequency (ω = 7.4 kHz) for two different angular orientations of the pillars (Θ = 0° and 90°). The numerical plots show clear transmission and attenuation as predicted for both 1D and 2D metamaterials.

In summary, we study, both numerically and experimentally, a dynamically tunable acoustic metamaterials that can be programmed to manipulate waves on-the-fly. Our metamaterials can open the door for various applications requiring active control of sound waves.

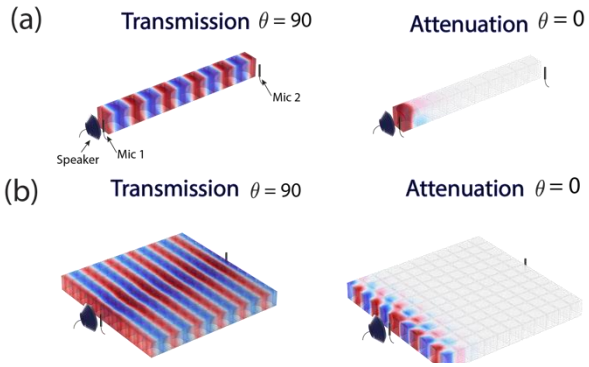

Figure 3 Numerical transmission maps for the same frequency of excitation at two different angular orientation in **a)** 1D and **b)** 2D

References

[1] H. Huang, C. Sun, and G. Huang, Int. *J. Eng. Sci.* **47**, 610617 (2009).

[2] T. Klatt and M. R. Haberman, *J. Appl. Phys.*, **114**, 033503 (2013).

[3] F. Zangeneh-Nejad, R. Fleury, *Reviews in Physics*, **4**, 100031 (2019).

[4] S. Chen, Y. Fan, Q. Fu, H. Wu, Y. Jin, J Zheng, and F. Zhang, *Appl. Sci*., **8**, 1480 (2018).

PHONONICS 2023: 6th International Conference on Phononic Crystals/Metamaterials/Metasurfaces, Phonon Transport, and Topological Phononics
Manchester, England, June 12-16, 2023
PHONONICS-2023-0087

Subwavelength Broadband Perfect Absorption for Unidimensional Open-Duct Problems

Y. Meng[1], V. Romero-García[2], G. Gabard[1], J.-P. Groby[1], C. Bricault[3], and S. Goudé[3]

[1] *Laboratoire d'Acoustique de l'Université du Mans (LAUM), UMR CNRS 6613, Institut d'Acoustique - Graduate School (IA-GS), CNRS, Le Mans Université, France.*
yang.meng@univ-lemans.fr, jean-philippe.groby@univ-lemans.fr, Gwenael.Gabard@univ-lemans.fr
[2] *Instituto Universitario de Matemática Pura y Aplicada (IUMPA), Departamento de Matemática Aplicada, Universitat Politècnica de València, Camino de Vera, s/n 46022 València, Spain.*
virogar1@mat.upv.es
[3] *Vibrations and Acoustics Laboratory, Valeo Thermal Systems, 78321 La Verrière, France*
charlie.bricault@valeo.com, sebastien.goude@valeo.com

Abstract: This work presents a general design methodology of metamaterial absorbers made of arrays of Helmholtz resonators for open-duct problems. By using a single point scatterer, a frequency-dependent maximum absorption exists and is derived analytically. To go beyond this absorption bound, at least two scatterers are necessary. Specific designs are provided and validated both numerically and experimentally.

The absorption of both reflected and radiated acoustic waves by using monopolar point scatterers in the unidimensional (1D) open-duct problem is studied in this work. The absorption coefficient is defined as

$$\alpha = 1 - E_{\mathrm{Ref}} - E_{\mathrm{Rad}}, \tag{1}$$

where E_{Ref} and E_{Rad} are the reflection and radiation energies normalized by the incidence energy, respectively.

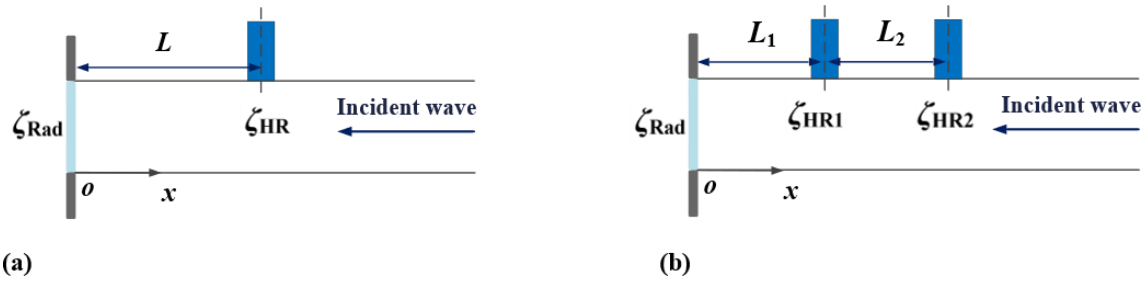

Figure 1 Schematic illustrations of metamaterials made of point scatterers in the 1D open-duct problem: **(a)** Single point scatterer. **(b)** Two coupled point scatterers.

In the case that a single point scatterer is used, which is illustrated in Figure 1(a), the maximum absorption coefficient is derived as

$$\alpha_{\max} = \frac{1}{2}\left[1 + \sqrt{\frac{(\theta_{\mathrm{Rad}} - 1)^2 + \chi_{\mathrm{Rad}}^2}{(\theta_{\mathrm{Rad}} + 1)^2 + \chi_{\mathrm{Rad}}^2}}\right], \tag{2}$$

which is in general frequency dependent and less than unity. Note that in the 1D problem, the acoustic response of the open end can be modelled by the specific radiation impedance[1] $\zeta_{\mathrm{Rad}} = \theta_{\mathrm{Rad}} + \mathrm{i}\chi_{\mathrm{Rad}}$ under the $\mathrm{e}^{\mathrm{i}\omega t}$ convention. To achieve $\alpha_{\max}$ at a single frequency, two conditions are necessary: (1) the scatterer provides the optimal impedance ζ_{opt} and (2) the distance between the scatterer and the open end is the optimal value Lopt. In contrast, to achieve perfect absorption ($\alpha = 1$), at least two point scatterers are needed as illustrated in Figure 1**(b)**. Moreover, it is required that the scatterers should achieve the optimal impedance values:

$$\begin{cases} \zeta_{\mathrm{HR1}} = 0 \\ \zeta_{\mathrm{HR2}} = -\mathrm{i}\sin\left(k_0 L_2\right)\mathrm{e}^{\mathrm{i}k_0 L_2} \end{cases}, \tag{3}$$

The above definition (Equation (1)) and results (Equations. (2) and (3)) in the open-duct problem are direct generalizations of the 1D reflection[2] and transmission[3,4] problems. The reflection or transmission problem corresponds to the special case when the boundary impedance ζ_{Rad} approaches to infinity or 1 + 0i, respectively.

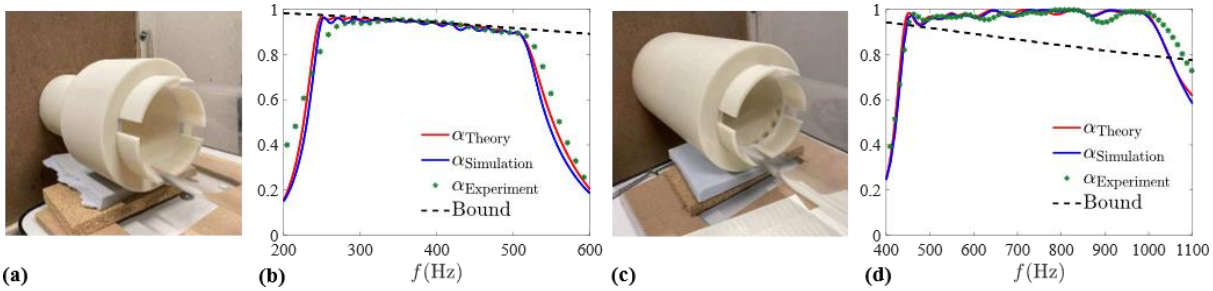

Figure 2 Single-point-scatterer metamaterial for broadband maximum absorption α_{max}: **(a)** Sample working from 250 Hz to 500 Hz. **(b)** Absorption coefficient of the sample: comparison of the theory, simulation, and measurement. Coupled-point-scatterer metamaterial for broadband perfect absorption: **(c)** Sample working from 450 Hz to 1000 Hz. **(d)** Absorption coefficient of the sample: comparison of the theory, simulation, and measurement.

To realize α_{max} and perfect absorption as well, we propose a general design strategy, in which monopolar point scatterers are employed. A circular waveguide (whose radius is 5 cm) with an open end in the baffled wall is considered. Arrays of Helmholtz resonators in parallel with the waveguide, i.e., in both the circumferential and the wave directions, are used to play the roles of the point scatterers. As predicted by Equation (2), the maximum absorption is close to perfect in the low frequency range. Specifically, for this circular waveguide, $\alpha_{\mathrm{max}} \geq 0.9$ when $f \leq 500$ Hz. Thus, a compact and efficient absorber is realized by utilizing this property with a single point scatterer made of detuned Helmholtz resonators, which possesses deep subwavelength size and achieves broadband (250 Hz to 500 Hz) maximum absorption as shown in Figures 2**(a)** and 2**(b)**. In contrast, coupled point scatterers are necessary to break the absorption bound and thus to achieve perfect absorption. A specific design is provided with numerical and experimental validations over the frequency band 450 Hz to 1000 Hz as shown in Figures 2**(c)** and 2**(d)**.

References

[1] L. E. Kinsler, A. R. Frey, A. B. Coppens, and J. V. Sanders, *Fundamentals of Acoustics*, John Wiley & Sons, USA (2000).
[2] S. Huang, X. Fang, X. Wang, B. Assouar, Q. Cheng, and Y. Li, *J. Acoust. Soc. Am.* **145**, 254-262 (2019).
[3] A. Merkel, G. Theocharis, O. Richoux, V. Romero-García, and V. Pagneux, *Appl. Phys. Lett.* **107**, 244102 (2015).
[4] N. Jiménez, V. Romero-García, V. Pagneux, and J.-P. Groby, *Sci. Rep.* **7**, 13595 (2017).

PHONONICS 2023: 6th International Conference on Phononic Crystals/Metamaterials/Metasurfaces, Phonon Transport, and Topological Phononics
Manchester, England, June 12-16, 2023
PHONONICS-2023-0171

Efficient analysis of sound insulation in locally resonant metamaterial panels using an effective medium model

Daniele Giannini[1], Edwin P.B. Reynders[1]

[1] *Department of Civil Engineering, KU Leuven, Kasteelpark Arenberg 40, 3001, Leuven, Belgium*
daniele.giannini@kuleuven.be, edwin.reynders@kuleuven.be

Abstract: Sound insulation in locally resonant metamaterial panels is usually analyzed by numerical approaches based on unit cell modelling and periodic structure theory. As a computationally cheap alternative, in this work we propose a novel analytical effective medium model that can account for complex and multimodal resonator layouts, finite dimensions of the panel, and diffuse incident sound fields.

Introduction

Locally resonant metamaterials (LRM) can be used to improve the sound insulation of a host structure. By distributing small resonators on a subwavelength scale, resonance-based bandgaps and sound insulation improvements are obtained close to the resonance frequency of the local resonators.

The vibroacoustic properties of LRM panels are usually predicted through numerical approaches that involve unit cell (UC) modelling and periodic structure theory. For LRM panels with infinite dimensions, the created bandgaps and the sound transmission loss (STL) can be studied e.g. through the Wave and Finite Element Method (WFEM) by modelling one single unit cell through finite elements (FE) and imposing periodicity conditions[1]. For LRM panels with finite dimensions, the modal behavior of the panel can be included through periodicity conditions that are coherent with the applied constraints at the boundaries of the panel[2]. When considering diffuse sound fields surrounding a finite panel, the hybrid deterministic - statistical energy analysis (det-SEA) framework can be employed to compute the diffuse STL, which represents the average insulation performance of the panel across a wide range of situations (e.g. across an ensemble of possible source and receiver rooms in buildings). In this case, a deterministic model of the (periodic) panel is combined with a diffuse model of the surrounding sound fields[3]. The computational cost of numerical models based on periodic structure theory is related to the dimension of the UC FE model, and can become significant when including resonators with complex geometrical layouts. For this reason, reduced order UC modelling, through e.g. Craig-Bampton reduction[1] and generalized Bloch mode synthesis[4], is used to speed up calculations.

Besides numerical models based on periodic structure theory, analytical effective medium models are an appealing alternative to reduce computational costs[5]. In these models, the LRM panel is studied through its effective dynamic mass density, which is frequency-dependent and is derived by combining the inertial forces of the host panel with the transmitted inertial forces of the local resonators. However, conventional effective medium models consider only infinite LRM panels with translational single degree of freedom resonators. They are therefore not yet suitable to consider finite panel dimensions and more complex resonators exhibiting multiple modes with both translational and rotational motion.

Effective medium model for multimodal LRM panels

In this work, we present an effective medium model to predict the vibroacoustic behavior of LRM panels with complex and multimodal resonators, when considering both infinite and finite size of the panel. A new analytical expression of the dynamic effective mass density is derived, to include the translational and rotational contributions of multiple resonator modes. These contributions are expressed as modal effective masses, extracted through a simple modal FE analysis of the fixed-base resonator. The resulting effective dynamic mass density depends not only on the frequency, but also on the wavenumber components of the waves propagating in the panel.

The proposed model enables accurate and efficient STL predictions. The STL of thin panels with infinite size is predicted through simple analytical formulas, by expressing the impedance of the panel in terms of its effective dynamic mass density. The STL of thin panels with finite size can be predicted by including in the det-SEA framework a deterministic effective medium model of the LRM panel. For simply supported rectangular panels, the dynamic stiffness matrix is expressed with respect to modal sinusoidal basis functions, where the mass contribution is scaled by the dynamic effective mass density, i.e. according to the frequency of the analysis and the modal wavenumbers.

Validation of the proposed effective medium model

The proposed effective medium model is validated for the STL prediction of the LRM panel in Figure 1a, consisting of an orthotropic host plate with periodically attached multimodal resonators. While the orthotropic host plate exhibits a broadband STL dip due to coincidence effects, the multiple resonator modes of the LRM panel are tuned to suppress the STL dip through the corresponding STL peaks[6]. Both infinite and finite panel dimensions are considered. For panels with infinite dimensions, the proposed effective medium model is validated against WFEM predictions (Figure 1b). For panels with finite dimensions, the use of the proposed effective medium model in det-SEA predictions is validated against the use of a FE model of the panel (Figures 2a-b). For the presented showcases, it is demonstrated that the proposed analytical effective medium model enables accurate STL predictions with significant computational savings with respect to conventional numerical approaches.

References

[1] Y. Yang, B.R. Mace, M.J. Kingan, *J.Sound Vib.* **457**, 333-353 (2019).
[2] Y. Yang, M.J. Kingan, B.R. Mace, *Mech. Syst. Sig. Process.* **151**, 107357 (2021).
[3] E.P.B. Reynders, C. Van hoorickx, *J.Sound Vib*. **544**, 117404:1-15 (2023).
[4] D. Krattiger, M.I. Hussein, *J. Comput. Phys.* **357**, 183-205 (2018).
[5] P. Li, S. Yao, X. Zhou, *J. Acoust. Soc. Am.*, **135(4)**, 1844–1852 (2014).
[6] D. Giannini, M. Schevenels, E.P.B. Reynders, *J.Sound Vib.* **547**, 117453 (2023).

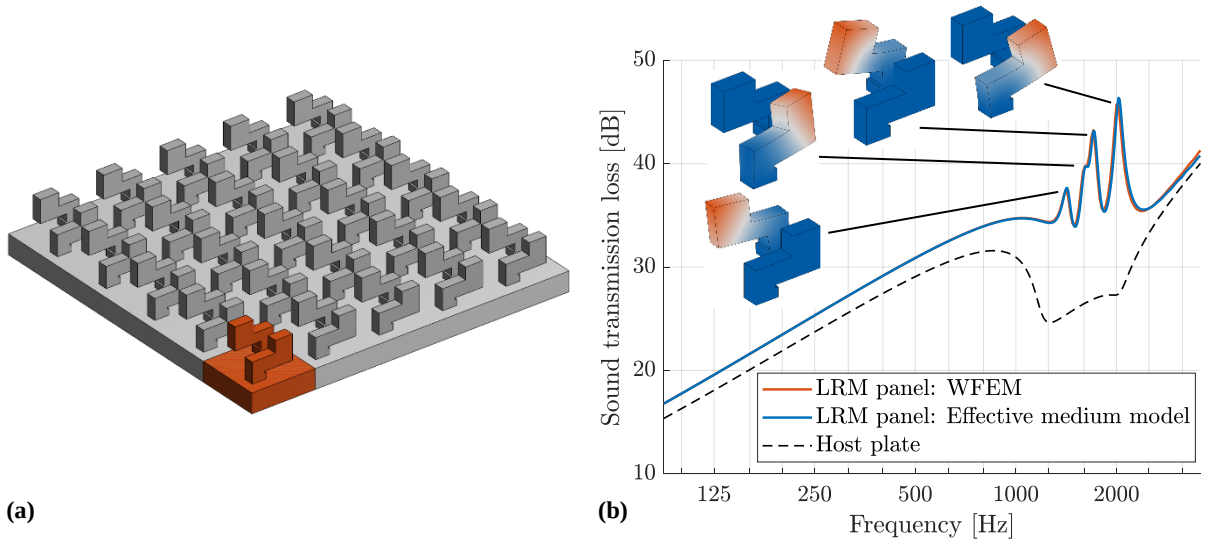

Figure 1 Validation of the proposed effective medium model: **(a)** considered multimodal LRM panel, **(b)** STL prediction for infinite panel dimensions.

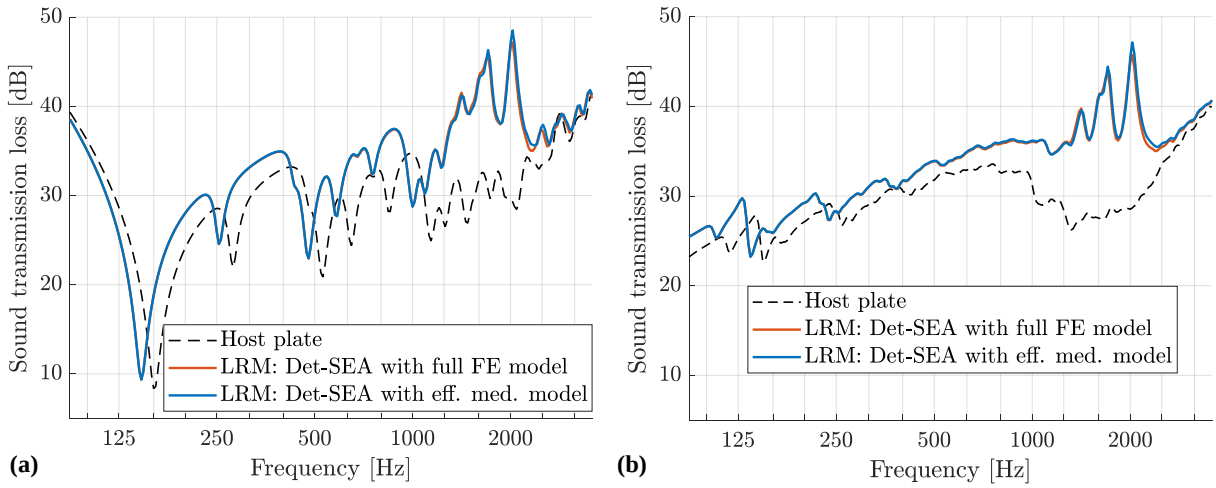

Figure 2 Validation of the proposed effective medium model: STL prediction for **(a)** a 60 cm x 45 cm LRM panel and **(b)** a 150 cm x 125 cm LRM panel.

PHONONICS 2023: 6th International Conference on Phononic Crystals/Metamaterials/Metasurfaces, Phonon Transport, and Topological Phononics
Manchester, England, June 12-16, 2023
PHONONICS-2023-0034

Wave propagation characterization of 2D structures through an algebraic identification technique

Xuefeng Li[1], Mohamed Ichchou[1], Abdelmalek Zine[2], Noureddine Bouhaddi[3], Pascal Fossat[1]

[1]LTDS - CNRS UMR 5513, École Centrale de Lyon, Écully, France
xuefeng.li@ec-lyon.fr, mohamed.ichchou@ec-lyon.fr, pascal.fossat@ec-lyon.fr
[2] Institut Camille Jordan - CNRS UMR 5208, École Centrale de Lyon, Écully, France
abdel-malek.zine@ec-lyon.fr
[3] Department of Applied Mechanics, Univ. Bourgogne Franche-Comté, Besançon, France
noureddine.bouhaddi@univ-fcomte.fr

Abstract: A reliable wavenumber identification method for k-space extraction is proposed in this work. This method has been validated experimentally on k-space extraction of a honeycomb sandwich plate by comparing it with other popular wavenumber identification methods. Moreover, experimental results illustrate the frequency-dependent mechanical properties of this plate.

1. Introduction

Wavenumber extraction is receiving more and more attention for wave propagation characterization and dynamic behavior identification in the vibroacoustic field. The extracted wavenumber can provide useful information related to the dispersion characteristic and energy propagation of waves propagating in complex structures.

Wavenumber extraction methods can be divided into two categories, depending on the principles on which they are based: nonlinear correlation-based methods and the linear Prony family methods. The representative methods of these two categories of methods are Inhomogeneous Wave Correlation (IWC)[1] and INverse COnvolution MEthod (INCOME)[2,], respectively. IWC is robust to signal noise, while it suffers from the low-frequency range and computation cost. Comparatively, the contribution of INCOME is that it can provide a full and accurate k-space using a single kernel, while this method is sensitive to perturbations and limited to periodic sampling because of the essence of the Prony method.

In realistic conditions, it is inevitable to take into account different uncertainties such as signal noise, grid distortion, operational error, and nonuniform sampling. To this end, authors have proposed Algebraic Wavenumber Identification (AWI) technique[3]. This work aims to extend the AWI to k-space extraction of the 2D structures. Thus, the method is renamed Algebraic K-space Identification (AKSI) technique. The AKSI is developed based on the algebraic parameter identification method in the polar coordinate system. This work is organized as follows: section 2 introduces the methodology of AKSI, and then an experimental application of AKSI on a honeycomb sandwich plate is investigated by comparing it with other popular wavenumber identification methods in section 3. Finally, a brief conclusion is provided.

2. Methodology

In the polar coordinate system, the harmonic displacement at any point (θ, r_n) can be expressed as follows:

$$U(\theta, r_n)=\sum_{m=1}^{N} A_m \exp(p_m r_n) \tag{1}$$

where p_m is related to the wavevector in direction θ by $p_m = \mathrm{i}k_m$. In the wavenumber domain, a characteristics polynomial can be defined:

$$\Psi(s)=\prod_{m=1}^{N}(s - R_m) \tag{2}$$

First, an ordinary differential equation can be obtained by taking the *N*th derivative of the product of the Laplace transform of Eq. (1) and Eq. (2) as follows:

$$\sum_{i=0}^{N}\sum_{j=i}^{N}\binom{N}{j}\binom{N-i}{N-j}(N-j)!\, s^{j-i}\frac{d^j S(\theta,s)}{ds^j}\gamma(i) = 0 \tag{3}$$

Next, Eq. (3) is transformed to the expression in the spatial domain by using inverse Laplace transform:

$$\sum_{i=0}^{N} \phi(i,\theta,r_n)\,\gamma(i) = 0 \tag{4}$$

with

$$\phi(i,\theta,r_n) = \sum_{j=i}^{N} \binom{N}{j}\binom{N-i}{N-j}(N-j)!\frac{1}{(N+i-j)!}\int_0^{r_n}(r_n-\tau)^{N+i-j}\,(-\tau)^j U(\theta,\tau)d\tau \tag{5}$$

Finally, because Eq. (4) is held for each measurement, it can be rewritten in the matrix format as $\mathbf{HX} = \mathbf{M}$ where $\mathbf{H}$ is a matrix containing $\phi(i,\theta,r_n)$ and $\mathbf{M}$ is a zero matrix. By using least square methods, the coefficient $\gamma(i)$ can be estimated. Based on this, the wavevector can be obtained by Eq. (2).

3. Experimental validation

In this section, AKSI is applied to a 1m × 1m of honeycomb sandwich plate (see Fig. 1). The total thickness of the plate is 1.4 cm. The plate was suspended at a fixed frame and excited by a point mechanical force using an electrodynamic shake at the point (0.5 m, 0.5 m). The 3D Polytec Laser Doppler Vibrometer was used to measure the out-of-plane displacement of the plate. As shown in Fig. 1, a 2D mesh with 49 × 49 measuring points is used as input of the INCOME and IWC, while AKSI is implemented on a set of data measured along 26 lines with 59 periodic samples in each direction. Fig. 1 (b) and Fig. 1(c) compare the k-space at 784.375 Hz and 3284.375 Hz obtained by INCOME, IWC, and AKSI, respectively. From these figures, one can observe two phenomena: 1) IWC has a good performance at the higher frequency, while it suffers from the low frequency range where the number of wavelengths is fewer. The performance of INCOME is not related to wavelength. However, this method is sensitive to signal noise. Thus, inaccurate wavenumbers obtained from INCOME in some directions exist in Fig. 1 (b). Comparatively, AKSI has a more reliable performance on k-space extraction; 2) The shape of k-space shows the transition from the circle (see Fig. 1 (b)) to elliptic (see Fig. 1(c)), which corresponds to the transition of the dynamic behavior of the tested plate from the isotropy to orthotropy. This is because this plate is more and more controlled by the shear stiffness of the core with frequency.

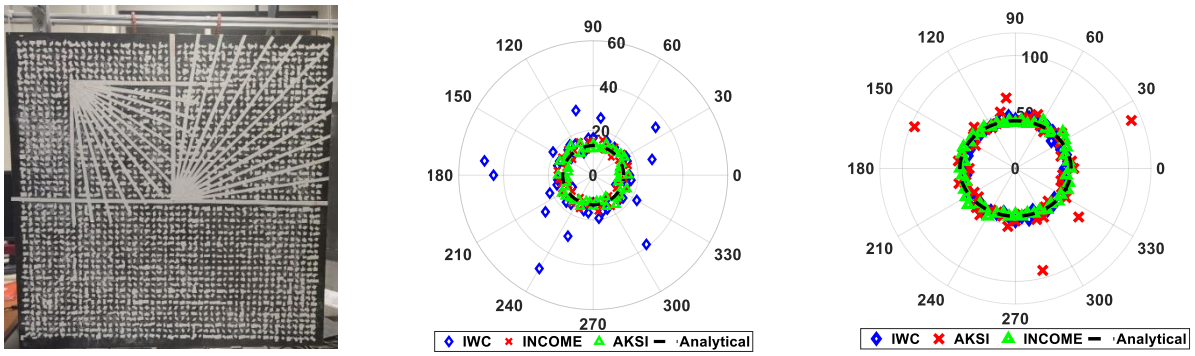

(a) (b) (c)

Figure 1 The k-space extracted by INCOME, IWC, and AKSI for a honeycomb sandwich plate: **(a)** measurement grid; **(b)** k-space at 784.375 Hz; (c) k-space at 3284.375 Hz.

4. Conclusions

This work introduces a reliable k-space extraction method, Algebraic K-space Identification (AKSI) technique, and applies it to extract the k-space of a honeycomb sandwich plate. The comparison of the k-space obtained by INCOME, IWC, and AKSI illustrates that the proposed method can be a good tool for k-space extraction in realistic condition. On the other hand, the change of k-space with frequency shows the transition of dynamic behavior of this honeycomb sandwich plate from isotropy to orthotropy.

References

[1] J. Berthaut, M. Ichchou, and L. Jezequel, K-space identification of apparent structural behaviou, *J. Sound Vib.* **280**, 1125–1131 (2005).
[2] R. F. Boukadia, C. Claeys, C. Droz, M. Ichchou, W. Desmet, and E. Deckers, A, INverse COnvolution MEthod for wavenumber extraction (INCOME): Formulations and applications, *J. Sound Vib.* **520**, 116586 (2022).
[3] X. Li, M. Ichchou, A. Zine, C. Droz, and N. Bouhaddi, An algebraic wavenumber identification (AWI) technique under stochastic conditions, *Mech. Syst. Sig. Process.* **188**, 109983 (2023).

PHONONICS 2023: 6th International Conference on Phononic Crystals/Metamaterials/Metasurfaces, Phonon Transport, and Topological Phononics
Manchester, England, June 12-16, 2023
PHONONICS-2023-0011

A Non-Linear Delayed Acoustic Resonator for Mimicking the Hearing Haircells

Jana Reda[1,*], Mathias Fink[1], Fabrice Lemoult[1]

[1] *Institut Langevin, ESPCI Paris, Université PSL, CNRS, 75005 Paris, France*
[*] *Jana.reda@espci.fr*

Abstract: The human ear is a fascinating extremely sensitive detector: 10 octaves in frequencies and 12 orders of magnitude in sound intensity. This is due to the non-linear phenomena that happen in the cochlea; the inner part of the ear that converts the sound stimulus into nerve impulses which travel to the brain. Using a quarter wavelength resonator we create an active non-linear acoustic resonator which well mimics the response of living hearing haircells.

We build a non-linear active acoustic resonator in order to reproduce the behavior of inner haircells, the cells that are the mechano-sensors at the origin of hearing. The design of this resonator is inspired from a previous work [1] where several subwavelength resonators were used to build a gradient index metamaterial that well reproduces the behavior of the entire cochlea. Here, we want to focus on the non-linear properties of a single one. In the laboratory, we made our experimental resonator with one of the simplest design in acoustics: a quarter wavelength resonator. The latter is made of a Plexiglas tube of length 10 cm with one open end, and one close end. The closing is made with a 3D-printed plastic where we introduce an electret microphone connected to its preamplifier as well as a speaker, also connected to its own amplifier in order to respectively measure the acoustic inside the pipe or emit sound inside. The goal of this design is to inject in real time inside the tube a sound that is directly related to a sound that is measured inside: a feedback loop is built. This revealed very limited in the number of resonators that can be controlled in the same time. In our model a delay does exist in the loop hence the name "delayed resonator".

From a mathematical point of view, we can write :

$$e_{loop(t)} = p(t-\tau)G(t) \tag{1}$$

where $e_{loop}(t)$ corresponds to the source term associated to the feedback loop with a delay τ and a gain $G(t)$. The advantage of using the feedback loop within a microcontroller is that the gain $G(t)$ of the loop or its delay τ can be modified numerically in real time and can include complex non-linear functions. We will end on a gain that allows to mimic a system operating near a Hopf bifurcation.

In mammalian's hearing, the outer hair cells produce amplification of low sound level [2]. This effect, known as the cochlear amplifier, permits to enlarge the range of audible sound amplitudes. Typically, there is a decrease in the cochlear amplification as sound level increases; hence the amplification is maximal for the lowest sound levels. The transition between the low and high amplitude sounds reveals a cubic non linearity [3]. We aim at demonstrating that it is possible to mimic such a behavior with our low-cost delayed resonator by introducing cubic non-linearity in the feedback loop. By doing so, we turn our resonator onto a non-linear resonator operating near a Hopf bifurcation.

To get our resonator operating following the expected regime, we need a gain that depends on the input $G(t)$. Then, to build the Hopf bifurcation we need to introduce cubic non-linearity and we define the value of the gain as:

$$G(t) = \begin{cases} G_0\left(1-\left(\dfrac{p(t-\tau)}{P_0}\right)^2\right) & \text{if} \quad p(t-\tau) < P_0 \\ 0 & \text{otherwise} \end{cases} \tag{2}$$

Experimentally, we conducted a set of experiments in order to probe the response of such an active resonator. The first experiment consists in exciting monochromatically the resonator with different amplitudes and frequencies. For each excitation, the response of the non-linear resonator is measured at the same frequency. All the results are shown in figure 1a). Note that the definition of decibel in these experiments is relatively arbitrary and does not correspond to true sound pressure level but rather to normalized units: we choose a value of 0 dB for our maximal measure. As expected an excitation with a low amplitude gives a sharp resonance peak (see the blue lines). With the increase of the excitation amplitude the response becomes wider and wider (see the yellow and red lines).

From all these measurements, we can then build a figure which only keeps the response at the resonance frequency figure 1b). The three regimes observed in the case of the mammalian ear are easily highlighted by this curve. At high amplitudes the resonator has a linear response (slope of 1): the response is proportional to the excitation. Decreasing the amplitude, an inverse-cubic power law is observed near -13 dB. This is the effect of the cubic non-linearity in the feedback loop introduced in equation (2). At low amplitudes, the slope recovers a value of 1 (near -47 dB).

All our results confirm that controlling the parameters in $G(t)$ is what is required to phenomenologically reproduce successfully the active amplifier happening in the cochlea. The next step will consist in building a full active metamaterial based on this active unit cell and reproduce the behavior of the entire cochlea.

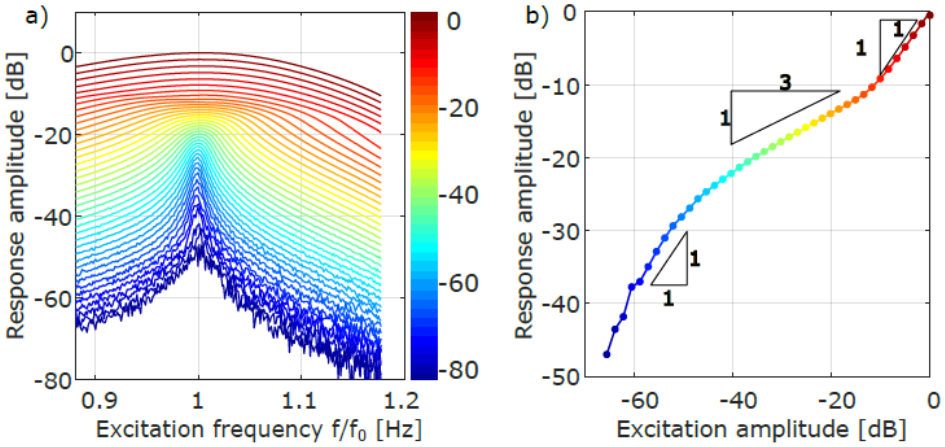

Figure 1 a) Response of the resonator at the excitation frequency when varying the amplitude and the frequency (frequency is renormalized by $\boldsymbol{f0}$ (the resonance frequency): a sharp resonance at low amplitude is followed by a broader one at higher excitation level. b) Same data as a) but with keeping the response at $\boldsymbol{f0}$ for all the curves: two linear regimes are separated by an inverse cubic response.

Reference

1. M. Rupin, G. Lerosey, J. d. Rosny & F. Lemoult, "Mimicking the cochlea with an active acoustic metamaterial," *New Journal Of Physics*, p. 11 (2019).

2. E. Shapira, R. Pujol, M. Plaksin & E. Kimmel, "Sound-induced motility of outer hair cells explained by stochastic resonance in nanometric sensors in the lateral wall," *Physics in Medicine*, p. 10 (2016).

3. F. N. Hudspeth, T. Reichenbach, A. N. Jonathan & A. J. Fisher, "Contribution of active hair-bundle motility to nonlinear amplification in the mammalian cochlea," *Proceedings of the National Academy of Sciences*, pp. 21076-21080 (2012).

INDEX

D

E

F

G

H

I

J

K

L

M

N

O

P

Q

R

S

T

U

V

W

X

Y

Z

Phononics 2023

6th International Conference on Phononic Crystals/Metamaterials/ Metasurfaces, Phonon Transport, and Topological Phononics

June 12 - 16, 2023 – Manchester, England